

## **General Disclaimer**

### **One or more of the Following Statements may affect this Document**

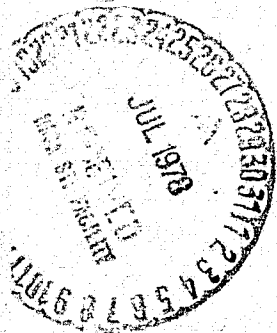
- This document has been reproduced from the best copy furnished by the organizational source. It is being released in the interest of making available as much information as possible.
- This document may contain data, which exceeds the sheet parameters. It was furnished in this condition by the organizational source and is the best copy available.
- This document may contain tone-on-tone or color graphs, charts and/or pictures, which have been reproduced in black and white.
- This document is paginated as submitted by the original source.
- Portions of this document are not fully legible due to the historical nature of some of the material. However, it is the best reproduction available from the original submission.

# High-Power, Ultralow-Mass Solar Arrays: FY-77 Solar Arrays Technology Readiness Assessment Report

(NASA-CR-157265) HIGH-POWER, ULTRALOW-MASS  
SOLAR ARRAYS: FY-77 SOLAR ARRAYS TECHNOLOGY  
READINESS ASSESSMENT REPORT, VOLUME 2 (Jet  
Propulsion Lab.) 514 p HC A23/MF A01

N78-27531

Unclas  
CSCL 10A G3/44 25143



National Aeronautics and  
Space Administration

Jet Propulsion Laboratory  
California Institute of Technology  
Pasadena, California



1. Report No. JPL Pub. 78-48	2. Government Accession No.	3. Recipient's Catalog No.	
4. Title and Subtitle High-Power, Ultralow-Mass Solar Arrays: FY-77 Solar Arrays Technology Readiness Assessment Report. Volume I and II		5. Report Date June 15, 1978	
		6. Performing Organization Code	
7. Author(s) E. N. Costogue, L.E. Young, H. Brandhorst		8. Performing Organization Report No.	
9. Performing Organization Name and Address JET PROPULSION LABORATORY California Institute of Technology 4800 Oak Grove Drive Pasadena, California 91103		10. Work Unit No.	
		11. Contract or Grant No. NAS 7-100	
		13. Type of Report and Period Covered JPL Publication	
12. Sponsoring Agency Name and Address NATIONAL AERONAUTICS AND SPACE ADMINISTRATION Washington, D.C. 20546		14. Sponsoring Agency Code	
15. Supplementary Notes			
16. Abstract <p>This report describes the results of a NASA intercenter effort conducted during FY 1977 to assess the technology readiness of solar array designs for future planetary missions and particularly for the Halley's comet ion drive space vehicle. The effort involved the participation of JPL, MSFC and LeRC for assessment of critical component technology for the development of candidate solar array designs, and for technology development planning. The main body of the report (Volume I) summarizes results and conclusions, of the NASA Centers' efforts. Contractors' reports, which are included in Volume II, present the development activities in detail.</p>			
17. Key Words (Selected by Author(s)) Spacecraft Propulsion and Power Engineering (General) Energy Production and Conversion Lunar and Planetary Exploration (Advanced)		18. Distribution Statement  Unclassified - Unlimited	
19. Security Classif. (of this report)  Unclassified	20. Security Classif. (of this page)  Unclassified	21. No. of Pages  152 + 544	22. Price

## HOW TO FILL OUT THE TECHNICAL REPORT STANDARD TITLE PAGE

Make items 1, 4, 5, 9, 12, and 13 agree with the corresponding information on the report cover. Use all capital letters for title (item 4). Leave items 2, 6, and 14 blank. Complete the remaining items as follows:

3. Recipient's Catalog No. Reserved for use by report recipients.
7. Author(s). Include corresponding information from the report cover. In addition, list the affiliation of an author if it differs from that of the performing organization.
8. Performing Organization Report No. Insert if performing organization wishes to assign this number.
10. Work Unit No. Use the agency-wide code (for example, 923-50-10-06-72), which uniquely identifies the work unit under which the work was authorized. Non-NASA performing organizations will leave this blank.
11. Insert the number of the contract or grant under which the report was prepared.
15. Supplementary Notes. Enter information not included elsewhere but useful, such as: Prepared in cooperation with... Translation of (or by)... Presented at conference of... To be published in...
16. Abstract. Include a brief (not to exceed 200 words) factual summary of the most significant information contained in the report. If possible, the abstract of a classified report should be unclassified. If the report contains a significant bibliography or literature survey, mention it here.
17. Key Words. Insert terms or short phrases selected by the author that identify the principal subjects covered in the report, and that are sufficiently specific and precise to be used for cataloging.
18. Distribution Statement. Enter one of the authorized statements used to denote releasability to the public or a limitation on dissemination for reasons other than security of defense information. Authorized statements are "Unclassified-Unlimited," "U. S. Government and Contractors only," "U. S. Government Agencies only," and "NASA and NASA Contractors only."
19. Security Classification (of report). NOTE: Reports carrying a security classification will require additional markings giving security and downgrading information as specified by the Security Requirements Checklist and the DoD Industrial Security Manual (DoD 5220.22-M).
20. Security Classification (of this page). NOTE: Because this page may be used in preparing announcements, bibliographies, and data banks, it should be unclassified if possible. If a classification is required, indicate separately the classification of the title and the abstract by following these items with either "(U)" for unclassified, or "(C)" or "(S)" as applicable for classified items.
21. No. of Pages. Insert the number of pages.
22. Price. Insert the price set by the Clearinghouse for Federal Scientific and Technical Information or the Government Printing Office, if known.

# **High-Power, Ultralow-Mass Solar Arrays: FY-77 Solar Arrays Technology Readiness Assessment Report**

**E.N. Costogue**  
Jet Propulsion Laboratory

**L.E. Young**  
Marshall Space Flight Center

**H. Brandhorst**  
NASA-Lewis Research Center

June 15, 1978

National Aeronautics and  
Space Administration

**Jet Propulsion Laboratory**  
California Institute of Technology  
Pasadena, California

Prepared Under Contract No. NAS 7-100  
National Aeronautics and Space Administration

## CONTENTS

This volume contains reports of contractors under contract to MSFC and JPL for the development of solar array designs and solar array technology during FY'77 and other related reports. The reports are grouped as follows:

Section 1 - Lockheed Missiles Space Co., Final Report on Extended Performance SEP Solar Array Study, MSFC NAS 8-31352.

Section 2 - Solarex, Inc., Final Report on Development of a High Efficiency Thin Silicon Solar Cell, JPL 954290.

Section 3 - General Electric Space Division Phase II Assessment Report on 200 W/kg Solar Array Conceptual Approach Study, JPL 954393.

Section 4 - Lockheed Missiles Space Co., Final Report Phase II Spraylon Fluorocarbon Encapsulation for Silicon Solar Cell Array, JPL 954410.

Section 5 - NASA-OAST, Technology Assessment of Concentrator Solar Arrays, June 3, 1977 Meeting Report.

**EXTENDED PERFORMANCE  
SEP SOLAR ARRAY STUDY**

**FINAL REPORT**

**NAS8-31352**

**Prepared for  
National Aeronautics and Space Administration  
George C. Marshall Space Flight Center  
Huntsville, Alabama**

**by  
Space Systems Division**

**PRECEDING PAGE BLANK NOT FILMED**

## FOREWORD

This final report summarizes the technology status and design evaluations performed for the preliminary design of advanced lightweight planar and concentrator solar arrays in the 60 to 120 kW range. This document is required by Contract NAS8-31352, Exhibit A Statement of Work. It was prepared by the Space Systems Division of Lockheed Missiles and Space Company, Inc. for the National Aeronautics and Space Administration's Marshall Space Flight Center, Huntsville, Alabama. The contents are not necessarily endorsed by the Marshall Space Flight Center or the National Aeronautics and Space Administration.

## ABSTRACT

LMSC has been performing a technology development program for a high-power, lightweight solar array system for solar electric propulsion (SEP), since October 1975. The work has been directed to a 66 W/kg requirement with the solar array system capable of performing over the range of 0.3 A.U. to 6.0 A.U. from the sun. In March 1977, LMSC commenced design studies for an ultra-lightweight solar array system that would meet the requirements of the Halley's Comet Rendezvous (HCR) SEP Mission. Two design concepts for the Extended Performance SEP Solar Array were studied. One is a planar, flat-fold array system in two power level designs, 60 kW and 120 kW at 1 A.U. from the sun. The two power levels are both in two specific power designs, 200 and 240 W/kg. The other design concept is a trough concentrator, flat-fold array system. Two concentrator designs were defined; one is a two-dimensional concentrator and the other is a combined two-dimensional and three-dimensional trough concentrator.

The planar arrays require the use of high efficiency Thin Cells (2 mil and 3 mil) and thin organic cell covers, combined with a lightened version of the SEP Solar Array printed circuit substrate. The concentrator array, because of improved power output at low solar illumination intensity, can meet the HCR Mission power requirements without an ultra-high specific power solar array design and therefore represents a lower technology development risk for the HCR Mission.

The selected baseline array design for the HCR Mission employs a 3-D concentrator with in-blanket flat-fold trough reflectors and movable side reflectors that are positioned to be either aiding concentration or not operating. This design requires the least number of solar cells but based on the launch stowage constraints requires significant articulation to position the arrays in the ready-to-extend position. The alternate concentrator array design is a 2-D design that greatly simplifies launch stowage and deployment of the array wings to the ready-to-extend position. The array blankets and reflector assemblies are stored between the spacecraft and the IUS. More solar cells are required for this design than for the 3-D design. Both the concentrator array designs meet the HCR



weight and power requirements with the use of a 5 mil thick, 13 percent covered efficiency solar cell and a 3 mil thick ceria stabilized microsheet cell cover combined with a lightened version of the SEP Solar Array printed circuit substrates.

## TABLE OF CONTENTS

	<u>Page</u>
FOREWORD	vi
TABLE OF CONTENTS	ix
LIST OF FIGURES	xi
LIST OF TABLES	xiii
 SECTION 1 INTRODUCTION	 1-1
1.1 OBJECTIVES	1-1
1.2 DESIGN REQUIREMENTS	1-2
1.2.1 Non-Concentrating Array	1-2
1.2.2 Concentrating Array	1-2
1.2.3 All Arrays	1-2
1.3 APPROACH	1-3
 SECTION 2 RESULTS, CONCLUSIONS, AND RECOMMENDATIONS	 2-1
2.1 RESULTS AND DATA	2-1
2.1.1 Design Study Results	2-1
2.1.2 Concentrator Solar Array Model Testing	2-19
2.1.3 Technology Assessment	2-26
2.2 CONCLUSIONS	2-31
2.3 RECOMMENDATIONS	2-33
2.3.1 HCR-SEP Mission Program	2-33
2.3.2 Recommended Technology	2-33
 SECTION 3 ASSESSMENT OF CRITICAL COMPONENT TECHNOLOGY	 3-1
3.1 SOLAR CELL TECHNOLOGY	3-1
3.1.1 Characteristics	3-1
3.1.2 Efficiency Projection	3-5
3.1.3 Wraparound Contact Cells	3-5
3.1.4 Production Rate	3-9
3.2 SOLAR CELL COVER TECHNOLOGY	3-10
3.2.1 Glass Covers	3-10
3.2.2 Spraylon	3-11
3.2.3 Polyimide	3-12
3.2.4 Glass-Resins	3-12
3.2.5 RTV Silicone	3-13
3.2.6 Cell Cover Coatings and Surfaces	3-13
3.3 BLANKET TECHNOLOGY	3-13
3.3.1 Design	3-13
3.3.2 Fabrication Technology and Processes	3-14
3.3.3 Qualification Testing	3-19

	<u>Page</u>
3.4 TECHNOLOGY DEVELOPMENT PLAN AND COST ESTIMATE	3-21
3.4.1 Introduction	3-21
3.4.2 Technology Status	3-21
3.4.3 Recommended Technology Development Projects	3-24
3.4.4 Schedule and Cost Estimates	3-30
3.5 NON-CONCENTRATING ARRAY DESIGN	3-32
3.5.1 Electrical Design, Planar Arrays	3-32
3.5.2 Mechanical Design, Planar Arrays	3-36
3.5.3 Structural Characteristics	3-40
3.5.4 Performance Data	3-41
3.5.5 Cost Data Summary	3-47
3.6 CONCENTRATING ARRAY DESIGN	3-49
3.6.1 Electrical Design	3-49
3.6.2 Mechanical Design	3-84
3.6.3 Structural Characteristics	3-102
3.6.4 Alternate Concentrator Array Design	3-111
3.6.5 Performance Data	3-114
3.6.6 Cost Data Summary	3-119
3.7 PROBABILITY OF ARRAY PROGRAM ACHIEVEMENT	3-125
SECTION 4 REFERENCES	4-1
APPENDIX A 36-CELL MODEL CONCENTRATOR TEST DATA	A-1
APPENDIX B 20-CELL MODEL CONCENTRATOR TEST DATA	B-1

## LIST OF FIGURES

<u>Figure</u>		<u>Page</u>
1-1	Launch Stowage Volume	1-4
2-1	200 W/kg Planar Solar Array Configurations	2-5
2-2	240 W/kg Planar Solar Array Configurations	2-6
2-3	Baseline Concentrator Array-Fully Deployed	2-9
2-4	Baseline Concentrator Array Stowage and Deployment	2-11
2-5	Alternate Concentrator Array Wing	2-16
2-6	36-Cell Concentrator Test Model	2-20
2-7	Effective Concentration Ratio Using $I_{sc}$ Ratios	2-21
2-8	20-Cell Concentrator Test Model	2-23
2-9	20-Cell Model Schematic and Test Results	2-24
2-10	36-Cell Model Temperature Correlation	2-25
3-1	Baseline Manufacturing Concept for Substrate Fabrication	3-16
3-2	Integral Interconnect Substrate Design	3-17
3-3	Technology Development Schedule and Cost Estimates	3-31
3-4	Planar Array Wing Sizes	3-34
3-5	200 W/kg Planar Array Deployed Configurations	3-37
3-6	240 W/kg Planar Array Deployed Configuration	3-38
3-7	120 kW Planar Array Stowage and Deployment	3-39
3-8	SEP Solar Array Concentrator Configurations	3-50
3-9	Concentrator Ratio vs Reflector Angle	3-54
3-10	"W" Concentration Ratio Vs Angle	3-55
3-11	3-Dimensional Concentration Ratio Vs Angle	3-56
3-12	60° Trough Misalignment Effects	3-58
3-13	67.5° Trough Misalignment Effects	3-59
3-14	"W" Configuration Misalignment Effects	3-60
3-15	Baseline Array Misalignment Effects	3-61
3-16	Proton Environment Effects	3-63
3-17	Solar Cell Radiation Degradation	3-64
3-18	Shape Factor Variation Across Trough Blanket	3-67
3-19	Trough Configuration Temperature Prediction, $\alpha_s = 0.85$	3-72
3-20	Trough Configuration Temperature Prediction, $\alpha_s = 0.70$	3-73
3-21	Baseline Array Temperatures	3-75
3-22	Baseline and Alternate Array Temperatures	3-76
3-23	Array Configurations	3-78
3-24	Solar Array Panel	3-82
3-25	Array Harness Design	3-83
3-26	Baseline Concentrator SEP Solar Array Wing	3-85
3-27	Baseline Array Wing Stowage Configuration	3-86
3-28	Baseline Array Wing Stowed Envelope	3-87
3-29	Baseline Array Wing Deployment Sequence	3-89
3-30	SEP Solar Array Wing Deployer Boom or Extension Mast	3-91

## LIST OF FIGURES (Cont.)

<u>Figure</u>		<u>Page</u>
3-31	In-Blanket Reflector (Deployed)	3-93
3-32	Array Packing Data	3-94
3-33	Blanket Tensioning	3-96
3-34	Reflector Hinge Assembly	3-98
3-35	Side Reflectors	3-99
3-36	Side Reflector Assembly Technique	3-101
3-37	Stowage and Deployment Concept 1	3-103
3-38	Stowage and Deployment Concept 2	3-104
3-39	Stowage and Deployment Concept 3	3-106
3-40	Single Blanket Concentrator Wing	3-108
3-41	Single Blanket Concentrator Wing Model	3-109
3-42	Baseline Array Mast Stiffness and Blanket Tensioning	3-110
3-43	Alternate Concentrator Array Wing-Fully Deployed	3-112
3-44	Alternate Concentrator Array Stowage and Deployment	3-113

## LIST OF TABLES

<u>Table</u>		<u>Page</u>
2-1	200 W/kg Planar Array Design Assumptions	2-2
2-2	240 W/kg Planar Array Design Assumptions	2-3
2-3	60 kW and 120 kW Planar Solar Array Performance	2-4
2-4	60 kW Planar Solar Array Weight Summary	2-7
2-5	120 kW Planar Solar Array Weight Summary	2-8
2-6	Baseline Concentrating Array Power and Assumptions	2-12
2-7	Baseline Concentrator Array Weight Summary	2-13
2-8	Baseline Concentrator Array Performance	2-14
2-9	Alternate Concentrator Array Design Assumptions	2-17
2-10	Alternate Concentrator Array Weight Summary	2-18
2-11	Alternate Concentrator Array Performance	2-18a
2-12	Cell Cover Candidates	2-28
3-1	Criteria For State-of-the-Art Assessment	3-2
3-2	Development Risks for Wraparound Contact Cells	3-6
3-2A	Wraparound Solar Cells	3-7
3-3	Flat Fold Planar Array Configurations	3-33
3-4	200 W/kg Planar Array Design Characteristics	3-35
3-5	60 kW and 120 kW Planar Array Performance Data	3-42
3-6	60 kW, 200 W/kg Planar Array Weight Summary	3-43
3-7	120 kW, 200 W/kg Planar Array Weight Summary	3-44
3-8	60 kW, 240 W/kg Planar Array Weight Summary	3-45
3-9	120 kW, 240 W/kg Planar Array Weight Summary	3-46
3-10	Concentrator Array Concepts	3-51
3-11	Thermal Design Support	3-65
3-12	Reflector Metal Candidates	3-69
3-13	Array Configurations	3-77
3-14	Baseline Array Performance	3-115
3-15	Baseline Array Module Voltage	3-116
3-16	Alternate Array Performance	3-117
3-17	Alternate Array Module Voltage	3-118

## 1.0 INTRODUCTION

### 1.1 OBJECTIVES

The cost effective application of low acceleration ion thruster propulsion for extended space exploration, such as the proposed Halley's Comet mission, requires an ultra-lightweight large-area solar array. A planar non-concentrating solar array must have a specific power of 200 W/kg (91 W/lb). A concentrating solar array, with electric propulsion, will provide better performance than a planar array at sun distances of 1.0 or more A. U. Thus the 1 A.U. specific power requirements for a concentrating solar array are significantly less than that of a planar array for the Halley's Comet mission or similar missions. Current lightweight solar array technology has developed large area planar arrays having a specific power of 66 W/kg (30 W/lb). Concentrator solar array technology is relatively undeveloped. This study was therefore required to develop preliminary advanced SEP solar array systems designs, to define applicable state-of-the-art technology, and to recommend the solar array technology development necessary to meet the advanced SEP solar array design requirements. This document presents the evaluations and design efforts performed and also the results of concentrator model testing used to support array performance predictions.

The specific objectives of the study were to:

1. Perform a solar array state-of-the-art assessment of applicable lightweight solar array technology.
2. Generate and document preliminary designs of an ultra-lightweight 60 kW and 120 kW non-concentrating array and of an equivalent concentrating solar array that will perform the Halley's Comet mission.
3. Provide a technology development plan and cost estimates for the specific recommended technology advancements needed to initiate flight hardware production by early 1979.

4. Determine the probability of timely flight hardware achievement for the solar arrays based on preliminary designs and required technology advancements and provide cost estimates for flight system development.
5. Construct and test an electrically functional developmental model of the most promising concentrating solar array module concept.

## 1.2 DESIGN REQUIREMENTS

The major design requirements for the advanced SEP solar array follow.

### 1.2.1 Non-Concentrating Array

- Power of non-concentrating array designs to be 60 kW and 120 kW BOL at 1 A.U., free space.
- Specific power objective is 200 W/kg with a design goal of 240 W/kg.

### 1.2.2 Concentrating Array

- | <u>A. U. From Sun</u> | <u>Power at Base of Array</u> |
|-----------------------|-------------------------------|
| 2.0                   | 48.4 kW                       |
| 3.0                   | 27.2 kW                       |
| 4.5                   | 14.0 kW                       |
- Total array system weight: 790 kg max.
- Array wing retraction not required if side reflectors are ejectable.

### 1.2.3 All Arrays

- Power degradation limited to 25% over five year period. Meet all performance requirements when exposed to specified charged particle environment.
- Full array deployment, 90% retraction and full redeployment for 50 cycles. An option is provided for concentrating arrays above.



- Stowage volume to be 4.5 m (14.76 ft.) diameter by 11.8 m (38.72 ft.) length, less the volume occupied by the remainder of the propulsion module (power conditioners, propellant tanks, thrusters, etc.). The launch stowage volume is shown in Figure 1-1.
- The extended array will be positioned such no part of the array will at any time be inside a 50° cone angle measured between the edge of any thruster at its exit plane and a line parallel to the thrust vector.
- Extended Array Natural Frequency:  $\geq 0.015$  Hz at Spacecraft Interface
- $V_{mp}$ , Base of Array, Conventional Drive: 200 to 400 VDC  
Direct Drive: 1600 to 4000 VDC if 1.25 Amperes  
Supplied
- $V_{oc}$ , Base of Array, Conventional Drive: 420 VDC  
Direct Drive: 5000 VDC
- Operating Temperature Range: -130°C to +140°C
- Thermal Shocks: 100 cycles, + 120°C to -190°C
- Maximum Loads, Longitudinal:  $\pm 4$  G's  
Yaw:  $\pm 4$  G's  
Pitch: + 10, -8 G's

### 1.3 APPROACH

The technical approach to the study was to perform the following tasks: (1) generate and document 60 kW and 120 kW non-concentrating solar array preliminary designs; (2) generate and document concentrating solar array preliminary designs; (3) assess and identify the technology required to develop and fly the designs in (1) and (2) above along with a technology development plan and cost estimate for the recommended technology advancements; (4) compare the performance and probability of success of the designs generated in (1) and (2) above; and (5) design, fabricate and test a model of a concentrating solar array module to support the definition of concentrating array design requirements.

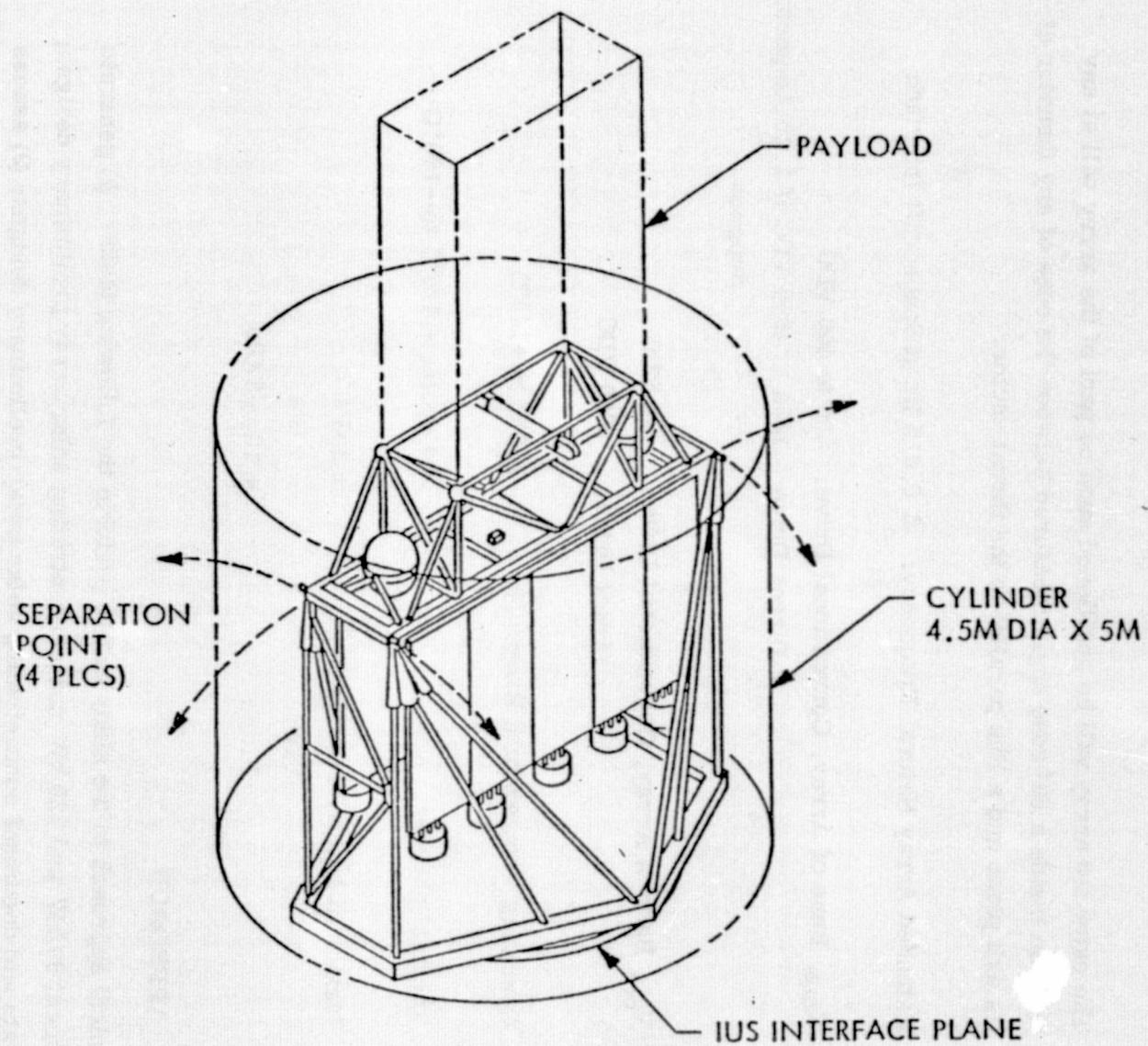


Figure 1-1 Launch Stowage Volume

ORIGINAL PAGE IS  
OF POOR QUALITY

## Task 1.0 Preliminary Design for Non-Concentrating Array

The starting point for the non-concentrating solar array designs was the current SEP Solar Array (25 kW) design. It was modified to meet the Extended Performance array area and new aspect ratio constraints. Since the solar cell assembly dominates the solar array weight and cost considerations it was investigated as the primary means of increasing non-concentrating solar array specific power. The evaluation of the cell thickness and coverglass thickness versus specific power and radiation degradation was emphasized.

### Solar Cells

The parameters studied were cell material (silicon and germanium arsenide), the base resistivity, cell thickness, AR coatings, front surface texturing, back surface fields and reflectors, thermal-optical properties, and advanced wraparound contact designs. These parameters were evaluated to optimize to the particular requirements of enhanced performance SEP arrays, e. g., high specific power over the design range of heliocentric distances.

### Solar Cell Covers

Candidate covers such as fused silica, ceria-doped microsheet, 7070 borosilicate glass, integral covers, FEP Spraylon and other plastic films were evaluated for application to the preliminary design.

### Substrates and Interconnects

A low mass flexible printed circuit substrate has been developed by LMSC for the SEP S/A Technology Development Program. The substrate uses two sheets of 0.5 mil Kapton/0.5 mil high temperature polyester adhesive. Reduction of these thicknesses was evaluated.

The interconnect metal mass is minimized by selecting low density metals and/or minimizing interconnect thickness and the percent area covered by the metal. For the selection of the interconnect, factors such as fabricability, power losses, compatibility with the cell bonding technique, heat removal, and thermal cycling strength were considered.

## Array Structures

Two basic flexible array stowage concepts used for launch support were considered in this study. The flat-fold designs developed to date require less structure mass per unit blanket mass than the roll-up. The volume of the array package is also less for the flat-fold array.

## Solar Array Structural/Mechanical Analyses

Alternate concepts for the solar array structural/mechanical design elements were generated and evaluated to evolve the preliminary design. These studies also provided a basis for the definition of the new technology requiring development.

## Structural Analysis

The structure includes the storage container, latching mechanisms, tension and guide line mechanisms. The stiffness of the structure was considered so that the natural frequencies will not allow resonance due to any predictable disturbance to the structure during the boost phase of flight.

## Solar Array Dynamic Analysis

<sup>\*</sup>  
An existing program was used to determine the structural vibration modes of the solar array concepts. This program evaluated the modal responses of structures that were modelled using discrete finite elements. Stiffness and mass matrices were formed from the finite elements to represent the properties of the combined array blanket and mast structures.

This analysis tool for solar arrays was used to determine the most effective weight and tension of the array by tuning various structural parameters in the analysis until an optimum boom and blanket modal response was reached considering torsional, in array plane and normal to array plane vibrations. In general, the normal to plane minimum allowable natural frequency controlled the array blanket tension requirement and the extension mast performance requirement.

---

\*SOLAR\*DYN is an LMSC-developed flexible solar array dynamics computer program.

### Thermal Analyses

Thermal studies performed to evaluate the array temperature over the mission and to optimize the thermal design such as low  $\alpha/\epsilon$  cell assembly designs.

### Radiation Analysis

Solar Array performance in specified radiation environments was determined by evaluating the equivalent 1 MeV electron fluences for the desired cover slide-substrate configurations, using the BOFES\* computer program, for prescribed mission environment. The provided proton fluence data was used to evaluate various cell cover/cell designs and to predict array degradation.

### Material Considerations

The temperature range anticipated for the array blanket, +140°C to -130°C, required screening of new lightweight materials to prevent failure. The preliminary design used mostly materials which are selected for the current SEP solar array. Recognizing the advantages of weight reduction, thermal dimensional stability and increased material stiffness, composite materials were extensively considered for array structural application.

### Task 2.0 Preliminary Design for Solar Concentrating Array

Concentrating reflectors were studied to provide additional energy to solar cells over the energy intercepted by the solar cells themselves. Due to the inefficiencies of the reflector, the total area of the array for a given power was increased over a non-concentrating array. The use of reflectors was studied to reduce the mass of the array system and reduce costs because of fewer solar cells.

Candidate solar cells, solar cell covers, substrates and interconnects, were all studied as indicated for the non-concentrating array design.

### Array Structures

The added problem of reflector stowage was considered along with its deployment, retraction and support.

---

\* BOFES is an LMSC-developed radiation effects computer program.

## Reflectors

Candidate materials for the reflector system are metallized plastics and these were compared based on availability, cost, efficiency, radiation resistance, weight, and ease of handling.

The concentrating array design concept was defined first with an 85 kW array with a CR (concentration ratio) of 2 at 1 A. U. and with capability to change configuration to provide a CR of 4. Design data was provided to MSFC for trajectory evaluation. Parametric studies were performed by LMSC to allow selection of the best set of design features that met the Halley's Comet mission requirements.

## Design Support

The mechanical/structural analyses effort was the same as for Task 1.0, non-concentrating array, with the addition of the evaluation of required reflector support, deployment, and tensioning systems.

The solar array dynamic analysis was the same as for Task 1.0 with the addition of modeling and analysis of deployed reflector and combined reflector/array blanket natural frequencies.

The thermal analyses evaluated the array blanket and reflector temperatures over the mission with various blanket-cell stack designs, concentration ratios, and reflector efficiencies.

The radiation analysis provided the same solar cell performance degradation predictions as in Task 1.0 and was also concerned with the performance degradation of the reflectors.

The material considerations were the same as for Task 1.0 with the addition of candidate reflector materials.

### Task 3.0 Technology Assessment, Technology and Flight Hardware Development Plans and Cost Estimates

A solar array system technology assessment was performed for the purpose of 1) assessing array technology as it applies to the SEP Halley's Comet mission, 2) providing guidance and direction for the Preliminary Design tasks, 3) categorizing the status of component and material technology, and 4) defining new technology requirements.

#### Assessment Method

Exclusive of design-peculiar elements which evolved in the design phase, there were certain components and materials that were the primary building blocks and candidates of consideration for the SEP array that were subjected to state-of-the-art categorization early in the Study. By analyzing the components individually, the validity of system selections was increased.

For example, at this time, ES bonded glass and FEP covers would be classified as insufficient (Category II) whereas fused-silica covers would be sufficient (Category I). A system which contains all Category I components may be very low risk but the weight would be too high.

Where a component or material was considered marginal (Category II), there might be accommodation in its system use, i. e., stress relief, selected thermal-optical coating, etc. where it would be acceptable at the system level. Therefore, design iteration occurred wherein, prior to rejection, the impact of each component on the system was evaluated. Because of the necessity to evaluate a component at the system level, there was no blanket rejection or low state-of-the-art categorization of the component or material until its system level status was ascertained.

The state-of-the-art assessment was used to develop a recommended technology development plan based on a February 1979 flight hardware development start. This development plan included cost estimates and schedules for the accomplishment of the plan.

#### Task 4.0 Comparison of Concentrating and Non-Concentrating Array Designs

The design and performance data generated for the planar solar arrays and the one concentrating solar array were compared. The probability of achieving required technology readiness by February 1979 was a factor of interest in the design comparisons. The trajectory performance of the concentrating array was of equal interest to the array specific power since this array has advantages at low solar intensities. The large area, concentrating solar array is also a new technology area where probability of achievement was of interest.

Ease of fabrication, ground testing, and costs associated with both technology development and flight hardware development are additional factors considered in comparing the designs developed in Tasks 1.0 and 2.0. The results of the comparison were the basis for the recommended technology development and flight hardware development plans.

#### Task 5.0 Model Fabrication and Test

A sun concentrating model of a solar cell module and two solar cell module designs that were electrically functional were designed, fabricated, tested, and delivered to NASA-MSFC. The objective of the model fabrication was to allow preliminary evaluation of reflector/cell module performance and design requirements in the areas of:

- distribution of reflector input over cell region
- determination of effective concentration ratios

The model was designed to allow the above evaluations. The model was tested in a thermal vacuum chamber with a sun simulator by Boeing under contract to NASA-MSFC and the test data were provided to LMSC for evaluation of the model performance.



## **2.0 RESULTS, CONCLUSIONS, AND RECOMMENDATIONS**

### **2.1 RESULTS AND DATA**

The results of the array design studies, model testing, and the assessment of required technology to start the flight hardware development are presented below.

#### **2.1.1 Design Study Results**

Early in the study it became apparent that a concentrator array would require the least risk technology advancement requirements to perform the Halley's Comet Rendezvous (HCR) Mission. As a result, emphasis was placed on the concentrator array designs and more design details were developed for this design concept. The planar array designs developed, however, are based on the SEP Solar Array design data and required less new design effort.

**2.1.1.1 Baseline Planar Solar Arrays.** The baseline planar array designs selected employ a 3 mil thick, 2 x 2 cm solar cell, 12.5% covered efficiency silicon solar cell with a 1 mil RTV silicone cover for both the 60 kW and 120 kW array system to provide 200 W/kg. The 240 W/kg design goal is obtained with the same cell assembly except that the 3 mil cell is reduced to 2 mil thickness while providing 12.6% covered efficiency at AMO, 28°C. The array power and design assumptions are shown in Tables 2-1 and 2-2. The performances of the baseline planar arrays are shown in Table 2-3 as a function of sun distance. The array configurations are shown in Figures 2-1 and 2-2. The weight summaries of the 200 W/kg arrays are contained in Tables 2-4 and 2-5.

**2.1.1.2 Baseline Concentrator Solar Array.** The design studies for the concentrator solar arrays resulted in the definition of two designs that met the design requirements. The selected baseline design is shown in its deployed configuration (one wing) in Figure 2-3. The array employs a 3-dimensional trough reflector configuration. The flat-fold array blankets contain in-blanket flat-fold reflectors with reflector angles of 60° with the blanket plane and side reflector sheets are at an angle of 67.5° to the blanket plane. The aspect ratio and weight of the array wing is minimized by employing two sections of the 3-D concentrator array in a side-by-side configuration. The resulting loads on the extension mast due to tensioning of the blankets and side reflectors are centered on the mast to eliminate mast bending moments.

TABLE 2-1  
200 W/kg PLANAR ARRAY DESIGN ASSUMPTIONS

Net BOL Array Power at 1 A.U. Sun Distance	60.0 kW	120.0 kW
Gross BOL Array Power at 1 A.U. Sun Distance	64.66 kW	129.32 kW
Cell Size, Conventional Contact	2.0 cm x 2.0 cm x 3 mil	2.0 cm x 2.0 cm x 3 mil
Cell Assembly Efficiency (28°C, AMO)	12.5%	12.5%
Coverslide	1 mil RTV 655 Silicone	1 mil RTV 655 Silicone
Cell Assembly Solar Absorptance	0.83	0.83
Cell Assembly Emittance	0.65	0.65
Cell Operating Temp. at 1 A.U. Sun Distance	60°C	60°C
Number of Cells per Array	1,114,106	2,228,212
Packing Factor	0.96	0.96
Cell Blanket Area	464 m <sup>2</sup>	928 m <sup>2</sup>
Interconnect	1 mil Aluminum	1 mil Aluminum

TABLE 2-2

## 240 W/kg PLANAR ARRAY DESIGN ASSUMPTIONS

Net BOL Array Power at 1 A. U. Sun Distance	60.0 kW	120.0 kW
Gross BOL Array Power at 1 A. U. Sun Distance	64.66 kW	129.32 kW
Cell Size, Conventional Contact	2.0 cm x 2.0 cm x 2 mil	2.0 cm x 2.0 cm x 2 mil
Cell Assembly Efficiency (28°C, AMO)	12.6%	12.6%
Coverslide	1 mil RTV 655 silicon	1 mil RTV 655 silicone
Cell Assembly Solar Absorptance	0.83	0.83
Cell Assembly Emittance	0.65	0.65
Cell Operating Temp. at 1 A. U. Sun Distance	60°C	60°C
Number of Cells per Array	1,105,263	2,210,526
Packing Factor	0.96	0.96
Cell Blanket Area	460.5 m <sup>2</sup>	921 m <sup>2</sup>
Interconnect	1 mil Aluminum	1 mil Aluminum

TABLE 2-3

## 60 kW AND 120 kW PLANAR SOLAR ARRAY PERFORMANCE

Sun Distance A. U.	Temp. (°C)	V <sub>mp</sub> /Cell (mv)	60 kW Array BOL Power (kW)	60 kW Array EOL Power* (kW)	120 kW Array BOL Power (kW)	120 kW Array EOL Power (kW)
1.0	60	373.4	60.00	48.00	120.00	96.00
1.5	-1.1	516.7	32.08	25.66	64.16	51.33
2.0	-37.5	594.3	24.35	19.48	48.70	38.96
3.0	-80.7	684.9	9.96	7.97	19.92	15.94
4.0	-106.5	721.8	5.38	4.30	10.76	8.61
4.5	-116.0	723.7	3.99	3.19	7.98	6.38

\*20% degradation

ORIGINAL PAGE IS  
OF POOR QUALITY

2-5

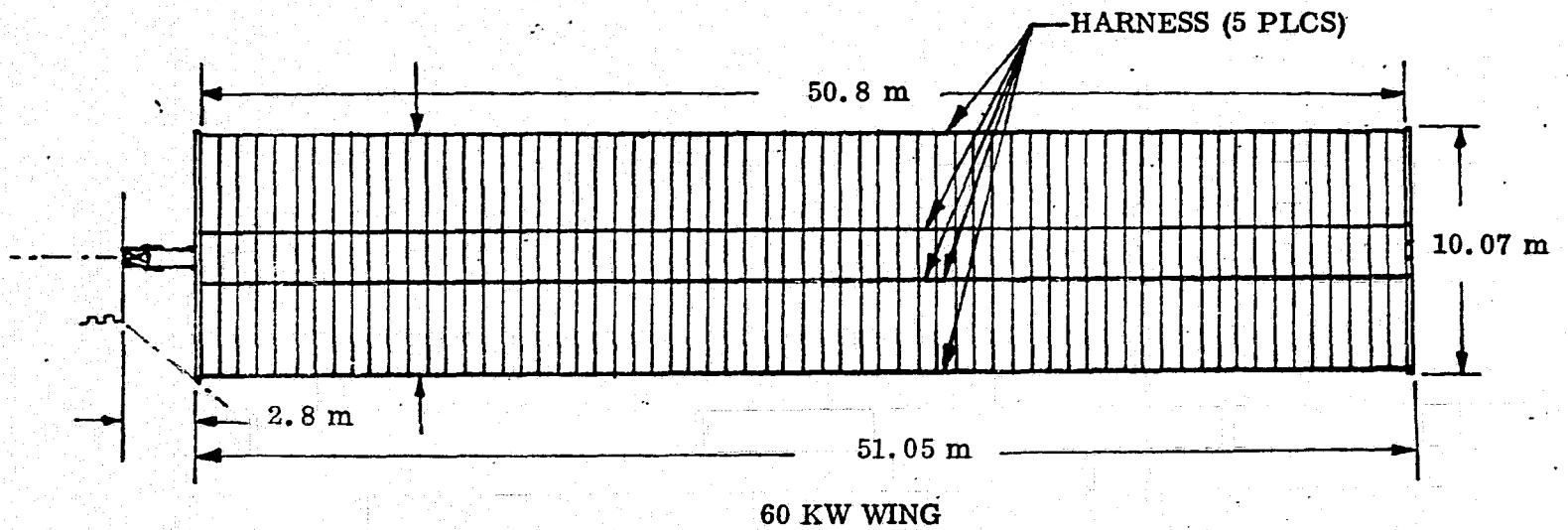
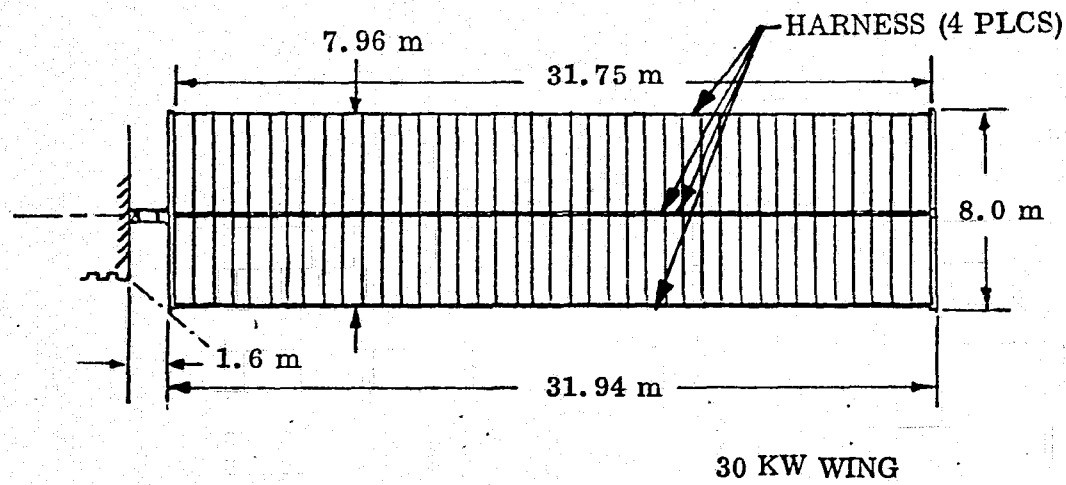
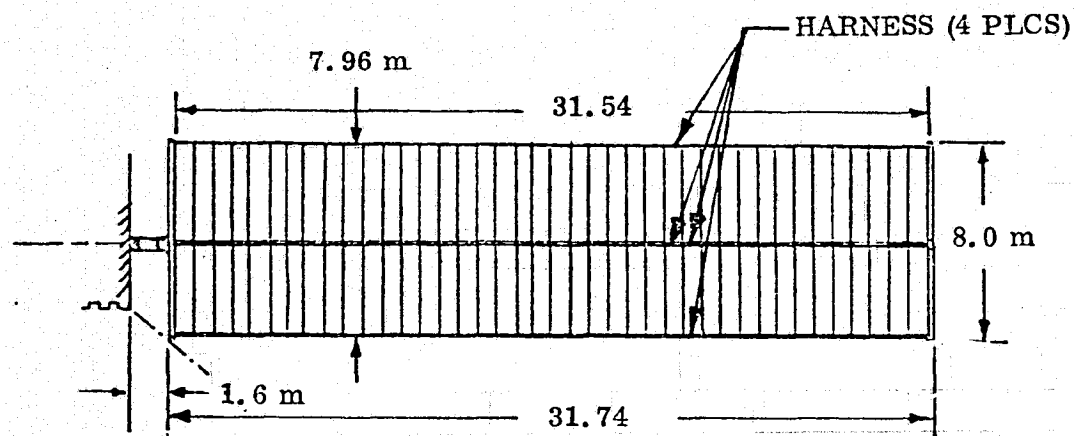
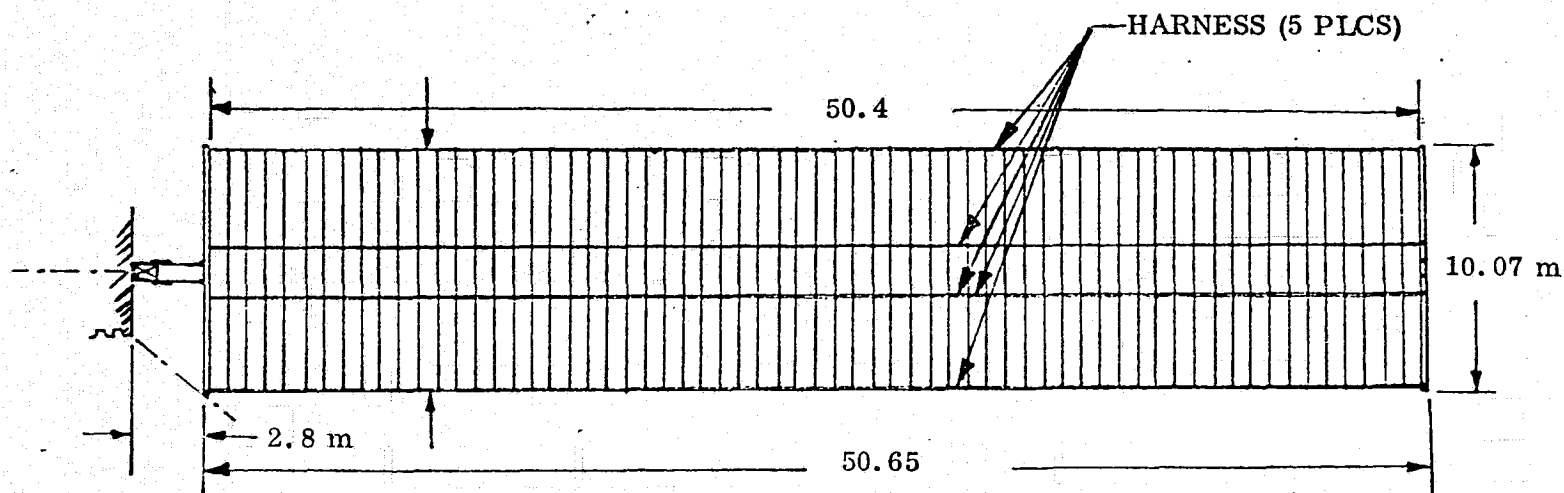


Figure 2-1 200 W/kg Planar Solar Array Configurations



30 kW WING



60 kW WING

Figure 2-2 240 W/kg Planar Solar Array Configurations

TABLE 2-4

200 W/kg, 60 KW PLANAR SOLAR ARRAY WEIGHT SUMMARY

Component	Weight (kg)	No. Req'd/Wing	Wing Weight (kg)
Blanket Assembly	44.90	2	89.8
Panels (40)	36.15		
Hinges (40)	1.7		
Tension Distribution (1)	0.45		
Leader	0.6		
Harness	6.0		
Blanket Tension & Control	3.4	2	6.8
Cover	3.02	2	6.0
Container	5.78	2	11.6
Blanket Padding	0.03	78	2.34
Mast	23.6	1	23.6
Tip Fitting	0.7	1	0.7
Wing Position Boom	9.0	1	9.0
Total Wing Weight			149.84 kg
Total Array Weight			299.7 kg

TABLE 2-5

## 200 W/kg, 120 KW PLANAR SOLAR ARRAY WEIGHT SUMMARY

Component	Weight (kg)	No. Req'd/Wing	Wing Weight (kg)
Blanket Assembly	70.00	2.5	175.0
Panels (64)	58.23		
Hinges (64)	2.72		
Tension Distribution (1)	0.45		
Leader	0.6		
Harness	8.0		
Blanket Tension & Control	4.0	2.5	10.0
Cover	4.4	2.5	11.0
Container	9.24	2.5	23.12
Blanket Padding	0.03	158.0	4.74
Mast	60.0	1	60.0
Tip Fitting	1.0	1	1.0
Position Links	2.5	2	5.0
Wing Position Boom	10.0	1	10.0
Total Wing Weight			299.86
Total Array Weight			599.72



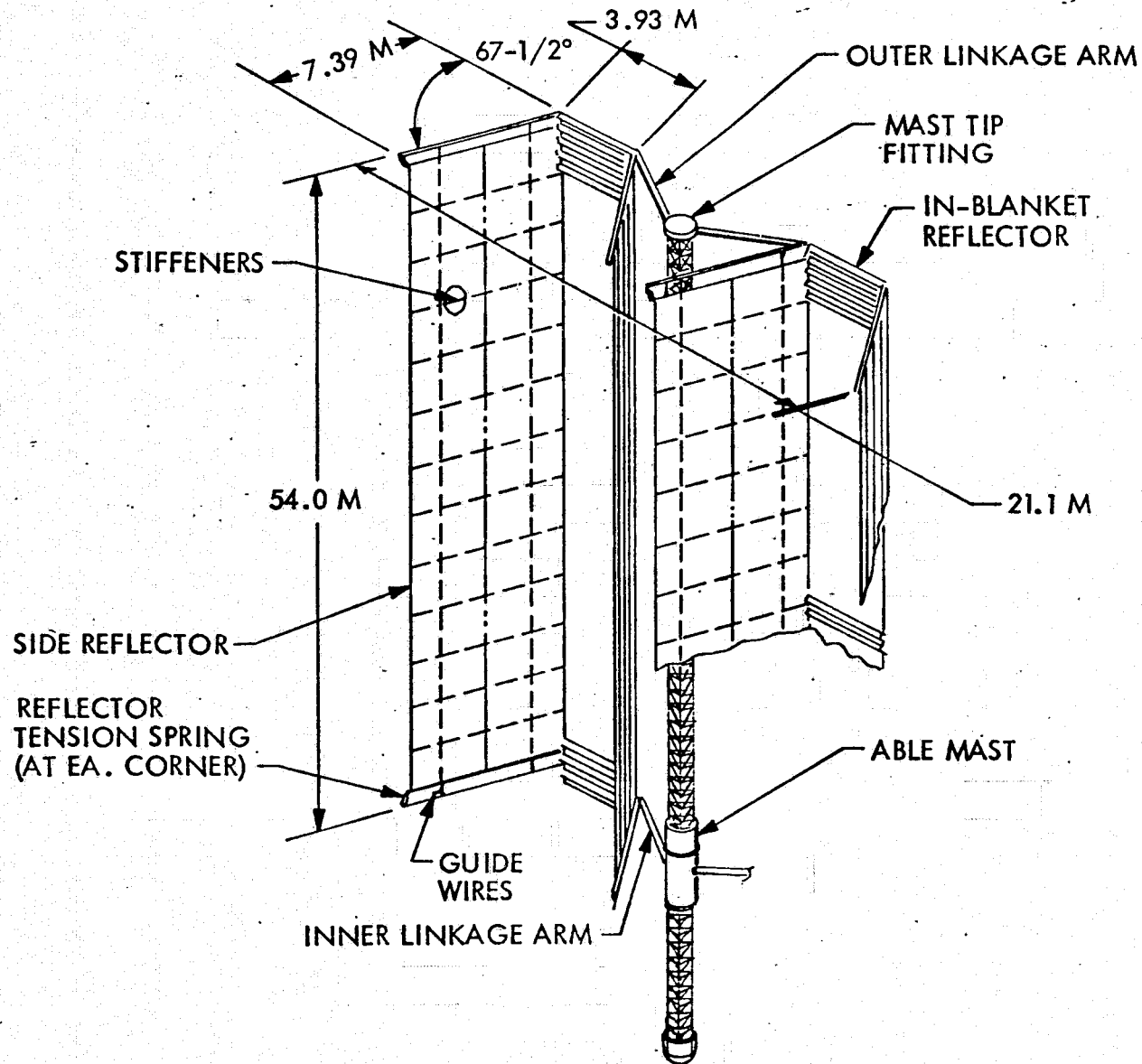


Figure 2-3 Baseline Concentrator Array Wing - Fully Deployed

The side reflectors are initially positioned so that they do not contribute to array concentration ratio and only the in-blanket reflectors are operating ( $CR = 1.9$ ). When array temperature permits, the side reflectors are positioned to increase the effective concentration ratio to 3.5.

The stowed configuration of the array wing is illustrated in Figure 2-4. A coilable longeron lattice structure beam is used to separate the array wing from the spacecraft by 11.5 m and thereby keep the array out of the thruster plume volume. Following release of the array wing from the spacecraft structure, the separation beam is rotated 90 degrees to align it with the array tracking axis in the spacecraft. Next, the array extension mast is rotated 90° to align it with the array tracking axis. The two stored array modules each containing an array blanket and two side reflectors are positioned by the linkage arms that connect them to the extension mast at the mast canister and tip fitting. The side reflector packages, which are folded in half for launch, are then articulated to their proper orientation by unfolding and rotating to the 67.5° angle. The side reflectors are initially configured and positioned to avoid contributing to array concentration ratio. The extension of the mast deploys the two array blankets and the four side reflectors.

The baseline concentrating array power and design assumptions are shown in Table 2-6. The baseline solar cell is a 5 mil, 2 x 4 cm wraparound contact silicon solar cell with a 3 mil ceria stabilized microsheet cover (CMS) and a covered efficiency of 13%, AMO, 28°C. The baseline concentrator array weight summary is shown in Table 2-7. The performance of the baseline concentrator array is shown in Table 2-8.

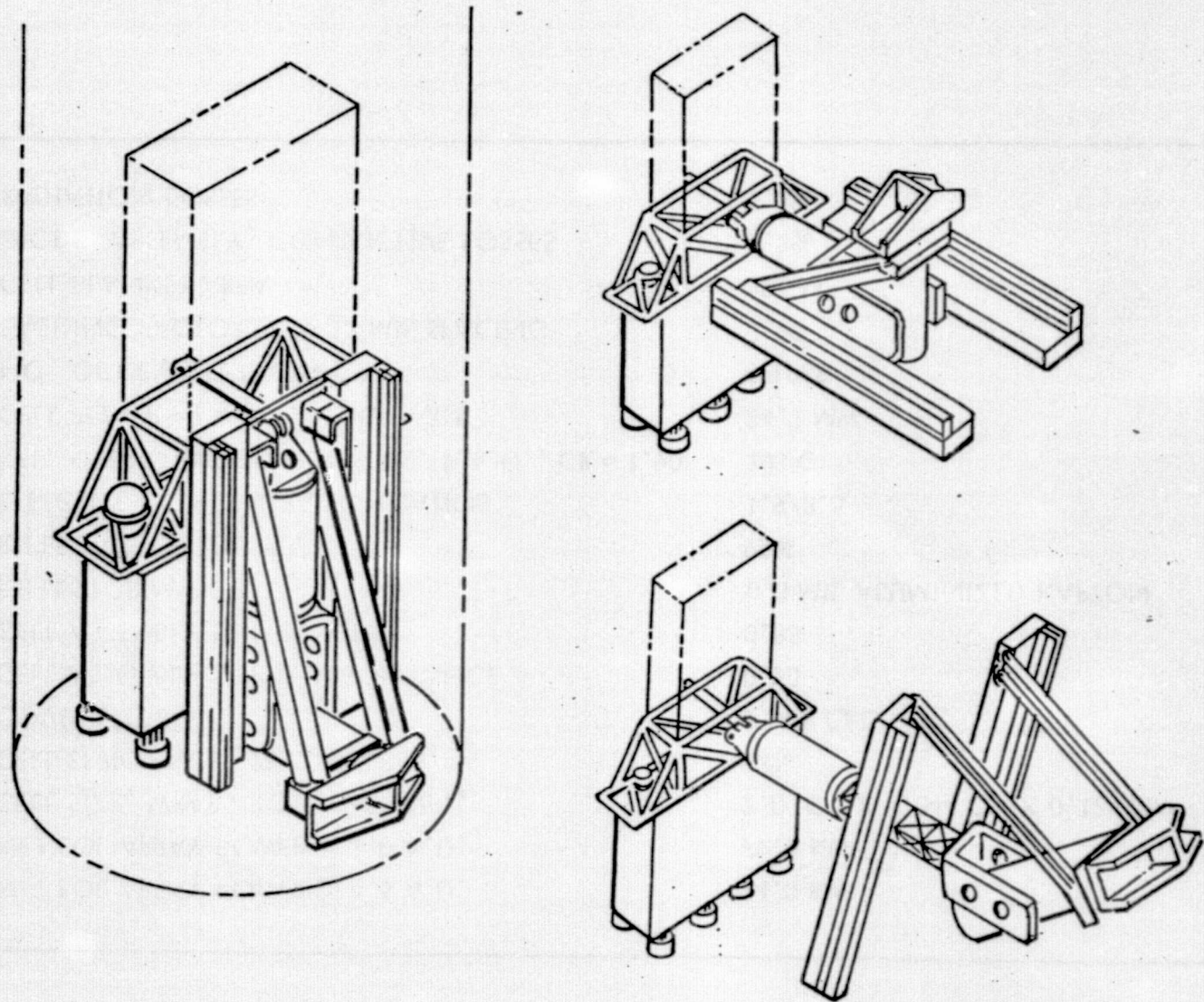


Figure 2-4 Baseline Concentrator Array Stowage and Deployment

TABLE 2-6

## BASELINE CONCENTRATING ARRAY POWER AND ASSUMPTIONS

NET EOL ARRAY POWER @ 4.5 A.U.	14.0 KW
NET EOL ARRAY POWER @ 1.0 A.U.	79.6 KW
CELL SIZE, WRAP AROUND CONF.,	2.0 CM X 4.044 CM X 0.125 MM
CELL EFFICIENCY, 28°C, AMO	13%
COVER SLIDE	3 MIL CMS
CELL ASSEMBLY SOLAR ABSORPTANCE	0.70
CELL ASSEMBLY EMITTANCE	0.85
REFLECTOR MATERIAL	0.3 MIL ALUMINIZED KAPTON
REFLECTOR EFFICIENCY	92%
EFFECTIVE CONCENTRATION RATIOS	1.9/3.5
CELL OPERATING TEMPERATURE, 1.A.U., CR = 1.90	103°C
CELL POWER AT 4.5 A.U., CR = 3.5	34.3 MW
NO. OF CELLS PER ARRAY	471968
PACKING FACTOR WITH 12 MIL SPACING	0.98
CELL BLANKET AREA	386 M <sup>2</sup>
DIODE, ASSEMBLY, CONDUCTIVE LOSSES	7.2%
RADIATION LOSSES	5.3%

TABLE 2-7

## BASELINE CONCENTRATOR ARRAY WEIGHT SUMMARY

COMPONENT	WEIGHT (Kg)	NO REQ'D/WING	WING WEIGHT (Kg)
BLANKET ASSEMBLIES	71.5	2	143
PANELS (43)	52.0		
HINGES (84)	5.0		
TENSION DISTRIBUTION (2)	0.9		
BLANKET REFLECTORS (86)	6.3		
LEADER (1)	0.9		
HARKNESS (1)	6.3		
BLANKET TENSION AND CONTROL (4)	5.2	2	10
COVER	5.5	2	11
CONTAINER	11.0	2	22
POSITION LINKS	4.0	4	16
BLANKET PADDING	.04	132	5
SIDE REFLECTORS	25.6	4	102
INNER SUPPORTS (2)	6.6		
OUTER SUPPORTS (2)	6.6		
DRIVES (3)	2.0		
REFLECTOR	4.8		
RELEASE	0.9		
TENSIONING AND CONTROL	4.7		
MAST	66	1	66
TIP FITTING	2	1	2
WING POSITION BOOM (11.5 METERS)	15	1	15
TOTAL/WING			392
TOTAL SYSTEM			784

TABLE 2-8  
BASELINE CONCENTRATOR ARRAY PERFORMANCE

AU DISTANCE	EFFECTIVE CONCENTRATION	TEMP °C	WING OUTOUT (KW)	ARRAY OUTPUT (KW)	ARRAY OUTPUT WITH LOSSES, DEGRADATION (12.5%) (KW)
1.0	1.9	103	45.5	91.0	79.6
1.1	1.9	85	43.3	86.5	75.7
1.1	3.5	140	31.5	63.1	55.2
2.0	3.5	27	15.9	60.1	52.6
3.0	3.5	-33	15.9	31.9	27.9
4.0	3.5	-66	9.77	19.5	17.1
4.5	3.5	-78	8.0	16.0	14.0

GROSS ARRAY UNCONCENTRATED POWER AT 1 A.U., 55°C IS 59 KW.

**2.1.1.3 Alternate Concentrator Solar Array.** An alternate trough concentrator solar array design was identified in the study which also met the design requirements. It differs from the baseline design in that it is a two-dimensional concentrator design employing one electrical module blanket per wing with side reflectors and no in-blanket reflectors. The fully-deployed alternate concentrator array wing is shown in Figure 2-5. The wing storage and deployment is less complex than for the baseline design. As shown in Figure 2-5, the alternate design wing is stored below the thrusters in the allowed storage volume. A short wing deployment mast is attached to the array wing extension mast on the same axis. The base of the short deployment mast is attached to the wing tracking mechanism on the spacecraft.

For deployment, the wing is released and the wing module is rotated outboard 90 degrees so that the tracking axis and the mast axes are in line. The short deployment mast then deploys the wing 8 m to separate the array wing from the spacecraft and thereby keep the array out of the thruster plume. The side reflector packages which are folded in half for launch are then articulated by motors to their proper orientation as shown in Figure 2-5. The flat-folded array blanket and reflectors are preloaded between inboard and outboard graphite-epoxy beam structures. The inboard support structures are attached to wing mast canister. The outboard support structures are attached to the wing mast tip and latched to the inboard support structures. The outboard structures are released and the extension of the wing mast extends both the array blanket and the side reflectors simultaneously. Extension continues to full extension and tensioning of the array blanket and side reflectors. The two side reflectors are not attached to the array blanket and the three elements are tensioned separately.

The side reflectors provide an effective CR of 2.27 and to meet the mission power requirements more solar cells are required by the alternate design than by the baseline design, 680,512 vs 471,968. The related design assumptions are shown in Table 2-9, the alternate design weight summary is shown in Table 2-10 and the performance of the alternate design is shown in Table 2-11.

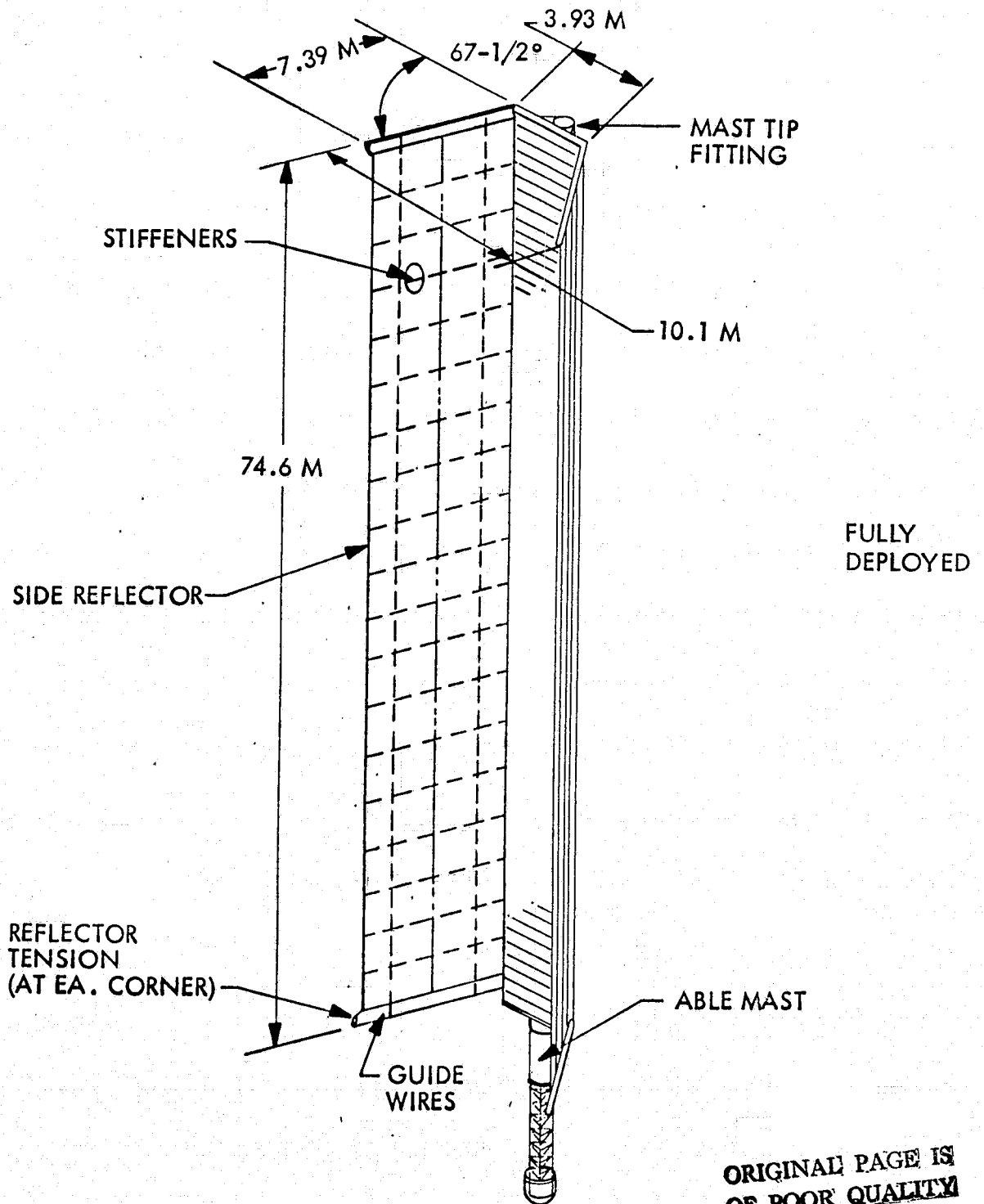


Figure 2-5. Alternate Concentrator Array Wing



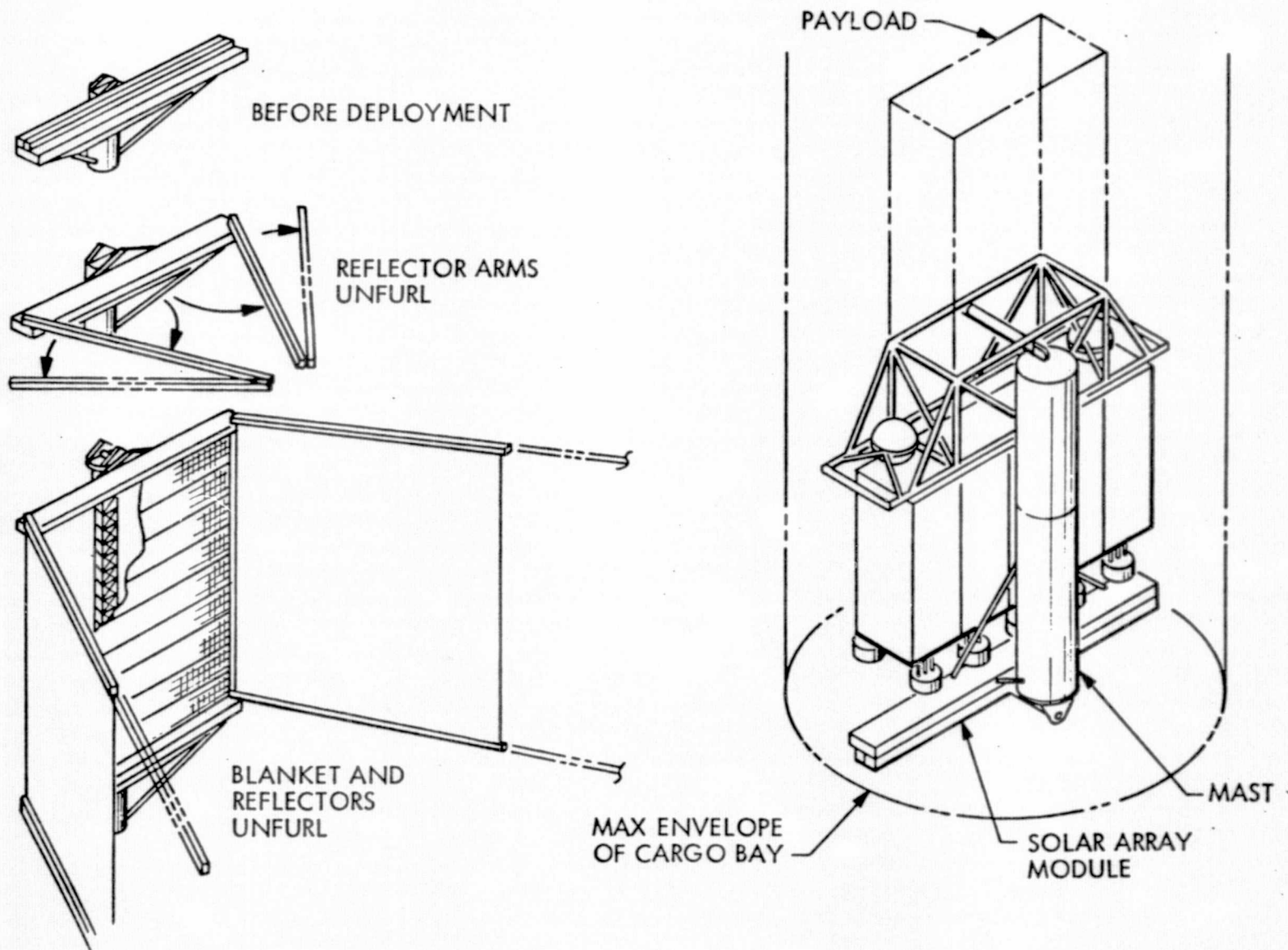


Figure 2-5. (Cont.)

TABLE 2-9  
ALTERNATE CONCENTRATOR ARRAY DESIGN ASSUMPTIONS

NET EOL ARRAY POWER @ 4.5 A.U.	14.0 KW
NET EOL ARRAY POWER @ 1.0 A.U.	126.5 KW
CELL SIZE, WRAPAROUND CONF.,	2.0 CM X 4.044 CM X 0.125 MM
CELL EFFICIENCY, 28°C, AMU	13.0%
COVER SLIDE	3 MIL CMS
CELL ASSEMBLY SOLAR ABSORPTANCE	0.70
CELL ASSEMBLY EMITTANCE	0.85
REFLECTOR MATERIAL	0.3 MIL ALUMINIZED KAPTON
REFLECTOR EFFICIENCY	92%
EFFECTIVE CONCENTRATION RATIO	2.2
CELL OPERATING TEMP, 1 A.U., CR = 2.2	130°C
CELL POWER AT 4.5 A.U., CR = 2.2	24.5 MW
NO. OF CELLS PER ARRAY	680,512
PACKING FACTOR WITH 12 MIL SPACING	0.98
CELL BLANKET AREA	586.1 M <sup>2</sup>
DIODE, ASSEMBLY, AND CONDUCTIVE LOSSES	7.2%
RADIATION LOSSES	5.3%

Table 2-10  
ALTERNATE CONCENTRATOR ARRAY  
**WEIGHT SUMMARY**

COMPONENT	WEIGHT (Kg)	NO. REQ'D/WING	WING WEIGHT (Kg)
BLANKET ASSEMBLY	181	1	181
PANELS (186)	165.9		
HINGES (186)	7.1		
TENSION DISTRIBUTION	0.9		
LEADER	0.6		
HARNESS	6.5		
BLANKET TENSION & CONTROL (4)	7.0	1	7
COVER	8.0	1	8
CONTAINER	12.0	1	
BLANKET PADDING (186)	0.04	186	7
SIDE REFLECTORS	25.5	2	51
INNER SUPPORTS (2)	6.5		
DRIVES (3)	2.0		
REFLECTOR	5.0		
RELEASE	1.0		
TENSIONING & CONTROL	4.5		
MAST	111	1	111
TIP FITTING	2	1	2
WING POSITION BOOM (8 METERS)	9	1	9
		TOTAL WING	388
		TOTAL SYSTEM	776

TABLE 2-11

## ALTERNATE CONCENTRATOR ARRAY PERFORMANCE

AU DISTANCE	EFFECTIVE CONCENTRATION	TEMP °C	WING OUTPUT (KW)	ARRAY OUTPUT (KW)	ARRAY OUTPUT WITH LOSSES DEGRADATION (12.5%) (KW)
1.0	2.27	130	72.3	144.6	126.5
1.5	2.27	42	48.3	96.6	84.5
2.0	2.27	27	32.0	64.0	56.0
2.5	2.27	-9	23.3	46.6	40.8
3.0	2.27	-33	17.3	34.5	30.2
3.5	2.27	-52	12.8	25.6	22.4
4.0	2.27	-67	10.0	20.0	17.5
4.5	2.27	-80	8.0	16.0	14.0

GROSS ARRAY UNCONCENTRATED POWER AT 1 A.U., 55°C IS 85.9 KW.

### 2.1.2 Concentrator Solar Array Model Testing

A 36-cell concentrator model was built by LMSC and tested under simulated space conditions in an  $\text{LN}_2$  cooled thermal vacuum chamber with a sun simulator. The chamber tests were performed by Boeing for NASA-MSFC. The cells were divided on the blanket into two 18 cell series-parallel combinations (6 in series and 3 in parallel). These two circuits were measured individually and hooked in series, both under concentration and without concentration, for a range of sun intensities. The cells were 8 mil wraparound contact, 2 x 4 cm cells with 6 mil fused silica covers,  $\alpha/\epsilon = 0.84/0.81$ , and 10.9% efficiency. The cells were welded to a SEP flexible printed circuit interconnect. The reflectors were constructed of 2 mil aluminized Kapton whose measured reflectance was 92%. The model configuration was such that two pairs of reflectors were configured like the baseline array combination of in-blanket and side reflectors surrounding an electrical panel. The set of large side reflectors was set at  $67.5^\circ$  with respect to the horizontal plane of the cell blanket and the other set was positioned at  $60^\circ$  to the blanket plane. Figure 2-6 is a photograph of the model.

The test was performed in order to verify analytical predictions of the concentrator array's temperature and effective concentration ratio (ECR). Some information on the intensity and temperature variation across the blanket was also anticipated. Test data are presented in Appendix A. Since the current is fairly linear with intensity, the  $I_{SC}$  for one of the circuits was chosen to determine the ECR (Ref. 1, 5, 15, 16, 20, 21). The  $I_{SC}$  for Circuit 1 while under concentration was factored by a temperature coefficient ( $.055\%/^\circ\text{C}$ ) to eliminate the current increase due to the elevated temperature. The currents for both concentrated and unconcentrated conditions were then plotted versus sun intensity, Figure 2-7.

Noting the short circuit current levels for both cases the same  $I_{SC}$  can be achieved with concentration at about 0.29 times the sun intensity as that of the unconcentrated case. Or, the concentrators have increased the sun level on the cells by a factor of 3.5. The effective concentration ratio for this system is then 3.5. As a check on this ECR, a simple heat balance was performed using the temperatures of the two cases. The temperatures indicated that the concentrated system saw light intensity increased by a factor of from 3.3 to 3.7, which is in good agreement with an ECR of 3.5.

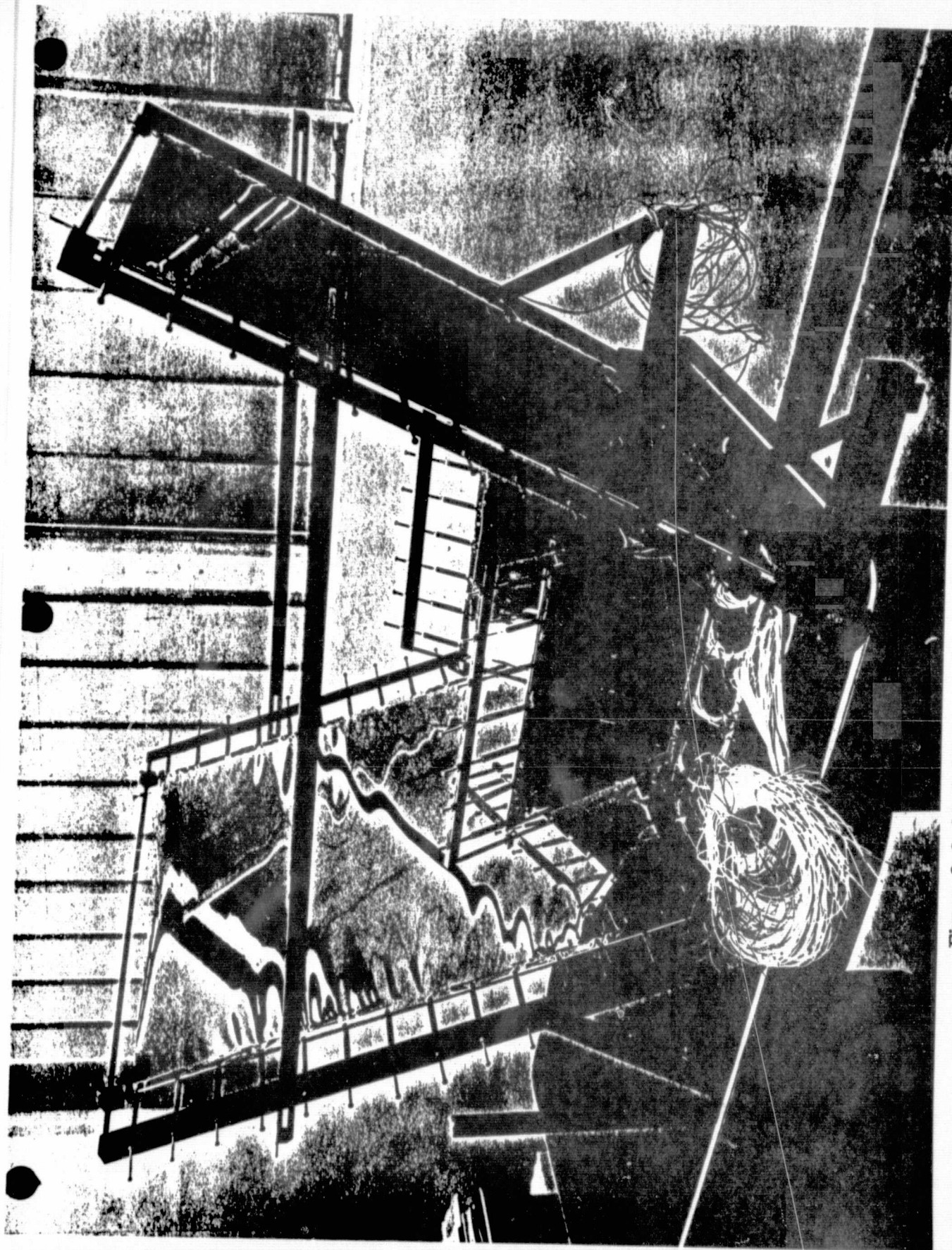


Figure 2-6 36-Cell Concentrator Test Model

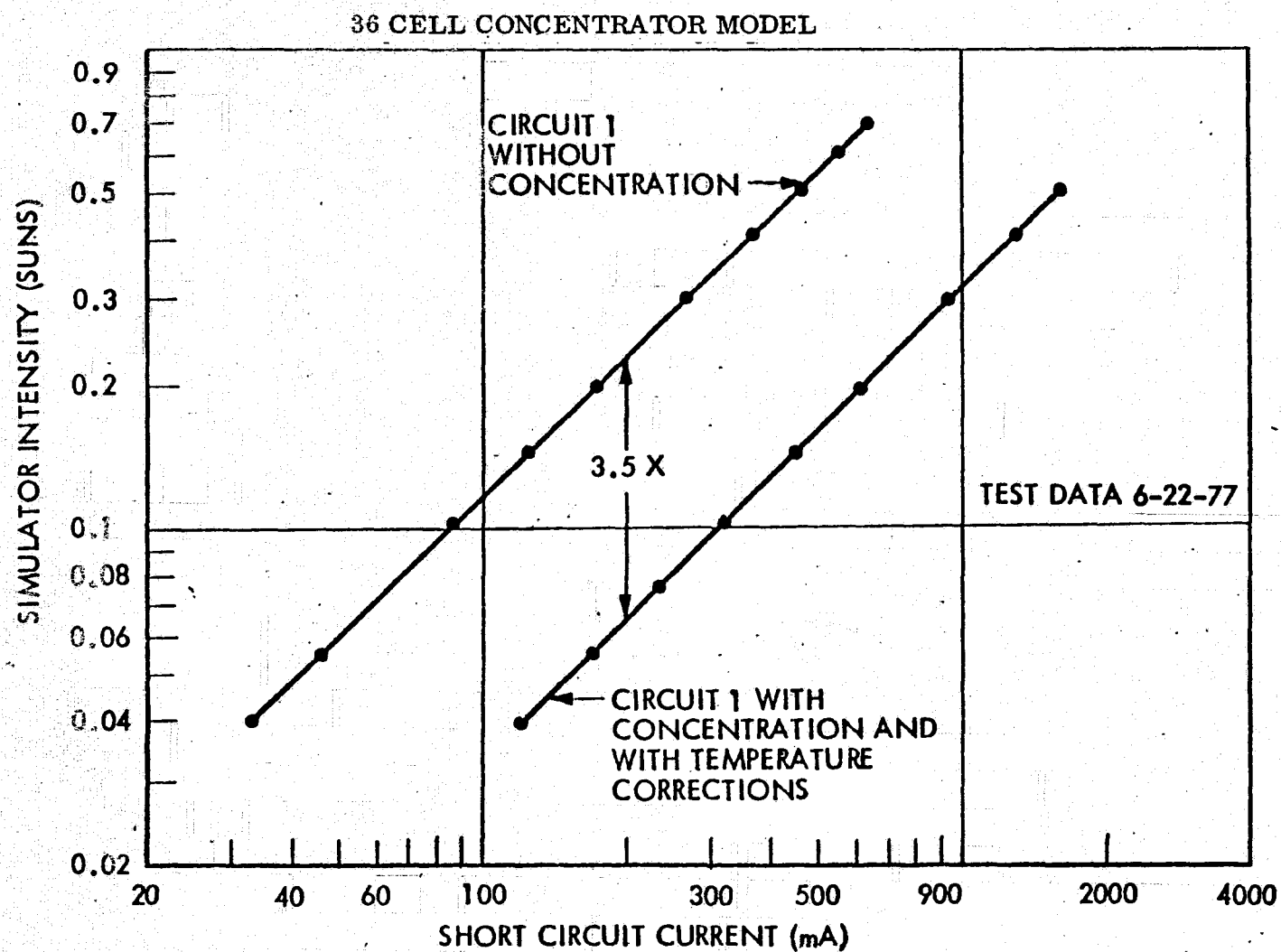


Figure 2-7 Effective Concentration Ratio Using  $I_{sc}$  Ratios



A twenty-cell concentrator model was also built and tested in a thermal vacuum chamber. This model had all twenty cells wired individually with 4-wire hookups. This would allow intensity and temperature mapping across the panel. Wrinkling and misalignment effects could also be determined with this model. Figure 2-8 shows the electrical module configuration. Figure 2-9 is a schematic of the cell blanket with cells and thermocouples indicated. Also shown in Fig. 2-9 is the calculated intensity levels on the blanket caused by the reflections from the side ( $67.5^\circ$ ) reflectors onto the  $60^\circ$  reflectors and then onto the blanket. Test data are contained in Appendix B. There doesn't appear to be good correlation between the ECR's determined for the cell and the predicted intensity levels. There is some uncertainty in the temperature predictions for those cells that did not have a thermocouples attached. There is also some uncertainty in the  $I_{SC}$  temperature correction in both the correction factor and in the unconcentrated temperature baseline as the unconcentrated, low intensity temperatures are estimates rather than data points.

The ECR's determined are at least reasonably accurate in their relative values and an important observation can be made about this test. If all the cells were connected in series and the string  $I_{SC}$  was measured, the ECR determined for the string would not be the average of all the individual cells in the string but it would be approximately that of the cell with the lowest ECR (in this case, 3.38). This effect is due to the current limiting (diode) property of the solar cell with the least intensity which forces all cells in series to operate at the current level of the lowest cell.

The calculated average ECR for the 3-dimensional reflector model was 3.78 based on the additional light from double reflections. Since current limiting effects are present in the 36 cell module, the measured ECR of 3.5 in that module was used to calculate the baseline design performance.

Some temperature correlation was attempted for both the models between the test data and computer predictions of the array design temperatures. Figure 2-10 is a plot of the temperature data for circuit 1 of the 36-cell model. The temperature prediction curve for the baseline  $CR = 3.5$  array is also shown. The difference between the data and the prediction is accounted for in three cases: 1) the solar absorptance and emittance of the model are significantly different from those in the LMSC model and the differences are estimated to cause a  $\Delta T$  at 1.9 A. U. of  $+24^\circ C$ ; 2) During the testing the solar cells



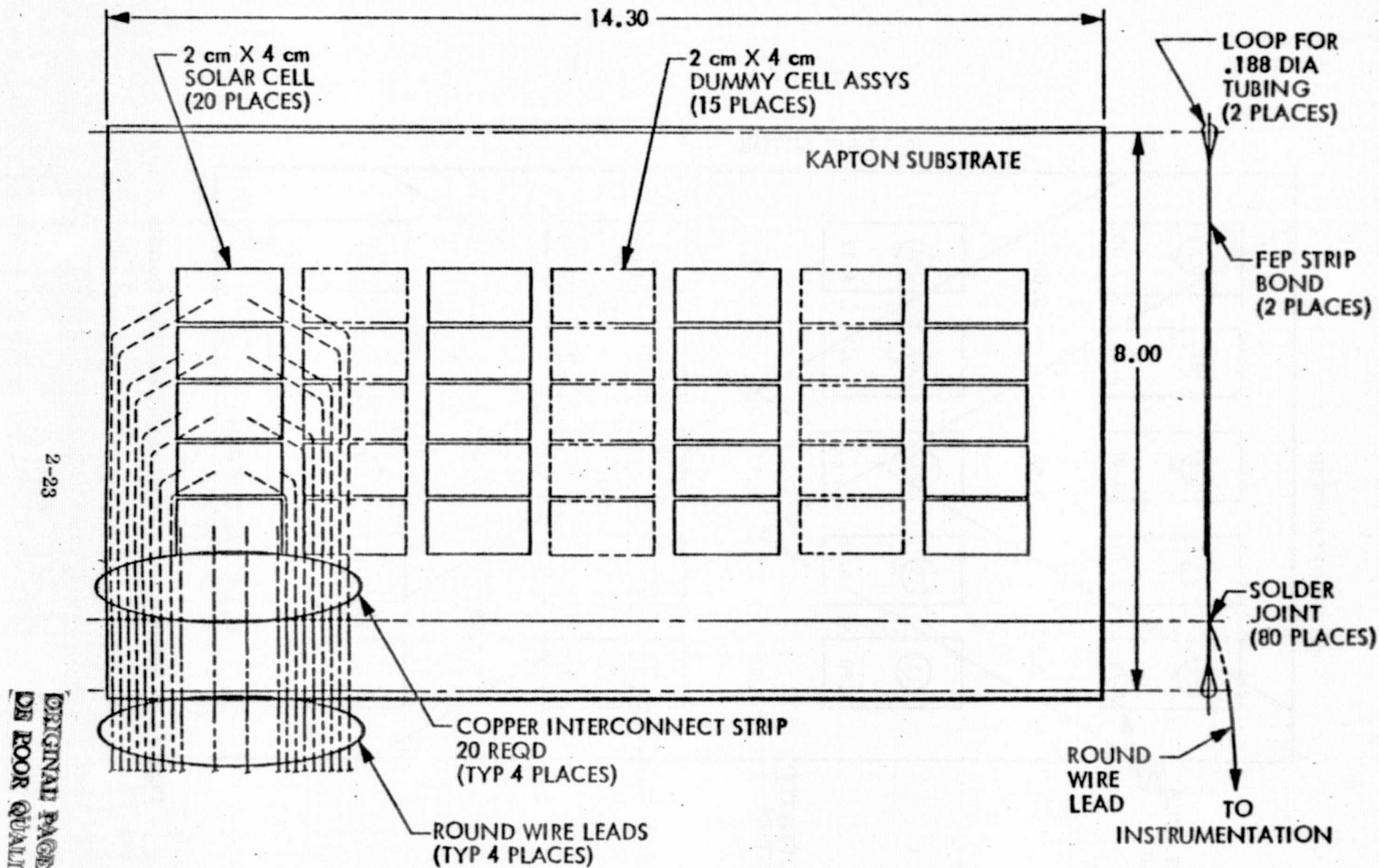


Figure 2-8 20-Cell Concentrator Test Model

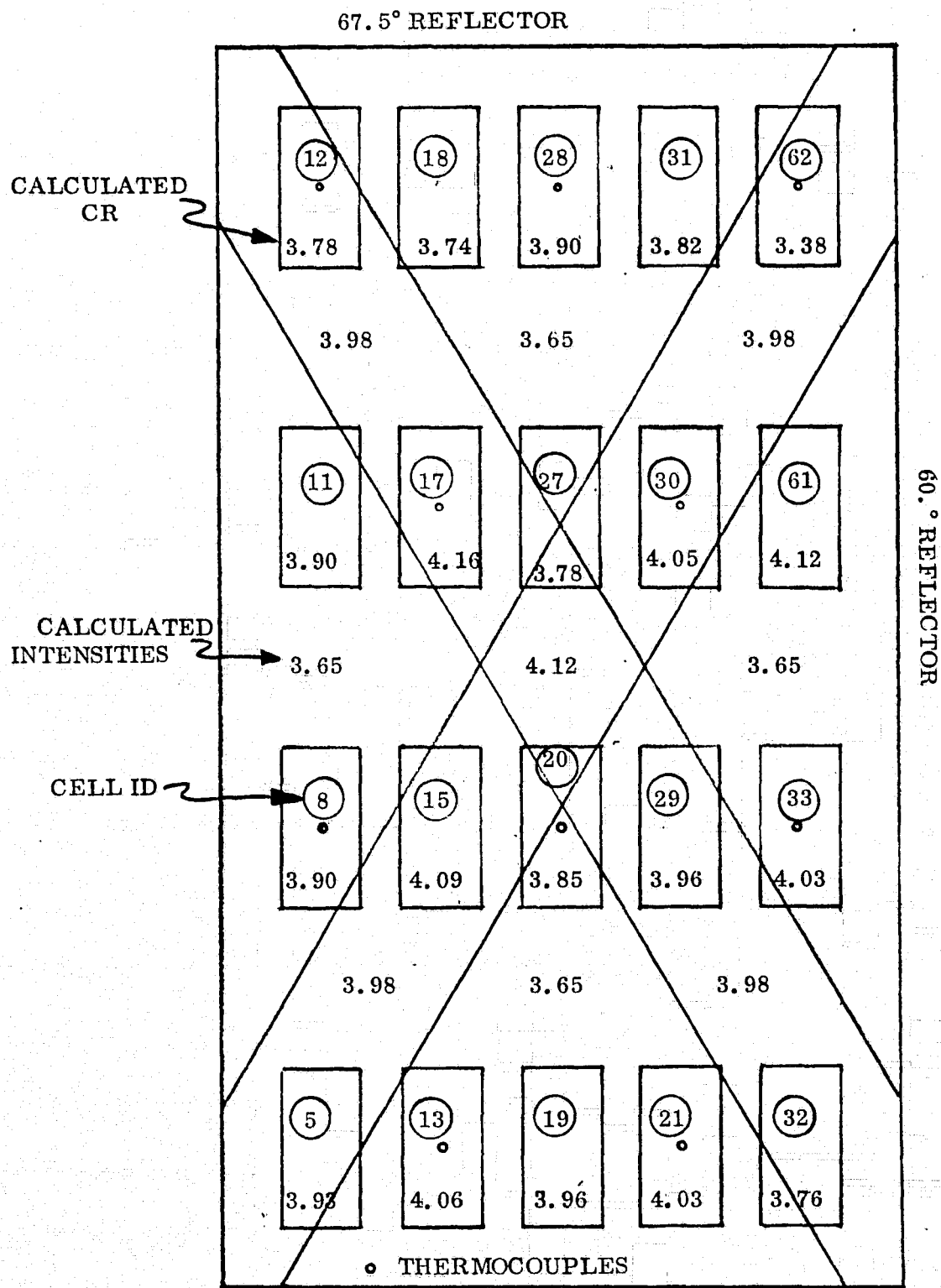


Figure 2-9 Schematic of 20 Cell Model and Test Results

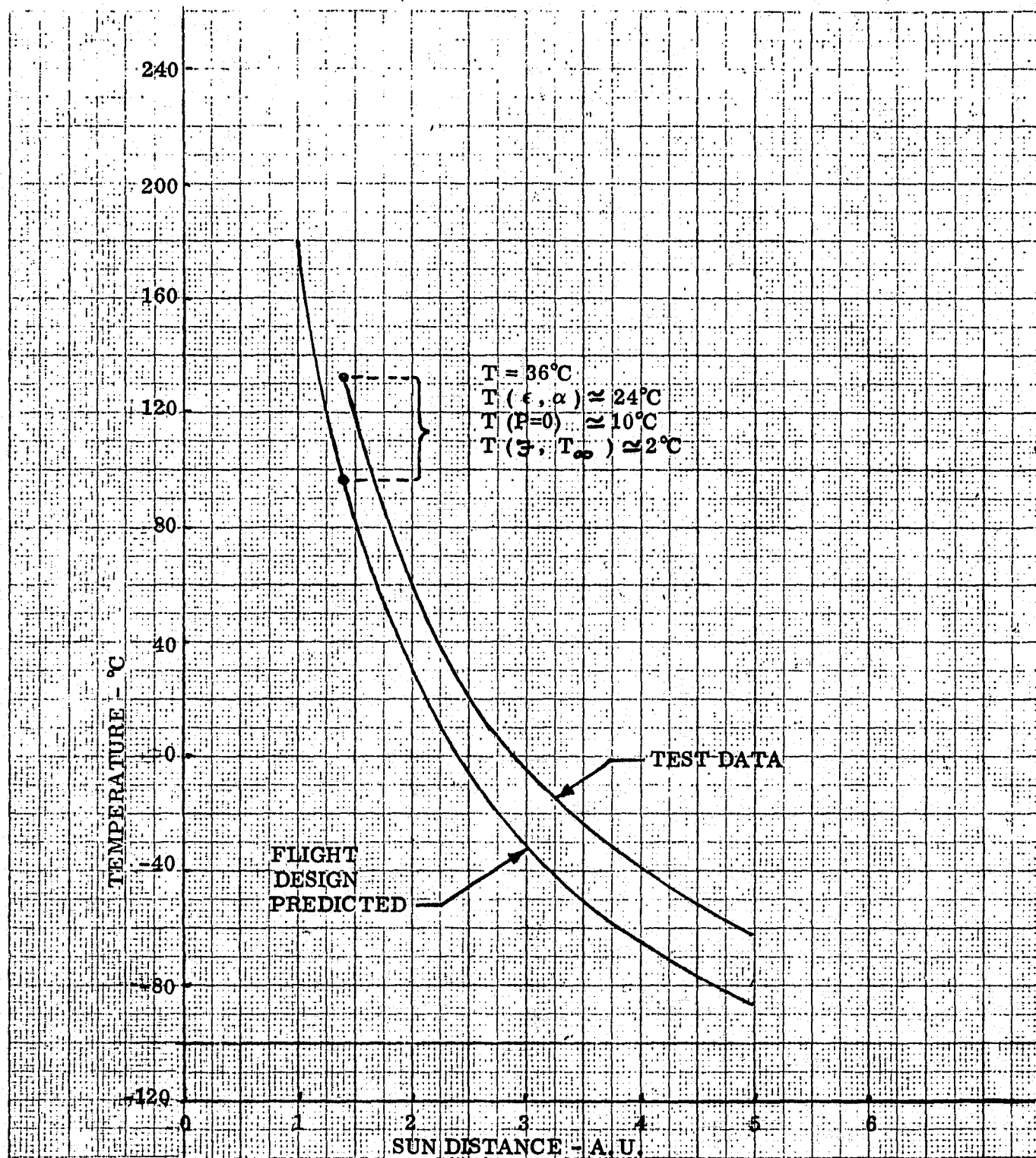


Figure 2-10 36-Cell Model Temperature Correlation

were in a no-load condition and thus a portion of the incident energy was not removed as electrical energy but rather went into heating of the cells. At 1.8 A. U., this no-load condition accounted for approximately a  $\Delta T$  of  $+10^{\circ}\text{C}$  over a loaded condition; 3) Although the test chamber conditions approached those of space, two deviations from space conditions contributed to a higher than expected cell temperature; higher than space, chamber temperatures and a slight reduction of the model's view to space due to the large overhead mirror used to reflect the sun simulator energy onto the blanket. It seems reasonable that these two deviations could contribute a  $\Delta T$  of  $+2^{\circ}\text{C}$  to the model data over array predictions.

### 2.1.3 Technology Assessment

The concentrator solar array to perform the Halley's Comet Rendezvous (HCR) mission requires less solar array technology advancement than does the planar array. This is due to the trajectory efficiency of the concentrating array which will allow significantly more engine thrust at far sun distances than will a planar solar array of the same weight and level of technology. Therefore, the probability of achieving the required solar array technology advances in a timely manner is higher and the cost of the technology development program is lower than with the planar array.

**2.1.3.1 Solar Cell Technology.** The prime solar cell candidates for the HCR-SEP Mission are 1) a 5 mil 13% efficient (covered) solar cell in a 2 x 4 cm wraparound contact configuration, 2) a 2 mil 13% efficient (covered) solar cell in a 2 x 2 cm conventional contact configuration. The solar cells are a part of system which is concerned with cell cover design, cover application, cell interconnecting fabrication techniques, substrate fabrication and solar array module fabrication. The 2 x 4 cm wraparound contact cell is a part of a system that has been under development by NASA for several years. It utilizes a lightweight printed circuit substrate and all cell bonding is performed from one side of the substrate. As indicated below, the selected baseline cell cover is a separate glass cover (3 mil CMS) and it completely covers the front of the wraparound contact cell. The lightest 2 x 4 cm wraparound cells fabricated to date ( $\approx 5,000$  units) are 8 mils thick and 11.4% efficient with no sculptured (non-reflecting) front surface, no P+, and no backside reflector. Eight (8) mil wraparound contact cells of the 2 x 4 cm size have been built in the laboratory with 14.8% efficiency. The cell vendors believe that the 5 mil 13% efficient cell can be achieved in the planned technology program.

The 2 x 2 cm cell with conventional contacts lacks the fabrication advantages seen for electrical modules using 2 x 4 cm wraparound contact cells in the number of cells to be handled, cell covering, cell packing factor, and bonding operations. The use of organic encapsulating techniques is seen as a higher technology development risk than is the glass cover technology advance required for 3 mil CMS covers. The application of glass covers to the 2 x 2 cm cells requires more cover units and handling than does the 2 x 4 cm cell.

Based on the above system considerations and the confidence of the vendors in achieving the required technology advance, the 5 mil, 13% efficient wraparound contact, 2 x 4 cm cell is selected for the HCR mission baseline design. A larger 4 x 4 cm cell is not essential to the HCR mission but would be evaluated in the technology development program.

The anomalous behavior (low voltage) of certain silicon solar cells in a family of cells at low temperature and low illumination intensity has been observed by investigators for several years. This problem is alleviated by sun concentrating arrays at far sun distances and by the use of P+ back surface fields. The technology development program will not have to completely solve this problem but will attempt to avoid the need to select out cells that would be poor performers in the final concentrator array design.

2.1.3.2 Solar Cell Cover Technology. The candidate cell covers are shown in Table 2-12. They are categorized as either glass or organic. The fused silica material cannot be obtained below 5 mils thickness. The integral covers which are ion sputtered onto the solar cells suffer mainly from the fact that the glasses that can be so applied do not match the thermal coefficient of expansion of the cells and bowing results.

The use of organic covers, either cost or heat laminated as films on individual cells or on cell modules, holds the promise of low cost cover material and low cost application to cells without the use of adhesives. The use of FEP film heat laminated to cells has not shown the desired stability in space environment testing. Cast in place FEP (Spraylon) has also been investigated but has not been stable at high temperature under UV exposure.

TABLE 2-12  
CELL COVER CANDIDATES

GLASS

- FUSED SILICA — NOT PRESENTLY FABRICATED UNDER 5 MILS THICKNESS
- VERY BRITTLE
- ENVIRONMENTAL DATA SUPPORTS PERFORMANCE
- ADHESIVE AND UV FILTER REQUIRED

**SELECTED**

- CERIA STABILIZED MICRO SHEET — AVAILABLE AT 3 MILS THICKNESS
  - DIFFICULT TO HANDLE AT 3 MILS
  - ENVIRONMENTAL DATA SUPPORTS PERFORMANCE
  - ADHESIVE REQUIRED
  - SOME WEIGHT PAYBACK IN CELL RADIATION PROTECTION
- INTEGRAL COVERS — ION SPUTTERED APPLICATION
  - CELL BOWING DUE TO THERMAL EXPANSION MISMATCH
  - EXPENSIVE BUT COS COULD BE REDUCED
  - CAN BE VERY THIN

ORGANIC

CAN BE  
VERY THIN

- FEP SRAYLON — CAST IN PLACE
  - STABILITY AT +140°C PLUS UV POOR
  - HIGH THERMAL EXPANSION MISMATCH FORCES
- HEAT LAMINATED FEP — NOT STABLE IN SPACE ENVIRONMENT
- SILICONE FILM
- GLASS + RESIN

LIMITED DATA IN SPACE ENVIRONMENT

Kapton polyimide film is not sufficiently transparent for cell cover use. A polyimide-siloxane copolymer has been investigated and found to be unstable under UV exposure.

RTV silicone and combinations of glass/resin have been recently considered as candidate covers for the HCR mission. The early UV test data indicates both good and poor UV stability depending on the sun intensity used and the validity of accelerated test conditions. Limited data for these systems in the space environment is presently available. Organic cover development has not yet shown the promise expected and for this reason the technology risk for the HCR mission is considered higher for this approach than for the selected 3 mil ceria stabilized microsheet material. It has been fabricated and its stability is established. The technology advancement required is in the area of high yield handling and application to the 5 mil, 2 x 4 cm solar cells.

**2.1.3.3 Array Blanket Technology.** The use of lightweight Kapton film as a solar array substrate is developed. One demonstrated use of this material is to support separately interconnected solar cell assemblies by adhering the assemblies to the film. LMSC has developed a Kapton encapsulated printed circuit substrate concept and NASA has funded the development of printed circuit interconnect materials, the use of 0.5 mil Kapton films with 0.5 mil adhesive and roll laminating techniques for low cost fabrication of long lengths of substrate strips. The cell assemblies are bonded to exposed pads on the printed circuit to provide mechanical and electrical joints.

An alternate cell mounting concept for the array blanket is to encapsulate interconnected cell modules with an organic film that is both the cell cover and the means by which the cells are held in place on the Kapton film substrate. The technology risk for this cover film is the same as for organic covers and it is not selected as the baseline design.

The selected printed circuit blanket that is proposed for the HCR mission requires the use of sheets of 0.3 mil Kapton film and 0.4 mil adhesive and a 1 mil thick aluminum interconnect printed circuit. The exposed aluminum circuit pads require local plating to allow bonding the silver contacted solar cell to the interconnect system. The plating technique is available. The technology development program would demonstrate the fabrication of this lighter substrate design.

**2.1.3.4 Reflector Technology.** Several metals are candidate reflectors but the optical performance, stability, and cost of aluminum make it the best choice for the HCR mission. The most stable substrate is Kapton film which is proposed in the 0.3 mil thickness to save weight. The aluminum is vacuum vapor deposited to a thickness of 900 to 1100 angstroms on the smooth side of the Kapton film (the other side has a matte finish from the fabrication process). The specular reflection of the aluminized Kapton is 92% and the degradation of this value in the HCR mission is expected to be small based on proton irradiation testing of similar material by NASA-MSFC. Further reflector materials testing is planned for the technology development program.

The baseline design proposes to extend the side reflectors with the four corners of a sheet tensioned with springs. Edge curl will be reduced with the use of stiffeners on the back of the reflectors where individual sheets are adhered together at seams to form the total side reflector. The flat-fold in-blanket reflector design requires technology development to insure that the surfaces are sufficiently planar under the varying temperature conditions of the HCR mission. The baseline design proposes the use of polyimide composite material as in-blanket reflector stiffener material to maintain a planar reflector shape and to have the same coefficient of thermal expansion as the reflector material.

The planar trough reflector configuration was selected over curved surface reflectors such as the Compound Parabolic Concentrator (CPC) since it could be specular and efficient for light reflection to the electrical modules and for heat rejection from the modules. The planar shape was also felt to be one that could more easily be attained and maintained.



## 2.2 CONCLUSIONS

- A flat-fold three dimensional trough concentrating solar array can meet the performance requirements of the Halley's Comet Rendezvous mission. The major requirements that are controlling and are met are those associated with array launch packaging volume, array weight, array power performance and clearance of the thruster exhaust plume by the deployed array. The deployment of this array from its stowed position is complex under the stowage volume constraints used in this study.
- Reflector/electrical module testing to date supports the array power predictions made for the baseline array design in the area of effective concentration ratios.
- Planar surface reflectors require relatively simple shape control with tension. Reflector material testing and mechanical design for maintenance of the reflector planar configuration over the HCR mission requires technology demonstration.
- Printed circuit flexible substrates with wraparound contact solar cells provide low cost fabrication and assembly methods for the large area solar arrays required by the HCR mission.
- An alternate two-dimensional trough concentrator array configuration exists that can meet the HCR mission requirements and that has reduced deployment complexity. This reduction, however, is at the expense of greater solar cell area and therefore cell costs.
- A major driver in the required technology advancements for the HCR solar array is the achievement of reasonable cost in the production of the solar cells with the required efficiency.

ORIGINAL PAGE IS  
OF POOR QUALITY

- The required technology readiness attainment for the baseline solar array design can be attained in a timely manner with moderate risk in the solar cell area and low risk in all other areas.
- The estimated cost of the technology development program is \$ 6.31 M.
- The estimated cost of the development and delivery of the proposed HCR mission solar array system is \$ 23.1 M.
- The availability of several alternate component and system design approaches reduces the array development risks.
- The HCR-SEP mission solar array technology advancements will strongly support other SEP missions as well as other proposed space projects requiring solar array power.

## 2.3 RECOMMENDATIONS

### 2.3.1 HCR-SEP Mission Program

Proceed at the start of FY 1978 with a technology development program aimed at the HCR mission requirements including development time. Some of the component design alternates that meet the HCR requirements and those that have potential for significant cost and/or weight savings should be initially considered. To reduce costs, however, a narrowing of candidates under development which have high associated costs should be completed within 6 months. Any introduction of new approaches will have to be weighed against the progress already attained in planned approaches, cost, schedule, and potential benefits to the HCR mission. Phase B studies on the spacecraft design should also start by January 1978 in order to assure that the solar array design requirements that are defining the solar array technology advancement requirements are as appropriate as possible. The progress toward solar array technology readiness should be monitored against planned milestones so that problem areas are identified and the planning for the HCR mission remains consistent with the projected times of technology readiness for all required technology advances.

### 2.3.2 Recommended Technology

The major solar array technology areas recommended for demonstration and development are divided into three groups: Components, Fabrication, Subsystems.

#### 2.3.2.1 Components.

Cell Covers. Study candidates, select promising approaches for development testing, narrow candidates based on test data, perform additional development, and testing and make final selection consistent with solar cell and blanket design.

Solar Cells. Commence development of weldable 5 and 6 mil wraparound contact solar cells in 2 x 4 and 4 x 4 cm configuration at 13 to 13.5% covered efficiency. Develop design and production fabrication techniques in a coordinated manner. Investigate design and fabrication techniques to avoid low voltage performance at low temperature and low light intensity. Select flight cell design based on development progress and characterize cell for performance versus intensity and temperature.

Lightweight Substrate. Develop a 0.3 mil Kapton, 0.4 mil adhesive sheet clad with 1 mil aluminum. Laminate this underlay with a 0.3 mil Kapton, 0.4 mil adhesive overlay sheet and develop local plating of the aluminum for compatibility with silver contacted solar cells. Investigate a lighter insulating coating to replace the overlay Kapton/adhesive film.

Lightweight Extension Mast. Develop an all composite mast canister and deployer and develop the application of graphite-epoxy to the continuous coilable longerons. The graphite epoxy longeron is not a required advancement but would be a significant weight reduction.

Reflectors. Develop design data as to required flatness. Determine reflector materials performance in space. Develop packing and deployment techniques and demonstrate required performance. Test reflectors with electrical modules in significant sizes to verify design.

#### 2.3.2.2 Fabrication.

Cell Covers. Demonstrate 2 x 4 cm 3 mil CMS glass application to solar cells with good yield. Demonstrate alternate cover application techniques.

Solar Cells. Improve the solar cell yield for the design cell and improve the yield of cells with good performance at low temperature and light intensity.

Electrical Modules. Develop the design cell weld schedule for minimum electrical degradation, high yield, minimum cell fabrication constraints, and sufficient bond strength. Develop module NDT techniques for quick and accurate determination of weld joint integrity.

#### 2.3.2.3 Subsystems.

Zero-Gravity Testing. Design and fabricate array blanket, in-blanket reflector and side reflector models. Test these models in an aircraft and/or neutral buoyancy environment to demonstrate design deployment and retraction technology.

**Full-Scale Wing Section Testing.** Based on the array detail design activity, a part of the technology development program, design and fabricate a full-scale section of the HCR mission solar array. Perform environmental testing and ground extension of the wing section to demonstrate large scale hardware design, fabrication, handling and testing.

### 3.0 ASSESSMENT OF CRITICAL COMPONENT TECHNOLOGY

The methodology used for the assessment of component technology applicable to the Extended Performance SEP Solar Array was discussed in Section 1.3, APPROACH, TASK 3.0. Table 3-1 summarizes the criteria used for categorizing the state-of-the-art for this application.

#### 3.1 SOLAR CELL TECHNOLOGY

##### 3.1.1 Characteristics

###### Base Resistivity

The choice of the base resistivity for an interplanetary mission is made by considering the base resistivity effects on cell power. An increase in the base resistivity lowers the efficiency at the cell while it increases its radiation resistance (Ref. 1, 2, 3). At higher intensities ( $> 250 \text{ mW/cm}^2$ ), the maximum power of the higher resistivity cells tend to fall off in comparison to the lower resistivity cells. Conversely, the higher resistivity cells operate at slightly higher power levels at low intensity, low temperature environments than their low resistivity counterparts. Since the radiation level for HCR-SEP mission design is relatively low and the original power requirements were at high intensities, a low base resistivity cell is recommended. Ref. 5 has shown that the optimum base resistivity for high intensities is in the 0.8 to 2.0 ohm-cm range. This range of resistivities has been space qualified and is therefore a Category I item.

###### Junction Depth

The technology for producing diffused junctions down to less than 0.1 microns is currently available and a Category I process. Shallower junctions increase the shorter wavelength (blue) response of the solar cell (which is also less sensitive to radiation damage than the cell's red response). Investigations on the influence of junction depth (Ref. 6) on  $I_{SC}$  and short wavelength response indicates that the optimum junction depth is between 0.10 and 0.15 microns.

TABLE 3-1  
CRITERIA FOR STATE-OF-THE-ART ASSESSMENT

Category	I - Sufficient	II - Insufficient, Devel. Progress Will Achieve Readiness	III - Sufficient, No Device Potential, Alternates Feasible
Determination Criteria	<ul style="list-style-type: none"> <li>• Successfully used for similar missions.</li> <li>• Not in use but substantiated by test and analysis.</li> <li>• Qualified by similarity and material compatibility.</li> </ul>	<ul style="list-style-type: none"> <li>• Insufficiency due to lack of analytical or test data and not due to known functional or physical limitation.</li> <li>• Insufficiency because of material or component specified for environment and duration marginal without modification, but development program may verify capability of material or component.</li> </ul>	<ul style="list-style-type: none"> <li>• Does not satisfy any of the preceding category determination criteria.</li> </ul>

3-2

ORIGINAL PAGE IS  
OF POOR QUALITY

### Back Surface Fields

The effect of a back surface field is to increase the red response of the solar cell. This increase in response, however, is very susceptible to radiation damage (Ref. 1, 3). The increase in red response is also more pronounced in the higher resistivity cells. The back field is reported to eliminate the cell low voltage problem at low temperature and low intensity. Since the study mission has a relatively low radiation fluence, a P+ back surface is a recommended treatment for this study's solar cell design; it is a Category I process.

### Solar Absorptance

The cell's solar absorptance ( $\alpha_s$ ) affects the cell's power because of its influence on the cell's operating temperature. The cell components that influence the solar absorptance are AR coating, back surface metalization, cell coverslide, cell surface roughness, and UV filter. For near sun missions or with arrays using concentrators, it is desirable to keep the  $\alpha_s$  as low as possible to keep the operating temperature down and cell efficiency up. The influence of  $\alpha_s$  on cell temperature at the far sun distances is not as great as that at near sun distances.

AR coatings are generally of two types: single and multilayer. Single layer coatings are currently  $Ta_2O_5$  and  $SiO_x$  with the  $Ta_2O_5$  being the superior coating. The multilayer coatings are made up of two or more layers of such materials as  $TiO_x$  and  $Al_2O_3$ . The advantage of the multiple coatings is an increased current output from the solar cell, presumably due to less reflection losses. The disadvantage of the multi-AR coatings are their higher  $\alpha_s$ 's, typically 0.85 to 0.90 (Ref 7, 8). The multi-AR coatings are expected to be space qualified shortly and are a Category I component.

A rough or sculptured surface cell accomplishes the same thing as the multi-AR coatings but by a different manner. Surface tetrahedrons on the silicon cell increase the current output of the cell 6 to 7% but increase the  $\alpha_s$  to values from 0.91 to 0.93 (Ref. 7). Sculptured cells are currently being used in space and are a Category I component.



The cell cover also influences the cell's solar absorptance. Of the two inorganic covers, fused silica has a slightly lower absorptance than ceria stabilized microsheet (CMS), depending on the fused silica's UV filter. This is primarily due to CMS's almost complete absorption of wavelengths at less than 0.33 microns (Ref. 1, 8, 9). The organic covers range in absorptance both with different materials but with different thicknesses of the same material. For 1 mil thickness,  $\alpha_s$  ranges from 0.34 for Kapton to 0.10 for RTV 655 to 0.05 for FEP and Spraylon (Ref. 10, 11). The organic covers are Category II items while the inorganic covers are in Category I.

A way to reduce the solar cell's  $\alpha_s$  then is to use a very high reflectance UV filter. Work is being done to this effect and may reduce the solar absorption of the solar cell assembly approximately 3%. This filter could not be used, as presently designed, on a CMS cover because of its natural UV absorption. If developed to be on the outside of the solar cell cover then this filter might also be developed to protect the organic cell covers. It is a Category II component.

The most promising new development in reducing the solar absorptance of a solar cell assembly is providing the cell with a Back Surface Reflector (BSR) (Ref. 8). The BSR provides both a P+ back surface and a back optical reflector. The BSR provides both a current increase of 2 to 3% and an  $\alpha_s$  lowered by approximately 10%. This is a relatively new development and is a Category II process. With some refinement it should be able to produce a solar cell with a total solar absorptance of 0.70.

#### Contact Metalization Systems

Some current metalization systems are TiPdAg and CrPdAg, which are both Category I systems. There is recent work which indicates that the TiPdAg systems may degrade significantly at high temperatures and thus may prove unsuitable for the extended performance array system (Ref. 13, 14). Some concern has also been voiced over the possibility of chromium poisoning of the solar cell junction at elevated temperatures. One Category II system currently being investigated is TaCrPdAg but few test results are available. With the elevated temperatures encountered at the near sun distances, the problem of gridline degradation should be given individual attention.

### Thickness

Solar cells are currently available in about any thickness ranging from 2 to 20 mils. The advantages of the thinner cells are weight reductions and increased radiation resistance (Ref. 1, 11). The problems associated with thin cells are cost, required handling care, reduced efficiency, and some thermal distortion problems associated with contact metalization. Production run cells 2 mils thick are currently available with 11.1% efficiency and production cells 12 mils thick are available with 14% efficiency.

#### 3.1.2 Efficiency Projection

Table 3-2 is a matrix showing the relative risks of achieving combinations of cell efficiencies and thicknesses in the required time frame. This matrix is subjective and is based on the current state-of-the-art wraparound technology, consideration of the large numbers of solar cells needed, and the time available to advance the technology.

#### 3.1.3 Wraparound Contact Solar Cells

Some work has been done recently to improve and characterize wraparound solar cells (Ref. 15, 16, 17). The current status of the wraparound contact solar cell configuration is shown in Table 3-2A. The majority of the wraparound cells produced to date are a modified junction wraparound type. The current SEP cell is of this variety. Some losses are inherent in this configuration associated with the lost area in the P back region due to the N contact but these are not significant. There appears to be a processing limit at about 6 mils of silicon for this configuration. Because of the cells application in the current SEP program it is classified as Category I in the 8 mil thickness and Category II in the 6 mil thickness.

A new type of wraparound cell currently under development is the dielectric isolation wraparound. Here, a dielectric is employed to insulate the edges and a portion of the back. Only the N layer metalization is brought around to the cell backside. This results in improved performance over the junction wraparound. In the past, this configuration has performed poorly due to lack of a suitable dielectric. Progress has been made, however, to the point of a non-vacuum deposited dielectric. Eight mil

**TABLE 3-2**  
**DEVELOPMENT RISKS FOR WRAPAROUND CONTACT CELLS EFFICIENCY**

		12%	13%	14%	15%
Thickness (mils)	10	1 *	1 *	4	7
	8	1 *	2	5	8
	6	3 *	5	7	9
	4	6	8	9	10
	2	10	10	10	10

**Probable Risk of Achieving Production of Wraparound Cells of Stated Efficiency and Thickness**

**1 - Risk Very Low**

**10 - Risk Very High**

**\*Indicates a Category I component, all others are Category II**

**TABLE 3-2A**  
**WRAPAROUND SOLAR CELLS**

**End Tab Wraparound Contact - Current SEPS Design**

- CrPdAg contacts
- fill factors ~ 0.72 to 0.77
- fabricated in vacuum
- limit to cell thickness for this processing, probably about 6 mil

**Dielectric Isolation Wraparound Contact - employs dielectric to insulate contact from cell edge and eliminate shorting effects**

- non-vacuum deposited dielectric
- improves fill factor and power
- 8 mil cells with 14.8% efficiencies have been made
- cells as thin as 5 mil are being produced
- about 4 mil limit on thickness for current process technology

**Mechanical Wraparound Contact - interconnect provides wraparound contact**

- probably needed for < 4 mil cells
- no configurations currently available

cells of this design have been reported with a 14.8% efficiency. This type of wrap-around cell has yet to be produced in large quantities or space qualified. It is therefore a Category II component.

The mechanical wraparound is still another conceptual approach to a wraparound cell. Here the interconnect is wrapped around the cell and bonded to N contacts at both ends of the cell. This type of wraparound will be required for less than 4 mil cells and is also a Category II component.

Spectrolab has stated the 5 mil 13% efficiency covered solar cell assembly with 3 mil CMS is feasible for development in the 18 month period starting 1 October 1978. The baseline cell would be a 2 x 4 cm wraparound contact design with an initial parallel development effort for a 4 x 4 cm wraparound contact design. The 2 x 4 cm design is selected since it meets the array performance requirements and limits new technology development. The 4 x 4 cm design would be evaluated for design and production techniques to compare the risk and array costs associated with this cell with the 2 x 4 cm design. A probable fabrication technique for the 4 x 4 cm cell is to process circular wafers as long as possible. Cutting the wafers square will remove any chipped edges generated to that point.

A 2 mil silicon solar, with a conventional contact cell has been developed by Solarex and Spectrolab is also developing a similar cell. The Solarex cell has been characterized as to illumination intensity and temperature performance and as to degradation in charged particle radiation. Data on welded assembly mechanical and electrical performance following exposure to space temperature extremes is not available but good flexibility of the cells at this thinness has been observed. The solar cells are a part of a system that is concerned with covering the cells for temperature control and radiation protection, interconnecting the cells for the desired electrical module configuration, and providing mechanical support for the cells during launch and when the solar array is extended. Based on available data, the development of organic covers or encapsulants for the Halley's Comet mission appears to be a greater risk than the use of 3 mil CMS. The application of a glass cover to 2 mil cell with attendant rework activity would appear to have a lower yield than with a thicker 5 mil cell. The glass cover for the conventional contact cell has a gap problem associated with the "N"

contact bar which cannot be covered by the glass prior to interconnecting the cells. The use of a wraparound contact cell allows the cell cover to cover the entire cell front. It also offers the potential of reduced cell interconnecting costs as the tooling is simplified and all the welds are made from one side of the assembly. A wraparound contact 2 mil cell may be developed but the risk for such a development is relatively high.

The wraparound contact 2 x 4 cm cell developed by NASA has progressed from a 12 mil 10.8 percent efficient design to an 8 mil 11.4 percent design without a sculptured front surface, P+, or a back surface reflector. This progression along with the development of large area printed circuit substrate fabrication improvements in the present SEP Solar Array Technology Development Program, NAS8-31352, led LMSC to select the 5 mil, 13% efficient, 2 x 4 cm wraparound contact cell as the baseline design with the least array system development risk for the Halley's Comet mission. Should an array system employing a 2 mil cell become sufficiently attractive prior to the flight hardware development, its application would further decrease array system weight.

#### 3.1.4 Production Rate

The present combined production capability of Spectrolab and OCLI is about 500,000 2 x 4 cm solar cells per year (10,000/wk), slightly over the total quantity required for the baseline design. The production of cells would have to commence 18 months after the start of the technology development program or about 1 January 1979. The production run would have to be complete by 1 January 1980. Either vendor alone would have to increase his production capability by a factor of two for the HCR mission and possibly by a factor of 2.5 to cover other commitments. If both vendors are qualified to produce the solar cells, the production capability increase for each is about 50 percent. Decisions regarding this increase in production capability would have to be made by 1 July 1979. These increases are feasible according to the cell vendors.

#### 3.1.5 Cost

The projected costs of the HCR mission solar cells in production is highly uncertain. The exact cell design and the resulting cost of each fabrication step is not known. The

order of 200,000 to 500,000 solar cells would also cause the cell vendors to fund at least semi-automation of some of the present manual operations. The estimated cost of a 5 mil 2 x 4 cm wraparound contact solar cell assembled with a 3 mil CMS cover and providing 13% covered efficiency is \$25.00/cell assy. The cell assemblies for the baseline concentrator array (466,680 cells) is \$11.7M. The cost estimated by Solarex for their 2 x 2 cm solar cell is \$9.00/cell uncovered. About 1.0 million of these cells are required for \$9 M total. Similar CMS covers and cover application would put the cell assembly costs over \$12 M. It is apparent that the availability of an organic cover would provide about a \$2 M cost savings. Handling fewer 2 x 4 cm cells than 2 x 2 cm cells or fewer 4 cm x 4 cm cells than 2 x 4 cm cells would be a definite fabrication cost advantage also. The improvement of yields, and the emphasis on the development of low cost cell fabrication processes and techniques will be emphasized in the technology development program.

### 3.2 SOLAR CELL COVER TECHNOLOGY

#### 3.2.1 Glass Covers

Fused Silica - Corning 7940 fused silica has been used extensively for cell covers on most U.S. satellites. It is favored for its environmental stability. It is fabricated at present down to an average thickness of 6 mils. A thinner design is required for the HCR SEP mission and this thinner design is a Category III item. The material is expensive and quite brittle.

Ceria Stabilized Microsheet Glass - This material is available from its developer, Pilkington Labs, United Kingdom. The material has been qualified and successfully flown on several foreign satellites. The material has lower cost, higher strength, and thinner options than fused silica. It has been built in 3 mil thicknesses. For the HCR-SEP mission, technology development is required for the sizing, handling, and applying of the covers to the solar cells and it is therefore a Category II item. The material (5% ceria doping) is a UV filter and the adhesive is protected. An AR coating is required.

Integral Covers - The primary limitations associated with integral covers are ion sputtering process rates, cost, and induced stresses (cell bowing). High facility capital expenditures would be required to bring production rates up. This is a Category III item.

Microsheet - Microsheet is not sufficiently stable for the HCR-SEP mission and is a Category III item.

### 3.2.2 Spraylon

Spraylon encapsulated solar cell modules are attractive for economical as well as technical reasons. The Spraylon replaces both the coverslide and coverslide adhesive and is inexpensive to apply. The continuous Spraylon cover sheet provides integral low energy proton protection which is not influenced by component and assembly tolerances. The density of Spraylon ( $2.1-2.2 \text{ gm/cm}^3$ ) is comparable to that of fused silica ( $2.2 \text{ gm/cm}^3$ ) and so it has equivalent radiation shielding properties. The properties of Spraylon films are almost identical to those of the DuPont FEP Teflon. For solar cell application, the emittance property is of direct concern. The room temperature emittances (Gier-Dunkle DB-100 Infrared Reflectometer) of several thicknesses of Spraylon have been measured (Ref. 10) and the emittance is seen to be about 0.85 for thickness greater than 5 mils. Below about 2 mils, the emittance of the Spraylon drops off and approaches the emittance of the material it is coated on. Typically, a solar cell has an emittance of 0.47.

As a result of Spraylon being applied directly to the solar cell and no adhesive being used, the specific power of the cell is improved in two ways. First, there is a weight reduction because of the lack of adhesive and because the cover can be tailored exactly to the mission's radiation environment. Secondly, since no UV filter is used, there is a slight gain in power due to the cell's  $< 0.35$  micron wavelength response.

One of the early problems with Spraylon coatings was its high coefficient of thermal expansion mismatch with silicon. Solar cells cycled to low temperatures were torn apart by the Spraylon. Proper coating techniques and limits on the Spraylon thicknesses as a function of cell thickness alleviated this problem.

Spraylon has been shown to have at least as good radiation resistance as FEP. Unfortunately, two recent reports on FEP as a cell cover have shown FEP to be an inferior cell cover (Ref. 18, 19). In one report, the FEP appeared initially to have a good resistance to UV and charged particle radiation. Measurements at a later date, however, showed that the FEP covered cell degraded 43% after two years of synchronous orbit



compared to 24% for a violet cell with a 6 mil CMS cover. This degradation is excessive for a Halley's Comet mission. Although it was not Spraylon that was tested, recent Spraylon UV tests at high temperatures have shown it to be unacceptable. It is a Category III item.

### 3.2.3 Polyimide

Polyimide plastics have been given some attention as a solar cell cover (Ref. 11). One polyimide, Kapton, seems to have all the ideal properties with respect to coefficient of thermal expansion, usable temperature limit, and other mechanical properties. The radiation tolerance of Kapton to charged particles and UV is good. The big drawback to the use of polyimides, however, is in its rather poor transmittance. Kapton sheet 1 mil thick has a transmittance of only 66%. Increased thicknesses of Kapton, which would afford more radiation protection for the cell, would decrease in transmittance inversely with thickness. For the equivalent proton radiation protection of 3 mil CMS, approximately 6 mils of Kapton would be needed which would have a transmittance of about 51%. Using a polyimide as a cover sheet would just about double the required cell area, and is there for an unacceptable cell coverslide (Category III item).

A polyimide-siloxane copolymer had also been proposed by Ref. 11. This copolymer has excellent transmission properties; 95% transmission through a 1 mil thickness. The coefficient can also be tailored to match that of silicon. Recent work, however, has shown severe UV degradation (Ref. 22) of the copolymer and hence, it is an unacceptable cell cover also.

### 3.2.4 Glass-Resins

Organic modified silicones when applied directly to the cell and cured at 150°C form SiO bonds and a very hard surface. The material, available in different formulations, is made by Owens-Corning. It is being evaluated by NASA-LeRC as a cell cover and some of the testing results are encouraging. Exposure to  $10^{17}$  1 MeV e/cm<sup>2</sup> showed no degradation. Accelerated UV tests, 10 suns for 728 hrs, showed 15 to 23% I<sub>sc</sub> degradation but lower rates may show better performance. This material is a Category II item.

### 3.2.5 RTV Silicone

This G. E. product is applied directly to the cells and cured to form a transparent cover. UV testing performed by NASA-LeRC was accelerated and although 21%  $I_{sc}$  degradation was observed, lower rates may show better performance. This material is a Category II item.

### 3.2.6 Cell Cover Coatings and Surfaces

The use of cell covers in the concentrator array raises interest in the advancement of AR coatings, UV filters, and front surface treatments for covers. The possible application of AR coatings and UV filters to non-glass surfaces would improve array performance and allow the use of adhesives to accommodate thermal coefficient of expansion mismatches between the cell and candidate organic covers that would otherwise be useable. The use of sculptured or grooved cover glass surfaces may reduce the losses associated with the non-normal angle of incidence of light reaching the electrical modules from reflector surfaces.

## 3.3 BLANKET TECHNOLOGY

### 3.3.1 Design

The lightweight flexible substrate strength members are polyimide (Kapton), fluoroplastic (FEP Teflon) and polyester (Mylar). Kapton film, made by DuPont, is the most stable of these materials in the space environment and has been used on the two flexible arrays flown to date, CTS and FRUSA solar arrays. It is available in widths up to 60 inches and in thicknesses down to 0.3 mils. The Kapton film may be the substrate to which interconnected solar cells are adhered (Category I design) or encapsulated with the use of a transparent film which also acts as the cell cover. This latter design requires extensive development and is a Category III design. The Kapton film is also used as insulating sheets between which a printed circuit cell interconnect trace is encapsulated. The present SEP Solar Array printed circuit blanket design employs two sheets of 0.5 mil Kapton with 0.5 mil high temperature polyester adhesive as the laminating adhesive. The use of the printed circuit substrate allows the low cost fabrication of the cell interconnect system and eliminates interconnect handling. Mechanical and environmental testing of the printed circuit has demonstrated this blanket technology

for the SEP Solar Array design. The Extended Performance SEP array, however, requires further weight reductions. The proposed use of 0.3 mil Kapton sheets with 0.4 mil laminating adhesive and a 1 mil aluminum interconnect metal requires technology demonstration and this is a Category II design.

A number of interconnect metals are available for solar cell interconnecting. Molybdenum, Kovar and Invar are low coefficient of thermal expansion metals which are plated to facilitate cell bonding and reduce electrical resistance losses. They provide smaller cell stress during thermal cycling of array modules. They are also high in density and not desirable for use in lightweight array blankets. They are Category III as feasible alternates are available.

Silver has excellent conductivity and has a demonstrated good flight history--primarily in an expanded metal form. It is, however, the heaviest of the candidate metals (density 10.6 gm/cm<sup>3</sup>) and would be very costly for a large area solar array. It has a Category III status.

Copper was rated for the SEP Solar Array as being the second best metal for interconnects after molybdenum. It was selected over Mo because of its weight, ease of fabrication in printed circuits, and excellent low temperature ductility. Based on present HCR-SEP solar array weight limitations, it is a Category III item since a feasible alternate is available.

Aluminum is the selected cell interconnect metal for the HCR-SEP mission because it has significant weight advantages and is easy to fabricate into printed circuits. The metal will require local plating to allow the preferred welding of the silver contacted cells to the interconnect. LMSC has fabricated samples of this metal in a printed circuit design and used a local plating technique. Since larger array modules and cell welding require demonstration this interconnect metal is a Category II item.

### 3.3.2 Fabrication Technology and Processes

Techniques for roll-laminating of large printed circuit solar array substrates are being developed by LMSC for NASA in the SEP Solar Array Technology Development Program.

Thirty-four inch wide panels up to 500 to 1000 ft long can be processed by roll-laminating or by electrodepositing aluminum on the Kapton film. Following the etching of the cell interconnect circuit, the Kapton coverlay is roll-laminated over the circuit to complete its encapsulation. The baseline manufacturing concept for the SEP Solar Array fabrication is illustrated in Figure 3-1. The laser skiving operation shown as the last step in the figure removes the Kapton plus adhesive from the pads in the interconnect system (both sides of blanket) so that welding electrodes have access to the pads on one side of the blanket and the cell surface has access to the pads on the other side of the blanket. The completed blanket strips are cut into electrical module lengths and are ready for cell bonding operations. Figure 3-2 illustrates the integral interconnect substrate design as it interfaces with a wraparound contact solar cell. The conventional contact cell interface is also shown. The demonstration of the fabrication technique for the thinner HCR-SEP mission substrate is required and this is a Category II item.

Several cell joining techniques have been developed. Solder joining is the most common technique. The joints are easily made, inspected and repaired. The relatively large solder joint and the mismatch in coefficient of thermal expansion between solder and silicon causes high stresses in joints under thermal cycling. The weight of solder is a penalty for the HCR-SEP mission array and the solder would be the weakest link in non-nominal temperature spikes. It is a Category III process as alternate techniques are available.

Parallel gap electric resistance welding of solar cell interconnects is the non-soldered joining techniques that has seen the most development activity. In Europe, AEG Telefunken has built welded arrays. In this country, LMSC has developed and flown for the Air Force a welded system on a rigid panel substrate array. Welding of copper interconnects to silver contacted cells has been successfully performed on the SEP Solar Array program with cell junction depths of 1200 to 1700 angstroms. The shallow junction of high efficiency cells is a potential problem area for parallel gap welding since too much weld energy too near the junction can damage the cell junction and degrade cell performance. Too little energy provides a weak mechanical bond. In the wraparound contact cell, if the front cell contact is brought around to the cell backside over a dielectric layer, all weld bonds are made with a significant amount of silicon between the bonds and the cell junction, thus alleviating the shallow junction cell problem. The

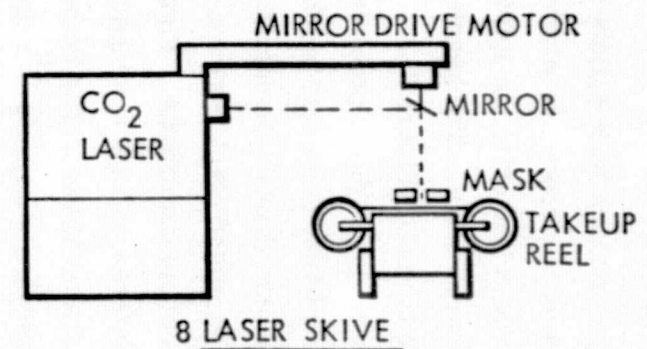
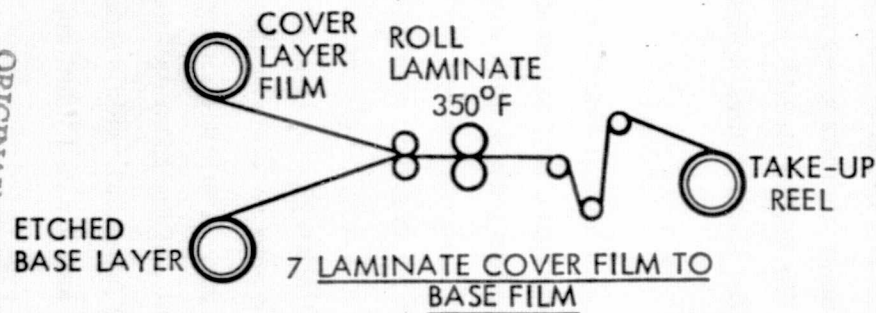
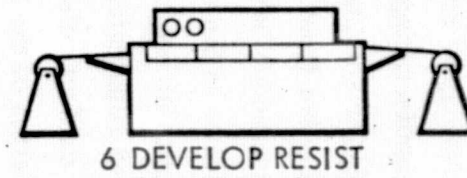
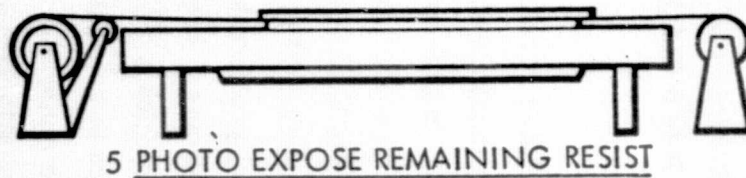
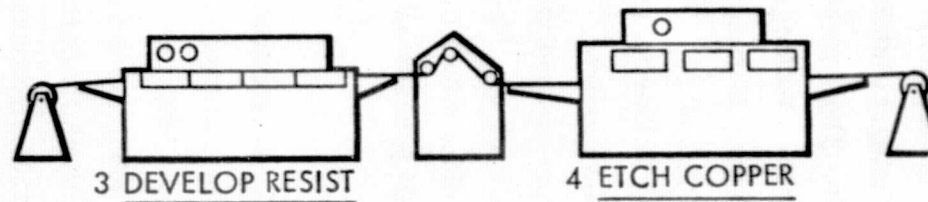
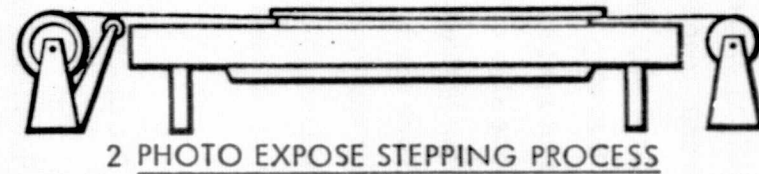
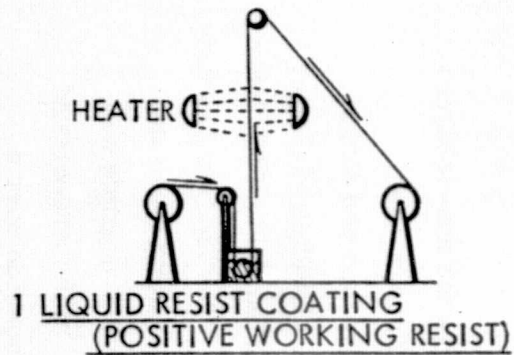


Figure 3-1 Baseline Manufacturing Concept for Substrate Fabrication



- GOOD JOINT ACCESS
- HIGHER PACKING FACTOR
- REDUCED ASSEMBLY STEPS AND COST
- ELIMINATES N-BUS GAP PROBLEM
- REDUCED WEIGHT

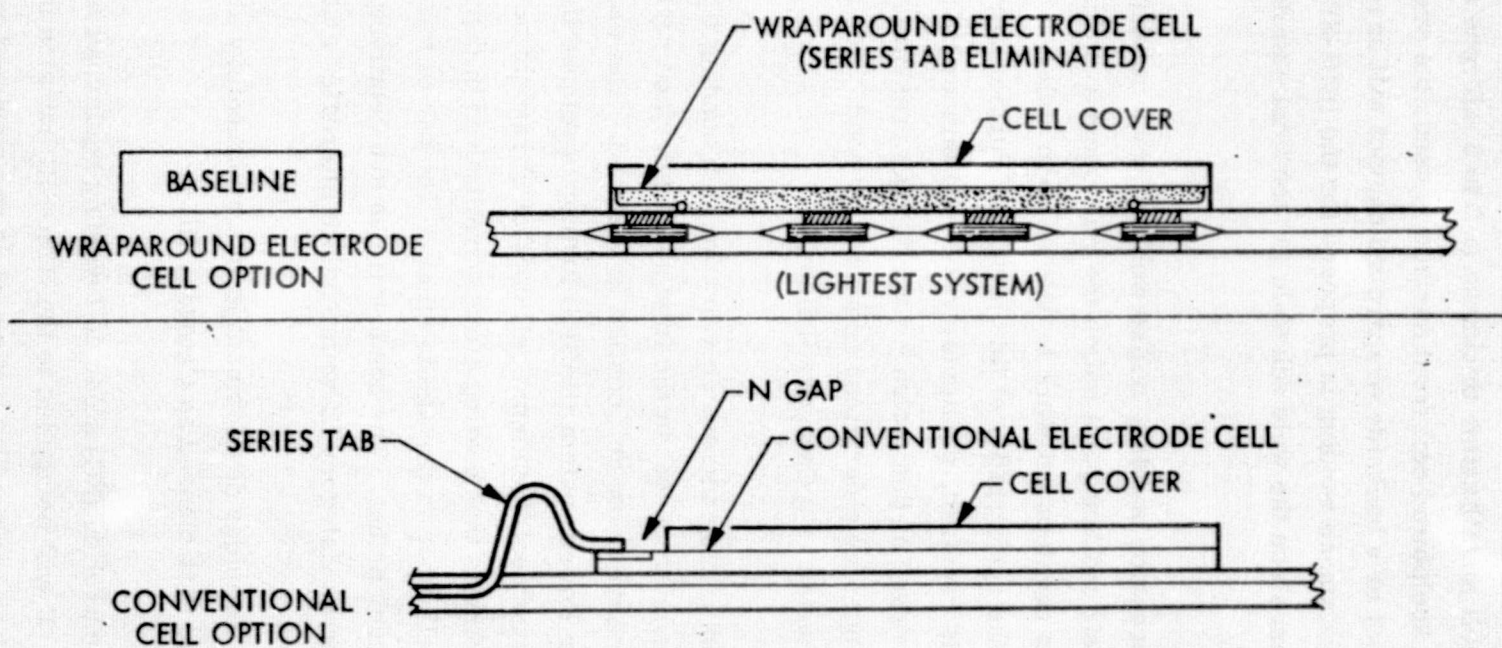


Figure 3-2 Integral Interconnect Substrate Design

weld process requires a smooth cell well area ( $< 250$  NM RMS surface) and control on variations in cell metallization thickness ( $\pm 2$  to  $3$  microns allowable variation). If a non-reflecting sculptured cell front surface is used, the area for the bond on either a frontside contact or a backside wraparound contact will have to be smooth. Parallel gap electric resistance welding is proposed for the HCR-SEP solar array. It is a Category II item since the weld schedule for the final cell design will have to be demonstrated.

Thermal compression bonding, unlike welding, does not depend on bringing the parts to be joined to their melting point but on the microscopic diffusion of each material into the other. The development work to date on solar cell bonding with this technique has demonstrated the applicability of this method. Further work on tooling and cell design requirements is required, particularly with the thinner HCR mission solar cells. The major disadvantages of this technique are 1) high pressures over a larger working area, and 2) much longer time durations required for bond. For the HCR-SEP mission, this technique is classed as a Category II item.

Ultrasonic bonding uses ultrasonic vibration in a bonding tip to cause local heating and cold flow of the interconnect in the immediate interface region, and a bond between the interconnect and the solar cell contact is obtained. The work by Hughes on the Air Force Hardened Solar Power System (HASPS) further developed the use of this technique for aluminum interconnect/aluminum cell contact ultrasonic bonding. An advantage of ultrasonic bonding is that heating effects are limited in depth in the solar cell and the potential for cell junction damage is small. The use of this technique on thin cells will require new development. The bonding times are relatively long and this bonding technique is classed as Category III with feasible alternates available.

Laser welding technique development is in a rudimentary stage for application to solar cell bonding and it is classed as Category III.

Numerically Controlled (NC) solar cell welding equipment has been developed and demonstrated. It will be applied to the HCR-SEP mission solar array fabrication to reduce fabrication costs. The equipment is programmed to move the registered solar cells and substrate or the weld head precisely from one weld position to the next and to

perform the weld operation. The operator monitors proper equipment operation. Certain go-no go weld parameters can be measured prior to the weld pulse. The time-temperature profile during welding and/or the weld voltage-current profile can be controlled to prevent under- and over-welds. This technique is classed as Category I.

Non-destructive testing of completed electrical modules prior to placing them in the solar array blanket is an important part of fabrication testing. The IR microscope with TV display can be employed on the welding equipment to provide individual weld evaluation as an in-process monitor. The larger area electrical modules require scanning techniques to reduce inspection times. One technique which shows promise for welded systems is an IR sensor with TV display which observes a panel with forward current flowing. Hot spots at welds that have high resistance due to underwelding or loose bonds or cold spots at bond areas due to opens are apparent in the TV display and can be identified for rework. This technique is Category II as specific correlation data will be required to be developed to demonstrate this technology for the HCR-SEP mission solar array.

Another technique which is being studied uses holographic interferometer techniques to display fringes which are close packed where high temperatures have caused more thermal expansion than normal compared to the module bond areas when no current is flowing. The application of this technique to solar array NDT and it also requires technology demonstration. It is a Category II technique.

### 3.3.3 Qualification Testing

Qualification testing of the array blanket is not considered a technology development problem. Confidence in the ability to design and fabricate an array blanket that will pass qualification tests during the array development program will be developed during the technology development program by performing environmental tests on the proposed blanket design. Thermal testing of materials, hinges, electrical modules and module stiffeners and post test evaluations will demonstrate mechanical, electrical and optical performance. UV and charged particle irradiation testing will also be performed. Mechanical tests at temperature will demonstrate adequate tensile, tear and creep properties for the design of blanket components. Tests of larger scale hardware will demonstrate reflector/electrical module performance, zero-gravity extension/



retraction performance of the blanket/reflector design, and full-scale wing section fabrication and test will demonstrate the technology readiness of large area array fabrication, handling, and ground testing techniques.

### 3.4 TECHNOLOGY DEVELOPMENT PLAN AND COST ESTIMATE

#### 3.4.1 Introduction

The purpose of this plan is to describe a cost effective approach to demonstrate technology readiness for the HCR-SEP mission solar array. As a result of the technology assessment performed in the study, several areas requiring technology demonstration and development have been identified and these are included in this plan. The major tasks in the demonstration of technology readiness are associated with 1) the required solar cell and 2) the fabrication and test of a full scale section of a concentrator solar array wing with less than a full complement of live solar cells. To accomplish the first task, a competitive procurement for the solar cell development will be initiated by defining the results that the cell vendor must attain and evaluating the proposed technical approach. To accomplish the second task, a review of the HCR-SEP solar array design requirements will be performed to identify any changes or studies of options that would affect design requirements. The solar array design requirements define the technology demonstrations and developments required and allow focusing of technology development efforts on the appropriate design. A significant cost savings in the technology demonstration program can be achieved if a design, meeting the HCR-SEP requirements, for the flight array wing is arrived at as soon as possible. Design optimization is not required during the technology development program, but a design is required to assure the proper component technology is being developed. A second cost savings will be achieved by performing component tests in the configurations that they have in the array design, and assuring that testing is performed specifically for the HCR-SEP environments. Similarly, technology development should be emphasized rather than design developments where there is confidence that the design is sufficiently developed to identify all necessary technology. To save costs, where technology readiness risk is low, components shall be incorporated and tested in the full-scale wing section tests.

#### 3.4.2 Technology Status

The technology state-of-the-art reviewed during the study is summarized below. Technology readiness was classified as: I - Sufficient, II - Insufficient but development progress will achieve readiness, and III Insufficient but an alternate is feasible. The classification is specifically for the HCR-SEP Solar Array.

### Solar Cell Covers

	<u>Cat.</u>
Fused Silica	III
Ceria Stabilized Microsheet Glass	II
Microsheet Glass	III
FEP - Heat Laminated	III
- Spraylon	III
Integral Covers	III
Electrostatically Bonded 7070	III
Glass-Resin	II
RTV Silicone	II

### Solar Cells

Cat. II

Preliminary design requires development of 13% efficient 5 mil WA contact 2 x 4 cm solar cell. A plan for implementing a pilot production and test program is required. A 4 x 4 cm design will be investigated for feasibility.

### Solar Cell Interconnect

	<u>Cat.</u>
Cu	III
Mo	III
Al	II
Ag	III
Kovar	III
Invar	III

### Cell Joining Technique

	<u>Cat.</u>
Parallel Gap Welding	II
Solder	III
Ultrasonic Bonding	III
Thermal Compression Bonding	II
Conductive Adhesives	III
Laser Welding	III

Substrate

0.3 mil Kapton/0.4 mil Polyester adhesive  
(2 sheets)  
0.3 mil Kapton/0.4 mil Polyester adhesive  
(1 sheet plus silicone insulating cover layer)  
0.3 mil Kapton film with cells adhered to film

Cat.

II

II

II

Reflectors

Material

Deployment/Retraction

Cat.

II

II

Electrical Harness

FCC Al

Cat.

I

Containment Box Structure

Cat.

II

Extension and Retraction Mast

Cat.

II

Mast Motors

Cat.

I

Lubricants

Cat.

I

Solar Cell Yield

Cat.

II

Electrical Module NDT

IR Scanning

Holographic Interferometer

Cat.

II

II

### 3.4.3 Recommended Technology Development Projects

#### A. Improved Solar Cell for HCR-SEP, Category II

**BACKGROUND:** The HCR-SEP array preliminary design requires a 5 mil silicon solar cell with 13% efficiency where the wraparound contact 2 x 4 cm cells presently produced are 8 mil 11.4% efficient. A minimum cost system depends on low cost fabrication techniques and high yield. Therefore integration of the cell design development with fabrication and handling methods to be used is essential.

**DESIRED OUTPUT:** A weldable 5 mil solar cell design with required covered efficiency is desired. Data on effects of particle radiation, both front and back exposure, on  $I_{sc}$ ,  $I_{mp}$ ,  $V_{mp}$  and  $V_{oc}$  as a function of 1 MeV electron fluence is desired. The cell performance under the temperature and illumination values that the cells will see, including angle of incidence effects, is required for array performance predictions. Demonstration of cell joining techniques that have minimum effect on cell performance, that are repeatable, and that are of low cost in application to array fabrication is needed. A high yield cell fabrication process is desired.

**RECOMMENDED PROGRAM ELEMENTS:** The program should include effort by the solar cell vendors to evaluate both 2 x 4 and 4 x 4 cm cell designs and to investigate "high efficiency" techniques such as P+, back surface reflector, and sculptured front surface, shallow junctions, optimized contact grid configurations, and dielectric layers for wraparound contact. The selected cell should then be characterized by electron irradiation testing, UV testing, and temperature, illumination, intensity and illumination angle testing. Compatibility of the cell design with parallel gap electric resistance welding should be demonstrated. The average low temperature, low intensity performance of the cell design should be improved with P+ and the addition of a dielectric layer such as silicon nitride or oxide, over any exposed edges of the cell junction.

#### B. Solar Cell Cover, Category II

**BACKGROUND:** Thin glass or organic material solar cell covers are required to meet the HCR-SEP mission array weight goals. Thin ceria stabilized microsheet (3 mils) is an acceptable material from a stability standpoint but handling and application to solar cells requires demonstration. Alternate materials such as Glass-Resin systems

and RTV silicone can be applied in 0.5 to 1 mil thicknesses. The stability of these candidates in the space environment requires demonstration. Low cost application techniques are also of interest.

DESIRED OUTPUT: A review of available data on candidate cell covers with a selection of promising candidates for the HCR-SEP solar array is desired. Environmental testing data for these candidates showing mechanical and optical performance is desired. A narrowing of candidates after initial evaluation and test should be followed by additional development and testing to demonstrate the desired technology readiness.

RECOMMENDED PROGRAM ELEMENTS: The program should include the collection of test data, the evaluation and selection of candidates, and the fabrication of selected cover designs for testing. The covers should be characterized by electron irradiation testing, UV testing, and extreme temperature capability. Mechanical performance and optical transmission stability should be demonstrated. The program should include cell cover AR coating and UV filter evaluations to optimize cell performance. Coatings and surface texturing to reduce high angle of incidence light loss should be evaluated. The technique for applying the cover to the solar cell should be demonstrated.

#### C. Lightweight Array Substrate, Category II

BACKGROUND: The present SEP printed circuit substrate employs two 0.5 mil Kapton sheets and an etched 1 oz. (1.4 mil) copper interconnect system. The weight of this substrate must be reduced for the HCR-SEP solar array.

DESIRED OUTPUT: Data on the performance of a lighter substrate design following environmental exposure to electron and UV irradiation, and to temperature extremes is desired. Mechanical and thermal optical performance should be demonstrated. The use of local plating of the aluminum interconnect and the resulting cell weld bond strength and humidity resistance should be demonstrated.

RECOMMENDED PROGRAM ELEMENTS: The program should include the specification of 1 mil aluminum clad on 0.3 mil Kapton and 0.4 mil adhesive. Sample substrates should be fabricated and tested under electron and UV irradiation. The local plating of

the aluminum interconnect should be developed and tested by welding solar cells and exposing the samples to humidity and to the temperature extremes of the HCR-SEP mission. Perform substrate tensile, tear, and creep tests at array operating temperatures. Evaluate an alternate coverlay of silicone insulating material to replace one sheet of 0.3 Kapton/0.4 mil adhesive.

**D. Reflectors For Concentrating Solar Array, Category II**

**BACKGROUND:** The development of solar array reflector technology is required for application to the HCR-SEP solar array. The proposed baseline array requires planar trough type in-blanket reflectors to be flat-folded with the array blanket and planar side reflectors to be stored in containers adjacent to the blanket containment box. The in-blanket reflectors must be deployed to a tent-like configuration and maintained within certain dimensional tolerances and flatness over the mission operating temperatures. The side reflectors are large area aluminized Kapton sheets. These must also be deployed and held in a planar configuration. The effective concentration ratio of large electrical modules and reflector assemblies must be verified to support the predicted array performance.

**DESIRED OUTPUT:** Data on mechanical and optical performance of the reflector material following simulated environmental exposure. Demonstration of the in-blanket and side blanket reflector support, deployment, tear resistance, shape control, and retraction design at operating temperatures and also under simulated zero-gravity conditions. Effective concentration ratio data for various illumination and thermal conditions associated with the HCR-SEP mission.

**RECOMMENDED PROGRAM ELEMENTS:** Subject reflector material samples with seams to UV and electron irradiation and measure mechanical and optical degradation. Fabricate models of in-blanket reflectors with grid spacers and stiffeners and demonstrate maintenance of planar configuration at temperature extremes. Fabricate a large electrical module with reflectors and utilize a pulse simulator to determine concentration ratios and allowable degree of reflector misalignments and wrinkling. Fabricate and test in a KC-135 zero-gravity aircraft and/or neutral buoyancy test facility a scale model of the reflector/blanket array design to demonstrate proper deployment and retraction design.

**E. Composite Material for Containment Box Structures and Extension Mast  
Interfacing Structure, Category II**

**BACKGROUND:** The fabrication of graphite-epoxy structures for blanket and reflector containment boxes requires verification of weights and strengths. Verification of environmental behavior in the HCR-SEP temperature ranges, and in vacuum coupled with space radiation. Interface joints with metal structures and components also require technology demonstration.

**DESIRED OUTPUT:** Data on mechanical performance of sandwich structure following simulated environmental exposure.

**RECOMMENDED PROGRAM ELEMENTS:** The program should include:

- 1) Fabrication of candidate single stage and two stage cure systems with prepreg epoxy and with supplemental adhesive
- 2) Perform pre-environmental exposure tests on panels
  - a) Flat-wise tensile
  - b) Sandwich flexure
  - c) Drum peel
- 3) Expose test specimens to temperature/vacuum environments of the HCR-SEP mission
- 4) Repeat mechanical tests at mission operating temperatures
- 5) If thermal control coatings are required, adhesion, peel, and thermal-optical stability of the control assembly will be tested following UV, particle radiation, temperature, vacuum environmental exposure

**F. Solar Cell Yield Category II**

**BACKGROUND:** To obtain the new design solar cells at acceptable cost, in the quantity required, and within the program time constraints, requires a program to improve the yield of the solar cell fabrication operation.



**DESIRED OUTPUT:** Demonstration of equipment, processes and controls which provide good yield of the required HCR-SEP solar cell.

**RECOMMENDED PROGRAM ELEMENTS:** The first 12 months of the solar cell design and fabrication technology development should concentrate on the cell design meeting the required performance. The next 6 months will be used for pilot production and the technology development and demonstration associated with improved solar cell fabrication yield. The program will include the delineation of required tolerances on all the cell parameters, the development of process controls and inspections which insure good yield, and the application of semi-automation to certain manual operations. Those areas which impact yield the most will receive the most emphasis. The aspect of cell design and fabrication which result in poor low temperature, low intensity performance will also be investigated to improve yield.

G. Electrical Module NDT, Category II

**BACKGROUND:** The rapid inspection of completed welded solar cell electrical modules and the identification of bad weld joints is required to reduce array fabrication costs and insure array quality. NDT methods for this inspection require technology demonstration.

**DESIRED OUTPUT:** Definition of on-line procedures and equipment to perform the NDT Inspection/Acceptance functions for welded solar array modules.

**RECOMMENDED PROGRAM ELEMENTS:** Investigate IR scanning and holographic interferometer techniques for application to the HCR-SEP electrical module NDT by fabricating and testing "good" and "bad" modules. The program should include:

- 1) Write specification for selected system
- 2) Procure and set-up the testing system
- 3) Develop processes and procedures for system application
- 4) Fabricate module using NDT inspection/acceptance system

#### H. Extension Mast, Category II

**BACKGROUND:** The fiberglass-epoxy coilable longeron extension mast has been developed with an aluminum storage canister. One weight improvement required by the HCR-SEP mission is the use of composites in the storage canister. Another weight improvement not required by the baseline array design but having a potential for significant weight savings is the use of graphite-epoxy in the mast longerons and battens.

**DESIRED OUTPUT:** Demonstration of an extension mast deployer/storage canister fabricated from composite materials with the design weight and performance under mission thermal environments is desired. Data on the performance of a coilable longeron for the HCR-SEP solar array fabricated from graphite-epoxy is desired.

**RECOMMENDED PROGRAM ELEMENTS:** The program should include a design study for the HCR-SEP extension mast and the short deployment mast based on specified stiffness and strength requirements. Graphite-epoxy longeron samples of the design cross-section should be fabricated and tested to demonstrate required strain/stress capability at operating temperatures. A short (12 foot) section of the graphite-epoxy mast should be built and tested if the longeron test results are satisfactory. The extension mast for the Full-Scale Wing Section should be fabricated using the composite deployer canister and a fiberglass-epoxy longeron mast element to reduce hardware costs. This mast will be tested prior to incorporation in the Wing Section.

#### I. Full-Scale Wing Section Fabrication and Test, Category II

**BACKGROUND:** The large size, the lightweight requirements, and the use of new reflector technology for the HCR-SEP solar array requires technology demonstration for the fabrication, handling, and ground testing of full-scale hardware.

**DESIRED OUTPUT:** Test data and design evaluation of a full-scale section of the HCR-SEP solar array covering component fabrication, handling of full-scale hardware, and techniques for ground acceptance testing.

**RECOMMENDED PROGRAM ELEMENTS:** The program should include the fabrication of a full-scale section of the wing using the proposed fabrication process, materials and techniques unless significant cost savings can be made with alternate materials without compromising wing technology demonstration. The live electrical portion of the wing section will be 5% of the section module area and the remainder of this area will employ mass simulators for the cell area. Environmental testing of the wing section in the stowed configuration should be performed, followed by a ground deployment test to demonstrate the deployment test technique and to perform post environmental test inspection. The environmental testing should include acoustic exposure, random vibration, and thermal-vacuum exposure of the stowed wing section.

#### **3.4.4 Schedule and Cost Estimates**

The HCR-SEP Solar Array Technology Development Program schedule and cost estimates are shown in Figure 3-3. These data are based on the baseline three dimensional concentrator solar array.

ORIGINAL PAGE IS  
OF POOR QUALITY

ITEM	FY78	FY79	FY80	FY78	FY79	FY80	TOTAL
A. SOLAR CELL DEVELOPMENT							
Design Development and Characterization	▲	▲		\$300K	\$250K		\$550K
B. CELL COVER DEVELOPMENT	▲	▲		300K			300K
C. LIGHTWEIGHT SUBSTRATE DEVELOPMENT							
Design	▲	▲		100K			100K
Materials Development and Demonstration	▲		▲	40K	40K	20K	100K
D. REFLECTORS							
Design Development	▲	▲		100K			100K
Materials Development and Demonstration	▲		▲	80K	80K	40K	200K
Evaluate and Minimize Maldistribution of Light	▲	▲		160K	100K		260K
Zero-Gravity Testing	▲	▲		340K			340K
E. CONTAINMENT STRUCTURES							
Design Development	▲	▲		75K			75K
Materials Development and Demonstration	▲		▲	50K	50K		100K
F. SOLAR CELL YIELD AND COST IMPROVEMENT							
Yield Improvement		▲	▲	200K	800K	450K	1450K
Automation		▲	▲	300K	300K	200K	800K
G. NDT Development	▲	▲		50K	50K		100K
H. MAST LONGERON MATERIAL	▲	▲		175K			175K
I. FULL-SCALE WING SECTION		▲	▲	700K	800K		1500K
J. WING DESIGN	▲	▲		160K			160K
TOTAL							\$6.31M

Figure 3-3 HCR-SEP Solar Array Technology Program

### 3.5 NON-CONCENTRATING ARRAY DESIGN

Planar array designs were developed to determine the technology requirements for 60 and 120 kW arrays providing 200 and 240 W/kg B.O.L. at 1 A.U. from the sun.

#### 3.5.1 Electrical Design, Planar Arrays

Range of solar cell thicknesses and efficiencies and cell cover designs were evaluated to generate 60 and 120 kW planar array designs. The weights of these designs were then calculated to develop their specific power. Table 3-3 summarizes the designs. In all cases the total 0.6 mil Kapton/0.8 mil adhesive substrate with 1 mil aluminum interconnect was assumed. Aspect ratios for the arrays were held in the 3 to 6 range by assuming that multiples of a basic 2 m or 4 m array strip width were used to vary the wing blanket width. Configuration 1 employs the 5 mil, 2 x 4 cm cell of 13 percent efficiency and this cell cannot provide a 200 to 240 W/kg design. This cell must be 17% efficient to provide 200 W/kg as indicated by Configuration 2. A 3 mil 2 x 2 cm cell at 12.5% efficiency and a 2 mil cell at 10.4% efficiency will provide a 200 W/kg design. The 3 mil cell, Configuration 4, is selected as the 12.5% efficiency appears feasible to attain and the reduced number of cells required compared to the 10.4% efficient cell will be a cost saving.

To achieve 240 W/kg, the 3 mil cell must be 15% efficient while the 2 mil cell must be 12.6% efficient. This latter technology, Configuration 7, involves less risk and is selected for the 240 W/kg design.

Conventional contact solar cells are assumed for the 2 mil and 3 mil cell thicknesses. The printed circuit concept for utilizing conventional contact cells was shown previously in Figure 3-2. The "N" contact tabs of the etched printed circuit interconnect are exposed, lifted and shaped to allow bonding to the solar "N" contacts.

The sizes of the planar array wings are shown in Figure 3-4.

The array electrical design characteristics for the 60 KW and 120 KW array design providing 200 W/kg are shown in Table 3-4.

TABLE 3-3

## FLAT FOLD PLANAR ARRAY CONFIGURATIONS

Config. No.	Efficiency AMO 28°C-%	Temp. 1 A. U. °C	Cell Cover	Cell Size	Cells Per Array		Wing Mass (kg)		Specific Power - W/kg	
					60 kW	120 kW	60 kW	120 kW	60 kW	120 kW
1	13	55	3 mil CMS	2 cm x 4.044 cm x 5 mil	533,540	1,067,080	227	447	132	134
2	16	55	1 mil RTV Silicone	2 cm x 4.044 cm x 5 mil	433,501	867,003	150	300	200	200
3	13.3	55	1 mil RTV Silicone	2 cm x 4.044 cm x 4 mil	521,505	1,043,011	150	300	200	200
4	12.5	60	1 mil RTV Silicone	2 cm x 2 cm x 3 mil	1,114,106	2,228,212	150	300	200	200
5	15	60	1 mil RTV Silicone	2 cm x 2 cm x 3 mil	928,422	1,856,844	125	250	240	240
6	10.4	60	1 mil RTV Silicone	2 cm x 2 cm x 2 mil	1,339,069	2,678,138	150	300	200	200
7	12.6	60	1 mil RTV Silicon	2 cm x 2 cm x 2 mil	1,105,263	2,210,526	125	250	240	240

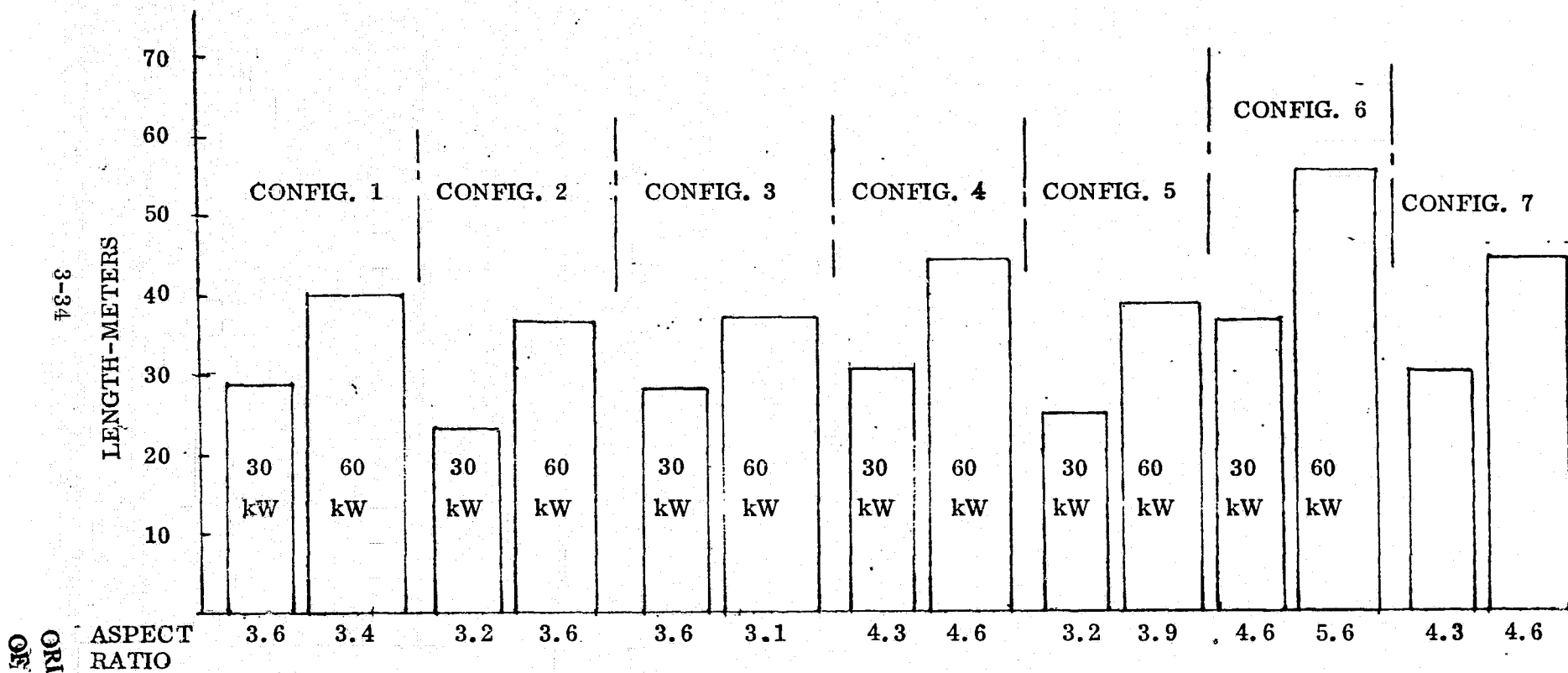


Figure 3-4 Planar Array Wing Sizes

TABLE 3-4

## 200 W/kg PLANAR ARRAY DESIGN CHARACTERISTICS

Net BOL Array Power at 1 A.U. Sun Distance	60.0 kW	120.0 kW
Gross BOL Array Power at 1 A.U. Sun Distance	64.66 kW	129.32 kW
Cell Size, Conventional Contact	2.0 cm x 2.0 cm x 3 mil	2.0 cm x 2.0 cm x 3 mil
Cell Assembly Efficiency (28°C, AMO)	12.5%	12.5%
Coverslide	1 mil RTV 655 Silicone	1 mil RTV 655 Silicone
Cell Assembly Solar Absorptance	0.83	0.83
Cell Assembly Emittance	0.65	0.65
Cell Operating Temp. at 1 A.U. Sun Distance	60°C	60°C
Number of Cells per Array	1,114,106	2,228,212
Packing Factor	0.96	0.96
Cell Blanket Area	464 m <sup>2</sup>	928 m <sup>2</sup>
Interconnect	1 mil Aluminum	1 mil Aluminum



### 3.5.2 Mechanical Design, Planar Arrays

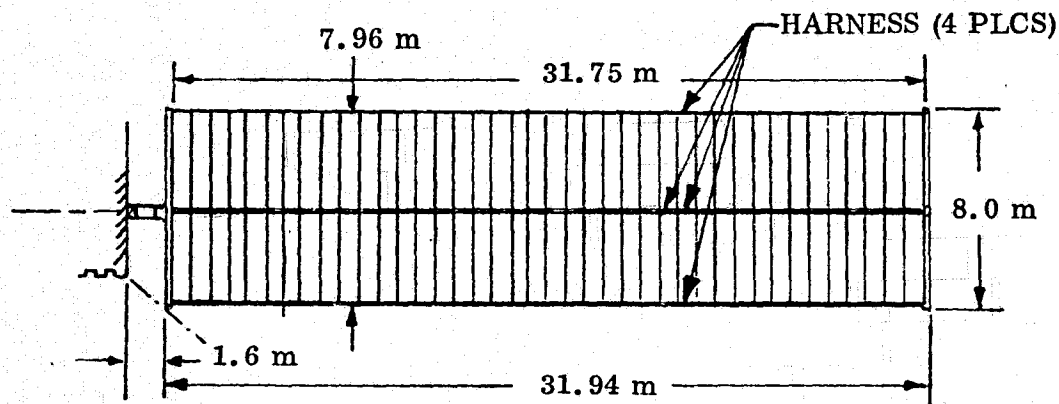
The deployed array wing configurations for the 60 and 120 kW planar arrays providing 200 W/kg B.O.L. power are shown in Figure 3-5. The configurations for these arrays providing 240 W/kg B.O.L. power are shown in Figure 3-6.

The blanket for the 30 kW wings is composed of two array strips, 3.93 m wide. The strips are made up of 40 panels each 0.76 x 3.93 m in size (similar to the present SEP Solar Array panels). The panels are hinged together and folded for stowage in a 0.38 in. stack. The blanket for the 60 kW wings is composed of 3 blanket strips to facilitate stowage and to reduce the aspect ratio of the deployed array. The two outside strips are similar to the two 30 kW wing strips. The inside strip is one half the width of the outside strips. The flat-fold array harness is located at both edges of the 3.93 m wide strips but only at one edge of 2.0 m wide central strips.

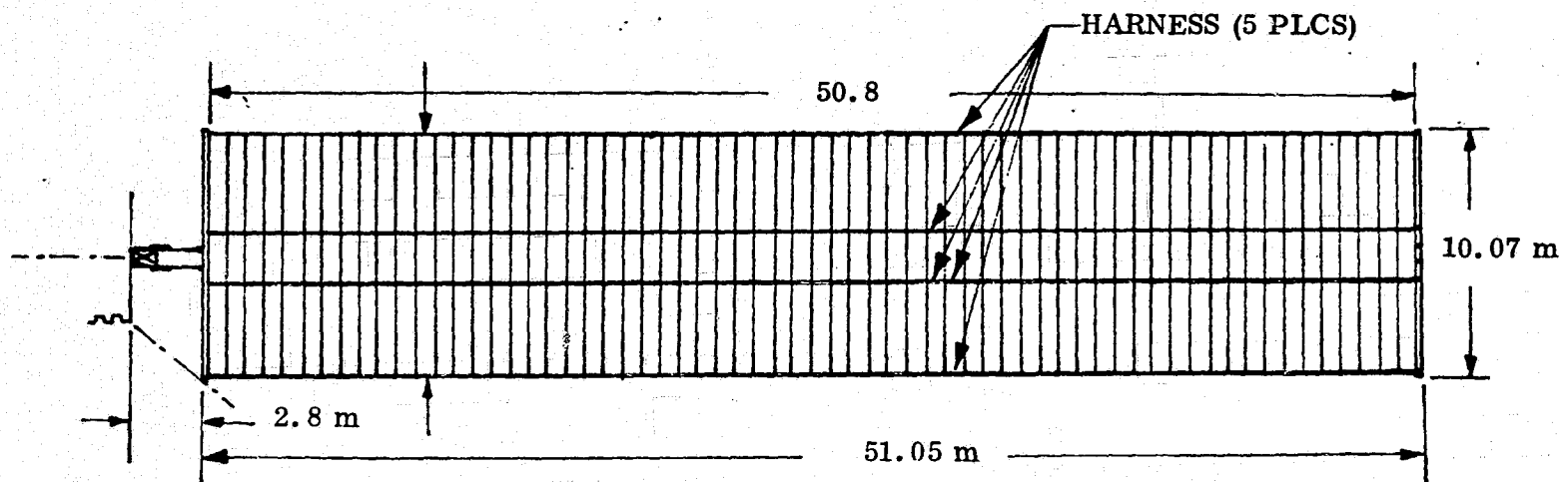
The tensioning of the array strips for planar shape control, and for deployed natural frequency control is provided by bottom and partial retraction tension distribution bar and negator powered tensioning cables. Guide wire, also tensioned by negators, pass through grommets at each panel hinge line and run from the containment box floors to the blanket outboard support arms. The guide wires control the location of the blankets when they are not tensioned. They also act, with local blanket panel stiffening, to cause flat folding of the array blanket strips during retraction.

A coilable longeron lattice structure mast that is both extendible and retractable provides all the motive force required to extend or retract the array blankets. This mast type is available from either Able Engineering Co., Inc. (Ablemast) or Astro Research Corp. (Astromast).

The stowage and deployment of 120 kW solar array wing is illustrated in Figure 3-7. A short (3 m) structural deployment boom is used to provide the required separation distance of the array to meet the thruster plume constraints.



30 KW WING

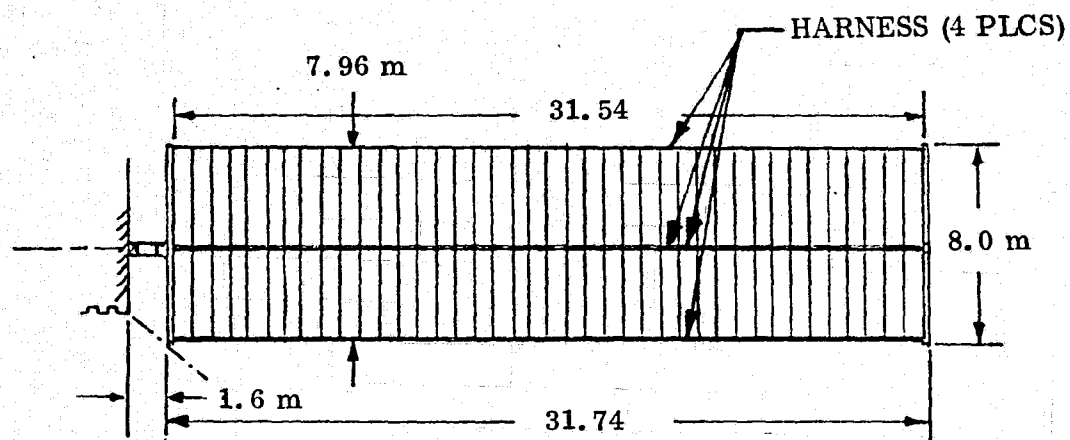


60 KW WING

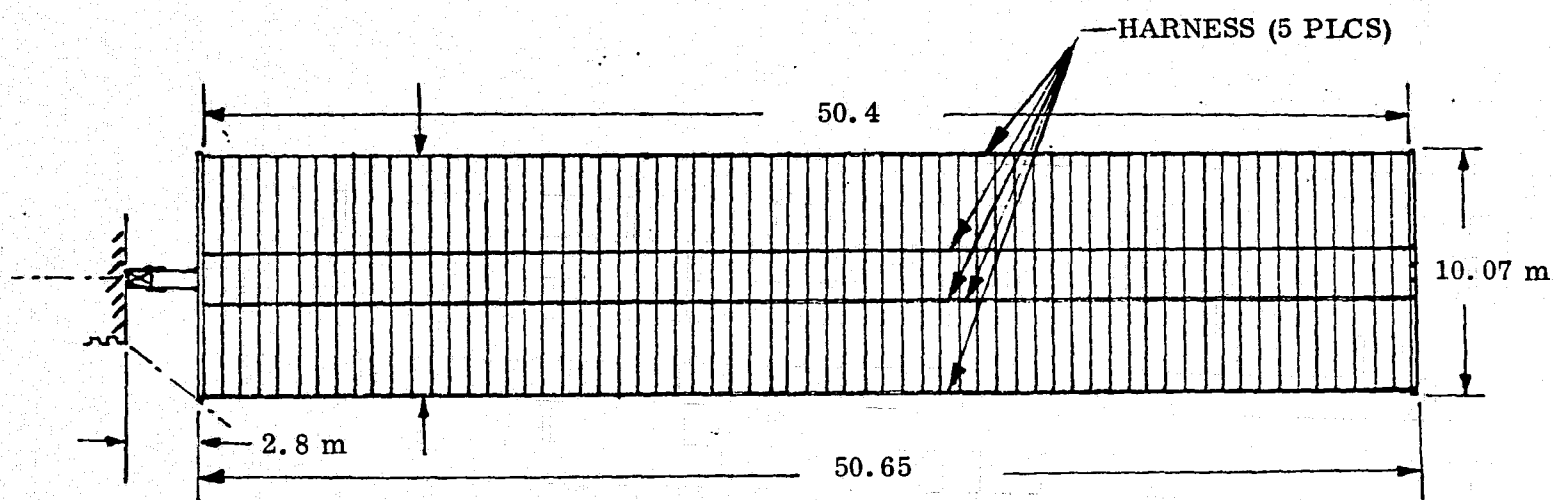
Figure 3-5 200 W/kg Planar Array Deployed Configurations

3-37

ORIGINAL PAGE IS  
OF POOR QUALITY



30 kW WING



60 kW WING

Figure 3-6 240 W/kg Planar Array Deployed Configurations

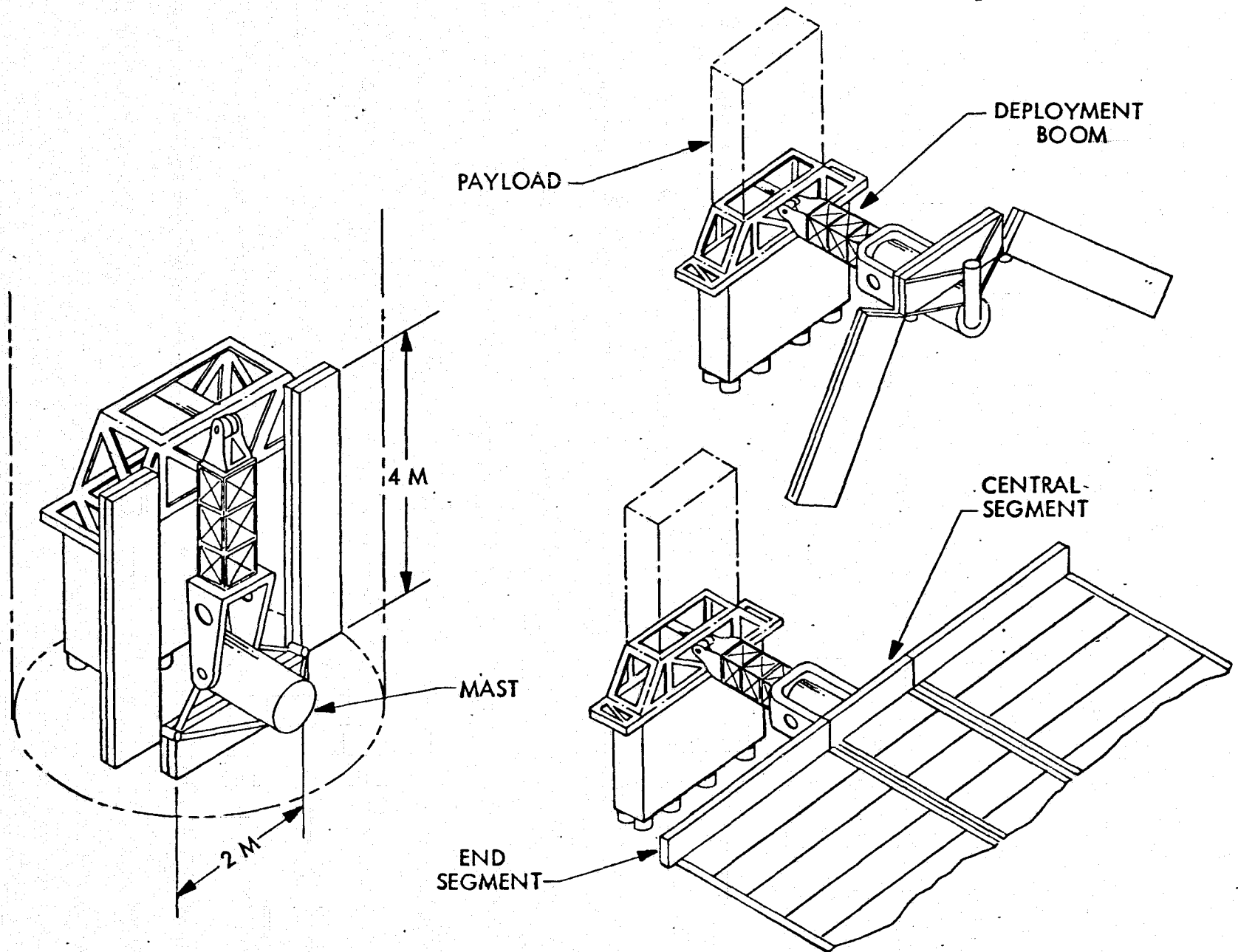


Figure 3-7 120 kW Planar Array Stowage and Deployment

The mast canister can be swivelled in a trunnion at the end of the deployment boom to its stowed position as depicted in Figure 3-7. The array container articulates at hinges situated at each end of a 2 meter long segment that is attached to the mast canister. Both end segments of the container swing into their stowage position, i. e., parallel to the deployment boom.

The outboard end of the array is attached to a yard arm that is articulated to match the container. This yard arm, in combination with a cover, provide protection to the blanket during launch and also is needed in withdrawing the array from its container. During stowage, the yard arm interfaces with the caging provisions and secures the blanket under an average pressure of 1.5 psi.

At separation between the IUS and SEP spacecraft, the array container is uncaged and ready for deployment.

The deployment boom swings out to a position that is at right angles to where it was stowed. The extension mast and canister rotates 90° in its trunnion and locks. The end segments of the array container swing out as shown in Figure 3-7. When all three segments have been coupled together, the blanket covers are unlatched and the extension of the mast commences. A tensioned guide wire system incorporated in the container controls the blanket location during extension.

### 3.5.3 Structural Characteristics

The design rationale is based on structural rigidity rather than strength. Weight is minimized by the use of high modulus graphite-epoxy composites, particularly, in the construction of the array container, support structure, mast fittings and struts.

Weight savings in the extension mast will be attained by the use of titanium cables, and composites in the construction of the canister.

Cable tensioning systems are employed to their full advantage in enhancing structural rigidity and control over the deployed configuration.

Structural weight is minimized by providing strength and rigidity for anticipated operational load and caging those structural areas, where feasible, where additional strength may be necessary to meet launch loads. Where possible launch support structure is left with the IUS.

The array extension mast for the 30 kW array wings has a stiffness of  $4.01 \times 10^8$  lb-in<sup>2</sup> and is 45.7 cm (18 in.) diameter.

#### 3.5.4 Performance Data

The 60 kW and 120 kW array electrical performance is shown in Table 3-5. The performance data is based on thermal modeling of the array blanket and resulting temperature predictions vs sun distance, and on cell performance data, published in Reference 21, defining cell performance as a function of temperature and illumination intensity. The weight summaries are shown for the 200 W/kg arrays in Tables 3-6 and 3-7 and for the 240 W/kg arrays in Tables 3-8 and 3-9.

TABLE 3-5  
60 kW AND 120 kW PLANAR ARRAY PERFORMANCE DATA

Sun Distance A. U.	Temp. (°C)	V <sub>mp</sub> /Cell (mv)	60 kW Array BOL Power (kW)	60 kW Array EOL Power* (kW)	120 kW Array BOL Power (kW)	120 kW Array EOL Power * (kW)
1.0	60	373.4	60.00	48.00	120.00	96.00
1.5	-1.1	516.7	32.08	25.66	64.16	51.33
2.0	-37.5	594.3	24.35	19.48	48.70	38.96
3.0	-80.7	684.9	9.96	7.97	19.92	15.94
4.0	-106.5	721.8	5.38	4.30	10.76	8.61
4.5	-116.0	723.7	3.99	3.19	7.98	6.38

\*20% degradation

TABLE 3-6

60 kW, 200 W/kg, PLANAR ARRAY WEIGHT SUMMARY

Component	Weight (kg)	No. Req'd/Wing	Wing Weight (kg)
Blanket Assembly	44.90	2	89.8
Panels (40)	36.15		
Hinges (40)	1.7		
Tension Distribution (1)	0.45		
Leader	0.6		
Harness	6.0		
Blanket Tension & Control	3.4	2	6.8
Cover	3.02	2	6.0
Container	5.78	2	11.6
Blanket Padding	0.03	78	2.34
Mast	23.6	1	23.6
Tip Fitting	0.7	1	0.7
Wing Position Boom	9.0	1	9.0
Total Wing Weight			149.84 kg
Total Array Weight			299.7 kg



TABLE 3-7  
120 kW, 200 W/kg, PLANAR ARRAY WEIGHT SUMMARY

Component	Weight (kg)	No. Req'd/Wing	Wing Weight (kg)
Blanket Assembly	70.00	2.5	175.0
Panels (64)	58.23		
Hinges (64)	2.72		
Tension Distribution (1)	0.45		
Leader	0.6		
Harness	8.0		
Blanket Tension & Control	4.0	2.5	10.0
Cover	4.4	2.5	11.0
Container	9.24	2.5	23.12
Blanket Padding	0.03	158.0	4.74
Mast	60.0	1	60.0
Tip Fitting	1.0	1	1.0
Position Links	2.5	2	5.0
Wing Position Boom	10.0	1	10.0
Total Wing Weight			299.86
Total Array Weight			599.72

TABLE 3-8

## 60 kW, 240 W/kg PLANAR ARRAY WEIGHT SUMMARY

Component	Weight (kg)	No. Req'd/Wing	Wing Weight (kg)
Blanket Assembly	37.42	2	74.84
Panels (40)	28.72		
Hinges (40)	1.7		
Tension Distribution (1)	0.40		
Leader	0.6		
Harness	6.0		
Blanket Tension and Control	2.80	2	5.6
Cover	2.50	2	5.0
Container	4.82	2	9.64
Blanket Padding	0.03	78	2.34
Mast	19.2	1	19.2
Tip Fitting	0.7	1	0.7
Wing Position Boom	7.5	1	7.5
Total Wing Weight			124.82 kg
Total Array Weight			249.64 kg

TABLE 3-9

120 kW, 240 W/kg, PLANAR ARRAY WEIGHT SUMMARY

Component	Weight (kg)	No. Req'd/Wing	Wing Weight (kg)
Blanket Assembly	58.16	2.5	145.4
Panels (64)	46.44		
Hinges (64)	2.72		
Tension Distribution (1)	0.40		
Leader	0.6		
Harness	8.0		
Blanket Tension and Control	3.3	2.5	8.3
Cover	3.7	2.5	9.1
Container	7.8	2.5	19.2
Blanket Padding	0.03	158.0	4.74
Mast	48.8	1	48.8
Tip Fitting	1.0	1	1.0
Position Links	2.4	2	4.8
Wing Position Boom	8.4	1	8.4
Total Wing Weight			249.74 kg
Total Array Weight			499.48 kg

### 3.5.5 Cost Data Summary

The estimated costs for the development and delivery of the planar solar array flight system with 200 to 240 W/kg performance are summarized below. The ground rules and assumptions are:

- a. 1977 dollars.
- b. Estimates include fee.
- c. Deployment of the wings away from the spacecraft is included in the estimates. Wing tracking and rotary power transfer is not included in the estimates.
- d. Estimates do not include technology development.

<u>Cost Element</u>	<u>Cost Estimate (60 kW/120 kW)</u>
A. Design, Drawings, Analysis, and Specifications	
1. Blanket Assy	\$1,845/1,845K
2. Deployment Assy	520/520K
3. Blanket Storage Assy	550/550K
	2915/2915K
B. Tooling Design, Fabrication and Checkout	
1. Blanket Assy.	80/80K
2. Deployment Assy	150/150K
3. Blanket Storage Assy	150/150K
	380/380K
C. Engineering Test Hardware Materials and Fabrication	
1. Blanket Assy.	225/225K
2. Deployment Assy.	120/120K
3. Blanket Storage Assy.	65/65K
	410/410K
D. Design Development Testing	
1. Blanket Assy.	80/100K
2. Deployment Assy.	70/80K
3. Blanket Storage Assy.	60/70K
	210/250K

<b>E. Qualification Test Hardware Materials and Fabrication</b>		
1. Blanket Assy. (Includes 5,000 cell assys.)	160/180K	
2. Deployment Assy.	70/80K	
3. Blanket Storage Assy.	50/60K	
		280/320K
<b>F. Component Qualification Testing</b>		
1. Blanket Assy.	40/40K	
2. Deployment Assy.	30/35K	
3. Blanket Storage Assy.	25/30K	
		95/105K
<b>G. Engineering Model</b>		
1. Blanket Assy (Includes 20,000 cell assys.)	470/490K	
2. Deployment Assy.	290/300K	
3. Blanket Storage Assy.	100/100K	
4. Integration and Assembly	35/35K	
		895/925K
<b>H. One New Wing Materials and Fabrication</b>		
1. Blanket Assy. (Includes 585,000 cell assys.)	8,055/16,200	
2. Deployment Assy.	420/420K	
3. Blanket Storage Assy.	75/80K	
4. Integration, Assembly, Acceptance Test	65/65K	
		8615/16765K
<b>I. Refurbish Engineering Model</b>		
1. Blanket Assy. (Less 20,000 cell assys.)	7,795/15,940K	
2. Deployment Assy. (10% of new)	42/42K	
3. Blanket Storage Assy. (10% of new)	8/8K	
4. Integration, Assembly, Acceptance Test	65/65K	
		7910/16055K
<b>J. Other Costs</b>		
1. Ground Support Equipment Design and Fabrication	100/100K	
2. Quality Assurance	250/250K	
3. Manufacturing Test Equipment (In-process tests)	500/500K	
4. Program Management, Reporting, Subcontract Monitoring	350/350K	
		1200/1200K

**TOTAL \$22.9M/39.3M**

### 3.6 CONCENTRATING ARRAY DESIGN

#### 3.6.1 Electrical Design

3.6.1.1 Conceptual Designs. To develop the concentrating array design, several configurations were conceptualized. These candidate configurations are shown in Figure 3-8.

The "trough" configuration is a flexible cell blanket which has planar reflectors adjacent to each side of the blanket. These "side reflectors" can be canted at angles of  $45^\circ$  to  $90^\circ$  to add illumination intensity to the cell blanket. Some of the disadvantages and advantages of this concept and others discussed below are listed in Table 3-10.

The "sawtooth" configuration employs reflectors labeled "in-blanket" reflectors. These reflectors are also effective at angles from  $45^\circ$  to  $90^\circ$ .

The side and in-blanket reflectors of the previous configurations may be combined to form a 3-dimensional reflector system. This system offers high geometric concentration possibilities and was later selected as the baseline.

Compound Parabolic Concentrators (CPC) are attractive because of their high average concentration. The inherent intensity variations caused by this system is a drawback to this configuration however. Diffuse reflectors will help even out the light intensity across the blanket but will not completely mitigate the variations.

The "W" configuration has planar reflectors which are perpendicular to the cell blanket. The reflector/cell blanket is then positioned to a sun angle between  $0^\circ$  and  $45^\circ$ . The advantage of this system is that the light both directly incident on the cell and reflected onto the cell arrives at the same angle of incidence. This would possibly allow some optimization of the cell's optical properties.

One variation which had advantages for the HCR-SEP array was the concept of building two short wing segments side-by-side rather than building one long wing. Table 3-10 points out some advantages and disadvantages of this concept.

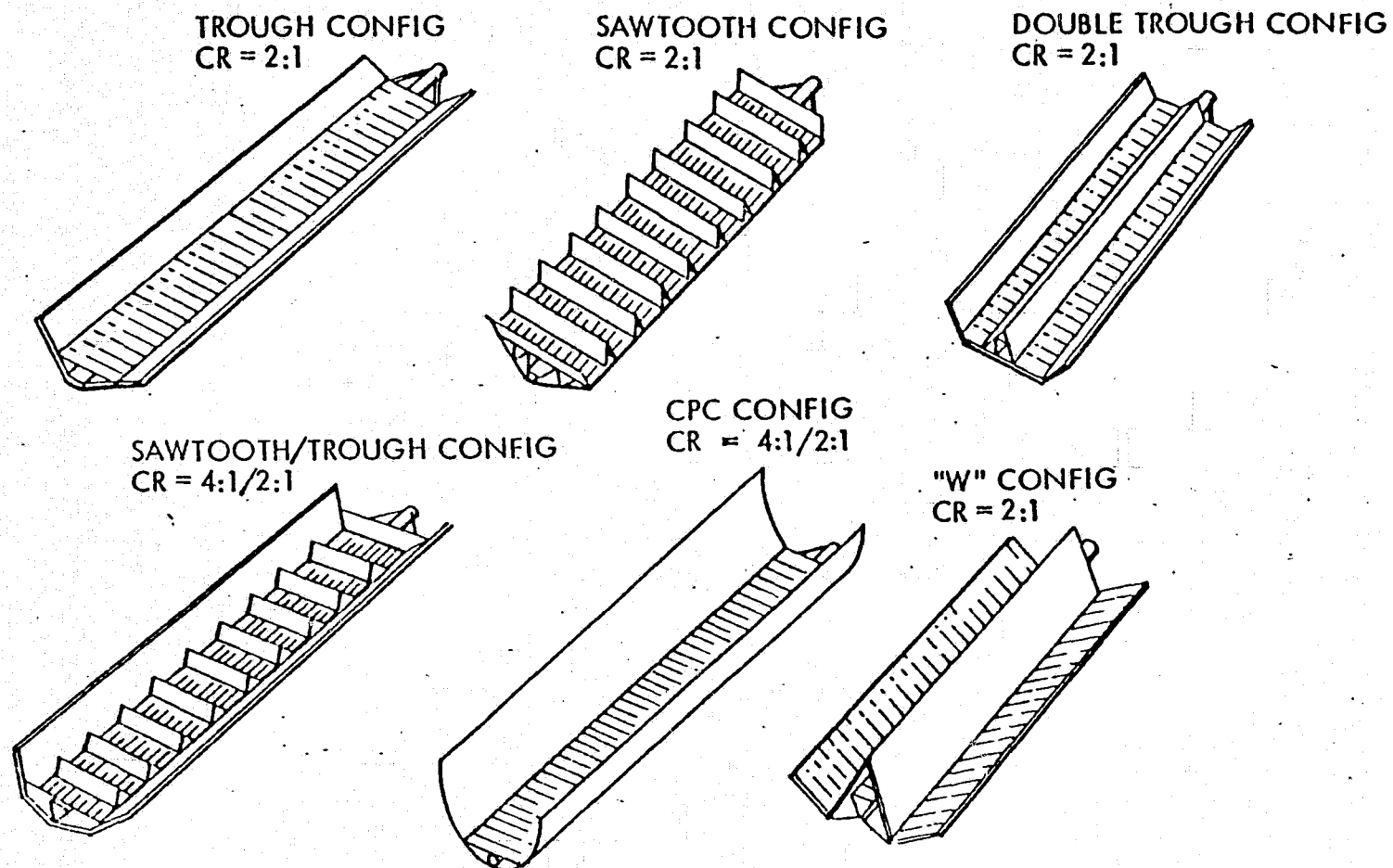


Figure 3-8 SEP Solar Array Concentrator Configurations

TABLE 3-10  
CONCENTRATOR ARRAY CONCEPTS

ADVANTAGES AND DISADVANTAGES

<p>① TROUGH CONFIG. SIDE REFLECTORS CR=2, 2.7</p>	<ul style="list-style-type: none"> <li>• LOWER CONCENTRATION THAN 3-D REQUIRES HIGHER CELL AREA</li> <li>• LOW TOTAL AREA PROVIDES SHORT LENGTH, LIGHT WEIGHT, STOWAGE EASE</li> <li>• NO IN-BLANKET REFLECTORS SIMPLIFIES BLANKET DESIGN</li> <li>• SPECULAR REFLECTION IS EFFICIENT FOR CR AND HEAT REJECTION</li> </ul>
<p>② SAWTOOTH CONFIG. IN-BLANKET REFLECTORS CR = 2, 2.7</p>	<ul style="list-style-type: none"> <li>• LOWER CONCENTRATION THAN 3-D REQUIRES HIGHER CELL AREA</li> <li>• LOW TOTAL AREA PROVIDES SHORT LENGTH, LIGHT WEIGHT, STOWAGE EASE</li> <li>• SPECULAR REFLECTION IS EFFICIENT FOR CR AND HEAT REJECTION</li> </ul>
<p>① + ② 3 - D REFLECTORS CR = 4:1/2:1</p>	<ul style="list-style-type: none"> <li>• HIGHER CONCENTRATION THAN 2-D REQUIRES LOWER CELL AREA</li> <li>• HIGH TOTAL AREA REQUIRES EITHER LONG LENGTH OR MULTIPLE ARTICULATION FOR STORAGE</li> <li>• SPECULAR REFLECTION IS EFFICIENT FOR CR AND HEAT REJECTION</li> <li>• CR CAN BE CHANGED DURING MISSION</li> </ul>



TABLE 3-10 (cont.)  
CONCENTRATOR ARRAY CONCEPTS

ADVANTAGES AND DISADVANTAGES

<p>CPC CR = 4:1/2:1</p>	<ul style="list-style-type: none"> <li>• HIGH AVERAGE CONCENTRATION, WITH 2-D REFLECTOR, GOOD ASPECT RATIO</li> <li>• DIFFUSE REFLECTION REDUCES MODULE HEAT REJECTION AND HAS LIGHT LOSSES TOWARD LIGHT SOURCE AND OUT ARRAY ENDS</li> <li>• COMPLEX STOWAGE, ARTICULATION, AND SHAPE CONTROL OF REFLECTORS</li> <li>• REFLECTOR AREA SLOPE NEAR MODULE RESULTS IN HIGH ANGLES OF LIGHT INCIDENCE ON MODULE</li> <li>• CHANGE CR DURING MISSION</li> <li>• INHERENT INTENSITY VARIATIONS</li> </ul>
<p>"W" CONFIG. CR = 2</p>	<ul style="list-style-type: none"> <li>• LOWER CONCENTRATION THAN 3-D REQUIRES HIGHER CELL AREA</li> <li>• HIGH TOTAL AREA REQUIRES EITHER LONG LENGTH OR MULTIPLE ARTICULATION</li> <li>• SPECULAR REFLECTION IS EFFICIENT FOR CR AND HEAT REJECTION</li> <li>• NO IN-BLANKET REFLECTORS SIMPLIFIES BLANKET DESIGN.</li> </ul>
<p>SIDE BY SIDE 2-D AND 3-D REFLECTOR SYSTEMS</p>	<ul style="list-style-type: none"> <li>• IMPROVED ARRAY ASPECT RATIO REDUCES WEIGHT</li> <li>• SYMMETRICAL LOADS ON EXTENSION MAST</li> <li>• INCREASED LENGTH OF DEPLOYMENT AWAY FROM SPACECRAFT TO AVOID EXHAUST PLUME</li> </ul>

3.6.1.2 Concentration Ratio. The effectiveness and sizing of the different reflector concepts as a function of the reflector inclination angle was studied. Some of the results of this study are shown in Figure 3-9. The reflector/cell blanket geometry considered in this figure is applicable to the planar side and in-blanket reflector systems.

The effective concentration of any configuration is calculated by summing the light directly incident on the electrical module plus the light reflected by the reflectors which strikes the electrical module and then dividing this sum by the light incident on the blanket. The light reflected by the reflectors is the light striking the reflectors times the efficiency or reflectance of the reflectors. The reflector width is sized so that the top of the reflector is coincident with the point which reflects light onto the solar cell module.

The effective concentration including angle of incidence effects is also shown in Figure 3-9. This takes into account the increased reflectance of the solar cell cover as the angle of incidence of incoming light from the reflectors increases. As can be seen from Figure 3-9, the effective concentration ratio (ECR) increases with increasing reflector angle. The ECR is increasing at a decreasing rate however. The area ratio, AR, which includes both reflectors, is also increasing as the reflector angle increases. The area ratio, however, is increasing at an increasing rate and goes to infinity as the reflector angle approaches  $90^\circ$ . If the incremental increase in ECR is calculated for each incremental increase in reflector angle, or  $\Delta(\text{ECR}/\text{AR})/\Delta\theta$ , we find that at about  $66.7^\circ$  the slope of this function is zero. This indicates that at angles greater than about  $66.7^\circ$ , the incremental increase in area ratio is larger than the incremental increase in ECR. Thus a  $66.7^\circ$  reflector angle represents an angle limit to design around for the side and in-blanket trough reflectors.

The ECR and area ratio for the "W" concentrator concept is shown in Figure 3-10. The curve shapes for the "W" concept's ECR and AR are similar to that of the side and in-blanket reflectors. Notice however that the maximum ECR for the "W" concept is considerably less than for the trough concept with the same area ratio.

Combining the side and in-blanket reflectors and basing the ECR on reflections directly from the reflectors to the cell blanket results in Figure 3-11 where ECR versus reflector angle is shown. The reflector angle indicated is the same for both the side and in-blanket reflectors.

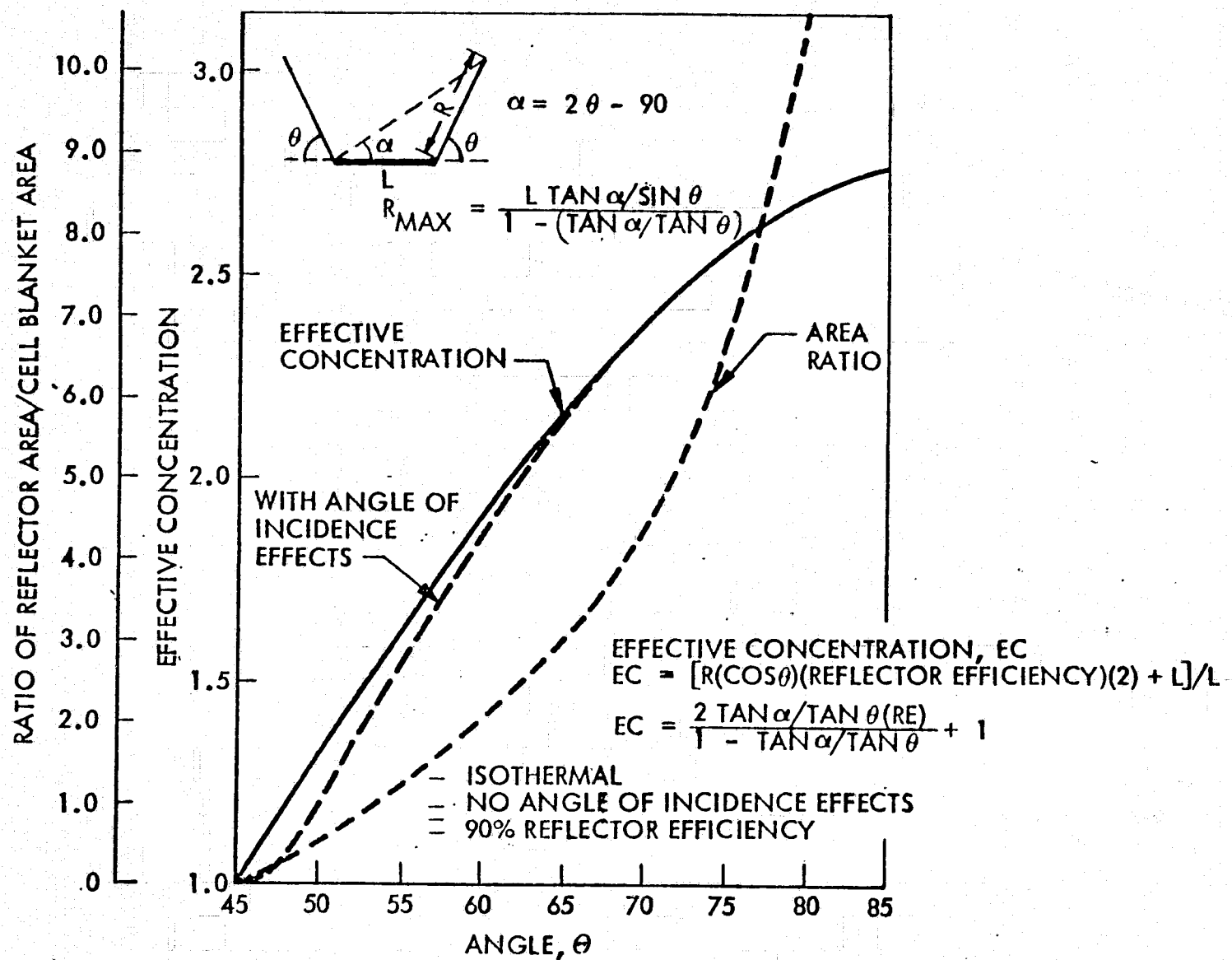


Figure 3-9 Concentration Ratio vs Reflector Angle

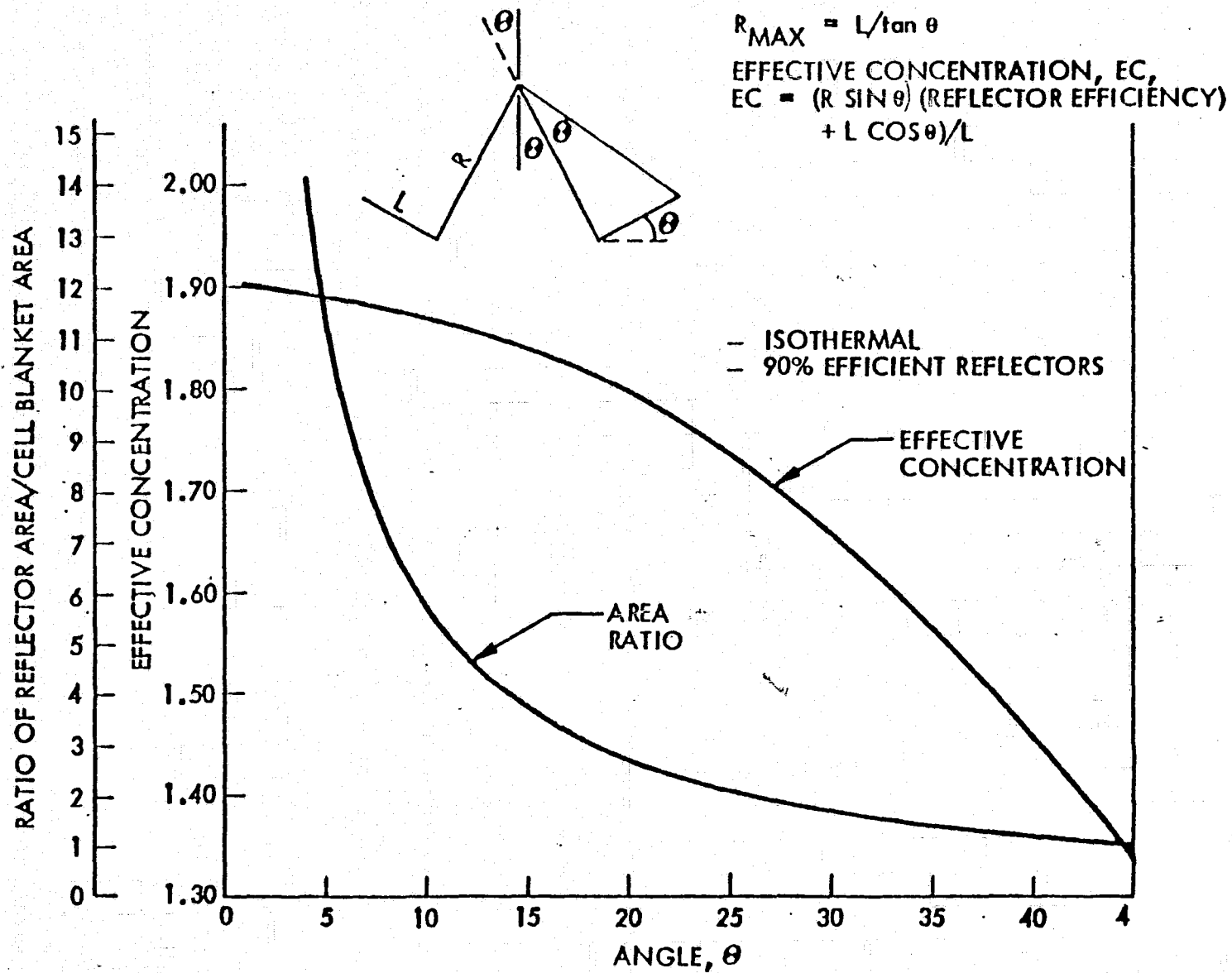


Figure 3-10 "W" Concentration Ratio Vs Angle

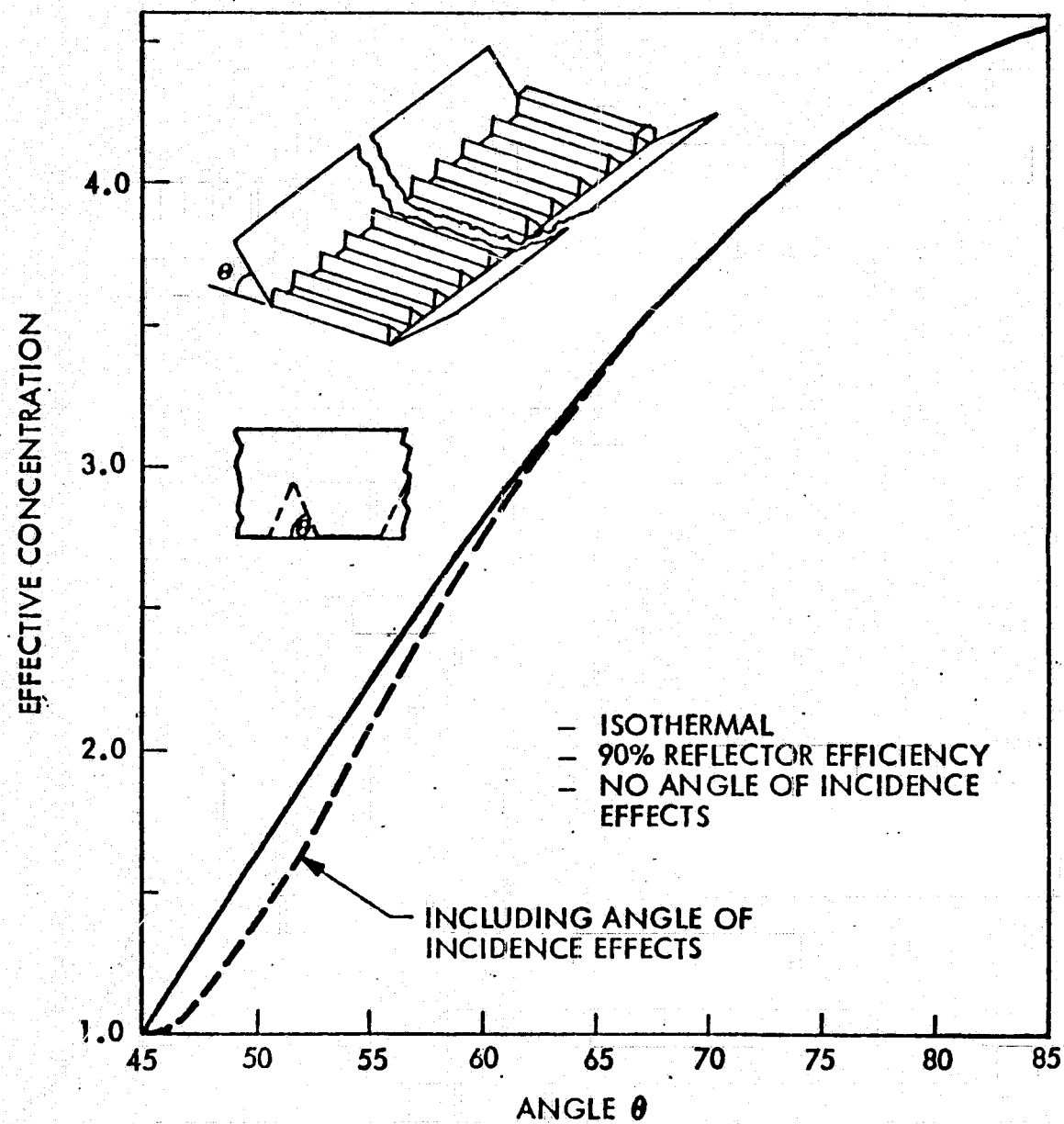


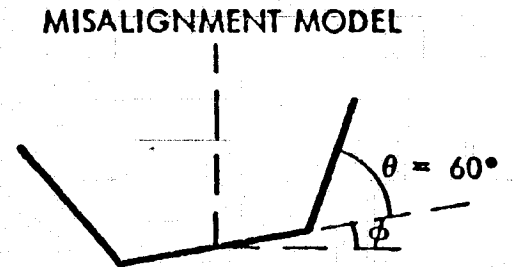
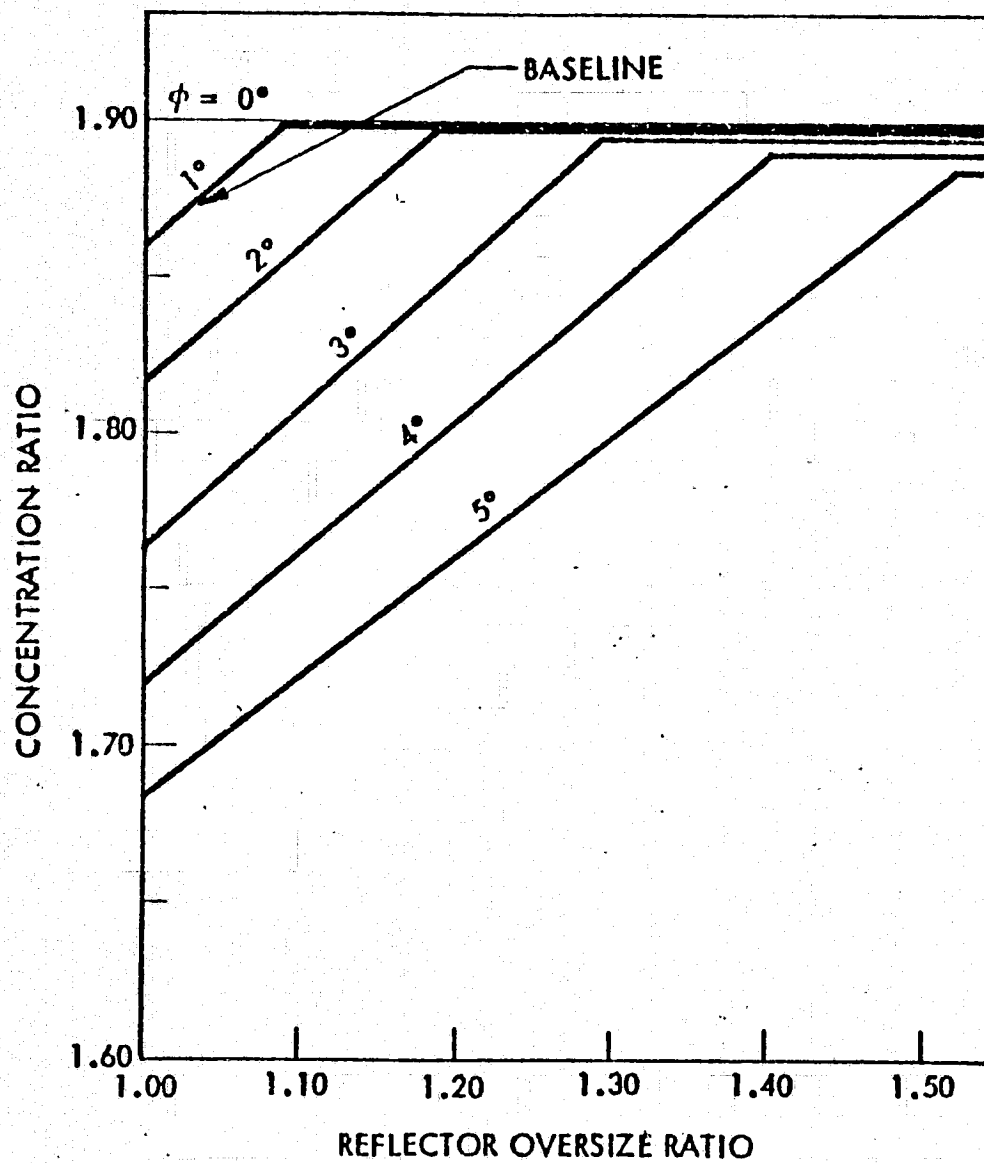
Figure 3-11 - 3-Dimensional Concentration Ratio Vs Angle

**3.6.1.3 Misalignment Effects.** Since perfect alignment of the array to the sun is not possible, the effect of off-normal angles on the concentrator's ECR was studied. The general effect of a misalignment of the array is threefold: 1) the cell blanket experiences a loss because the intercepted area of the blanket is varying as the cosine of the misalignment angle, 2) the reflector whose angle with the horizontal is increased by the misalignment, does not reflect its light completely across the cell blanket and suffers an intercepted area cosine loss also, and 3) the reflector whose angle with the horizontal is decreased, increases its intercepted area but reflects some of its light directly onto the other reflector, adding to the losses. One way to nullify these effects of misalignment is to oversize the reflectors slightly. The concentration ratio variation with the reflector oversizing ratio and with misalignment angle was determined. Figure 3-12 shows the misalignment effect for a trough configuration with  $60^\circ$  side reflectors. Note that this figure could equally apply to a sawtooth configuration with  $60^\circ$  in-blanket reflectors. A maximum misalignment angle of  $1^\circ$  is considered a realistic constraint. From Figure 3-14, a 9% oversizing of the reflectors will maintain the expected ECR.

Figure 3-13 shows the effects of misalignment on a trough with reflectors set at  $67.5^\circ$ . Changes in ECR are more pronounced in this configuration with increasing misalignment angles. However, only 8% oversizing is needed to compensate for a  $1^\circ$  misalignment angle. Note that 8% of a  $67.5^\circ$  reflector represents more area than 9% of a  $60^\circ$  reflector.

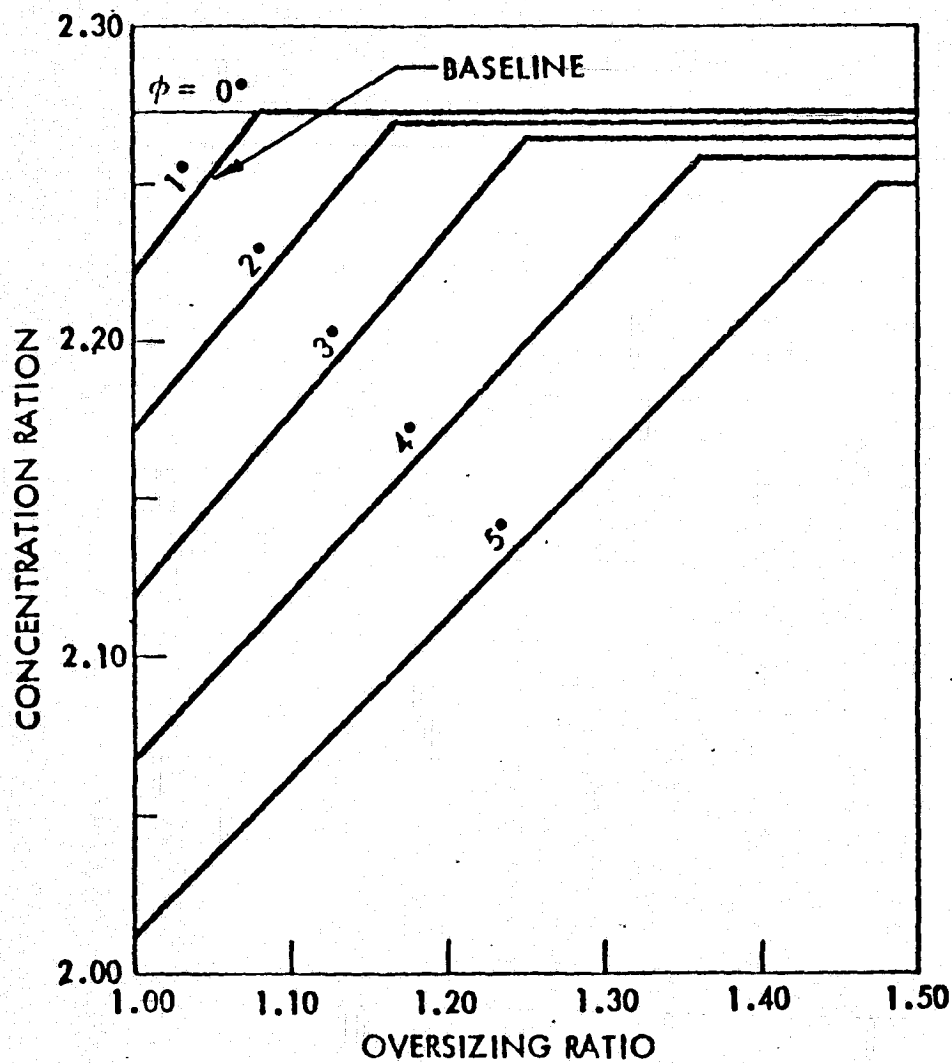
The sensitivity of the "W" configuration to misalignment angles was also determined. Figure 3-14 shows misalignment effects on a "W" configuration with a  $15^\circ$  characteristic angle. The same curve shapes as in the above trough cases are present. At the baseline  $1^\circ$  misalignment, an oversize ratio of 9% is needed for compensation.

The net result of misalignment angles and oversizing on the baseline array power is shown in Figure 3-15. This figure shows misalignment in one axis only, but the effect is similar for either axis. The  $P/P_0$  value with two axis misalignment would be approximately the product of the values in this figure. As can be seen from the figure, a  $1^\circ$  misalignment causes no power loss. A  $5^\circ$  misalignment causes only a 5% power loss due to loss of ECR. The values of  $P/P_0$  beyond  $1^\circ$  misalignment may be somewhat optimistic as no intensity variation effects on the electrical module have been taken into account. These effects are dependent upon the intensity variation pattern and the series-parallel pattern of the cells designed to offset intensity variation effects.

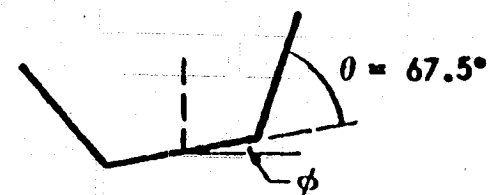


- ISOTHERMAL
- 90% REFLECTOR EFFICIENCY
- NO ANGLE OF INCIDENCE EFFECTS

Figure 3-12  $60^\circ$  Trough Misalignment Effects



## MISALIGNMENT MODEL



- ISOTHERMAL
- 90% REFLECTOR EFF.
- NO ANGLE OF INCIDENCE EFFECTS

Figure 3-13  $67.5^\circ$  Trough Misalignment Effects



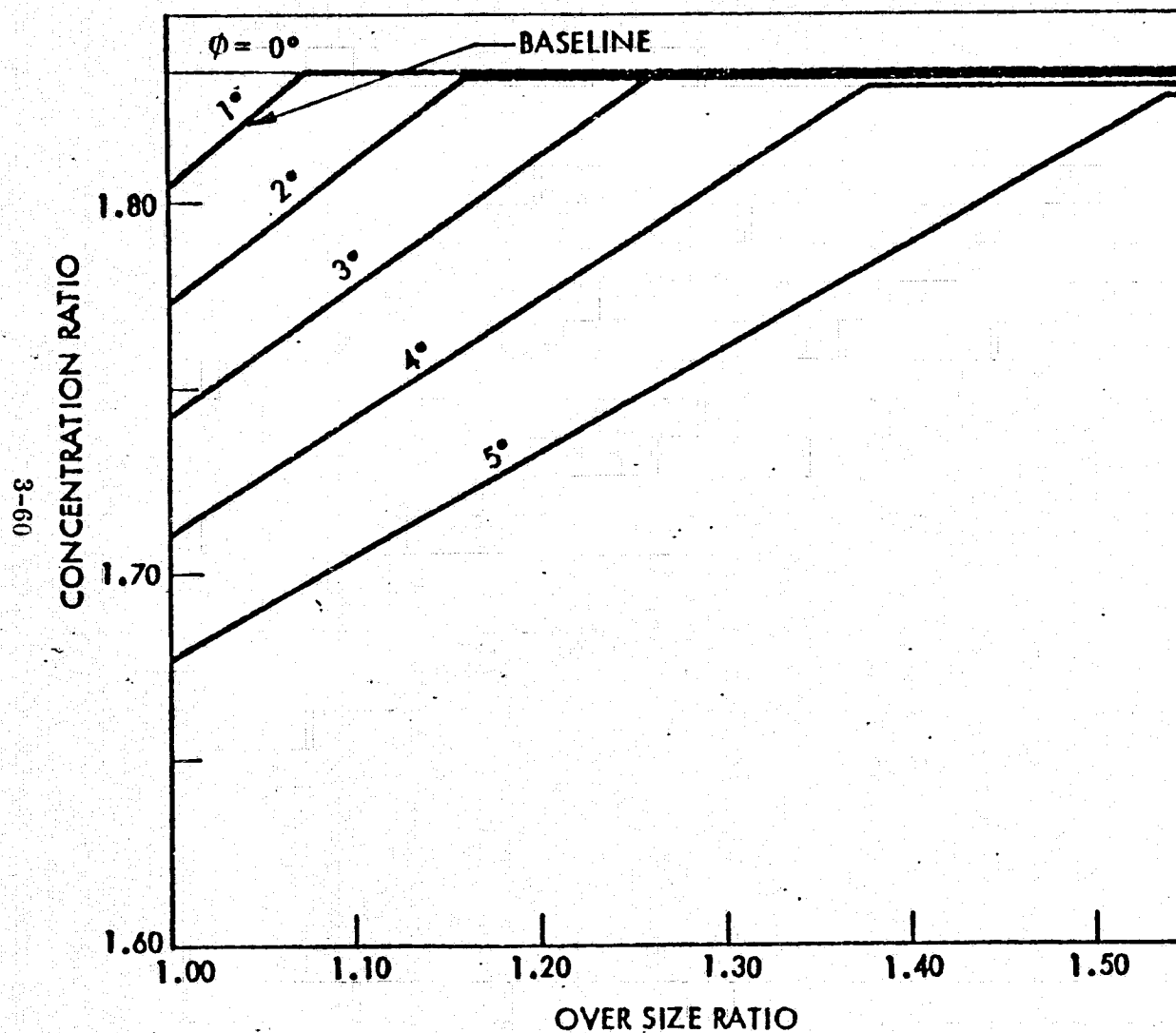
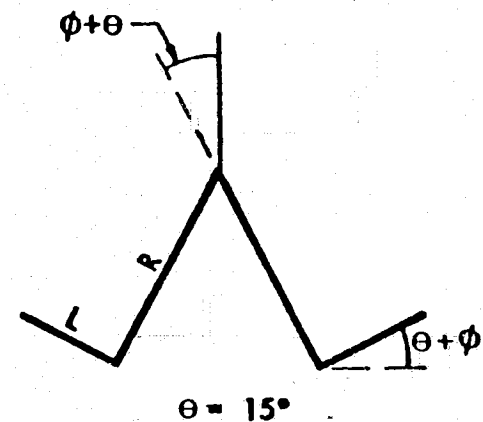


Figure 3-14 "W" Configuration Misalignment Effects

# MISALIGNMENT MODEL



- ISOTHERMAL
- 90% REFLECTOR EFFICIENCY
- NO ANGLE OF INCIDENCE EFFECTS

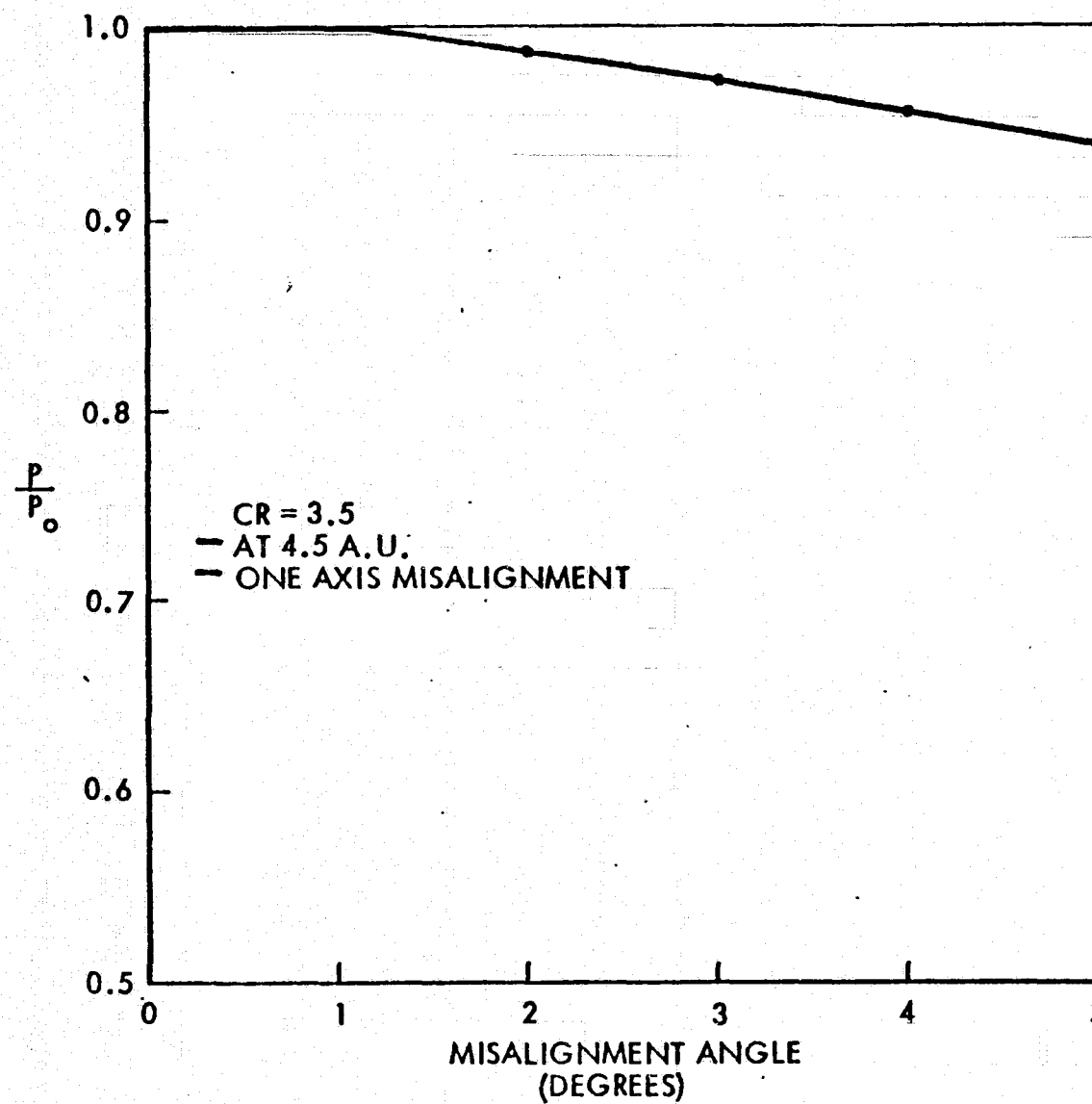


Figure 3-15 Baseline Array Misalignment Effects

**3.6.1.4 Proton Environment and Effects.** A proton and electron environment for the Halley's Comet Rendezvous (HCR) mission was specified by NASA-MSFC. The electron fluence was orders of magnitude less than the proton fluence and so the electron fluence was not considered in this study. The proton integral fluence is shown in Figure 3-16. Since most of the data on solar cell radiation degradation is with respect to 1 MeV electron fluence ( $\text{e}/\text{cm}^2$ ), the proton environment specified was converted into an equivalent 1 MeV electron fluence versus shielding area density relationship. This relationship is also shown in Figure 3-16. The N-P junction may be considered the plane of damage in a solar cell. The area density in front of and in back of the junction is then used to estimate a fluence into the junction from either direction. The total fluence into the junction is the sum of the fluence contributions from the front and back sides. The area densities in front of and behind the baseline 5 mil silicon cell with a 3 mil CMS cover is shown in Figure 3-16. A total fluence of  $1 \times 10^{14} \text{ e}/\text{cm}^2$  1 MeV electrons is calculated to impact at the N-P junction in the baseline cell/cover design.

Figure 3-17 shows the relative power degradation of several solar cell designs as a function of 1 MeV electron fluence (Ref. 1, 7). The radiation resistance of thinner cells can be seen in this figure. There is little data on the radiation degradation of 5 mil cells and so the degradation for this cell was estimated from the 2 mil and 8 mil cell data. From the calculated total fluence of  $1 \times 10^{14} \text{ e}/\text{cm}^2$ , the relative degradation of the baseline cell is found to be approximately 4% for the specified HCR-SEP mission radiation environment.

The radiation degradation of the voltage at maximum power versus fluence and cell thickness is not as well documented as the power degradation. The P+ back field of the baseline cell also influences the rate of  $V_{mp}$  degradation. A survey of the available data leads to the estimation that with a fluence of  $1 \times 10^{14} \text{ e}/\text{cm}^2$ , the degradation of  $V_{mp}$  will be, at most, 2%. The voltage variations due to temperature and intensity effects will be significantly greater.

**3.6.1.5 Thermal Design Support.** Table 3-11 indicates the areas studied in determining the operating temperatures of the cells and reflectors at the various sun distances. The thermo-optical properties of the array components are critical in the determination of the cell temperature and hence the cell power. The solar absorptance,  $\alpha_s$ , of the cell

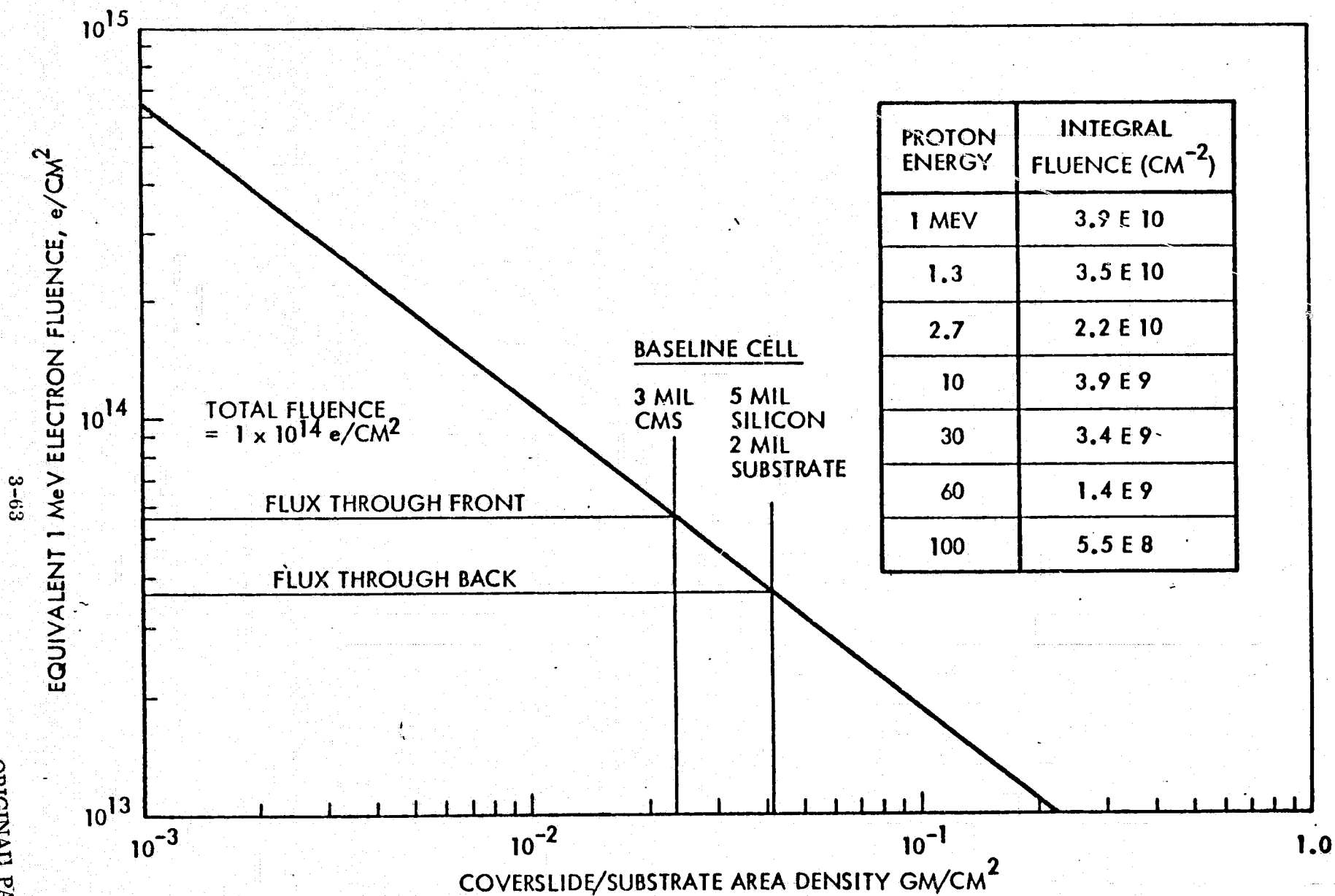


Figure 3-16 Proton Environment Effects

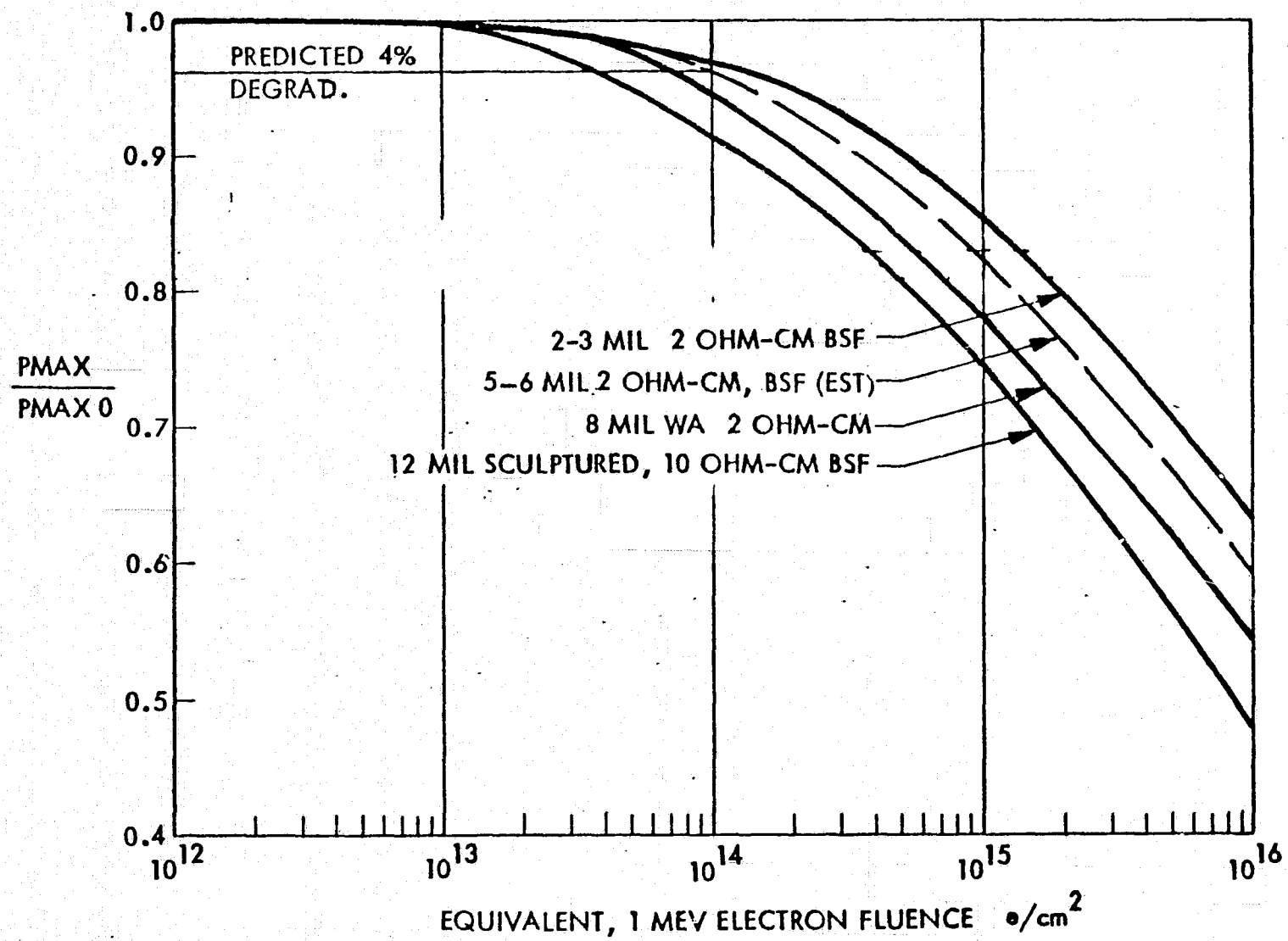


Figure 3-17 Solar Cell Radiation Degradation

TABLE 3-11  
THERMAL DESIGN SUPPORT

ORIGINAL PAGE IS  
OF POOR QUALITY

PARAMETRIC STUDY

- THERMO-OPTICAL PROPERTIES OF MATERIALS —  $\alpha, \epsilon$
- CONCENTRATION RATIO
- GEOMETRIC EFFECTS
- SHAPE FACTORS
- REFLECTOR MATERIALS
- SUBSTRATE MATERIALS — INTERCONNECT MATERIALS

TEMPERATURE PREDICTION MODELS

- FLAT PLATE CONDUCTION MODEL
- RADIATION MODEL

assembly was studied in detail. Typically, solar cells have  $\alpha_s$  values varying from 0.7 to 0.95. The recent trend in cell efficiency/solar absorptance has been that higher efficiency meant higher solar absorptance. Current work at Spectrolab, Inc., however, may reverse that trend with their work on the Back Surface Reflector (BSR). The BSR is an aluminum alloying process which converts the back of the cell into an optical reflector. This optical reflection does two things: (1) it lowers the  $\alpha_s$  by rejecting some of the unconverted light, and (2) the second pass of light through the cell allows for more energy conversion. Current work involving 12 mil silicon cells with a BSR has shown cells with an  $\alpha_s$  of less than 0.75. Thinner cells and improved techniques are expected to lower the cell's  $\alpha_s$  to around 0.70, while still maintaining improved cell efficiencies.

The emittance of the solar cell assembly is important to the cell temperature but not as much as the solar absorptance. This is because the temperature is determined by the sum of the cell emittance and the back of the substrate emittance. The emittance of the two inorganic cell covers considered, fused silica and ceria stabilized microsheet, are 0.81 and 0.85 respectively. The emittance of the organic materials considered, Spraylon, FEP, and RTV, vary drastically with decreasing thicknesses below 2 mils. At 1 mil, all the organic coverslides have an emittance of approximately 0.55 to 0.65 (Ref. 1, 7, 9, 10, 18, 19). The backside emittance of the substrate composite was taken to be 0.80. A cell with an  $\epsilon$  of 0.55 would run 5° C hotter than one with an  $\epsilon$  of 0.85 at one sun.

**3.6.1.6 Shape Factor.** A variable in the heat transfer equation which was considered was the shape or view factor. A variation in the view factor across the blanket would result in a temperature variation and possible power losses. To determine the magnitude in the variation of the shape factor, two view factor models of a trough configuration were considered. Figure 3-18 shows the results of these studies.

First the geometric shape factor was considered and the reflectors were considered only as obstructions. The maximum temperature variation across the blanket at 1 A.U. sun distance with the calculated variation in the geometric shape factor was estimated to be 2.5°C. The second study took into account the reflectance, absorptance, and emittance of the reflector material. This study indicated that the expected  $\Delta T$  across the blanket

3-67

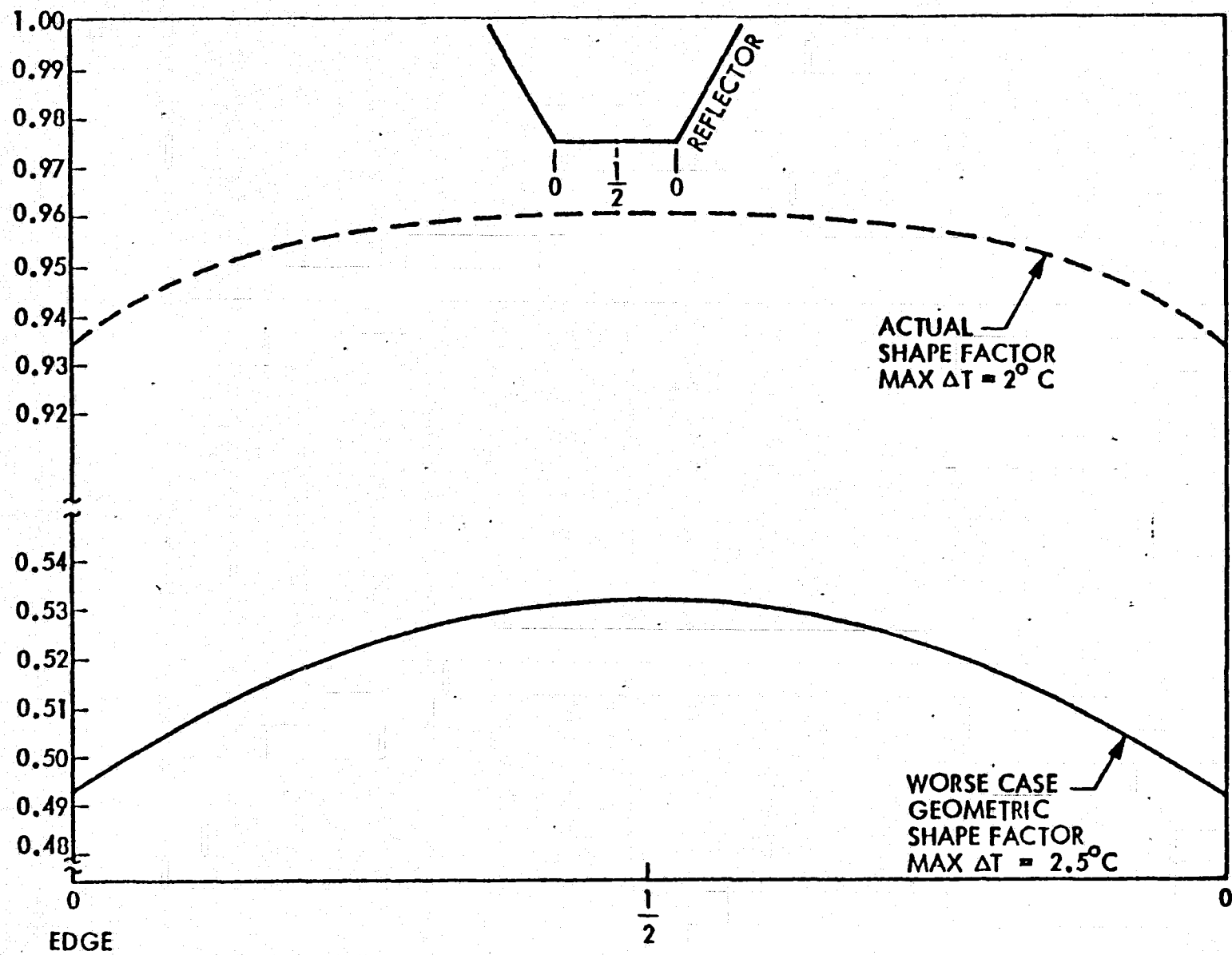


Figure 3-18 Shape Factor Variation Across Trough Blanket



would be about 2°C at 1 A.U. sun distance. The result of both these calculations is that the view factor variation has minimal impact on the temperature across the blanket and therefore, minimal impact on the module power output.

**3.6.1.7 Reflector Materials.** The reflector metal candidates were aluminum, silver, gold, chromium, and rhodium. Some representative thermo-optical properties are shown in Table 3-12. Four criteria were used to select the baseline reflector: 1) the solar reflectance of the reflector, 2) the availability of the reflector as a thin metalized plastic, 3) the stability of the reflector in the earth environment, and 4) the reflectors resistance to handling damage. Gold, chromium, and rhodium are not reflective enough particularly in the solar cell response wavelengths. Aluminum and silver are about equal in reflectance but silver suffers from the disadvantage of tarnishing rapidly in air and so would have to be coated with a protective layer of  $\text{SiO}_x$ . This protective layer would add to the handling problems as care would have to be taken to avoid cracking the coating. Aluminized plastics do not suffer this tarnishing problem as severely and are available in a wide variety of sizes. Considering the temperature range and space radiation environment the reflectors must survive, Kapton polyimide film appears to be the best choice as the reflector substrate. Aluminized Kapton is available in 0.3 mil thicknesses and is the baseline reflector material. This reflector will have a reflectance of at least 90%.

**3.6.1.8 Temperature Prediction Models.** Mathematical models of the two and three dimensional configurations were developed to calculate the distribution of solar energy entering the cavity, temperatures of reflections and solar cell blanket, and electrical output. These models incorporate the details of geometry, solar distance, optical properties, and solar cell efficiency which is in turn a function of temperature and solar flux density. The models are used to evaluate the effects of these parameters on the designs.

The specific assumptions and ground rules which define the relationship of the mathematical model to the physical problem or which limit the range of the parameters are:

TABLE 3-12  
REFLECTOR METAL CANDIDATES

	$\alpha_S$	$\epsilon_{TN}$	$\epsilon_{TH}(300^\circ K)$
ALUMINUM ON KAPTON(0.3MIL)	0.082 0.334	0.030 0.655	CALORIMETRIC 0.610
SILVER SIOX COATED	0.091	0.012	
CHROMINUM ON KAPTON (1/2 MIL)	0.099 0.727	0.037 0.790	0.760
GOLD BE/CR/NI SUBSTRATE	0.217	0.013	
RHODIUM BE/CR/NI/AU SUBSTRATE	0.289	0.038	

1. All surfaces are flat and are assumed to be isothermal.
2. Constant surface optical properties are used (no angular dependence).
3. Solar vector deviates off normal only in the direction of the primary reflector with the maximum angle limited to the angle of the reflector.
4. Solar cells were assumed to be perfectly diffuse (specular reflectance,  $\rho_s = 0$ ). The 2-D trough design can be analyzed with a specular component but the 3-D trough must have perfectly diffuse cells.
5. The angle between the reflector and the solar cells must be between  $90^\circ$  and  $135^\circ$ .
6. All incident energy is divided into 3 components upon striking a surface  $Q_i = \alpha Q_i + \rho_s Q_i + \rho_d Q_i$ . The absorbed energy ( $Q_i$ ) is used directly in the thermal energy balance. The reflected energy is divided into diffuse ( $\rho_d Q_i$ ) and specular ( $\rho_s Q_i$ ) components. The diffuse portion is assumed to stay diffuse and will be absorbed and reflected by other surfaces. The specular portion is treated as incident energy which strikes another surface(s) and again assumed to divide into three components.
7. The geometric view factors for the simple trough are calculated directly by the program. The 3-D trough requires the view factors of any given design to be computed separately and inputted into the program.
8. A limitation on the geometry for the 3-D trough is that an incident ray striking the primary reflector and reflected to the blanket reflector will either hit the solar cells or the opposite primary reflector but not another blanket reflector. (The baseline 3-D trough configuration is not affected by this limitation).
9. No conduction heat transfer between reflectors and solar cells. Conduction through the cell and backside has been included.
10. Steady state conditions only.
11. Solar cell efficiency curves with an input bias factor are based on data in a Boeing report (Reference 15) and are representative of the solar cells to be used.

Before temperatures can be calculated other boundary conditions must be specified to complete the model.

1. Backside radiation for all surfaces of the simple trough has been assumed to radiate directly to space with a view factor of unity. The emittances are specified in the input block.
2. The solar cell conducts and radiates to a backside surface. Solar cell and substrate cross section is similar to the SEP solar cell sections analyzed. The radiation term is calculated assuming two parallel plates with emittances of .07 and .88. The conductance term used is a value of 0.916 watts-ft<sup>2</sup>/°F and represents the conductance through the total cross section.
3. For the 3-D trough, the backside of the blanket reflectors radiate to a surface in the same plane as the solar cell modules having an emittance of .8 with all other surfaces radiating to space with a unity view factor.
4. The 3-D trough analyses were performed for one bay only with a bay being defined as the distance from the top of a blanket reflector to the top of the next blanket reflector.
5. Diffuse solar and infrared energy exchange is based upon five bays or interaction with two adjacent bays on each side of the bay analyzed. For the infrared energy exchange, identical surfaces in adjacent bays were assumed to be at identical temperatures. Symmetry was used to compute both the diffuse solar and infrared energy exchange.

Based on these assumptions and boundary conditions, temperature predictions at several distances from the sun for several configurations were made. Figure 3-19 is a plot of temperature versus A. U. sun distance for a simple trough configuration. A schematic showing the four node temperature model is also in Figure 3-19. Note that in this case, the cell solar absorptance is 0.85.

Figure 3-20 is again a simple trough temperature prediction. The cell's solar absorptance in this case is 0.70. The difference in the cell temperature at 1 A.U. sun distance for these two cases is 25°C. The lower temperature in Figure 3-20 results in a cell power increase of about 34%.

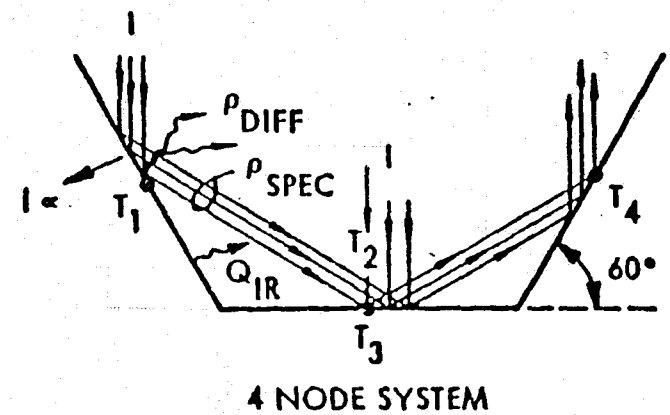
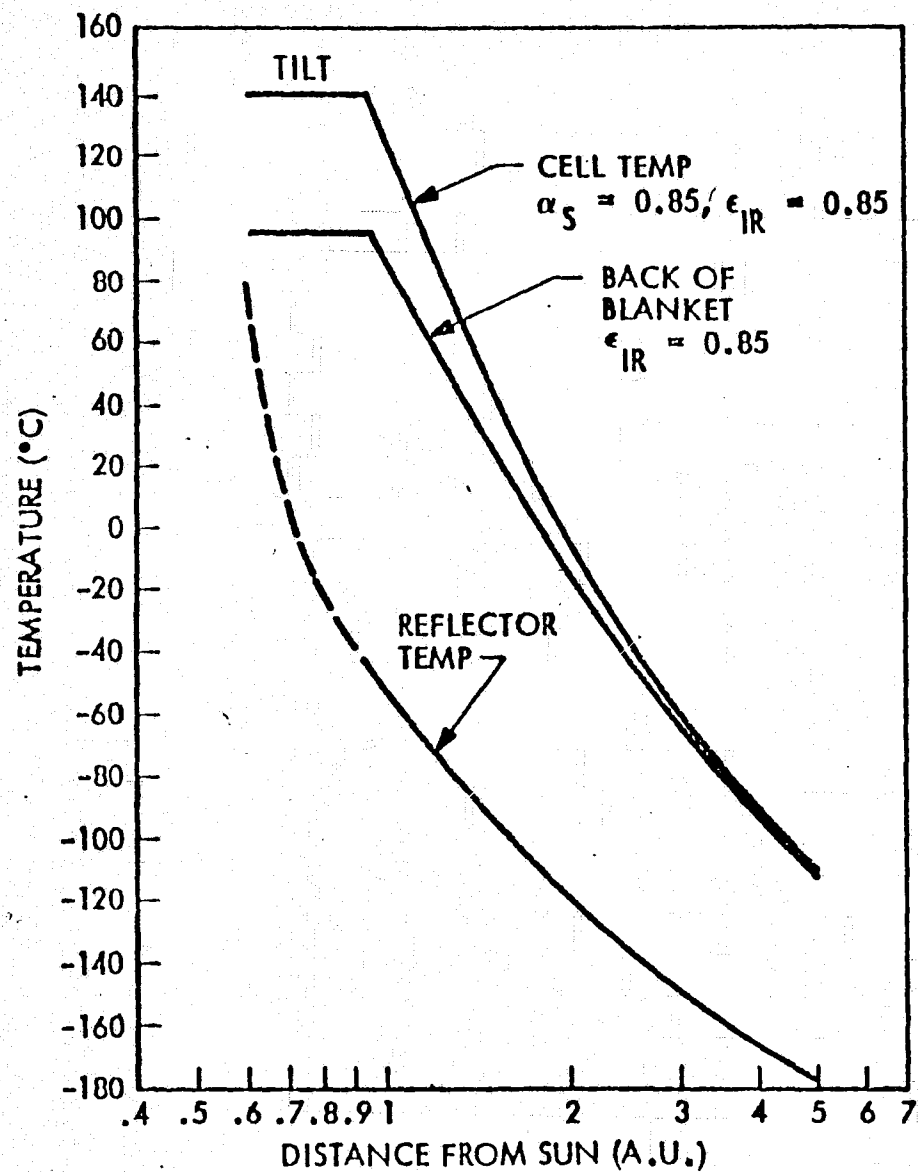


Figure 3-19 Trough Configuration Temperature Prediction,  $\alpha_s = 0.85$

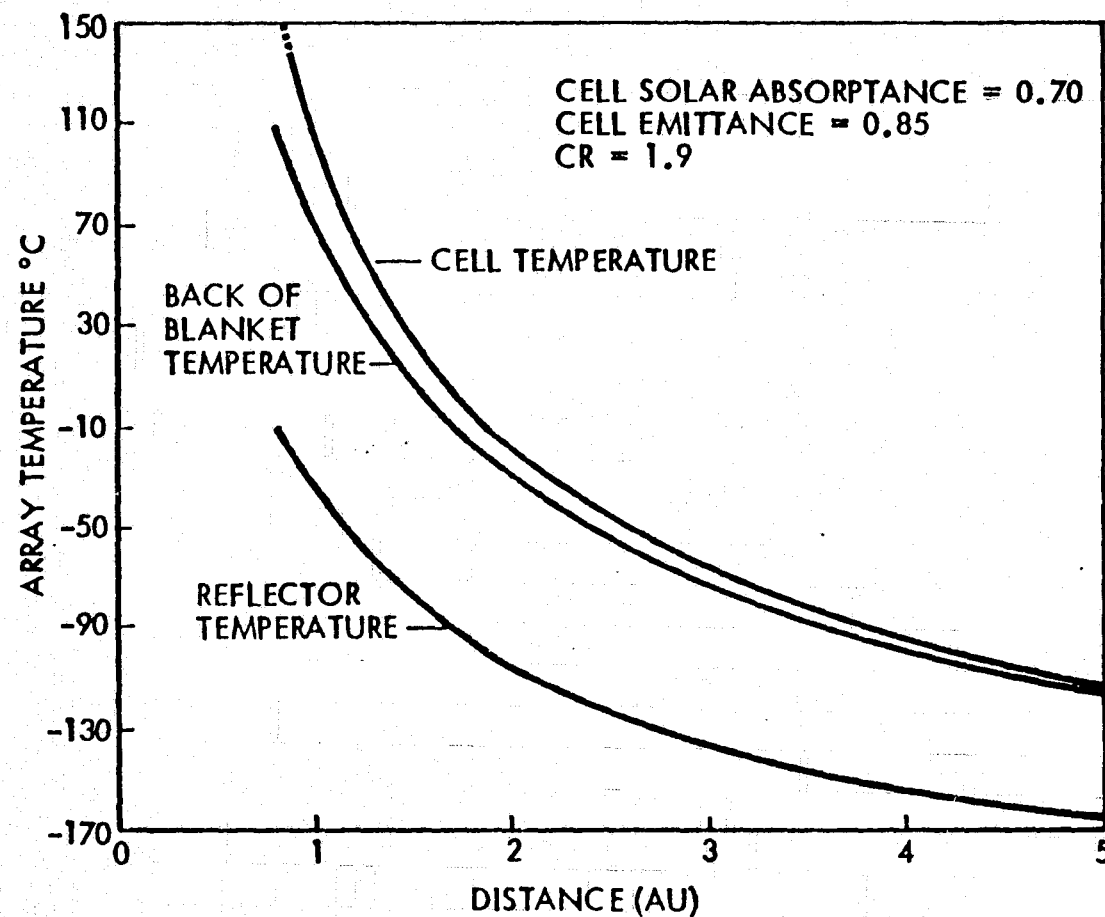


Figure 3-20 Trough Configuration Temperature Prediction,  $\alpha_s = 0.70$

Temperature predictions for the baseline 3-dimensional array were made and are shown in Figure 3-21. The temperatures shown have averaged the double reflection effects and effects of different view factors. The temperature of the alternate, 2-dimensional concentrator array system with a CR = 2.27, was also estimated and is shown in Figure 3-22. The baseline array is shown in Figure 3-22 for comparison also.

Several conclusions can be drawn from the temperature modeling done during this study. The cell assembly's solar absorptance is a very influential factor. The cell assembly's emittance is important, but not to the magnitude that the absorptance is. The reflector temperature has very minimal effects on the blanket temperature hence there is no need for a frontside, high emittance coating on the reflectors. With the shape fixed, the size of the array influences the cell temperature very slightly.

**3.6.1.9 Array Configurations.** Some 18 array configurations were evaluated for their specific power and the effect on specific power of varying some parameters. The first 13 arrays were configured to meet a set of power requirements that called for 85 kW, BOL, from a nominal 3:1 concentrating array or for 110 kW, BOL, from a nominal 2:1 concentrating array. The cases 14 through 18 all had power requirements at various distances with a controlling power requirement of 14.0 KW, EOL, at 4.5 A.U. sun distance. Table 3-13 gives parameters and assumptions for each of the 18 cases. Figure 3-23 shows the relative sizes, shapes and reflector configurations for the 18 cases.

**Case 1** - This configuration is a 3-dimensional array with 60° side and in-blanket reflectors. It uses a 5 mil, 13% silicon cell with a 3 mil CMS coverslide. The solar cell has an  $\alpha/\epsilon$  ratio of 1.0. Each wing consists of a single blanket. The wing is 85 meters long and the array meets the weight requirements.

**Case 2** - This is a reconfiguration of Case 1 using 14%, 6 mil cells instead of 15%, 5 mil cells. Each wing is 107.4 meters long and this array does not meet the weight requirements.

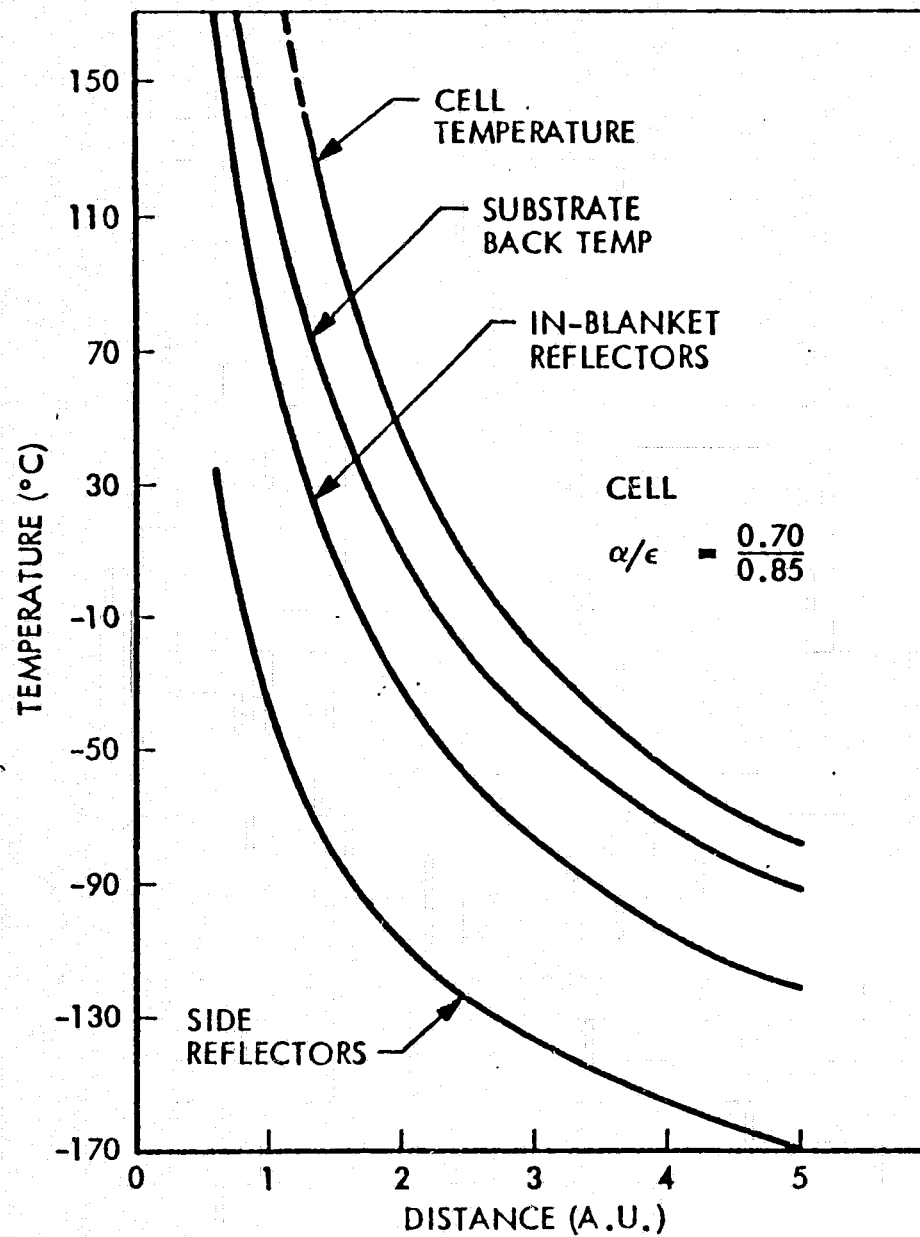


Figure 3-21 Baseline Array Temperatures



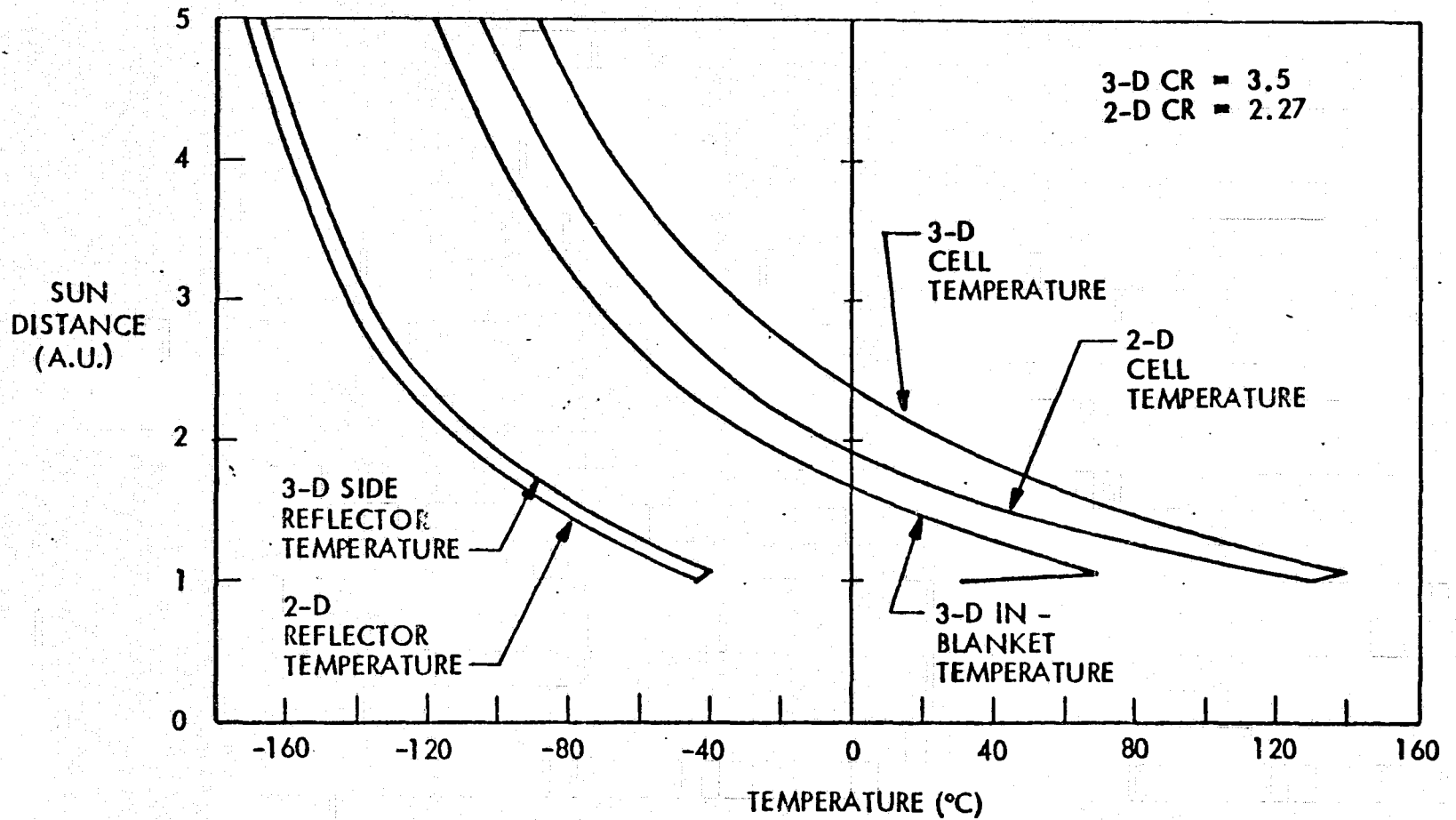


Figure 3-22 Baseline and Alternate Array Temperature

TABLE 3-13  
ARRAY CONFIGURATIONS

CASE NO.	CR EFFECT	$\alpha$ $\epsilon$	TEMP 1 A.U. °C	EFF % AMO 28 °C	CELL SIZE	CELLS PER ARRAY	POWER BOL 1.0 A.U.	POWER EOL 4.5 A.U.	WING MASS (KG)
1	1.9/2.8	0.85 0.85	128	15%	2 CM X 4.044 CM X 0.125 MM	387,700	85.0 KW	10.6 KW	325
2	1.9/2.8	0.85 0.85	128	14%	2 CM X 4.044 CM X 0.15 MM	486,100	85.0 KW	12.4 KW	620
3	1.9/2.8	0.70 0.85	103	14%	2 CM X 4.044 CM X 0.15 MM	423,620	85.0 KW	11.1 KW	412
4	1.9	0.85 0.85	128	14%	2 CM X 4.044 CM X 0.15 MM	629,160	110. KW	11.6 KW	348
5	1.9	0.70 0.85	103	14%	2 CM X 4.044 CM X 0.15 MM	548,300	110. KW	10.2 KW	289
6	1.9	0.70 0.85	103	13.5%	2 CM X 4.044 CM X 0.15 MM	570,200	110. KW	10.2 KW	300
7	1.9	0.70 0.55 (1 MIL FEP)	129	14%	2 CM X 4.044 CM X 0.15 MM	629,200	110. KW	11.6 KW	285
8	1.9/2.8	0.85 0.85	128	14%	2 CM X 4.044 CM X 0.15 MM	486,100	85.0 KW	12.4 KW	348
9	2.27	0.70 0.85	120	14%	2 CM X 4.044 CM X 0.15 MM	495,600	110. KW	10.6	304

3-77

ORIGINAL PAGE IS  
OF POOR QUALITY

TABLE 3-13 (Cont.)  
ARRAY CONFIGURATIONS

CASE NO.	CR EFFECT	$\alpha$ $\epsilon$	TEMP 1 A.U. °C	EFF % AMO 28 °C	CELL SIZE	CELLS PER ARRAY	POWER BOL 1.0 A.U.	POWER EOL 4.5 A.U.	WING MASS (KG)
10	1.9	0.70/0.85	103	14%	2 CM X 4.044 CM X 0.15 MM	548,300	110 KW	10.2 KW	302
11	1.9	0.70/0.85	103	13%	2 CM X 4.044 CM X 0.15 MM	606,620	110 KW	10.5 KW	331
12	1.73	0.70 0.85	94	14%	2 CM X 4.044 CM X 0.15 MM	569,400	110 KW	9.6 KW	—
13	1.9	0.70 0.85	103	13%	2 CM X 4.044 CM X 0.15 MM	606,620	110 KW	10.5 KW	327
14	2.27	0.70 0.85	130	13 %	2 CM X 4.044 CM X 0.125 MM	678,220	134.2 KW	14.0 KW	388
15	2.27	0.70 0.85	130	13.5%	2 CM X 4.044 CM X 0.15 MM	653,100	134.2 KW	14.0 KW	396
16	1.9/3.5	0.70 0.85	103	13%	2 CM X 4.044 CM X 0.125 MM	466,680	84.4 KW	14.0 KW	626
17	1.9/3.5	0.70 0.85	130	13 %	2 CM X 4.044 CM X 0.125 MM	466,680	84.4 KW	14.0 KW	392
18	2.27/3.5	0.70 0.85	130	13.5%	2 CM X 4.044 CM X 0.15 MM	401,200	82.7 KW	14.0 KW	583

ORIGINAL PAGE IS  
OF POOR QUALITY

3-77a

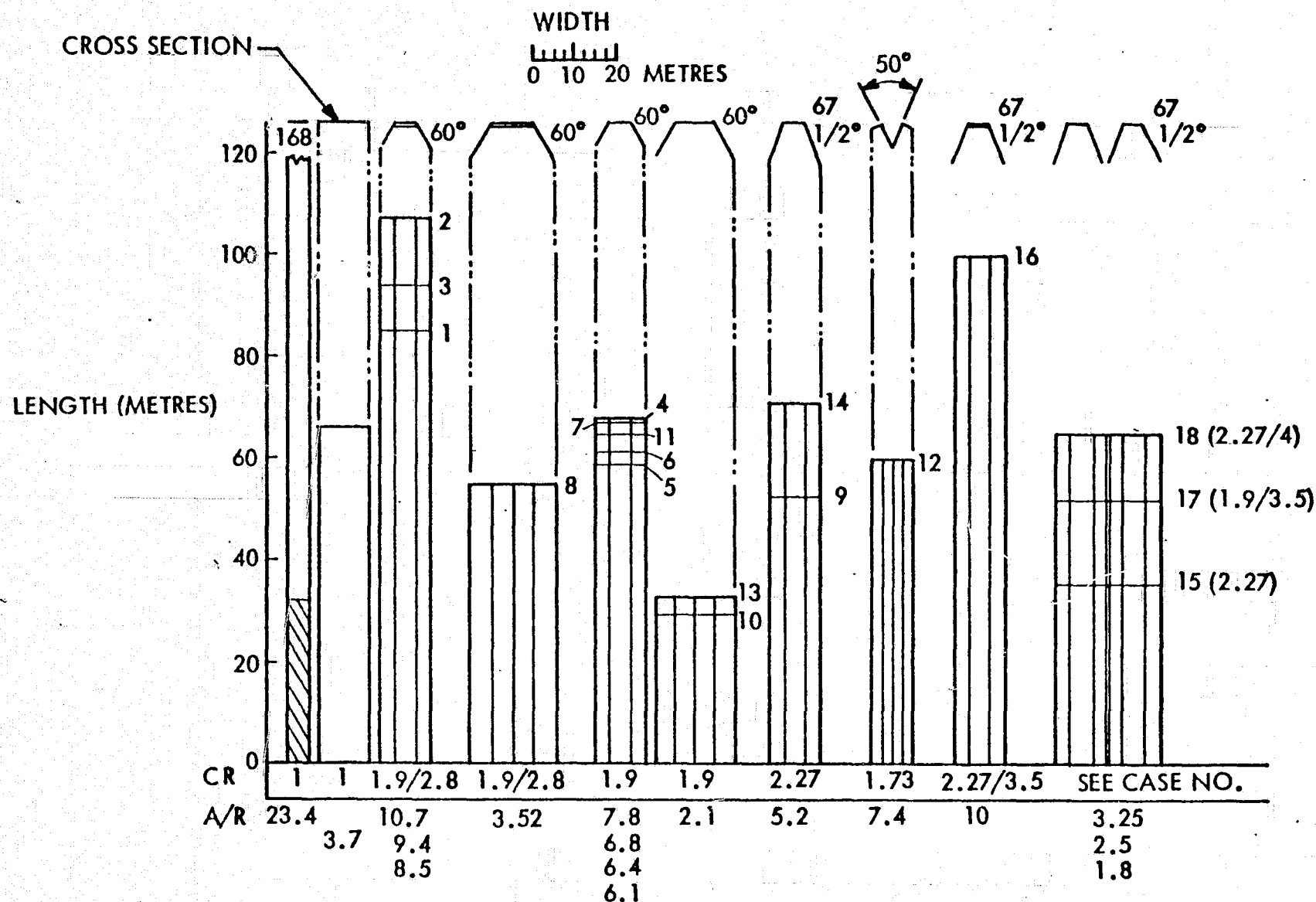


Figure 3-23 - Array Configurations

Case 3 - A cell with a BSR (with a low solar absorptance) was used in this case. Otherwise, this configuration is that of Case 2. This configuration is slightly too heavy. The wing length is 94.1 meters.

Case 4 - This configuration is a two-dimensional trough with 60° side reflectors. The  $\alpha/\epsilon$  ratio is 1.0 and the cell is 6 mil thick with an efficiency of 14%. The cell cover is 3 mil CMS. The wing length is 68 meters and each wing has only a single blanket. This array meets the weight constraint.

Case 5 - This is identical to Case 4 except that a BSR cell is used with its low  $\alpha_s$ . The wing length is only 58.3 meters and it is considerably lighter than the maximum allowed weight.

Case 6 - A 13.5% BSR cell was used in this case instead of the 14% as in Case 5. The wing length is 60.6 meters and this design also meets the weight requirement.

Case 7 - The thin 1 mil FEP cover used in this design plus the 14% cell makes it the lightest system considered. Otherwise it is similar to Case 5 and has wings only 66.9 meters long.

Case 8 - Starting with Case 2, the blanket width was doubled to reduce the aspect ratio. This array has a blanket width of 7.75 meters and wings 54.5 meters long. The weight is almost 1/2 of that of Case 2 and does meet the weight requirements.

Case 9 - A trough with 67.5° side reflectors was considered in this case. The 14% 6 mil cell with a 3 mil CMS coverslide was used. This cell was also at the low  $\alpha_s$  variety. A wing length of 52.7 meters was estimated and the weight is well under the limit.

Case 10 - Case 10 took a Case 5 system and doubled the cell blanket width. The aspect ratio was halved and the wing length was calculated to be 29.5 meters. This system is actually heavier than case 2 but still meets the weight requirement.

Case 11 - This is the same as Case 5 except that a 13% cell is used rather than a 14% cell. The array of course is longer and heavier but a wing is still only 64.4 meters long and the array still is under the weight limit.

Case 12 - A "W" configuration was tried in this case. Using a 14% cell the array would be 59.3 meters long. A weight estimation was not made however. The packaging and deployment are complex for this design and makes this system very unattractive.

Case 13 - This is Case 11 except that the blanket width has been doubled. The array weight has gone down slightly and comfortably meet the weight requirement. The wing length is 32.7 meters.

Case 14 - This is a trough with  $67.5^\circ$  side reflectors. It is sized to meet an array EOL power of 14.0 KW. A 13%, 5 mil cell with the BSR is used. The single blanket wing is 74.6 meters long and the array just meets the weight requirement. This is the alternate to the baseline configuration that requires significantly more solar cells.

Case 15 - A double wing version of Case 14 was tried in this case. A double wing system rather than a double blanket system was used because the side reflectors on a double blanket system became too large and unmanageable. This system was slightly too heavy but was only 35.5 m long.

Case 16 - A 3-dimensional system with  $67.5^\circ$  side reflectors and  $60^\circ$  in-blanket reflectors was considered. The wing length was estimated to be 100 meters for this system using a 13%, 5 mil BSR solar cell. The array system was estimated to be way over the weight limit due to the very high aspect ratio.

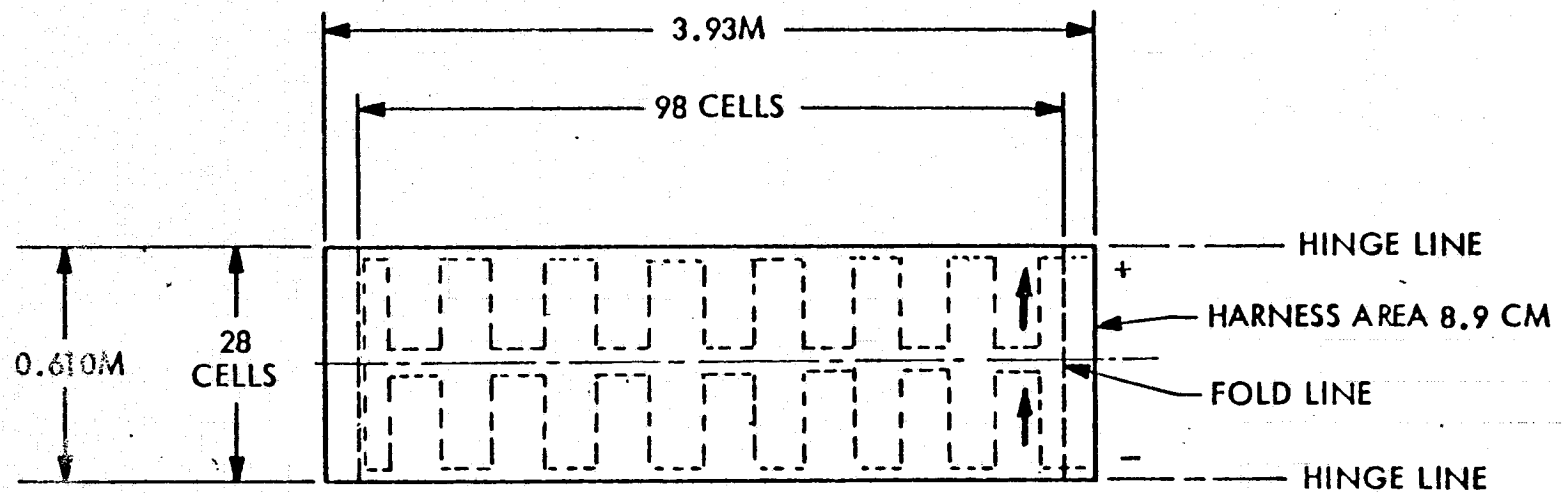
Case 17 - This case took Case 16 and made a double wing configuration out of it to reduce the aspect ratio. The wing length is now 50 meters and the array now meets the weight limitations. This case is the baseline configuration.

Case 18 - This 3-dimensional array has both  $67.5^\circ$  side and in-blanket reflectors. This array has the highest CR of all the cases considered. For a double wing system using a 13.5%, 6 mil solar cell with a BSR, a wing length of 65 meters was calculated. The estimated array weight is considerably over the requirements due to the large width and length of the array.

3.6.1.10 Panel Configurations. A schematic of the solar array panel for the baseline array is shown in Figure 3-24. Each panel consists of 7 cells in parallel and 392 cells in series for 2744 cells per panel. Harness connections for this panel are made on one side only, alternating sides from panel to panel. The panel for the alternate baseline configuration would be identical to this panel except that for the alternate design there would be no fold line in the panel. The panels would then stow in the 0.61 m wide containment box with no in-blanket reflectors.

#### Harness Design

Figure 3-25 shows the harness design strategy. For the baseline 3-dimensional array using aluminum conductor FCC harnesses, optimum weights were calculated at 4.5 A. U. and 1.0 A. U. sun distances. Obviously, more harness weight is required at 1 A. U. sun distance because of the higher currents and temperatures than at 4.5 A. U. sun distance. A harness weight that is halfway between the optimum weights at 4.5 A. U. and 1 A. U. sun distances was selected as a reasonable compromise.



2 x 4 CM WRAPAROUND CONTACT CELL

7 CELLS IN PARALLEL

1 MODULE/PANEL

392 CELLS IN SERIES

43 PANELS/STRIP

2744 CELLS/MODULE

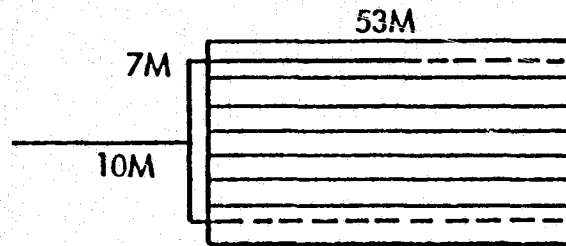
2 STRIPS/WING

235,984 CELLS/WING

ORIGINAL PAGE IS  
OF POOR QUALITY

Figure 3-24 Solar Array Panel





$$L_1 = 22 \text{ M}$$

$$L_{43} = 75 \text{ M}$$

$$(L_{\text{COND.}}/A_{\text{COND.}})^2_{\text{OPT}} = \frac{W/LB_{\text{BLANKET}} \times \text{FCC DENSITY} \times (\text{COND.}/\text{PANEL}) \times \Sigma L^2}{\text{TOTAL NO. COND.} \times I^2 \times \text{RESISTIVITY}}$$

$$\text{HARNESS WT} = W/LB_{\text{BLANKET}} \times \Sigma L^2 \times \text{TOTAL NO. COND.} / (L_{\text{COND.}}/A_{\text{COND.}})$$

$$\text{WT OPT AT 4.5 A.U.} = 4 \times 2.2 \text{ LBS} = 4.0 \text{ KG}$$

$$\text{WT OPT AT 1.0 A.U.} = 4 \times 30.0 \text{ LBS} = 54 \text{ KG}$$

Figure 3-25 Array Harness Design

### 3.6.2 Mechanical Design

The baseline Solar Array Wing shown in Figure 3-26 extends fully and extends or retracts partially to a pre-determined 10 percent extended point. When deployed it tensions two "flat-folding" array blanket sections, each having 43 solar cell panels spaced alternately between 44 in-blanket reflectors, and forming a total projected area of 3.93 m x 53 m (208 m<sup>2</sup>). The wing has two pairs of side reflectors, each having a deployed area of 8 m x 53 m. The side-reflectors when operating are at an angle of 67.5° from the plane of the blanket assembly. The wing has a natural extended frequency equal to or greater than 0.015 Hz measured at the spacecraft.

The wing consists of nine major components; Solar Array Wing deployer boom, wing extension mast, a pair of inboard and outboard linkage arms, two blanket containment boxes, two array blankets which include the in-blanket reflectors, tensioning and guide cable mechanisms, two blanket box covers, two blanket cover hold-down mechanisms, and two pairs of side reflectors.

The array wing is stowed in the spacecraft as shown in Figure 3-27 and has a stowage envelope as shown in Figure 3-28. The wing deployer boom is a coilable, continuous longeron, lattice structure mast. The inboard end of the boom canister is attached to the spacecraft pivoted interface and the deploying boom end is attached to a mast tip fitting which is a clevis link arm. The link arm is pinned to the canister of the wing extension mast where it also pivots. The array wing extension mast end has a mast tip fitting attached to it, and assembles to the pair of outboard mast/containment box linkage arms. The other ends of these linkage arms are attached to the blanket box covers. The pair of inboard mast/containment box linkage arms lie in the same vertical plane as the outboard arms with one end attached to the array extension mast canister and the other to the blanket containment box. The blanket assemblies with its layers of solar array panels, in-blanket reflectors, reflector spacers, and solar cell/reflector surface protectors are stowed between the blanket containment box floors and the box covers. The blanket cover hold-down mechanism apply a predetermined preload (compression) force to prevent adjacent layer slippage during the ascent phase of the mission. The inboard and outboard reflector support arms are pinned to the containment boxes and box covers respectively. The inner and outer edge of the reflectors are respectively

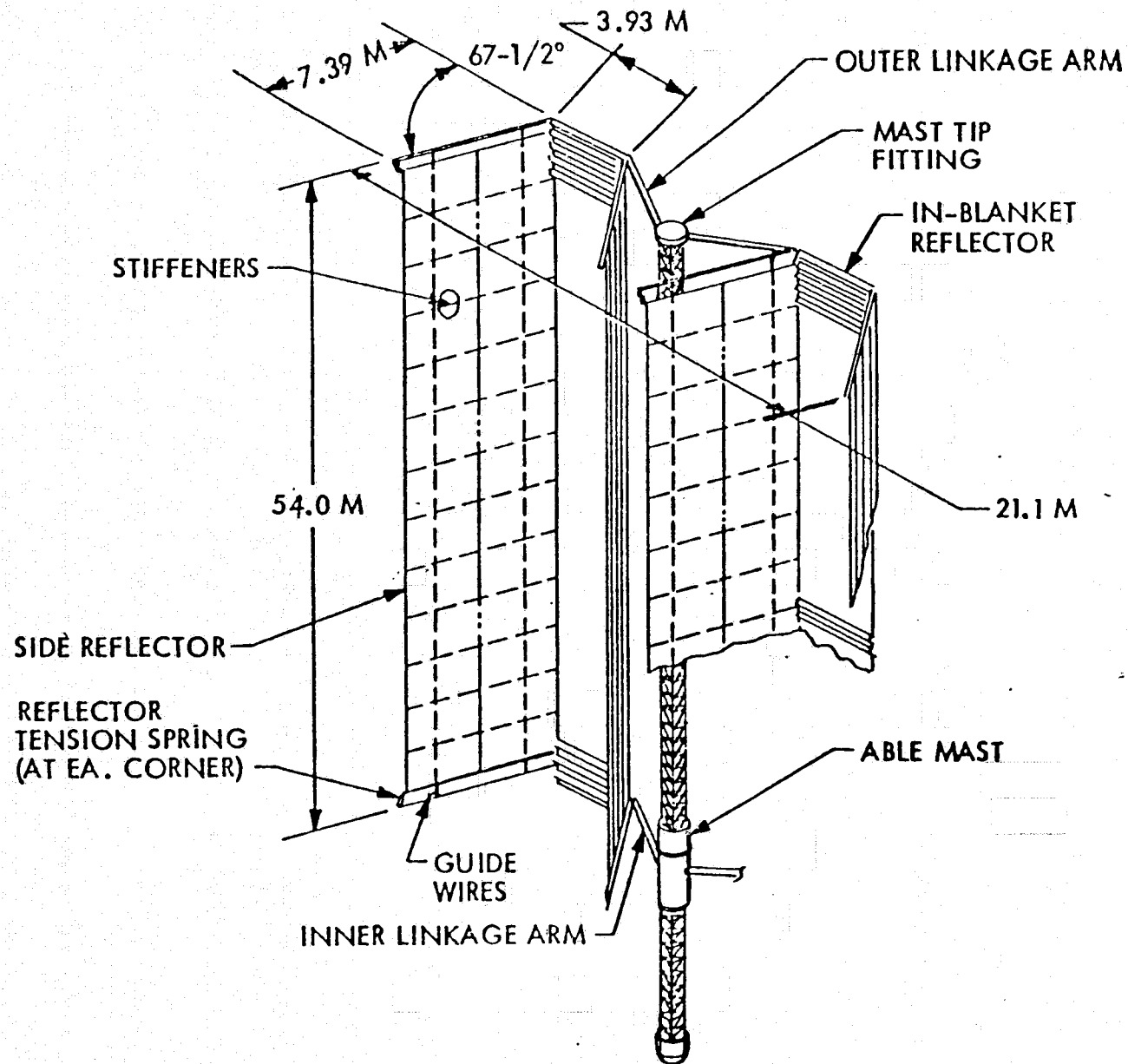


Figure 3-26 Baseline Concentrator SEP Solar Array Wing

ORIGINAL PAGE IS  
OF POOR QUALITY

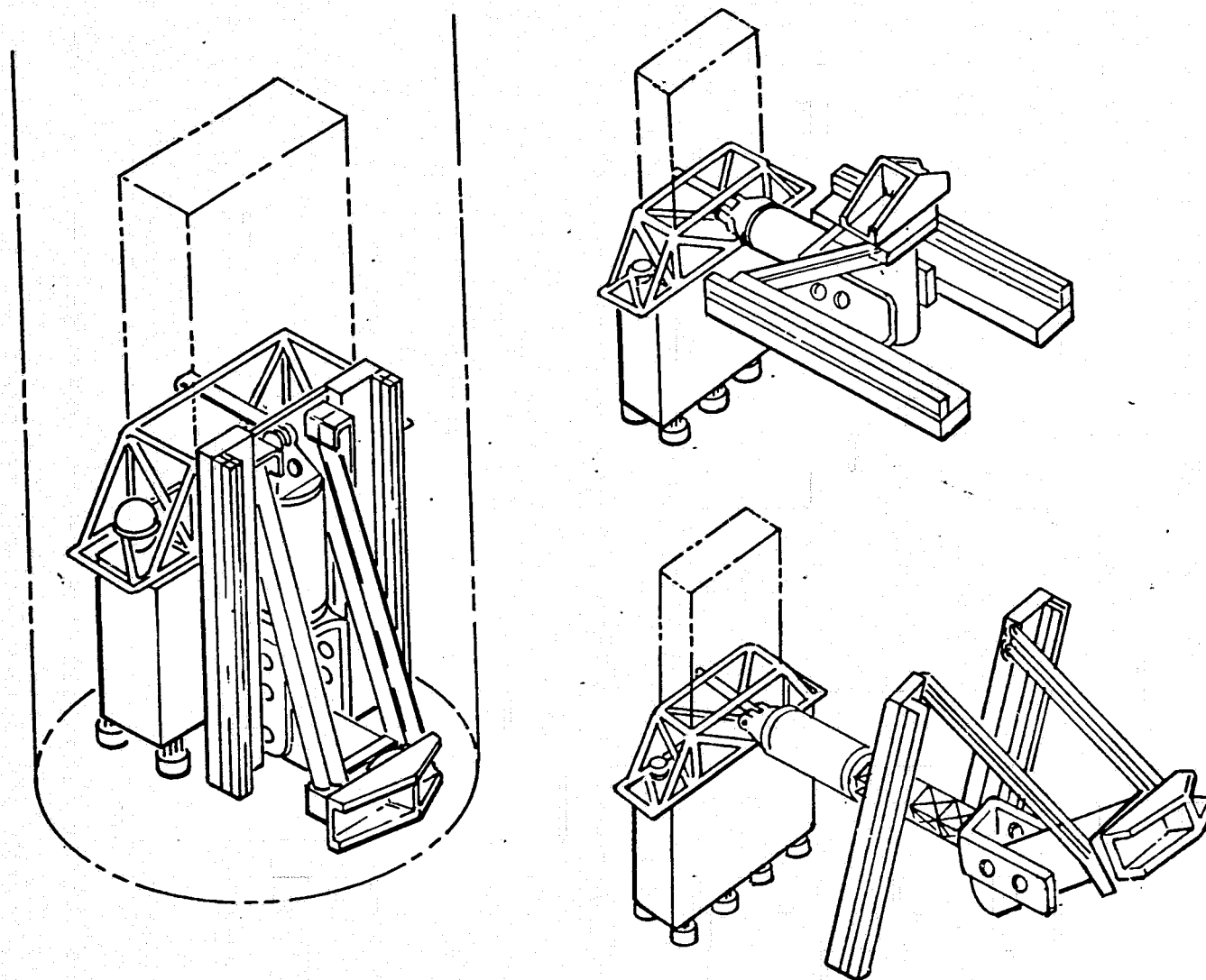


Figure 3-27 Baseline Array Wing Stowage Configuration

ORIGINAL PAGE IS  
OF POOR QUALITY

3-87

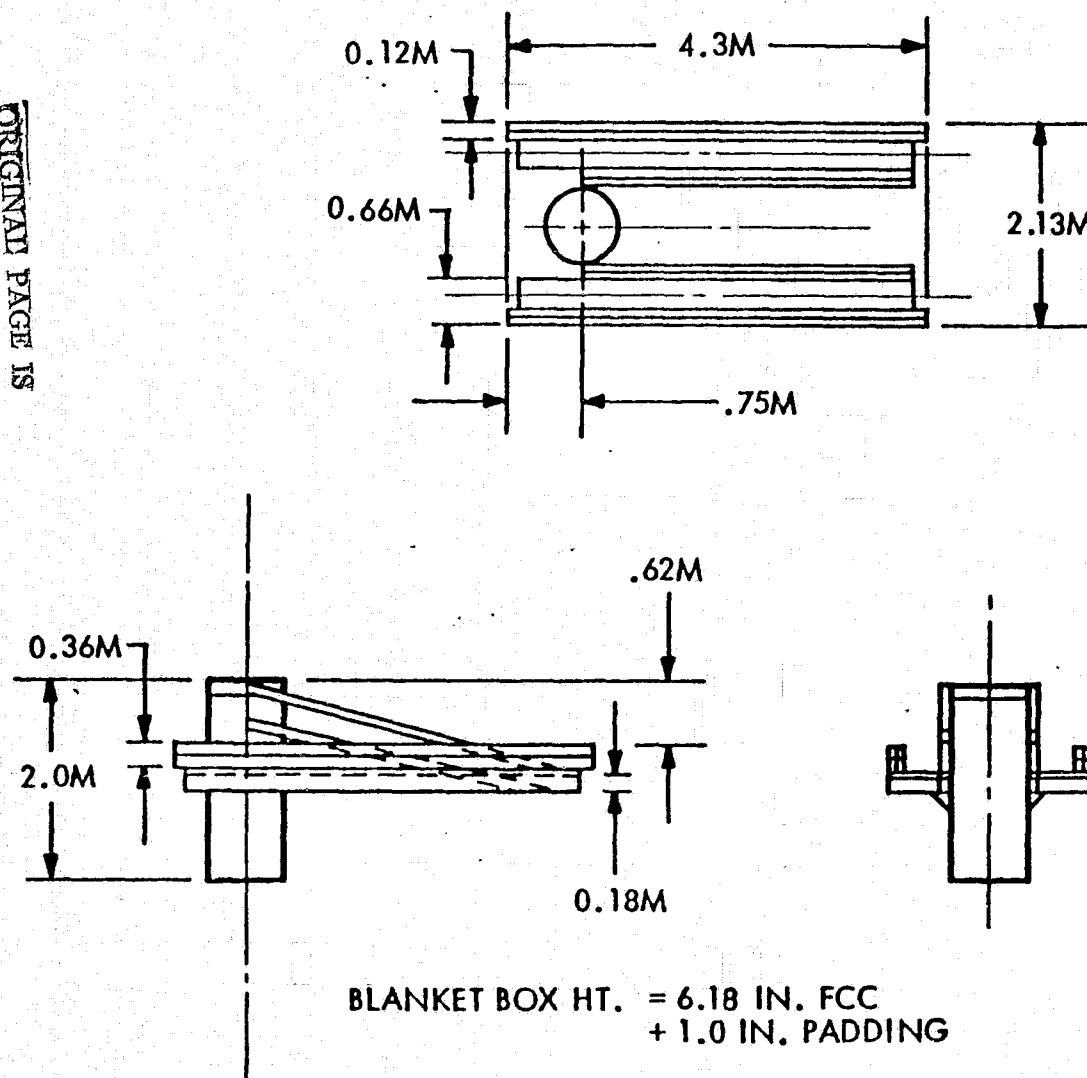


Figure 3-28 Baseline Array Wing Stowed Envelope

attached to the inboard and outboard reflector support arms by mechanical spring devices. The side reflectors are flat folded in layers 8 m long and stowed between inboard and outboard support arms. They are then folded  $180^\circ$  to a 4 m length package. There are 12 tensioning mechanisms for the blanket assemblies (6 per blanket); 2 are for full extension tensioning, 2 are for partial extension tensioning, and 2 are for guide cables. Each side reflector has a tensioning mechanism at each of four corners and 2 for guide cable tensioning.

The Solar Array Wing shown stowed in the spacecraft (Figure 3-27) rotates about the spacecraft interface into its initial position. The wing deployer boom then extends out 11.5 m (37.7 ft.). The wing then rotates  $90^\circ$  in the deployer boom clevis and is locked in position 1 Stowed, Figure 3-29.

Motors position the two solar array module sections as shown in Position 3, Figure 3-29. The side reflector motors then rotate these reflectors to the  $67.5^\circ$  position (Position 5, Figure 3-29). The pyrotechnic devices maintaining preload on the blanket covers and the side reflector covers are fired to release these covers. The wing extension mast is then actuated by mast deployer motors. The array extension mast is a continuous longeron lattice structure, capable of fully extending 54 m (177.17 ft.). As the mast extends, it raises the mast tip fitting, and symmetrically, the outboard linkage arms, the two blanket covers, and the four side-reflector outboard supports. In addition, the mast is located on the theoretical "center of mass", resulting in pure mast compression and eliminating mast tip bending. The box covers and the reflector outboard supports now serve as the support for the outer ends of the array blanket and side reflectors. Two guide cables per blanket section assembly (2) and per side reflector assembly (4) attach to the blanket covers and reflector outboard supports. These cables are tensioned by negator powered reels, are used to maintain positive position of the unfolding blanket and reflector in zero-gravity. As extension of the mast continues, the stowed blanket and reflector assemblies unfold and the blanket assemblies are tensioned at 10% extension as the result of the intermediate tension system (partial extension). The extension mast eventually fully extends the blankets and reflectors, and at this point all the tensioning mechanisms tension the blankets and reflectors to assure minimum wing natural frequency requirement of 0.015 Hz. Upon command the mast will retract back to the intermediate tension position (10% extension). Retraction

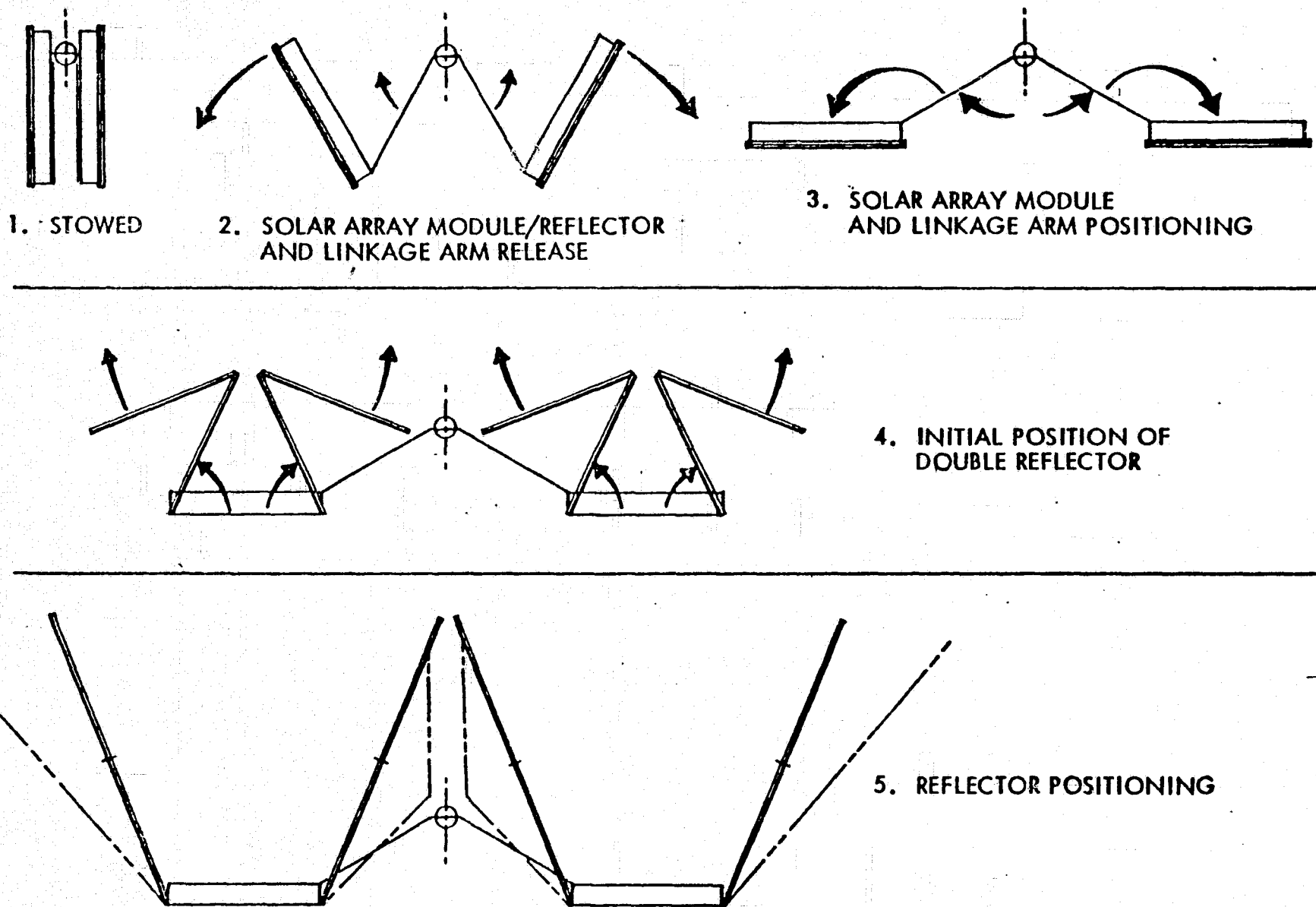


Figure 3-29 Baseline Array Wing Deployment Sequence

will result in the flat-folding of the untensioned individual panels of the blanket assemblies (90%) below the intermediate tension position. The total length of the side reflectors will be in a random folded sequence within the 10% extension position (5.4 m or 17.72 ft.). During partial retraction, there is no requirement for using the side reflectors. Upon command the mast fully extends and at some later time also retracts to the partial extension position. The wing has the capability of achieving this for a minimum of 50 cycles.

**3.6.2.1 Deployer and Extension Mast.** The wing deployer boom and extension mast shown in Figure 3-30 is made up of two major components, the mast assembly and the mast stowage canister. The mast has three equally spaced continuous coilable longerons and a lattice structure with a full extension capability of 11.5 m (37.7 ft.) for the wing deployer and 54 m (177.17 ft.) for the array wing extension mast. The continuous longerons are integrated to each other by numerous triangular battens, forming a series of equally spaced bays. In addition, the three sides of each bay are diagonally supported by tension cables. The mast assembly is a coilable truss structure when stowed in its canister and is uncoiled by the canister rotating nut as it extends. The driving force is provided by two electric motors through a gear system. The selection of a continuous coilable longeron mast for the Extended Performance SEP Solar Array is based on its minimum weight for the application. An additional advantage of this mast is the elimination of dead band from the base to the tip, which is not the case in a metal articulated lattice structure design.

**3.6.2.2 Inboard and Outboard Linkage Arms.** As shown in Figure 3-27, the pair of inboard and outboard linkage arms, symmetrical about the centerline of the extension mast are made from graphite-epoxy composite tubes and ends. The advantage gained is thermal compatibility between the tube and its respective ends. As shown in Figure 3-28, the link arms are stowed parallel to the blanket containment box, and unfold to their final position prior to side reflector positioning. As the array wing extends, the outboard and inboard linkage arms separate, and at full extension, become the load path from the tip of the mast to the blanket cover and reflector outboard supports, and from the mast canister to the blanket containment box and reflector inboard supports, respectively.



ORIGINAL PAGE IS  
OF POOR QUALITY

3-91

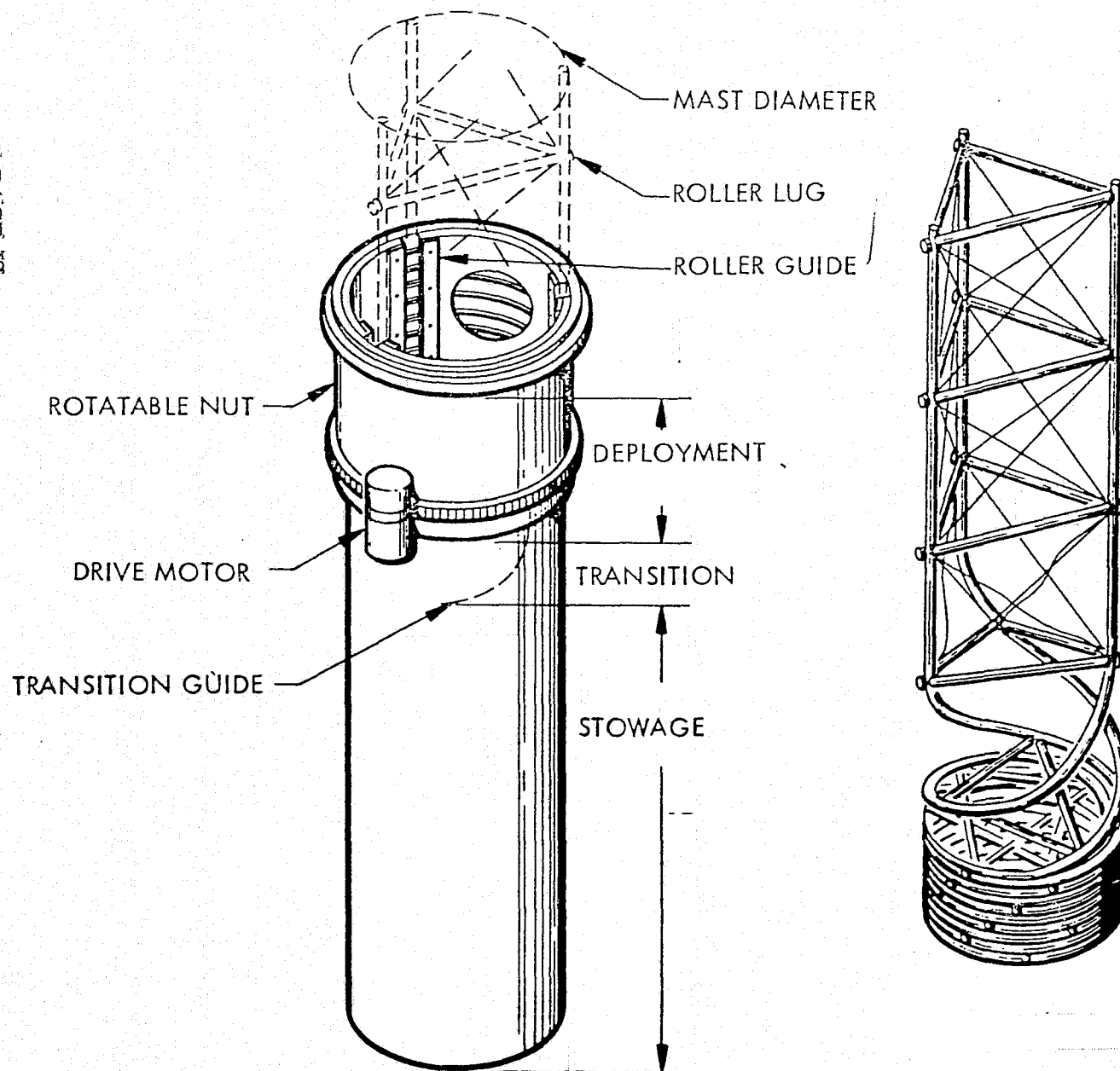


Figure 3-30 SEP Solar Array Wing Deployer Boom or Extension Mast

3.6.2.3 Blanket Containment Box. The array containment box must provide an equal and opposite reaction capability in stiffness to work together with the box cover. It must support the tension mechanisms and interface with the spacecraft during the ascent phase of the mission. Upon command the container is separated from the spacecraft and goes through its positioning sequence as shown in Figure 3-27. The floor of the container is a 2.54 cm (1.00 in.) thick honeycomb panel with graphite skins and aluminum core. The blanket side is faced with polyurethane foam like the cover for cell protection with the blanket stowed. The guide wire, intermediate, and full tension mechanisms are mounted on the underside of this honeycomb panel. The perimeter of the honeycomb floor is a graphite-epoxy laminate shield with one side and both ends removable for accessibility to the blanket assembly.

3.6.2.4 Array Blanket Assembly. The blanket assembly including the in-blanket reflectors consists of 43 solar cell panels spaced alternately between 44 in-blanket reflectors. The selected configuration of Figure 3-31 in-blanket reflector, shows a portion of the blanket assembly. When stowed, the stacked blanket consists of 350 layers; solar cell panels (86), in-blanket reflectors (88), kapton open grid reflector spacers (88), and embossed kapton cell/reflector protective sheets (88). In addition, the flat conductor cables (FCC) are installed on each edge of the blanket section assembly and when stowed, is made up of 174 layers. Figure 3-32 shows the thicknesses of the stowed blanket and stowed flat conductor cable. The make-up of these thicknesses is also shown in the figure.

Spaced alternately between the 43 solar array panels are 44 in-blanket reflectors. These reflectors are made of 0.3 mil aluminized kapton with an actual surface area of  $2.397 \text{ m}^2$ . In addition, there are a series of polyimide stiffeners on each reflector to maintain its shape when deployed (Figure 3-31, selected configuration). The open grid (mesh) reflector spacer is made from a kapton mesh and is the third leg of the triangular shaped  $60^\circ$  reflector. When stowed, the grid folds between the kapton surfaces of the reflector and has the same stowed area as the solar panels. An embossed kapton sheet is also provided and forms a cell/reflector protective sheet. It basically separates both surfaces during ground handling and the ascent phase of the mission. One edge of the sheet is permanently attached to the containment box floor and stays with the floor when extending the blanket. Stiffening of the solar panels are

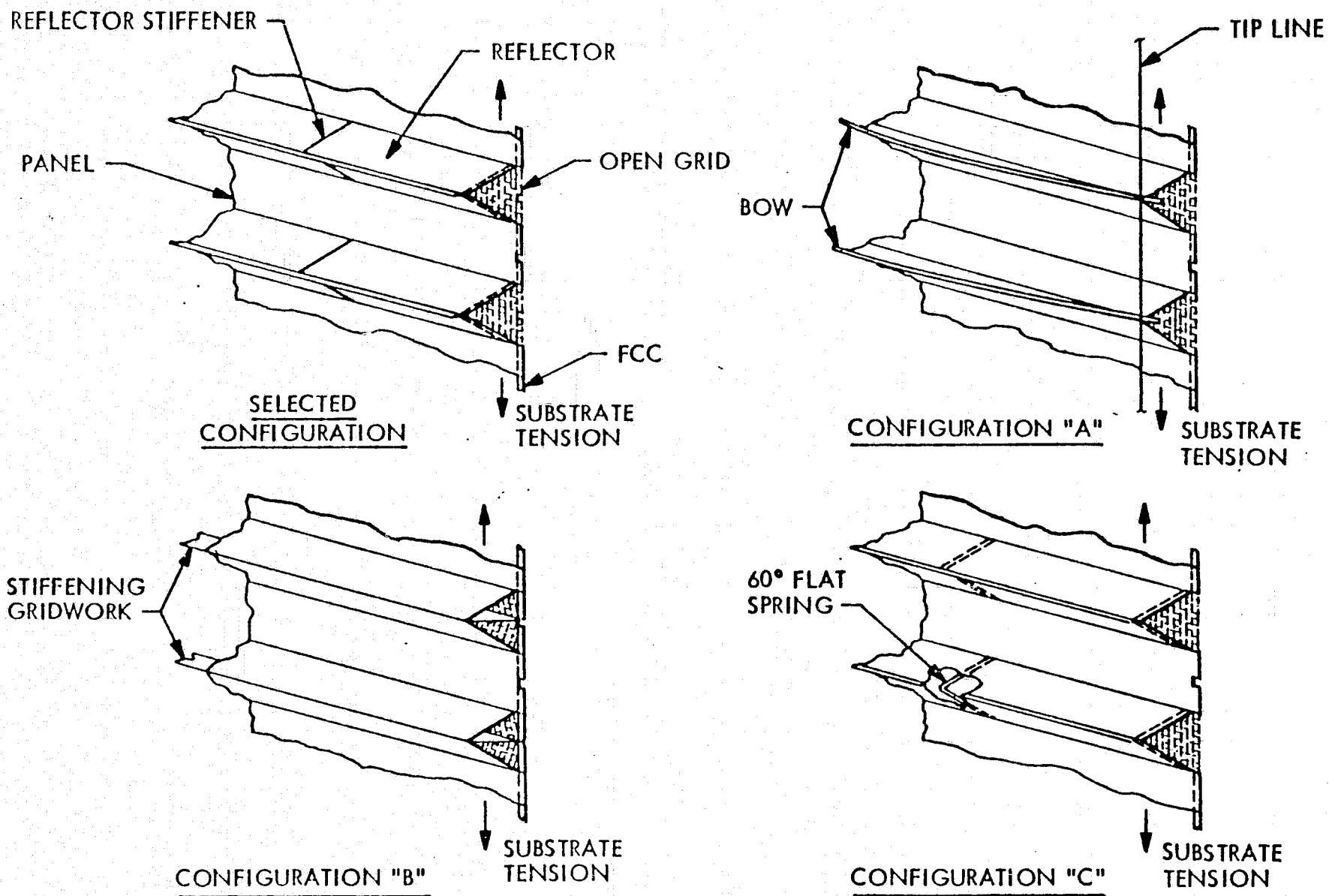
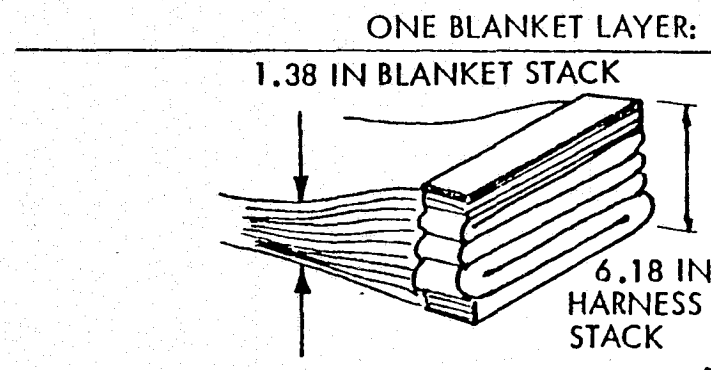


Figure 3-31 In-Blanket Reflector (Deployed)

## BLANKET



ONE BLANKET LAYER:	CELL	0.005 IN.
	COVER	0.003 IN.
	COVER ADHESIVE	0.001 IN.
	KAPTON	0.0008 IN.
	ADHESIVE	0.0008 IN.
	AL INTERCONNECT	0.001 IN.
		<hr/> 0.0114 IN.
43 PANELS, 86 LAYERS		0.9804 IN.
LAUNCH PADDING, 86 X .00075		0.0645 IN.
IN-BLANKET REFLECTOR, 88 X .0003		0.0264 IN.
REFLECTOR SPACERS, 88 X .0005		0.044 IN.
LEADER (2)		0.012 IN.
BOX PADDING		0.250 IN.
		<hr/> 1.38 IN.

SIDE-REFLECTORS

5 IN. FOLDS, 348 LAYERS X .0003 IN. X FACTOR OF 3 = 0.3132 IN.

Figure 3-32 Array Packing Data

necessary for zero-gravity fold-up during retraction. Stiffener locations are along the panel fold and hinge lines and at the guide wire positions. The guide wire system is an integral part of the blanket as the pair of guide cables are inserted through a pair of hinge grommets at every hinge. The 43 panels and 44 reflectors with spacers are attached to each other by a hinge pin polyimide rod 0.081 cm in diameter. At the outer end of the blanket, where it interfaces with the cover, a kapton leader with a hinge configured the same as the panels/reflector and spacers provide sufficient distance from the cover to preclude shadowing by it. The inner end of the blanket interfaces with a series of mechanical springs (low spring rate) which attaches to the inner tension bar. See Figure 3-33.

3.6.2.5 Tensioning System. The blanket tension, side reflector tension and guide cable systems are all negator powered. They differ in the amount of travel and force that is required. Negator motors provide a required constant force to a reel that winds a cable of determined length to perform a specific function. The negator spring element lengths and two negator motor drum diameters are sized to provide sufficient revolutions to the cable take-up reel while at the same time provide the required constant force to the cable. With the exception of the 4 corner mechanisms of the side reflectors, all of the shafts for each reel end drum are directly attached into the containment box honeycomb floor to minimize the system weight. Inserts are tooled into the floor to provide parallelism to the mechanism shafts. In addition, precision instrument bearings are used throughout all mechanisms to minimize friction within the assembly.

The two intermediate tension mechanisms per blanket assembly provide tension to the blanket at a convenient hinge-line at 10% of blanket extension. Each mechanism applies a force at 10% to a tension distribution system (see Figure 3-33) which distributes the two local loads over the blanket width. The local loads from the mechanism are introduced to a graphite tube through a fitting. The loads from the tube are then transferred to a blanket hinge line by spring assemblies. The spring rates of the assemblies are sufficiently low such that straightness tolerances in the blanket and tube, and tube deflections will not represent large tension variations across the blanket. On the other hand, the spring length is limited by the stowage volume of the container.

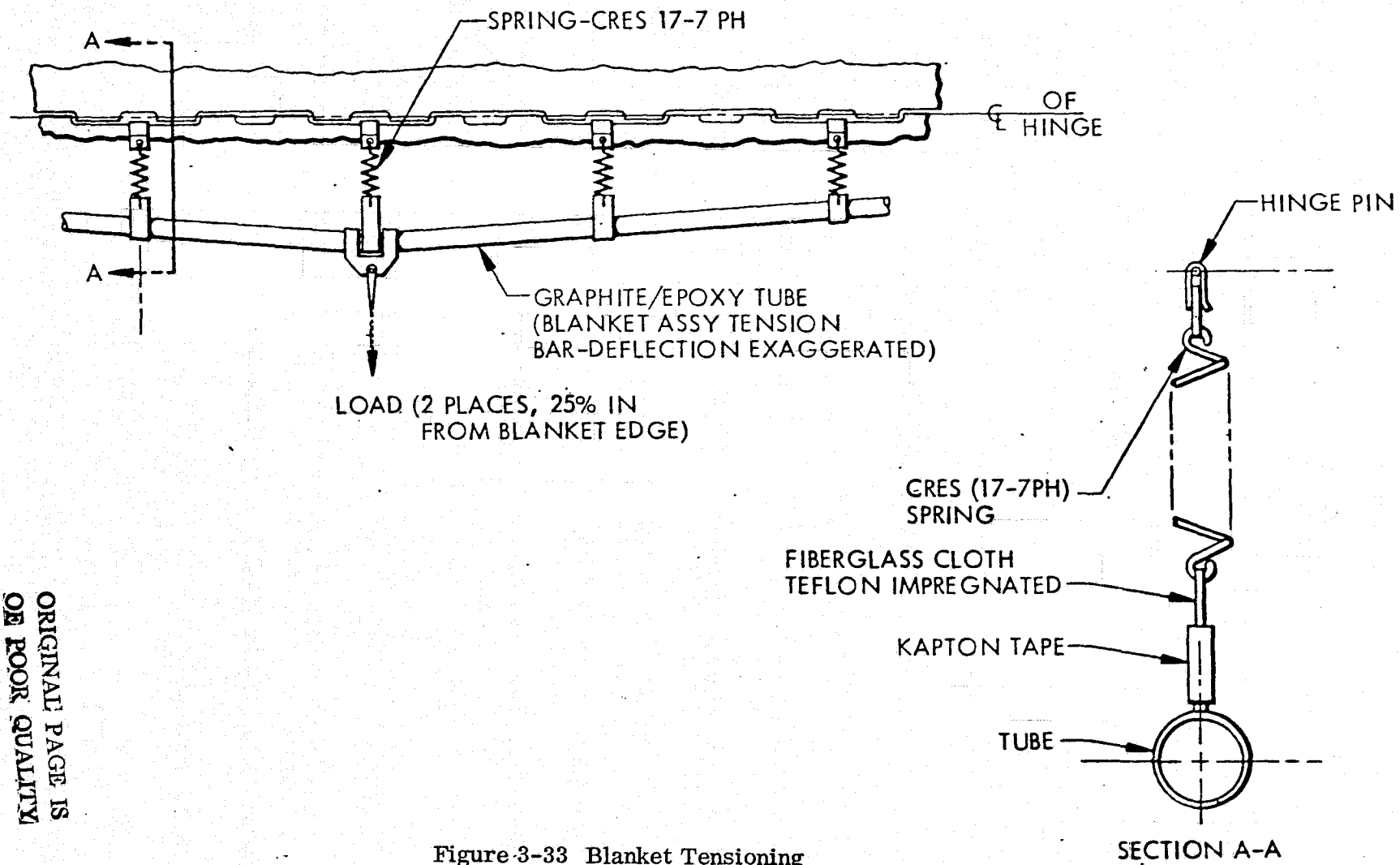


Figure 3-33 Blanket Tensioning

**3.6.2.6 Blanket Box Covers.** The containment box cover must provide an equal and opposite reaction capability in stiffness to work together with the containment box. It must preload the stowed blankets in conjunction with the hold-down mechanism during the ascent phase of the mission. When extended, it provides the outer support for the array blanket assemblies. The cover consists of an aluminum honeycomb cone with graphite face sheets. The peripheral closures are channel sections, also made from graphite. The blanket side of the cover is faced with 0.5 cm thick polyurethane foam covered with a thin layer kapton sheet to prevent UV degradation.

**3.6.2.7 Blanket Cover Hold-Down Mechanism.** The hold-down mechanism when integrated with the cover must provide the preload (compression) force to the stowed blanket assembly during the ascent phase of the mission. There are four cover support bars located about 25% in from the ends of the containment box. The bar has a series of conical spikes that mate into a series of conical holes on the cover assembly. A tool holds the cover in the preloaded position, and cross arms with a redundant pin puller system are attached to each other and properly adjusted. The tool is then removed. After ascent and upon command, the pin pullers are activated. The spring loaded cross arms separate and swing away releasing the blankets.

**3.6.2.8 Side Reflectors.** The reflector units are stowed on the cover side of the solar array blanket assembly. Two separate operations are required to make the reflectors operational. First they are positioned to the proper reflection angle and then they are extended. The positioning is by electric motor/worm gear drive units. The inboard and outboard hinges are keyed together to synchronize the positioning of the inboard and outboard reflector supports. After the array wing is extended, the motor drive units are utilized to change the angle between the reflector and the solar cell blanket. Synchronization will be done electrically as there will be no mechanical link between the inboard and outboard reflector supports.

The reflector supports consist of two trapezoidal shaped graphite-epoxy box sections placed together to form a 4 cm x 8 cm rectangular shape (see Figure 3-34). The section is oriented to maximize support stiffness along the deployed reflector plane. The aluminized kapton reflector material is flat folded each 7.62 cm and stowed between the two box sections (see Figure 3-35). The creasing of the reflector material by flat

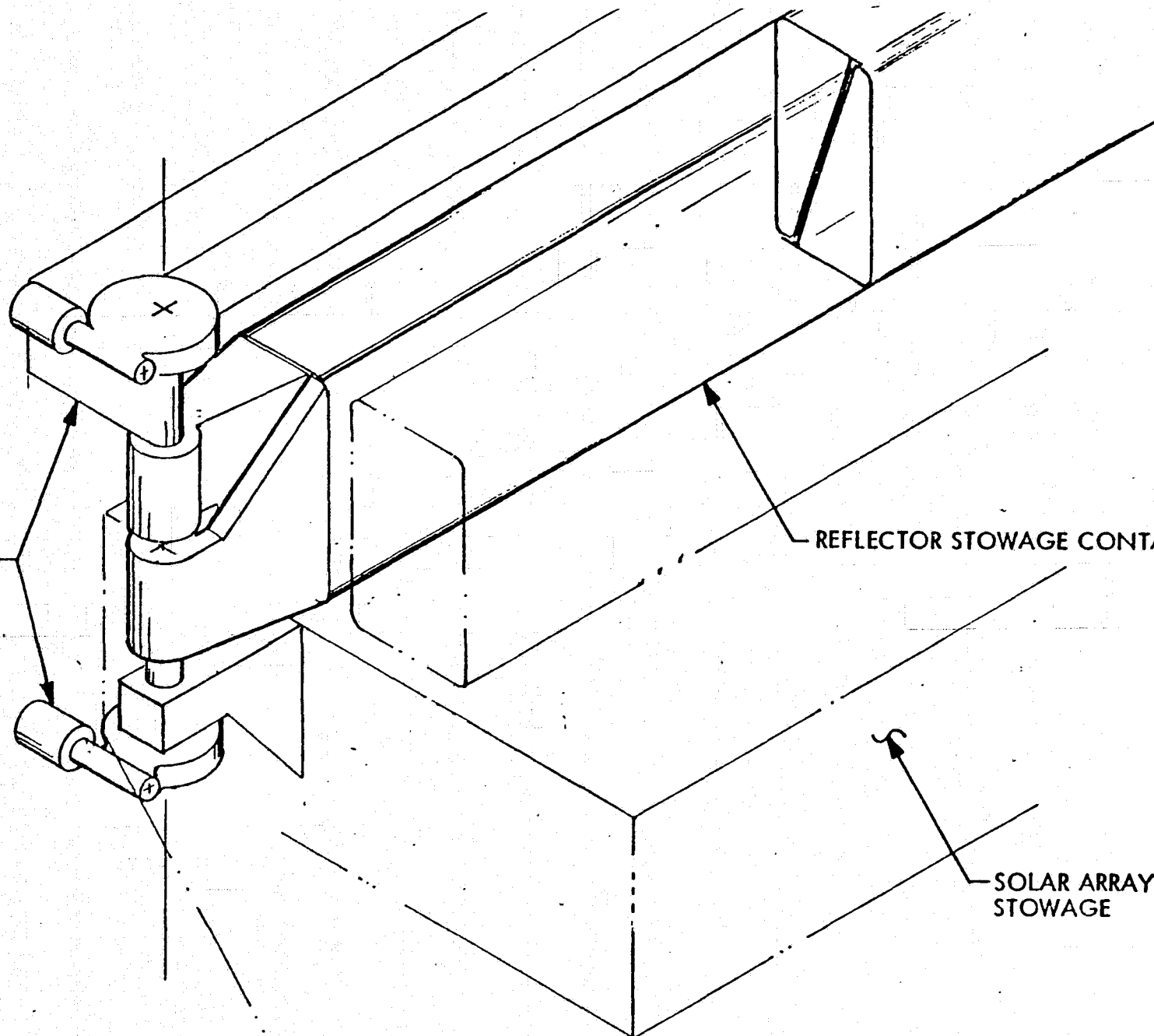
REFLECTOR  
ACTUATOR

REFLECTOR STOWAGE CONTAINER

SOLAR ARRAY  
STOWAGE

Figure 3-34 Reflector Hinge Assembly

86-3





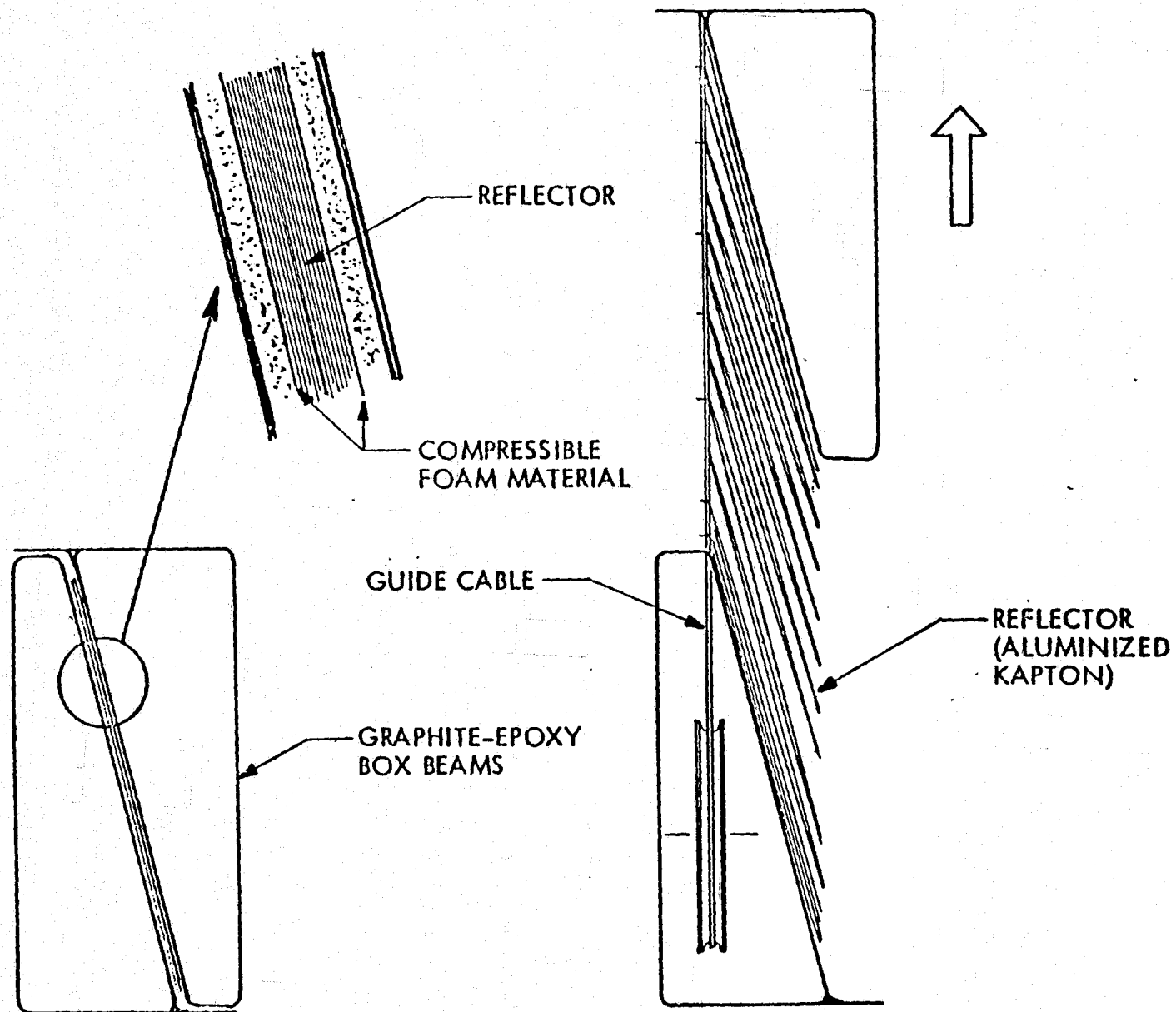


Figure 3-35 Side Reflectors

folding tends to stiffen the reflector material and give a more effective deployed surface. In addition, stiffeners can be formed by folding the reflector material and bonding it to itself (see Figure 3-36). Since only limited widths (approximately 4 ft) can be purchased, splicing of the reflector material is required. Ten years ago TRW similarly spliced together 10 reflector panels 2 ft by 8 ft using Schjeldahl dry film adhesives heated by a tungsten wire. The joints exhibited strengths of 2 lbs/in. along their length, low assembly tolerances were experienced, and wrinkling was considered negligible.

The reflector material is controlled during extension by a guide cable system. The cables attach to the outboard support section and feed through grommets placed in the flat-fold section of the reflector at the splices and intermediate stiffeners, into the inboard support section, through a pulley system and on to a cable reel. The cable tension is controlled by a negator spring to give a constant amount of tension throughout the extension cycle. This system allows the reflector material to be aligned during all phases of extension or retraction, including partial retraction and still maintain the minimum natural frequency.

ORIGINAL PAGE IS  
OF POOR QUALITY

3-101

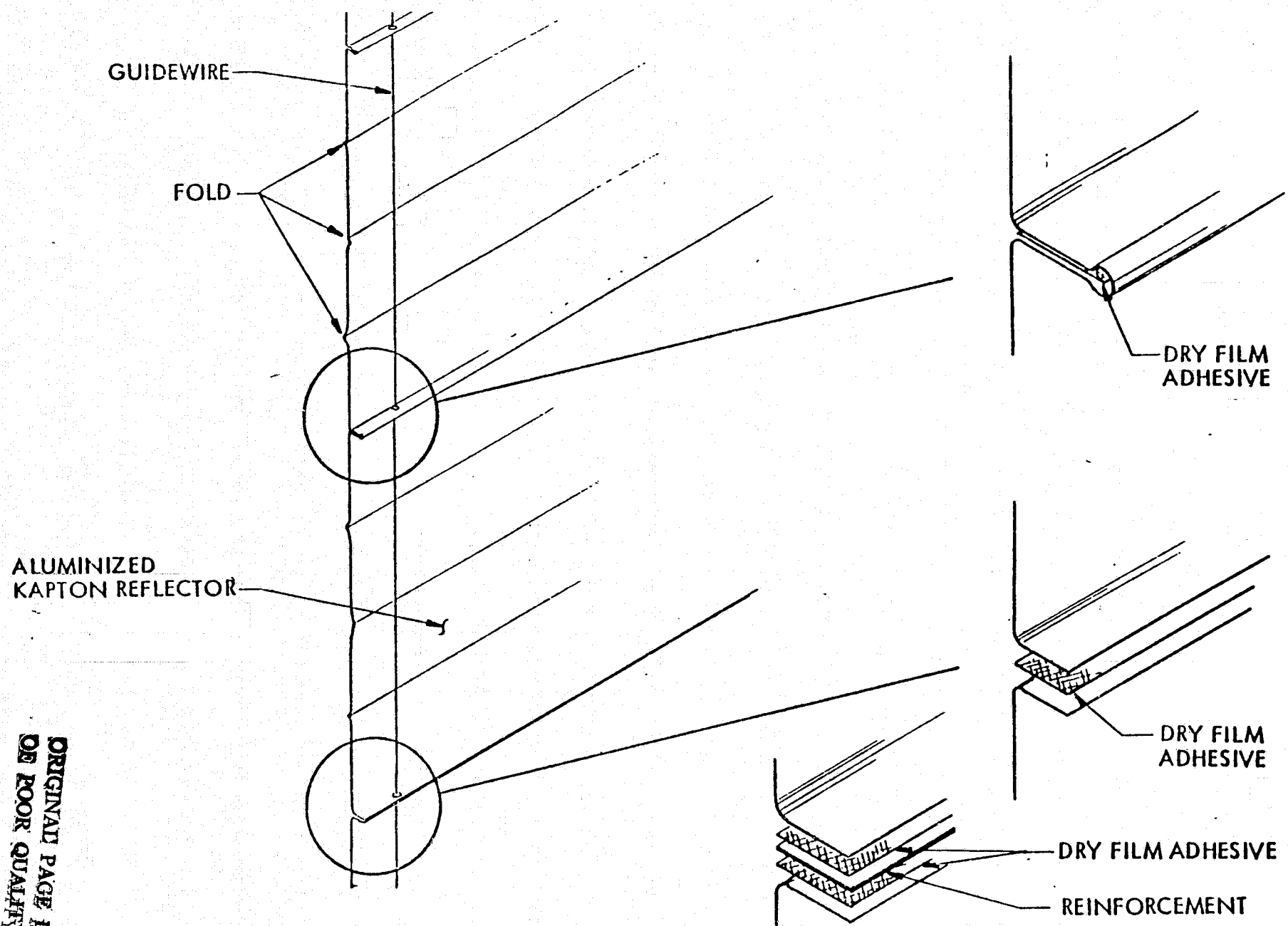


Figure 3-36 Side Reflector Assembly Techniques

### 3.6.3 Structural Characteristics

#### 3.6.3.1 Stowage and Deployment Concept Evaluation.

Concept 1 - As shown in Figure 3-37 each solar array module swings from a forward attach point located at either side of the propulsion module. During stowage the extension mast lies on the longitudinal axis of the SEP unit with the array container located directly aft of the propulsion thrusters. Separation between the IUS and SEP unit occurs after the uncaging of the array wing. Some of the caging is incorporated in the IUS. Each array wing swings in a direction outboard of the propulsion module on a rigid lattice structure boom. When larger side reflectors are used, an extendible boom may be used to extend the wing beyond the thruster plume. The wing extension mast is located on a center coaxial to the tracking control axis. The array/reflector containers are then unfurled to their deployment position and then unlatched. The extension of the mast extends both the array blanket and the side reflectors simultaneously. Extension continues to full extension and tensioning. Flat-folded triangular shaped in-blanket reflectors are deployed, automatically, as they leave the blanket container. Tensioned guide wires maintain location control of the blanket and the reflectors until they are tensioned between the outboard supports and the inboard support structures/containment boxes.

Concept 2 - The solar array wing swings out on an articulated boom that has one end attached to a point forward at the side of the propulsion module (see Figure 3-38). The array wing extension mast canister, attached to a clevis fitting at the end of the boom, is stowed perpendicular to the boom. The solar array containers tie into the mast by means of linkage arms, one set of arms attach to the cover portion of the array module and the mast tip and are employed in the extension of the array and reflector. The other set of arms are connected to the mast canister and the containers of the array blanket and side reflectors. The array containers and arms are stowed symmetrically to each side of the propulsion unit and are conveniently caged during launch. During launch, the solar array wings are caged and support is provided by the IUS interface. At separation, the IUS will move aft of the SEP thus providing room for the deployment of the array wings.

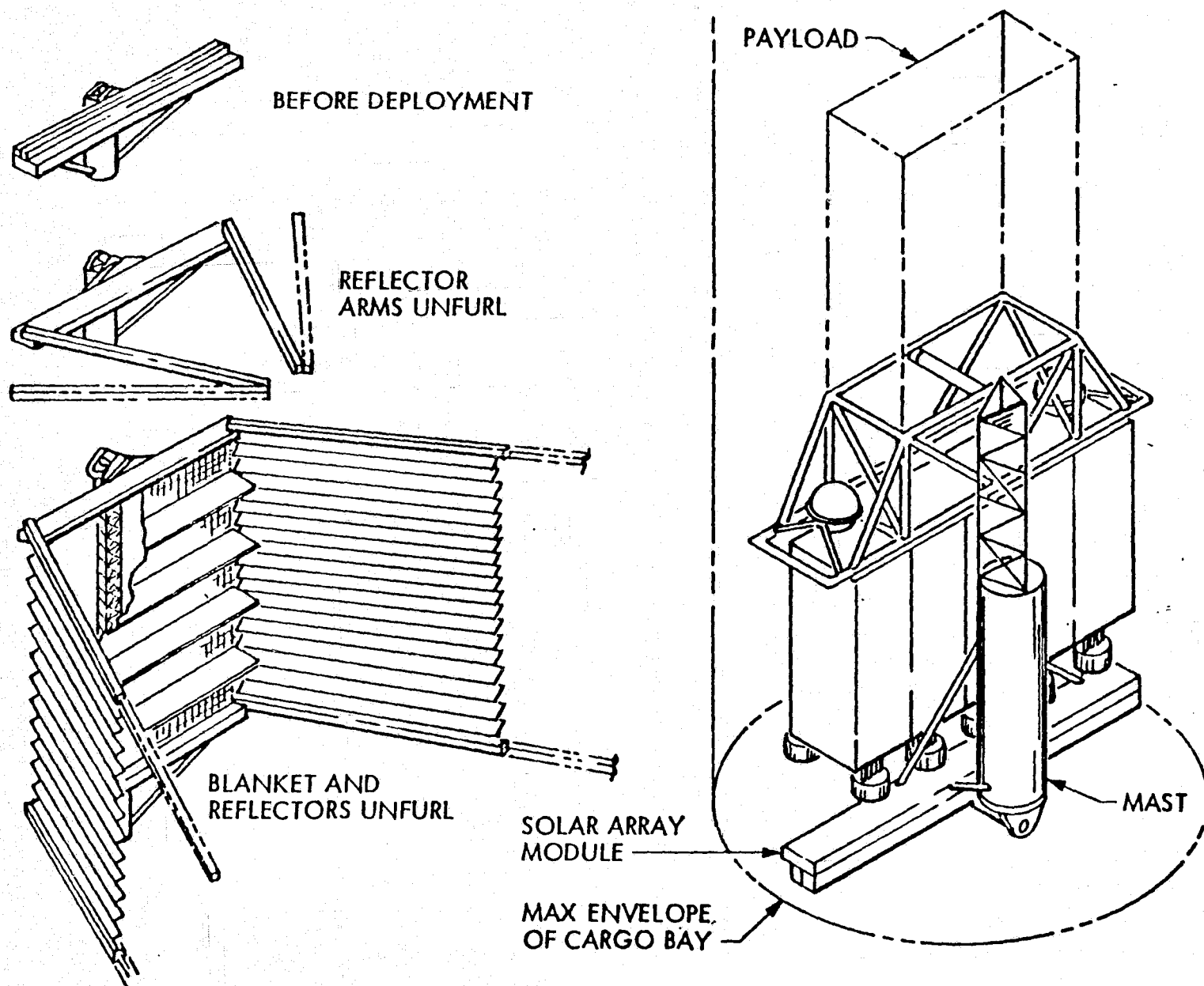


Figure 3-37 Stowage and Deployment Concept 1

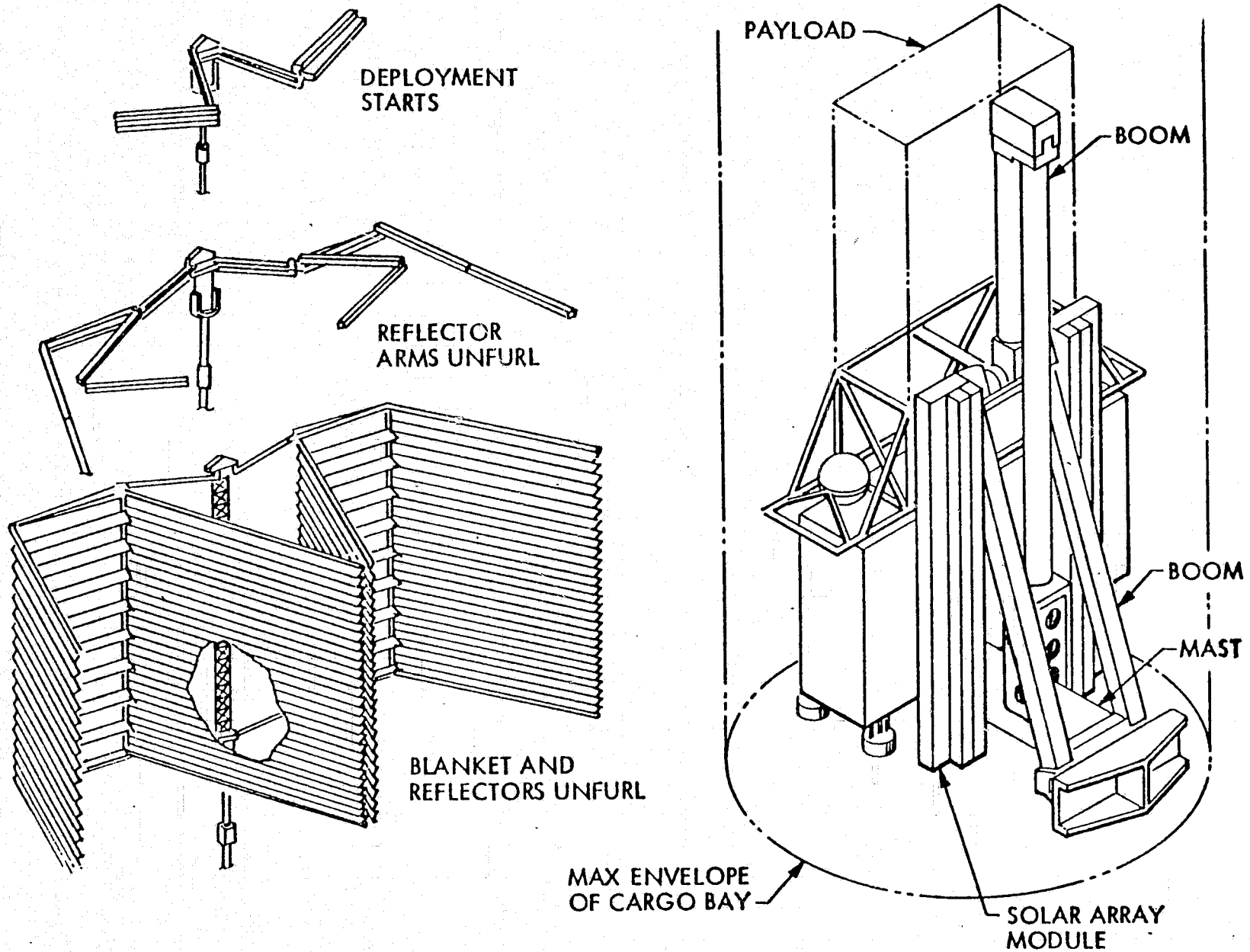


Figure 3-38 Stowage and Deployment Concept 2

The folded boom is used to extend the array wing module beyond the plume of the thrusters. The boom unfolds and the mast canister rotates in its clevis fitting to a position with the extension mast axis coaxial with the tracking control axis. The array blanket and side reflector containers swing to appropriate positions on the linkage arms. The outboard reflector container is swung to the correct extended angle, followed by the deployment of the inboard reflector container to the correct extended angle. With the container elements in their final position, the covers are simultaneously unlatched and the extension of the array is accomplished by the extension mast.

Concept 3 - The solar array wing in this configuration is stowed with the extension mast in line with a short extendible separation boom, see Figure 3-39. This boom extends the array outside of the plume of the thrusters. Caging of the wing during launch is conveniently integrated with the IUS. At separation, the array wing is uncaged and the spacecraft separates from the IUS.

During deployment, the array wing is positioned beyond the thruster plume by the short extendible mast. The deployment sequence is then identical to the sequence for Concept 2. The array containers are swung to their appropriate angular positions with the linkage arms that attach them to the extension mast. The containers are unlatched. The extension extends until the array blankets and side reflectors are completely extended and tensioned.

Concept Selection - The weight estimates of concentrator array configurations resulted in the selection of a side-by-side 3-dimensional reflector wing similar to that of Concepts 2 and 3. These wing packages could not be stowed aft of the thrusters due to volume constraints. The caging and articulation of the containers for the array blankets and side reflectors, using linkage arms to the wing extension mast, was more complicated for Concept 3 than for Concept 2. The simple articulated rigid boom in Concept 2, however, violated the payload area exclusion constraint of the study. It was replaced with a shorter extendible boom as described in Section 3.6.2.

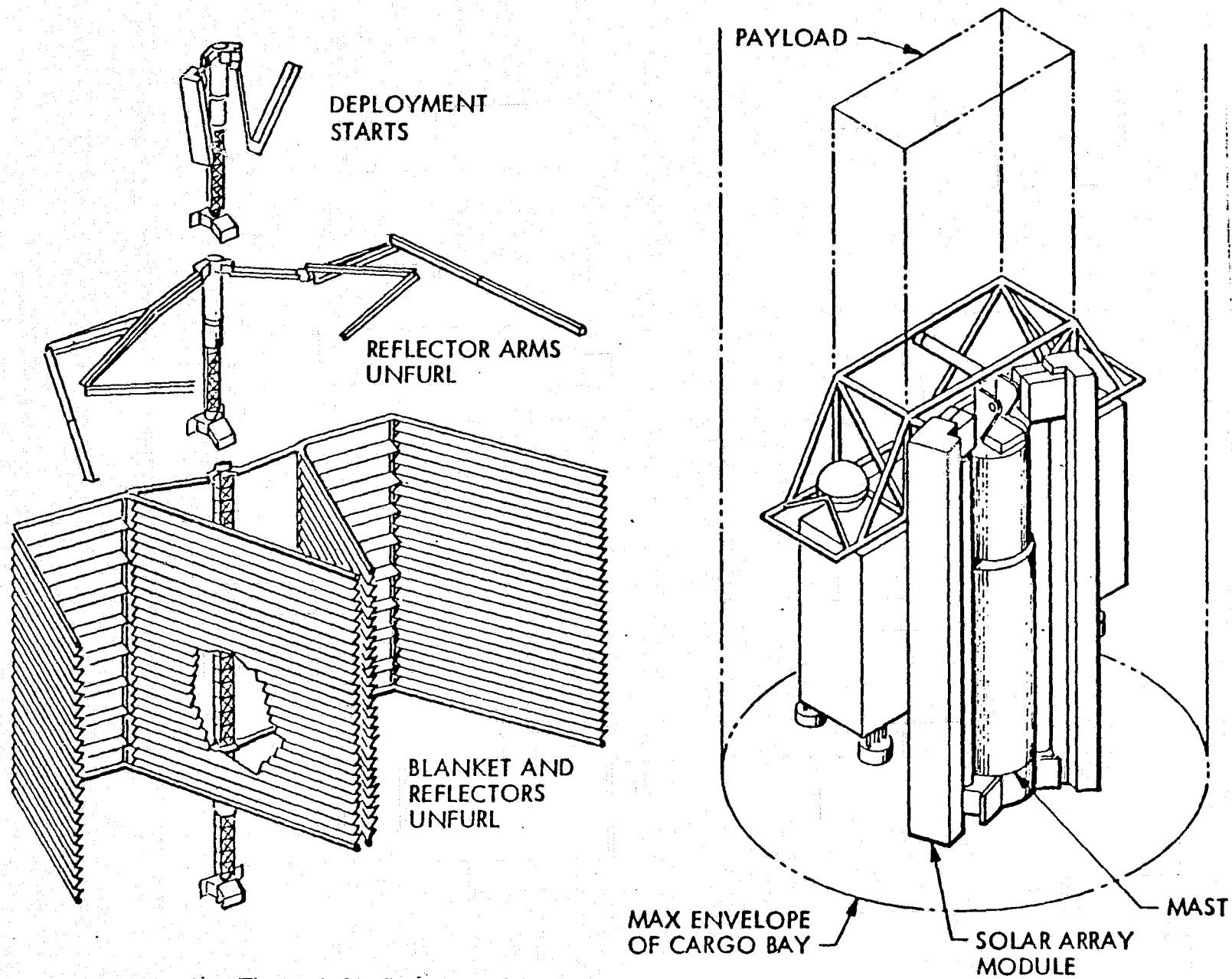


Figure 3-39 Stowage and Deployment Concept 3



3.6.3.2 Dynamics Analysis. Dynamic studies were performed on the different concepts for the SEP fold-up concentrator solar array to determine the effects of various parameters on the optimized first structural mode. The maximum advantage of the system occurs when the parameters of mast EI and blanket tension are adjusted to optimize the first structural modes of both the blanket and the mast into a single combined mode involving simultaneous and in-phase motions of both parts. These studies determined what the values of the various parameters for an optimized first mode at a given minimum frequency for the different design concepts.

A single blanket design is shown in Figure 3-40. The figure also shows the assumed distribution of the mast/blanket system tension force. Figure 3-41 shows the corresponding construction of the finite-element model using the ASTRO computer program. The wing natural frequency was selected as 0.017 Hz to allow the wing deployment boom to decrease this value to 0.015 Hz. The data was prepared by considering 18 cases, adjusting the model geometry, calculating mast weight for a particular mast EI, selecting a tension value, and making a computer run. The preload was varied and a peak was determined for a particular boom EI. Then a different boom EI was selected and another peak was determined by connecting the peak values, an intersection could be determined with the minimum frequency of .017 Hz. The results for the baseline array are shown in Figure 3-42.

ORIGINAL PAGE IS  
OF POOR QUALITY

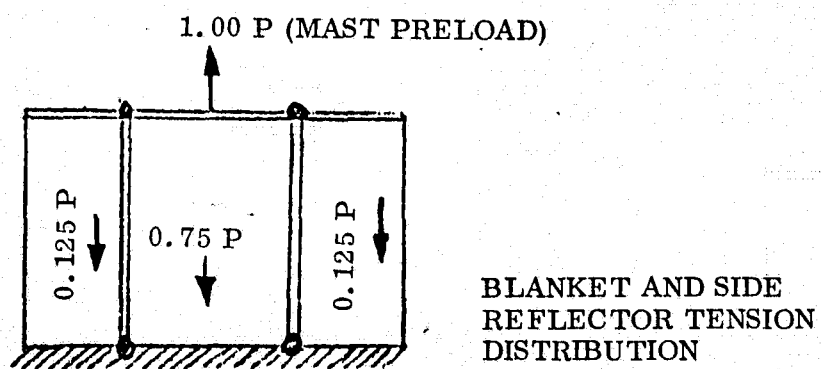
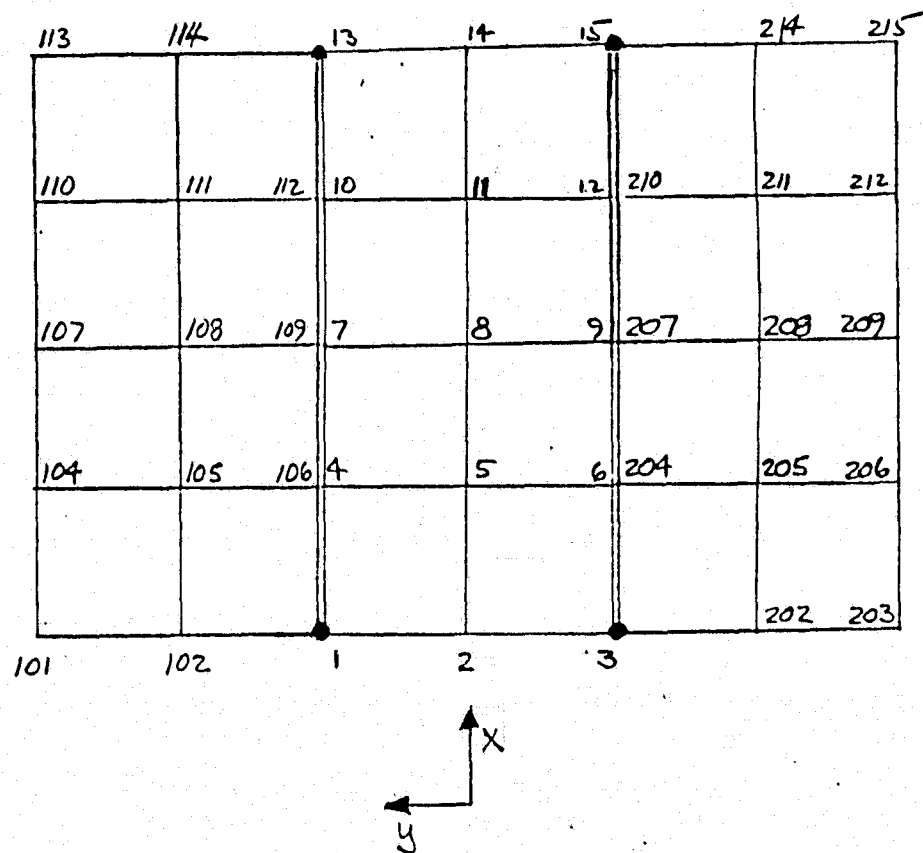


Figure 3-40 Single Blanket Concentrator Wing

3-109

ORIGINAL PAGE IS  
OF POOR QUALITY

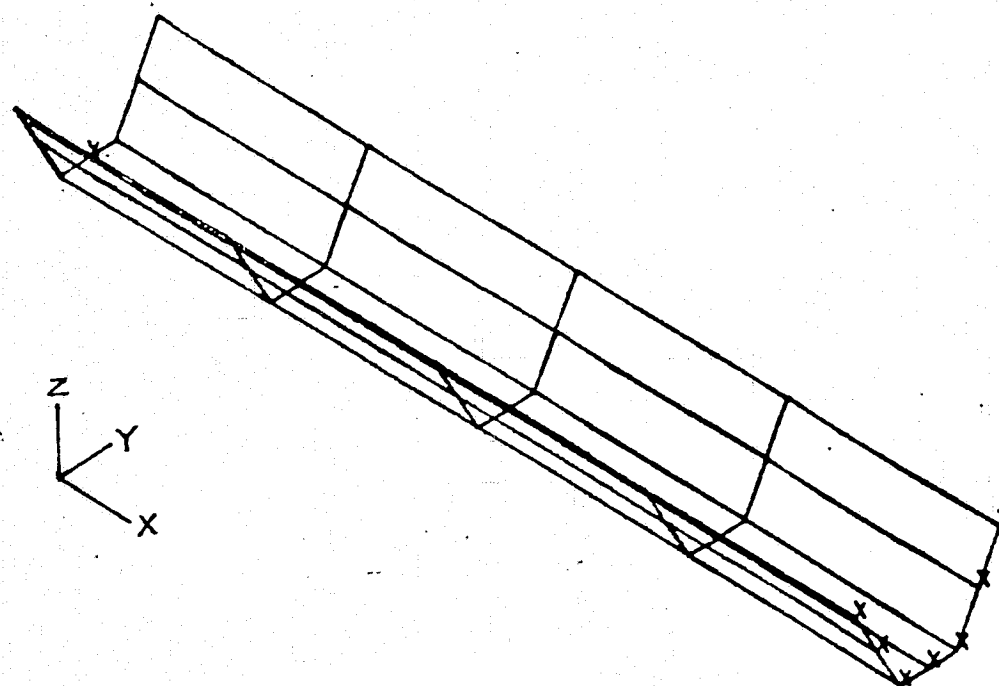


Figure 3-41 Single Blanket Concentrator Wing Model

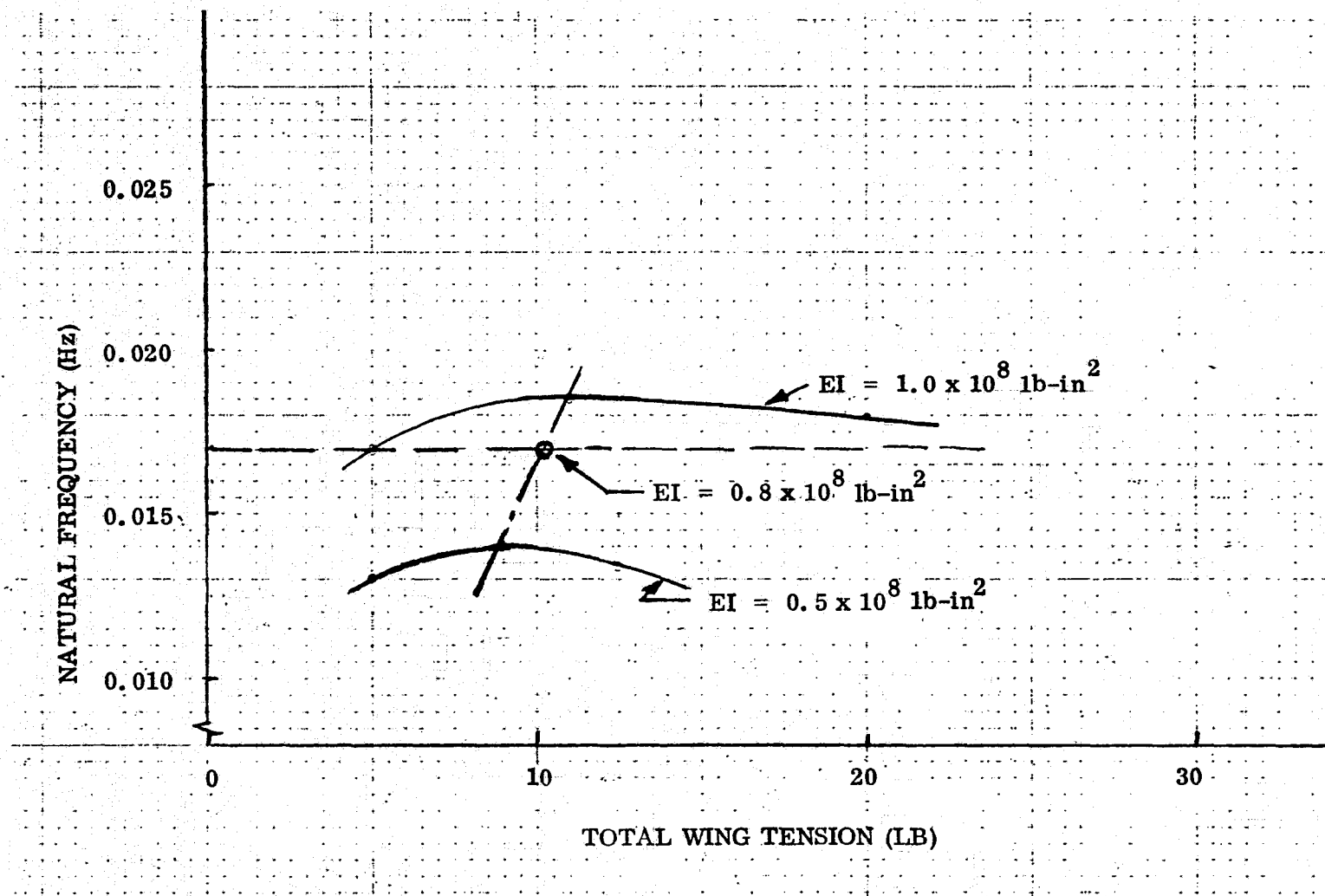


Figure 3-42 Baseline Array Stiffness Mast Stiffness and Blanket Tensioning

#### 3.6.4 Alternate Concentrator Solar Array

An alternate trough concentrator solar array design was identified in the study which also met the design requirements. It differs from the baseline design in that it is a two-dimensional concentrator design employing one electrical module blanket per wing with side reflectors and no in-blanket reflectors. The fully-deployed alternate concentrator array wing is shown in Figure 3-43. The wing storage and deployment is less complex than for the baseline design. As shown in Figure 3-44, the alternate design wing is stored below the thrusters in the allowed storage volume. A short wing deployment mast is attached to the array wing extension mast on the same axis. The base of the short deployment mast is attached to the wing tracking mechanism on the spacecraft.

For deployment, the wing is released and the wing module is rotated outboard 90 degrees so that the tracking axis and the mast axes are in line. The short deployment mast then deploys the wing 8 m to separate the array wing from the spacecraft and thereby keep the array out of the thruster plume. The side reflector packages which are folded in half for launch are then articulated by motors to their proper orientation as shown in Figure 3-44. The flat-folded array blanket and reflectors are preloaded between inboard and outboard graphite-epoxy beam structures. The inboard support structures are attached to wing mast canister. The outboard support structures are attached to the wing mast tip and latched to the inboard support structures. The outboard structures are released and the extension of the wing mast extends both the array blanket and the side reflectors simultaneously. Extension continues to full extension and tensioning of the array blanket and side reflectors. The two side reflectors are not attached to the array blanket and the three elements are tensioned separately.

The side reflectors provide an effective CR of 2.27 and to meet the mission power requirements more solar cells are required by the alternate design than by the baseline design, 680, 512 vs 471, 968.

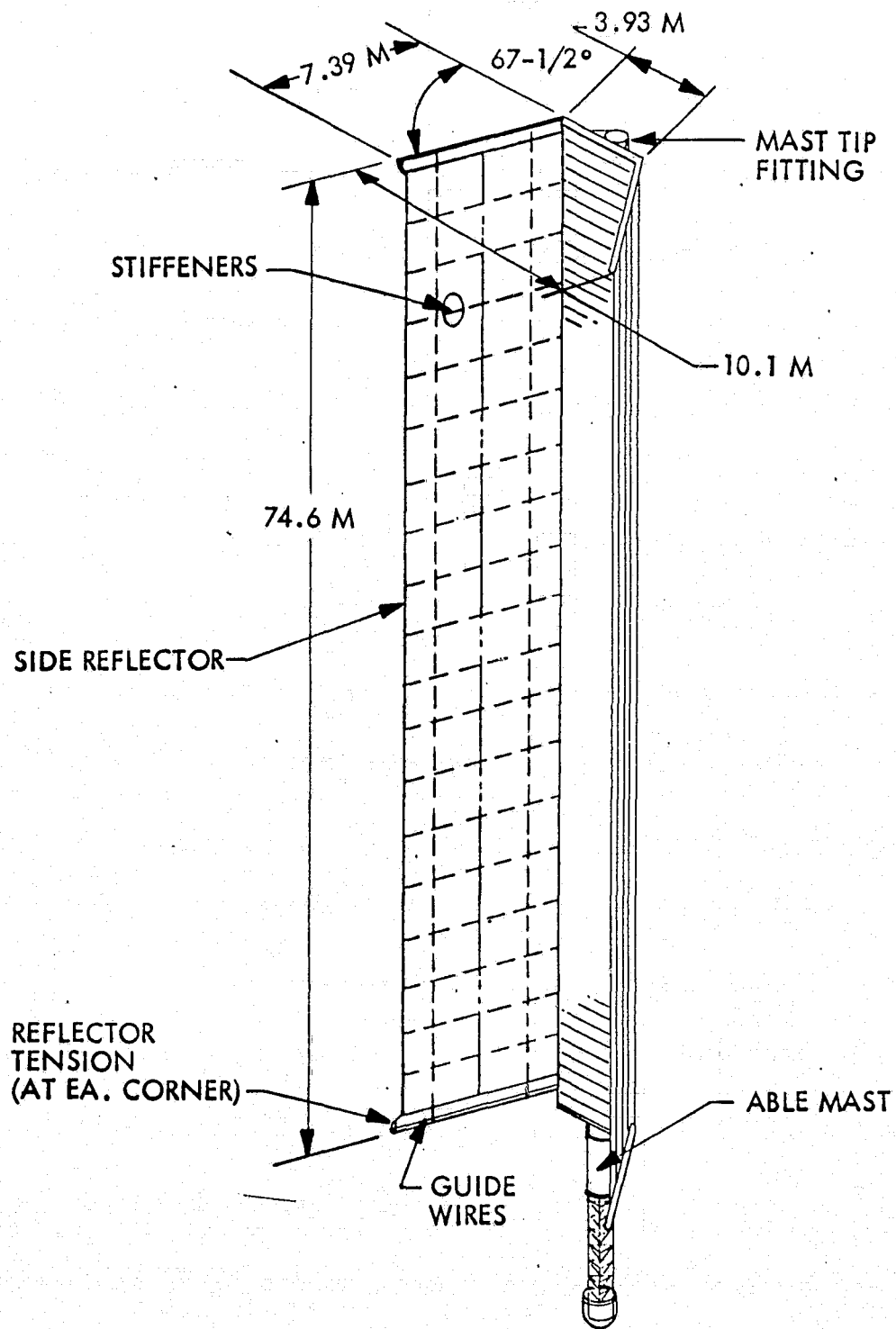


Figure 3-43 Alternate Concentrator Array Wing-Fully Deployed

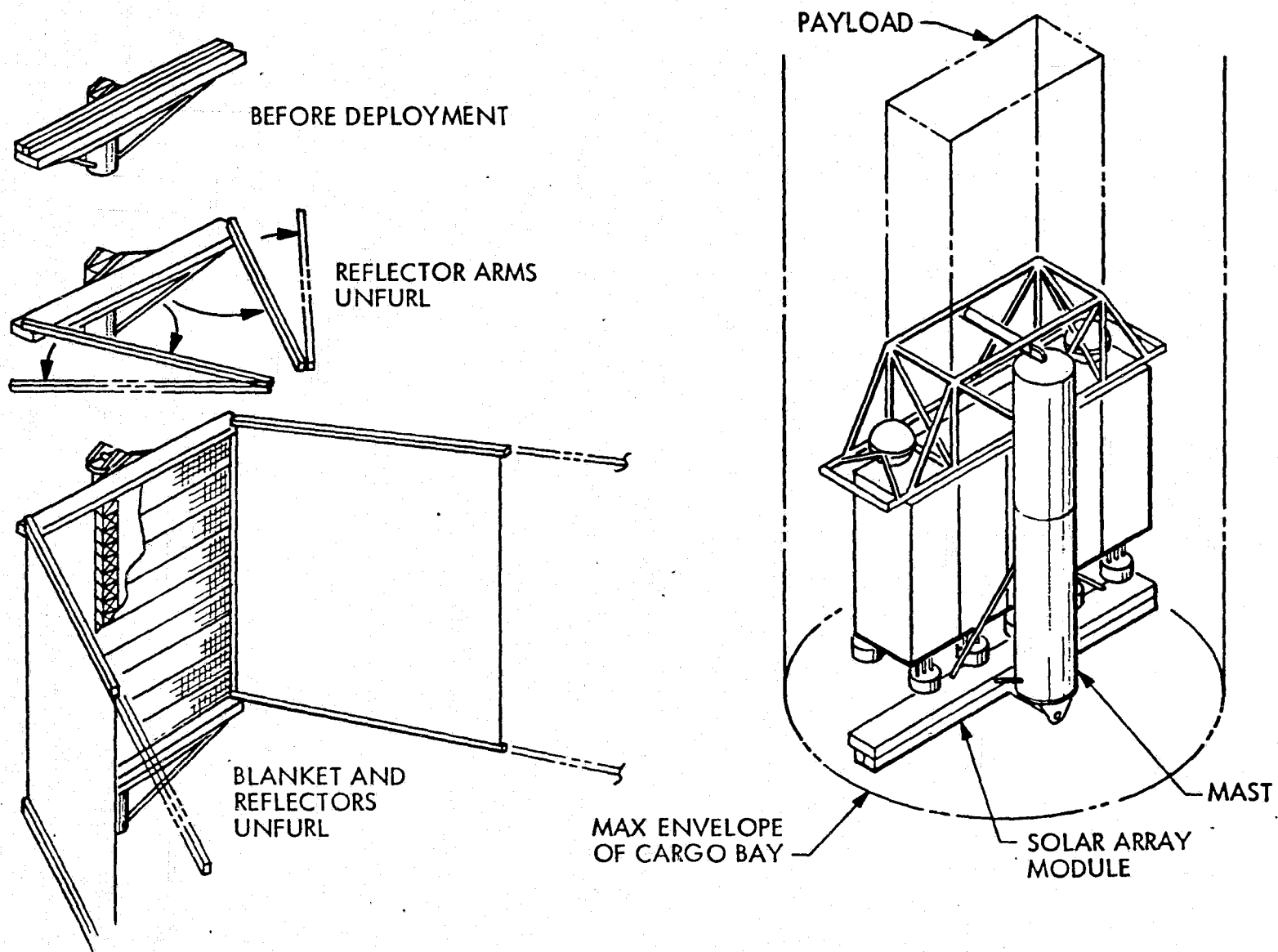


Figure 3-44 Alternate Concentrator Array Stowage and Deployment

### 3.6.5 Performance Data

The performance data is based on data published in Reference 21. The data was first normalized to  $P/P_0$  and  $V_{mp}/V_{mp0}$  where  $P_0$  and  $V_{mp0}$  were taken from the data at 30°C, AMO.  $P_0$  was based on the assumed efficiency of the cell and  $V_{mp0}$  was assumed to be 500 mV.

Performance data at various A.U. from the sun were then calculated using the predicted cell temperatures and the assumed array concentration ratio, CR. A bivariate interpolation routine was used to determine  $P/P_0$  and  $V_{mp}/V_{mp0}$  at each intensity and temperature point. Tables 3-14 and 3-15 list the predicted array power and module voltage at maximum power of the baseline 3-dimensional array. Tables 3-16 and 3-17 list the predicted array power and module voltage at maximum power of the baseline 3-dimensional array. Tables 3-16 and 3-17 list the predicted array power and module voltage at maximum power of the alternate, two dimensional concentrator array. The combined degradation and losses for the  $V_{mp}$  was taken to be 6% for both arrays.

The baseline 3-D concentrator array design assumptions and weight summary are shown in Tables 2-6 and 2-7. The same data for the alternate 2-D concentrator array are shown in Tables 2-9 and 2-10.



TABLE 3-14  
BASELINE ARRAY PERFORMANCE

AU DISTANCE	EFFECTIVE CONCENTRATION	TEMP °C	WING OUTOUT (KW)	ARRAY OUTPUT (KW)	ARRAY OUTPUT WITH LOSSES, DEGRADATION (12.5%) (KW)
1.0	1.9	103	45.5	91.0	79.6
1.1	1.9	85	43.3	86.5	75.7
1.1	3.5	140	31.5	63.1	55.2
2.0	3.5	27	15.9	60.1	52.6
3.0	3.5	-33	15.9	31.9	27.9
4.0	3.5	-66	9.77	19.5	17.1
4.5	3.5	-78	8.0	16.0	14.0

GROSS ARRAY UNCONCENTRATED POWER AT 1 A.U., 55°C IS 59 KW.

3-115

ORIGINAL PAGE IS  
OF POOR QUALITY

TABLE 3-15  
BASELINE ARRAY MODULE VOLTAGE

Sun Distance A. U.	Effective Concentration	Temp °C	392 Cell in Series Module Voltage	
			V <sub>mp</sub> (BOL) (Volts)	V <sub>mp</sub> (EOL) (Volts)
1.0	1.9	103	117.	110.
1.1	1.9	85	136.	128.
1.1	3.5	140	76.	71.
2.0	3.5	27	198.	186.
3.0	3.5	-33	259.	243.
4.0	3.5	-66	289.	272.
4.5	3.5	-78	300.	282.

TABLE 3-16

## ALTERNATE ARRAY POWER PERFORMANCE

AU DISTANCE	EFFECTIVE CONCENTRATION	TEMP °C	WING OUTPUT (KW)	ARRAY OUTPUT (KW)	ARRAY OUTPUT WITH LOSSES DEGRADATION (12.5%) (KW)
1.0	2.27	130	72.3	144.6	126.5
1.5	2.27	42	48.3	96.6	84.5
2.0	2.27	27	32.0	64.0	56.0
2.5	2.27	-9	23.3	46.6	40.8
3.0	2.27	-33	17.3	34.5	30.2
3.5	2.27	-52	12.8	25.6	22.4
4.0	2.27	-67	10.0	20.0	17.5
4.5	2.27	-80	8.0	16.0	14.0

GROSS ARRAY UNCONCENTRATED POWER AT 1 A.U., 55°C IS 85.9 KW.

TABLE 3-17  
ALTERNATE ARRAY MODULE VOLTAGE

Sun Distance A. U.	Effective Concentration	Temp °C	392 Cell Module	
			V <sub>mp</sub> (BOL) (Volts)	V <sub>mp</sub> (EOL) (Volts)
1.0	2.27	130	89.	84.
1.5	2.27	42	189.	178.
2.0	2.27	27	237.	223.
2.5	2.27	-9	262.	246.
3.0	2.27	-33	282.	265.
3.5	2.27	-52	300.	282.
4.0	2.27	-67	308.	290.
4.5	2.27	-80	312.	293.

3-118

ORIGINAL PAGE IS  
OF POOR QUALITY

### 3.6.6 Cost Data Summary

The estimated costs for the development and delivery of the baseline concentrator solar array flight system for HCR-SEP are summarized below. The ground rules and assumptions are:

- a. 1977 dollars
- b. Estimates include fee
- c. Deployment of the wings away from the spacecraft is included in the estimates. Wing tracking and rotary power transfer is not included in the estimates.
- d. Estimates do not include technology development.

<u>Cost Element</u>	<u>Cost Estimate</u>
A. Design, Drawings, Analysis and Specifications	
1. Blanket Assy	\$2,095K
2. Deployment Assy	560K
3. Blanket Storage Assy	550K
4. Side Reflectors	900K
	4105K
B. Tooling Design, Fabrication and Checkout	
1. Blanket Assy	80K
2. Deployment Assy	175K
3. Blanket Storage Assy	150K
4. Side Reflectors	450K
	855K
C. Engineering Test Hardware Materials and Fabrication	
1. Blanket Assy	275K
2. Deployment Assy	140K
3. Blanket Storage Assy	65K
4. Side Reflectors	250K
	730K

D.	Design Development Testing	
1.	Blanket Assy	95K
2.	Deployment Assy.	80K
3.	Blanket Storage Assy.	65K
4.	Side Reflectors	225K
		465K
E.	Qualification Test Hardware Materials and Fabrication	
1.	Blanket Assy (Includes 5,000 cell assys.)	160K
2.	Deployment Assy.	80K
3.	Blanket Storage Assy.	40K
4.	Side Reflectors	60K
		340K
F.	Component Qualification Testing	
1.	Blanket Assy.	45K
2.	Deployment Assy.	35K
3.	Blanket Storage Assy.	25K
4.	Side Reflectors	45K
		150K
G.	Engineering Model	
1.	Blanket Assy (Includes 10,000 cell assys)	480K
2.	Deployment Assy	420K
3.	Blanket Storage Assy	75K
4.	Side Reflectors	200K
5.	Integration and Assembly	35K
		1210K
H.	One New Wing Materials and Fabrication	
1.	Blanket Assy (Includes 250,000 cell assys)	6700K
2.	Deployment Assy	420K
3.	Blanket Storage Assy.	75K
4.	Side Reflectors	200K
5.	Integration, Assembly, Acceptance Test	65K
		7460K

**I. Refurbish Engineering Model**

1. Blanket Assy (Less 10,000 cell assys)	6450K
2. Deployment Assy (10% of new)	42K
3. Blanket Storage Assy (10% of new)	8K
4. Side Reflectors (10% of new)	20K
5. Integration, Assembly, Acceptance Test	65K

6585K

**J. Other Costs**

1. Ground Support Equipment Design and Fabrication	100K
2. Quality Assurance	250K
3. Manufacturing Test Equipment (In-process tests)	500K
4. Program Management, Reporting, Subcontract Monitoring	350K

1200K

**TOTAL**

**\$23.1M**

The estimated costs for the development and delivery of the alternate 2-D concentrator solar array flight system for HCR-SEP are summarized below. The ground rules and assumptions are the same as for the baseline concentrator array.

<u>Cost Element</u>	<u>Cost Estimate</u>
A. Design, Drawings, Analysis and Specifications	
1. Blanket Assy	\$1,465K
2. Deployment Assy	560K
3. Blanket Storage Assy	550K
4. Side Reflectors	900K
	3475K
B. Tooling Design, Fabrication and Checkout	
1. Blanket Assy	55K
2. Deployment Assy	175K
3. Blanket Storage Assy	150K
4. Side Reflectors	450K
	830K
C. Engineering Test Hardware Materials and Fabrication	
1. Blanket Assy	195K
2. Deployment Assy	140K
3. Blanket Storage Assy	65K
4. Side Reflectors	150K
	550K
D. Design Development Testing	
1. Blanket Assy	70K
2. Deployment Assy	80K
3. Blanket Storage Assy	65K
4. Side Reflectors	190K
	405K



<b>E. Qualification Test Hardware Materials and Fabrication</b>		
1.	Blanket Assy (Includes 5,000 cell assys.)	150K
2.	Deployment Assy	75K
3.	Blanket Storage Assy.	40K
4.	Side Reflectors	60K
		325K
<b>F. Component Qualification Testing</b>		
1.	Blanket Assy.	45K
2.	Deployment Assy.	35K
3.	Blanket Storage Assy.	25K
4.	Side Reflectors	45K
		150K
<b>G. Engineering Model</b>		
1.	Blanket Assy (Includes 10,000 cell assys)	410K
2.	Deployment Assy	330K
3.	Blanket Storage Assy	75K
4.	Side Reflectors	180K
5.	Integration and Assembly	35K
		1030K
<b>H. One New Wing Materials and Fabrication</b>		
1.	Blanket Assy (Includes 358,000 cell assys)	9150K
2.	Deployment Assy.	390K
3.	Blanket Storage Assy.	75K
4.	Side Reflectors	180K
5.	Integration, Assembly, Acceptance Test	65K
		9860K

I.	Refurbish Engineering Model		
1.	Blanket Assy (Less 10,000 cell assys)	8900K	
2.	Deployment Assy (10% of new)	39K	
3.	Blanket Storage Assy (10% of new)	8K	
4.	Side Reflectors (10% of new)	18K	
5.	Integration, Assembly, Acceptance Test	65K	
			9030K
J.	Other Costs		
1.	Ground Support Equipment Design and Fabrication	90K	
2.	Quality Assurance	240K	
3.	Manufacturing Test Equipment (In-process tests)	500K	
4.	Program Management, Reporting, Subcontract Monitoring	350K	
			1180K
		TOTAL	\$26.8M

### 3.7 PROBABILITY OF ARRAY PROGRAM ACHIEVEMENT

The probability of achieving the desired HCR-SEP solar array system performance and flight hardware delivery schedule was assessed for four solar array design concepts. Two are planar array concepts with specific powers of 200 W/kg and 240 W/kg where the initial power is assumed to be sufficient to perform the mission in the associated environments. One is the baseline three-dimensional concentrator array and one is the alternate two-dimensional concentrator array. The two major risk areas are timely successful attainment of the required technology advances and timely accomplishment of the flight hardware design development, fabrication, and ground testing.

The solar cell/cover assembly performance to be achieved is a key technology area for all the concepts. The risk for the 3 mil, 12.5% efficient cell (200 W/kg), the 2 mil, 12.6% efficient cell (240 W/kg), and the 5 mil, wraparound contact, 13% efficient cell (concentrator array designs) are considered equal for both design achievement and good fabrication yield achievement. The timely attainment of a stable thin (1 mil) cover system for the 200 and 240 W/kg designs is considered a higher risk problem than the 3 mil CMS covers on the concentrator array designs. This factor is significant in rating the planar arrays as higher risks than the concentrator arrays. The 240 W/kg design is rated a slightly higher risk than the 200 W/kg as the 240 W/kg cell design (2 mils) to be developed and fabricated in quantity is thinner than the 3 mil cell for the 200 W/kg design while both require nearly the same efficiency.

All four concepts employ a thin printed circuit substrate and the risk associated with the technology development and fabrication of the large area substrates is considered very small. The conventional contact thin cells for the planar arrays will require more operations for cell joining but the risk associated with these operations is associated with developing a high rate cell bonding technique that is compatible with the cell structural capability and minimum electrical performance degradation.

The attainment of the required reflector technology readiness is a slight risk. The 3-D concentrator requires both in-blanket and side reflectors, and, to meet the weight limitation, requires a more complicated articulation for array deployment and extension

than the 2-D concentrator array. For this reason the 3-D concentrator design is rated a slightly higher risk in development than the 2-D concentrator design.

The available time for development, fabrication, and test of the flight hardware is about 25 months. This time period is typically sufficient for new solar array programs where the number of new technology concepts being applied is modest. The size of the HCR-SEP array wings, the amount of blanket hardware to be fabricated, and the new concentrator array design tend to increase the risk associated with this part of the program. Off-setting this, however, is the fact that the proposed technology development program is directed not only at component performance attainment, but also at the fabrication, handling, and testing problems that are associated with the large area concentrator solar array hardware. The probability of achievement for the array programs is highly dependent on the technology program success probability.

Based on the above discussion the probability of achievement of a successful HCR-SEP Solar Array Program (performance and schedule) is:

200 W/kg	80%
240 W/kg	77%
3-D Concentrator	89%
2-D Concentrator	91%

The above estimates are developed from estimates of the probability of achieving the key milestones of each design in series.

The solar cell technology achievement probability is 0.98 for all four designs.

The cell cover technology achievement probability for the 3 mil CMS cover is 0.99 and for the 1 mil organic cover 0.85.

The timely fabrication and delivery risk for the 2 mil cells for the planar array is 0.93 and for the 3 mil cells is 0.97. The same risk for the 5 mil wraparound contact cells is 0.97.

The reflector technology achievement risk is 0.98 for both concentrator designs.

The timely development of the array packaging and deployment mechanisms and structure within weight constraints has a probability of 0.99 for the planar arrays, 0.98 for the 3-D concentrator array and 0.99 for the 2-D concentrator array.

The resulting program achievement probabilities are then:

$$200 \text{ W/kg}, 0.98 \times 0.85 \times 0.97 \times 0.99 = 0.80$$

$$240 \text{ W/kg}, 0.98 \times 0.85 \times 0.93 \times 0.99 = 0.77$$

$$3\text{-D Concentrator } 0.98 \times 0.99 \times 0.97 \times 0.98 \times 0.97 = 0.89$$

$$2\text{-D Concentrator } 0.98 \times 0.99 \times 0.97 \times 0.98 \times 0.99 = 0.91$$

#### 4.0 REFERENCES

1. Solar Cell Array Design Handbook, Vols 1 and 2, NASA-JPL SP 43-38, October 1976.
2. Solar Cell Space Manual, Centralab.
3. W. Luft, "Radiation Effects On High Efficiency Silicon Solar Cells," 1976 IEEE Annual Conference on Nuclear and Space Radiation Effects, San Diego, CA, 27-30 July 1976.
4. R. E. Patterson, R. K. Yasui, "Parametric Performance Characteristics and Treatment of Temperature Coefficients of Silicon Solar Cells for Space Application," NASA-JPL Contract No. NAS7-100, Technical Report 32-1582, 15 May 1973.
5. John A. Castle, "Design Criteria For High Efficiency Silicon Solar Cells With Concentration," Twelfth IEEE Photovoltaic Specialists Conference-1976, Baton Rouge, Louisiana, 15-18 November 1976.
6. John A. Scott-Monck, "Advanced Silicon Solar Cell Production Technology," AIAA Conference On The Future of Aerospace Power Systems.
7. W. Szmyd, "1976 High Efficiency Solar Cell Independent Development Program," LMSC-D492695, 1977.
8. "Development of a Weldable and Solderable High Efficiency Solar Cell Assembly," Spectrolab, Inc., LMSC Contract Status Review, 29 March 1977.
9. Pilkington P. E., Limited CMS Solar Cell Coverslips Product Specification, Issue: B, 29 October 1973.
10. L. A. Haslim, et al, "A Highly Stable Clear Fluorocarbon Coating For Thermal Control and Solar Cell Applications," AIAA 12th Aerospace Sciences Meeting, Washington, D. C., 30 January-1 February 1974.
11. G. J. Rayl, et al, Final Oral Report, Phase 1, "Conceptual Approach Study, 200 W/Kg Solar Array," NASA-JPL Contract No. 954393, 13 January 1977.
12. Private Conversations with persons at OCLI, Santa Clara Division, April-May 1977.
13. H. L. Petersen, Internal Report, "Investigation of Solar Cell Metalization," EM No. 213-6381, 16 June 1976.
14. T. C. Tisone, J. Drubeck, "Diffusion in Thin Film Ti-Au, Ti-Pd, and TiPt Couples," The Journal of Vacuum Science and Technology, Vol. 9 No. 1, 28 July 1971.

15. Solar Cell Selection And Characterization For Solar Electric Propulsion, Boeing Aerospace Company, Final Report NASA-MSFC Contract No. NAS8-31670, May 1977.
16. Robert H. Josephs, "A Lightweight Solar Array Study," JPL Publication 77-3, 15 February 1977.
17. John A. Scott-Monck, "Advanced High Efficiency Wraparound Contact Solar Cell," AIAA Conference On The Future of Aerospace Power Systems, Ibid.
18. H. S. Rauschenbach, M. D. Cannady, "Final Report, Flexible, FEP-Teflon Covered Solar Cell Module Development," NASA-LRC Contract No. NAS8-16742, 13 October 1976.
19. Lee Goldhammer, "Final Report, ATS-6 Solar Cell Experiment/Improvement," NASA-GSFC Contract No. NAS5-22873, 31 January 1977.
20. T. Faith, "Solar Array Synthesis Computer Program," NASA-GSFC Contract No. NAS5-21642, April 1973.
21. B. Anspaugh, "Parametric Testing of Solarex 2 mil Solar Cells," Engineering Memos #341-015A and #341-018A, 4 and 13 April 1977.
22. Private conversations with LMSC Thermophysics Dept., May 16, 1977.
23. H. Brandhorst, NASA-LeRC, private conversation, June 1977.
24. M. Field, Pantech, Inc., private conversation, July 1977.

ORIGINAL PAGE IS  
OF POOR QUALITY

TABLE 1  
CELL TEMPERATURES WITHOUT CONCENTRATION

SUN DISTANCE -A. U.	INTENSITY -SUNS	SOLAR CELL THERMOCOUPLE READINGS - °C												
		1	2	3	4	5	6	7	8	9	10	11	12	Avg
4.98	0.0403	-114.4	-114.4	-111.7	-111.4	-110.0	-111.1	-111.1	-110.0	-114.4	-113.3	-115.0	-114.4	-112.8
4.27	0.0545	-105.6	-105.6	-102.2	-100.6	-99.4	-101.1	-101.1	-100.0	-105.0	-103.3	-106.1	-105.0	-102.8
3.605	0.077	-93.9	-95.0	-92.8	-91.7	-90.0	-92.2	-91.7	-90.0	-92.8	-90.6	-92.2	-90.6	-91.9
3.098	0.1042	-80.0	-82.2	-79.4	-78.9	-76.7	-78.9	-78.3	-77.2	-79.4	-77.8	-79.4	-77.8	-78.4
2.48	0.163	-54.4	-60.0	-56.7	-58.3	-55.0	-58.3	-57.2	-57.2	-57.8	-58.3	-58.9	-57.8	-57.5
2.22	0.2023	-42.2	-47.2	-45.6	-46.1	-43.3	-47.2	-45.6	-46.1	-46.7	-47.8	-47.8	-47.8	-46.1
1.796	0.310	-17.2	-22.8	-21.1	-21.1	-20.6	-23.3	-19.4	-20.6	-22.2	-23.3	-23.3	-24.4	-21.6
1.566	0.408	0.0	-6.1	-5.6	-4.4	-5.6	-7.2	-3.9	-2.2	-5.6	-6.7	-6.7	-8.3	-5.2
1.412	0.502	16.1	10.6	10.6	12.2	10.0	8.9	11.7	15.0	9.4	10.6	8.9	7.8	11.1
1.292	0.599	28.3	22.8	22.8	25.6	21.7	22.2	23.3	28.3	21.1	23.9	20.6	20.6	23.4
1.193	0.702	41.1	35.6	35.6	38.3	34.4	34.4	35.0	41.1	33.3	37.2	32.8	32.8	36.0
1.0	1.00	71.1	66.7	66.1	70.0	63.9	66.1	65.0	71.1	64.4	67.8	62.8	62.2	66.4
4.88	0.042	-108.9	-108.2	-107.8	-107.2	-106.1	-105.0	-105.0	-106.7	-110.6	-108.9	-108.9	-108.9	-107.7

APPENDIX A  
36-CELL MODEL CONCENTRATOR TEST DATA



TABLE 2  
ELECTRICAL PERFORMANCE WITHOUT CONCENTRATION - CIRCUIT NO. 1

SUN DISTANCE, - A. U.	INTENSITY, - SUNS	I <sub>sc</sub> - m. a.	P <sub>mp</sub> - watts	Avg. Cell Temp. - °C	V <sub>oc</sub> - volts	V <sub>mp</sub> volts
4.98	0.0403	32.7	0.0405	-112.8	3.22	1.62
4.88	0.042	34.1		-107.7	3.31	1.68
4.27	0.0549	45.5	0.065	-102.8	3.74	2.00
3.605	0.077	61.4	0.0979	-91.9	4.06	2.25
3.098	0.1042	86.1	0.163	-78.9	4.25	2.76
2.48	0.163	147.9	0.339	-57.5	4.17	3.23
2.22	0.2023	184.8	0.448	-46.1	4.09	3.32
1.796	0.310	280.7	0.734	-21.6	3.85	3.19
1.566	0.408	363.5	0.939	-5.2	3.67	3.03
1.412	0.502	448.0	1.117	11.1	3.50	2.90
1.292	0.599	540.0	1.306	23.4	3.35	2.75
1.193	0.702	631.3	1.439	36.0	3.21	2.62
1.0	1.00	909.5	1.760	66.4	2.87	2.20

A-2

ORIGINAL PAGE IS  
OF POOR QUALITY

C-3

TABLE 3  
ELECTRICAL PERFORMANCE WITHOUT CONCENTRATION, CIRCUIT NO. 2

SUN DISTANCE - A. U.	INTENSITY - SUNS	I <sub>sc</sub> - amps	P <sub>mp</sub> - watts	Avg. Cell Temp - °C	V <sub>oc</sub> - volts	V <sub>mp</sub> - volts
4.98	0.0403	31.8	0.0444	-112.8	3.92	1.85
4.88	0.042	33.1	0.047	-107.7	3.94	1.89
4.27	0.0549	44.1	0.0715	-102.8	4.15	2.20
3.605	0.077	65.8	0.120	-91.9	4.23	2.93
3.098	0.1042	91.8	0.199	-78.9	4.22	3.11
2.48	0.163	144.0	0.371	-57.5	4.10	3.30
2.22	0.2023	178.6	0.476	-46.1	4.03	3.34
1.796	0.310	275.5	0.759	-21.6	3.85	3.23
1.566	0.408	358.0	0.964	-5.2	3.67	3.06
1.412	0.502	442.8	1.153	11.1	3.53	2.92
1.292	0.599	541.0	1.306	23.4	3.35	2.75
1.193	0.702	626.6	1.473	36.0	3.23	2.63
1.0	1.00	904.9	1.793	66.4	2.88	2.27

A-3

PRECEDING PAGE BLANK NOT FILMED

TABLE 4  
ELECTRICAL PERFORMANCE WITHOUT CONCENTRATION, CIRCUIT 1 & CIRCUIT 2

SUN DISTANCE - A. U.	INTENSITY - SUNS	I <sub>sc</sub> - ma	P <sub>mp</sub> - watts	AVG. CELL TEMP - °C	V <sub>oc</sub> - Volts	V <sub>mp</sub> - Volts
4.98	0.0403	31.9	0.040	-112.8	7.06	3.48
4.88	0.042	33.4	0.088	-107.7	7.10	3.65
4.27	0.0549	44.5	0.1349	-102.8	7.86	4.15
3.605	0.077	62.2	0.214	-91.9	8.25	4.75
3.098	0.1042	86.4	0.355	-78.9	8.45	5.54
2.48	0.163	144.4	0.699	-57.5	8.28	6.50
2.22	0.2023	178.6	0.924	-46.1	8.12	6.60
1.796	0.310	275.8	1.484	-21.6	7.68	6.45
1.566	0.408	357.8	1.885	-5.2	7.32	6.05
1.412	0.502	443.1	2.244	11.1	7.02	5.68
1.292	0.599	535.0	2.585	23.4	6.70	5.62
1.193	0.702	628.0	2.873	36.0	6.43	5.13
1.0	1.00	906.0	3.520	66.4	5.76	3.52

TABLE 5  
CELL TEMPERATURES WITH CONCENTRATION

SUN DISTANCE - A. U.	INTENSITY - SUNS	SOLAR CELL THERMOCOUPLE READINGS - °C												
		1	2	3	4	5	6	7	8	9	10	11	12	AVG.
4.98	0.0403	-51.8	-60	-56.7	-63.3	-55.6	-71.1	-72.2	-60.5	-65.6	-60.5	-63.3	-61.7	-62.4
4.83	0.043	-51.1	-57.2	-53.3	-55.6	-47.8	-57.8	-57.8	-51.1	-56.1	-55.0	-56.7	-53.9	-54.4
4.27	0.0549	-38.9	-43.3	-42.2	-47.8	-37.8	-56.7	57.2	-45.0	-50.0	-45.6	-47.8	-46.7	-46.6
3.64	0.0753	-18.9	-25.6	-24.4	-30.0	-18.9	-39.4	-40.6	-25.0	-31.1	-27.8	-30.0	-28.3	-28.3
3.08	0.105	4.4	-3.3	-4.4	-8.3	1.7	-21.9	-23.9	-3.3	-12.8	-7.8	-10.6	-7.2	-8.1
2.48	0.163	34.4	29.4	30.0	24.4	28.9	7.2	3.9	32.2	15.0	21.7	18.9	24.4	22.5
2.22	0.202	48.9	43.9	46.7	41.7	40.6	20.0	21.1	57.1	31.1	40.0	35.0	41.1	38.4
1.80	0.307	90.6	85.0	82.8	81.1	81.1	56.1	50.6	95.0	71.1	77.8	72.2	81.7	77.1
1.58	0.401	119.4	109.4	108.3	107.2	117.2	86.7	78.3	123.9	97.2	102.8	102.2	110.6	105.3
1.41	0.502	145.0	129.4	129.4	129.4	142.8	122.2	114.4	143.3	122.2	134.4	126.1	135.6	131.2
1.69	0.350	108.3	91.1	92.8	94.4	103.9	84.4	81.1	107.2	88.9	96.7	87.2	97.2	94.4

TABLE 6  
REFLECTOR TEMPERATURES WITH CONCENTRATION

SUN DISTANCE - A. U.	INTENSITY - SUNS	END REFLECTOR TEMP - °C				SIDE REFLECTOR TEMP - °C			
		13	14	15	AVG.	16	17	18	AVG.
4.98	0.0403	-198.3	-158.3	-165.0	-157.2	-129.4	-140.1	-146.7	-138.9
4.83	0.043	-128.9	-150.6	-158.9	-146.1	-94.4	-116.7	-125.6	-147.1
4.27	0.0549	-145.6	-156.7	-162.8	-155.0	-124.4	-135.6	-142.8	-134.5
3.64	0.0753	-140.5	-153.9	-160.0	-151.5	-116.1	-128.4	-135.6	-126.9
3.08	0.105	-134.4	-149.4	-155.6	-146.5	-106.1	-120.0	-128.3	-118.3
2.48	0.163	-122.2	-142.2	-148.3	-137.6	-88.9	-106.2	-115.6	-103.7
2.22	0.202	-113.8	-137.8	-143.9	-131.9	-78.9	-98.9	-108.9	-95.6
1.80	0.307	-94.4	-127.2	-133.3	-118.3	-55.6	-81.1	-96.7	-76.1
1.69	0.350	-83.9	-121.1	-128.3	-111.1	-38.8	-70.0	-80.0	-62.8
1.58	0.401	-82.2	-120.0	-126.7	-109.6	-40.0	-69.4	-80.0	-63.1
1.41	0.502	-71.1	-113.3	-119.9	-101.3	-25.0	-57.8	-68.9	-50.6

TABLE 7  
ELECTRICAL PERFORMANCE WITH CONCENTRATION, CIRCUIT 1

SUN DISTANCE - A. U.	INTENSITY - SUNS	I <sub>sc</sub> - mA	P <sub>mp</sub> - watts	AVG. CELL Temp. - °C	V <sub>oc</sub> - Volts	V <sub>mp</sub> - Volts	I <sub>sc</sub> With Temp. Corr. -mA
4.98	0.0403	119.9	0.296	-62.4	4.17	3.12	119.0
4.83	0.043	142.4	0.342	-54.4	4.18	3.18	141.4
4.27	0.0549	168.7	0.456	-46.6	4.10	3.20	167.3
3.64	0.0753	239.0	0.662	-28.3	3.88	3.27	236.9
3.08	0.105	335.9	0.936	-8.1	3.71	3.07	332.6
2.48	0.163	504.3	1.279	22.5	3.30	2.75	497.8
2.22	0.202	613.8	1.446	38.4	3.12	2.63	605.2
1.80	0.307	966.2	1.832	77.1	2.69	2.13	951.0
1.58	0.401	1314	1.886	105.3	2.35	1.64	1291.9
1.41	0.502	1760	1.863	131.2	2.06	1.39	1730.4
1.69	0.350	1229	1.882	94.4	2.50	1.81	—

TABLE 8  
ELECTRICAL PERFORMANCE WITH CONCENTRATION, CIRCUIT 2

SUN DISTANCE - A. U.	INTENSITY - SUNS	I <sub>sc</sub> - mA	AVG. CELL Temp. - °C	V <sub>oc</sub> - Volts	V <sub>mp</sub> - Volts	I <sub>sc</sub> With Temp. Corr. - mA
4.98	0.0403	120.6	-62.4	4.12	3.06	117.3
4.83	0.043	144.3	-54.4	4.14	3.30	143.3
4.27	0.0549	169.7	-46.6	4.09	3.25	168.3
3.64	0.0753	237.0	-28.3	3.87	3.24	234.7
3.08	0.105	333.6	-8.1	3.74	3.14	330.0
2.48	0.163	526.1	22.5	3.33	2.73	519.8
2.22	0.202	654.6	38.4	3.15	2.52	646.3
1.80	0.307	977.0	77.1	2.70	2.07	962.0
1.69	0.350	1221	94.4	2.54	1.83	-
1.58	0.401	1302	105.3	2.40	1.71	1280
1.41	0.502	1760	131.2	2.08	1.38	1731

A-8

ORIGINAL PAGE IS  
OF POOR QUALITY

TABLE 9

ELECTRICAL PERFORMANCE WITH CONCENTRATION CIRCUIT 1 &amp; CIRCUIT 2

SUN DISTANCE - A. U.	INTENSITY - SUNS	I <sub>sc</sub> - mA	P <sub>mp</sub> - watts	AVG. CELL Temp. - °C	V <sub>oc</sub> - volts	V <sub>mp</sub> -volts	I <sub>sc</sub> With Temp. Corr. -mA
4.98	0.0403	—					
4.83	0.043	142.6	0.709	- 54.4	8.36	6.30	141.6
4.27	0.0549	—					
3.64	0.0753	—					
3.08	0.105	336.9	1.875	- 8.1	7.45	6.25	333.5
2.48	0.163	512.9	2.651	22.5	6.68	5.70	506.5
2.22	0.202	630.0	2.913	38.4	6.27	5.11	621.7
1.80	0.307	975.7	3.676	77.1	5.46	4.13	960.7
1.58	0.401	1315	3.800	105.3	4.74	3.33	1293
1.41	0.502	1760	3.780	131.2	4.20	2.70	1731





TABLE 1  
20-CELL MODULE CALIBRATION

CELL NUMBER	INTENSITY SUNS	I <sub>sc</sub> mA	P <sub>mp</sub> watts	CELL TEMP -°C	V <sub>oc</sub> V
30	1.000	298.2	0.134	30.0	0.59
29		289.6	0.128	32.2	0.59
27		301.3	0.134	28.9	0.59
20		290.2	0.129	30.6	0.59
15		293.0	0.131	31.1	0.59
17		301.3	0.129	29.4	0.59
11		296.4	0.130	29.4	0.59
8		291.8	0.126	31.1	0.58
62		309.1	0.139	30.0	0.59
32		301.7	0.133	32.2	0.58
31		301.0	0.135	29.4	0.59
21		305.6	0.134	30.6	0.58
28		304.1	0.133	30.0	0.57
19		307.1	0.133	31.1	0.59
18		300.2	0.132	30.6	0.58
13		303.1	0.130	31.1	0.58
12		296.8	0.130	30.0	0.59
5		301.5	0.129	30.0	0.58
33		293.2	0.130	31.7	0.58
61		303.7	0.139	30.0	0.59

TABLE 2  
ELECTRICAL PERFORMANCE AT 5.04 A. U.

CELL NUMBER	INTENSITY SUNS	I <sub>sc</sub> mA	P <sub>mp</sub> watts	CELL TEMP- °C	V <sub>oc</sub> V	V <sub>mp</sub> V	I <sub>sc</sub> With Temp. Corr. mA
30	0.0394	48.8	0.028	-73.9	0.76	0.64	48.1
29		40.2	0.021	-73.9	0.76	0.66	39.5
27		48.2	0.0265	-74.4	0.74	0.62	47.5
20		39.9	0.022	-74.4	0.75	0.66	39.2
15		42.5	0.024	-85.0	0.75	0.65	42.0
17		48.6	0.0255	-85.0	0.73	0.61	48.1
11		43.8	0.024	-70.0	0.75	0.65	43.0
8		39.5	0.0205	-70.0	0.75	0.64	38.7
62		42.9	0.025	-87.8	0.78	0.66	42.5
32		47.2	0.0275	-87.8	0.75	0.63	46.8
31		42.7	0.026	-75.6	0.77	0.65	42.0
21		48.1	0.0255	-75.6	0.76	0.64	47.4
28		43.9	0.022	-71.1	0.75	0.63	40.6
19		48.3	0.0272	-71.1	0.75	0.64	47.6
18		44.1	0.023	-70.0	0.75	0.65	43.3
13		48.2	0.026	-70.0	0.75	0.62	47.4
12		43.1	0.0245	-99.4	0.75	0.64	42.9
5		45.6	0.026	-99.4	0.74	0.62	45.4
33		39.4	0.0235	-88.9	0.77	0.64	39.0
61		46.2	0.027	-88.9	0.78	0.67	45.8

TABLE 3  
ELECTRICAL PERFORMANCE AT 3.605 A.U.

CELL NUMBER	INTENSITY SUNS	I <sub>sc</sub> mA	P <sub>mp</sub> Watts	CELL TEMP-°C	V <sub>oc</sub> V	V <sub>mp</sub> V	I <sub>sc</sub> With Temp.Corr. mA
30	0.077	91.6	0.0515	-37.2	0.70	0.61	89.8
29		79.7	0.043	-37.2	0.71	0.62	77.9
27		91.2	0.050	-37.8	0.69	0.59	89.4
20		77.4	0.043	-37.8	0.70	0.62	75.6
15		80.4	0.0455	-59.4	0.69	0.61	79.3
17		91.8	0.0475	-59.4	0.68	0.57	90.7
11		83.0	0.045	-33.3	0.69	0.60	81.0
8		78.4	0.0415	-33.3	0.69	0.60	76.4
62		83.6	0.0495	-53.3	0.74	0.65	82.3
32		95.0	0.0545	-53.3	0.71	0.61	93.7
31		83.6	0.049	-35.6	0.70	0.62	81.7
21		96.5	0.053	-35.6	0.70	0.61	94.6
28		85.6	0.045	-33.3	0.69	0.59	83.6
19		98.0	0.053	-33.3	0.68	0.59	96.0
18		84.5	0.0455	-31.6	0.69	0.60	82.5
13		94.9	0.0515	-31.6	0.69	0.59	90.7
12		84.3	0.0455	-77.2	0.68	0.58	83.8
5		90.6	0.0480	-77.2	0.68	0.58	90.1
33		79.0	0.0470	-53.9	0.73	0.65	77.7
61	↓	89.3	0.053	-53.9	0.72	0.64	88.0

TABLE 4  
ELECTRICAL PERFORMANCE AT 2.469 A.U.

CELL NUMBER	INTENSITY SUNS	I <sub>sc</sub> mA	P <sub>mp</sub> Watts	CELL TEMP-°C	V <sub>oc</sub> V	V <sub>mp</sub> V	I <sub>sc</sub> With Temp. Corr. mA
30	0.164	202.6	0.0925	22.8	0.59	0.495	196.2
29		178.1	0.0813	22.8	0.60	0.51	171.7
27		198.7	0.0888	18.9	0.58	0.48	192.6
20		175.0	0.0813	18.9	0.59	0.50	168.9
15		186.7	0.085	-26.7	0.58	0.485	184.3
17		205.6	0.0863	-26.7	0.56	0.46	203.2
11		196.6	0.085	22.2	0.58	0.475	189.3
8		180.1	0.080	22.2	0.58	0.48	173.8
62		180.3	0.0913	1.7	0.63	0.54	175.6
32		204.2	0.0975	1.7	0.60	0.51	199.5
31		180.7	0.0838	22.2	0.59	0.50	174.4
21		211.7	0.095	22.2	0.59	0.49	205.4
28		189.0	0.0825	23.9	0.58	0.49	182.6
19		206.1	0.090	23.9	0.57	0.47	199.7
18		185.0	0.0825	24.4	0.57	0.47	178.5
13		207.4	0.0913	24.4	0.58	0.48	200.9
12		182.2	0.080	-43.9	0.57	0.475	181.1
5		201.9	0.0875	-43.9	0.57	0.47	200.8
33		185	0.0925	5.6	0.62	0.525	180.0
61		204.9	0.095	5.6	0.60	0.515	199.9

TABLE 5  
ELECTRICAL PERFORMANCE AT 1.82 A. U.

CELL NUMBER	INTENSITY SUNS	I <sub>sc</sub> mA	P <sub>mp</sub> Watts	CELL TEMP-°C	V <sub>oc</sub> V	V <sub>mp</sub> V	I <sub>sc</sub> With Temp. Corr. mA
30	0.302	377.2	0.1263	78.3	0.48	0.39	361.8
29		378.2	0.1238	78.3	0.47	0.37	362.8
27		364.8	0.1225	82.2	0.48	0.375	348.8
20		368.6	0.120	82.2	0.47	0.365	352.6
15		377.8	0.120	2.2	0.47	0.36	374.1
17		371.0	0.1113	2.2	0.46	0.345	367.3
11		362.5	0.115	82.8	0.47	0.36	346.4
8		368.4	0.1175	82.8	0.47	0.36	352.3
62		332.1	0.1288	55.0	0.53	0.425	320.3
32		370.6	0.130	55.0	0.49	0.39	358.8
31		337.6	0.115	64.4	0.48	0.38	324.3
21		375.1	0.125	64.4	0.48	0.38	361.8
28		362.4	0.1175	80.6	0.47	0.365	346.6
19		376.5	0.120	80.6	0.47	0.365	360.7
18		363.7	0.1187	82.2	0.48	0.37	347.7
13		382.8	0.1238	82.2	0.48	0.37	366.8
12		337.0	0.1075	-11.0	0.47	0.36	335.4
5		368.4	0.115	-11.0	0.47	0.365	366.8
33		381.7	0.1325	71.1	0.49	0.385	367.4
61		392.8	0.135	71.1	0.49	0.385	378.5



DEVELOPMENT OF A HIGH EFFICIENCY  
THIN SILICON SOLAR CELL

JPL CONTRACT NO. 954290

SEPTEMBER 1977

FINAL REPORT

REPORT NO. SX/105/F

BY

JOSEPH LINDMAYER &  
CHARLES Y. WRIGLEY

SOLAREX CORPORATION  
1335 PICCARD DRIVE  
ROCKVILLE, MARYLAND 20850

This work was performed for the Jet Propulsion  
Laboratory, California Institute of Technology  
Sponsored by the National Aeronautics and Space  
Administration under contract NAS-7100.

**SOLAREX CORPORATION**

1335 PICCARD DRIVE □ ROCKVILLE, MD 20850 □ 301 948 0202 □ TWX: 710 828 9709 □ CABLE ADDRESS: SOLAREX

TECHNICAL CONTENT STATEMENT

This report contains information prepared by Solarex Corporation under JPL subcontract. Its content is not necessarily endorsed by the Jet Propulsion Laboratory, California Institute of Technology, or the National Aeronautics and Space Administration.



## ABSTRACT

This report documents a highly successful program performed by Solarex for JPL/NASA-OAST in developing high-efficiency ultra-thin (40 - 60 microns) silicon solar cells for lightweight space power systems and proceeding to pilot production.

A key to the success of this program was the breakthrough development of a technology for producing ultra-thin silicon slices which are very flexible, resilient, and tolerant of moderate handling abuse. The solar cell fabrication process developed to be compatible with these slices has generated thousands of ultra-thin solar cells at a respectable yield with average AM0 conversion efficiencies of 11%, and a few experimental samples reaching efficiencies above 12%. The guiding philosophy through this stage of development was to both improve cell efficiencies and develop a cell fabrication process amenable to high manufacturing yields, so that these ultra-thin solar cells are producible and not laboratory curiosities. For example, textured surfaces were not aggressively pursued to improve optical coupling, because that would require shadow masking for the gridline pattern, which was prone to increase breakage losses in processing as compared to photolithographic gridline generation.

Experimental topics investigated were thinning technology, gaseous junction diffusion, aluminum back alloying, internal reflectance, tantalum oxide anti-reflective coating optimization, slice flexibility, handling techniques, production rate limiting steps, low temperature behavior and radiation tolerance.

ORIGINAL PAGE IS  
OF POOR QUALITY

## TABLE OF CONTENTS

	<u>Page</u>
Abstract	2
I. Introduction	4
II. Program Description	
A. General	6
B. Work Plan & Schedule	7
III. Technical Discussion	
A. Silicon Thinning Technology	12
B. Anti-reflection Coating Optimization	15
C. Internal Reflection	21
D. Diffusion Optimization	27
E. Czochralski vs. Float Zone Silicon	33
F. Aluminum Deposition & p <sup>+</sup> Alloy Schedule	33
G. Power Output vs. Thickness	37
H. Excess Forward Current & Low-Temperature Behavior	41
I. Flexibility & Fracture Limits	47
J. Stability Tests	50
K. Minimization of Bowing	54
L. Absorptance & Emittance Measurements	56
M. Handling Techniques	57
N. Production Rate-Limiting Steps	59
O. Radiation Resistance	60
P. Pilot Line Program	62
Q. Fabrication Process Developed	63
IV. Conclusions & Recommendations	67
V. Appendix: Pilot Line Report	68

## I. INTRODUCTION

This highly successful program was performed by the Solarex Corporation for the Jet Propulsion Laboratory under the auspices of NASA-OAST. It was performed over a 24 month period and resulted in very high power-to-weight ratio silicon solar cells reaching down to 30 microns thickness. The key breakthrough making such ultra-thin solar cells possible was the development of a process for producing extremely thin silicon slices while leaving the surfaces parallel, avoiding preferential perforation and not introducing stresses which would make the slices brittle. This process uses a very hot sodium hydroxide (NaOH) etch and results in ultra-thin slices of excellent flexibility and resistance to breakage in handling. This breakthrough occurred at a time when the majority of the photovoltaic community had concluded that it was not feasible to fabricate ultra-thin silicon solar cells in this thickness range.

NASA-OAST recognized the implications of this breakthrough in ultra-lightweight silicon solar cells and seized the opportunity to accelerate reduction to manufacturing practice with a Pilot Line effort in the second quarter of the second year of this program. That acceleration by NASA-OAST provided thousands of ultra-thin silicon solar cells to familiarize the photovoltaic community with the properties of these cells, their handling techniques, assembly technology adaptation and assessment of the high power-to-weight ratios that can be obtained. The fabrication technology was frozen for the Pilot Line effort at a stage which produced 50 micron thick solar cells with 11% conversion efficiencies at AM0. (These had a higher power-to-weight ratio than 75 micron cells with 12% efficiencies, and were chosen as the Pilot Line vehicle for that reason as well as for optimum flexibility.)

These ultra-thin solar cells also have improved radiation tolerance as compared to 200-250 micron silicon solar cells, since they simply do not have beginning-of-life efficiencies dependent on long minority carrier diffusion lengths in a thick slice of silicon.

Although the frozen technology employed in the Pilot Line effort produced 11% conversion efficiencies for 50-micron-thick solar cells, the laboratory efforts have resulted in 50 micron cells with AMO conversion efficiencies of up to 12.5%. Further efforts on optimizing the fabrication parameters would, no doubt, result in very reproducible conversion efficiencies in excess of 12% for cells only 50 microns thick.

## II. PROGRAM DESCRIPTION

### A. General

This program was initiated in September 1975 with the objective of improving process parameters which influence the performance of high-efficiency, thin silicon solar cells. Near the end of the first year of effort a breakthrough was achieved at Solarex in developing a technology to produce very flexible ultra-thin silicon slices. This in turn made possible the subsequent fabrication of extremely lightweight high efficiency solar cells only some 40 - 60 microns in thickness.

The second twelve months of this program had efforts concentrated on ultra-thin solar cells (40-60 microns in thickness). Early in 1977, at the direction of NASA-OAST and JPL a Pilot Line was set up which fabricated pilot-production quantities of these ultra-thin solar cells. After this Pilot Line effort, the remaining four months of the contract term were concentrated on further improving the efficiency of ultra-thin solar cells.

This program encompassed a wide spectrum of R&D activities from experimental n on p cell fabrication technology analysis through evaluation of thin-cell handling techniques, determination of electrical and mechanical stability, identification of production rate-limiting steps and studies of optical properties, including internal reflectance at the back interface. This effort readily achieved the initial objective of improving thin-cell process parameters and has resulted in the fabrication of thousands of high-efficiency ultra-thin solar cells for evaluation purposes.

ORIGINAL PAGE IS  
OF POOR QUALITY

## B. Work Plan & Schedule

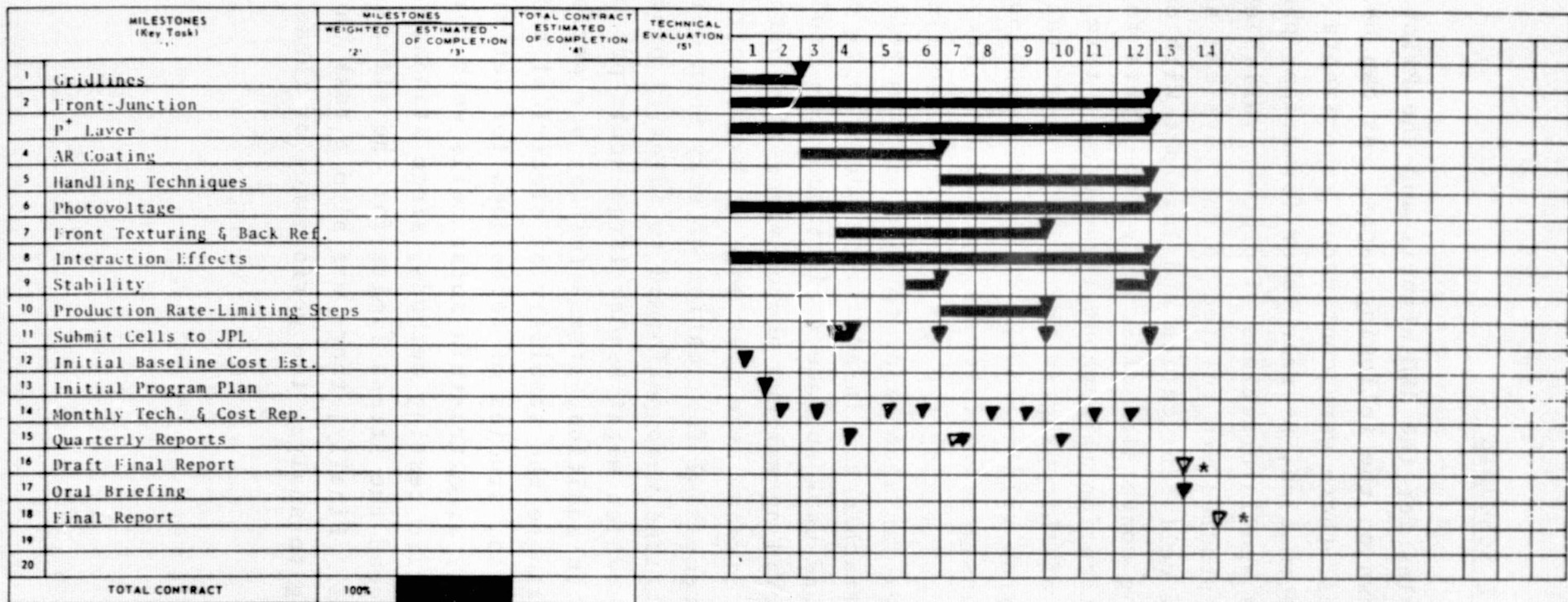
The schedules for the R&D efforts and the Pilot Line effort are shown on the following pages. As can be seen from these schedules, there were continuous experimental efforts on front junction formation, p<sup>+</sup> rear layer formation, photovoltage improvement studies and interactions of process variables. Since all of these studies are related to the physical and chemical details of cell fabrication and interact with one another in affecting conversion efficiency, they were topics of continual investigation throughout the contract term. At the very beginning of this program there was a short task on optimizing the chevron gridline masks for minimum shadowing, while maintaining insignificant series resistance. There then followed a task on optimizing the anti-reflective coating, employing high-index tantalum oxide to give minimum reflectance after coverglass attachment. In addition, the effects of front surface texturing and back surface reflectance were studied, with the aim of providing maximum photon absorption paths in thin solar cells. Studies were also made of handling techniques which aid in the successful fabrication of very thin solar cells, and periodic evaluations were performed to identify production-rate-limiting steps which might hinder large-scale production of ultra-thin cells. In addition, stress testing was performed periodically to evaluate the stability of electrical and mechanical characteristics. Also, studies of techniques for determining the contact integrity of ultra-thin solar cells were performed to find non-destructive testing methods, since standard procedures usually exceed the stress limits for the silicon itself in ultra-thin cells. Finally, there was also a task on measurements and modelling to analyze the performance of these revolutionary new cells.

# MILESTONE PROGRESS REPORT

CONTRACTOR: SOLARIX CORPORATION

CONTRACT NO. 151201

FOR PERIOD ENDING:

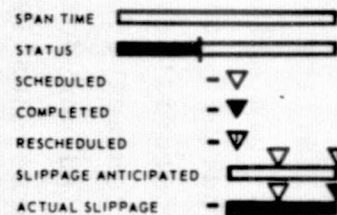


-8-

DELIVERIES DATE STATUS

SCHEDULE LEGEND:

REMARKS: \* Rescheduled



TECHNICAL EVALUATION SYMBOLS:  
 SATISFACTORY PROGRESS   
 SIGNIFICANT PROBLEM   
 SERIOUS PROBLEM

ORIGINAL  
OF FOUR COPIES

Approved \_\_\_\_\_

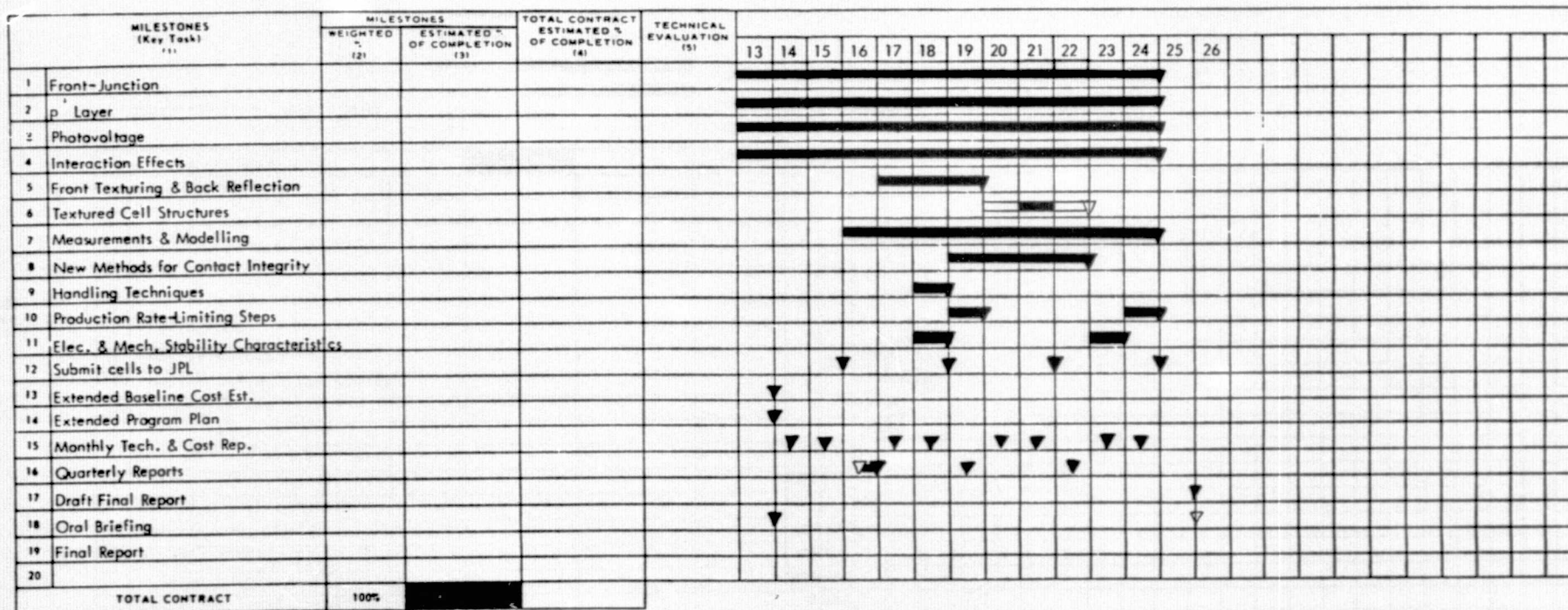


# MILESTONE PROGRESS REPORT

CONTRACTOR: SOLAREX CORPORATION

CONTRACT NO. 954290

FOR PERIOD ENDING:



DELIVERIES DATE STATUS

## SCHEDULE LEGEND:

SPAN TIME [Solid bar]  
 STATUS [Solid bar]  
 SCHEDULED - ▽  
 COMPLETED - ▽  
 RESCHEDULED - ▽  
 SLIPPAGE ANTICIPATED [Bar with ▽]  
 ACTUAL SLIPPAGE [Bar with ▽]

TECHNICAL EVALUATION SYMBOLS  
 SATISFACTORY PROGRESS - △  
 SIGNIFICANT PROBLEM - △  
 SERIOUS PROBLEM - ○

REMARKS:

Approved: \_\_\_\_\_

- 9 - ORIGINAL PAGE IS OF POOR QUALITY



CONTRACTOR: SOLAREX CORPORATION  
FOR PERIOD ENDING:

MILESTONE PROGRESS REPORT  
PILOT LINE PROGRAM

CONTRACT NO. 054200

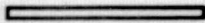
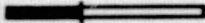
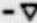
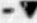
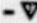

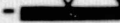
MILESTONES (Key Task)	MILESTONES		TOTAL CONTRACT ESTIMATED % OF COMPLETION	TECHNICAL EVALUATION																						
	WEIGHTED (12)	ESTIMATED % OF COMPLETION (13)			17	18	19	20	21																	
1 Project Management																										
2 Assemble Production Team																										
3 Train additional personnel																										
4 Acquire necessary equip.																										
5 Prepare space																										
6 Install equipment																										
7 Test & Upsale Production																										
8 Optimize Cell Design																										
9 Dev. Prod. Monitrg. Proced's.																										
10 Full Scale Production																										
11 Production Monitoring																										
12 Complete Pilot Line Report																										
13 Cell Shipments																										
14 Program Plan																										
15																										
16																										
17																										
18																										
19																										
20																										
TOTAL CONTRACT	100%																									




- 10 -

DELIVERIES DATE STATUS

SCHEDULE LEGEND:

REMARKS:

SPAN TIME   
 STATUS   
 SCHEDULED   
 COMPLETED   
 RESCHEDULED   
 SLIPPAGE ANTICIPATED   
 ACTUAL SLIPPAGE 

TECHNICAL EVALUATION SYMBOLS  
 SATISFACTORY PROGRESS   
 SIGNIFICANT PROBLEM   
 SERIOUS PROBLEM 

Approved: \_\_\_\_\_

The Pilot Line effort was carried out in conformance to a separate short-fuse schedule of its own. That schedule allowed only 2 1/2 months preparation including all phases of equipment preparation and personnel training, followed immediately by the production phase. The Pilot Line effort achieved its goal of fabricating 1000 pre-production samples and 2000 production cells within the short schedule shown following.

### III. TECHNICAL DISCUSSION

#### A. Silicon Thinning Technology

This topic was not a scheduled format task in the contractual effort, but it was of such key importance as the breakthrough which made ultra-thin solar cell fabrication feasible that it warrants separate discussion. Prior to discovery of this thinning technology it had been very difficult and quite a hit-and-miss affair to achieve silicon slices less than a hundred microns (approximately 4 mils) in thickness which were amenable to surviving fabrication into solar cells. It was determined that a key aspect of fabricating 50  $\mu\text{m}$  to 75  $\mu\text{m}$  thick silicon solar cells is the technique of thinning the starting slices. The maintenance of uniform thickness across a slice is quite important for cell strength and resistance to damage in handling during processing.

The very thin cells fabricated during the first two quarters employed silicon slices which had been subjected to chemical/mechanical thinning and polishing to produce a 50 micron slice thickness. Such procedures, however, are both costly and time-consuming. Therefore, efforts were directed to establishing a simple process for chemically thinning the silicon. Attempts to employ acidic "CP" etches (nitric, hydrofluoric & acetic acid mixtures) generally resulted in non-uniform cell thicknesses, especially in localized areas.

However, it was found during the third quarter efforts that etching in 20%-40% NaOH solutions at temperatures above 100°C resulted in reproducible uniformity of thickness across (100)-oriented silicon slices down to 30 microns or so in final thickness. The etching rate is approximately 4  $\mu\text{m}$ /minute/side for a (100) plane under such conditions, which allowed for considerable

ORIGINAL PAGE IS  
OF POOR QUALITY

ease in trimming to the desired thickness.

It became quite apparent that the mechanical survival of slices prepared with this technique was far superior to that of slices prepared by the other methods employed, including chem/mechanical polished. In addition, uniformity of thickness across a slice is quite good (few microns) with this etching technique and is maintained even with very thin slices.

A very reproducible surface was regularly achieved which has only a fine feature "pillowed" texture, with each pillow a fraction of a micron in height. The etch rate of a few microns per minute for each side was found convenient for thickness control but not so slow as to be production rate-limiting for batch processing.

At low temperatures and/or low concentrations, the tendency is to develop preferential pyramids on the 100 plane with alkaline etches. At temperatures above 100° C, the texture appears reduced almost to a plane with features that are pillow-like; with the size and exact dimensions of such pillows dependent on the specific etch conditions. A high degree of etching reproducibility was achieved by introducing clean slices into a 20%-40% (by weight) NaOH solution when the solution has reached temperatures in the neighborhood of 105° C. Stainless steel containers were employed for the NaOH etch, with magnetic stirring. Various concentrations of etch solutions were employed with no adverse effects on the surface texture or the flexibility of the resulting slices. In fact, perfect etching was also achieved for 3-inch (7.6cm) round slices.

Several grades of NaOH were used to etch silicon slices to 50 microns. There was no apparent difference in either the etch rate, surface texture, or resulting slice flexibility.

The best grade readily available was 97.9% pure and four times as expensive as the cheapest "technical grade" for which no analysis was received or expected.

Various starting slice surface conditions have been employed in the etching experiments. These have ranged from "as-sawn" (100) to mirror-finish chem-mechanical polished (100) surfaces. A prepolished surface remains much like its original condition after a slice is reduced from 250 microns to 50 microns in a NaOH etch. Employing a slice with no smoothing treatment after sawing from the ingot results in a pillowed or quilted looking surface with each feature less than a micron or so in height. No distinct trend in solar cell performance was observed between cells made from slices with these different surface conditions, which means that the chemical polishing of the NaOH etch is apparently quite satisfactory and no other mechanical or acidic chemical polishing is required.

For some of the float zone grown silicon employed in this effort, randomly distributed surface features appeared on some slices. These consisted of either spherical-segment dents or obviously preferential square, sloped-side indentations with plane bottoms. The size of these indentations ranged up to about a half millimeter. These features did not occur on any of the Czochralski-grown silicon employed and also did not occur on many other slices from that very same ingot of float-zone silicon. It was tentatively assumed that inherent crystal defects in those few slices were the cause of the anomaly.

The NaOH etch does tend to leave a residue of microscopic particles on the silicon surface. These residue particles were not chemically identified, but were unaffected by rinsing with cold or hot deionized water. They can be removed mechanically with scrubbing or can be removed completely by other chemical treatments. The most successful residue removal was achieved by employing a 2:1 boiling mixture of

sulfuric acid and hydrogen peroxide. This resulted in a very reproducible complete removal, but was relatively inconvenient. A fully satisfactory alternate residue removal method is a soak in a solution of HCL, which also eliminates the need for removing the chemically grown oxide produced by the sulfuric peroxide cleaning method.

#### B. Anti-reflection Coating Optimization

During this contract, efforts were directed to studying tantalum oxide anti-reflective coatings on silicon. It was found that regardless of the deposition technique employed, all films were extremely adherent and the main changes incurred related to the resulting net reflectance and the refractive index of the tantalum oxide.

The experiments performed varied the source material condition, evaporation rate, oxygen back pressure and post-deposition treatment. The means of coating evaluation consisted of reflectance measurements for films on silicon employing a Beckman DK-2A spectrophotometer with a Gier-Dunkle integrating sphere. Also, observation of reflectance and short-circuit current changes produced by overcoating the samples with silicone rubber cover-slide adhesive (medium optical index material) was used as a means to evaluate whether the anti-reflective coating's index would be high enough to provide the best optical matching for cells finally assembled with cover slides. The as-deposited reflectance was measured as a function of incident light wavelength from 400nm to 1000nm and changes with post-deposition treatment and adhesive application were observed for evaluation of overall film optical properties.

The changes in evaporant source material consisted of:

- a) fresh  $Ta_2O_5$  powder (Atomergic Chematals Co.)
- b) Multiply-vacuum-melted glass from the powder.

- c) Adding a back pressure of oxygen during evaporation in expectation of restoring stoichiometry after probable dissociation during evaporation.

The results of these experiments are shown in Figure 1, Figure 2 and Figure 3. These films were all electron-beam evaporated, with low background pressures before deposition. Fresh source charges of  $Ta_2O_5$  powder produced curves of the type shown in Figure 1. The right-hand lower curve is the reflection obtained as deposited. The left-hand lower curve results after brief heating (seconds) at temperatures in excess of  $350^\circ C$ . The optical effect of the heating is to shorten the wavelength for quarter-wave matching, most likely due to an index of refraction increase or physical shrinkage in densification. Application of the silicone adhesive, which has a refractive index near 1.5, causes a net increase in reflectance across the silicon absorption band. This indicates a relatively low value of index of refraction for the film. These curves are very reproducible, always with an apparent film index too low for optimum optical matching of the adhesive layer and the silicon.

Figure 2 shows the set of reflectance curves measured when a background pressure of oxygen at  $2 \times 10^{-5}$  Torr is maintained during evaporation. Note that when the film is overcoated with the silicone the reflectance is just slightly worse over the silicon absorption band, a somewhat surprising result.

Figure 3 shows typical reflectance curves for films produced by evaporating a tantalum oxide source which has been premelted in vacuum. These films show a higher reflectance before heating and not quite as low after heating as the previous film types. However, after coating with the silicone adhesive, there is a markedly lower reflectance over the silicon absorption band. Consequently, this evaporation technique was



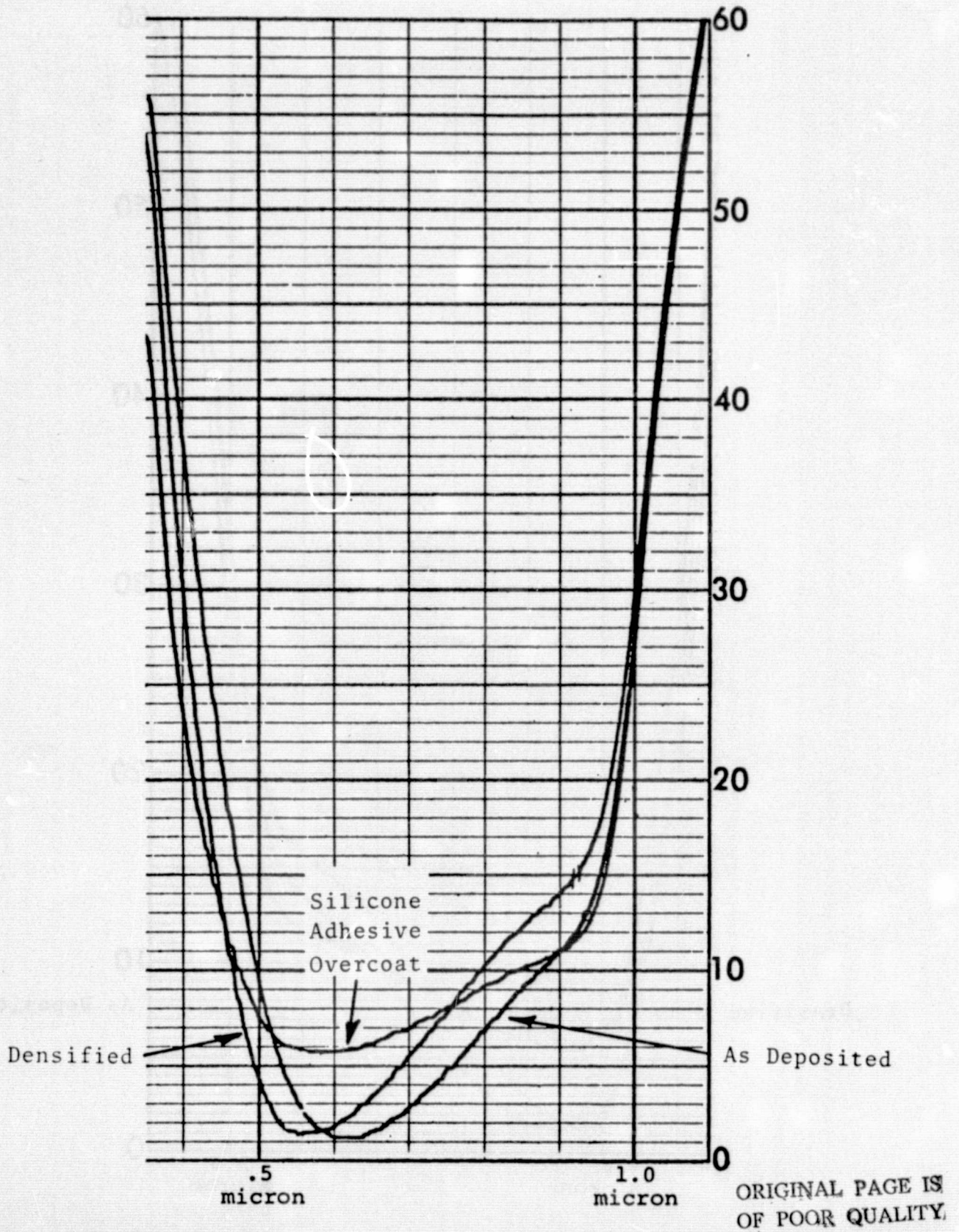


FIGURE 1. REFLECTION VS. WAVELENGTH - EVAPORATED  
FILM OF FRESH SOURCE  $Ta_2O_5$  POWDER.



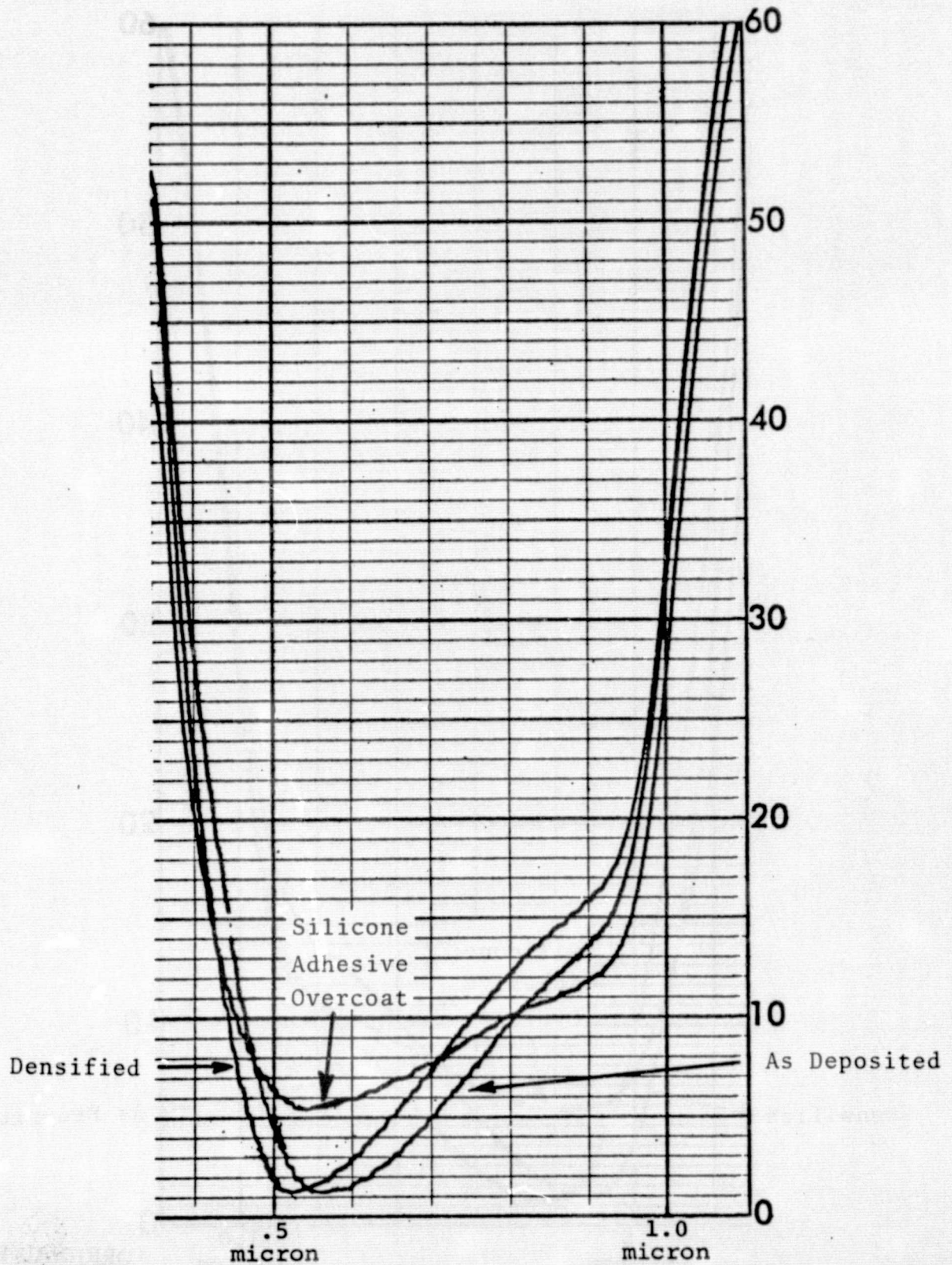


FIGURE 2. REFLECTION VS. WAVELENGTH - EVAPORATED FILM OF FRESH SOURCE  $Ta_2O_5$  POWDER WITH  $O_2$  BACK PRESSURE.

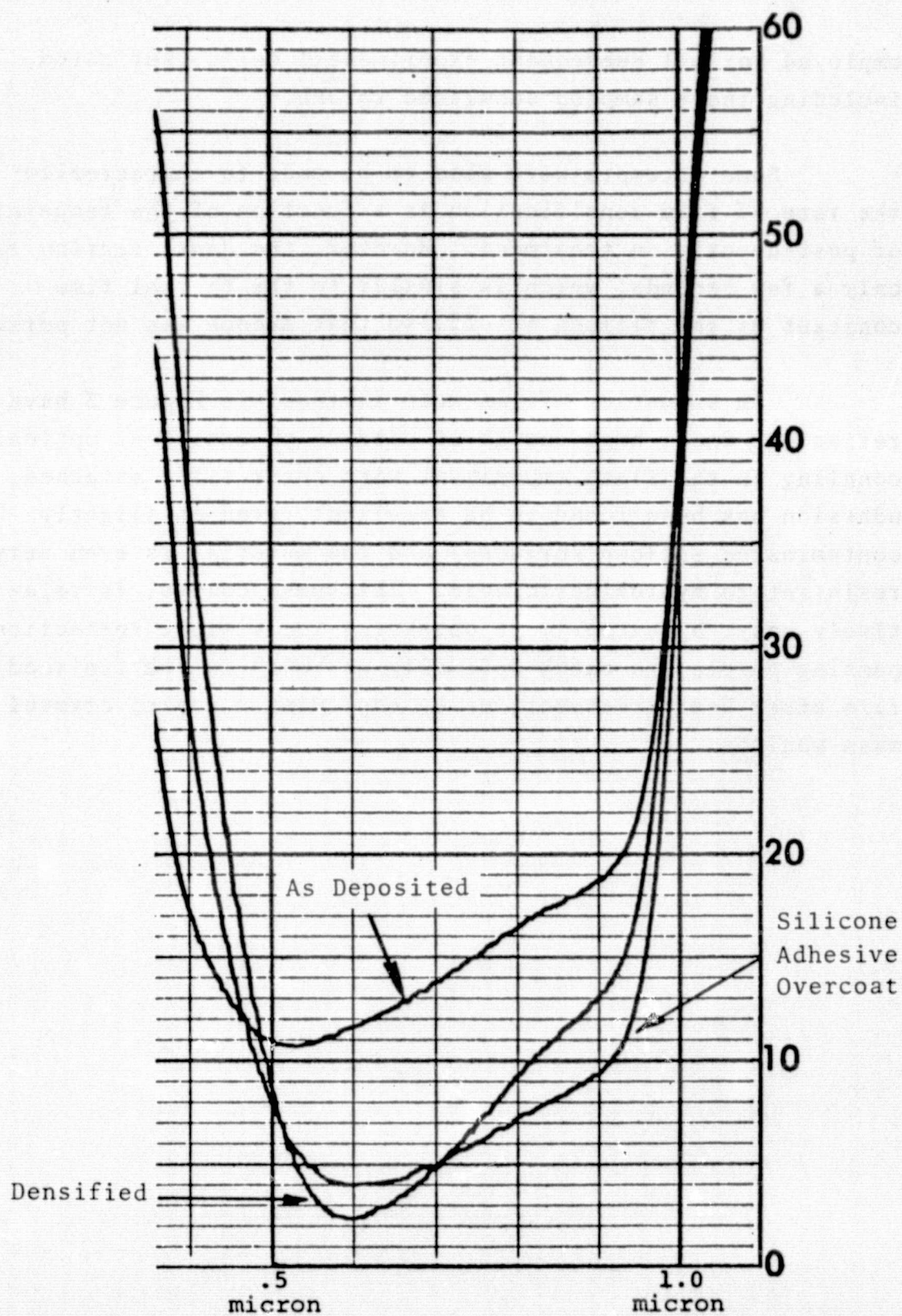


FIGURE 3. REFLECTION VS. WAVELENGTH - EVAPORATED FILM OF PRE-MELTED-SOURCE  $\text{Ta}_2\text{O}_5$  POWDER.

employed for all subsequent experimental cells fabricated, including those samples submitted to JPL.

Some attempts were also to be made to characterize the rate of film densification as a function of the temperature of post-deposition treatment. However, the densification takes only a few seconds, which is similar to the thermal time constant of the silicon itself, so that avenue was not pursued.

In summation, films made as those in Figure 3 have a refractive index high enough to produce an excellent optical coupling in the final embodiment with cover slide attached, adhesion has been found to be excellent (even on slightly contaminated silicon surfaces) and the material is even very resistant to hydrofluoric acid. Thickness control is relatively easy, by either just observing the visible reflection passing purple, to match optimally at 550nm in the finished film after heat treatment, or by employing a quartz crystal mass monitor.

### C. Internal Reflection

The purpose of this task is two-fold: first, to analyze the optical properties of the back interface for its effect on the longer wavelength end of the spectrum and, second, to attempt maximizing reflection at that interface for increasing the red response of thin solar cells.

Numerous samples were prepared on both (100) and (111) silicon slices for alloying over a range of temperatures and subsequent measurement of the internal reflection at the resulting interface. As in cell fabrication, aluminum was evaporated onto the silicon surface and then alloyed into the silicon for a given time at a particular temperature. Separate samples were used for each time and temperature.

The optical measurements were performed with the Beckman DK-2A spectrophotometer and Gier-Dunkle integrating sphere in the Solarex laboratories. The measured quantity was the net reflection at wavelengths slightly longer than the silicon absorption band. In that range the silicon is a non-absorbing window and the reflection measured is a result of both the front-surface air/silicon and the rear silicon/alloy interfaces. The reflection at the rear interface can be calculated from the measured net reflection when the properties of the front-surface interface are known. Experimentally, the front silicon surface was smooth and cleaned in a mild hydrofluoric acid solution to produce a controlled known interface prior to measurement.

The net reflection from a series of two interfaces is:

$$R = \frac{R_1 + R_2}{1 + R_1 R_2}$$

where  $R_1$  is the reflectance of the first interface in the light path and  $R_2$  is that of the second interface encountered in the light path. In this case,  $R_1$  is due to the differing refractive



indices of air and silicon at a wavelength of 1.3 microns.  
It is:

$$R_1 = \left( \frac{n_{\text{Si}} - n_{\text{air}}}{n_{\text{Si}} + n_{\text{air}}} \right)^2 = 0.31$$

The value of  $R_2$  can thus be calculated from measured net reflection by inserting 0.31 for  $R_1$  in the first expression above, as:

$$R_2 = \frac{R - 0.31}{1 - 0.31R}$$

Typical plots of net reflection as a function of wavelength are shown in Figure 4. Note that the reflection becomes essentially wavelength independent for wavelengths beyond 1.3 microns.

Calculated values for the silicon/alloy interface reflectance derived from measurements are shown in Figure 5 for (100) surfaces and in Figure 6 for (111) surfaces. Before alloy,  $R_2$  was found to be in the immediate neighborhood of 0.8. After alloying, the interface reflectance decreases; most likely the mirror darkening is due to absorption in the recrystallized layer at the interface. Below the temperature of the silicon-aluminum eutectic, the sintering effect produces little disturbance of the mirror properties. However, from the eutectic up to 850°C there is a drop in reflectance to the range of 0.5 to 0.6, with a good deal of scatter from sample to sample.

For sufficiently long alloying times at temperatures of 900°C or higher, an increased reflectance reappears, although still with considerable scatter from sample to sample.

The main conclusion to be drawn is that the reflectance of the silicon/aluminum interface is high only for treatment at

ORIGINAL PAGE IS  
OF POOR QUALITY

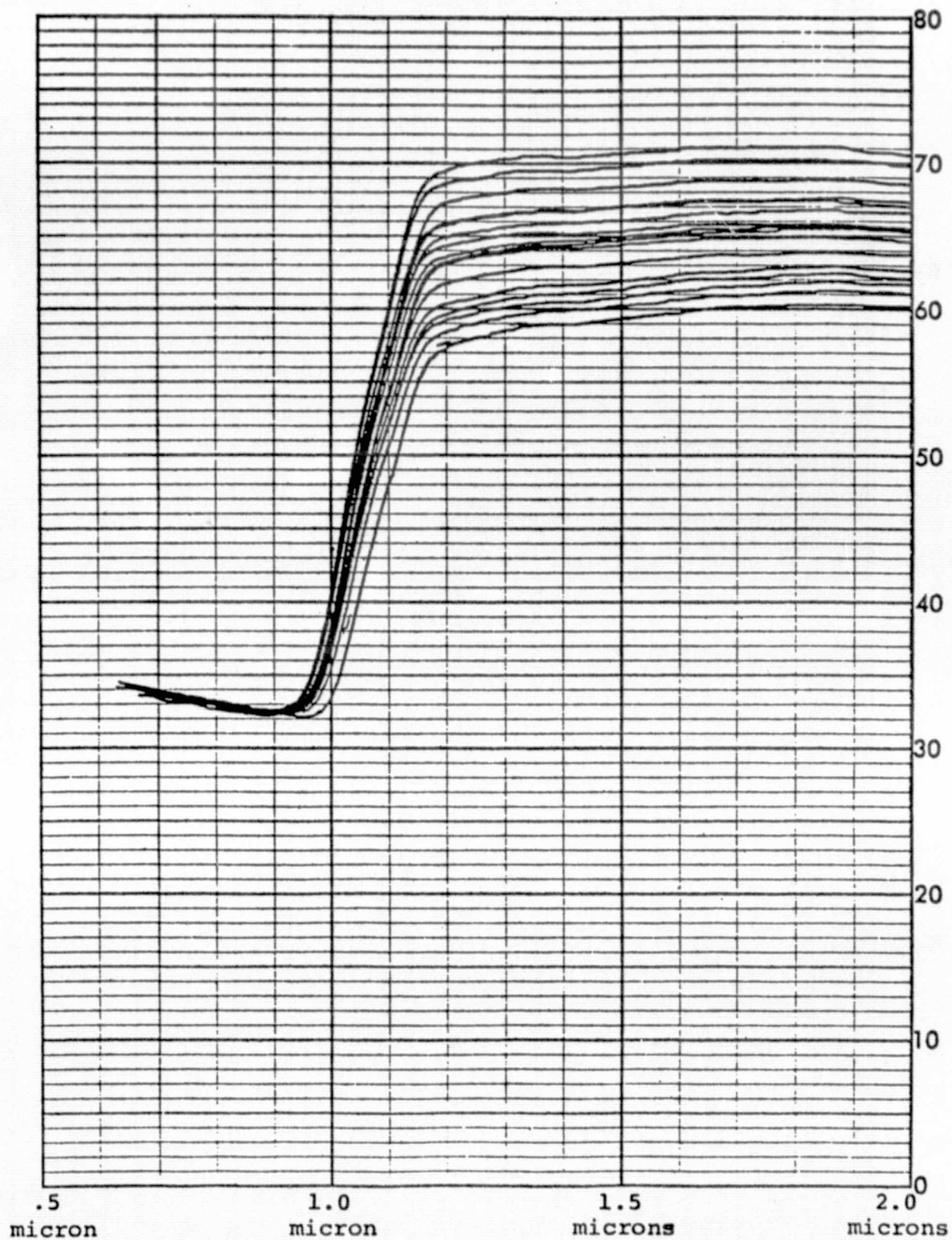


FIGURE 4. NET REFLECTION AS A FUNCTION OF WAVELENGTH

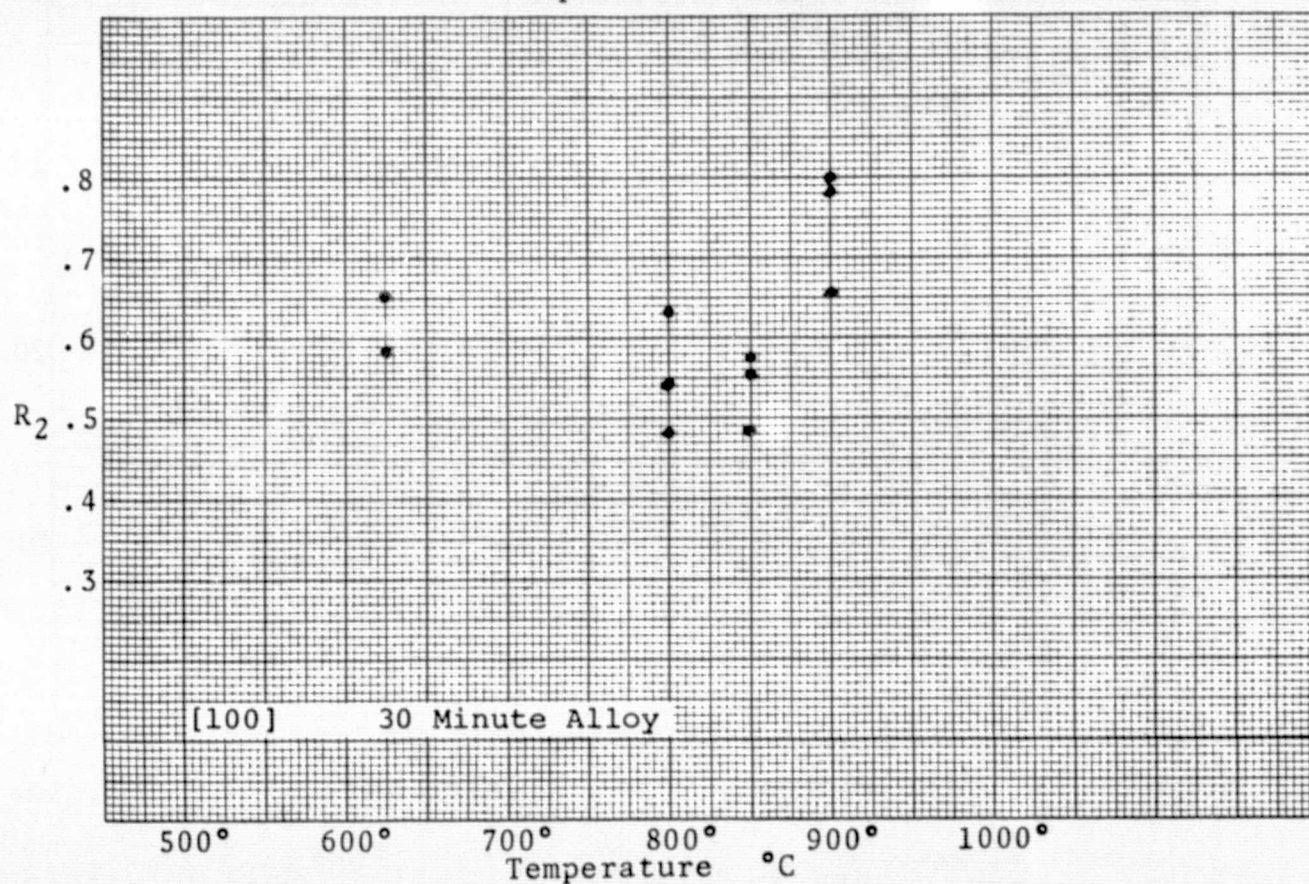
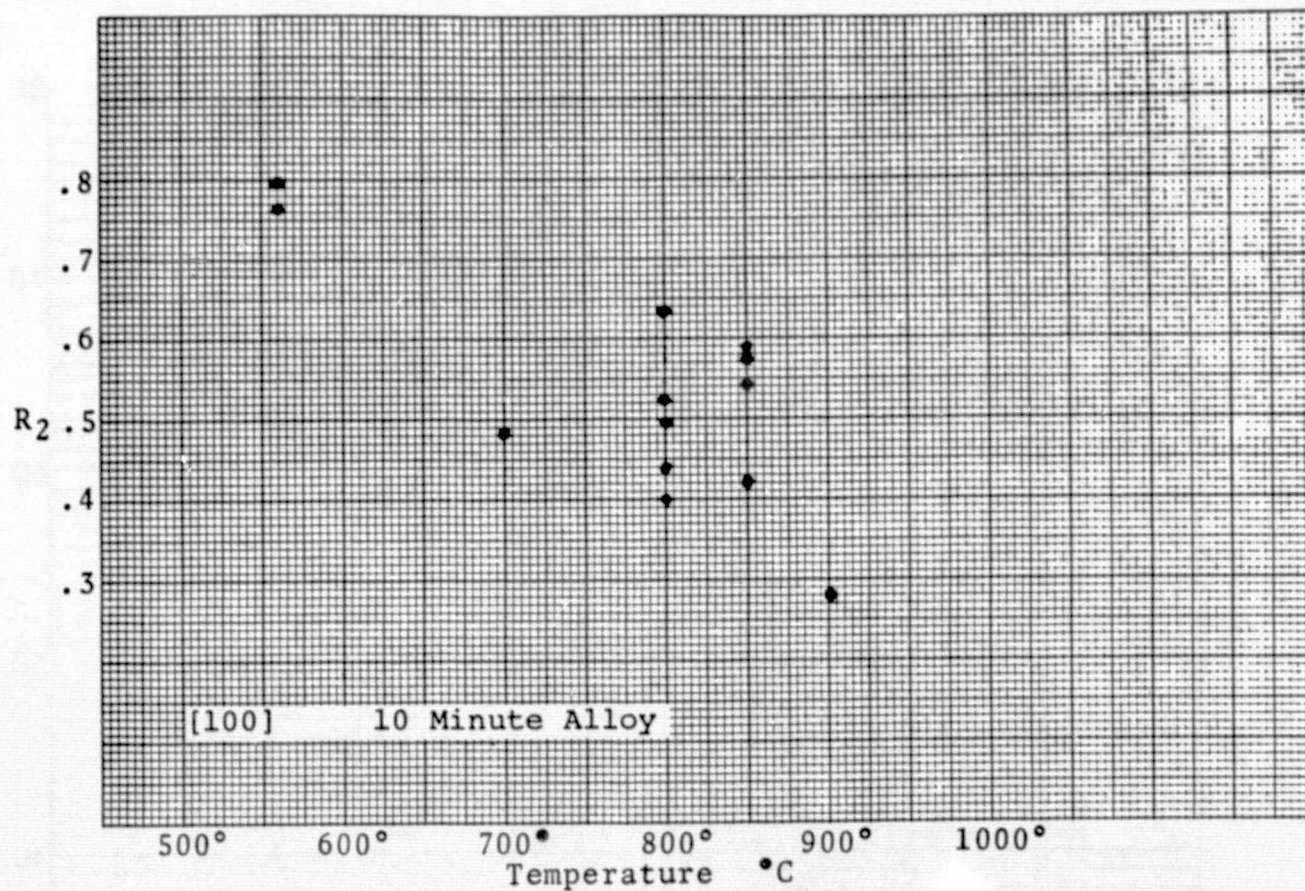


FIGURE 5. REFLECTION OF Si Al INTERFACE ( $R_2$ ) VS. ALLOY TEMPERATURE



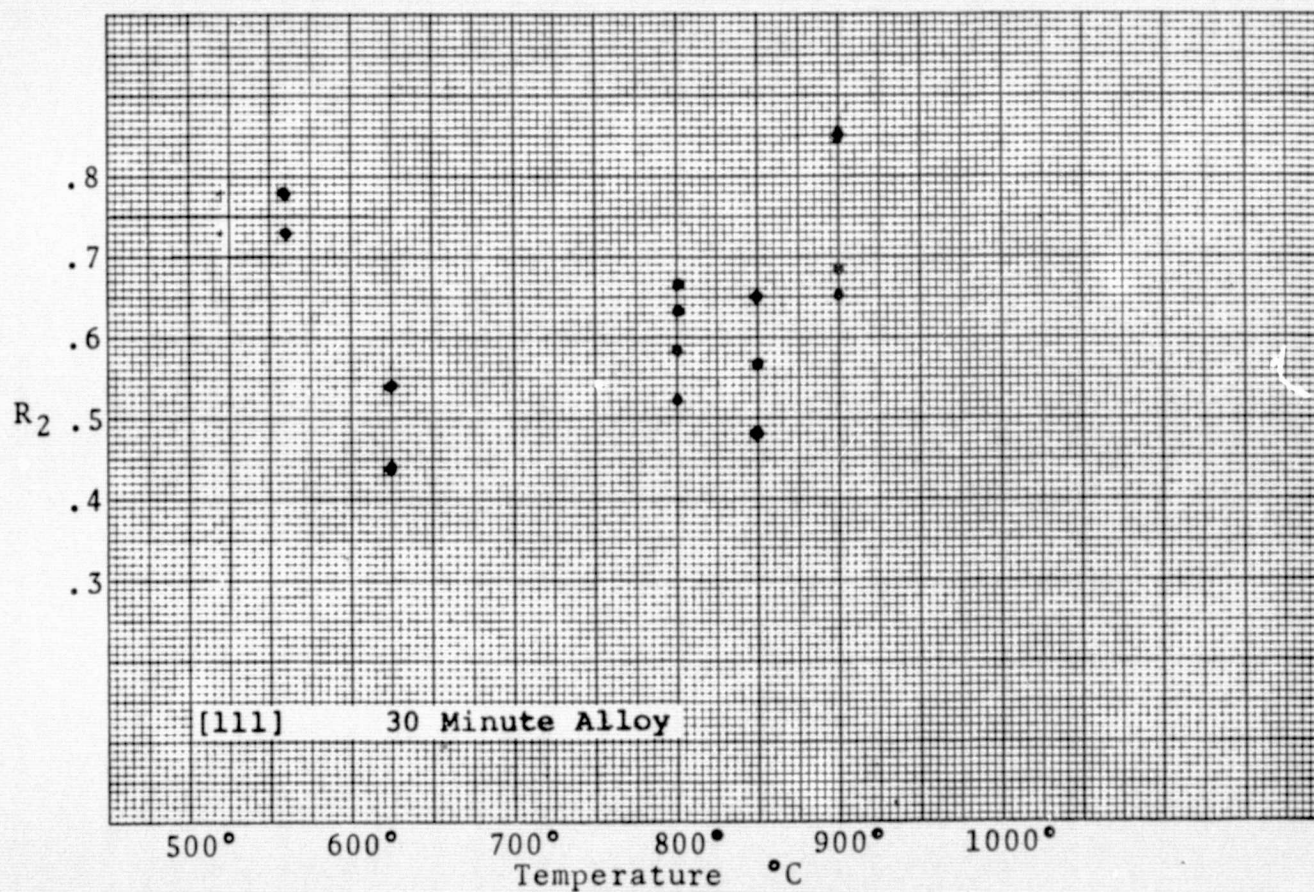
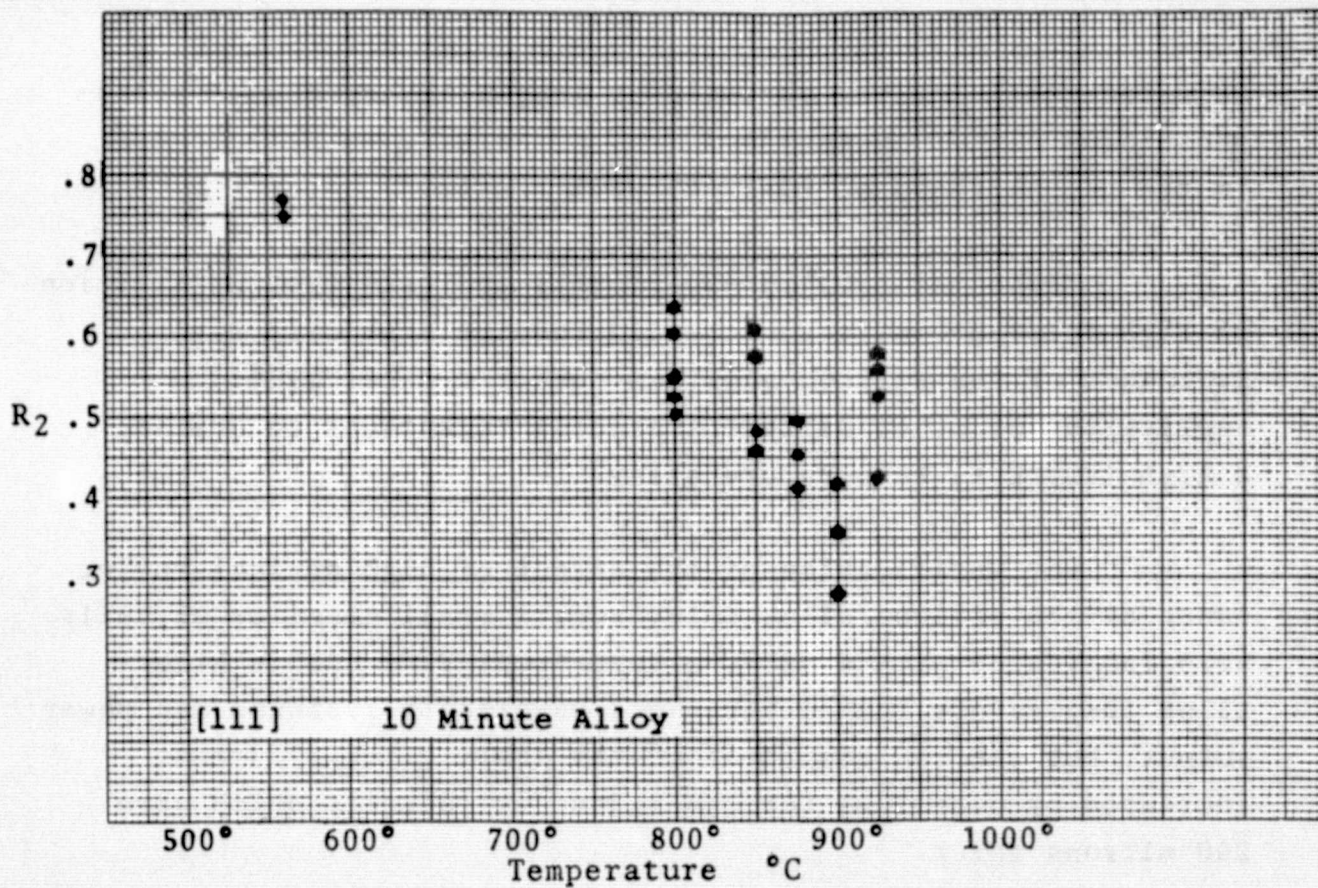


FIGURE 6. REFLECTION OF Si Al INTERFACE (R<sub>2</sub>) VS. ALLOY TEMPERATURE



temperatures below the eutectic or long alloying above optimum phosphorus diffusion temperatures. Otherwise, a reflectance in the neighborhood of 50 - 60% will result.

These reflectance experiments indicate that utilization of high internal reflectance would require a process with avoidance of the silicon-aluminum eutectic after aluminum application or other different process techniques to utilize a high (900°C +) temperature alloy.

For verification of the effect of high optical reflectance at the silicon/alloy interface, a small quantity of cells were fabricated with a 925°C alloy. Employing such a high alloy temperature ruined the short wavelength response and power output, but the red component of the short-circuit current increased by over 10mA for 2cm x 2cm sample cells which were 200 microns thick.

#### D. Diffusion Optimization

Throughout this program there was a continuous effort on optimizing the front junction diffusion process. It involved the use of both phosphorus and arsenic from different source compositions ( $\text{PH}_3$ ,  $\text{POCl}_3$ ,  $\text{AsH}_3$ ) both alone and in combination, changed in gas compositions and flow rates, and variations of time-temperature schedules. The resulting solar cells were evaluated in terms of maximum output power under AM0 illumination ( $P_{\text{max}}$ ), open-circuit voltage ( $V_{\text{oc}}$ ), short-circuit current ( $I_{\text{sc}}$ ), short-wavelength short-circuit current component ( $I_{\text{sc}} \text{ Blue}$ ), long-wavelength short-circuit current component ( $I_{\text{sc}} \text{ Red}$ ) and I-V curve fill factor (F).

In general, it was determined that employing phosphine diffusion ( $\text{PH}_3$ ) produced the highest efficiency cells, while phosphorus oxychloride produced slightly lower efficiencies and combination diffusions with arsenic (as  $\text{AsH}_3$ ) have not as yet produced significant improvements in cell performance. (Arsenic alone requires elevated diffusion temperatures for attainment of reasonable lateral sheet resistance which degrade other parameters.) A long series of experiments was performed to evaluate the effects that the temperature of phosphorus diffusion has on the performance of ultra-thin silicon solar cells. Quantities of cells were processed at each experimental temperature to assure a sample large enough so that extraneous effects from individual cell faults could be weeded out of the resulting performance characteristics, without reducing confidence in the results. Czochralski-grown slices were employed.

The silicon surface preparation was soon standardized to common NaOH thinning etch, hydrochloric acid cleaning, followed by a water rinse, a hydrofluoric acid etch and a rinse in de-ionized water, in order to remove any variables from deposits on residual oxides. The diffusion employed argon carrier gas and phosphine as

the source of phosphorus. Early in the program diffusions were performed on 250 micron slices isochronally over a temperature range spanning 750°C to 900°C. Near the end of the first year emphasis in diffusion experimentation shifted to 50 micron slices and a higher temperature range.

The results of the diffusion experiments for cells of conventional thickness showed an onset of loss in short-wavelength photocurrent at 830-840°C, but a steady climb in open-circuit voltage past these diffusion temperatures, so that the maximum in peak output power did not occur until approximately 870°C. Experimentation with isochromal diffusion of 50 micron slices as a function of temperature produced the parameters for 2cm x 2cm solar cells shown\* in Figures 7,8, and 9, where both mean values and measured limits are indicated.

It is to be noted that there is a decline in short-circuit current for longer wavelengths commencing for diffusion temperatures above 850°C, and for shorter wavelengths at temperatures above 860°C. The long wavelength short-circuit current was measured by inserting a Corning No. 2408 long-pass filter 3mm in thickness between the cell being measured and the incident AMO light beam, while the short-wavelength short-circuit current was obtained by inserting a Corning No. 9788 short-pass filter 5mm in thickness in the incident AMO light beam. The decline of the long-wavelength component indicates diminishing bulk minority carrier lifetime in these thin cells commencing at diffusion temperatures above 850°C. The fall in short-wavelength response follows the expected behavior with increasing junction depth at higher temperatures, while the values achieved at 850-865°C are equal to the best achieved for cells of conventional thickness at slightly lower temperatures.

---

\* Without cover slides, but with tantalum oxide coatings.

ORIGINAL PAGE IS  
OF POOR QUALITY

# SLICE RESISTIVITIES

- 2 ohm-cm
- 0.6 " "
- △ 0.1 " "

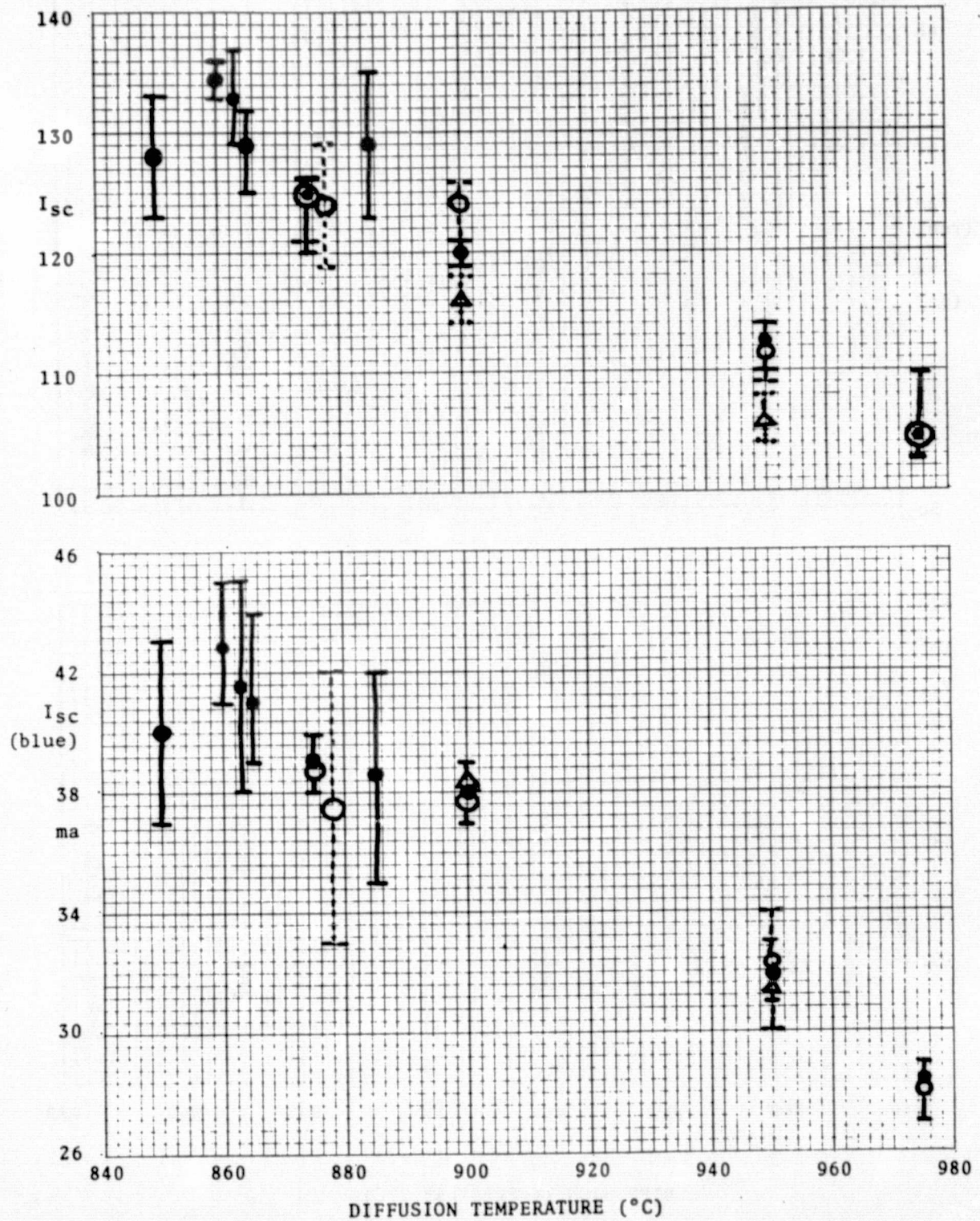


FIGURE 7. Short-circuit current and its short-wavelength component vs. diffusion temperature.

ORIGINAL PAGE IS  
OF POOR QUALITY



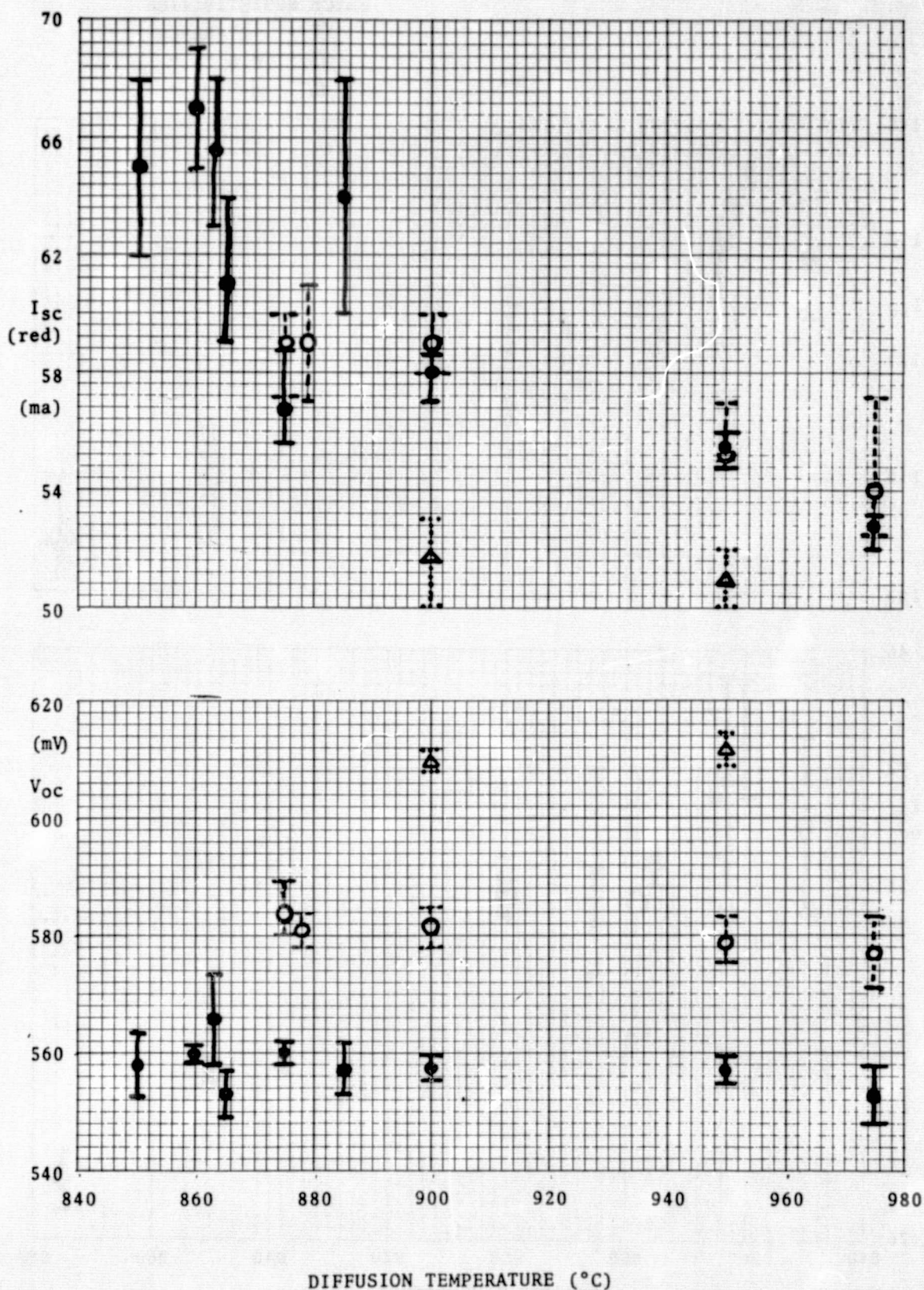


FIGURE 8. Behavior of red current and voltage vs. diffusion temperature.

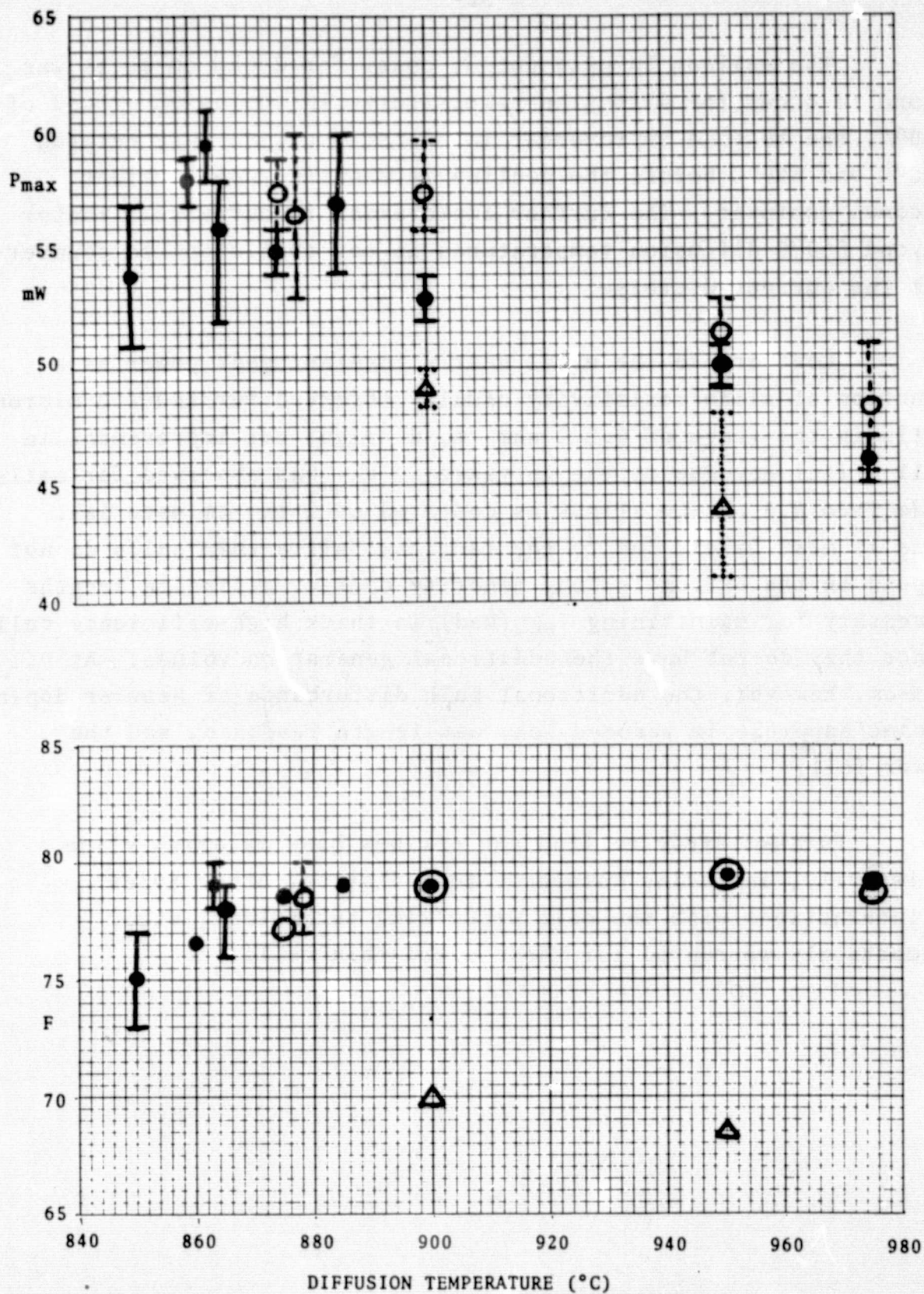


FIGURE 9. Maximum power and fill factor vs. diffusion temperature.

The maximum in peak output power for 2 ohm-cm cells was found to occur for diffusion temperatures in the neighborhood of 860°C, due to some improvement in open-circuit voltage between 850°C and 860°C before the decline in short-circuit current becomes dominant. The further improvement in curve full factor beyond 860°C diffusion temperatures is not sufficient to counteract the current decrease.

Contrary to the usual nearly constant peak power as a function of slice resistivity usually observed for 200-250 micron cells in the range of 0.5-2 ohm-cm, a slight net improvement in cell efficiency due to the increase in  $V_{OC}$  was observed for cells made from 0.6 ohm-cm slices as compared to 2 ohm-cm material. This is most likely due to the fact that ultra-thin cells do not depend on the extremely long minority carrier diffusion lengths necessary for maintaining  $I_{SC}$  (Red) in thick high-efficiency cells, since they do not have the additional generation volume. At 0.1 ohm-cm, however, the additional bulk disturbance of heavier doping became apparent in reduced long-wavelength response, and the power fell.

Further study to find the optimum base material slice resistivity, including tolerance to radiation, other types of interactions with the cell processing technology, etc., is certainly warranted for these ultra-thin cells.



### E. Czochralski vs. Float Zone Silicon

The starting silicon material employed for cell fabrication in this program was picked from both Czochralski-grown and float-zone ingots. This was done so that any differences in device performance could be evaluated. However, we must say that no differences could be discerned in the initial electrical performance for the very thin cells fabricated, other than a very slight trend toward better fill factors with the Float-Zone silicon.

### F. Aluminum Deposition & P<sup>+</sup> Alloy Schedule

#### 1. Aluminum Thickness

The thickness of the deposited aluminum film used as the alloy source for forming the p<sup>+</sup> back surface was varied from 1000 Å to 10,000 Å. It was found that there is a large drop in the resulting cell performance upon using deposited films of less than 2000 Å in thickness. On the other hand, there is only a marginal electrical performance improvement with increasing aluminum film thickness between approximately 2000 Å and 10,000 Å. Also, two other limitations become apparent for aluminum films thicker than 4000 Å on these very thin cells. Near an 8000 Å film thickness the aluminum begins to form lumps and balls upon alloying, which not only produce difficulties in handling and contacting, but also stress the silicon so violently as to dimple the front surface on cooling. Above a 4000 Å film thickness, the whole cell curls after alloying and becomes more susceptible to breakage.

Upon consideration of these factors, it was decided to employ a few thousand Å of aluminum film thickness for the very thin (under 80 μm) silicon solar cells. This thickness is probably near optimum, but further study of interactions with other fabrication parameters should be performed in the future.



## 2. P<sup>+</sup> Alloy Schedule

Experimentation was done with aluminum alloying temperature to determine its effect on resulting electrical performance for very thin cells. It was found that there is a slight improvement in the photocurrent at longer wavelengths with increasing alloying temperature for ultra-thin cells. All of the alloy variation experiments were done on 1.75 ohm-cm float-zone silicon from the same ingot.

Figure 10 is a plot of both the ranges and mean values of the longer wavelength short-circuit currents for groups of cells alloyed at temperatures from 700°C to 800°C. The filter employed passes wavelengths longer than 560nm and was the same as employed for the data presented in previous sections above. Both the alloying temperature and time were varied for the experimental runs. As can be seen from the figure, there is a trend toward increasing the red component of the photocurrent with increasing alloying temperature, and also a trend to lowering the red component with increasing time in the alloying furnace. It is apparent that short alloying cycles at higher temperatures produce improvement in cell performance, since the open-circuit voltage and fill factors were unaffected, as can be seen from the additional data in Table I. As discussed in section C above, however, increasing alloying temperatures produce a reduction in optical reflectance at the alloy interface, and at temperatures in the range of the phosphorus diffusion commences to degrade the short-wavelength response.

ORIGINAL PAGE IS  
OF POOR QUALITY

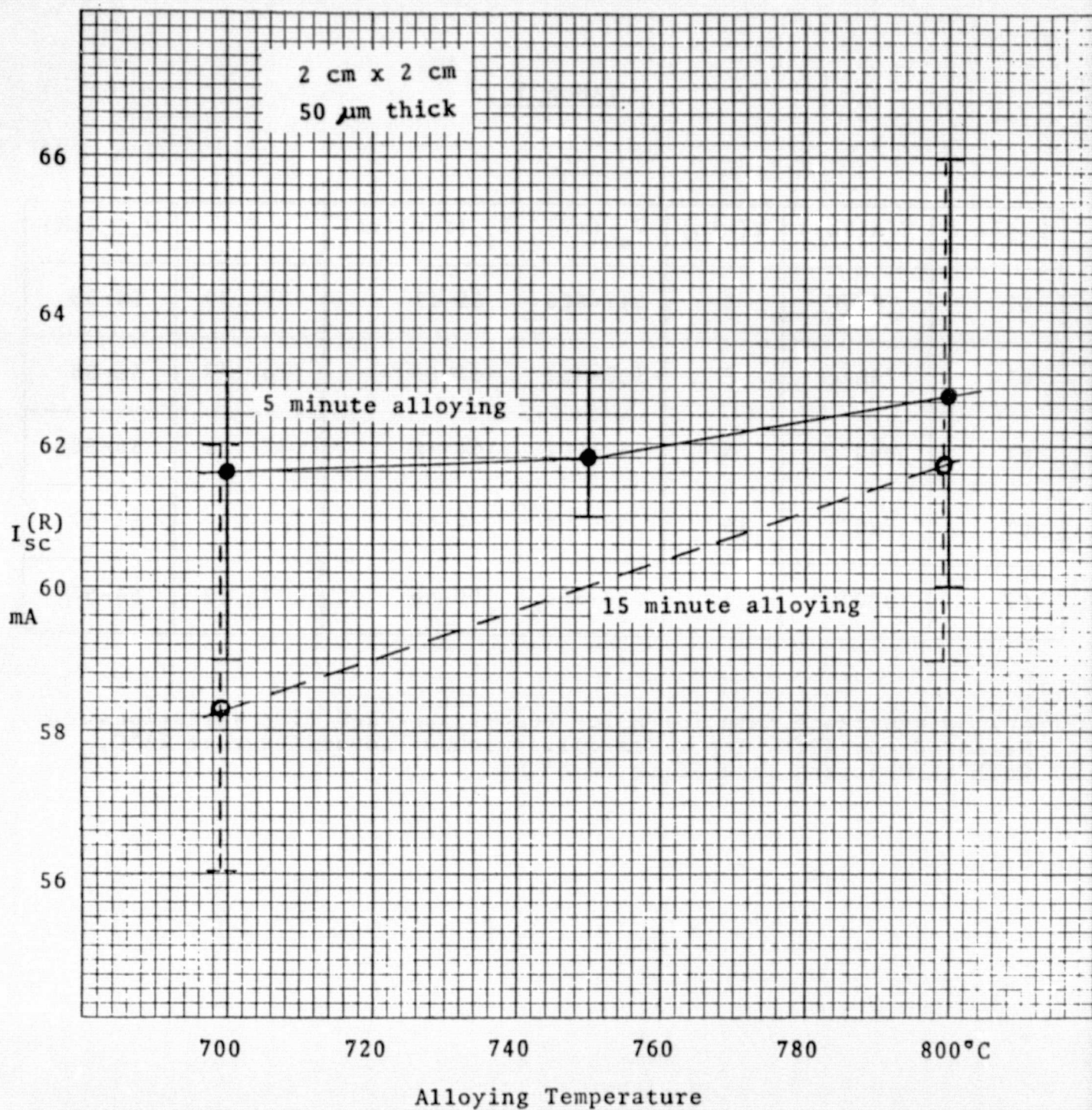


Figure 10. Effect of alloying temperature and time on the red component of the short-circuit current.

TABLE I

Exp't.#	T(alloy)	t(min)	V <sub>oc</sub> (mV)	I <sub>sc</sub> (red)(mA)	F	P <sub>max</sub> (mW)
67	700°C	5	547-555	59-63	.77-.79	54-58
67	750°C	5	550-557	61-63	.76-.77	53-58
67	800°C	5	552-561	60-66	.77-.78	56-58
67	700°C	15	550-558	56-62	.77-.79	52-57
67	800°C	15	550-556	59-66	.77-.80	54-58

Cell performance data for alloy temperature and time variations.  
Measured for fifty 2cm x 2cm cells without coverslides at 25°C,  
with thicknesses from 55  $\mu$ m to 65  $\mu$ m.

#### G. Power Output vs. Thickness

Reduction in solar cell thickness from the conventional 200-250 micron range down to the neighborhood of 50 microns reduces the minority-carrier generation volume for the long-wavelength end of the silicon absorption band. In addition, the closer proximity of the back contact to the front junction accentuates the effect of minority carrier recombination in the neighborhood of the back contact on reducing both the open-circuit voltage under illumination and the collection of minority carriers generated by intermediate to long-wavelengths. Despite these deleterious possibilities the ultra-thin silicon solar cells fabricated in this program retained most of the photovoltaic conversion efficiency achieved with similarly fabricated high-efficiency cells of conventional thickness. Figure 11 shows the peak power at AM0 for 2cm x 2cm cells of 2 ohm-cm and various thicknesses fabricated during this program. These cells were measured at 25°C without covers and are smooth-surface cells with tantalum oxide anti-reflection coatings. The improving efficiencies achieved during this program as shown in the figure resulted largely from experimentation on optimizing the technology for diffusion and improved  $p^+$  formation. The improvement over initial results achieved by the time just prior to freezing the technology utilized in the Pilot Line effort was further advanced for small quantities of experimental cells also shown in the figure as the latest results.

Figure 11 shows the output power over a wide thickness range and the improvements wrought by experimentation with the cell technology. The Pilot Line portion of this program, on the other hand, provided data for output power as a function of thickness for cells processed nearly identically in quantity. Figure 12 shows the AM0 power as a function of thickness (limited by the



	1st Year	Pilot Line	Best Cells
CZ	x	□	Δ
FZ	.	o	

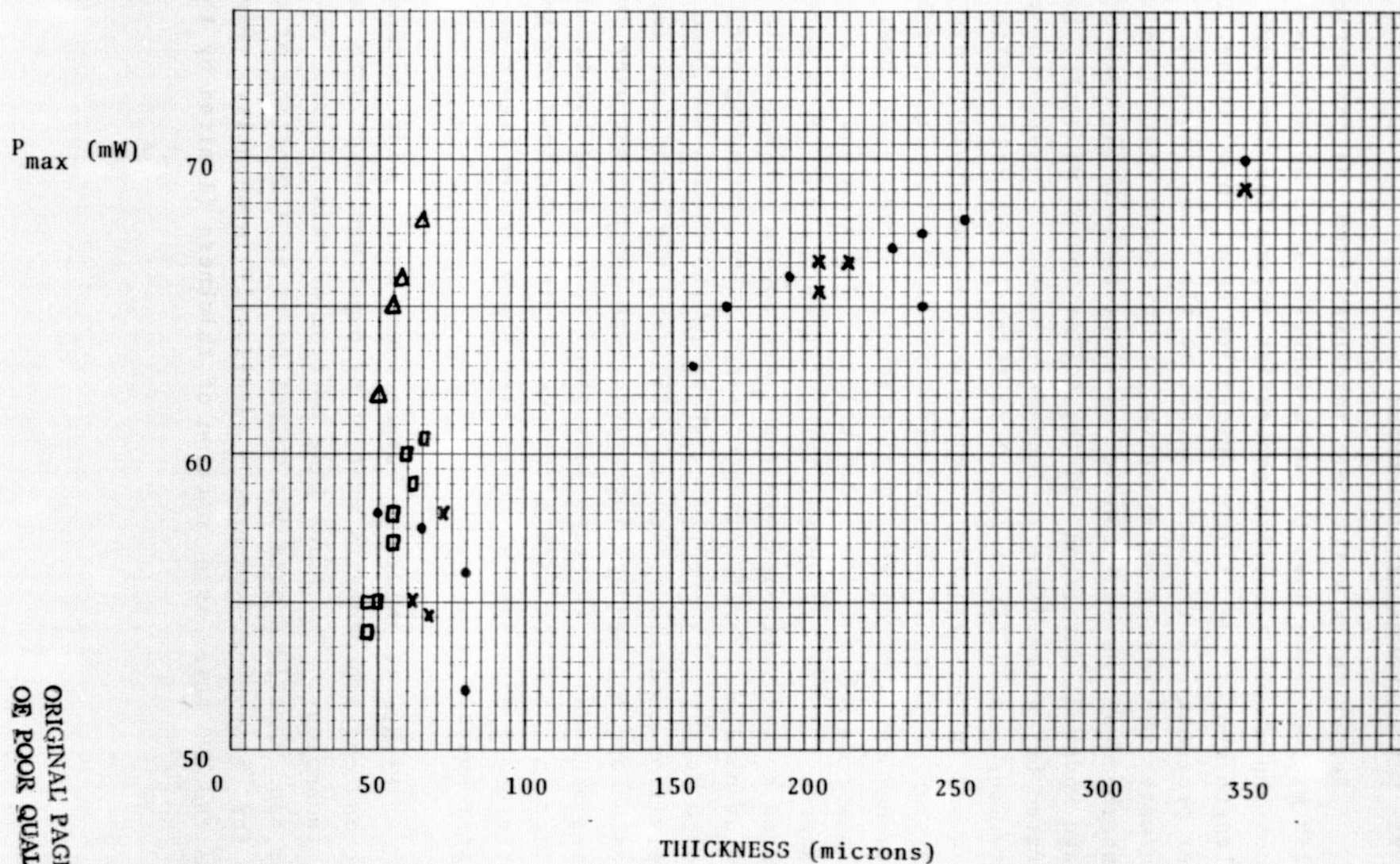


FIGURE 11. OUTPUT POWER AT AMO AND 25°C FOR 2CM X 2CM CELLS AS A FUNCTION OF THICKNESS (WITHOUT COVERSLIDES).

ORIGINAL PAGE IS  
OF POOR QUALITY

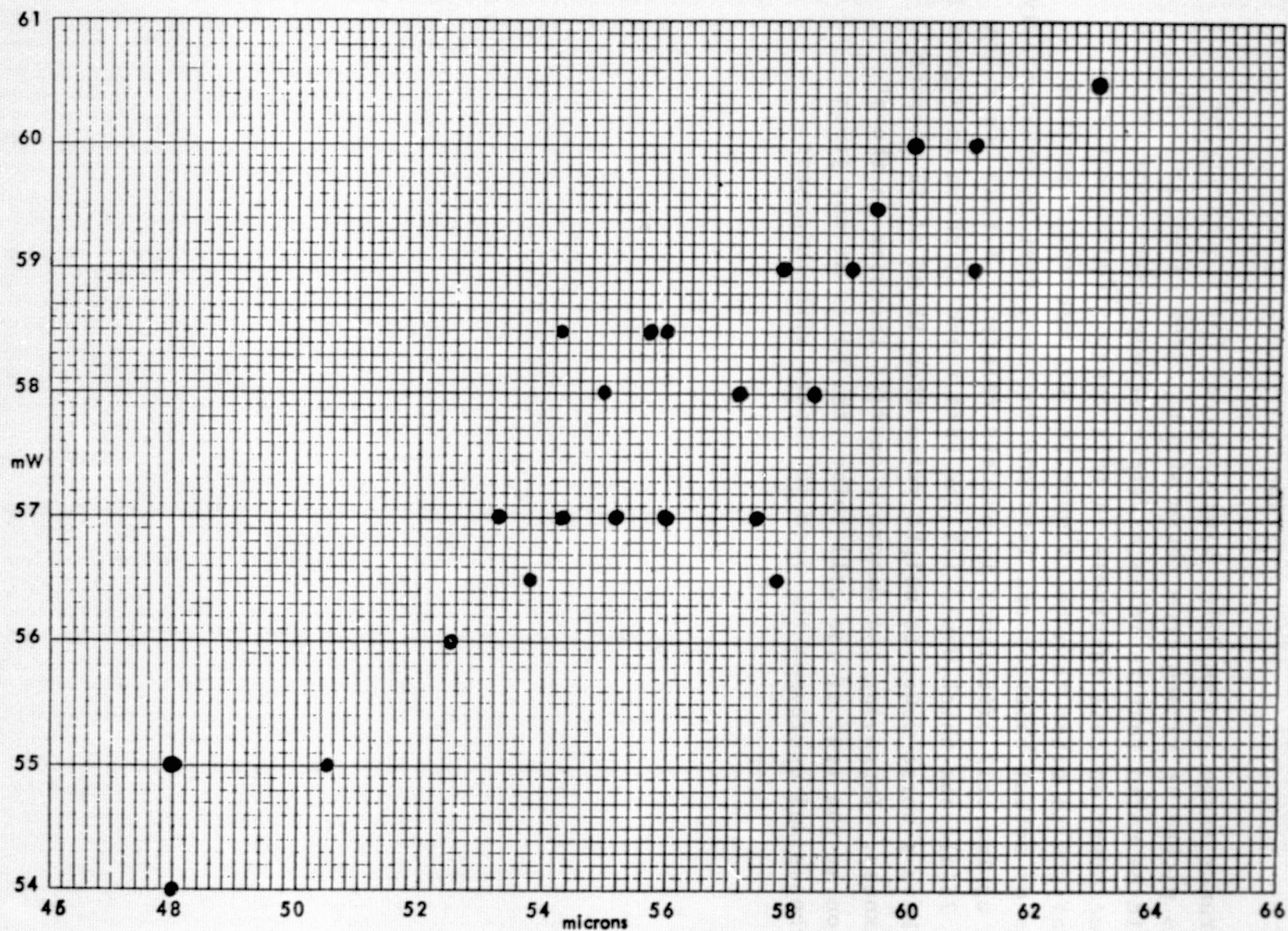


FIGURE 12. PEAK OUTPUT POWER AT AM0 FOR UNCOVERED 2CM X 2CM PILOT LINE CELLS OF THICKNESS IN THE NEIGHBORHOOD OF 50 MICRONS AT 25°C.(WITHOUT COVERSLIDES)

tolerance range in the Pilot Line program) for a quantity of cells picked at random from those which passed Final Q.C. It should be noted that there is a fairly strong dependence of output power on cell thickness in this range. Consequently, comparison to other thin cells must be scrupulously viewed in terms of actual thicknesses, lest one conclude that an unexpectedly high or low cell efficiency is process related. A 65mW 2cm x 2cm cell 75 microns thick would fit the same trend as shown in Figure 12 but have a worse power-to-weight ratio than 58 mW at 55 microns thickness. Improving the minority carrier lifetime in the  $p^+$  region at the rear of the cell raises the power at any given thickness and decreases the rate of change with thickness.

ORIGINAL PAGE IS  
OF POOR QUALITY

#### H. Excess Forward Current & Low-Temperature Behavior

The application of very thin silicon solar cells to interplanetary missions which can experience multiples of 1AU provokes interest in how the junction forward voltage varies as a function of injected current density. An ideal forward characteristic has the form:

$$I = I_0 \exp\left(\frac{qV}{kT} - 1\right)$$

Crystal damage, resulting electronically active defect centers, mid-gap states from undesirable impurities and imperfect edge finishing modify the ideal characteristic to:

$$I = I_1 + I_2 = I_{01} \exp\left(\frac{qV}{n_1 kT} - 1\right) + I_{02} \exp\left(\frac{qV}{n_2 kT} - 1\right)$$

where the values of  $n$  are greater than unity ( $n_2$  is nearly unity) and the values of  $I_0$  are larger than in the ideal case. The most common effect on a solar cell is to reduce the junction forward voltage at low injection current densities (where  $I_1$  is dominant) from the ideal case and consequently the output voltage of the cell at low light levels. One of the physical factors affecting the junction forward characteristic is residual work damage from sawing slices out of ingots. In general, very thin cells are etched more than thicker cells and thereby have their junctions at a position in the slice which is further from the original sawed surface. Consequently, they tend to have more ideal forward characteristics than thick cells simply because there is less chance of residual work damage in the resulting slice. In addition, of course, there are a myriad of other factors which require a sophisticated approach to their control. These include such topics as impurity solubilities, interfacial segregation, crystal stresses, slice flexure during high temperature furnace treatment, etc., which are a topic of continuing study.



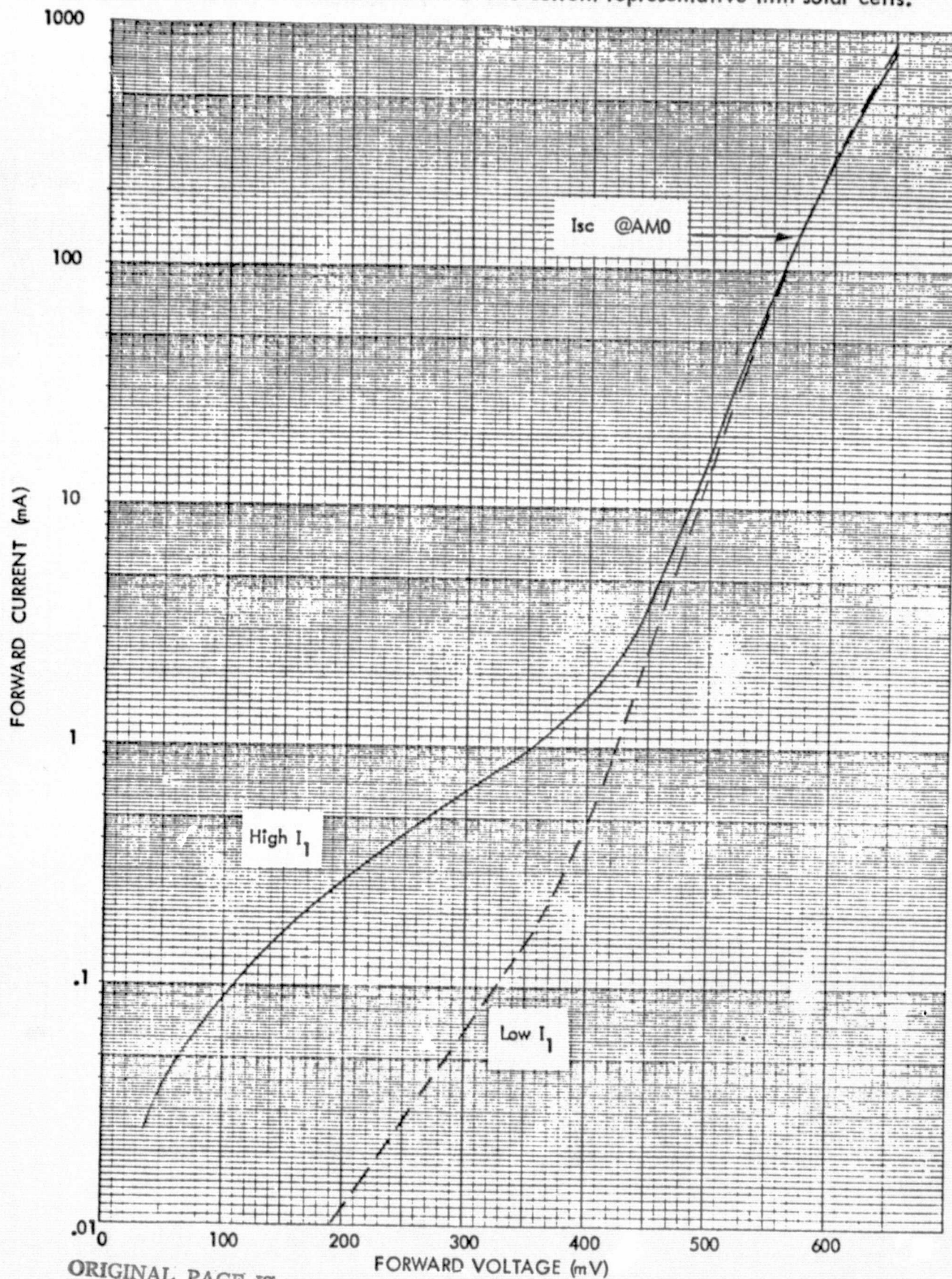
The present status of typical ultra-thin solar cell junction characteristics from this program is demonstrated in Figure 13. The two samples in the plot are from different experimental groups and the lot-to-lot variation in the  $I_1$  component is apparent. We are working on this area and think  $I_1$  will be brought under control in the near future.

Figure 14 is a plot which shows the low temperature behavior of a cell having a lower  $I_1$  component as for the lower curve in Figure 13. Here the importance of controlling the  $I_1$  component of the junction injection current becomes obvious. On missions reaching multiples of 0.1 AU both the incident light intensity and the cell temperature will drop. In order to fully realize the benefit of higher voltages expected at lower temperatures the cell's  $I_1$  component must not intersect the  $I_2$  component at current densities greater than a fraction of the short circuit current produced at the decreased incident intensity. The cell characteristics shown in Figure 14 have an intercept of the  $I_1$  and  $I_2$  components at approximately 1.3% of the 1 AU AM0 short circuit current even at  $-100^\circ\text{C}$ . The rise in the intercept current level occurs because  $I_2$  is controlled by the silicon bandgap energy, while  $I_1$  has a considerably smaller activation energy and therefore changes less as the temperature is decreased. The lower  $I_1$  is, the better the maintenance of the fill factor and the better the improvement of operating voltage to help compensate for decreasing  $I_{sc}$  at multiples of 0.1 AU.

Figure 15 shows the illuminated I-V characteristics at  $25^\circ\text{C}$  and  $-100^\circ\text{C}$  for 5% of AM0 1 AU incident intensity of a thin cell from the same group as in Figure 14. It can be seen that these cells have an  $I_1$  component of injection current low enough to maintain their fill factors at low intensities. The efficiency at  $25^\circ\text{C}$  for 5% sun is only 8.3%, but that is an artificial laboratory condition.

ORIGINAL PAGE IS  
OF POOR QUALITY

Figure 13. Dark forward characteristics of two current representative thin solar cells.



ORIGINAL PAGE IS  
OF POOR QUALITY



Figure 14. Effect of low temperature on the junction forward I-V characteristic for the thin cell of the lower curve in Figure 2.

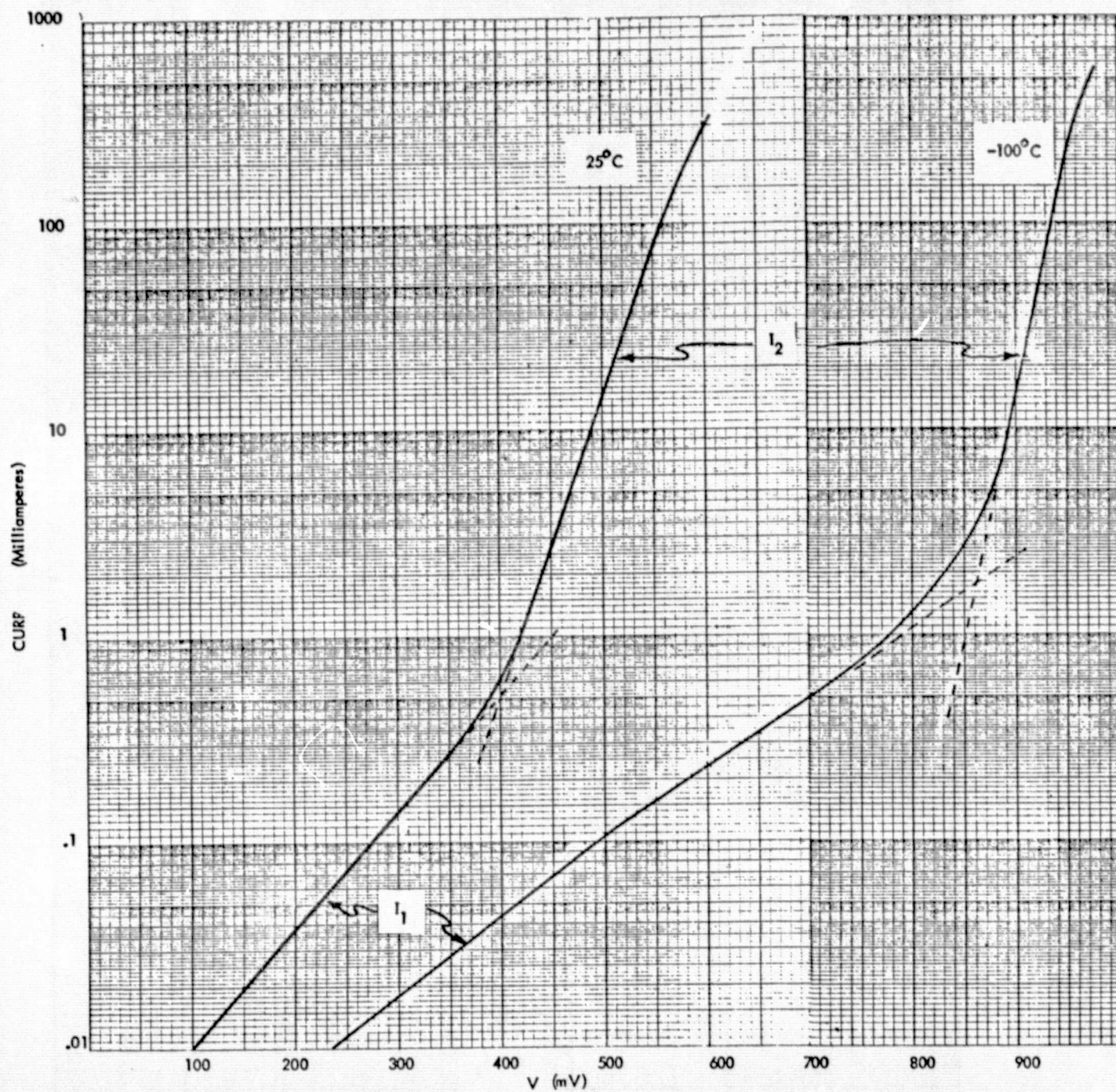
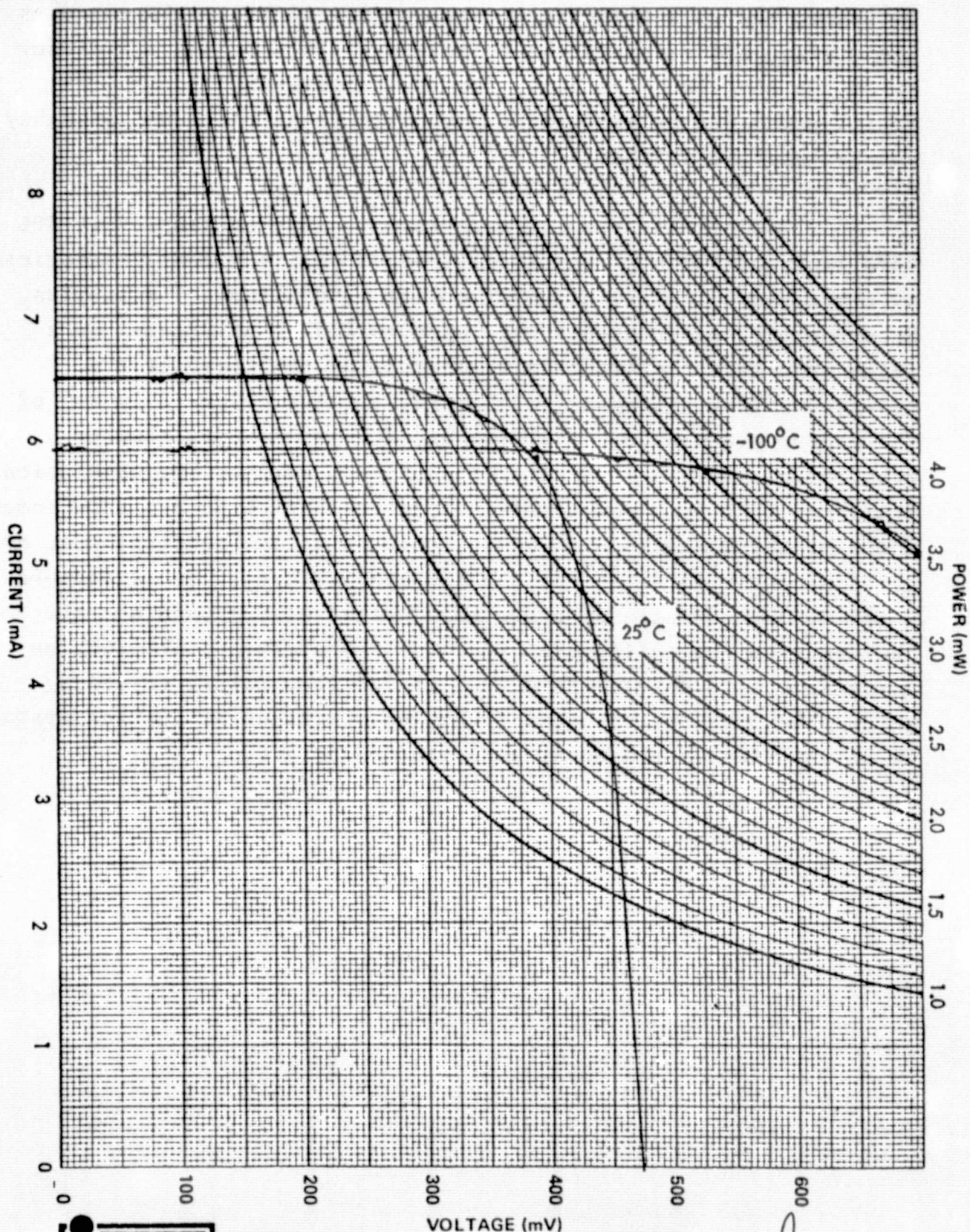


Figure 15. Low light level I-V characteristic of a 50 micron 2cm x 2cm cell for 5% of AM0 1AU illumination.



Cell Type 2 mil No 2009-3 By C.W. Date 4/12/77



In space, the cell temperature drop at low light levels improves the voltage and recovers the efficiency. This cell's efficiency at 5% sun and  $-100^{\circ}\text{C}$  is 13%. The low-temperature, low-current efficiencies can be kept quite high with these cells and probably can be improved further.

During this program measurements made on samples at JPL were reported which showed a collapse of cell I-V characteristics at temperatures in the neighborhood of  $-100^{\circ}\text{C}$  for a few samples. Subsequently, measurements were made to  $-120^{\circ}\text{C}$  at Solarex on a large quantity of ultra-thin cells to find the cause of the observed effect. However, the effect was not observed in any of the measurements made at Solarex and the temperature chamber measurements were halted after a couple of weeks. The conclusion drawn was that some few of the sample cells sent to JPL were somehow under-sintered and had non-ohmic contacts at low temperatures, or gridline adhesion failed at the low temperatures. Since measurements at JPL on cells of other manufacture also showed a small incidence of the collapse at very low temperatures, it would be advantageous to develop some type of low-temperature screening methodology for any cells destined for operation at low temperature on interplanetary missions, as suggested by JPL.

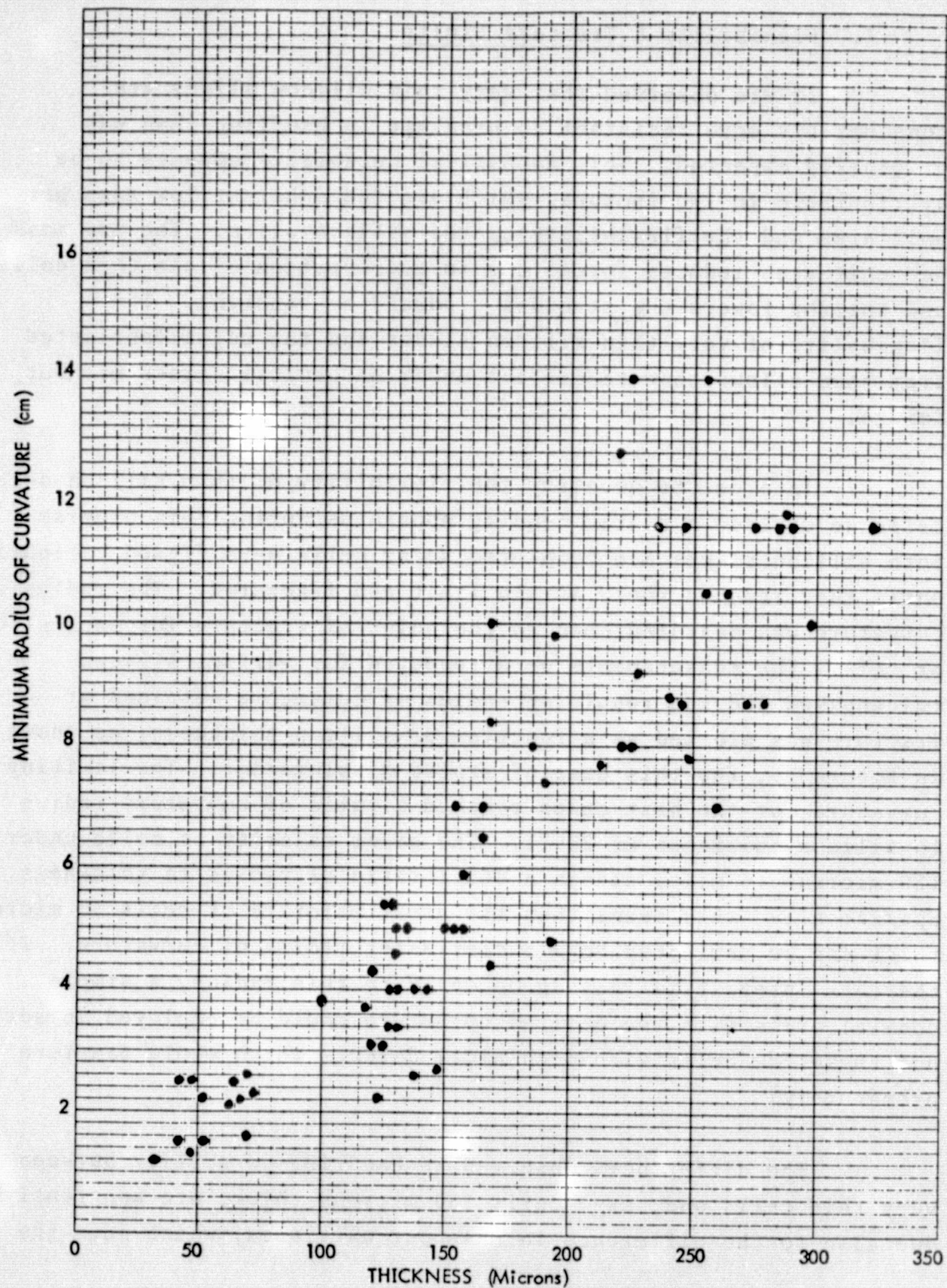
## I. Flexibility & Fracture Limits

It was observed that very thin silicon slices are considerably more resistant to breakage in handling than was originally expected. This mechanical durability appears to be attributable to two factors, which are the inherent low mass per unit area and the flexibility of the silicon slice. The low mass per unit area reduces forces due to acceleration on the thin cells and thereby lowers the stresses produced by handling. The flexibility of very thin silicon slices and the cells fabricated from them allows them to deflect under mechanical stress without damage.

In order to quantify the flexibility of thin silicon solar cells we devised a static bending apparatus during this program. Both silicon slices and completed solar cells were flexed cylindrically until they reached their strain limit and fractured. The radius of curvature was measured down to the point of fracture for each slice or cell. The measurements were repeated for various silicon thicknesses and the resulting radius of curvature attained at fracture was plotted as a function of silicon thickness, as shown in Figure 16, for this case of static displacement. The limiting curvature for the best cases reached a ratio of curvature radius to silicon thickness of 200:1. The great majority of cells under 150 microns (6 mils) attain a 400:1 ratio of radius to thickness. Specifically, this means that the great majority of cells 50 microns thick can be deflected to a 2 centimeter radius of curvature. If there is interest in rolling up cells to this radius, a simple coaxial press with the desired curvature could be employed to sort out those few cells with mechanical defects which would fracture prematurely.

The differences observed in handling durability between very thin cells and, say, cells 150 microns thick, are apparently due also to the difference in mass per unit area, which sets the

Figure 16. Radius of curvature at fracture vs. cell thickness.



stress under acceleration. The measurements reported in Figure 16 are strictly for the case of static deflection and do not reflect the difference in the dynamic case.

These measurements do relate to one important consequence of flexibility as a function of thickness. Large ultra-lightweight arrays made from thin cells can be rolled up onto quite small drums for launch configuration without damaging the cells.



## J. Stability Tests

Determinations of the stability of cell electrical and mechanical characteristics were performed during the program on 50  $\mu\text{m}$  thick cells as called for in the contract schedule. No discernable changes occurred for 50 hour thermal soaks at 150-160°C, which was the first type of test. The second type of test was the thermal shock produced by putting the thin solar cells in liquid nitrogen (-196°C) and rapidly transferring them to boiling de-ionized water at 100°C for five (5) complete cycles. When the solar cells are put into the liquid nitrogen they quickly curl cylindrically to a radius of some few centimeters. This behavior is not surprising since the test cells were not supported and mainly consist of a layer of 8  $\mu\text{m}$  of silver on some 42  $\mu\text{m}$  of silicon. The larger thermal expansion coefficient of silver compared to silicon would be expected to put the back silver layer in tension compared to the silicon when in liquid nitrogen.

The 5-cycle thermal shock tests produced no discernable changes in 80% of the first lot tested, but decreased the fill factors to lower the peak output power by 1mW to 2mW in the remaining 20% of the lot. Examples are shown in Figure 17 and Figure 18. This result points out not an inherent problem with cell construction, but rather a measurement problem. These early ultra-thin solar cells did not have the common procedures of evaporation lot tape test, nor solder pull test. The reason is that the tape glue is so strong relative to the thin silicon that tape testing for contact adhesion is 100% destructive. Also, soldered-tab pull testing shatters the thin silicon far below the minimum forces in any published specifications for thick cells. Consequently, the experimental thin cells fabricated during the first half of the program had not even been subjected to the usual contact metallization testing procedures, except for visual inspection at contact sintering, anti-reflective coating and electrical measurement steps in the fabrication process.

ORIGINAL PAGE IS  
OF POOR QUALITY

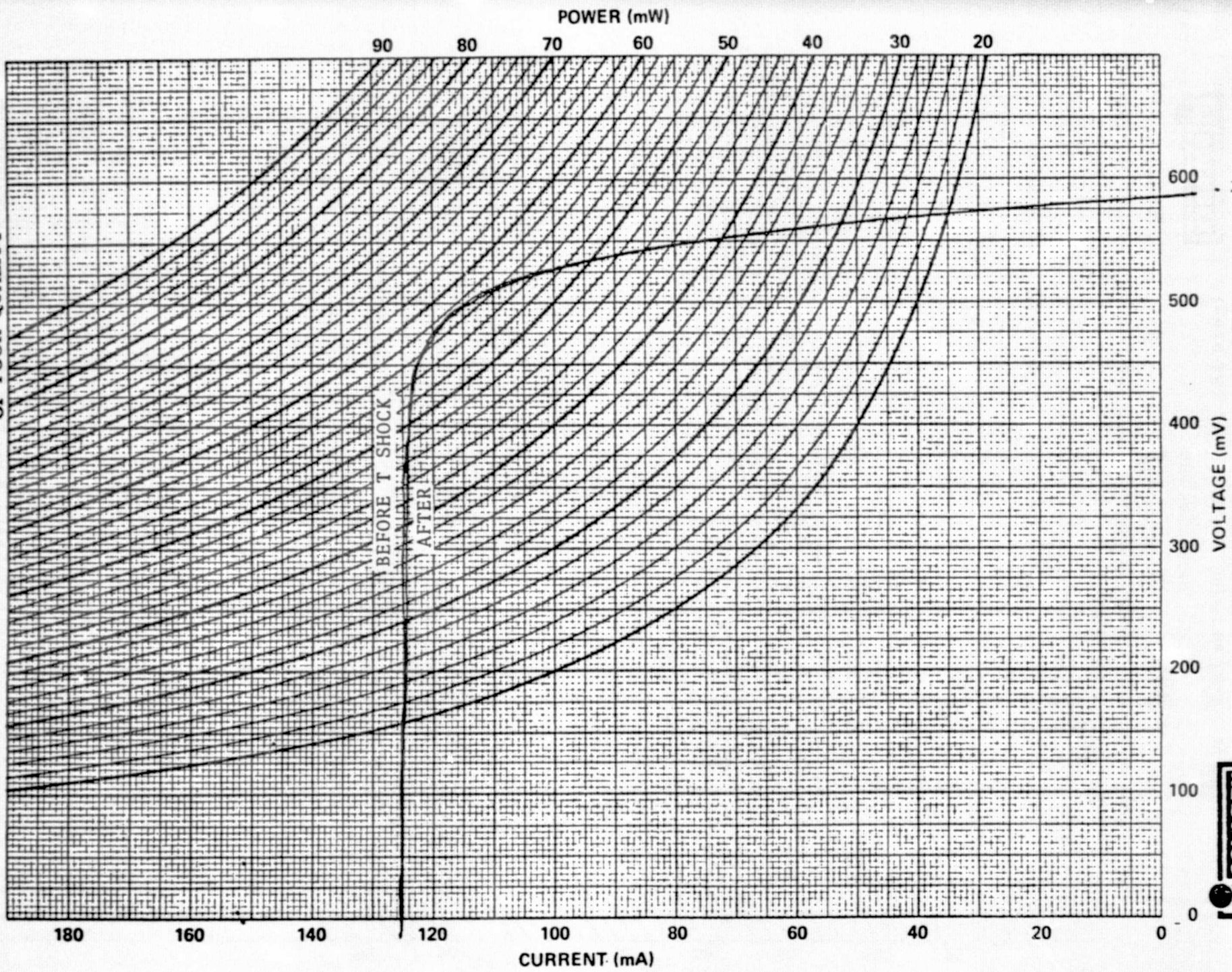


Figure 17.

Cell Type .002" No. 76-4 By J.C. Date 8-19-76  
-51-



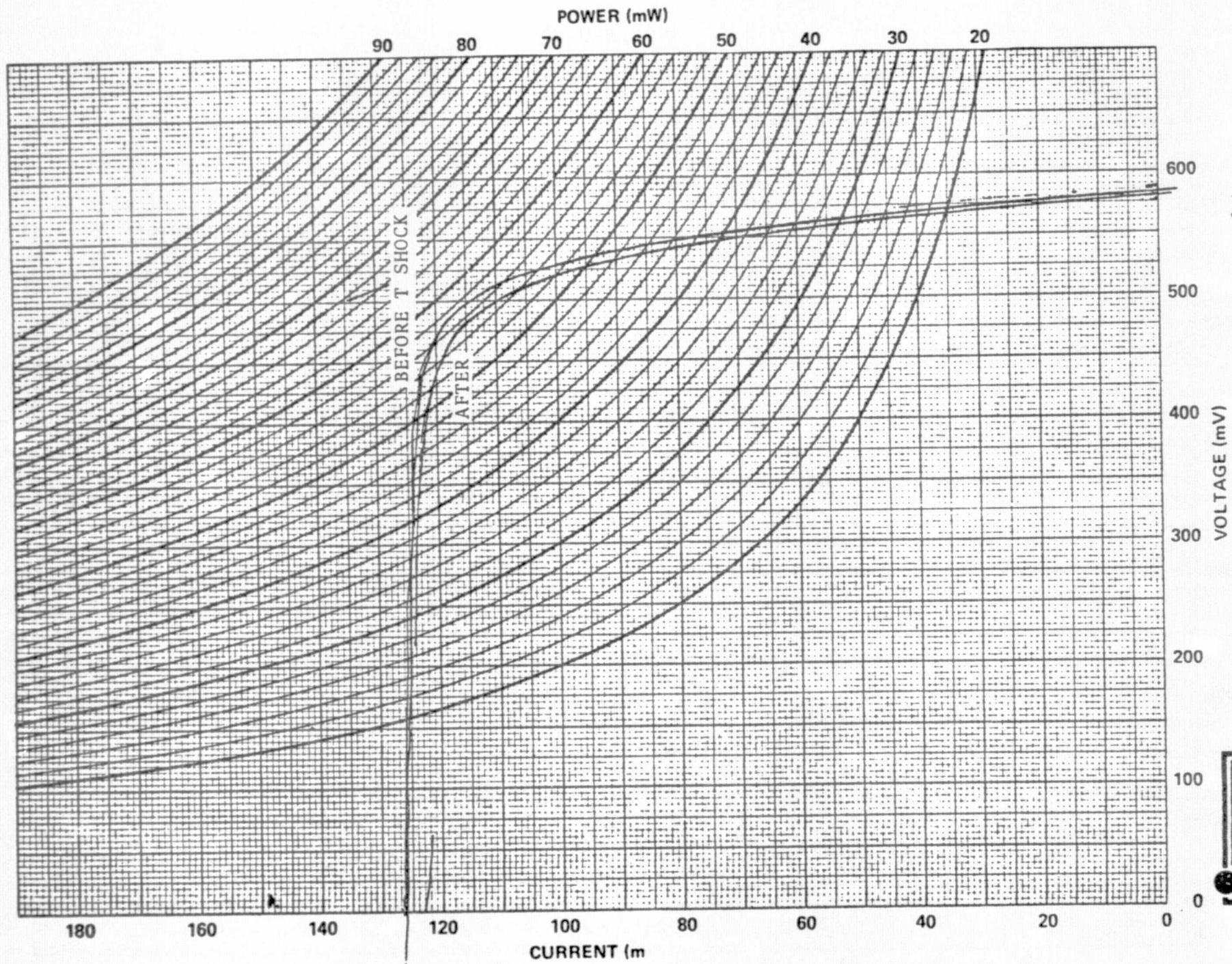


Figure 18. Cell Type .002" No. 76-6 By JC Date 8-19-76



A new measurement technique for assuring the contact adhesion reliability of very thin cells has to be found. Direct tape testing provided no information because the silicon itself shattered. It was suggested that perhaps the thermal shock test itself would be the most useful.

Subsequent study of this problem led to significant progress in techniques to assure contact adhesion. Improved attention to details of cleanliness before contact evaporation and contact sintering techniques were the most fruitful areas. The main attention in sintering technique was directed to reducing flexing of the solar cells before the contact sintering was completed. The usual structure has 6-8 microns of silver (plus thin Ti-Pd) over its entire back surface. Rapid heating to sintering temperature causes extreme flexing of the cell and apparently caused local delamination of the deposited metal on the front grid before intimate fusion with the silicon occurred in some cases. Changing the heat-up technique to avoid flexing of the cell until grid sintering occurs apparently eliminated the partial delamination. Series resistance increase as in Figure 18 was not observed after the flexure at thermal shock tests on sample quantities of the ultra-thin cells subsequently fabricated. In addition, in order to provide confidence in-process, co-cleaned thick silicon slices co-evaporated with ultra-thin cells are tape-tested for metal adhesion.

#### K. Minimization of Bowing

Thin silicon slices of only some 50 microns thickness have some residual bowing after etching to thickness, as do the solar cells after processing. This curvature is a result of the cells' flexibility, residual stress in the silicon and having full coverage of 8 microns of silver on the backs of the solar cells v.s. silver only in the gridwork on the fronts. Upon cooling after the contact sintering treatment the silver (which has the larger coefficient of thermal expansion) shrinks more than the silicon, adding slightly to the curvature as mentioned above. This does not occur to any significant degree for thick cells where the silver is a small fraction of the silicon thickness and the slices are too stiff to bow significantly.

Although the residual bowing of finished 50 micron 2cm x 2cm cells is only in the neighborhood of a millimeter at room temperature it does increase significantly upon dropping some 200°C to liquid-nitrogen temperature. Since we have not observed fracturing of cells even with the latter degree of bowing, it is not necessarily deleterious to cell life in space environments. However, in this program we have experimented with interrupting the continuity of the silver layer on the cell back to observe its effect on the bowing from differential expansion. It was found that interrupting the silver on the back by shadowing with a screen grid which eliminated some 10% to 20% of the silver area reduced the bowing by approximately a factor of five. After cooling in liquid nitrogen the usual five-millimeter bowing of uncovered 2cm x 2cm cells was reduced to approximately one millimeter. Very similar results were obtained with a dot pattern which eliminated approximately 50% of the silver coverage on the backs. Sample cells from this experiment were forwarded to JPL for evaluation.

Although gaps were introduced in the back silver layer's current path, no significant increase in series resistance was observed. This was not surprising, considering the full coverage of the cell back by the p+ aluminum alloyed layer under the interrupted Ti-Pd-Ag.

L. Absorptance and Emittance Measurements

The absorptance and emittance of representative ultra-thin solar cells were measured with ceria doped microsheet covers attached. The absorptance was obtained by measuring reflectance from 240nm to 2500nm on our Beckman DK-2A spectrophotometer with its Gier-Dunkle integrating sphere, weighing with AM0 spectral irradiance in 100nm intervals and subtracting the result from unity. The emittance was obtained by measuring wide-band long wave infra-red reflectance with our Gier-Dunkle infra-red reflectometer and subtracting the reflectance from unity. The values obtained for absorptance for 50 micron cells were found to lie in the range of 0.85 to 0.87 with the differences due mainly to the reflectance at the silicon-aluminum interface. The emittance with the ceria doped covers was 0.85, which results in alpha to epsilon ratios of 1.00 to 1.03.

Earlier efforts under this contract were concerned with the reflectance at the back silicon interface, which was not a consideration in selecting these samples. They were not optimized for internal reflectance, but just picked from later representative samples. Changing the internal reflectance does alter the absorptance.

ORIGINAL PAGE IS  
OF POOR QUALITY

### M. Handling Techniques

The resiliency of ultra-thin silicon is very dependent upon the thinning technique, but with the technology developed in this program, as described above, the handling becomes considerably less critical. These rather springy cells have been routinely subjected to almost the same handling during processing as cells of conventional thickness. All chemical etching, rinsing, etc. is done in the conventional plastic carriers employed in high-volume production of thick silicon solar cells. Diffusion and alloying is routinely done with the cells standing in high-density quartz boats; requiring only slightly greater care in loading and unloading than thick cells. Loading of each piece is done with conventional tweezers in a surprisingly cavalier fashion without breakage.

A step which does require caution is evacuating or back-filling evaporators, as these very light cells are prone to blow about in the air stream. Throttling the back-filling air flow into the evaporators and restraining the slices to the tooling has solved the problem and only added a few minutes to the operation.

Another processing step requiring some care is rinsing and centrifugal spin-drying. High flow rates normally employed to rapidly flush deionized water rinsers can fracture cells restrained in baskets and must be throttled to gentler flows. Similarly, although centrifugal drying in commercially available spin-dryers does not contribute to slice breakage by itself (thanks to low slice mass and flexibility), spray rinsing or fast acceleration while the slices are constrained by the baskets can produce breakage. Consequently, slices were rinsed after chemical processing steps in a recirculating deionized rinser and spun dry in a Fluoroware Systems spin dryer at moderate speeds.

ORIGINAL PAGE IS  
OF POOR QUALITY



It now appears that there are rather few significant problems in handling very thin cells during processing and that they can be treated much like thick cells, except for avoiding very rapid jerks or other high torque situations during individual steps or transfers. None of these reasonable precautions are inherently production rate limiting.

Other aspects of handling which require some caution were discovered early in the program. Although the ultra-thin cells are extremely flexible and quite resistant to breakage in normal handling, they can be crushed with relatively moderate forces. As just discussed, this can occur with slices constrained to wet-processing plastic baskets. Crushing can also occur in thickness measurement or shipping. Thickness measurement with micrometers, calipers or dial gauges can apply extreme localized stresses unless great care is taken in handling. Consequently, an out-of-contact differential capacitance thickness gauge (ADE Corp. "microsense") was obtained for measuring large quantities of slices in the Pilot Line phase of this program. Such an instrument only requires passing the slices between sensors spaced a millimeter or so apart and eliminated breakage at thickness measurement.

Shipping breakage was found to be due to using polystyrene foam containers with cell slots under 2cm in depth. These containers allowed the box lid to crush the cells against the slot bottom without bowing, for forces less than affected cells of conventional thickness in shipping. Boxes with slots deeper than 2cm eliminated the problem, as the cells do not suffer any significant breakage rattling in the deeper slots.

#### N. Production Rate-Limiting Steps

After a considerable review of the process technology for fabricating ultra-thin silicon solar cells in this program we had to conclude that there really are not any steps limiting production rates other than the thinning etch for the starting slices and subsequent rinsing steps. Beginning with conventional slice thicknesses as-sawn of some 13 to 16 mils (330 to 400 microns), the NaOH etching alone takes approximately 45 minutes to reduce the slice thickness to some 50 microns. In addition, starting slices were sorted into narrow ranges of thickness in order to produce batches of etched slices of the same thickness, which took additional time. Thinner starting slices would, of course, reduce the etching time. This process is, however, a batch-etching process and etching more slices simultaneously would alleviate the time factor. So far, there was not production-quantity pressure to etch more than approximately 50 slices at once, but a larger etch bath could as easily be monitored by the same operator doing well over a hundred slices at a time.

Handling speeds are necessarily slightly slower than with conventional slices and cells, but the extra second or so per transfer is not felt to be rate-limiting in the overall process time. Rinsing is also a bit slower due to gentler flow rates for rinse water, but only amounts to minutes per batch processed.

It should be mentioned that the process employed in this program at Solarex avoided any difficulties in loading shadow-mask tooling with ultra-thin slices by employing photolithography for front-pattern gridline generation. This latter technology creates intimate mask contact with vacuum chucks and air pressure which eliminates any difficulties with slice bowing and mechanical flattening apparatus.

## O. Radiation Resistance

Ultra-thin silicon solar cells would be expected to be more tolerant of bulk crystal damage than silicon solar cells of conventional thicknesses. This improved tolerance to radiation damage in the crystal bulk is simply due to the fact that these cells do not have minority carriers generated by longer wavelengths of incident light 200 microns or so from the collecting junction. Consequently, power loss due to high-energy electron bombardment would be expected to be lower for ultra-thin cells.

Figure 19 is a plot of the relative peak power output as a function of accumulated 1MeV electron dose for 50 micron and 250 micron thick similarly processed uncovered 2cm x 2cm cells which all had equivalent short-wavelength response. Also shown for comparison in Figure 19 are data from Meulenberg, Curtin and Cool\* on relative peak power degradation of 225 micron and 250 micron thick uncovered planar surface high-efficiency cells from other manufacturers. The ultra-thin cells still produce over 90% of their beginning-of-life power at an accumulated 1MeV electron dose of  $7 \times 10^{14} \text{cm}^{-2}$ . The 85% of beginning-of-life power level is not reached by these ultra-thin cells until the accumulated 1MeV electron dose exceeds  $1 \times 10^{15} \text{cm}^{-2}$ . Consequently, designs for space power systems which would utilize these ultra-thin cells could work with considerably improved end-of-life conditions.

---

\* A. Meulenberg, D.J. Curtin and R.W. Cool, "Comparative Testing of High Efficiency Silicon Solar Cells", 12th IEEE Photovoltaic Specialists Conference Proceedings, Baton Rouge, La., 1976, pp. 238-246.

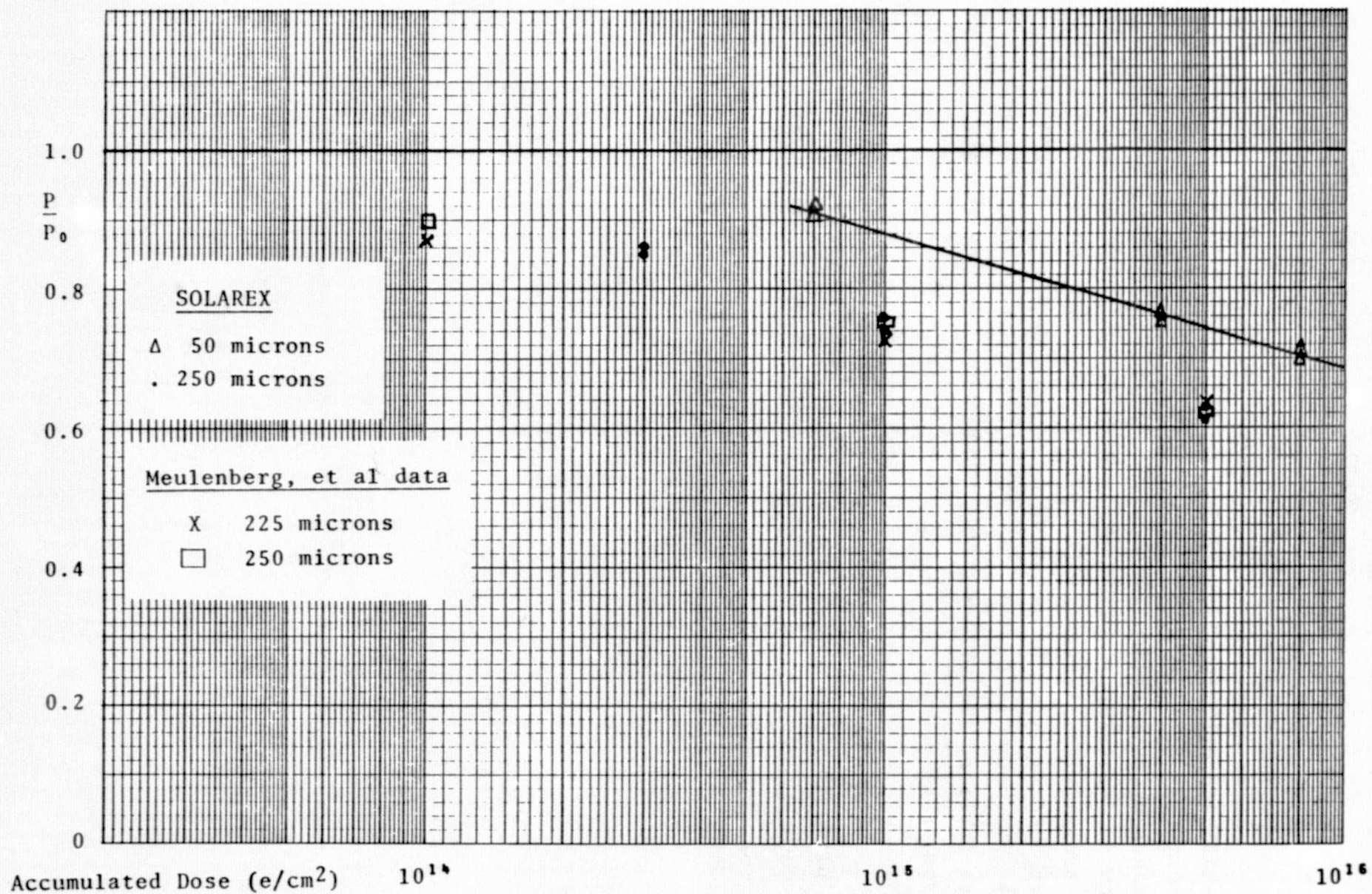


FIGURE 19. CHANGE OF  $P_{max}$  WITH ACCUMULATED 1 MeV ELECTRON DOSE FOR CONVENTIONAL-THICKNESS AND ULTRA-THIN CELLS.

P. Pilot Line Program

A few months into the second year of this program NASA-OAST and JPL requested that pilot production of ultra-thin high-efficiency silicon solar cells be implemented to produce thousands of such cells for assembly trials. A Pilot Line was designed, dedicated equipment was obtained and installed, personnel were trained for its operation and the line was successfully operated to produce the required solar cells, all in a time span of slightly over a quarter. A copy of the previously released report covering the entire pilot production portion of this program is attached to this report as an Appendix.

The highly successful pilot production program demonstrated that ultra-thin silicon solar cells have the potential to be manufactured with acceptable yield and reasonable cost.

Q. Fabrication Processes Developed Specifically for Ultra-Thin Cells

Successful fabrication of ultra-thin silicon solar cells required not only the breakthrough in etching technology, but also tailoring several process steps to result in good processing yields. Those felt to differ from standard solar cell processing practices common throughout the industry are specified as follows.

1. Slice Thinning

Starting as-sawn (100)-oriented slices (pre-cleaned in solvents) are placed vertically in Teflon plastic slice carrier baskets. These baskets are immersed in approximately six inches of NaOH + H<sub>2</sub>O solution maintained at 100°C to 110°C in a stainless steel vessel. The etching solution is from 18% to 40% by weight NaOH, with 22% being near optimum for reproducibility, but not critical. Slice thickness reduces at a rate of approximately 7 microns per minute.

At the completion of alkaline etching the basket is rinsed in tap water and then immersed in a 50:50 solution of concentrated HCl and water for ten minutes to remove alkali-silicate residues before final rinsing.

2. Diffusion

Slices are dipped for 10 seconds in 10:1 to 20:1 diluted HF, rinsed in deionized water, spun dry at low speed (approximately 500 rpm) and 50-100 are stood vertically in a slotted quartz diffusion boat.

They are then loaded into a 90mm quartz diffusion tube flushed with argon in a tubular furnace set at 860°C. Insertion of the loaded boat into the hot zone of the furnace tube should be done with gradual motion over a three minute period. Diffusion source gasses are then turned on for 20 minutes with the following flow composition:

Argon	:	2.3 liters per minute
1% Phosphine in Argon	:	2.3 liters per minute
Pure oxygen	:	0.3 liters per minute

Withdrawal is also a slow pull in argon atmosphere. Sheet resistance of the resulting diffused n layer should be in the immediate neighborhood of 80 ohms per square.

### 3. Back Aluminum Alloy

The diffusion glass alone is removed from the slices in 10:1 diluted HF and the slices are rinsed in deionized water. Pure aluminum (99.999%) is evaporated on one side of the slices to a thickness of 2000<sup>0</sup>Å-5000<sup>0</sup>Å.

The slices are then placed vertically into another quartz diffusion boat and loaded into a furnace set at 800°C with argon atmosphere (5 liters per minute flow) and kept in the hot zone for 10 minutes. Loading and unloading are also performed over 3 minutes each. The rear n layer is not removed, but alloyed through.

### 4. Front Gridline Pattern

In order to eliminate breakage of ultra-thin cells in shadow-mask tooling (they bow slightly and are difficult

to maintain in close contact without a high incidence of breakage) photolithography with Shipley Co. photoresist type AZ1350J is employed for gridline generation. Standard processes as recommended by the manufacturer are employed, with application spinning at approximately 2500 rpm, and care in developing and rinsing not to agitate the slices too violently while immersed in the solutions. Gridline pattern employs 5 micron lines spaced no more than 0.18 cm apart.

5. Metallization

Ti-Pd-Ag, unchanged from practice for thick cells.

6. Edge Finishing

Same as for thick cells.

7. AR Coating

Tantalum oxide powder is pre-melted with an electron beam before the actual deposition. Coating is deposited on the cells by electron-beam evaporation from the previously melted source.

8. Contact Sintering

Ultra-thin cells warp on heating and can loosen gridlines before sintering occurs. Cells should be heated from the front so that gridline sintering temperature is reached before the rest of the cell is at temperature.

9. Handling

Slice transport with tweezers should not exceed 50-70% of the speeds usually employed with thick slices.



Wet-processing baskets should not be jerked while in solutions or rinses. Slices should be positioned in basket slots so as to already bear on outboard slice edges before accelerating in spin dryers. Inattention to this detail will increase breakage markedly as the rinse-water-droplet mass is very significant compared to slice masses.

Gentle restraint of slices over complete area and throttled backfilling of vacuum systems eliminates breakage from flutter and flying out of tooling.

Storage and shipping containers must be such that the cells cannot be subjected to high edge forces, especially without room to curl under the force.

Slices and cells should not be picked up by corners with tweezers.

Use flat-blade tweezers in handling, preferably the type with at least half-centimeter-wide ends.

10. Contact Adhesion Tests

Common tape-testing and bond pull-strength tests are both destructive. Tape testing by evaporation lot is inferred by association from tape-testing of co-evaporated thick slices.

11. Other Steps

Other than specifically mentioned in the above ten topics the standard techniques employed in solar cell manufacturing technologies are fully applicable. Caution should be exercised in applying sharp 4-point probes, performance test probes, etc.

#### IV. CONCLUSIONS & RECOMMENDATIONS

##### A. Conclusions

The breakthrough in slice thinning technology made the fabrication of flexible ultra-thin silicon solar cells feasible.

A fabrication process for ultra-thin cells tailored to relatively high cell efficiencies with concurrent good fabrication yields has been demonstrated, including pilot production quantities.

These cells have extremely high power to weight ratios, already producing over 60 mW from 2cm x 2cm cells 50 microns in thickness under 1AU AMO illumination with covers attached.

##### B. Recommendations

Further investigations to further improve the efficiencies of ultra-thin silicon solar cells are warranted. Cells of 2cm x 2cm x 50 microns have been routinely produced with conversion efficiencies of 11%, while a few cells reaching 12.5% have been fabricated. This would entail careful experimentation with technologies to improve the longer-wavelength photocurrent collection and to produce voltage improvement, while not jeopardizing processing yields.

Further pilot production of ultra-thin cells is warranted to familiarize the photovoltaic community with quantities of such cells and the performance of arrays.

Larger cell sizes should be fabricated. Some few larger cells were experimentally fabricated during this program with little difficulty compared to 2cm x 2cm cells, but not in any quantity.

V. APPENDIX



## PILOT LINE REPORT

### DEVELOPMENT OF A HIGH EFFICIENCY THIN SILICON SOLAR CELL

JPL CONTRACT NO. 954290

June, 1977

Report No. SX/105/PL

By

Joseph Lindmayer, et al

SOLAREX CORPORATION

1335 Piccard Drive

Rockville, Maryland 20850

This work was performed for the Jet Propulsion Laboratory,  
California Institute of Technology Sponsored by the National  
Aeronautics and Space Administration under Contract NAS-  
7100.

#### **SOLAREX CORPORATION**

1335 PICCARD DRIVE □ ROCKVILLE, MD 20850 □ 301 948 0202 □ TWX: 710 828 9709 □ CABLE ADDRESS: SOLAREX

### **TECHNICAL CONTENT STATEMENT**

**This report contains information prepared by Solarex Corporation under JPL subcontract. Its content is not necessarily endorsed by the Jet Propulsion Laboratory, California Institute of Technology, or the National Aeronautics and Space Administration.**

## I. ABSTRACT

In the latter part of 1976 Solarex achieved a breakthrough in fabricating ultra-thin (50 micron or less) silicon solar cells during JPL Contract 954290, under the auspices of NASA. The results were presented in a briefing at JPL in October and also presented at the 12th IEEE Photovoltaic Specialists Conference at Baton Rouge, La. in November, 1976. Recognizing the importance of this breakthrough, NASA OAST through JPL provided funding to exploit this advance in an accelerated pilot line phase. The program was to test the manufacturability of such thin cells to show that the new cell is not only a laboratory curiosity.

Solarex constructed a Pilot Line facility within two and a half months and during the succeeding month manufactured and delivered on schedule, 2000 of the newly developed ultra-thin (50 micron)  $4\text{ cm}^2$  silicon solar cells. In addition, it delivered 1000 cells that were made during the construction period.

During the initial stages of the pilot line installation, personnel were hired and trained on existing Solarex equipment in the new technology developed at Solarex for fabricating and handling ultra-thin silicon solar cells. Successful completion of the construction and training phase within this short time frame is felt to be a major achievement.

As the operational phase of the Pilot Line Program proceeded, steadily increasing yields and consistent electrical performance were attained.

This Pilot Line Program has demonstrated that Ultra-thin silicon solar cells with excellent power-to-weight ratios could be readily manufactured in a production setting with an acceptable yield and reasonable cost.

## II. TABLE OF CONTENTS

Technical Content Statement . . . . .	1
I. Abstract . . . . .	2
II. Table of Contents . . . . .	3
III. Summary. . . . .	4
VI. Pilot Line Description . . . . .	5
V. Technology & Procedures . . . . .	17
VI. Evaluation Criteria & Procedure . . . . .	19
VII. Handling & Safety Precautions . . . . .	21
VIII. Future Thin Cell Production . . . . .	27
IX. Future Production Yield and Efficiency . . . . .	29
X. Conclusion . . . . .	30

### III. SUMMARY

Under the auspices of the Jet Propulsion Laboratory for NASA OAST, a Pilot Line facility for producing ultra-thin (50 microns), 4 cm<sup>2</sup> silicon solar cells was constructed and put into operation at Solarex with the following objectives:

- 1) To demonstrate the feasibility of fabricating larger quantities of high efficiency, ultra-thin silicon solar cells in a semi-production setting.
- 2) To develop manufacturing techniques conducive to an acceptable mechanical and electrical yield.
- 3) To determine production rate limiting operations and provide recommendations for improvement.
- 4) To manufacture and deliver (within a 30 day production period) 2000 ultra-thin, 2cm x 2cm solar cells.

This set of objectives was successfully accomplished and the cells delivered precisely on schedule.

ORIGINAL PAGE IS  
OF POOR QUALITY



## IV. PILOT LINE DESCRIPTION

### A. Introduction

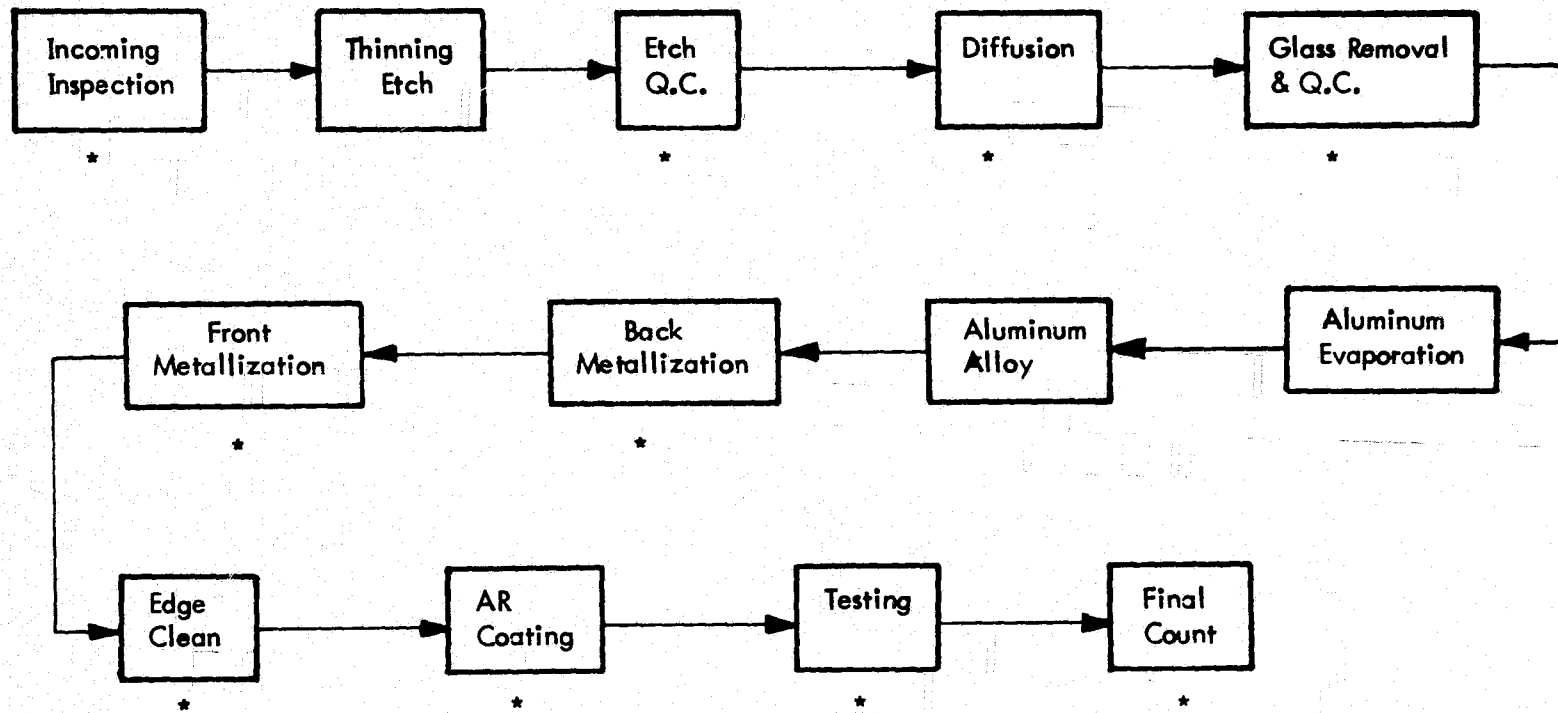
The R & D efforts by Solarex in 1976 under JPL Contract 954290 "Development of a High Efficiency Thin Silicon Solar Cell" produced a breakthrough showing that ultra-thin cells, 50 micron or less in thickness, can be made in the laboratory and Solarex delivered hundreds of such experimental samples to JPL. This laboratory work was so successful that it became feasible to try pilot production. The supporting agency, NASA/OAST, through JPL recognized the importance of this advance and made funding available to quickly exploit this breakthrough.

In January, 1977, Solarex began the creation of a Pilot Line facility for the manufacture of ultra-thin silicon solar cells. A considerable amount of internal construction and rearrangement of existing facilities was required to incorporate the additional equipment and space necessary to institute the program. Within two and a half months, Solarex purchased, received in-house, installed and put into operation the equipment required to meet the manufacturing goals of this effort while also training new personnel to operate the Pilot Line.

A process flow was established corresponding to the frozen technology to be used during the production phase. Exhibit I is the process sequence diagram for the flow employed in the program. Steps are noted in the diagram where accurate accounting and recording of loss modes were made for yield analysis.

Program and production managers generated a working plan that would allow for delivery of completed cells on schedule at a reasonable yield. Working within this framework the Pilot Line completed the production phase one day ahead of the projected schedule.

# PROCESS SEQUENCE DIAGRAM



\* - Steps with accurate accounting and loss mode record.

## B. Objectives

The primary objective of this effort under JPL Contract No. 954290 was to demonstrate in a short time that 2 mil thick silicon solar cells are reproducible and can be processed in quantity with a reasonable yield, at reasonable cost.

In addition, this Pilot Line effort was to demonstrate with a relatively large quantity of such thin solar cells that they are not particularly fragile, as was widely supposed.

## C. Work Plan & Schedule

This Pilot Line Program was of very short duration from the time of commencement to the end of the manufacturing stage. As can be seen from the Program Plan attached as Exhibit II, only two and a half months were allowed to complete all preparations for pilot production, which then had only one month to complete the delivery schedule prescribed by JPL.

This short-fuse program was subdivided into four monthly divisions of effort. The first month consisted of program planning by management concurrent with organizing an in-house team, defining equipment requirements and commencing acquisition, and working on device and process definition experimentation. The second month entailed finishing equipment acquisition, training new production personnel in ultra-thin cell processing techniques, facilitating the Pilot Line area, equipment installation, further experimentation with device processing and delivery of 1000 experimental-process solar cells. During the third month, training, installations and process definition were completed, production trials and upscaling were effected and both the Thin Cell Lot Follower form and production monitoring procedures were developed.

# PILOT LINE PROGRAM PLAN

Contract No. 954290

1977

Key Tasks Milestones	Jan.	Feb.	March	April	May	June
1. Project Management						
2. Assemble Production Team						
3. Train additional personnel						
4. Acquire necessary equipment						
5. Prepare space						
6. Install equipment						
7. Test & Upscale Production						
8. Optimize Cell Design						
9. Develop Production Monitoring Procedures						
10. Full Scale Production						
11. Production Monitoring						
12. Complete Pilot Line Report						
13. Cell Shipments						
14. Program Plan						

\* Shipment of 1,000 Cells per Uni. Mod. #3

EXHIBIT II

ORIGINAL PAGE IS  
OF POOR QUALITY

The fourth month was the production phase of the Pilot Line, which was planned for a capacity of 3000 solar cells per month and produced 2000 within its first month. The following month was scheduled for compilation and analysis of results for this report. Although this was a very short schedule before the production phase, the milestones were accomplished in a timely manner and the production phase reached its goal a day ahead of schedule.

A highly aggressive and flexible approach to equipment acquisition and new employee training was required to adhere to the schedule. Equipment available only on long lead time was side-stepped and the whole country scoured for equivalent used and refurbished equipment available for immediate delivery. All required items were obtained and put into service almost immediately upon arrival. The new personnel training was adapted on a person-to-person basis to best utilize training from other fields and accelerate proficiency in the various processing steps for ultra-thin silicon solar cells.

#### D. Results & Data

Fabrication of the 2000 deliverable ultra-thin solar cells during April 1977 was subdivided into daily lots starting out with 150 cells, ranging up to 450 cells, with a usual starting lot of 300. The total number started was 5173 to result in the 2000 delivered solar cells, with a rising yield in successive lots. Individual lots are tabulated in Exhibit III in terms of number started, reject categories and quantities, the number passing final Q.C. and the percent yield for each lot. In addition, overall totals and percentages are presented.

LOT HISTORIES & YIELD

EXHIBIT III

LOT NO.	STARTED	Rejection Categories											PASSED	YIELD %
		A	B	C	D	E	F	G	H	I	J	K		
1601	150	9	6	6				117	12				0	0
1602	300	34	6	49		18	2	52	10	6			123	41
1603	300	26		14		16	41	61	77				65	22
1604	300	18	13	47	1	37	6	75	19	1	1	4	78	26
1605	300	9	4		2	1	107	60	11		2		104	35
1606	300	88	1	5		4	2	58	22		4		116	39
1607	450	72	12	36		6	3	92	25	1	5	9	189	42
1608	300	83	6	4		13		54	19	20		13	88	29
1609	300	54	22	25			10	41	25		8	6	109	36
1610	300	7	7	15		7		96	18		3	2	145	48
1611	300	5	8	66		4	12	165	3				37	12
1612	300	42	20	36	6			39	14		4	8	131	44
1613	450	33	6	40	2			57	28		11	6	259	55
1614	412	10	17	27		1	8	71	28		16	5	229	56
1615	411	28	1	70		6		35	42	24		12	193	47
1616	300	26	14	23		3		28	6	4	3	10	183	61
TOTALS	5173	544	143	471	11	116	191	1101	359	56	57	75	2049	
Percentages		11	3	9	0	2	4	21	7	1	1	1		

## EXPLANATION OF REJECTION CODE

A. Broken by operator

Cells broken during insertion or removal from any machine during operation of any machine (except spin-dryer or rinser) or during any handling operation.

B. Broken in spin dryer

Cells broken during spin drying cycle.

C. Broken in rinse cycle

Cells broken during rinsing cycle.

D. Etch imperfection

Cells having severe etch pits, severely tapered edges, non-uniform thickness or stained and/or foggy surfaces.

E. Metal splatter

Cells having particles or lumps of metal deposited during metal evaporation.

F. Resist failure

Cells on which the resist peels during developing, cells that do not develop a clean pattern, cells which show badly tapered pattern edges, or cells with many pinholes in the resist field.

G. Front contact failure

Cells on which the front contacts are peeling or delaminating, or in which the buss or any sub-buss is severed, or from an evaporation lot which fails tape test on thick silicon sample substrates.

H. Back contact failure

Cells on which the back contact is peeling or delaminating, or has bubbling under the back contact or has voids greater than 0.5mm, or from an evaporation lot which fails tape test on thick silicon sample substrates.

I. Improper AR coating

Cells having any area not covered by a uniform layer of anti-reflective coating, cells with other than a deep metallic blue color or cells with visible scratches in the AR coating.

J. Electrical reject

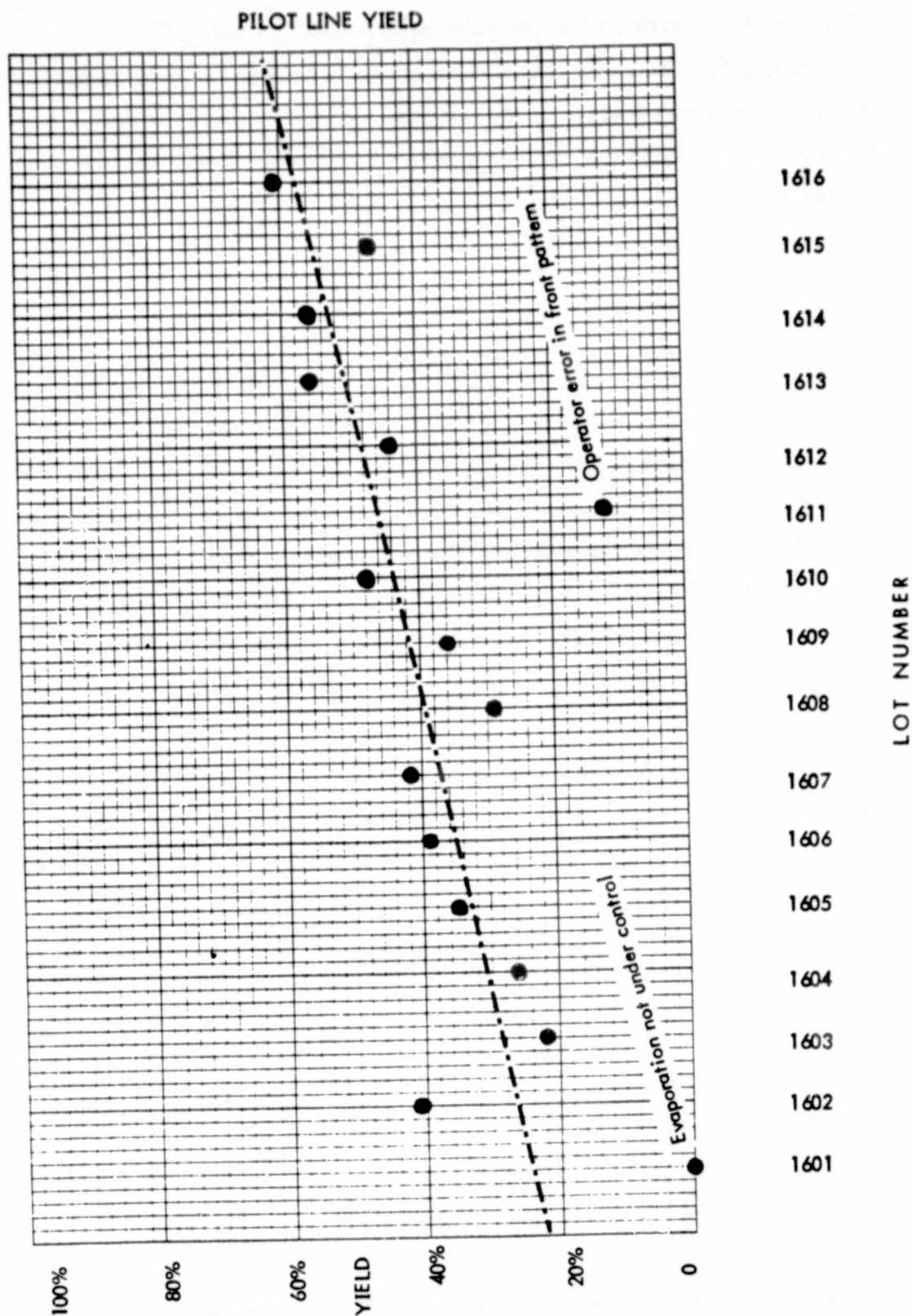
Less than 55 mW output without coverslide at AM0.

K. Dimensional reject

Cells having planform dimensions other than  $0.787 \pm 0.001$  inches and a thickness other than  $0.002 \pm 0.0005$  inches.



# EXHIBIT IV



The yield from starting silicon to solar cells passed by final Q.C. improved during the month of production, as shown in Exhibit IV. The overall yield is completely meaningless, as the operators made mistakes particularly at the beginning. In addition, the modus operandi had to be found. Had the production phase been longer, the yield would have probably continued to improve on a steady basis as the production personnel gained further proficiency and experience.

Since this effort was a first-trial production, a great deal of engineering support time was expended which would not occur with full scale production and previously experienced personnel. During the pilot production phase in April, the operating Pilot Line which processed the 2000 ultra-thin solar cells was comprised of four (4) just-trained operators, an experienced foreman and a Q.C. inspector. Of course, additional support was available in the form of incoming material inspection, packaging and shipping, etc. Engineering support was available continuously, including additional training.

The average peak power output uncovered\* at 25°C under AM0 illumination conditions is shown in Exhibit V for each lot processed. Both the limits and the mean values are given for the cells produced with the frozen technology employed. As can be seen, the mean power in the latter half of the production was about 58 mW. This could be improved, but the technology was frozen for the April pilot production.

The peak power output for ultra-thin silicon solar cells varies with thickness, decreasing as the available generation volume decreases for any particular fabrication technology employed. Plots have been submitted in previous reports under JPL Contract No. 954290 for experimentally fabricated thin silicon solar

---

\* The high index of tantalum oxide produces gain on coversliding.

C-4

TWO MIL CELL POWER OUTPUT

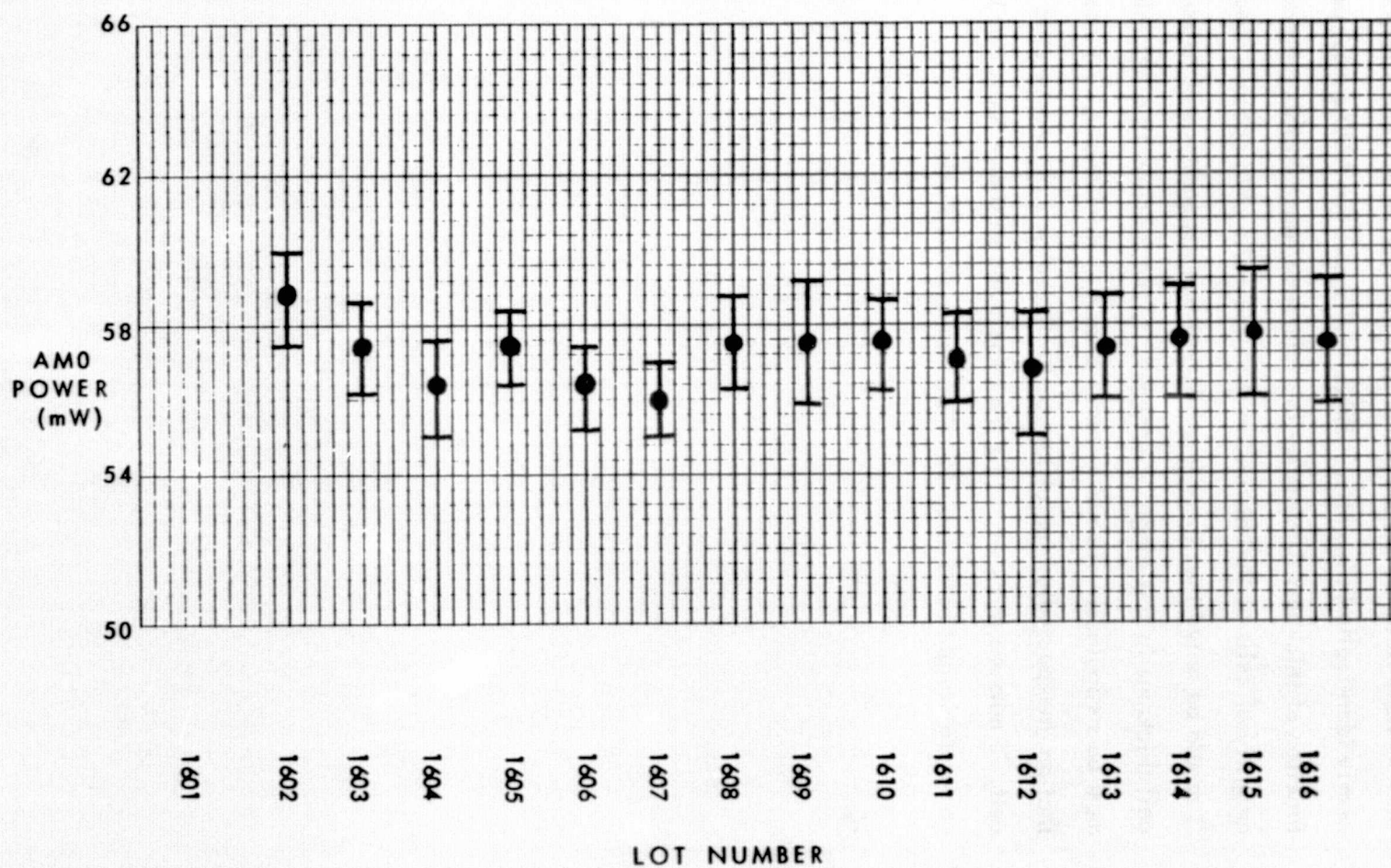
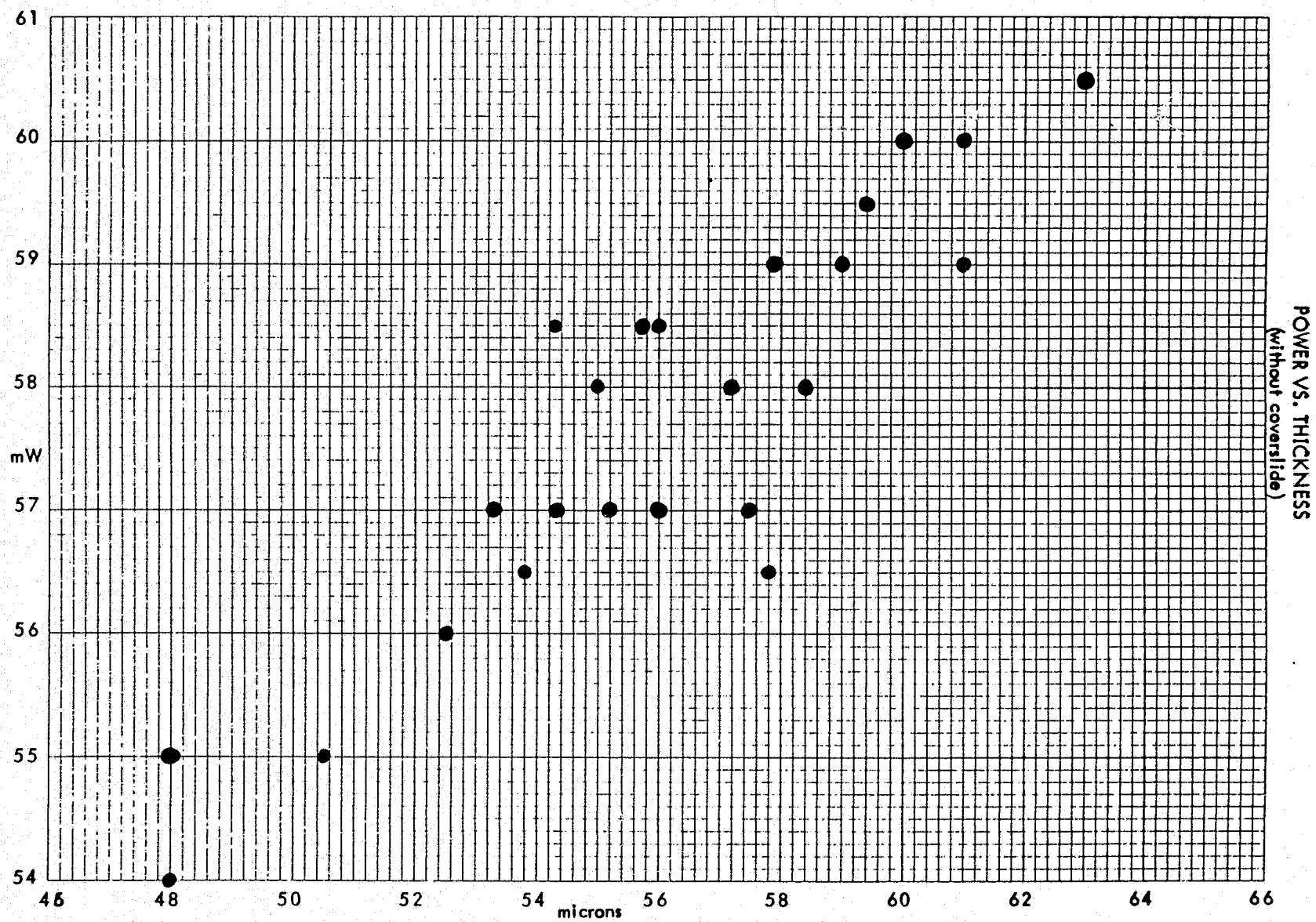


EXHIBIT V

cells, but those were not all processed identically. From this Pilot Line effort we now have data for output power as a function of thickness for cells processed nearly identically in quantity. Exhibit VI shows the AM0 output power as a function of thickness (limited by the tolerance range in this program) for a quantity of cells picked at random from the cells which passed Final Q.C. It should be noted that there is a fairly strong dependence of output power on cell thickness in this range. Consequently, comparison to other thin cells must be scrupulously viewed in terms of actual thicknesses, lest one concludes that an unexpectedly high of low cell efficiency is process related. A 65 mW cell, 75 microns thick would fit the same trend as shown here, but have a worse power-to-weight ratio than 58 mW at 55 microns thickness.



## V. TECHNOLOGY & PROCEDURES

In early April, 1977, Solarex notified JPL that it had frozen the technology to be used during the Pilot Line production phase, which, at that time, would provide both good electrical and mechanical yield. Although not an optimized technology, it provided a reliable framework within which the Pilot Line could attain its production goals.

Silicon chosen for the manufacturing phase was 2.0 ohm-cm, p-type, boron doped, CZ grown.

Etching techniques had already been dealt with extensively by Solarex R&D during the prior development of these thin cells. During the Pilot Line production phase, a 40% solution of NaOH in water was used for the silicon etch. It was maintained at a temperature slightly over 110°C and produced pillow-texture surfaces which were compatible with the rest of the operations. Newly trained operators, using a two-step approach were consistently able to provide 50 micron slices with an excellent yield (over 90%).

Solarex developed the following workable, reproducible procedure for thinning silicon slices to 2 mils (50 microns) by alkaline etching in the Pilot Line effort:

- 1) Prior to commencing etching the starting slices were measured with a calibrated ADE Corporation Microsense 6033 electronic thickness gauge and were sorted into 7 micron groups (e. g.  $300 \pm 3.5$ ).
- 2) Slices taken from a thickness group were batch-etched with the 40% NaOH solution to approximately 100-125 microns using etch rates established previously for the temperature.

- 3) The slices were then re-measured and small corrections made for the observed etch rate were employed to time the remaining etching to produce thicknesses within the range of 40 microns to 65 microns for the whole group of slices.

Phosphorous diffusions of the p-type silicon were done at  $865^{\circ}\text{C}$  for 15 minutes in  $\text{PH}_3$ , Ar,  $\text{O}_2$  gases. Previous experimental work, as reported earlier to JPL, had shown this temperature to be conducive to respectable electrical performance for the substrate resistivity used. The diffusion results were evaluated by sheet resistance measurement, employing a Signatone 4-point probe and constant-pressure mount. The sheet resistance was in the range of 50-70 ohms/square.

The p+ back surface was formed by vacuum deposition of  $5000\text{\AA}$  of aluminum followed by alloying at a temperature of  $800^{\circ}\text{C}$  for 10 minutes without removal of the rear n+ layer. Both the front grid and the rear surface contacts were comprised of titanium-palladium-silver. Front contact pattern generation was accomplished with photolithography masking techniques, rather than by shadow masking.

The anti-reflective coating was produced by vacuum deposition of tantalum oxide with an electron beam source, the system was then sintered at  $450^{\circ}\text{C}$  for about 1 minute.



## VI. EVALUATION CRITERIA & PROCEDURE

All cells were measured after etching using an ADE Microsense thickness gauge (Model 6033), to assure that the cell thickness was within specification ( $.002" \pm .0005"$ ).

Phosphorous-diffused n-type layers were evaluated after diffusion by sheet resistance measurement employing a Signatone 4 point probe with constant-pressure mount.

In-line Q.C. of the titanium-palladium-silver deposition for front and back contacts was done by tape testing scrap pieces of silicon from each evaporation. The Veeco/Kronos Automatic Deposition System performed very reliably once the proper program had been established. Except for the first production lot, excellent yields were realized from all vacuum deposition operations.

Final mechanical Q.C. criteria are documented in Exhibit VII.

Cell electrical performance was measured using Solarex's xenon simulator. All measurements were made under AM0 ( $135.6 \text{ mW/cm}^2$ ) conditions at  $25^\circ\text{C}$ . Minimum acceptable peak power for the program was established without cover slide.



FINAL Q.C. INSPECTION PROCEDURE  
(Mechanical)  
PILOT LINE PRODUCTION

- I. The back contact of each cell will be visually inspected for the following:
  1. There shall be no voids greater than 0.5 mm diameter penetrating the contact which expose either the sub-metal or silicon. Two voids less than 0.5 mm will be acceptable.
  2. There shall be no evidence of any contact peeling.
  3. There shall be no evidence of any bubbling under the back contact.
- II. The front contacts of each cell will be visually inspected for the following:
  1. Front contacts shall be located in accordance with Solarex drawing.
  2. There shall be no evidence of any contact peeling or delamination.
  3. There shall be no severing of any of the sub-buss contacts.
  4. There shall be an allowable maximum of two (2) severed fine finger contacts. The severed gap shall not exceed 0.5 mm.
- III. Sample quantities totaling 10% of each manufacturing lot will be mechanically measured for the following:
  1. The areal dimensions shall be .787 inches x .787 inches  $\pm$  0.001 inch.
  2. The cell thickness shall be .002 inches  $\pm$  .0005 inches measured off the front contact.
- IV. The front contacts will be mechanically tested using the following procedure:
  1. The cell will be firmly held in position on a vacuum chuck.
  2. A wooden swab shaft will be pulled across the contact areas (using a force of 50 grams).
  3. The front contacts will then be visually inspected in accordance with Section II.
- V. The anti-reflective coating will be visually inspected for the following:
  1. Uniformity across the cell surface.
  2. A deep metallic blue color corresponding to an established reference cell.
  3. Absence of any scratches in the AR coating (from swab shaft testing) indicating improper evaporation technique or improper sintering.

## VII. HANDLING & SAFETY PRECAUTIONS

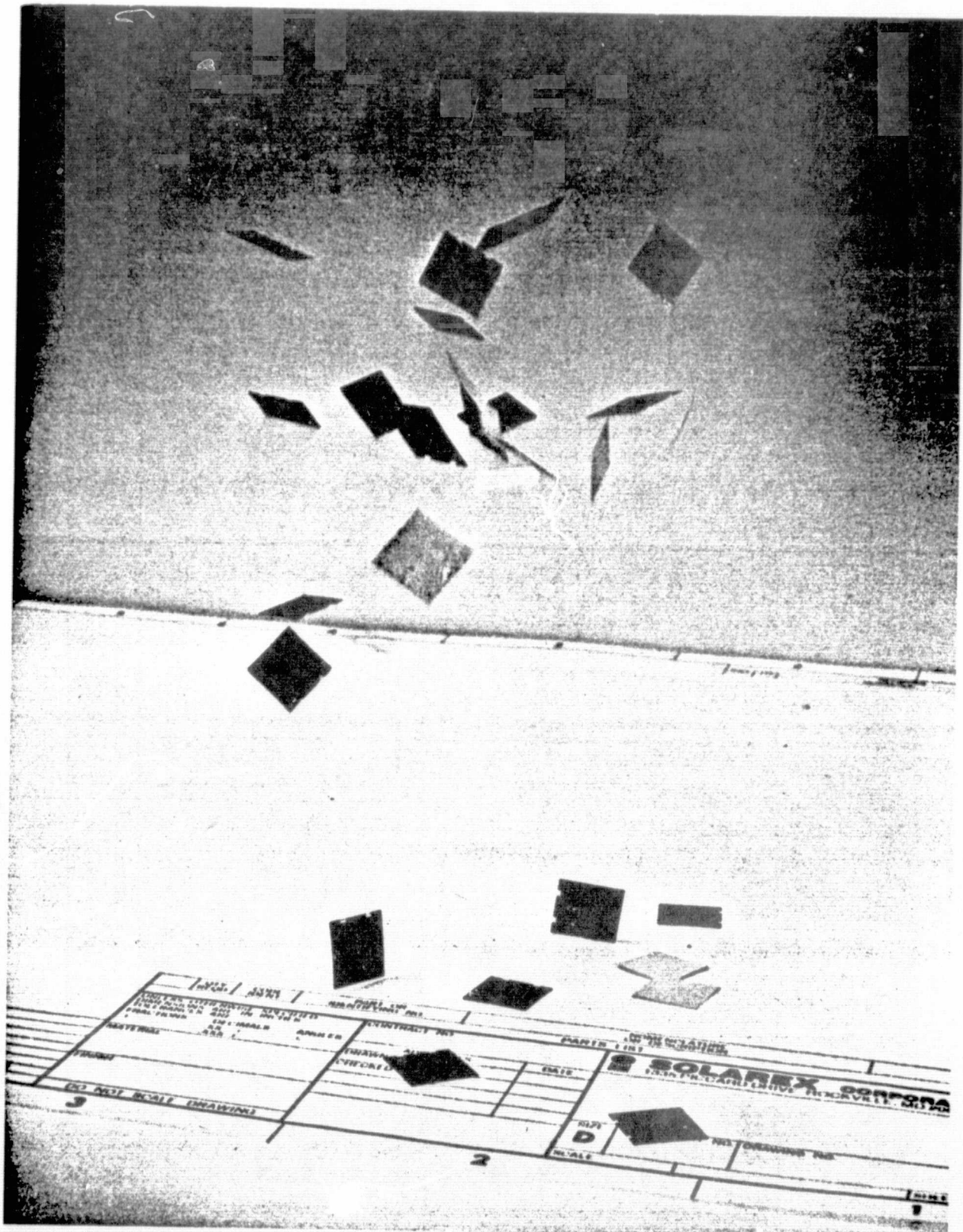
Pilot line operators quickly demonstrated that ultra-thin solar cells can be handled quite easily without employing any production-restraining measures. The 50 micron devices are surprisingly flexible and are highly resistant to breakage when dropped. This aspect of the mechanical durability was demonstrated in a rather unconventional fashion for 2 mil cells at the end of the program. A randomly picked group of some thirty 2cm x 2cm ultra-thin cells was thrown from a dish into the air and allowed to fall four (4) feet to a table top. Exhibit VIII shows a photograph of the flying cells surviving this mistreatment.

Tweezers were used for cell handling during all fabrication steps that required operator handling and, as the program proceeded, Pilot Line operators developed a high degree of confidence in handling these cells. Exhibit IX shows the operator breakage for the program. Except for a couple of instances, percentage losses for this failure mode were within acceptable limits.\*

Ultra-thin solar cells can be centrifugally spun dry in conventional plastic carriers. In some cases significant losses occurred. The percentage losses experienced for the many spin drying operations on the Pilot Line was acceptable but could be improved further. The actual drying techniques can only be evaluated statistically with large enough quantities. Particularly interesting parameters are: supporting carrier shape, support in the carrier and spinning speed. The relatively good results were obtained because these solar cells can be stressed by bending to a surprising degree without cracking or shattering. The photograph in Exhibit X demonstrates the radius of curvature easily withstood by these highly flexible solar cells without damage.

---

\* Considering the number of handling steps and the short experience of the operators, this is a very respectable record.



# EXHIBIT IX

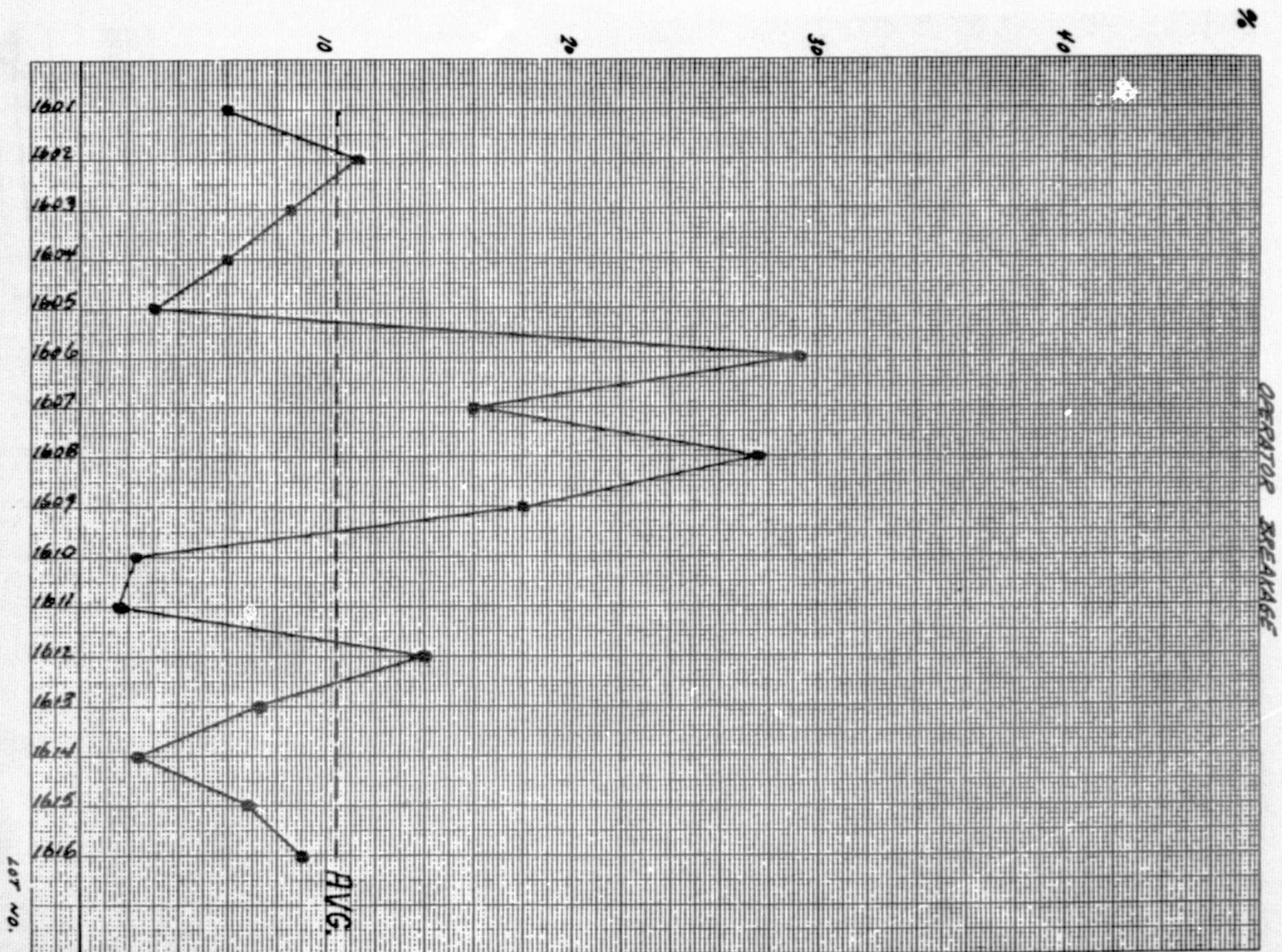






EXHIBIT X

ORIGINAL PAGE IS  
OF POOR QUALITY

- 6-11    o    Power requirements as a function of Heliocentric Distance need definition.
- 6-12    o    Set cell performance/thickness, CG, (and reflector material) and see if mission can be done (e.g., 13.5%, 6 mil w/a).
- 6-13    o    The dynamics and control of systems like this seems hard, especially in such a widely ranging environment, are the calculations being done sufficiently, realistically to ensure that nothing is being overlooked?
- 6-14    o    Thermal bending and effects on control system for orientation mechanism need to be considered.
- 6-15    o    Guidance and stability, e.g., cancellation of moments of inertia needs to be considered.
- 6-16    o    A better assessment of orientation requirements and constraints, power regulation and control, thermal control and conditions, is needed.
- 6-17    o    Were all estimates of weights made on a consistent basis, with all elements carefully checked?
- 6-18    o    Need analysis of interconnection scheme.
- 6-19    o    Have all the alternative concepts been eliminated systemically. For example, conflicting photovoltaic concepts operating at C.F.'s of 10, 15 or perhaps 25 to 1 with a distributed heat pipe radiator and selective optics. Selective concentration will improve the performance and provide minimum cost at 1 AU with a distributed heat pipe radiator to cell panel area ratio of 4 to 1  $\Delta R = 4$ . Maximum CR is used consistent with HPR ability  $\overline{AP}$  to reject heat.

## VIII. FUTURE THIN CELL PRODUCTION

The pilot line facility was designed for a production capacity of 3000 2x2cm cells per month. Production during the month April showed that the main factors limiting the production rate were: AR Coating equipment capacity and pilot line manpower. The AR coating problem could easily be resolved by adding additional evaporators or retooling the present one. This present vacuum system was donated by Solarex. Retooling it for greater capacity was not considered since a capacity of only 3000 cells per month was required.

At the outset of the pilot line program it was determined that only four operators were needed to produce the required 2000 cells. While this proved sufficient to get the job done, it was a manpower level below the threshold at which job specialization can occur. This caused single operators to carry out multiple process steps and led to only cyclic use of available equipment. An increase in manpower and some additional equipment could easily raise the production capacity to 6,000 cells per month.

Our experience on the pilot line has demonstrated that production of ultra-thin solar cells is not inherently more difficult than the production of conventional 12-15 mil space cells. A production facility capable of producing 50,000 thin cells per month could be installed in as little time as six months. The initial cost of such a facility would be in the range of \$600,000 to \$800,000; of this amount, roughly \$500,000 would be for production and test equipment and the balance for equipment installation and modification, space preparation, manpower training and other system start up costs.

Once such a line is established and operating, the recurring costs should be in the \$5 per cell range (for 2x2cm cells).

An additional fact to consider in future thin cell research and production is the development and production of large area and differently shaped devices. During the program, perfect cells up to 3" in diameter could be made. Some of the cells were shaped into 39cm<sup>2</sup> hexagons, 5x5cm squares and other rectangular shapes. Production of larger area devices can reduce cell processing costs and presumably array fabrication costs as well.

Finally, it must be noted that the cell thickness of 50 microns was set somewhat arbitrarily, as part of the pilot line technology. This demonstrated that a specified thickness can be tightly controlled. However, cells as thin as one mil have been fabricated and it appears that cell thickness is a parameter that can be varied to fit a particular overall array design.



## IX. FUTURE PRODUCTION - YIELD AND EFFICIENCY

The one-month pilot production phase demonstrated that ultra-thin cells could be processed with a reasonable yield; however, this short production phase did not determine the "typical" production yield for this technology. As the graph in Exhibit IV shows, yield improved steadily throughout the month. It is reasonable to assume that additional production will improve this yield even further. Both mechanical and electrical yield will increase with additional production experience. Increased familiarity in handling cells and using equipment should reduce breakage. Electrical yield will be improved and contact losses reduced as operators gain experience in the vacuum deposition of contacts and anti-reflection coatings. It is estimated that an additional six months of pilot production with underlying research support will result in typical production yields of 60-70% and electrical performance of 65 milli watts or higher. Ultimately electrical performance should reach 70 milli watts.

ORIGINAL PAGE IS  
OF POOR QUALITY

## X. CONCLUSION

The pilot effort reported here conclusively demonstrates that paper-thin silicon cells can be manufactured with respectable yield and reasonable efficiency. These thin cells can be handled safely, can be welded to, and already exceed the typical efficiency of most cells presently in orbit. Moreover, independent JPL testing indicates a much improved end-of-life efficiency through increased radiation resistance.

The old fear of easily breaking thin cells is now shattered. In fact, for yet unexplained reasons, 2 mil cells exhibit a much greater mechanical integrity than thicker cells, four mil for example. Moreover, as a result of the consistent reproducibility shown during this effort, it can be said that solar cells can now be tailor-made with great accuracy to any thickness desired.

This tremendous reproducibility and relative straightforwardness of the process as now developed forecasts that ultimate quantity production costs will be competitive with prevailing high efficiency space cell prices. Moreover, if large area devices are accepted by the space cell community, unit cost will be even lower.

It has now been shown that the 2 mil silicon solar cell can be fabricated in quantity and is not by any means a laboratory curiosity. Further optimization of these cells and future production in large quantities will make lightweight, high-powered solar arrays a working reality at reasonable cost. Such applications for space missions are quite numerous and the implications for cost reduction in the expanding terrestrial field are significant.

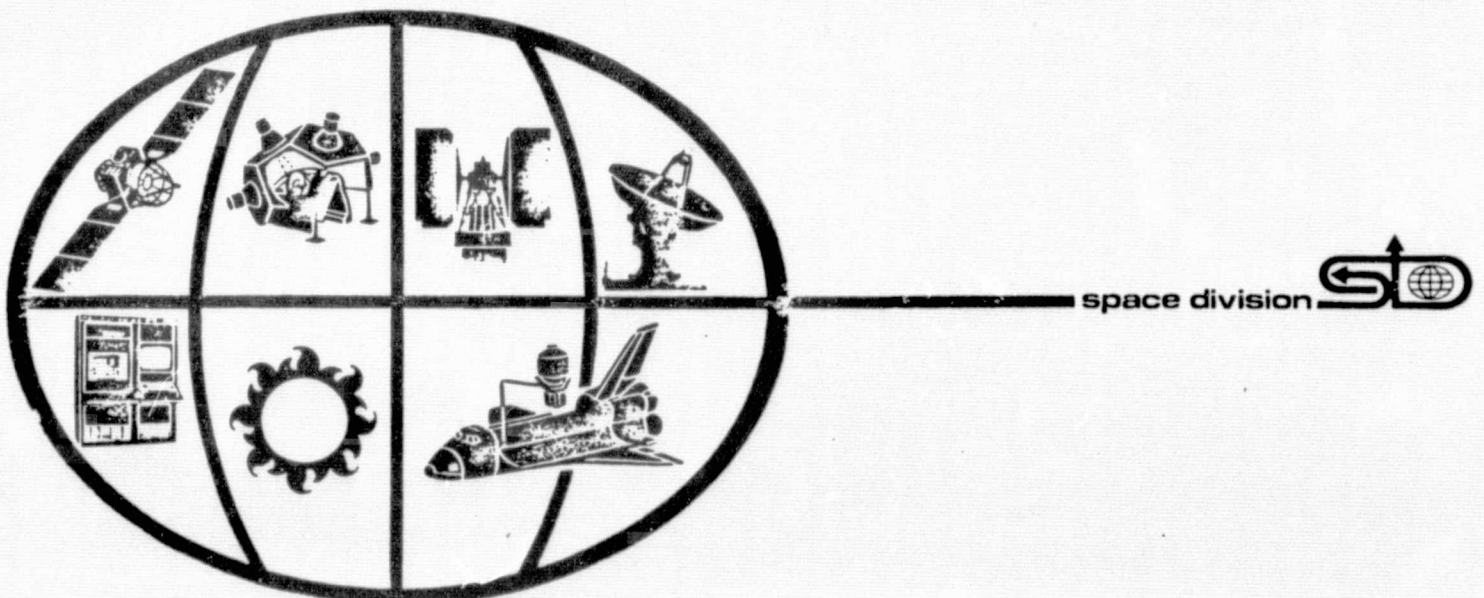
Lastly we must take recognition of the fact that this entire program was accomplished in only three and one half months. This required the dedicated efforts of many individuals at Solarex and was only possible with the close cooperation and support of JPL and NASA/OAST personnel.

200W/Kg 7.77-048

# 200 WATTS/KILOGRAM SOLAR ARRAY CONCEPTUAL APPROACH STUDY

PHASE II

ASSESSMENT REPORT



GENERAL  ELECTRIC

200W/Kg 7.77-048  
8 JULY 1977

**200 WATTS/KILOGRAM SOLAR ARRAY  
CONCEPTUAL APPROACH STUDY**

**PHASE II  
ASSESSMENT REPORT**

**ASSESSMENT REPORT  
FOR  
PROOF-OF-CONCEPT EXPERIMENTS  
AND  
HALLEY'S COMET CONCENTRATOR ARRAY**

**PERFORMED UNDER CONTRACT NO. 954393  
FOR  
THE JET PROPULSION LABORATORY  
PASADENA, CALIFORNIA**

**GENERAL  ELECTRIC**

**SPACE DIVISION**

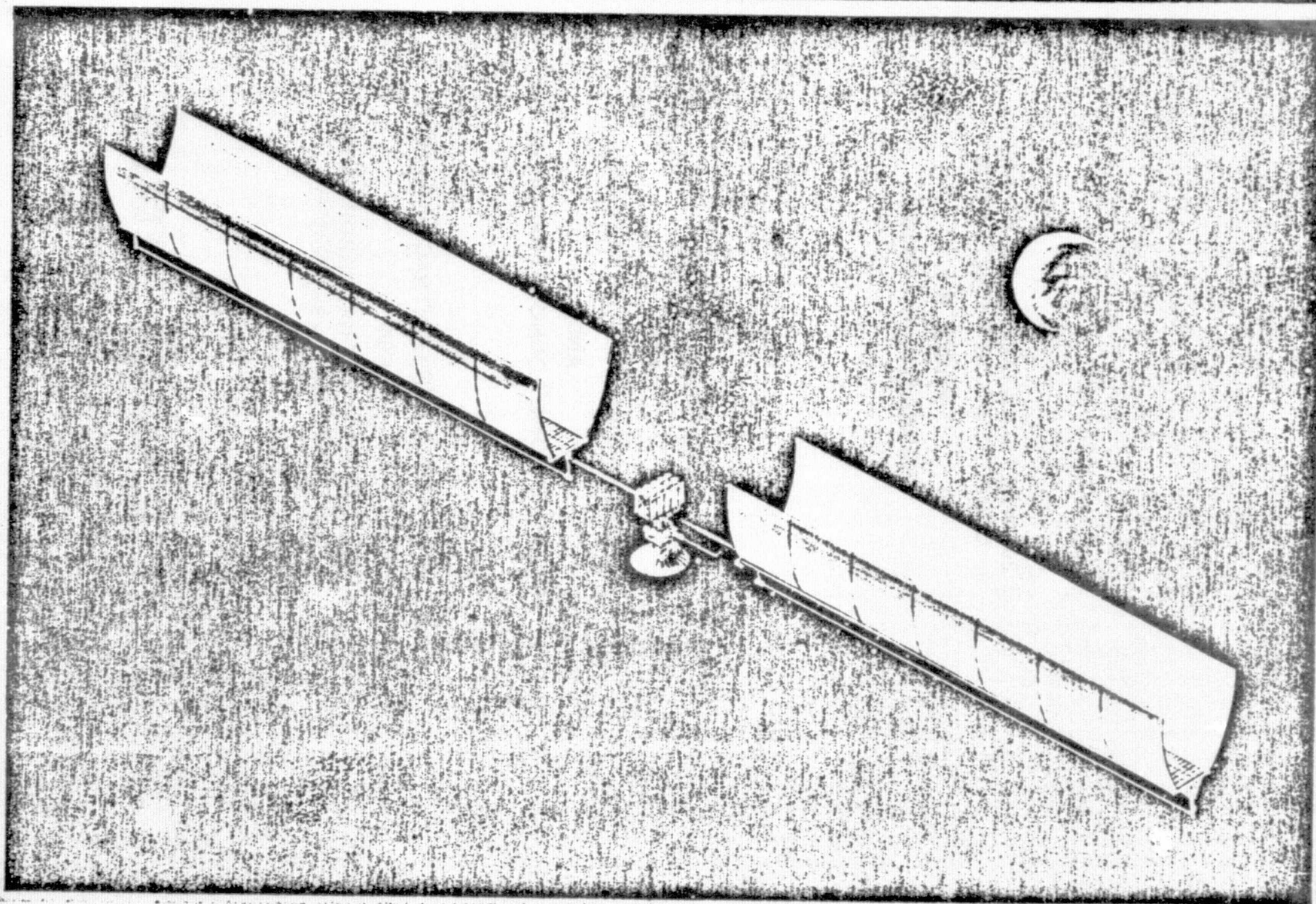
**Valley Forge Space Center**

**P. O. Box 8555 • Philadelphia, Penna. 19101**



SPACE  
DIVISION

# 200 W/Kg SOLAR ARRAY, PHASE II HALLEY'S COMET CONCENTRATOR ARRAY



ORIGINAL PAGE IS  
OF POOR QUALITY



## TABLE OF CONTENTS

<u>Section</u>	<u>Page</u>
EXECUTIVE SUMMARY . . . . .	vii
1 INTRODUCTION . . . . .	1-1
2 PRELIMINARY CONCLUSIONS . . . . .	2-1
3 TECHNOLOGY ASSESSMENT . . . . .	3-1
3.1 Introduction and Summary . . . . .	3-1
3.2 Proof-of-Concept Test Program . . . . .	3-2
3.2.1 Material Evaluation . . . . .	3-2
3.2.2 Design Evaluation . . . . .	3-8
3.2.3 Manufacturing Process Development . . . . .	3-9
3.3 Laboratory Test Results . . . . .	3-10
3.3.1 Thermal Cycle Test . . . . .	3-10
3.3.2 UV Exposure Test . . . . .	3-11
3.3.3 Roll-up Test . . . . .	3-12
3.3.4 Vibration Test . . . . .	3-14
3.3.5 Creep Test . . . . .	3-14
3.3.6 Electrical Test . . . . .	3-15
4 CONCEPTUAL SOLAR ARRAY DESIGN FOR HALLEY'S COMET MISSION . . . . .	4-1
4.1 Solar Array Requirements . . . . .	4-1
4.2 Mechanical Design . . . . .	4-1
4.2.1 Mechanical Elements . . . . .	4-9
4.3 Electrical Design . . . . .	4-13
4.3.1 Solar Cell Circuits . . . . .	4-13
4.3.2 Solar Cell Module . . . . .	4-13
4.3.3 Solar Cell Section . . . . .	4-16
4.3.4 Solar Array Blanket . . . . .	4-16
4.3.5 Mode Switching . . . . .	4-16
4.3.6 System Performance . . . . .	4-17
4.3.7 Mission Trajectory . . . . .	4-17
4.3.8 Array Power Performance . . . . .	4-18
4.3.9 Array Voltage Performance . . . . .	4-22
4.3.10 Radiation Analysis . . . . .	4-22

## TABLE OF CONTENTS (Cont'd)

<u>Section</u>		<u>Page</u>
5	OPTIONAL SOLAR ARRAY DESIGN . . . . .	5-1
5.1	Number of Cells Required . . . . .	5-1
5.2	Array Size . . . . .	5-1
5.3	Array Weight . . . . .	5-2
5.4	Optional Solar Array Summary . . . . .	5-2
6	RECOMMENDATIONS . . . . .	6-1

ORIGINAL PAGE IS  
OF POOR QUALITY

## LIST OF ILLUSTRATIONS

<u>Figure</u>		<u>Page</u>
2-1	80 Cell Module and 16 Cell Test Coupons . . . . .	2-3
3-1	Proof-of-Concept Experiment 200 Watt/Kilogram Solar Array Program . . . . .	3-3
3-2	Flexible Design . . . . .	3-6
3-3	Stiff Interconnect Design . . . . .	3-6
4-1	Concentrated Array Concept (Halley Comet Mission) Partially Deployed . . . . .	4-2
4-2	Jettison Position for Concentrator . . . . .	4-3
4-3	Concentrated Array Concept (Deployed) . . . . .	4-5
4-4	Solar Array Concept (Articulated CPC Reflector) . . . . .	4-8
4-5	Slip Ring Assembly . . . . .	4-9
4-6	Rib Hinge Concept . . . . .	4-11
4-7	Deployment Sequence . . . . .	4-12
4-8	Circuit Layout (7S by 4P) . . . . .	4-14
4-9	Circuit Module Interconnections . . . . .	4-15
4-10	Blanket Layout . . . . .	4-15
4-11	Mode Switching Diagram . . . . .	4-17
4-12	Halley Rendezvous Trajectory (Ecliptic Plane Projection) . . . . .	4-18
4-13	Undegraded Power vs AU . . . . .	4-21
4-14	Array Temperature vs AU . . . . .	4-22
4-15	Array Voltage vs AU . . . . .	4-23



## LIST OF TABLES

<u>Table</u>		<u>Page</u>
3-1	200 W/Kg Solar Array Conceptual Design Study, Phase II . . . . .	3-4
3-2	Proof-of-Concept Experiments Summary . . . . .	3-4
3-3	Interconnect Evaluation . . . . .	3-7
3-4	Substrate Cement Evaluation . . . . .	3-7
3-5	80-Cell Module, Summation of Properties . . . . .	3-9
3-6	Temperature Cycling . . . . .	3-10
3-7	UV Exposure Test . . . . .	3-11
3-8	Absorptance and Emittance of RTV Coated Cells Cemented to Kapton-H . . . . .	3-12
3-9	Roll-up Test . . . . .	3-13
3-10	Vibration Test . . . . .	3-14
3-11	Electrical Testing . . . . .	3-15
4-1	Study Requirements . . . . .	4-1
4-2	Mass Summary (Articulated Parabolic Concentrated Concept) . . . . .	4-7
4-3	Array Performance Over Halley's Comet Mission Trajectory . . . . .	4-19
4-4	Fluences for Halley's Comet/Ion Drive Mission. . . . .	4-24
5-1	Weight Comparison of Optional Array to Baseline . . . . .	5-2
5-2	Major Characteristics . . . . .	5-3

## EXECUTIVE SUMMARY

During the course of the 200 Watt per Kilogram Solar Array Program, several significant technological advances have been demonstrated that add to the overall readiness assessment being made for a lightweight solar array applicable to the Halley's Comet Mission. Although some system level concerns remain, much of the activities associated with the fabrication, handling, and testing of 2-mil solar cell modules on a flexible substrate have been successfully demonstrated. We have shown that 2-mil solar cells can be reliably handled, welded, and bonded to a Kapton substrate. Flexible Invar interconnects can be used to interconnect individual cells to form modules. These solar cell modules can be temperature cycled, wrapped around a 10-inch diameter drum, and vibrated to the Shuttle environment with no significant damage. We have developed a bonding technique to physically join adjacent modules that is stronger than the Kapton, itself. We have performed ultraviolet radiation tests on RTV - silicone as a cell cover material - with very encouraging results. In summary, we have successfully demonstrated the lightweight solar cell module technology readiness.

The activities undertaken to date on the Concentrator Solar Array for the Halley's Comet Mission have been conceptual in nature. Detailed analyses relating to areas such as flatness, natural frequency, temperature control, alignment, etc., have not been performed. However, projections have been made to quantify certain key parameters using the analytical results developed for the unconcentrated array. The results of these projections, coupled with an adequate conservatism, strongly indicate a technically feasible and practical design for the Halley's Comet Mission. However, additional effort is required to resolve the major open concerns. Detailed analysis and optimization studies should be performed in the areas of flatness, alignment, tension, concentrator efficiencies, stiffness, ground testing, and automated tooling. Materials testing should also be undertaken to better understand the radiation effects on the concentrator and cell cover materials. Additional testing of 2-mil cells at low temperature and low illumination will enable a more accurate prediction of solar array performance at far distances from the Sun.

The technology developed in the 200 Watt per Kilogram Solar Array Program will undoubtedly find its way into a wide variety of programs requiring large ultra lightweight solar arrays. It will benefit not only the Halley's Comet Mission, but other missions such as the Space Power Satellite. It is, therefore, incumbent upon us to keep this technology moving ahead.

Based on the work performed to date on this program, the solar array design proposed for the Halley's Comet Mission represents a technically feasible and practical approach. It incorporates the lightweight technology presently being successfully developed. An artist's rendering of the concentrator array design is shown as the Frontispiece of this report.

ORIGINAL PAGE IS  
OF POOR QUALITY

## **SECTION 1**

### **INTRODUCTION**

**Since January, 1977, General Electric Space Systems has been under contract with the Jet Propulsion Laboratory to:**

- 1. Develop the technology required to fabricate and test ultra-thin solar cell modules utilizing a flexible substrate**
- 2. Develop a conceptual solar array design to power the ion engines planned for use on the Halley's Comet Mission.**

**This report describes the activities undertaken and the results achieved to enable an overall assessment to be made of the technology readiness relating to the Halley's Comet mission solar array. The solar array design is based on the technology achievements made during the module development and test program, as is described in this report. The considerable amount of knowledge gained in the handling, welding, interconnecting, bonding, encapsulating, and testing of 2-mil thick solar cells on a flexible substrate has been applied to the concentrator solar array design for the Halley's Comet Mission. The feasibility of fabricating these ultra-thin modules has been demonstrated with a high degree of success.**

## SECTION 2

### PRELIMINARY CONCLUSIONS

The following preliminary conclusions are based on the solar array program activities undertaken to date. The detailed results are covered in this report.

1. Approximately 1457 2-mil solar cells have been processed through the manufacturing and test cycles at GE. Of these, 117 were initially rejected for various defects and not processed further; 330 were used for welding, encapsulation, or bonding tests; 120 were made into 4-cell modules for special evaluations; 270 were made into 9-cell modules for delivery to JPL; and 640 were made into 80-cell modules. At the start of the program, a reject or fall-out rate of about 44% was encountered. During the last two months, 640 cells were processed into 80-cell modules with a manufacturing reject rate of 9%. This successful reduction in rejects results from the knowledge gained in handling and assembling 2-mil cells together with the establishment of appropriate procedures.
2. Evaluations of several interconnect materials and configurations resulted in selecting a flexible design of silver-plated Invar.
3. Evaluations of several encapsulant cover materials resulted in selecting RTV silicone as both the encapsulant and the cell-to-substrate adhesive.
4. A welding schedule has been established that produces a strong repeatable cell-to-interconnect weld capable of surviving a temperature shock environment of  $-190^{\circ}\text{C}$  to  $+120^{\circ}\text{C}$ , without damaging the cell electrical junction.
5. Temperature cycling tests at GE on test coupons produced no harmful effects.
6. Ultraviolet testing at GE (1000 hours at 1 equivalent UV suns) resulted in no loss in transmittance.
7. Ultraviolet testing at 10 EUVS at NASA/LeRC on RTV silicone and polyimide/siloxane showed RTV silicone to be on a par with an untried glass resin.
8. Pull testing on lapped-joined Kapton-to-Kapton using RTV silicone resulted in Kapton breaking before bond indicating a good bonding technique.
9. Wrapping five 80-cell modules bonded together around a 10-inch diameter drum 15 times resulted in no cell breakages.
10. Vibration testing of five 80-cell modules wrapped around a 10-inch diameter drum resulted in no cell breakage or module movement.
11. Electrical testing of over 1200 cells shows the repeatability of the 2-mil cell.

12. Solar cell modules consisting of 2-mil cells (2 cm x 2 cm), welded Invar interconnects, bonded to 1-mil Kapton substrates with RTV silicone, and covered with RTV silicone for radiation protection, can be readily assembled, tested, and handled. Such modules can survive temperature cycling of  $-190^{\circ}\text{C}$  to  $+120^{\circ}\text{C}$ , can be wrapped around a 10-inch diameter drum with no cell breakages, can be vibrated to the shuttle launch environment with no cell breakages, and can survive a 1000 hour UV exposure with only a 11% power loss, maximum.
13. Creep Testing of a module and lap joint resulted in zero elongation.
14. The solar cell module fabrication and test program proves that 2-mil cells mounted on a flexible substrate can meet the requirements of the Halley's Comet Mission Solar Array Design.

A representative sample of the product produced in this phase of work is shown in Figure 2-1, along with a diagramic sketch of a typical cross-section through a solar cell assembly.

ORIGINAL PAGE IS  
OF POOR QUALITY

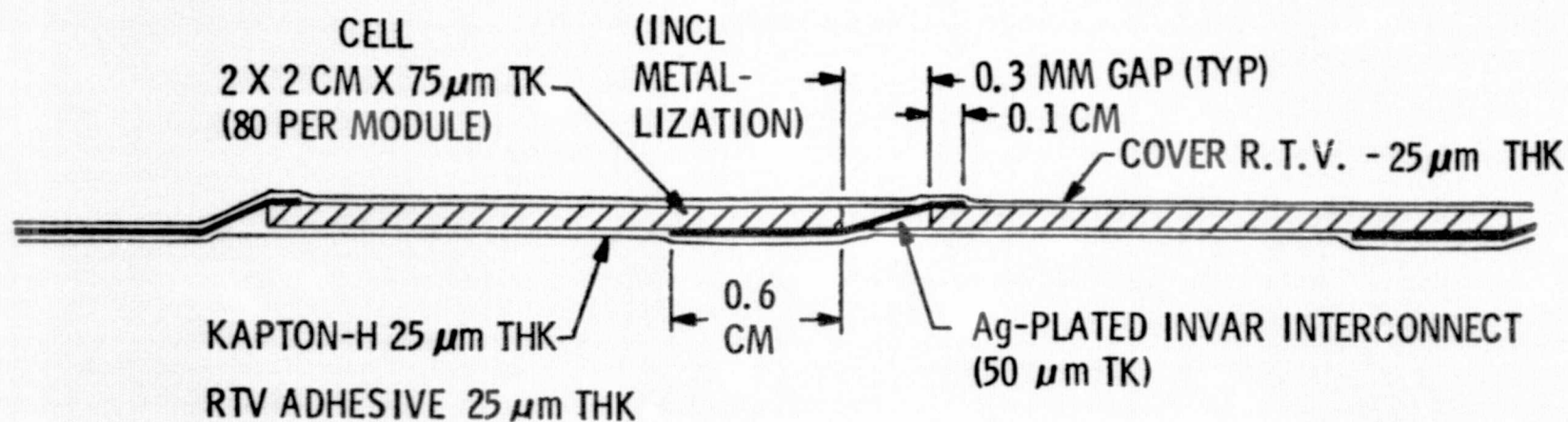
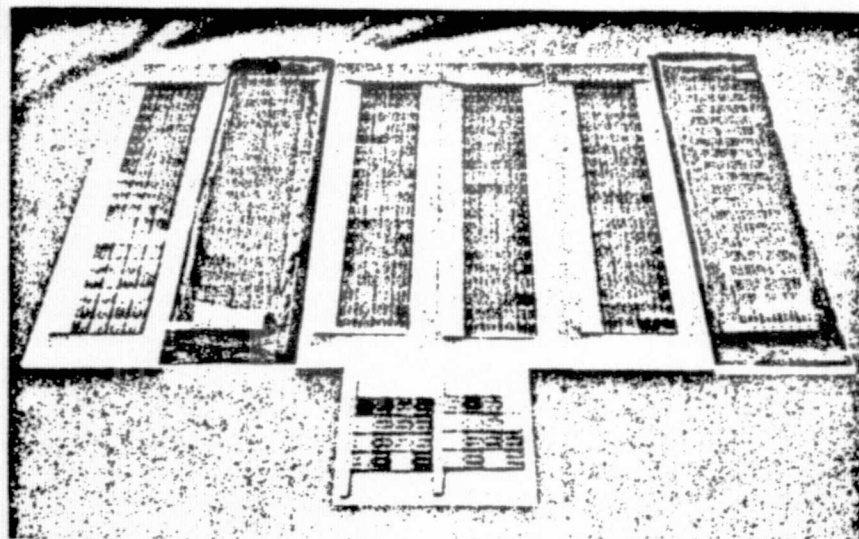


Figure 2-1. 80 Cell Module & 16 Cell Test Coupons

## SECTION 3

### TECHNOLOGY ASSESSMENT

#### 3.1 INTRODUCTION AND SUMMARY

Beginning in mid-January 1977 and ending in June 1977, an experimental program was implemented to assess the soundness of the design concepts identified during the preceding Phase I conceptual design study. Whereas Phase I was a generic study of design techniques, manufacturing methods and materials that together could lead to an ultralight solar array, the Phase II work was directed specifically in a manner to meet the system requirements of the Halley's Comet rendezvous. The proof-of-concept experiments that were conducted were designed to test and validate the ultra-lightweight design against environmental conditions imposed by a Shuttle launch of the Halley's Comet rendezvous spacecraft into an interplanetary orbit that could be as close to the sun as 0.6 AU and as far away as 4.5 AU. This work was unique in that no prior experimental work had been done to directly support the 200W/Kg solar array conceptual design. Working drawings had to be created from engineering sketches, materials had to be ordered, and manufacturing tools had to be designed and fabricated. Test plans were created to: (1) simulate Shuttle launch vibration; (2) simulate UV exposure at earth orbit; (3) test materials over temperature extremes anticipated with a concentrator solar array; and (4) prove that ultra-thin solar cell arrays may be rolled-up on a circular storage drum without deleterious results. It may be noted that no prior experience existed for either manufacturing or testing of solar modules involving 2-mil thick solar cells.

While not all the test results are in at this writing (a 1000-hour UV exposure test is still in process), it may be concluded on the basis of the work completed that the basic soundness of an ultra-thin solar cell array with specific powers (watts per unit mass) at the module level of 370 watts is a proven fact. Future work should be directed toward improvements in cell electrical efficiency and optimization of array design parameters so that this extremely high value of specific power will not be diluted unduly at the system level.



### **3.2 PROOF-OF-CONCEPT TEST PROGRAM**

The objective during this accelerated test program was to demonstrate that the advent of the 2-mil silicon solar cell could be capitalized on to produce high quality, ultra-lightweight solar arrays following the design principles outlined in the preceding phase of work. The scope of this activity included product design, material evaluation, production of test coupons and solar modules, environmental tests, demonstration of roll-up stowage and performance evaluation. This work had to be accomplished in five months because of the dictates of the Halley's Comet rendezvous program evaluation schedule. A test program schedule was developed whereby key delivery dates could be met and which accounted for all the required elements of work. The overall program schedule, as shown in Figure 3-1, was divided into two principal parts - the production and test of test coupons, and the production and test of 80-cell modules. Three important processes had to be addressed at the beginning; viz, (1) weld bonding of interconnects to cells; (2) thermal bonding of welded cell assemblies to the flexible substrate; and (3) final encapsulation of the cell/substrate assembly in a protective covering. Although the issue of weld bonding vs. solder bonding had been resolved in favor of weld bonding during the Phase I study, a small side experiment (not identified in the above bubble charts) for solder bonding was conducted as a hedge on weld bonding. Solder bonding offers no advantages in the assembly of interconnects and solder cells, by our experience. Solder bonding requires excessive clean-up both before and after soldering and more careful handling of the product in the manufacturing process. When consideration is given to the temperature limit and the additional weight imposed by solder bonding, there appears to be no merit to solder bonding in an ultra-lightweight solar array. A summary of the experience with weld bonding is given in Table 3-1 and the overall conclusions of the proof-of-concept program is shown in Table 3-2.

#### **3.2.1 MATERIAL EVALUATION**

Three material items were identified for laboratory test and evaluation; viz, silver-plated interconnects, substrate cement and cell encapsulation. The Phase I study identified silver-plated molybdenum as the optimum interconnect and FEP-Teflon as the substrate cement and encapsulant. During the course of laying out the program plan, a decision was made to incorporate alternate materials in the test plan.

ORIGINAL PAGE IS  
OF POOR QUALITY

ORIGINAL PAGE IS  
OF POOR QUALITY

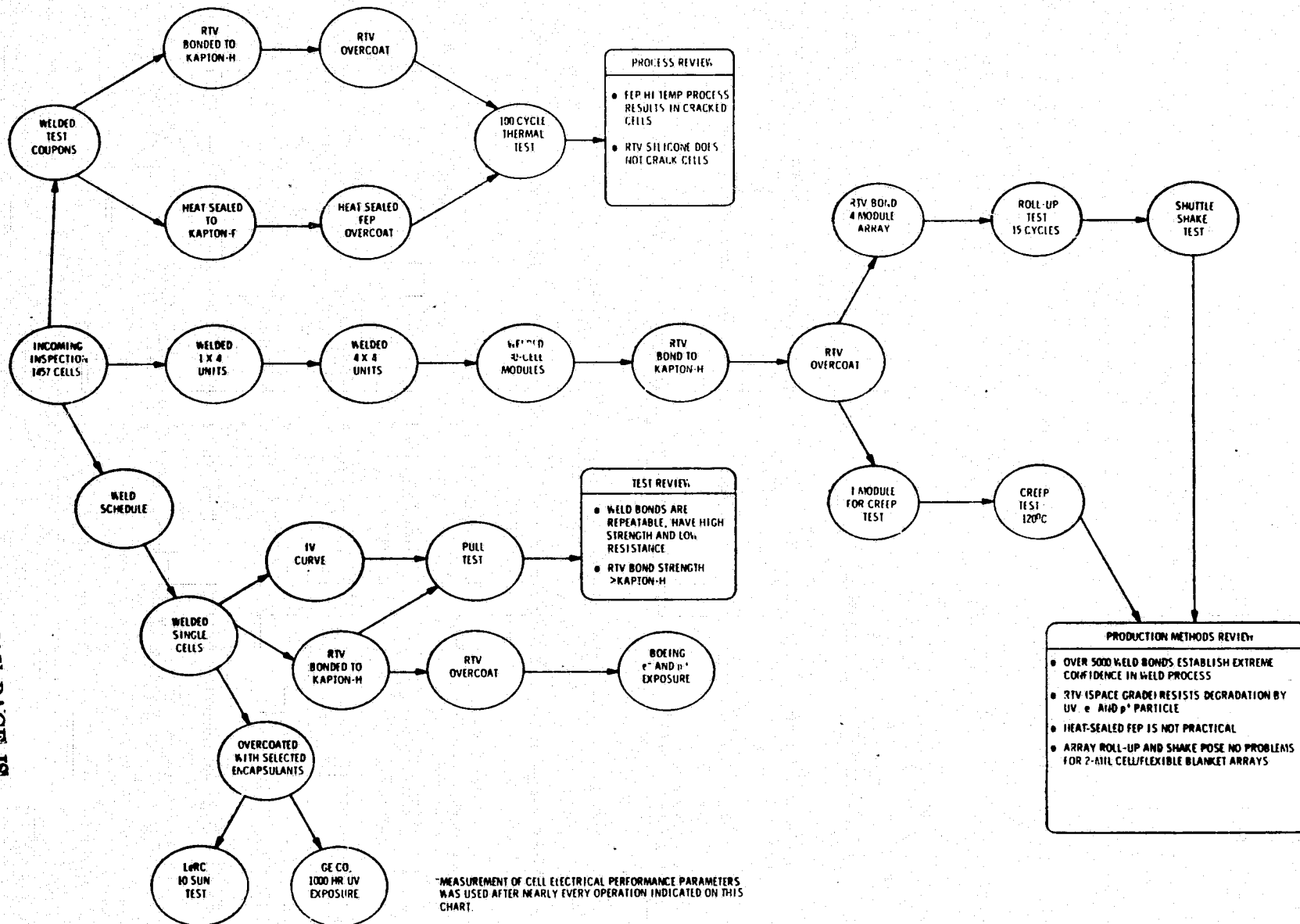


Figure 3-1. Proof-of-Concept Experiment 200 Watt/Kilogram Solar Array Program

Table 3-1. 200 W/Kg Solar Array Conceptual Design Study, Phase II

Cell Processing Summary

Item	Quantity	Total Cells	Weld Bond
Welded Single Cells	42	42	84
Welded 1 x 4 Cell Unit	185	740	1480
Welded 2 x 2 Cell Unit	30	120	480
Welded 2 x 4 Cell Unit	5	40	80
Welded 3 x 3 Cell Unit	30	270	1080
Welded 4 x 4 Cell Unit	49		1568
Welded 80 Cell Modules	8		320
Cell Rejects, Broken in Process, etc.	<u>245</u>	<u>245</u>	
		1457	5092

Yield at Various Stages of Module Manufacture - June 1977:

Incoming Inspection	0.92
1 x 4 Unit, After Welding	0.96
4 x 4 Unit, After Welding	0.98
80 Cell Module, After Welding	0.99
80 Cell Module, After Cementing	0.99+
80 Cell Module, After Encapsulation	0.99+

Table 3-2. Proof-of-Concept Experiments Summary

Objectives Were Successfully Met

- Interconnect design survived thermal fatigue test
- Weld bonding shows high bond integrity under thermal and vibration stress
- RTV silicone shows no degradation at 1 EUV and does not cause cell fracture
- RTV silicone bond is stronger than the Kapton substrate at 15,000 psi
- Four 80-cell modules survived 15 cycles of wrap and unwrap on 10" dia drum
- The stowed array withstood shuttle launch environment

Conclusion

- Proof-of-concept for a 2-mil cell, flexible array, roll-up storage has been accomplished

### **3.2.1.1 Silver-Plated Interconnects**

Three materials, moly, Invar and Elinvar, were tested during the course of this phase of work. Two interconnect designs, Figures 3-2 and 3-3, were used as a flexible and stiff interconnect respectively. The results of weld strength and electrical measurements were used as an evaluation criteria, called weldability, to rank the materials. Thermal shock and thermal cycle test results were used to rank the materials and design configurations. These findings are summarized in Table 3-3. The original criteria for selecting moly as the best interconnect material was based on (1) its high strength-to-weight ratio (specific stiffness), and (2) its coefficient of thermal expansion which matches very closely that of silicon. A pragmatic problem impeded the full evaluation of moly, however. It was very tedious at best and very erratic at worst to get a good, tenacious silverplate on moly. A nominal 0.5-mil plate of silver is essential to obtain sound, repeatable weld bonds. Further work on silver-plating of moly will be required before this non-magnetic material may be fairly evaluated as an interconnect material. There appears to be enough weld strength data to state a preference for Ivar over Elinvar<sup>(1)</sup>. Both of the high nickel content metals take a silver-plating equally well. The major problem which surfaced during the thermal cycle tests is the propensity of the stiff interconnect to break cells. The obvious advantage of the so-called stiff design is its rather large weight advantage. A compromise interconnect design incorporating some of the features of both is the next logical step.

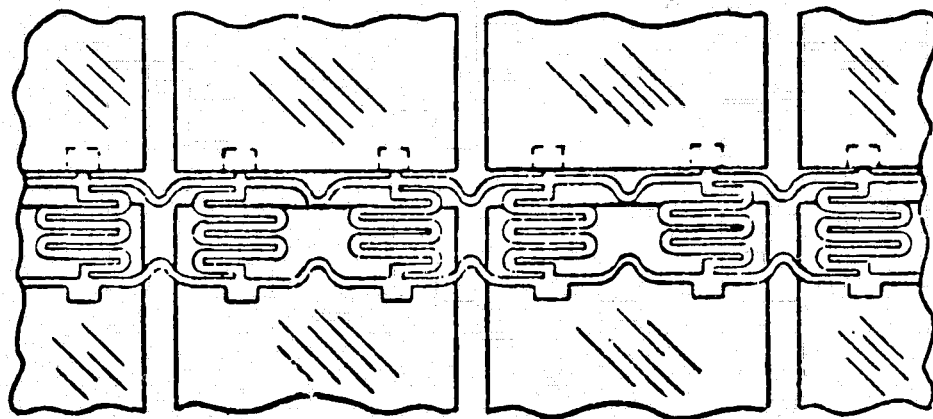
### **3.2.1.2 Substrate Cement**

Three materials were evaluated as cements for bonding the cell/interconnect assembly to the Kapton substrate, see Table 3-4; viz, a flexible epoxy known as SMRD 745, RTV silicone, and FEP-Teflon. Of the three, REP-Teflon was pre-processed with the Kapton substrate and purchased as Kapton-F. The epoxy and silicone are both two-part cements that were mixed and applied at the time of cementing. Heat sealing of FEP-Teflon to the cell backs at 250°C was accomplished with sufficient adhesion to crack cells when the bonded assembly was cycled in temperature from -190°C to 120°C. The same results were encountered with the flexible epoxy. Excellent results were experienced, however, with RTV-silicone which was cured at

---

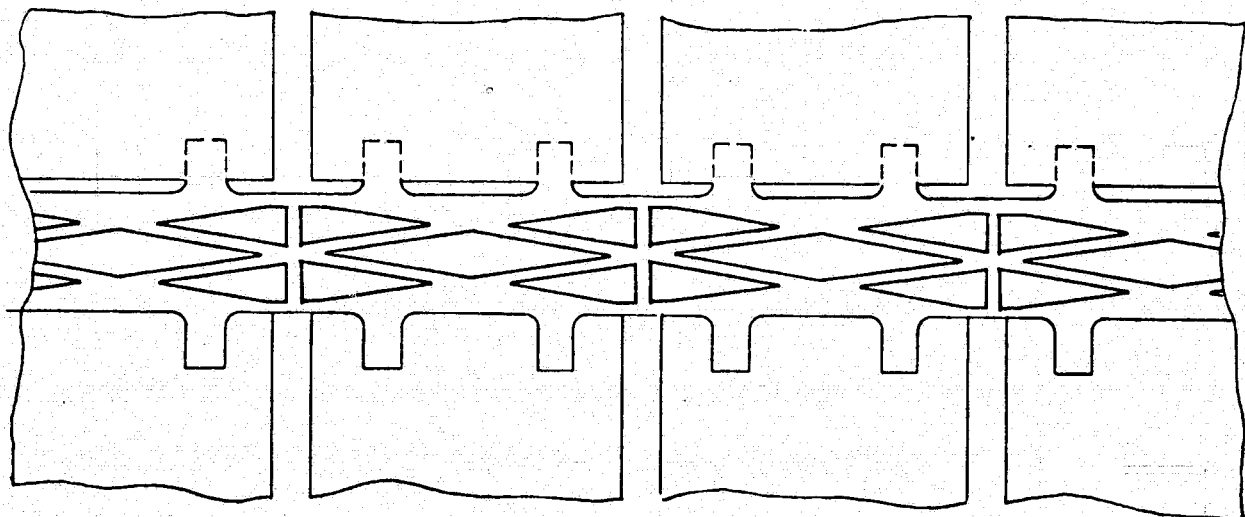
(1) Proprietary Alloy of Hamilton Technology

65°C to accelerate the cure cycle. Moreover, when the RTV silicone was used as the bond for a lap joint of Kapton against Kapton, the bond proved to be stronger than the 1-mil Kapton-H material itself.



1 MIL INVAR  
0.5 MIL Ag  
BOTH SIDES

Figure 3-2. Flexible Design



1 MIL INVAR  
0.5 MIL Ag,  
BOTH SIDES

Figure 3-3. Stiff Interconnect Design

ORIGINAL PAGE IS  
OF POOR QUALITY

Table 3-3. Interconnect Evaluation

Interconnect Design	Moly	Invar	Elinvar	Comparative Mass
Stiff Weldability Thermal Cycle	Poor Poor	Excellent Poor	Good Poor	1
Flexible Weldability Thermal Cycle	Good Poor	Excellent Good	Good Good	4
Material Specifications	1-mil (99.5% pure) Moly 0.5 Ag, both sides	1-mil Invar 63.2% Fe 36% Ni 0.5-mil Ag, both sides	1-mil Elinvar 48% Fe 43% Ni 5% Cr 2-3/4% Ti 0.5-mil Ag, both sides	

Flexible Invar Interconnect is Best

Need Further Work in Ag-plating of Moly

Need Weight Reduction on Flexible Design

Table 3-4. Substrate Cement Evaluation

Cement	Form	Method of Application	Applicable Temperature	Survivability in Thermal Cycle (-190°C to 120°C)	Bond Strength
FEP-Teflon	Laminated to Kapton	Heat sealed under pressure	250°C	Poor	Fair
Flexible Epoxy SMRD-745	2-part formula	Spatula or brush	140°C	Poor	Good
RTV-Silicone	2-part formula	Spatula or brush	Room Temperature to 65°C	Excellent	Excellent

High Temperature Processes Crack Cells

RTV Silicone is Superior

ORIGINAL PAGE IS  
OF POOR QUALITY

### 3.2.1.2 Encapsulant

Following the conclusions of the earlier conceptual design study, a continuous protective cover was desired as an encapsulant for both solar cells and interconnects. Eleven material formulations of polymeric materials were evaluated for comparative merit. In addition to FEP-Teflon, RTV-Silicone and several formulations of a copolymer of polyimide and silicone were tested. Again the processing temperature was the determining factor in maintaining cell/interconnect integrity. The RTV silicone, with its low temperature processing feature, is a clear winner among those materials processed as encapsulants. The one sun 1000-hour UV exposure test showed that the RTV-Silicone and the co-polymer BE124H <sup>(1)</sup> were unaffected by UV. In a 10 sun test at NASA's Lewis Research Center, after 728 hours exposure, the RTV-silicone proved to be superior to the same co-polymer.

RTV-silicone was selected as the best of the evaluated materials for three reasons; low temperature processing, UV resistance, and ease of processing.

### 3.2.2 DESIGN EVALUATION

The status of the ultra-lightweight, flexible blanket concept may be summarized as follows.

Ultra-thin silicon solar cells may be rolled-up on a 10-inch diameter drum without catastrophic failure. Wrap-around contacts are not required with 2-mil thick solar cells. Planar, flexible interconnects made from silver-plated Invar have passed every test given them. The low-temperature processed adhesive and encapsulant does not lead to thermally induced stress great enough to break cells or bonds. The RTV silicone class of adhesives and encapsulants are superior to any other material tested during the course of this program. The low temperature processed co-polymer of polyimide and silicone shows promise and should be further evaluated. The weld bonding process has been proven successful and is to be preferred over solder bonding for the reasons enumerated above. The fully encapsulated cell/interconnect assembly cemented to Kapton-H proves to be a very rugged assembly, resistant to temperature cycling, vibration cycling, roll-up on curved surfaces and creep under load. A summary of properties for the 80-cell module is given in Table 3-5.

---

(1) Bergston & Associates - Schenectady, N.Y.



Table 3-5. 80-Cell Module, Summation of Properties

<u>Mass Breakdown</u>	
2-mil Cells	78 mg
#580 Interconnect	31.3 mg/cell
Kapton-H	14.5 mg/mil-cell
RTV-655	10.9 mg/mil-cell
For the 80-Cell Module:	
80, 2-mil Cells	6.24 g
80, #580 Interconnects	2.50
1-mil Kapton-H (8.2 cm x 41 cm)	0.85
3-1/2-mil RTV-655	3.05
Total Mass Per Cell	158 mg
Maximum Power at 28°C:	
$P_m$ , 80-Cell Module	4.72 Watts
$P_m$ , per Cell	59 mW
Specific Power:	373W/Kg

### 3.2.3 MANUFACTURING PROCESS DEVELOPMENT

#### 3.2.3.1 Weld Bonding

A weld bonding schedule has been developed that is repeatable and reliable in the quality of bonds produced. Hot welds (cell junction is destroyed) are minimal as long as the cell has sufficient thickness (0.3-mil to 0.5-mil) of metallization. Cold welds may be readily detected and corrected by a second current pulse in most cases. Overall yield is better than 90%.

#### 3.2.3.2 Cement Bonding

Strong tenacious bonds may be made with space qualified RTV-silicone at low to moderate curing temperatures. The elastomeric properties of silicone offer a resilient bond that is helpful in protecting the cell/interconnect from mechanical damage. Bond strengths for RTV-silicone exceed that of the Kapton-H substrate.



### 3.2.3.3 Cover Material Bonding

A manufacturing process has been developed which permits a uniform, thin RTV silicone coating to be applied and cured with a minimum of equipment and almost zero production loss. A cure period of 1-hour at 65°C is sufficient to polymerize this material.

## 3.3 LABORATORY TEST RESULTS

### 3.3.1 THERMAL CYCLE TESTS

A total of 12 thermal cycles were run on individual cells, test coupons, and 16 cell sub-modules. In all cases the items under test were clamped at one or more points to the heat sink/source via the metal interconnect to get good thermal contact. One or more thermocouples were soldered to the interconnects to measure cell temperature. The entire assembly was wrapped in a metal-foil shroud to control thermal emittance. A summary of these tests is listed in Table 3-6. The second objective listed in this table has not been met because the thermal/UV test cycle (1200 hours) is still in process at this writing.

Table 3-6. Temperature Cycling

<u>Objectives</u>
<ul style="list-style-type: none"><li>• Stress total cell, interconnect, cement and substrate over extreme temperatur range (-190°C to 120°C)</li><li>• Repeat after UV exposure</li></ul>
<u>Procedure</u>
<ul style="list-style-type: none"><li>• Measure IV characteristic before and after test</li><li>• Attach test coupon to heat sink/source</li><li>• Cycle 100 times at ~ 5°C/min</li><li>• Inspect for cracked cells, open interconnects, etc.</li></ul>
<u>Conclusions</u>
<ul style="list-style-type: none"><li>• FEP-Teflon, heat sealed at 250°C, results in cracked cells</li><li>• RTV silicone, cured at 65°C, does <u>not</u> result in cracked cells</li><li>• There are no signs of fatigue in the Invar interconnect</li><li>• The non-compliant interconnect is not fully evaluated at this time</li></ul>

### 3.3.2 UV EXPOSURE TEST

One 1000-hour UV exposure test is complete and a second is in process at this time. The first test was conducted on single cells overcoated with a selection of cover materials; viz, FEP-Teflon, RTV-silicone, polyimide and several formulations of a polyimide/silicone co-polymer. Each cell was attached to a heat source through a metallic interconnect so that each test item could be maintained at a steady 120°C throughout the duration of the tests. Periodically, readings of  $I_{sc}$  and  $V_{oc}$  were recorded, along with a measurement of surface reflectance at 400 nm. The latter reading was made via an integrating sphere incorporated in the vacuum test stand. Both UV exposure and 20 Kev electron fluence were obtained concurrently. The former radiation, originating with a 2.5 Kw high-pressure mercury-Xenon arc, was adjusted to provide an illuminance at the samples under test of one equivalent UV sun (EUVS). The total low energy electron dosage over the 1000-hour test was  $10^7$  rads. This test is summarized in Table 3-7. The solar and thermal band optical constants for RTV silicone, before and after this test are shown in Table 3-8. These results compare very favorably to FEP-Teflon measured earlier.

Table 3-7. UV Exposure Test

#### Objective

- Comparative evaluation of candidate cover materials under simulated UV exposure and low energy electron dosage

#### Procedure, GE Co.

- Expose 11 samples of selected polymers and co-polymers at 120°C to  $H_g-X_e$  lamp at 1 equivalent UV sun (EUVS) and 20 Kev fluence
- Monitor IV characteristics and surface reflectance at 400 nm

#### Conclusions

- The optical properties of the polyimide, 20% polyimide/80% siloxane and RTV silicone coatings were unaffected through this exposure to 1 EUVS and  $10^7$  rads
- LeRC tests at 10 EUVS for 728-hours showed a 17% change in  $I_{sc}$  for RTV silicone, comparable to the best glass resin

Table 3-8. Absorptance and Emittance of RTV Coated Cells Cemented to Kapton-H

<u>Top Surface Measurements</u>		
<b>Materials:</b>		
3-mil RTV-655 over Solarex 2-mil Silicon Solar cells		
1/2-mil RTV-655 as adhesive between cells and substrate		
1-mil Kapton-H substrate		
<b>Measurements:</b>		
	Before IV Exposure	After 1000 Hours UV Exposure (1 Sun)
<u>Top Surface</u>		
Reflectance (0.1 $\mu\text{m}$ to 10 $\mu\text{m}$ )	0.16	0.13
Absorptance (2.5 $\mu\text{m}$ to 28.5 $\mu\text{m}$ )	0.05	0.13
(0.1 $\mu\text{m}$ to 10 $\mu\text{m}$ )	0.84	0.87
Emittance, normal (100°F)	0.94	0.87
<u>Back Surface</u>		
Reflectance (2.5 $\mu\text{m}$ to 28.5 $\mu\text{m}$ )	0.18	--
Emittance, normal (100°F)	0.82	--

### 3.3.3 ROLL-UP TEST

A mockup of a 10-inch diameter storage drum was used as a test vehicle for a simulated four-module solar array. Four 80-cell modules were bonded together and equipped with flat conductor cable buses on both sides of the assembly. The 80-cell modules represented a full-scale module in the direction of wrap, but only a small fraction of the design width of the module. The total length of the assembly was sufficient to provide 2-1/2 wraps around the 10-inch drum. The assembly was wrapped under the load per unit length (29.2 N/m) prescribed in the array design. A total of 15 cycles of wrap and unwrap of this assembly did not result in any broken cells or interconnect bonds. The RTV silicone cement and overcoat showed no signs of delamination. Subsequent measurement of the IV characteristic on each module showed a 3% to 9% loss in maximum power and fill factor losses ranging up to 11%. In no case was the fill factor less than 70%. This test is summarized in Table 3-9.

Table 3-9. Roll-up Test

## ROLL-UP TEST

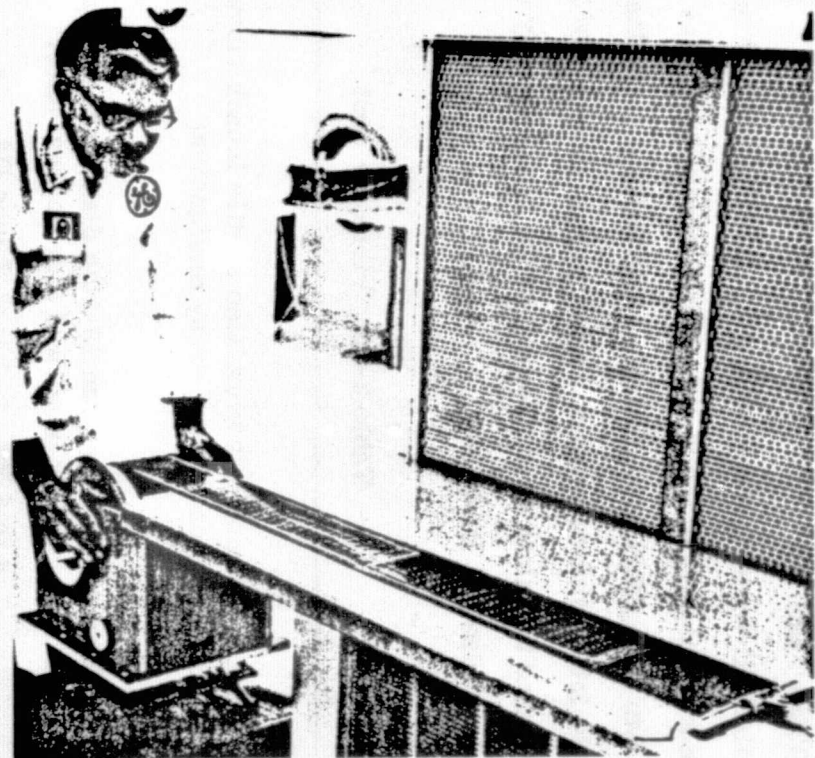
### ● PURPOSE

- DEMONSTRATE FEASIBILITY OF BLANKET ROLL-UP

### ● TEST RESULTS

- NO CRACKED CELLS AFTER 15 ROLL-UPS
- MODULE  $P_{mp}$  LOSSES RANGED FROM 3% TO 9%
- MODULE FILL FACTORS  $\geq 0.70$

VERIFIED FLEXIBLE BLANKET ROLL-UP CONCEPT



ORIGINAL PAGE IS  
OF POOR QUALITY

### 3.3.4 VIBRATION TEST

Subsequent to the roll-up test, the wrapped-up assembly of four modules was placed on a shake machine where a simulation of the Shuttle launch environment was imposed on it. The test unit was shaken in two orthogonal axes (the third axis being a redundant transverse axis). No cells were broken. No interconnects were damaged. A minimal loss of  $P_{max}$  and fill factor were noted. There was no translational movement of the test assembly along the axis of the drum. This test is summarized in Table 3-10.

Table 3-10. Vibration Test

#### Objectives

- Expose array model to simulated shuttle launch vibration environment
- Test for vibration induced array malfunction

#### Procedure

- Wrap four-module array on 10-inch diameter drum under the prescribed tension
- Vibrate the assembly in each of 3 orthogonal axes:

4 to 5 Hz	1 inch DA
5 to 25 Hz	1.4 g (0-peak)
25 to 50 Hz	0.036 inch DA
50 to 1000 Hz	5 g (0-peak)

- Visually inspect and compare IV characteristics before and after test

#### Observations

- No cracked cells
- $\Delta P_{mp} < 2\%$ ,  $\Delta FF < 3\%$

#### Conclusions

- A flexible blanket rolled-up under tension will suffer no loss in a shuttle launch vibration environment.

### 3.3.5 CREEP TEST

As a test of module and lap joint elongation under load and at an elevated temperature, a test was conducted whereby an 80-cell module and associated substrate lap joint were suspended from a test fixture in a thermal chamber. The unit under test was loaded at the level (29.2 N/m) used in the roll-up test. After 24-hours at 120°C no measurable creep was observed.

### 3.3.6 ELECTRICAL TEST

Repeated use of Spectrolab's Large Area Pulsed Solar Simulator (LAPSS) was made during the course of manufacture and test of cells, test coupons, and modules. A standard cell, supplied by JPL, was used as a zero air mass reference. An IV curve was obtained at each test enabling  $I_{sc}$ ,  $V_{oc}$ ,  $I_{mp}$ ,  $V_{mp}$  and  $P_{mp}$  to be readily observed. It may be noted, however, that a visual inspection must accompany each electrical test. There were times, for instance, when a normal IV curve could be obtained on a test article that had one or more broken cells. A summary of the conclusions of this test is given in Table 3-11.

Table 3-11. Electrical Testing

<u>Purpose</u>
In-process test of product health
<u>Implementation</u>
Spectrolab's Large Area Pulsed Solar Simulator (LAPSS)
<u>Procedure</u>
IV curve is taken after each weld bonding stage as well as cement bonding and encapsulation
<u>Conclusion</u>
<ul style="list-style-type: none"><li>● Monitoring of I at 470 mV is sufficient at incoming inspection</li><li>● LAPSS provides all necessary data <math>I_{sc}</math>, <math>V_{oc}</math>, <math>I_{mp}</math>, and <math>V_{mp}</math> to quickly diagnose state of health</li></ul>

## SECTION 4

### CONCEPTUAL SOLAR ARRAY DESIGN FOR HALLEY'S COMET MISSION

This section describes the conceptual design for a concentrator solar array utilizing the 2-mil solar cell module development technology described in Section 3. Section 5 briefly summarizes the array performance if a 6-mil solar cell of 13.5% efficiency were used.

#### 4.1 SOLAR ARRAY REQUIREMENTS

The solar array requirements to meet the Halley's Comet Mission objectives are listed in Table 4-1.

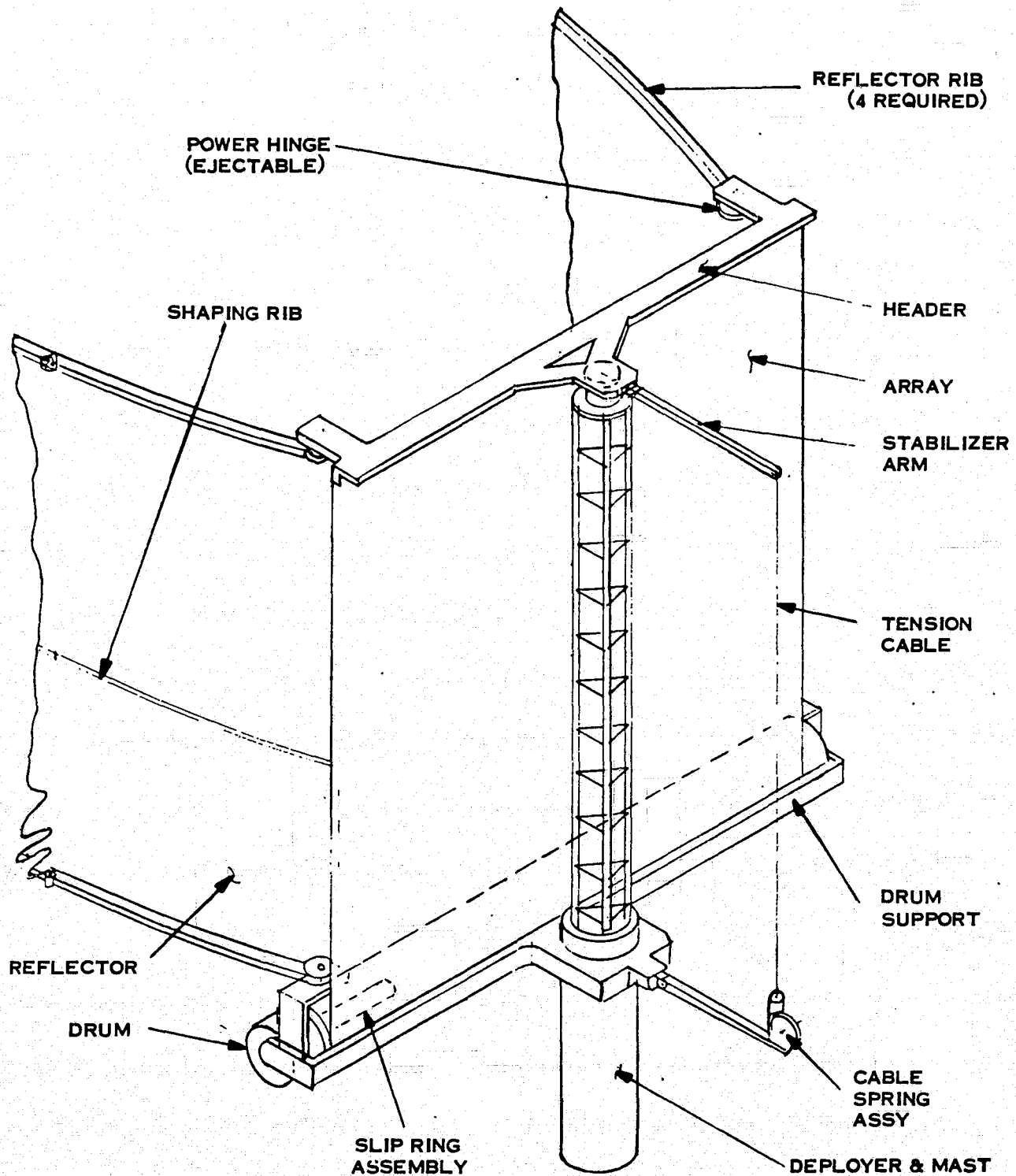
Table 4-1. Study Requirements

CATEGORY	REQUIREMENT
POWER BOL (M.)	60 (UNCONCENTRATED) AT 1 AU
CONCENTRATION RATIOS (EFFECTIVE)	1.8 AND 3.2
ALLOWABLE ARRAY POWER DEGRADATION	LESS THAN 25% OVER FIVE YEARS
DEPLOYMENT/RETRACT CAPABILITIES	DEPLOYMENT: FULL RETRACTION: 90% NO. OF CYCLES: 50
OPERATING TEMPERATURE RANGE (°C)	-130 TO +140°C
THERMAL SHOCKS	100 CYCLES OVER THE TEMPERATURE RANGE OF +120°C TO -190°C
FLATNESS PARAMETER	MAXIMUM 10° ACROSS THE OVERALL ARRAY WIDTH AND/OR LENGTH
OPERATING PRESSURE (TORR)	10 <sup>-5</sup>
NOMINAL VOLTAGE RANGE (VOLTS)	200-400VDC
MAXIMUM VOLTAGE (VOLTS)	420VDC
ARRAY NATURAL FREQUENCY (Hz)	0.015
DYNAMIC PACKAGING ENVELOPE (METERS)	4.5 DIA x 11.8 LENGTH (MAC CONFIG DWG #2D)
MAXIMUM LOADS (G's)	LONGITUDINAL ± 4.0 (X) YAW ± 4.0 (Y) PITCH +10.0, -8.0 (Z)
VIBRATION LEVELS	25 - 100 Hz      +6 dB/OCT 100 - 250 Hz      0.035 G <sup>2</sup> Hz 250 - 500 Hz      -6 dB/OCT 500 - 2000 Hz      0.009 G <sup>2</sup> Hz
ACOUSTIC LEVELS (dB)	145
DEPLOYMENT CONSTRAINTS	THE DEPLOYED ARRAY CONFIGURATION SHALL BE CONSTRAINED TO ASSURE THAT ITS PERFORMANCE AND THE SPACECRAFT PERFORMANCE ARE NOT DEGRADED BY THE THRUSTER'S ION PLUME.

**ORIGINAL PAGE IS  
OF POOR QUALITY**

#### 4.2 MECHANICAL DESIGN

The baseline design of the solar array for the Halley's Comet mission is illustrated in Figure 4-1, showing the array and reflectors partially deployed. The array is a roll-out type blanket 4.3m wide by 73.9m long. The array is deployed by means of an astromast which is attached to the stowage drum support. The side reflectors are supported by cantilevered ribs, (top and bottom) hinged to facilitate stowage for launch. Shaping ribs are spaced at equal intervals to insure that the proper curve is established along the entire reflector length. The



**Figure 4-1. Concentrated Array Concept (Halley Comet Mission)  
Partially Deployed**



extended reflector is hinged at the root to provide adjustment of the reflector assembly to two levels of concentration (i.e., effective concentration ratio of 1.8 and 3.6). The reflectors are moved by means of hinge motor assemblies directly attached at the root pivot point. These drive assemblies are mounted to the header (19)\* and drum support (13)\* with adapters so that the concentrator can be jettisoned at a specific point in the mission profile. The concentrator position for jettisoning is shown in Figure 4-2.

\*Callouts refer to Figure 4-4.

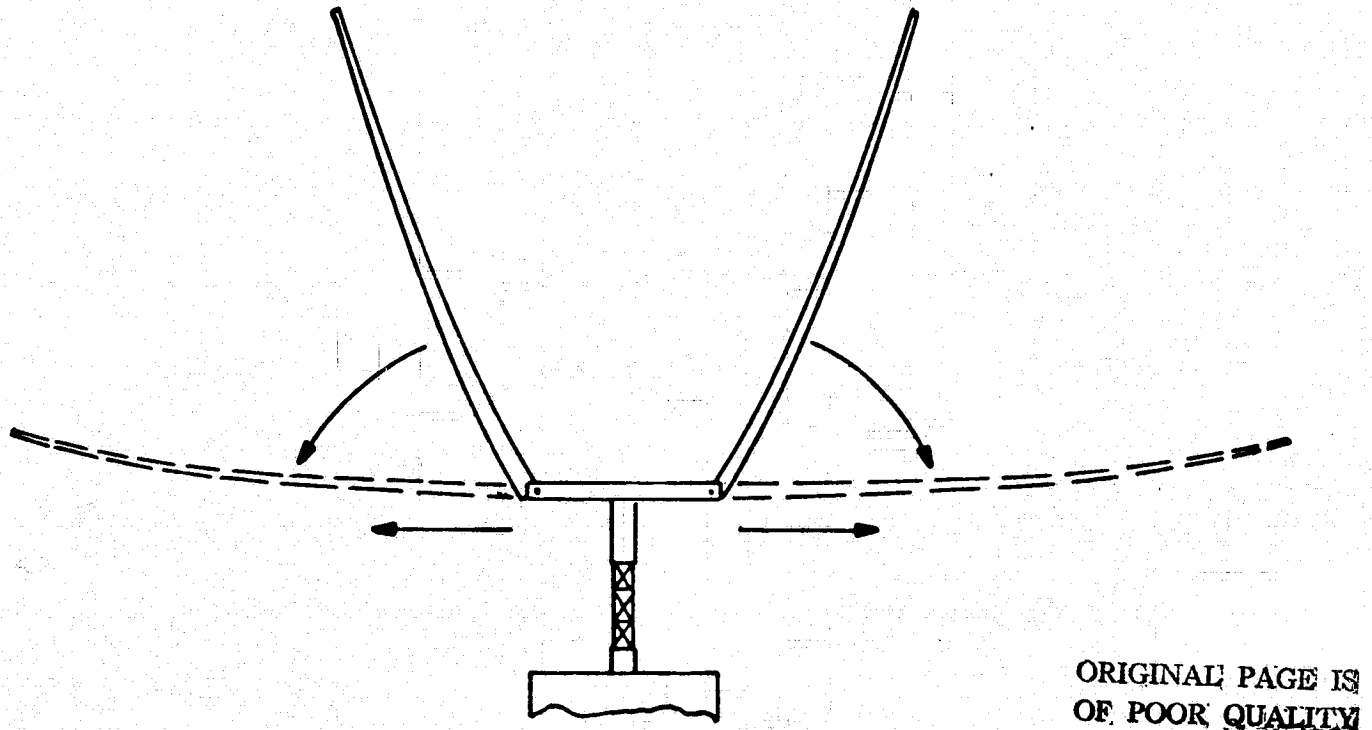
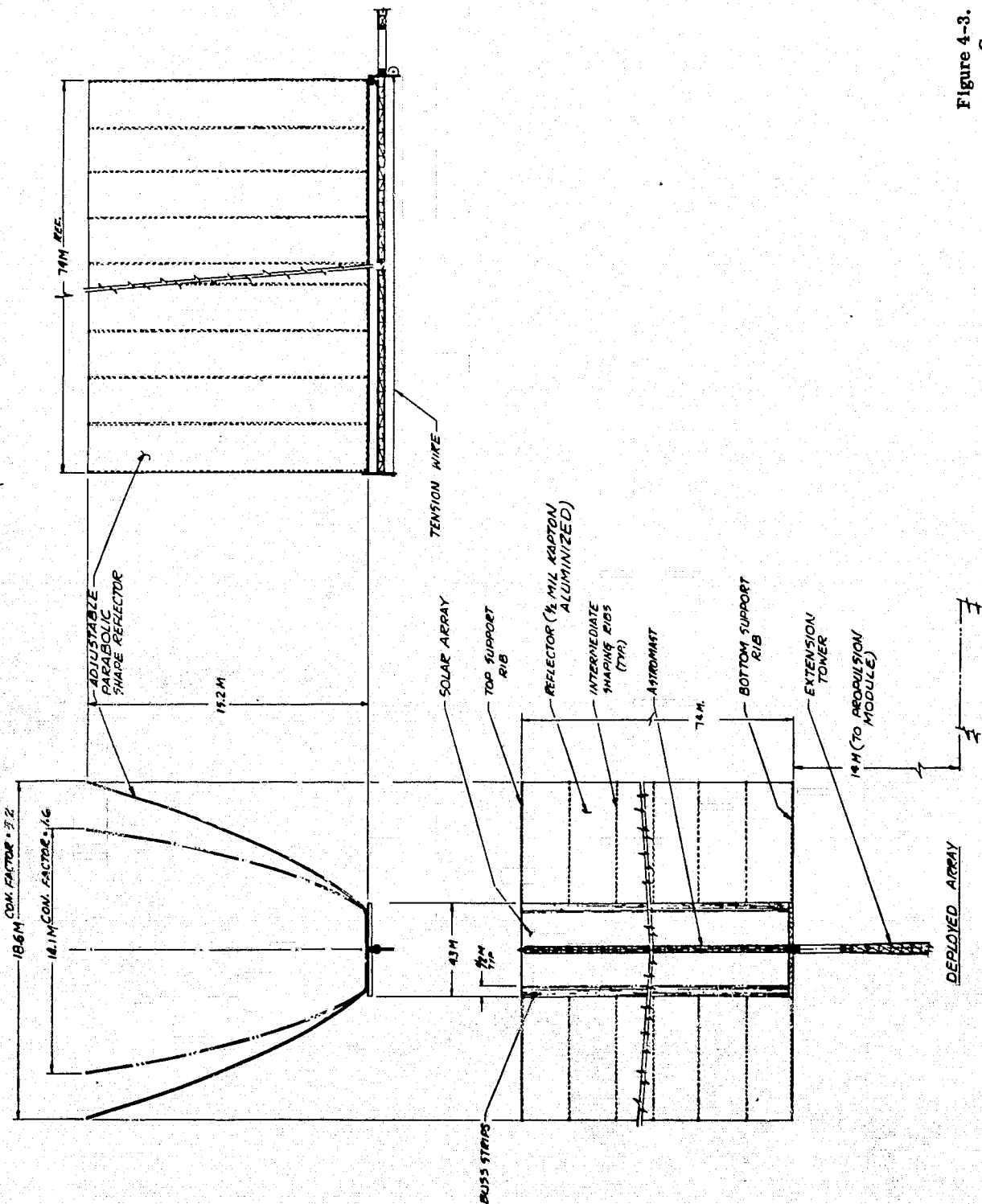


Figure 4-2. Jettison Position for Concentrator

The reflectors are rotated to bring their center of gravity in line with the direction of ejection (parallel to the drum axis). During this rotation, the tension in the stabilizer cable is reduced upon ground command to a lower value by a pyro release device in the tension cable assembly (18).

#### Size and Weight

The overall size of the deployed array is essentially 15m x 18.6m x 74 meters as shown in Figure 4-3. The entrance aperture of the concentrator is initially set at for a concentration ratio of 1.8 a 1 AU and opened to 18.6m for ratio of 3.8 at 4.5 AU. The total mass of the



baseline array including a boom to extend the array 14 meters from the spacecraft is estimated at about 386 Kilograms per wing. This value is based upon the use of thin 2-mil solar cells in a ultra-lightweight blanket which is nonretractable. A breakdown of the mass is given in Table 4-2 with item references given in Figure 4-4.

Table 4-2. Mass Summary (Articulated Parabolic Concentrated Concept)

Item No.	Item	Unit Mass KG	Quantity Per Wing	Baseline Design KG
	<u>Blanket (Electrical)</u>			
1.	Solar Cells	$78 \times 10^{-6}$	596,960	46.56
2.	Substrate	.036/m <sup>2</sup>	317.8 m <sup>2</sup>	11.44
3.	Adhesive (1 mil RTV)	.01/m <sup>2</sup>	243.8 m <sup>2</sup>	2.44
4.	Cover Material (3 mil RTV)	.03/m <sup>2</sup>	243.8 m <sup>2</sup>	7.32
5.	Interconnects	25 mg	596,960	14.92
6.	Bus Strips	.144/m	73.9 m	10.6
7.	Slip Rings Assy	7.0	1	7.0
8.	Cable	.2	1	.2
9.	Connectors	.04	4	.24
10.	Switching Relays	.03	52	1.56
11.	Control Modules	.20	1	.20
	Sub Total			102.57
	<u>Blanket Support/Stowage</u>			
12.	Drum	5.93	1	5.93
13.	Drum Support	24.83	1	24.38
14.	Shaft & Bearings	3.67	2	7.34
15.	Mast	46.20	1	46.20
16.	Mast Deployer	39.3	1	39.3
17.	Stabilizer Arms	1	2	2.0
18.	Tension Wire Assy	.84	1	.84
19.	Header	6.0	1	6.0
20.	Blanket Tension Springs	.2	5	1.0
21.	Drum Drag Brake	.2	1	0.2
	Sub Total			133.64
	<u>Concentrator</u>			
22.	Reflector (Kapton Film)	20	2	40.0
23.	Support Rib	13	4	42.
24.	Shaping Rib (Inc. Flex Hinge)	.59	12	7.08
25.	Rib Folding Joint	1	16	16.0
26.	Rib Power Hinge	4	4	16.0
27.	Jettison Adapter	2.3	4	9.2
28.	Container Support	2.0	1	2.0
				132.28
29.	Misc. Hardware	-	-	5.0
30.	Extension Mast	12.9	1	12.9
	Total Mass	12.9		386.39

ORIGINAL PAGE IS  
OF POOR QUALITY

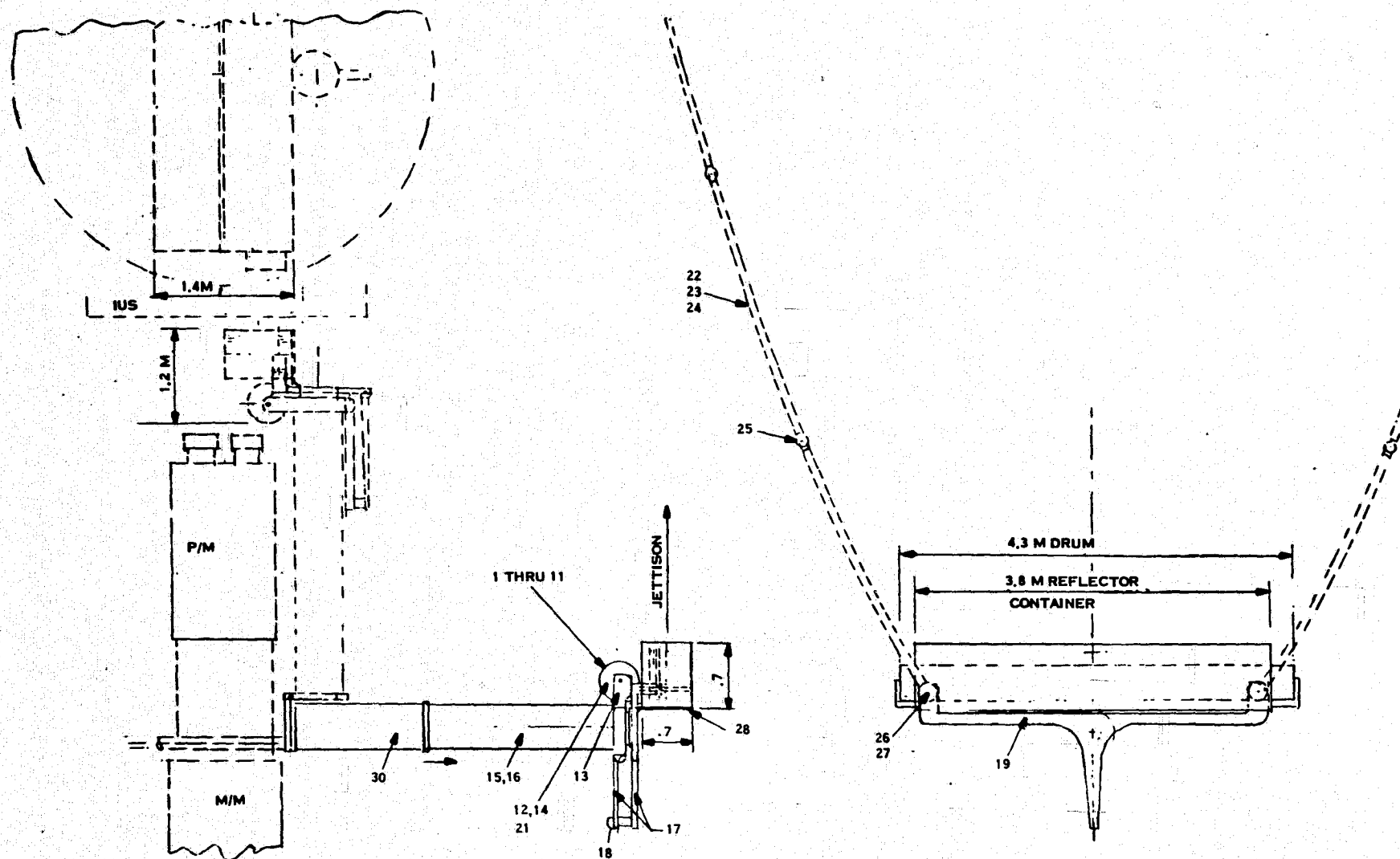


Figure 4-4. Solar Array Concept (Articulated CPC Reflector)

### Structure and Tension

The primary structure of the array assembly is an astromast of about 20 inch diameter capable of taking a 100 lb axial load. The stiffening of the assembly results from the "V" formation of the concentrators.

## 4.2.1 MECHANICAL ELEMENTS

### 4.2.1.1 Canister and Mast

The extendible boom which deploys the array and concentrator is a coilable lattice boom of the type manufactured by Astro Research Corporation. The longeron and cross members are constructed with polyimide resin glass reinforced composite to withstand the higher temperatures ( $150^{\circ}\text{C}$ ) expected in this mission.

### 4.2.1.2 Slip Rings

The slip ring assembly consists of 26 power rings with returns capable of handling 20 amperes each and a number of small signal rings rated at 0.5 amps. The general configuration of the unit is shown in Figure 4-5.

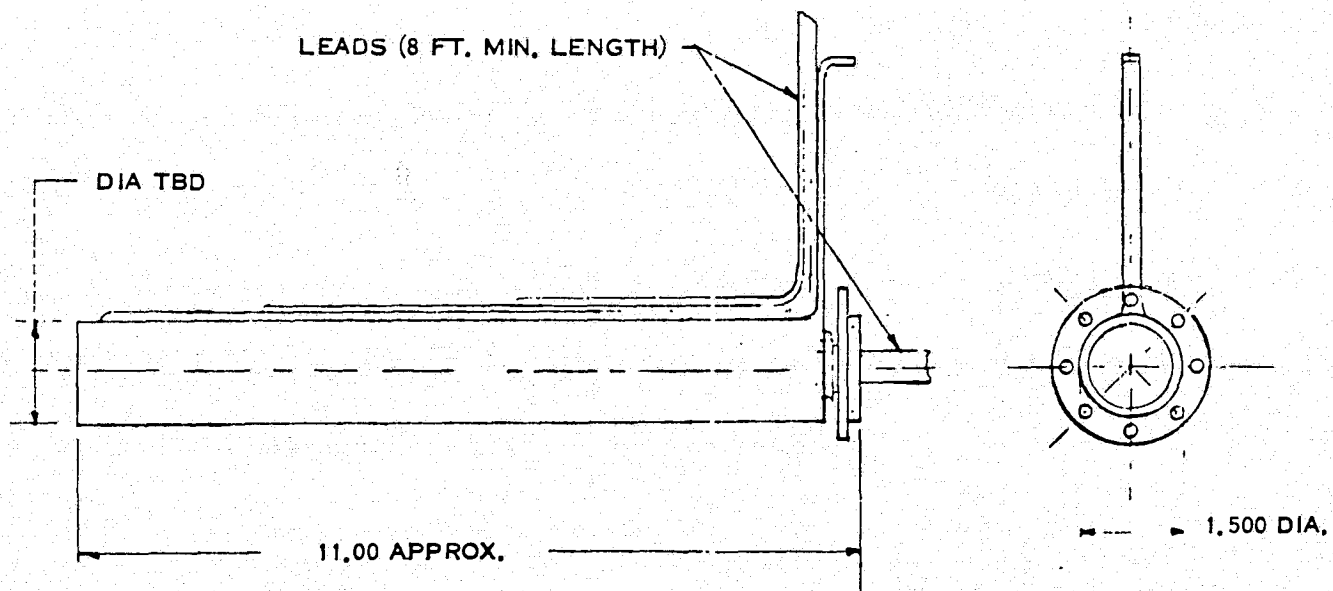


Figure 4-5. Slip Ring Assembly

ORIGINAL PAGE IS  
OF POOR QUALITY

#### **4.2.1.3 Tensioning Devices**

Two tensioning devices are needed to (1) establish a specified tension level in the blanket array when fully developed, and (2) maintain a tension in the concentrator film in the longitudinal direction. For the blanket tension in the non-retractable version, a short travel rotary or linear spring comes into play near the end of full extension to establish the desired tension with low gradient characteristic to allow for thermal expansion. During extension, a low tension is produced in the blanket by means of a lightweight brake on the drum. Since rotary spring motors such as the negator motor become very heavy for the long extension lengths involved in the Halley mission, a considerable weight saving can be realized with the brake approach.

Concentrator tension and tension on the stabilizing cable which compensates for the movement at the top of the mast caused by the concentrator and blanket tension are also established by springs which become effective near the end of the deployment cycle. The cable spring assembly is equipped with a pyro release device to reduce that tension to a lower value after jettisoning the concentrator.

#### **4.2.1.4 Concentrators**

The concentrators are composed of thin aluminized Kapton film (1/2-mil) stretched over supporting ribs which are articulated in four points to permit stowage in a small volume. The ribs are curved to generate the desired parabolic shape at the ends of the reflector. This shape is insured along the reflector by means of six (6) shaping ribs of very lightweight "T" section members bonded to the film to maintain the desired curvature. These ribs are also articulated with flexure hinge points to accommodate folding.

A concept for the support rib hinge joints is shown in Figure 4-6. A torsion spring torque the arms into position against a pin stop. The deployed position is held by means of a spring actuated cam lock which automatically snaps into its final position. The sequence of deployment of the concentrator along with the array is illustrated in Figure 4-7. Mechanical latches holding the bundle in the stowed configuration are sequentially tripped by the rib unfolding action to control the deployment sequence of the concentrator.

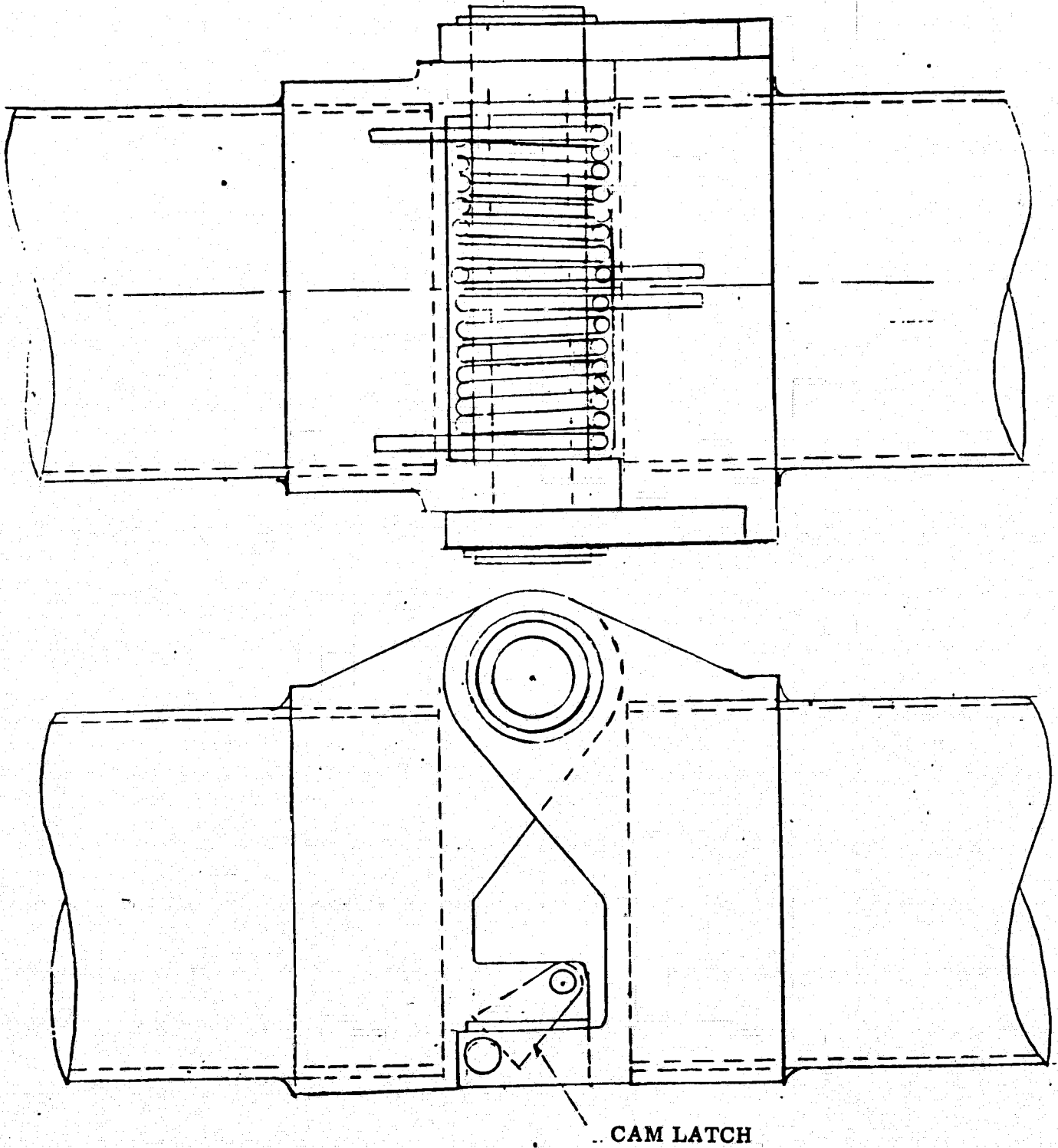


Figure 4-6. Rib Hinge Concept

ORIGINAL PAGE IS  
OF POOR QUALITY

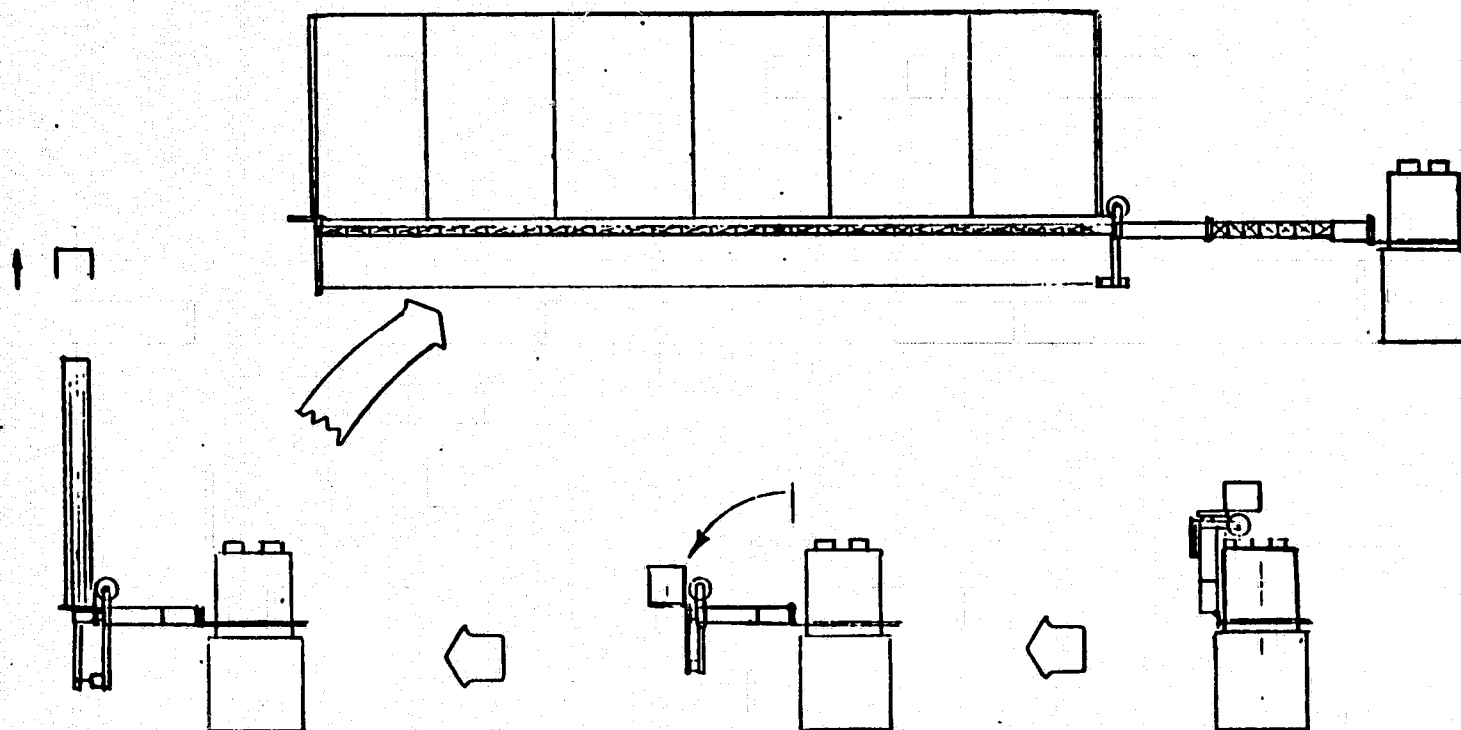


Figure 4-7. Deployment Sequence



#### **4.2.1.5 Materials**

It is expected that graphite reinforced composites will be used extensively in this concept. Thin wall composite tubing is considered to be a prime candidate for the concentrator support ribs because of its high stiffness to weight ratio. Beryllium hinge tube fittings and drum support structure will be chosen where necessary to meet the weight goal. Carbon composites will also be given consideration in the support structure.

#### **4.2.1.6 Mass Summary**

The total mass of the system as discussed in Paragraph 4.2 is estimated to be 773 Kg. The breakdown of weights includes 30 items as shown in Table 4-1.

### **4.3 ELECTRICAL DESIGN**

This section describes the electrical design for the concentrator solar array proposed for the Halley's Comet Mission. Maximum use of the technology developed for two-mil cells as described in Section 3 of this report has been incorporated into the design.

#### **4.3.1 SOLAR CELL CIRCUITS**

The smallest replaceable group of solar cells incorporated into the blanket design is a matrix of 28 solar cells, connected 7 in series by 4 in parallel. Each solar cell is 2 Cm x 2 Cm x 0.002 inch in size. Invar interconnects, as previously described, are welded to the silverized P-surface of one row of cells, and to the N-surface tabs of the adjacent layer. This is depicted in Figure 4-8. Interconnect tabs at the top and bottom of the circuit will be trimmed off as appropriate to permit the circuits to be interconnected alternately as shown in Figure 4-9. Each solar cell circuit produces 1.41 watts at the maximum power point (1 AU, AMO, 55°C) and develops a maximum power voltage of 2.66 volts.

#### **4.3.2 SOLAR CELL MODULE**

A solar cell module consists of 41 circuits connected in series across the width of the blanket as shown in Figure 4-10. Each circuit is orientated 180 degrees from its adjacent circuit to alternate the direction of current flow and thereby minimize the magnetic fields generated. The 41 series circuits represent a total of 1148 cells connected 287 in series by 4 in parallel. Each module produces 57.7 watts at the maximum power point (1 AU, AMO, 55°C) and develops a maximum power voltage of 109 volts.

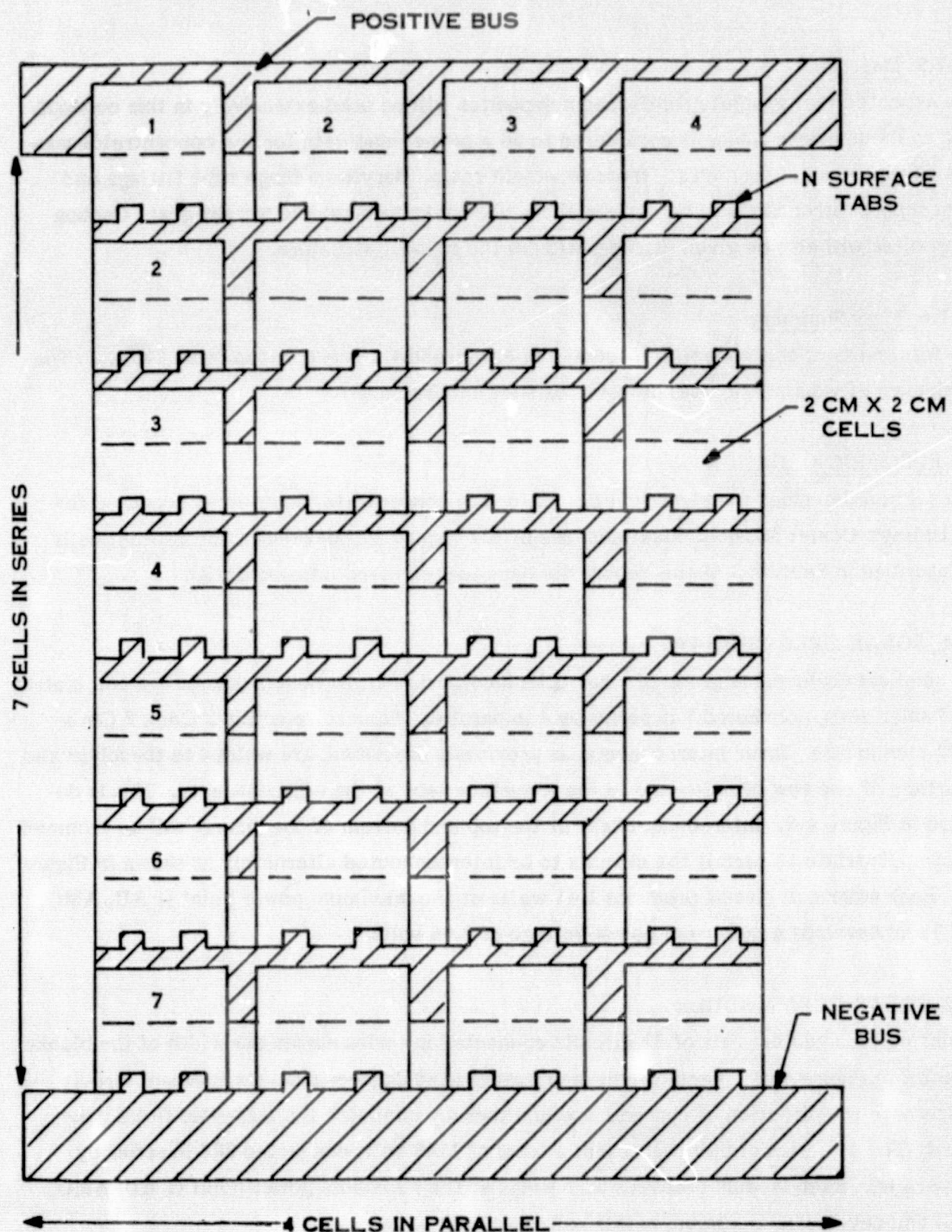


Figure 4-8. Circuit Layout (7S by 4P)

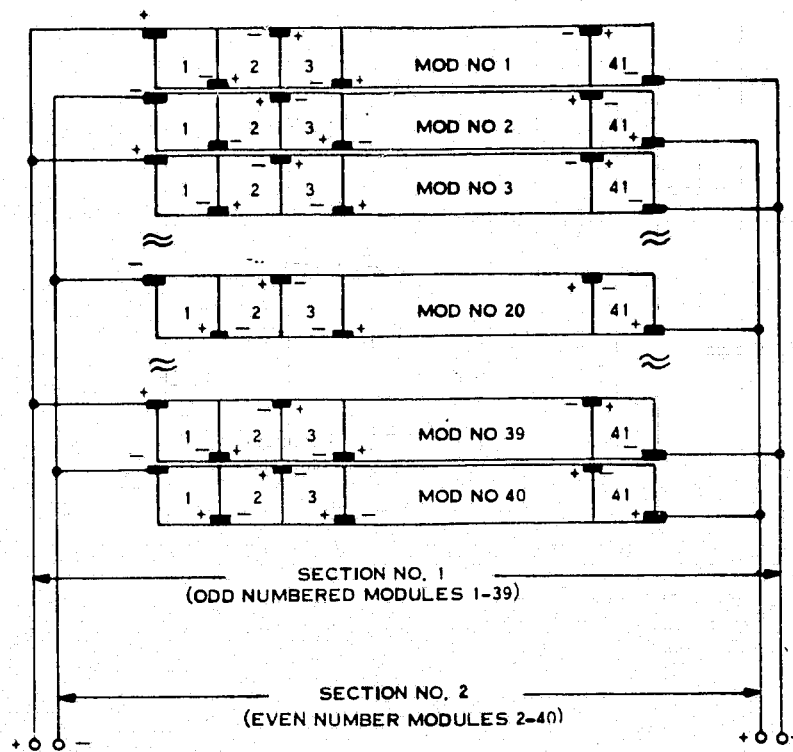


Figure 4-9. Circuit Module Interconnections

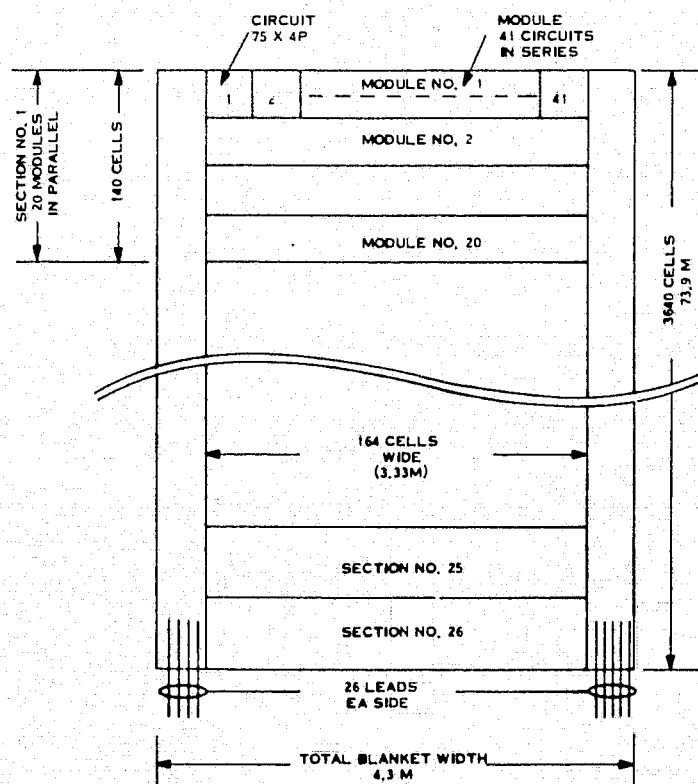


Figure 4-10. Blanket Layout

#### **4.3.3 Solar Cell Section**

A solar cell section is the smallest area of the total blanket from which external cabling is routed to the spacecraft. Each section is composed of 20 alternate modules connected in parallel. This permits current flow across the width of the blanket to be in opposite directions for adjacent modules and thereby minimize the magnetic fields generated. The 20 module in each section represent 22,960 solar cells connected 287 in series by 80 in parallel. This produces 1155 watts at the maximum power point (1 AU, AMO, 55°C) and a maximum power voltage of 109 volts.

#### **4.3.4 Solar Array Blanket**

Each solar array blanket (or wing) contains 26 sections as shown in Figure 4-10. The power from each section is brought out on two flat aluminum conductors running along the sides of the blanket. The conductors are sized in cross section according to the length of their run to equalize the section voltages at the array output. Approximately 0.5 meters of blanket width is allocated on each side of the blanket to accommodate the 26 flat aluminum conductors. The conductors are positioned underneath the concentrators so they will not be exposed to concentrated sunlight. The maximum expected current for each conductor is 20 amperes (1 AU, CR=1.8, AMO, 110°C).

The overall blanket size is 4.3 meters wide by 73.9 meters long. The 596,960 cells per wing occupy an area 3.3 meters wide by 73.9 meters long. A cell-to-cell spacing of 0.03 Cm was assumed in the sizing.

#### **4.3.5 Mode Switching**

Each solar array wing is composed of 26 sections. The power from each section is routed along the blanket sides via flat aluminum cables to the mode switching relays located within the array drum. The relays connect the individual sections into two groups of nine sections in parallel and two groups of four sections in parallel. The four groups are then interconnected into one of two configurations as shown in Figure 4-11. The array output then passes through the slip rings located within the drum onto the power bus. The two mode switching configurations are necessary to maintain the array output voltage between 200 and 400 VDC. A power controller can be added between the array output and the bus if additional regulation is required.

ORIGINAL PAGE IS  
OF POOR QUALITY

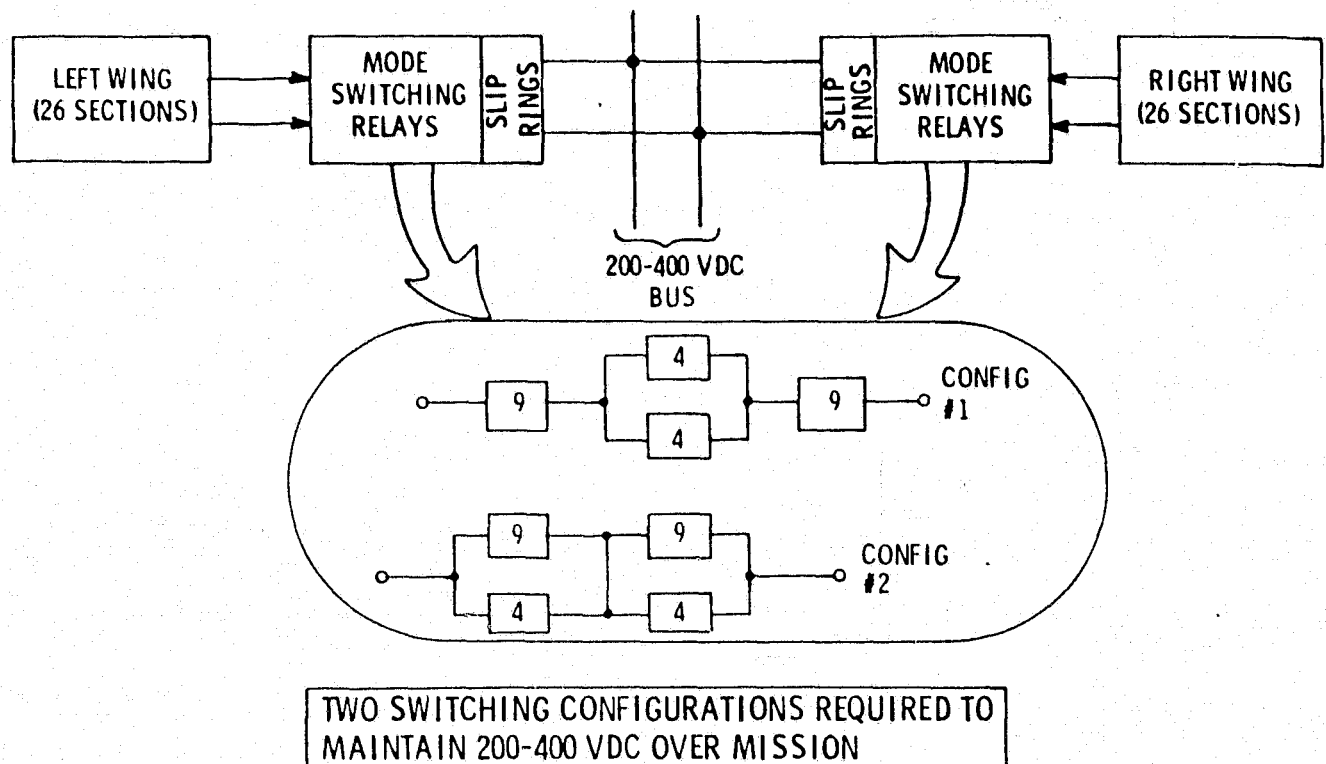


Figure 4-11. Mode Switching Diagram

#### 4.3.6 System Performance

A preliminary estimate of the system performance of the solar array has been made utilizing the Halley's Comet Mission trajectory shown in Figure 4-12. The array power, voltage, and temperature as a function of distance from the sun and concentration ratio have been calculated and are described in this section of the report. Of equal importance is the impact on power degradation due to the radiation environment. Although the analytical activities to date in this area have been only cursory, it will also be addressed.

#### 4.3.7 Mission Trajectory

The mission trajectory used to estimate the array performance is shown in Figure 4-12. After launch at 1.0 AU, the spacecraft travels outbound to a maximum distance of 4.5 AU over a time period of approximately 750 days. At 4.5 AU, the spacecraft moves inbound along the orbit of the comet for rendezvous at about 1.1 AU. The time period for the spacecraft to travel from 4.5 AU to 1.1 AU is about 530 days. Therefore, rendezvous with the comet is about 1280 days after launch ( $3\frac{1}{2}$  years). After rendezvous, the spacecraft follows the comet reaching a minimum sun distance of 0.6 AU.

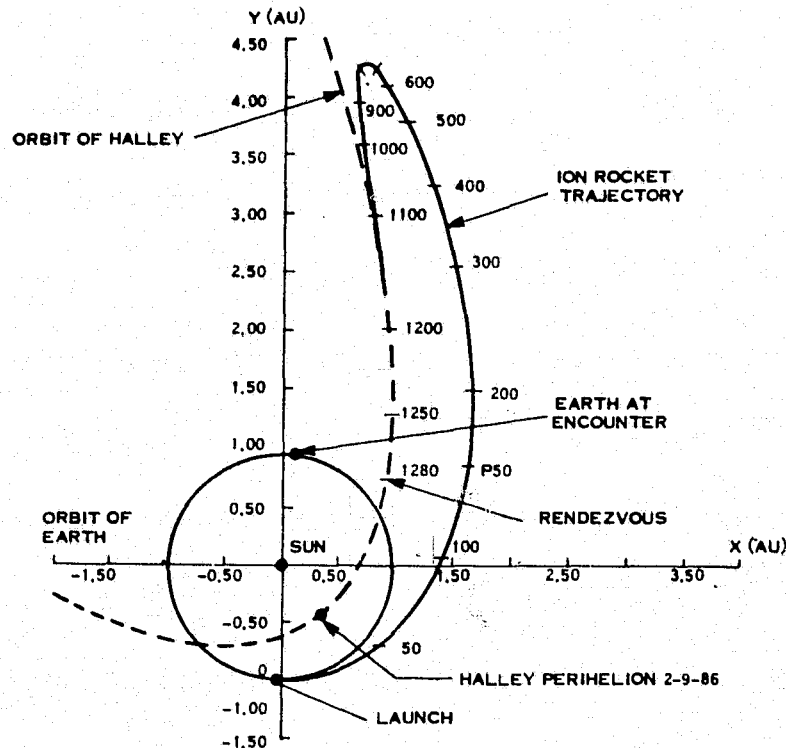


Figure 4-12. Halley Rendezvous Trajectory (Ecliptic Plane Projection)

#### 4.3.8 Array Power Performance

The basic building block for the Halley's Comet solar array is a 2 Cm x 2 Cm x 0.002 inch solar cell having an efficiency of 60 mW at 28°C (11.1%). Estimates of cell power were made using the JPL test data (JPL IOM #341-018A, "Parametric Testing of Solarex 50 Micron Solar Cells", April 13, 1977, Mr. Bruce Anspaugh), and upgraded the efficiency from those tested (9.96%) to the present 11.1%. Effective concentration ratios of 3.2 and 1.8 were used to establish the solar incident energy impinging on the solar cells (geometric ratios are 4.6 and 2.0 respectively). These data, along with the solar cell temperature estimates over the Halley's Comet Mission, were used to calculate array power.

Table 4-3 summarizes the results of the analysis relating to array power and voltage as a function of distance from the sun. Effective concentration ratios of 3.2 and 1.8 were used. The solar incident energy falling upon the cells was calculated as:

$$\text{Incident Energy} = \frac{\text{solar constant (135.3 mW/cm}^2\text{)}}{(\text{Au distance})^2}$$

Table 4-3. Array Performance Over Halley's Comet Mission Trajectory

AU Distance	Concentration		Incident Energy	Array Temp.	Cell Power	Cell Voltage	Undegraded Array Power	Section Voltage	Array Voltage With Switching	Switch Config.
	Ratio	Equiv AU								
1	1	1	135.3 mW/Cm <sup>2</sup>	55°C	50.3mW	0.38VDC	60KW	109VDC	327VDC	1
1	1.8	0.75	243.5 mW/Cm <sup>2</sup>	110°C	58.6mW	0.30VDC	70KW	86VDC	258VDC	1
1.1	1.8	0.82	201.2 mW/Cm <sup>2</sup>	85°C	58.1mW	0.32VDC	69.4KW	92VDC	276VDC	1
1.1	1	1.10	111.8 mW/Cm <sup>2</sup>	50°C	48.1mW	0.38VDC	57.8KW	109VDC	327VDC	1
1.5	1.8	1.12	108.2 mW/Cm <sup>2</sup>	45°C	45.2mW	0.40VDC	54KW	115VDC	344VDC	1
1.5	3.2	.84	192.4 mW/Cm <sup>2</sup>	90°C	57.3mW	0.335VDC	68.4KW	96VDC	288VDC	1
2.0	3.2	1.12	108.2 mW/Cm <sup>2</sup>	40°C	44.9mW	0.404VDC	53.6KW	116VDC	348/232VDC	1/2
2.8	3.2	1.57	55.2 mW/Cm <sup>2</sup>	0°C	28.3mW	0.50VDC	33.8KW	144VDC	287VDC	2
3.0	3.2	1.88	48.1 mW/Cm <sup>2</sup>	-15°C	24.6mW	0.540VDC	29.1KW	155VDC	310VDC	2
4.0	3.2	2.23	27.1 mW/Cm <sup>2</sup>	-50°C	14.7mW	0.620VDC	17.6KW	178VDC	356VDC	2
4.5	3.2	2.50	21.4 mW/Cm <sup>2</sup>	-72°C	12.9mW	0.680VDC	15.4KW	195VDC	390VDC	2

ORIGINAL PAGE IS  
OF POOR QUALITY

When using solar concentrators, the cells behave as though they were closer to the sun (higher incident energy) than they actually are. The "equivalent AU" listed on the table is a measure of that effect. The equivalent AU was calculated as:

$$\text{Equiv AU} = \left[ \frac{\text{Solar Constant}}{\text{Incident Energy}} \right]^{1/2}$$

As can be seen on the table, when the solar array is actually at 4.5 AU, but has a concentration of 3.2, the effective AU is 2.5. Since the solar cell power varies inversely with the square of the distance, the power output is increased significantly at far distances from the sun by using concentrators.

By using the incident energy along with the corresponding cell temperature, the cell power and voltage (at maximum power point) was determined using the JPL test data previously mentioned. The cell power was ratioed upward by 11.1/9.96 to account for the present cell efficiency. The "cell power" and "cell voltage" values shown on Table 4-2 were thus determined. The undegraded array power is the product of the total number of cells times the cell power (no losses assumed at this point).

As described in Paragraph 4.3.3, a solar cell section is composed of 20 modules connected in parallel. Each module consists of 41 circuits connected in series. Each circuit is a 7 series by 4 parallel celled building block. Therefore, the voltage developed per section (same as module) is 7 cells/circuits x 41 circuits, or 287 cells in series. The column labeled "section voltage" is 287 times the cell voltage. The cell voltage was taken directly from the JPL test data. The switching configurations described in Paragraph 4.3.5 either doubles (Configuration #2) or triples (Configuration #1) the voltage from each section. The column labeled "Array Voltage with Switching" on Table 4.2 shows the resulting values.

Figure 4-13 shows a plot of the total undegraded array output power as a function of AU. From initial array deployment at 1.0 AU to about 1.5 AU, the parabolic concentrators are set for an effective concentration ratio of 1.8 to 1.5 AU, the ratio is changed from 1.8 to 3.2. The concentration ratio remains at 3.2 until the spacecraft completes its outbound



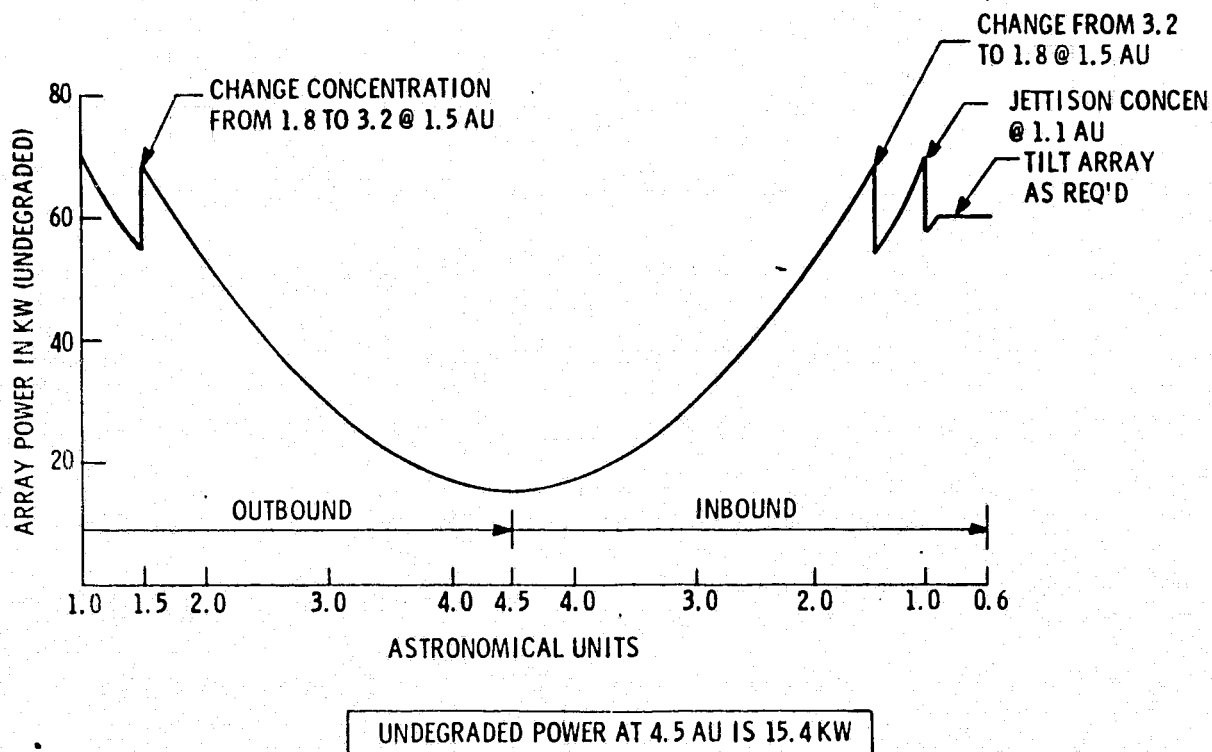


Figure 4-13. Undegraded Power vs AU

journey and returns inbound to 1.5 AU (approximately 1135 days). At 1.5 AU, the concentrators are moved back to the 1.8 ratio position until just prior to comet rendezvous (approximately 1.1 AU). At this point, the concentrators are jettisoned as their usefulness has terminated. In order to maintain temperature control ( $120^{\circ}\text{C}$  maximum), the array can be tilted as the spacecraft travels inbound from about 0.8 AU. Figure 4-14 shows the array temperature profile.

The total undegraded array output power varies from 70kW at 1 AU to 15.4kW at 4.5 AU, as seen on Figure 4-13. If an overall degradation of 12% is assumed, those values will drop to 61.6kW and 13.6kW, respectively. A requirement to drive six ion engines at 2kW per engine at 4.5 AU will result in a power margin of 1.6kW for the degraded array.

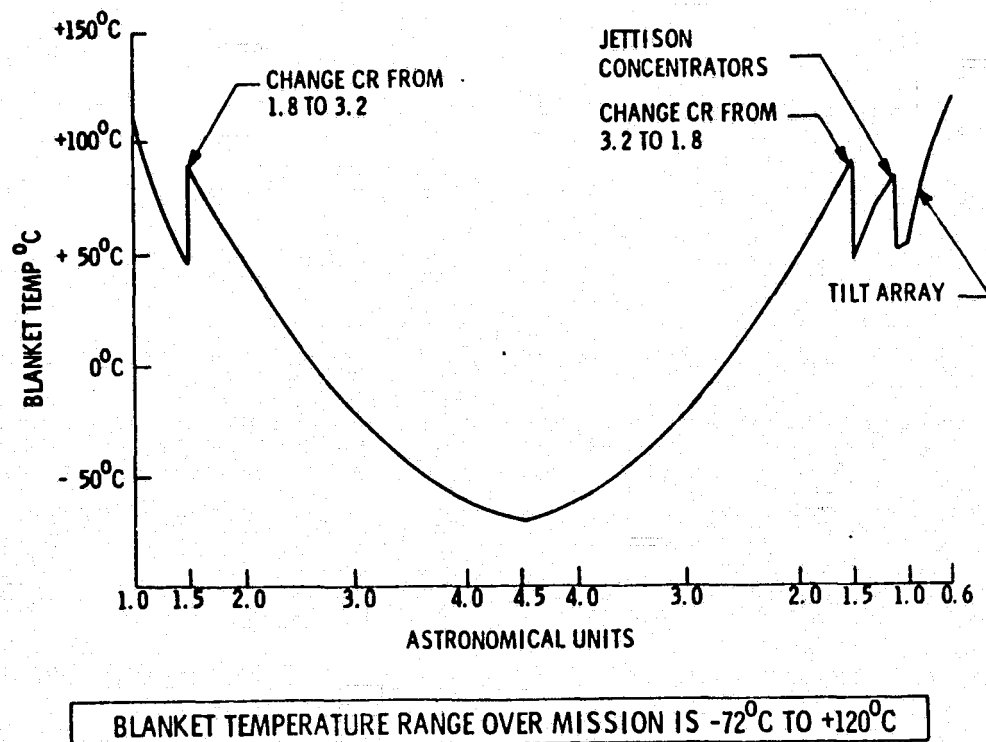


Figure 4-14. Array Temperature vs AU

#### 4.3.9 ARRAY VOLTAGE PERFORMANCE

Using the values established for cell voltage listed on Table 4-3 and the switching scheme described in Paragraph 4.3.5, a plot of array voltage over the Halley's Comet Mission was developed and is shown in Figure 4-15. The array voltage output varies between 232 VDC and 390 VDC using the switching points as shown. Configuration #1 is used for sun distances less than 2 AU and configuration #2 for sun distances greater than 2 AU. The voltage range shown falls well within the specification limits of 200 to 400 VDC.

#### 4.3.10 RADIATION ANALYSIS

A radiation analysis was conducted using the electron and proton fluence listed in Table 4-4 for the Halley's Comet Mission (Ion Drive). The fluence levels stated at 50% probability were doubled for the analysis. The results show a maximum power degradation of 5% over the mission. This value was obtained by using the JPL supplied test data of power loss versus the damage equivalent normally incident (DENI) electron fluence at 1 MEV. This value excludes the effect of UV Radiation.

ORIGINAL PAGE IS  
OF POOR QUALITY

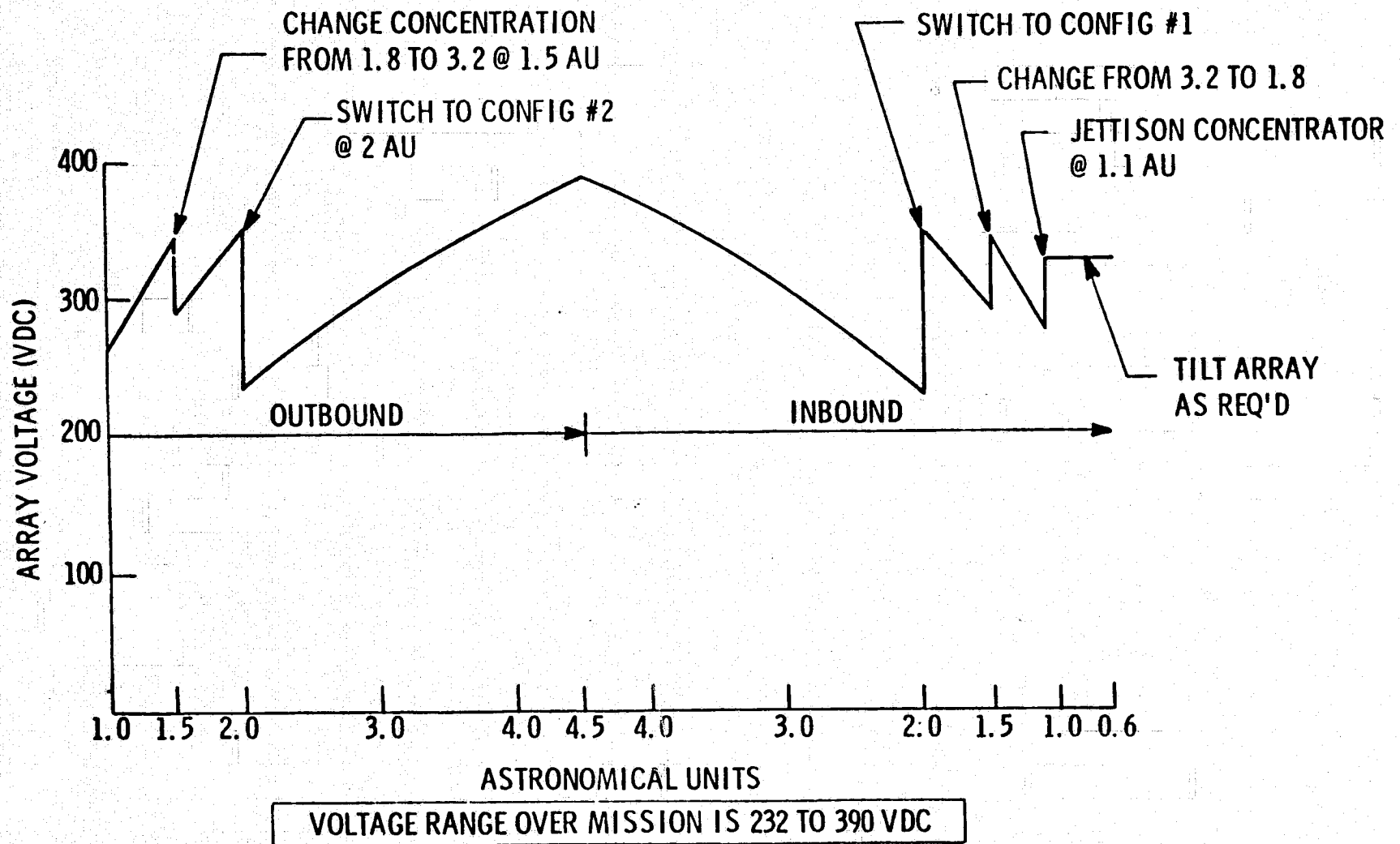


Figure 4-15. Array Voltage vs AU

Table 4-4. Fluences for Halley's Comet/Ion Drive Mission

PARTICLES	ENVIRONMENT	ENERGY	INTEGRAL FLUENCE, F (cm <sup>-2</sup> )			
			PROBABILITY THAT F IS NOT EXCEEDED <sup>(4)</sup>			
			50%	75%	90%	95%
INTERPLANETARY PROTONS	SOLAR WIND <sup>(2)</sup>	0 900 eV 1 keV	3.9 (15) 3.9 (15) 3.1 (15)			
	INTERMEDIATE ENERGY PROTONS	10 keV 100 keV 1 MeV 1.5 MeV 3.0 MeV 7.0 MeV	6.2 (13) 1.2 (12) 2.5 (10) 1.3 (10) 4.0 (9) 2.5 (9)	2.5 (10) 1.3 (10) 4.0 (9) 2.5 (9)	2.5 (10) 1.3 (10) 8.5 (9) 5.1 (9)	2.5 (10) 2.0 (10) 1.2 (10) 7.6 (9)
	SOLAR PROTON EVENTS AND COSMIC RAYS	10 MeV 30 MeV 60 MeV 100 MeV 1000 MeV	1.5 (9) 4.2 (8) 3.1 (8) 2.8 (8) 1.9 (8)	2.1 (9) 9.1 (8) 4.6 (8) 3.1 (8) 1.9 (8)	4.4 (9) 1.8 (9) 6.9 (8) 3.6 (8) 1.9 (8)	6.0 (9) 2.3 (9) 8.7 (8) 4.0 (8) 1.9 (8)
INTERPLANETARY ELECTRONS	SOLAR WIND <sup>(3)</sup>	0 10 eV 20 eV 50 eV	1.5 (16) 1.5 (16) 1.2 (16) 4.0 (15)			
	INTERMEDIATE ENERGY ELECTRONS (SOLAR AND JOVIAN)	100 eV 1 keV 10 keV 100 keV 1 MeV	1.0 (15) 1.0 (13) 1.0 (11) 1.0 (9) 8.0 (7)			
	COSMIC RAYS	10 MeV 100 MeV 1000 MeV	1.9 (7) 1.8 (7) 6.4 (6)			

## SECTION 5

### OPTIONAL SOLAR ARRAY DESIGN

The solar array design described in Section 4 of this report utilized 2 Cm x 2 Cm x 0.002 inch solar cells having a power efficiency of 11.1% at 28°C. The optional design described in this section utilizes 2 Cm x 2 Cm x 0.006 inch solar cells having a power efficiency of 13.5% at 28°C. For the same power output, the increase in efficiency means that fewer cells are required and therefore a smaller overall blanket size. However, using cells 3-times thicker results in additional cell mass. As will be seen, these offsetting mass factors nearly compensate one another in the overall system. The principal description of this optional solar array was determined by ratioing appropriately from the baseline described in Section 4.

#### 5.1 NUMBER OF CELLS REQUIRED

The baseline design utilizes 596,960 solar cells per wing to achieve 60 kW at 1 AU, 55°C with no concentration. By ratioing the number of cells by the power efficiencies:

$$\frac{11.1}{13.5} \times 596,960 = 490,834$$

The optional design requires 490,834 cells per wing to achieve the same power output at 13.5% efficiency.

#### 5.2 ARRAY SIZE

The optional design maintains the same overall blanket width and concentrator height. Therefore, the 490,834 cells will be accommodated in an area 164 cells wide by 2993 cells long.

Using the same cell spacing (0.03 Cm), the array length will be:

$$2993 \text{ cells} \times 2.03 \frac{\text{Cm}}{\text{Cell}} = 60.7 \text{ meters}$$

This decrease in length from the baseline of 73.9 meters to 60.7 meters for the blanket, concentrators, and mast, affords a reduction in weight, as does the fewer number of cells required.

### 5.3 ARRAY WEIGHT

The optional solar array weight has been estimated by ratioing appropriately from the detailed weight estimates determined for this baseline. The weight breakdown is shown in Table 5-1. The total weight of the optional array design is nearly the same as that for the baseline for the same power output. This is because the higher cell efficiency permits using fewer of them and thus the array size is reduced. This weight reduction is closely offset by the increased weight due to the larger cell thickness. The 6-mil cell weight was calculated by adding 4-mils of silicon to the baseline 2-mil cell. It assumes the metallization, grids, weld tabs, etc. are the same for both cells. A silicon density of 2.4 grams/Cm<sup>3</sup> was used in the calculation.

Table 5-1. Weight Comparison of Optional Array to Baseline

	Baseline (2 Mil Cells, 11.1 %)	Optional (6 Mil Cells, 13.5%)
Electric	102.6	136.1
Blanket Support and Stowage	133.6	118.4
Concentrators	132.3	125.1
Extension Mast	12.9	12.9
Misc. Hardware	<u>5.0</u>	<u>5.0</u>
Total per Wing	386.4	397.5
Total Array (2 Wings)	772.8 Kg	795.0 Kg

### 5.4 OPTIONAL SOLAR ARRAY SUMMARY

Table 5-2 lists the major characteristics of the Optional Solar Array design. Except for size and number of cells, the optional design is identical to the baseline design.

ORIGINAL PAGE IS  
OF POOR QUALITY

**Table 5-2. Major Characteristics**

<u>Item</u>	<u>Baseline</u>	<u>Optional</u>
No. Cells per Wing	596,960	490,834
Cell Area per Wing	244 m <sup>2</sup>	200 m <sup>2</sup>
Blanket Area per Wing	318 m <sup>2</sup>	261 m <sup>2</sup>
Blanket Size per Wing	4.3 x 73.9 m <sup>2</sup>	4.3 x 60.7 m <sup>2</sup>
Reflector Size (1 Side)	15 x 73.9 m <sup>2</sup>	15 x 60.7 m <sup>2</sup>
Total Reflector Area (2 Sides)	2217 m <sup>2</sup>	1821 m <sup>2</sup>
Power, 1 AU, No Concentration	60 kW	60 kW
Cell Size	2 cm x 2 cm x 0.002 in	2 cm x 2 cm x 0.006 in
Cell Efficiency	11.1 %	13.5 %
Total Weight	773 kG	795 kG

## SECTION 6

### RECOMMENDATIONS

Great progress has been made in less than six months in the development of designs, selection of materials and refinement of manufacturing processes for the fabrication of ultra-lightweight solar modules using the recently available 2-mil silicon solar cells. An exciting conceptual design for a variable-concentration concentrator solar array has been identified that meets or exceeds the performance and mass requirements placed on it by the Halley's Comet Ion Drive.

Further design analysis and proof-of-concept experiments should be pursued without delay to enhance the technology readiness status already established. Some pertinent topics for additional investigation are:

1. Long duration (greater than 1000 hr) 1 EUVS exposure on RTV silicone and a modified polyimide-siloxane-co-polymer.
2. Design refinement and thermal test of the flexible interconnect to reduce the interconnect mass.
3. Module fabrication and test using  $2 \times 4 \text{ cm}^2$  and  $4 \times 4 \text{ cm}^2$  2-mil solar cells to reduce inter-connect mass and increase module area efficiency.
4. Design of production tooling to accommodate the fabrication and in-process testing of 41 circuit modules (1148 cells/module).
5. Investigation of material properties; such as, pinholes in the cover material using scanning electron microscopy and ultrasonic profiling of solar cells to uncover incipient cell fractures.
6. Experimentally determine solar flux distribution across the exit plane of the compound parabolic concentrator as a function of concentration ratio and sun angle.
7. Obtain cell output data as a function of solar illuminance and cell temperature over the range of values expected for the Halley's Comet Mission.
8. Experimentally determine the optimum method for stowage of large area thin films, as would be found in the solar array concentrator, in the smallest possible volume.



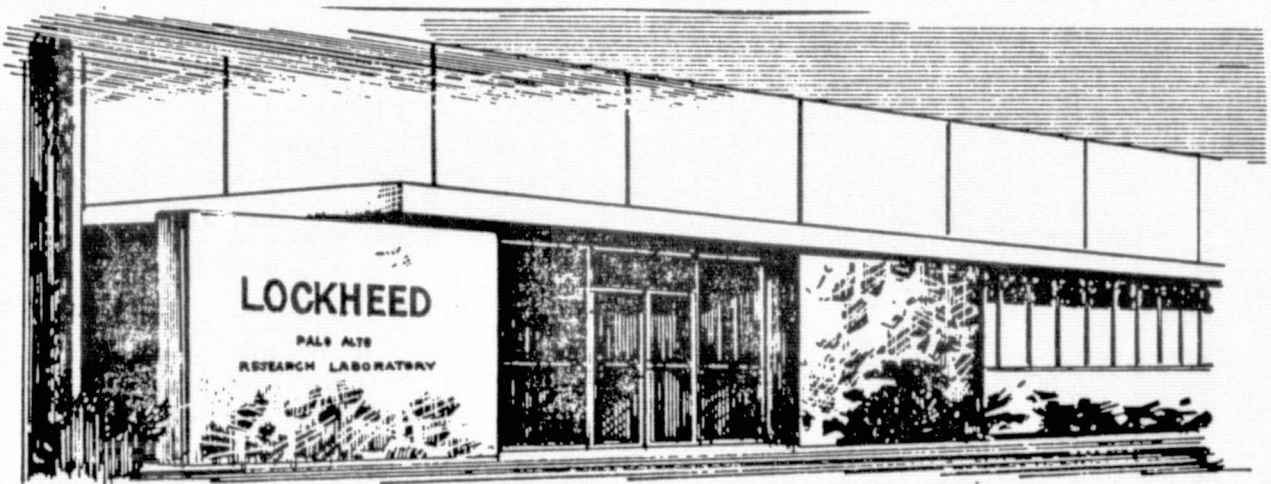
9. Design and test the appropriate sequencing mechanism to be used in concentrator development.
10. Design and test a suitable scale model of the array and concentrator stowage and deployment sequence.
11. Perform the necessary stress and dynamics analysis for the deployment and erection system to arrive at the minimum mass system.

FINAL REPORT  
PHASE II

SPRAYLON FLUOROCARBON  
ENCAPSULATION FOR SILICON  
SOLAR CELL ARRAYS

FOR THE  
JET PROPULSION LABORATORY,  
CALIFORNIA INSTITUTE OF TECHNOLOGY

CONTRACT NO. 954410



**LOCKHEED**

PALO ALTO RESEARCH LABORATORY

LOCKHEED MISSILES & SPACE COMPANY, INC. • A SUBSIDIARY OF LOCKHEED AIRCRAFT CORPORATION  
PALO ALTO, CALIFORNIA

November 1977

PHASE II  
FINAL REPORT  
SPRAYLON FLUOROCARBON  
ENCAPSULATION  
FOR  
SILICON SOLAR CELL ARRAYS

PREPARED BY: D. A. VANCE AND S. A. GREENBERG  
THERMAL SCIENCES LABORATORY OF MATERIALS SCIENCES  
LOCKHEED PALO ALTO RESEARCH LABORATORIES

PREPARED FOR: NASA-JPL  
JPL CONTRACT NO. 954410  
E. N. COSTOGUE, PROGRAM MANAGER

THIS WORK WAS PERFORMED FOR THE JET PROPULSION LABORATORY,  
CALIFORNIA INSTITUTE OF TECHNOLOGY, SPONSORED BY THE NATIONAL  
AERONAUTICS AND SPACE ADMINISTRATION UNDER CONTRACT NAS 7-100.

Lockheed Palo Alto Research Laboratory  
LOCKHEED MISSILES & SPACE COMPANY, INC.  
A Subsidiary of Lockheed Corporation  
Palo Alto, California 94304

## FOREWORD

This document was prepared by the Thermophysics Group of Thermal Sciences in the Materials Sciences Laboratory of Lockheed Palo Alto Research Laboratory of the Lockheed Missiles & Space Company for NASA-JPL as a Phase II final report. The work was administered under the technical direction of Mr. E. N Costogue, JPL Program Manager, and Dr. M. McCargo, Program Manager. The technical effort was conducted by D. A. Vance, Project Leader, and Dr. S. A. Greenberg, Research Scientist.

## ABSTRACT

The original development program (Phase I, Ref. 1) was performed to evaluate, modify, and optimize the Lockheed-formulated liquid transparent film-forming fluorocarbon (Spraylon) protective coating for silicon solar cells and modules. In Phase II, the program objectives were extended to include advanced thin solar cells at 120°C operational temperature. As a result of excessive degradation to the Spraylon under conditions of accelerated ultraviolet exposure at 120°C, an evaluation and assessment of other candidate encapsulants was performed. A computer model thermal stress parametric study of various laminate cell structures was performed. A finite element analysis of solar-cell interconnect configurations for numerous designs is presented.

## ACKNOWLEDGMENTS

Contributions have been made to this program from various organizations in carrying out the objectives of testing and evaluation of candidate materials and their uses in a number of solar cell laminar configurations. This program is interrelated with other programs to achieve the purposes of assessment and evaluation of various proposed lightweight and low-cost solar arrays.

The contributors have been:

Lockheed Missiles & Space Company, Palo Alto, California

- Solar Cell Interconnect Fabrication  
Mr. M. Lopez, Manufacturing Research
- Computer Modeling  
Dr. J. A. de Runtz, Jr., Structures Laboratory  
Dr. C. Yen, Structures Laboratory
- Fracture Investigation  
Dr. F. W. Crossman, Structures Laboratory
- Thermal Properties Measurements  
Mr. G. R. Cunningham, Jr., Thermophysics Laboratory

General Electric Company, Space Division, Valley Forge, Pennsylvania

- Mr. George Rayl

NASA-Lewis Research Center (NASA-LeRC), Cleveland, Ohio

- M. J. J. Marsik

Boeing Aerospace Company, Seattle, Washington

- L. Fogdall
- D. Russell

Cell and submodules were supplied by General Electric and NASA-LeRC.

High-energy electrons plus UV and protons plus UV irradiations were performed by Boeing Aerospace Company's Combined Radiation Effects Test Laboratories.

## CONTENTS

Section		Page
	FOREWORD	ii
	ABSTRACT	iii
	ACKNOWLEDGMENTS	iv
	ILLUSTRATIONS	vii
	TABLES	x
1	INTRODUCTION	1-1
2	PROGRAM OBJECTIVE	2-1
3	TECHNICAL DISCUSSION	3-1
	3.1 Spraylon Systems Component Evaluation For Conventional Solar Cells	3-1
	3.1.1 Spraylon - Primer Evaluation	3-2
	3.1.2 Primer Application Considerations	3-3
	3.1.3 Primer Application	3-4
	3.1.4 Spraylon Formulation Evaluation	3-5
	3.1.5 Spraylon Composition Evaluation of Various Temperatures	3-6
	3.1.6 Test Results of Thermal/UV Exposure at 10 Suns Intensity	3-12
	3.1.7 Thermal Cycling of Spraylon-Coated <u>Thick</u> Cells (12 mils)	3-17
	3.2 Evaluation of Spraylon System on <u>Thin</u> Solar Cells	3-17
	3.2.1 Thermal Cycling of Spraylon-Coated <u>Thin</u> Cells (2 mils)	3-18
	3.3 Cell Fracture Investigation	3-19
	3.4 Redirection of Encapsulant Material Evaluation Program	3-23
	3.5 Evaluation Assessment of Candidate Encapsulants	3-26

Section		Page
3.6	UV Test Results	3-28
3.6.1	Low-Intensity UV Exposure Test Results of Candidate Encapsulants (1 and 2 Suns Intensity)	3-28
3.6.2	Accelerated UV Test Results of Candidate Encapsulants (5 and 10 Suns Intensity)	3-31
3.7	Combined Environmental Exposures of Candidate Materials	3-37
3.7.1	Combined Environmental Exposure Test Results	3-38
3.8	Parametric Stress Analysis of Solar Array Elements	3-38
3.8.1	Laminate Studies	3-43
3.8.2	Thermal Cycling Analysis of Solar Cell Configurations	3-52
3.8.3	Plane Strain Analysis	3-58
4	DISCUSSION OF TEST RESULTS AND OBSERVATIONS	4-1
4.1	Selection of Materials	4-1
4.2	Spraylon Encapsulant Test Results	4-2
4.3	Silicone Encapsulant Test Results	4-2
4.4	FEP Teflon Encapsulant Test Results	4-5
4.5	Glass Resin Encapsulant Test Results	4-8
4.6	Comparative Encapsulant Evaluation	4-10
4.7	Parametric Stress Analysis	4-13
5	CONCLUSIONS AND RECOMMENDATIONS	5-1
5.1	Conclusions	5-1
5.2	Recommendations	5-1
Appendix		
A	TABLE OF THERMAL-UV STABILITY OF SILANE PRIMER/SPRAYLON	A-1
B	TEST REPORT - UV/CHARGED PARTICLE IRRADIATIONS	B-1
C	OPTICAL DATA FOR FEP TEFLON	C-1
D	REFERENCES	D-1



## ILLUSTRATIONS

Figure		Page
3-1	Effect of Spraylon Formulation on Transmittance	3-7
3-2	Effect of Temperature on UV Degradation of 1-mil Spraylon	3-9
3-3	Effect of Temperature on UV Degradation of 2-mil Spraylon	3-10
3-4	Calculated Solar Cell Response Curves	3-11
3-5	20°C-Thermal - UV Exposed Spraylon Spectral Transmittance Dependence on Film Thickness	3-13
3-6	120°C-Thermal - UV Exposed Spraylon Spectral Transmittance Dependence on Film Thickness	3-14
3-7	Calculated Primer Degradation - 910 ESH UV Exposure	3-15
3-8	Silicon Fracture Surface, 38 X, Below Metal Trace	3-20
3-9	Silicon Fracture Surface, 75 X, Below Metal Trace	3-20
3-10	Silicon Fracture Surface, 380 X, Below Metal Trace	3-21
3-11	Silicon Fracture Surface, 1000 X, Below Metal Trace	3-21
3-12	Silicon Fracture Surface, 390 X, Away From Metal Trace	3-22
3-13	Silicon Fracture Surface, 1000 X, Away From Metal Trace	3-22
3-14	Metal Trace of Current Collection Grid on Solar Cell, in Cross-Section, 500 X (Non-Spalling Area)	3-24
3-15	Metal Trace of Current Collection Grid on Solar Cell, in Cross-Section, 500 X (in Spalling Area)	3-24
3-16	Metal Trace of Current Collection Grid on Solar Cell, in Cross-Section, 500 X (in Non-Spalling Area)	3-25
3-17	Silicon Cell Curvature as a Function of Temperature - <u>Spraylon</u> Thickness Variable	3-45
3-18	Silicon Cell Curvature as a Function of Temperature - <u>Silicon</u> Thickness Variable	3-46
3-19	Silicon Cell Curvature as a Function of Temperature - <u>Silver</u> Thickness Variable	3-47
3-20	Silicon Cell Curvature as a Function of Temperature - <u>FEP Teflon</u> Thickness Variable	3-47

Figure		Page
3-21	Silicon Cell Curvature as a Function of Temperature – <u>Kapton</u> Thickness Variable	3-48
3-22	Curvature of Silicon Cell as a Function of Temperature – <u>Cover Material</u> as a Variable	3-49
3-23	Thermal Expansion Properties of Solar Cell Cover Materials	3-51
3-24	Stress Profile in <u>Cover</u> Layer of Silicon Cell	3-53
3-25	Stress Profile in <u>Silicon Cell</u> Layer	3-54
3-26	Stress Profile in <u>Silver Electrode</u> Layer	3-55
3-27	Stress Profile in <u>Adhesive</u> Layer	3-56
3-28	Stress Profile in <u>Kapton</u> Layer	3-57
3-29	Finite Element Structural Model of an Interconnect Area	3-60
3-30	Finite Element Structural Model of an Interconnect Area With Invar Connection	3-61
3-31	Cross Section of a Cell Structure at Interconnected Area	3-62
3-32	Shear Stresses of the Silicon Cell in the Edge Area at 320°F for Different Cover Materials	3-63
3-33	Shear Stresses Between Invar and Silicon Cell at the Inter- connected Area for Different Cover Materials at -320°F	3-65
4-1	UV Degradation of Silicon Cell Maximum Power as a Function of <u>Equivalent Sun Hours</u> (ESH) at 120°C for Spraylon Cover	4-3
4-2	UV Degradation of Silicon Cell Maximum Power as a Function of <u>Hours of Exposure</u> at 120°C for Spraylon Cover	4-4
4-3	UV Degradation of Silicon Cell Maximum Power as a Function of <u>Equivalent Sun Hours</u> (ESH) at 120°C for Silicone Cover	4-6
4-4	UV Degradation of Silicon Cell Maximum Power as a Function of <u>Hours of Exposure</u> at 120°C for Silicone Cover 1 to 10 Suns Intensity	4-7
B-1	Top View of Vacuum Test Chamber	B-2
B-2	Side View of Vacuum Test Chamber	B-3
B-3	Electron Beam Profile Map	B-5
B-4	Relative Fluence Plot and Specimen Map for Electron Irradiation	B-6
B-5	Sample History – Electron and UV Test	B-8
B-6	Proton Beam Profile Map	B-9

Figure		Page
B-7	Relative Fluence Plot and Specimen Map for Proton Irradiations	B-10
B-8	Sample History - Proton and UV Test	B-12
C-1	Spectral Reflectance and Transmittance Data for 1-, 5-, and 10-mil Thicknesses of Teflon Films in the Solar Region	C-2
C-2	Spectral Normal Transmittance Data for 1-, 5-, and 10-mil-Thick Teflon Films	C-3

## TABLES

Table		Page
3-1	Thermal Stability of Concentrated Primers at 140°C	3-2
3-2	Results of Exposure on Spraylon-Coated Solar Cells (Exposure: 10 Suns Intensity at 120°C)	3-16
3-3	Results of Low-Intensity UV Irradiation at 120°C, Candidate Silicon Solar Cell Covers	3-29
3-4	Summary of Results of Low-Intensity UV Irradiation, Candidate Silicon Solar Cell Covers at 120°C	3-30
3-5	UV Test Cells Identification	3-32
3-6	NASA-LeRC Glass Resin Cells Test Allocation	3-33
3-7	UV Exposure Test Data - 1st Exposure Increment (285 Hr) - Solar Cells at 120°C	3-34
3-8	Cell Operating Temperatures for Nominal 120°C UV Test	3-35
3-9	UV Exposure Test Data (450 Hr Total) - 1st Exposure Increment (285 Hr); 2nd Exposure Increment (165 Hr) - Solar Cells at 120°C	3-36
3-10	Results of High-Energy Electrons Plus UV Irradiation - Candidate Silicon Solar Cell Covers at 120°C	3-39
3-11	Summary of Results of High-Energy Electrons Plus UV Irradiations - Candidate Silicon Solar Cell Covers at 120°C	3-40
3-12	Results of Low-Energy Protons Plus UV Irradiation - Candidate Silicon Solar Cell Covers at 120°C	3-41
3-13	Summary of Results of Low-Energy Protons Plus UV Irradiation - Candidate Silicon Solar Cell Covers at 120°C	3-42
3-14	Stresses in the Cell Cover With and Without Invar Substrate	3-59
4-1	Summary of Results of UV Irradiation - FEP Teflon at 120°C	4-9
4-2	Summary of Radiation Effects on Candidate Materials	4-11
A-1	Thermal - UV Stability, Silane Primer/Spaylon - Alclad 6061 Substrates	A-2

## Section 1

### INTRODUCTION

This report describes the follow-on work, Phase II, to the development program for the optimization of the Lockheed-formulated liquid transparent film-forming fluorocarbon (Spraylon) to be used as a cover for silicon solar cells. The previous work, Phase I, has been documented in the final report, Spraylon Fluorocarbon Encapsulation for Silicon Solar Cell Arrays, LMSC-D558143, June 1977.

The total contracted effort was directed to Spraylon, a low-cost, lightweight, and high solar-transmittance replacement for fused silica cover glass. The primary function of the solar cell cover is to provide protection from penetrating space radiation as well as to increase infrared emittance, thereby lowering the cell operating temperature so that the solar cell will operate at higher efficiency. The fundamental requirement of a high solar-transmittance cover material is that its resistance to optical, mechanical, and photochemical degradation allows it to function within acceptable limits.

The Phase II effort was specifically directed to the applications of Spraylon to silicon cells and modules utilizing advanced state-of-the-art thin (2 mils) solar cells at operational temperatures to 120°C and to examine the qualification potential of the system for a space environment of UV exposure up to 10 suns intensity.

It became evident early in the Phase II program that the thermal-ultraviolet (UV) stability of the Spraylon/primer system was a major problem. The results of thermal-UV accelerated testing of Spraylon-coated solar cells at NASA-Lewis Research Center (NASA-LeRC) and at Lockheed showed that the Spraylon degraded to unacceptable levels when exposed to 10 suns intensity of UV and 120°C operating temperature.

As a consequence of these test results, an evaluation and assessment of candidate encapsulants being developed and qualified for JPL by General Electric and NASA-LeRC was undertaken.

The General Electric candidate was a G. E. RTV 655 silicone and the NASA-LeRC candidate was an Owens-Illinois glass resin system.

Another system considered was FEP Teflon\* which was either thermally or adhesively bonded to the silicon cell.

The selection of a particular encapsulant material and process system for solar cell covers would have to be made on the basis of a specific mission requirement. The selection should be based on an allowable level of degradation in optical and mechanical characteristics consistent with the goals of weight savings, material and application costs, and acceptable reliability.

---

\*Teflon is a registered trademark of E. I. du Pont de Nemours & Co. (Inc).  
FEP is a copolymer fluorinated polyethylene propylene.

## Section 2

### PROGRAM OBJECTIVE

The program objective was to continue the development and qualification of the Lockheed "Spraylon" system solar cell encapsulant for a more rigorous environment of 120°C at an irradiance of 10 suns intensity with the use of advanced state-of-the-art thin solar cells.

The performance was in accordance with the following tasks.

#### Task 1: "Spraylon" Evaluation – Standard Cell at 120°C

- Environmental Test
  - Long-term ultraviolet
  - Thermal cycling
  - Ultraviolet, protons, and electrons
- Environmental Test
  - NASA-LeRC ultraviolet test
- Computer Modeling Program

#### Task 2: "Spraylon" Evaluation – Thin Solar Cell at 120°C

- Environmental Test
  - Long-term ultraviolet
  - Thermal cycling
  - Ultraviolet, protons, and electrons

**Task 3: "Spraylon" Evaluation – Thin Solar Cell Modules at 120°C**

- Environmental Test
  - Long-term ultraviolet
  - Thermal cycling
  - Ultraviolet, protons and electrons

**Task 4: Assessment Report and User Kit**

The Program was redirected after Tasks 1 and 2 were in progress.

The objective of the redirected program was:

**Task A: Conduct Evaluation and Assessment of Candidate Encapsulants**

- Environmental Tests
  - Ultraviolet exposure
  - Thermal cycling
  - Ultraviolet, protons, and electrons
- Computer Program Encapsulant and Module Design Compatibility

**Task B: Conduct Evaluation and Assessment of Alternate Encapsulant Materials**

**Task C: Provide Test and Evaluation Laboratory Support to JPL.**



### Section 3

## TECHNICAL DISCUSSION

The results of Phase I Environmental Testing showed an exponential increase in optical degradation when Spraylon-coated specimens were irradiated at higher temperatures. Phase II of this program had specific requirements for more rigorous environmental testing. The initial test results of ultraviolet (UV) exposure at 120°C quickly identified thermal-UV stability as a primary problem area. This problem had to be resolved for the Task 1 objective; otherwise, succeeding task objectives could not be met.

Optical degradation of the UV-exposed Spraylon at elevated temperatures can be ascribed to a number of causes such as raw material impurity, thermal and UV primer degradation, or the intrinsic instability of the Spraylon fluorocarbon under the test conditions.

The technical program was directed to solving the thermal-UV stability of Spraylon under the original task plans. It was only after verifying the instability of Spraylon at elevated temperature that the program was redirected to testing and evaluation of other encapsulant systems. The technical work progression followed these major tasks:

- Spraylon system component evaluation for conventional solar cells
- Spraylon systems evaluation for thin solar cells
- Evaluation and assessment of candidate encapsulants

### 3.1 SPRAYLON SYSTEM COMPONENT EVALUATION FOR CONVENTIONAL SOLAR CELLS

As a result of the work performed in Phase I, in which solar cells were tested at higher temperatures (>75°C) during UV exposure, it was evident that the major problem area was thermal-UV stability of the Spraylon-primer system. It appeared, originally, that the primer was a major contributor to the discoloration of the Spraylon (and, hence, reduced light transmission) at higher temperatures.

### 3.1.1 Spraylon - Primer Evaluation

The thermal stability of the primary candidates as adhesion promoters was verified by exposing thick concentrated primer films to the Spraylon processing temperature 140°C (350°F) and observing the color change. Those primers investigated and their observed color change are shown in Table 3-1.

Table 3-1  
THERMAL STABILITY OF CONCENTRATED PRIMERS AT 140°C

Primer	Color Change
Dow Corning Q16082	None
General Electric SS4120	None
Dow Corning Z6032	Deep yellow
Dow Corning Z6020	Light yellow
Union Carbide A1100	None
Dow Corning Q16011	None

The combined effect of UV and temperature in the degradation of these primers was investigated by coating alclad aluminum alloy substrates with dilute primer at various concentrations and exposing the samples to various UV intensities, temperatures, and exposure times.

The summary of test results in Table A-1, Appendix A, are highly subjective and require interpretation. The objective was to perform short-term accelerated tests to quickly eliminate from consideration those Spraylon/primer systems which exhibited marked degradation and thereby investigate in more detail those systems which showed promise of being thermally stable.

To interpret the results from Table A-1 and to understand the significance of the comments, it is necessary to consider these points:

- Evaluation of the thermal/UV stability of primers solely in vacuum at high temperatures is misleading since the primer volatilizes and leaves a bare aluminum substrate surface which shows little change in optical characteristics from the original surface. At lower temperatures (20°C), where the evaporation rate of the primer allows UV polymerization to take place, a definite change in substrate optical properties is observed because of primer color change.
- Comparison of thermal/UV stability between primed and unprimed Spraylon-coated aluminum substrates is also misleading. The unprimed Spraylon-coated aluminum has very poor adhesion which results in lifting of the Spraylon from the aluminum surface. There is poor thermal conduction from the heated Spraylon to the aluminum substrate, and hence, to the temperature-controlled substrate holder with the result that a substrate can show a temperature of the order of 100°C while the separated Spraylon coating may be at temperatures as high as 200°C, in which case the Spraylon degrades excessively.

The only pertinent results, therefore, are for those samples which exhibited good adhesion with primed substrates.

- In interpreting the result of the short-term accelerated tests, it is important to realize that time, temperature, UV intensity, and reciprocity have not been established. Using aluminum in a reflective mode is different from that of the silicon solar cell in the absorptive mode. Using the aluminum substrate is a much more severe test of the Spraylon coating inasmuch as the incident UV has almost double the effect on the Spraylon coating because much of the transmitted UV through the Spraylon is reflected from the aluminum surface and retransmitted through the Spraylon. Similarly, when the change in reflectance of the Spraylon-coated aluminum is measured, two passes through the coating occur.

### 3.1.2 Primer Application Considerations

Experience with primers (or "adhesion promoters") has shown wide variations in the bond strengths of the primer/substrate interface. The Union Carbide, A1100 (or

Dow Corning equivalent), while very good in terms of thermal or UV stability, was relatively poor in terms of bond strength. In contrast, the Dow Corning Z6020 gave excellent bond strengths though it was not as stable in respect to color formation. Inasmuch as such a low concentration (0.1%) is used, the contribution to decreased transmission in the UV and of the solar spectrum has a minimal effect on power output as does the cell response characteristics for wavelengths below 0.4  $\mu\text{m}$ .

Another critical problem is the uniform application of the primer to the cell surface. This is particularly difficult with the A1100 because of the mode of application which is to wash the primer off the cell surface with clean alcohol. Consequently, there is considerable doubt as to the uniformity of primer over most of the cell area. The absence of primer will result in a nonuniform adhesion which then results in FEP cracking during thermal cycling. It was also found to be important to apply the cover within a half-hour of priming.

### 3.1.3 Primer Application

The selection of Dow Corning Z6020 was made for reasons discussed in the final report of Phase I of this contract, namely:

- Excellent adhesive properties between Spraylon and solar cell surfaces
- Good optical transparency
- Good UV and thermal stability

Dow Corning Z6020 used at 0.1% concentration (0.05% to 0.1% range acceptable) was applied by solution dip for 5 s followed by vertical draining for 30 s onto absorbent paper. The primed specimen was then dried for 1 min at 180°C and subsequently coated within 1/2 hr of priming. Prior to priming, the specimens (6061 Alclad aluminum alloy) were etched with commercial phosphoric-hydrofluoric acid brightener (Cee-Bee B-66, Cee Bee Chemical Co., Inc., Downey, California).

### 3.1.4 Spraylon Formulation Evaluation

For the case of Spraylon at 120°C exposed to UV, the contribution of the primer to reduced light transmittance through the Spraylon is minimal. At 20°C Spraylon usage and UV exposure, the contribution of the primer to reduced light transmittance is comparable to that of the Spraylon only. At the lower temperatures, this reduction in transmittance is minimal in the spectral region of solar cell response.

Initially, it was believed that impurities in the Spraylon component materials might be a significant cause of the increasing rate of optical degradation of the Spraylon at increasing test temperatures. Possible impurities could be process waxes, contamination (ferrous) from process equipment or material process variables. A number of processing procedures, intended to purify, convert, or extract the suspect impurities in the starting raw materials, were done on a number of different lots of raw material. These variations in raw material were molecular weight, particle size, and process variations. UV absorbers were also evaluated.

The purification processes were:

- De-ionized water rinse and filtration followed by vacuum oven drying at various temperatures using a liquid-nitrogen trapped vacuum pump
- Intermediate washings with freon, benzene, hydrochloric acid, acetic acid, methyl alcohol, and oxalic acid
- Nitric acid and sodium fluoride additions

As a result of the extensive screening analysis which was performed on the candidate primers and Spraylon constituent materials, the following Spraylon formulations were selected for more comprehensive and quantitative investigation:

#### Lot Identification/Description

D	Phase I baseline material -- Primary Control
U	Similar to Lot D with improved molecular weight distribution
V	Variation in particle size of Lot U

### Lot Identification/Description (Cont.)

W	Same as D but of more recent manufacture
Y	Lot U treated with 3% nitric acid
X	Lot V treated with 1% sodium fluoride

#### 3.1.5 Spraylon Composition Evaluation of Various Temperatures

Thermal/UV screening tests were performed on the six selected Spraylon systems which appeared to have either the most promise of initial and continuing stability or stability enhancement during UV exposure.

Five thermal/UV test exposures were made at 10 and 20 suns intensity for 910 ESH (equivalent sun hours) and 1820 ESH, respectively. The tests were performed at 20°C, 50°C, 80°C, 100°C, and 120°C. Spectral reflectances of the coated aluminum substrates were measured (using a Cary Spectrophotometer) at 0.3-, 0.36-, 0.4-, 0.8-, and 1.0- $\mu$ m wavelengths.

Initial data evaluation was based on measured changes in the spectral reflectance. This is a very sensitive diagnostic technique because changes in Spraylon film transmittance are amplified when the light makes two passes through the material.

Since spectral transmittance is considered to be the determining factor in solar cell cover performance, the exposed films were stripped from the aluminum substrates. Transmittance properties of the stripped films (with primer) were measured over the range 0.3 to 1.1  $\mu$ m. Figure 3-1 shows the spectral transmittance of several of these stripped film specimens after UV exposure of 910 ESH (10 equivalent suns intensity) at 120°C.

The transmittance measurements of the stripped films confirmed the reflectance mode data. In all respects, Lot U demonstrated the best retention of transmittance properties over the entire spectral region of significance to solar cell response.

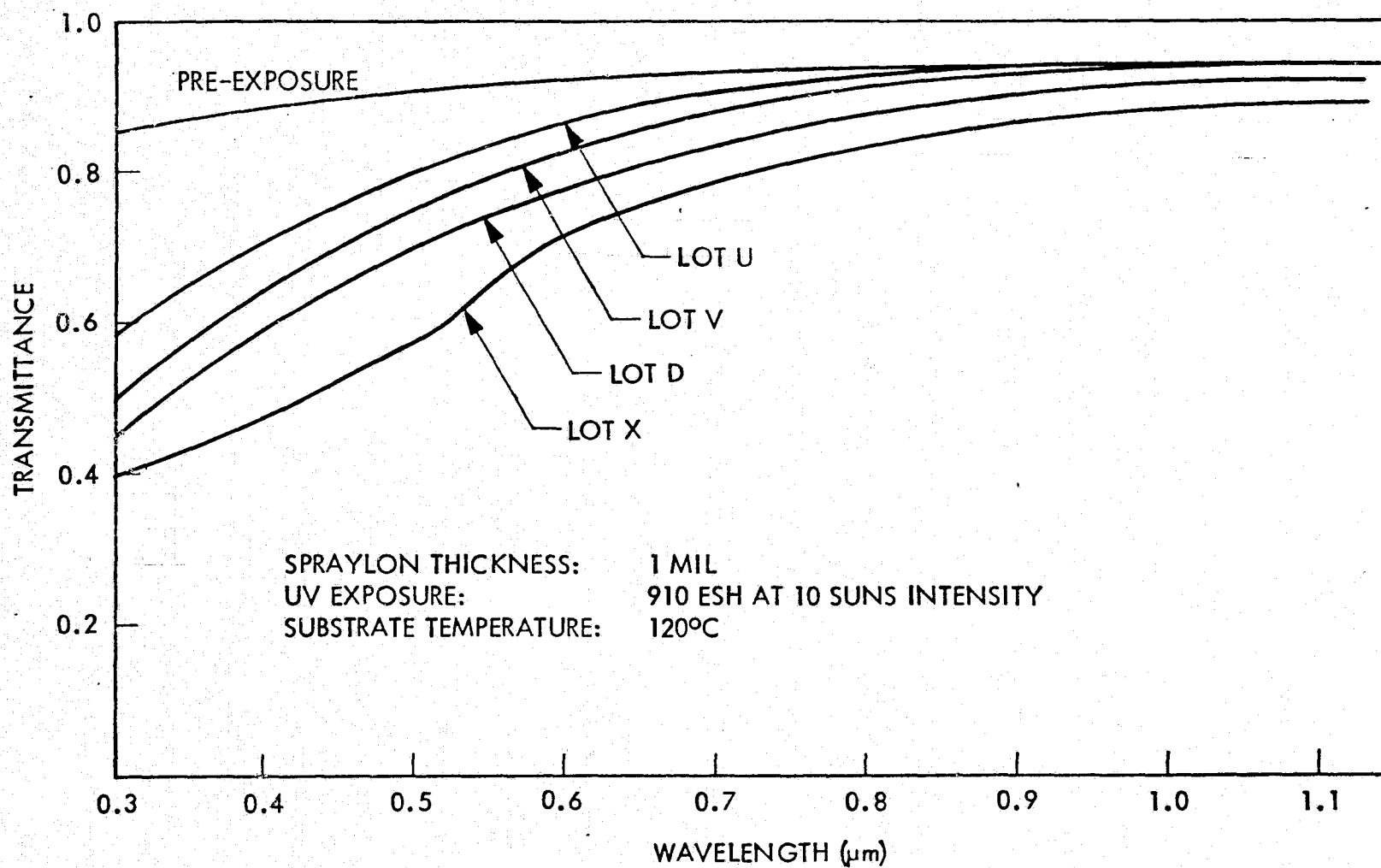


Fig. 3-1 Effect of Spraylon Formulation on Transmittance

The improvement of Lot U compared to the baseline Phase I material (Lot D) can also be seen from Fig. 3-1. On the basis of these extensive tests, the Lot U formulation was considered to offer the most stable Spraylon system at all temperatures up to 120°C.

Figure 3-2 shows the effect of temperature on the UV degradation of 1-mil primed films of Lot U Spraylon. With increasing temperature, the transmittance decreases regularly for equal UV exposures. Between 100°C and 120°C, however, there appears to be a greater effect than that observed for lower-temperature increments. Figure 3-3 shows the same presentations for 2-mil-thick films. Here again the trends are similar with increase in degradation due to increased film thickness.

To assess the potential impact of the UV degradation of the 1-mil Lot U Spraylon films on solar cell performance, cell response calculations were performed. Figure 3-4 shows typical solar cell response curves, normalized to the AMO (air mass zero) solar spectrum for unexposed and UV-exposed Spraylon coatings computed from measured values of spectral transmittance.

The effect of UV exposure on the primer spectral transmittance can be determined directly from the Spraylon data. At any given wavelength,  $\lambda$ , the transmittance of the Spraylon/primer composite system can be represented as

$$T_{\lambda} = (1 - R_{\lambda}) e^{-k_1 d_1} e^{-k_2 d_2}$$

where

- $T_{\lambda}$  = measured transmittance
- $k_1$  = Spraylon absorption coefficient
- $d_1$  = Spraylon thickness
- $k_2$  = primer absorption coefficient
- $d_2$  = primer thickness
- $R_{\lambda}$  = total interfacial reflections



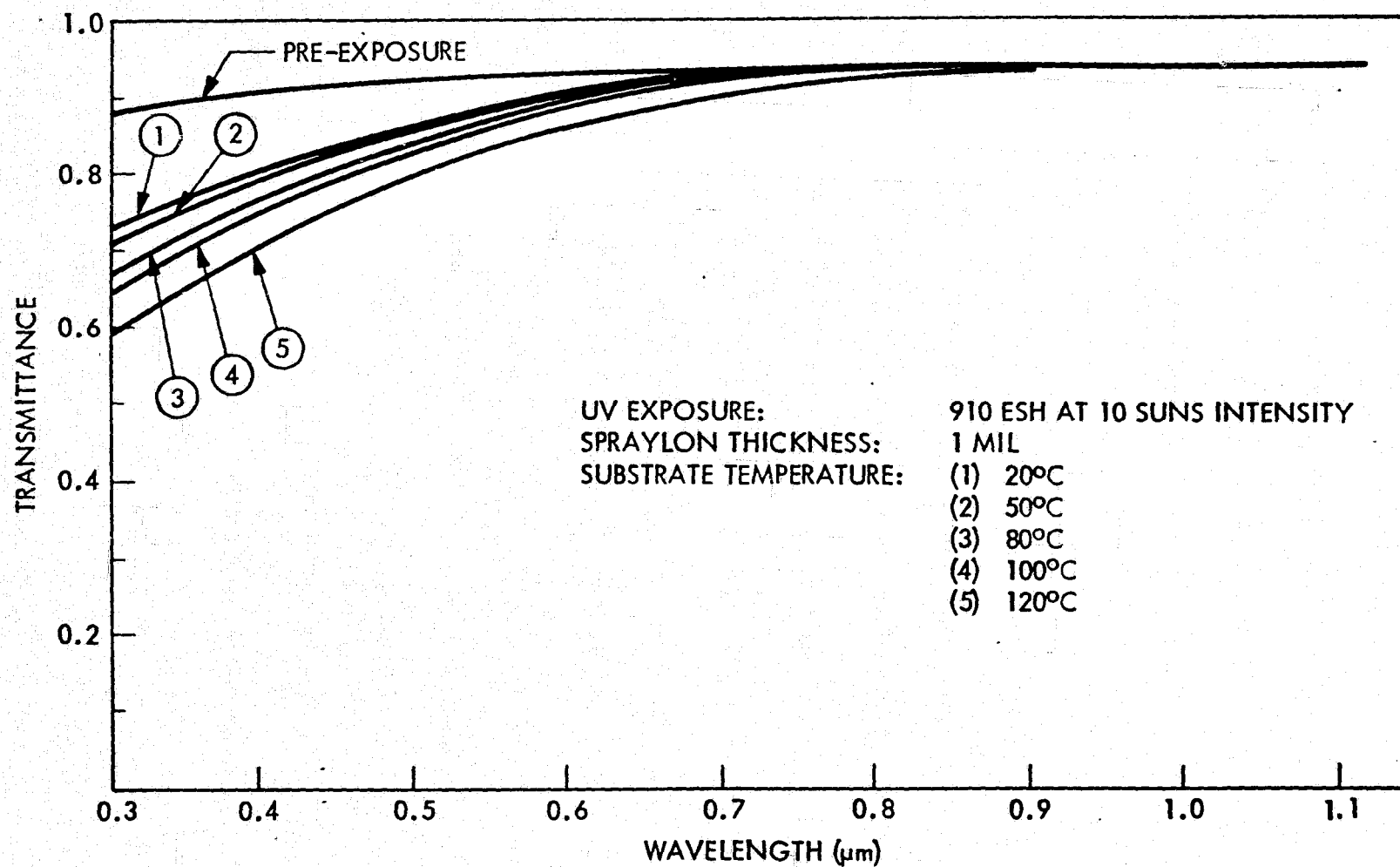


Fig. 3-2 Effect of Temperature on UV Degradation of 1-mil Spraylon

3-10

ORIGINAL PAGE IS  
OF POOR QUALITY

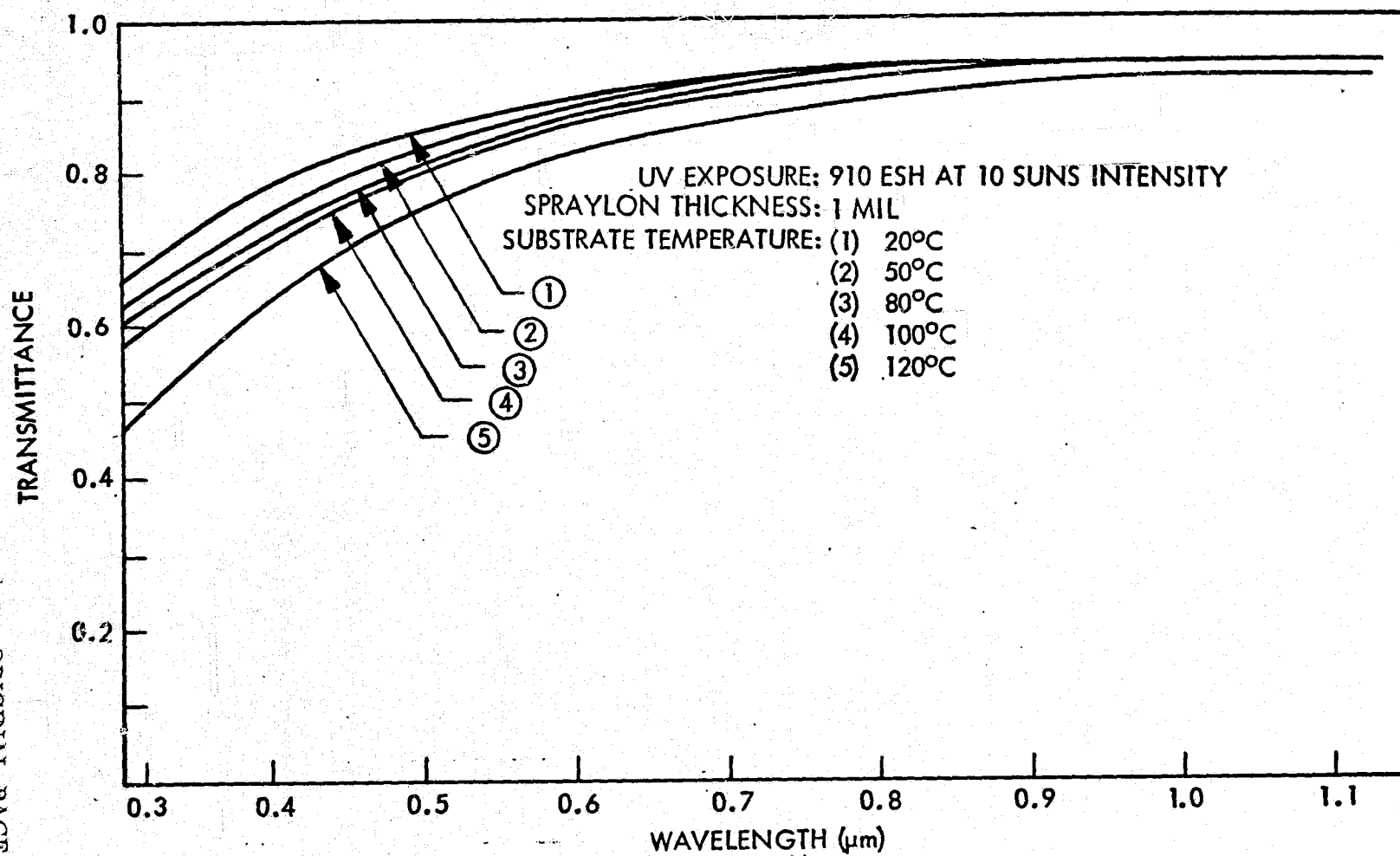


Fig. 3-3 Effect of Temperature on UV Degradation of 2-mil Spraylon

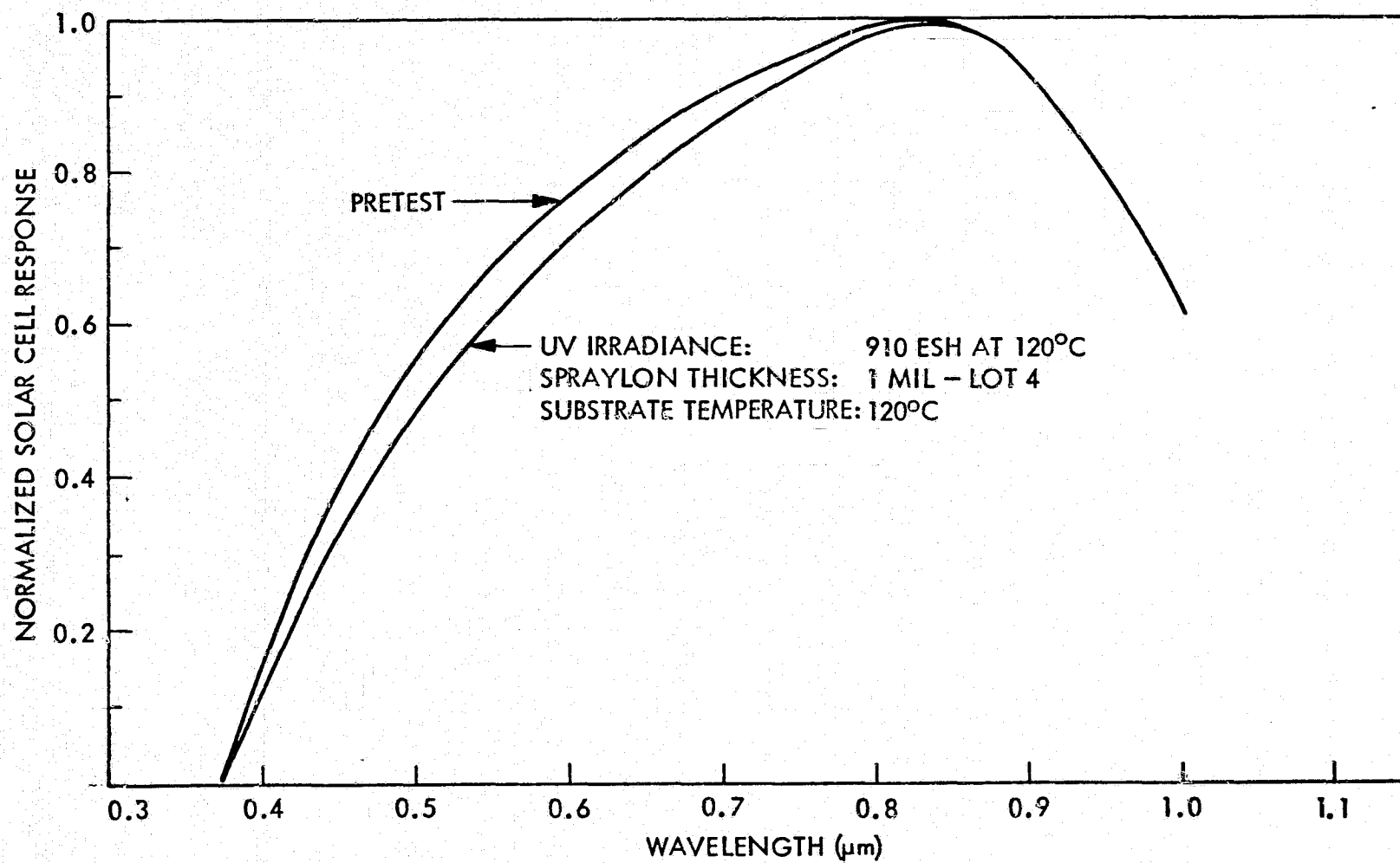


Fig. 3-4 Calculated Solar Cell Response Curves

For a specific UV exposure (910 ESH at 10 suns), it is assumed that the primer degradation is independent of the Spraylon thickness. For constant primer thickness as used in these tests, the quantity  $k_2 d_2$  is then constant

$$(k_2 d_2) = C$$

The transmittance is therefore given by

$$T_\lambda = C(1 - R_\lambda) e^{-k_1 d_1}$$

In this format, it can be seen that the logarithm of the measured transmittance should be a linear function of the Spraylon thickness. Figures 3-5 and 3-6 show the change in transmittance as a function of film thickness for 20°C and 120°C UV exposures (910 ESH at 10 suns) for several wavelengths.

From the intercepts of Figs. 3-5 and 3-6 (extrapolation to  $d_1 = 0$ ), spectral transmittance values of the degraded primer can be calculated, the quantity  $(1 - R_\lambda)$  being determined from pre-exposure measurements. Figure 3-7 shows the results of these computations presented as spectral transmittance loss due to primer degradation, while at 120°C the primer absorption may account for a significant fraction of the system transmittance reduction (compare Figs. 3-2 and 3-3).

#### 3.1.6 Test Results of Thermal/UV Exposure at 10 Suns Intensity

The UV stability of Spraylon-coated 12-mil solar cells, at 10 suns intensity, was determined by exposing three groups of cells at 120°C for nominal 1000, 2000, and 3000 ESH. The results are shown in Table 3-2.

The conclusions obtained from the data can be summarized as follows:

After UV exposure at 120°C, the average reduction in maximum power for 800 ESH at 10 suns intensity is 10%; for 1870 ESH at 10 suns, 15%; and for 3000 ESH at 10 suns, 26%.

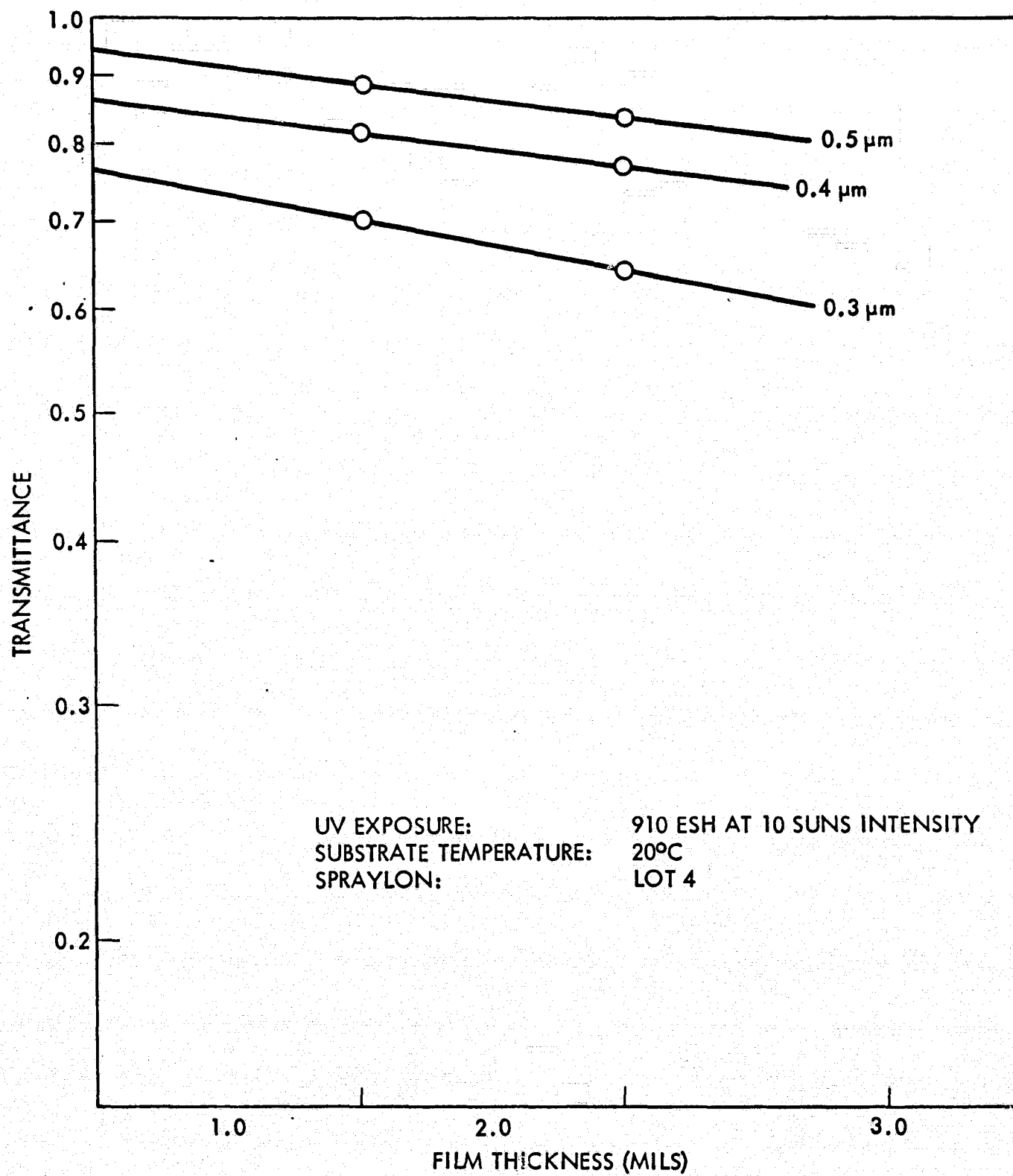


Fig. 3-5 20°C-Thermal - UV Exposed Spraylon Spectral Transmittance Dependence on Film Thickness

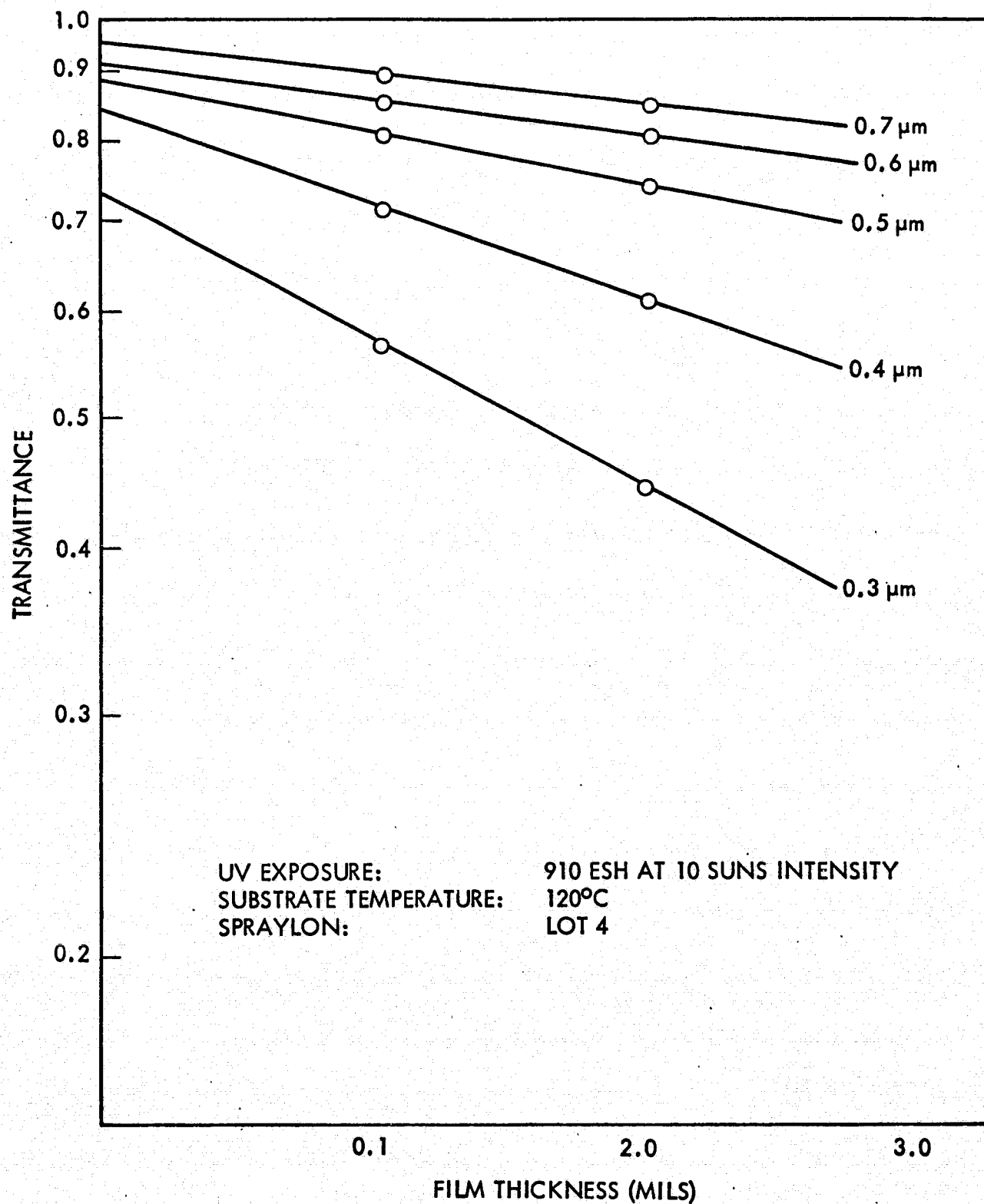


Fig. 3-6 120°C-Thermal - UV Exposed Spraylon Spectral Transmittance Dependence on Film Thickness

3-15

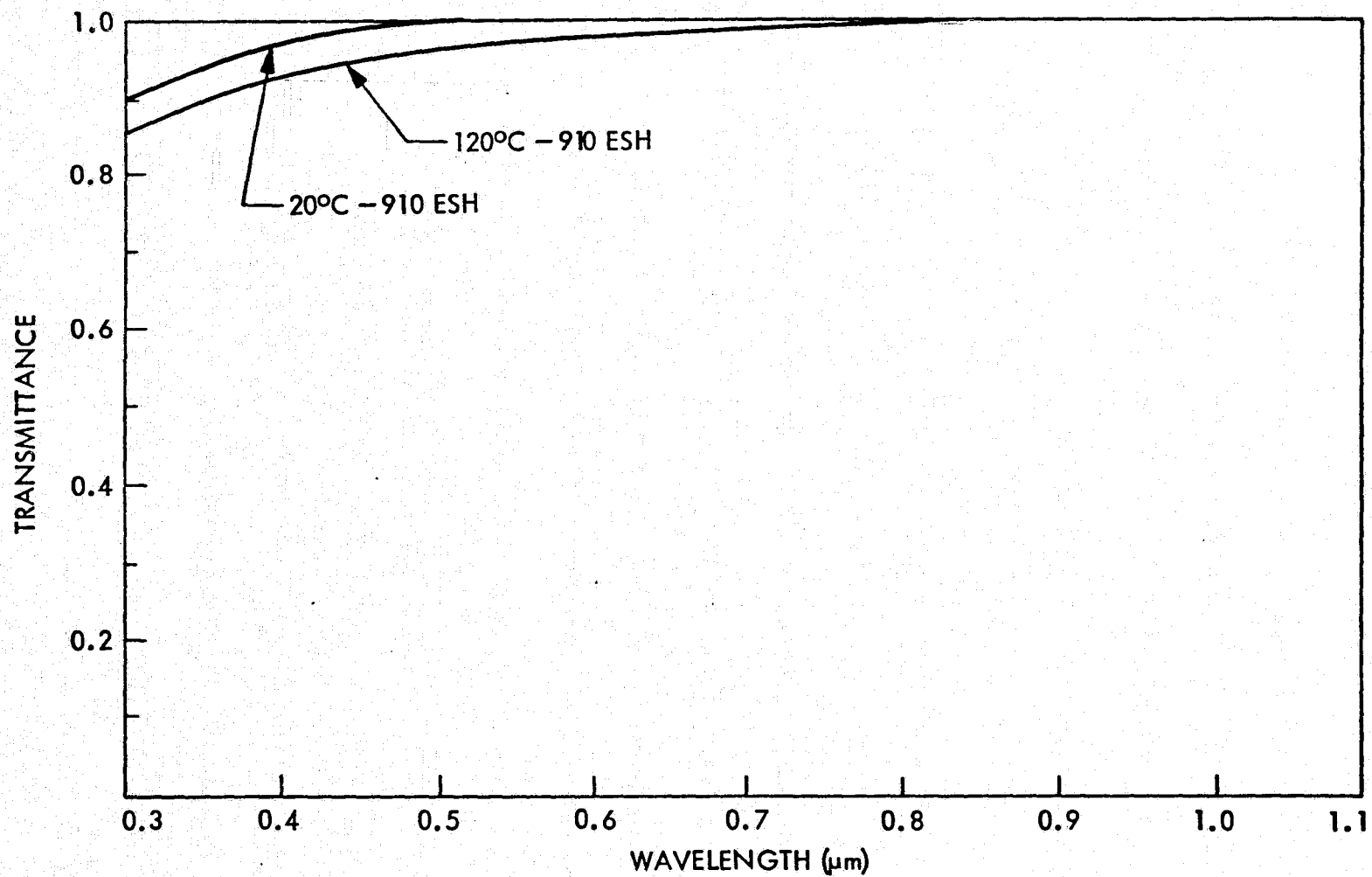


Fig. 3-7 Calculated Primer Degradation - 910 ESH UV Exposure

Table 3-2

**RESULTS OF UV EXPOSURE ON SPRAYLON-COATED SOLAR CELLS**  
 (Exposure: 10 Suns Intensity at 120°C)

Equivalent Sun Hrs	Cell No.	$I_{sc}$ (mA)		$V_{oc}$ (mV)		$I_{mp}$ (mA)		$V_{mp}$ (mV)		$P_{max}$ (mW)		$\frac{P_{max}}{P_{max}^0}$	Avg. Max Power Lost
		Post Test	Pre- Test	Post Test	Pre- Test	Post Test	Pre- Test	Post Test	Pre- Test	Post Test	Pre- Test		
800 ESH	X1	134.6	151.0	575.1	583.9	124.8	140.0	467.04	469.0	58.28	65.66	88.76	-10%
	X7	138.5	152.7	577.3	584.6	127.1	141.0	472.04	483.0	59.9	68.10	87.95	
	X8	138.2	153.1	577.6	589.4	124.7	139.0	449.04	461.0	55.99	64.08	87.37	
	X14	141.0	152.4	581.0	588.4	129.6	138.6	460.04	473.0	59.62	65.56	90.93	
	X13	137.6	150.1	575.1	583.0	128.0	139.5	457.04	469.0	58.50	65.43	89.40	
	X33	142.8	152.6	578.2	585.3	134.1	141.9	464.04	476.0	62.2	67.54	92.09	
	X34	142.2	153.2	575.8	583.8	132.3	141.5	469.04	479.0	62.05	67.78	91.54	
	X48	139.8	151.0	574.9	580.4	128.3	139.2	469.04	468.0	60.17	65.15	92.35	
1870 ESH	X15	131.5	150.8	579.0	589.2	121.3	139.9	478.04	475.0	57.98	66.45	87.25	-15%
	X24	132.4	151.7	574.0	582.1	124.3	140.3	470.04	473.0	58.42	66.36	88.03	
	X25	134.1	152.3	580.6	590.3	124.0	140.1	468.04	479.0	58.03	67.11	86.47	
	X29	133.7	152.4	578.9	587.2	125.5	140.1	468.04	481.0	58.27	67.39	86.47	
	X43	133.2	153.0	575.2	585.7	120.2	140.0	410.04	449.0	49.28	62.86	78.39	
	X46	131.0	151.8	571.5	581.9	120.9	140.1	463.04	470.0	55.98	65.85	85.01	
	X47	130.9	151.6	574.0	584.4	119.8	140.2	465.04	472.0	55.70	66.17	84.17	
3000 ESH	X2	109.9	151.2	569.7	583.6	102.0	139.8	474.04	476.0	48.35	66.54	72.66	-26%
	X3	102.9	151.2	566.7	581.5	95.5	141.6	469.04	470.0	44.79	66.55	67.30	
	X22	120.7	152.6	568.5	585.2	109.3	137.0	427.04	445.0	46.67	60.97	76.54	
	X26	118.0	150.7	568.4	580.6	111.5	140.1	453.04	471.0	50.51	65.99	76.54	
	X37	123.1	156.4	572.8	588.0	112.9	141.0	463.04	482.0	52.27	67.96	76.91	

(a) 12 mil Spectrolab Cells, 2-mil Spraylon coating

 $I_{sc}$  = Current, short circuit (mA) $V_{oc}$  = Voltage, open circuit (mV) $I_{mp}$  = Current at maximum power (mA) $V_{mp}$  = Voltage at maximum power (mV) $P_{max}$  = Power at maximum output (mW) $P_{max}^0$  = Initial pre-exposure power at maximum output (mW)



These results compare with the NASA-LeRC tests (Ref. 2) which showed 20% to 25% output drop for 1 week of UV exposure (1848 ESH) at 108°C and 11 suns intensity.

### 3.1.7 Thermal Cycling of Spraylon-Coated Thick Cells (12 mils)

One-mil Spraylon-coated cells were thermocycled from +100°C to -196°C (liquid nitrogen immersion) in a period of 4 min. Twenty-five cycles were performed. One-half of each group of cells - 800 ESH Group, 1870 ESH Group, and 3000 ESH Group (Table 3-2) - was thermocycled after UV exposure as well as 12 cells which had no UV exposure. The Spraylon coating exhibited no failure modes after the 25 cycles and in the case of the 12 cells with no UV, the 4 cells with 800 ESH, or the 3 cells with 1870 ESH. Of the 4 thermocycled cells with 3000 ESH, there were 2 cells that showed partial delamination starting at the soldered electrical test tabs. There was no change in power output as a result of thermocycling.

## 3.2 EVALUATION OF SPRAYLON SYSTEM ON THIN SOLAR CELLS

Although the optimum Spraylon composition was selected on the basis of the work done with the thick conventional cells, the results were directly applicable to the thin-cell system, the only exception being that the film thickness was limited to 1 to 2 mils in order that no excessive thermal stresses would be induced during thermal cycling.

The testing of the thin cells required simulation of the lightweight flexible array construction for reasons of thermal cycling similitude as well as for reason of practicality in handling fragile silicon cells. The preparation of test cells required thermal bonding of the back surface of the silicon cell to the 1/2-mil FEP Teflon/1-mil Kapton substrate. To make electrical measurements of cell output, conductive copper tabs (1-mil-thick  $\times$  1/16-in.-wide  $\times$  1-in.-long) were welded to the front and back electrodes. The thermal bonding temperature (290°C) caused excessive oxidation of the silver back electrode bonding surface, resulting in poor bond strength at the silver electrode-FEP Teflon interface. The silver was electroplated with a flash coating of nickel to 1- $\mu$ m thickness. The nickel-plated silver electrode-FEP Teflon interface bond

strength was excellent in that it exceeded the bond strength of the cell silver to silicon interface. After thermal bonding to the substrate, the cells were cleaned with anhydrous methyl alcohol and then primed with DC Z6020 (0.1% concentration) and covered with a 1-mil Spraylon coating.

To monitor solar cell surface temperature (as opposed to measuring back surface temperature which more realistically measures the substrate holder temperature), thermocouples (0.003-in. wire) were laser-welded to the front surface copper tab 1/8 in. away from cell edge. There was great variation in front and back silver electrode adhesion in the as-received thin solar cells. The cleaning of the front electrode collection grid frequently resulted in lifting of this grid from the cell surface.

Prior to mounting cells in the UV exposure apparatus, the thermally bonded cells were adhesively (silicon adhesive-Kapton tape) bonded to Invar substrates. This procedure enabled a good thermal conductance path to the temperature-controlled substrate holder. Previous experience showed large variations in cell temperature (as much as 50°C) when the cell was lightly clamped (to prevent fracture of the cell) to the substrate holder.

In the long-term UV test (6000 ESH), the exposure conditions were 10 suns intensity and 120°C cell temperature.

This test was terminated after 1440 ESH exposure as the results of the NASA-LeRC testing of Spraylon-coated conventional cells as well as LMSC's long-term testing showed that Spraylon degraded excessively under the test conditions of 120°C and 10 suns UV intensity accelerated testing.

### 3.2.1 Thermal Cycling of Spraylon-Coated Thin Cells (2 mils)

Six ("mechanical rejects") 2-mil silicon cells were coated with 1-mil Spraylon (these cells had broken corners).

Four good cells were thermally bonded to 3-cm x 3-cm substrates of 1/2-mil FEP Teflon-1-mil Kapton and coated with 1 mil of Spraylon.

Both groups of cells were thermal-cycled 25 times from  $+100^{\circ}\text{C}$  to  $-196^{\circ}\text{C}$  (liquid nitrogen immersion) in a period of 4 min. There were no failures even though there were large cell deflections. Subsequently, cells were heated to  $100^{\circ}\text{C}$  and immediately immersed in liquid nitrogen with no visual evidence of change. Because the testing of these cells was terminated, there are no results of additional thermocycling of UV-exposed cells. The encapsulated thin cells showed surprising ruggedness in handling and thermal cycling because of the lack of restraint to curvature from bending of thermal cycling.

### 3.3 CELL FRACTURE INVESTIGATION

Cracking of the highly stressed cell coating when undergoing the extremes of thermal cycling can be caused by either very good adhesion or very poor adhesion. If there is good adhesion except at cell edges, the cell can "explode" from strain-energy release. If there is spotty good adhesion, the silicon will divot and/or fracture; on the other hand, if there is poor adhesion, the cover stress is relatively low.

An investigation of silicon cell fracturing due to thermal cycling was made on a Spraylon-coated thick (12-mil) silicon cell. The cell spalled with the macroscopic fracture plane parallel to the surface of the cell at an average depth of 0.01 cm. Surprisingly, a visible pattern of lines was noted on the fracture surface directly below the location of the metal traces which had been vapor-deposited on the original solar cell surface. A macroscopic examination was made to determine the cause of these "ghost" trace lines on the fracture surface.

Figures 3-8, 3-9, 3-10, and 3-11 show scanning electron micrographs of the silicon fracture surface (parallel to the plane of the paper). The ghost trace is located vertically at the center of Fig. 3-8 (38x) and viewed at successively higher magnification (the particulate matter on the surface is dust and other artifacts). At higher magnification, the ghost traces are shown to be made up of finer steps in the macrofracture surface, all of which are oriented at approximately the same angle to the trace line. The similar orientation (Figs. 3-12 and 3-13) of other fine steps at some distance

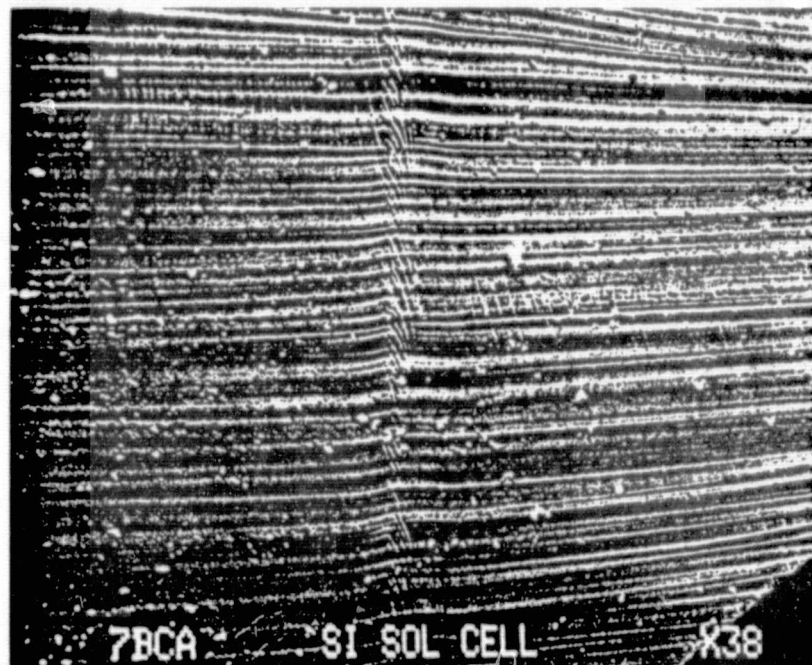


Fig. 3-8 Silicon Fracture Surface, 38 X, Below Metal Trace

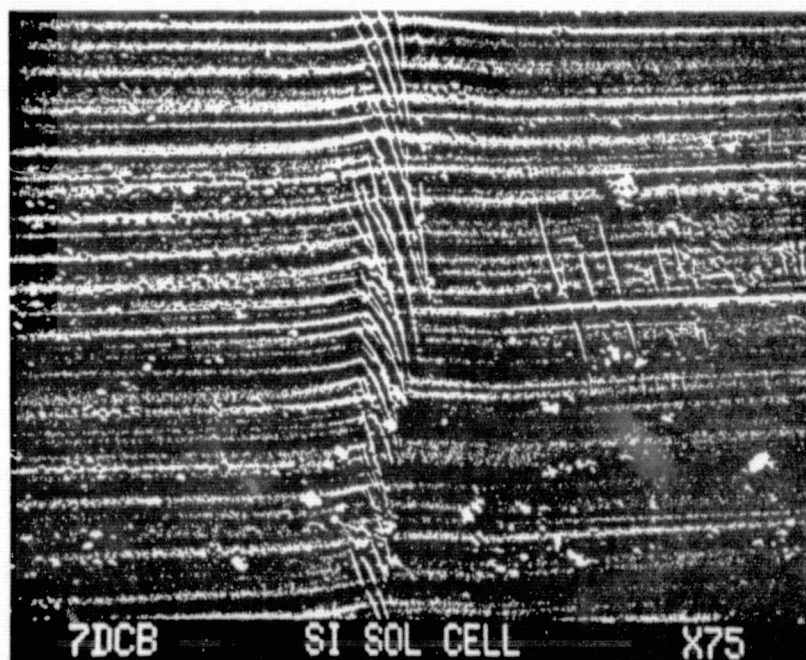


Fig. 3-9 Silicon Fracture Surface, 75 X, Below Metal Trace

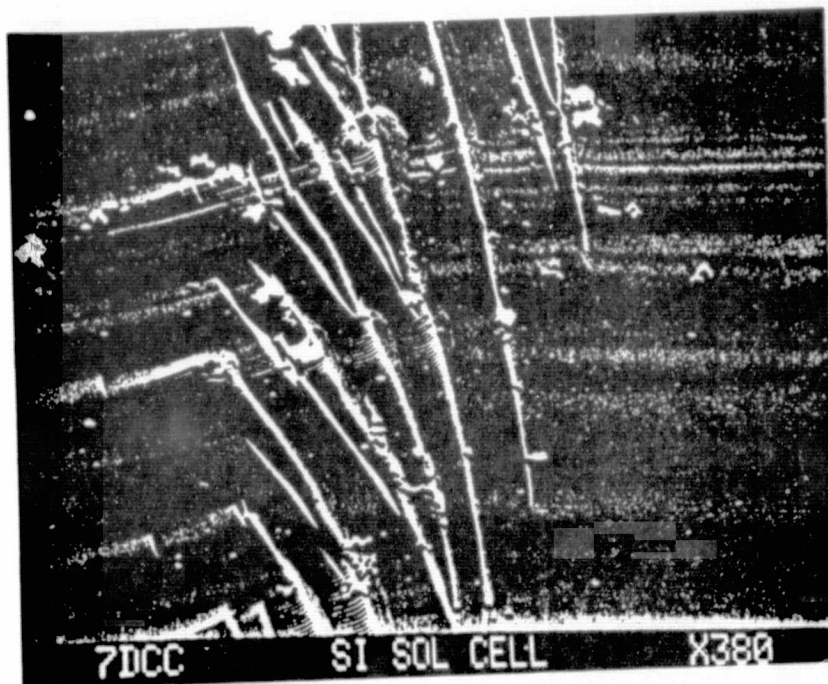


Fig. 3-10 Silicon Fracture Surface, 380 X, Below Metal Trace

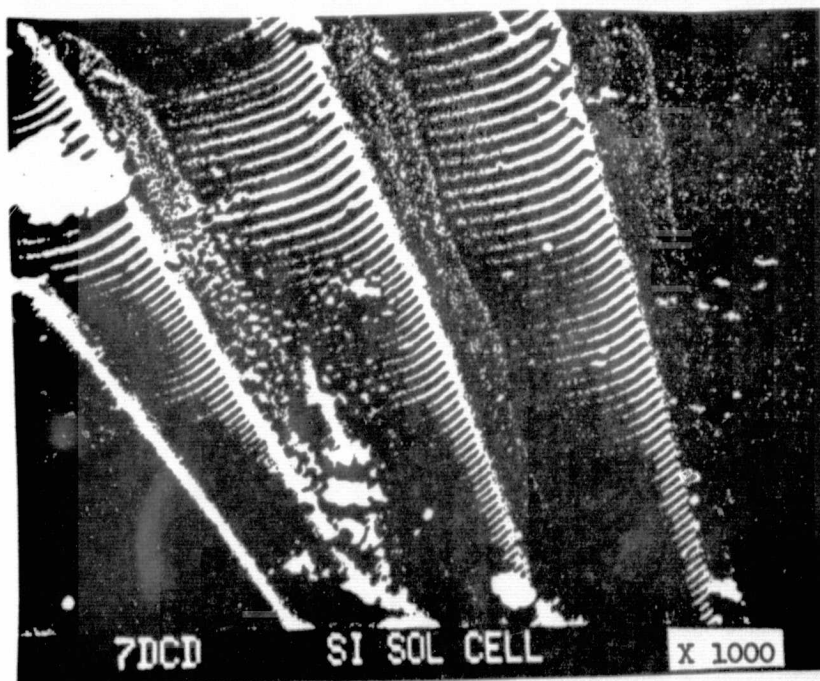


Fig. 3-11 Silicon Fracture Surface, 1000 X, Below Metal Trace



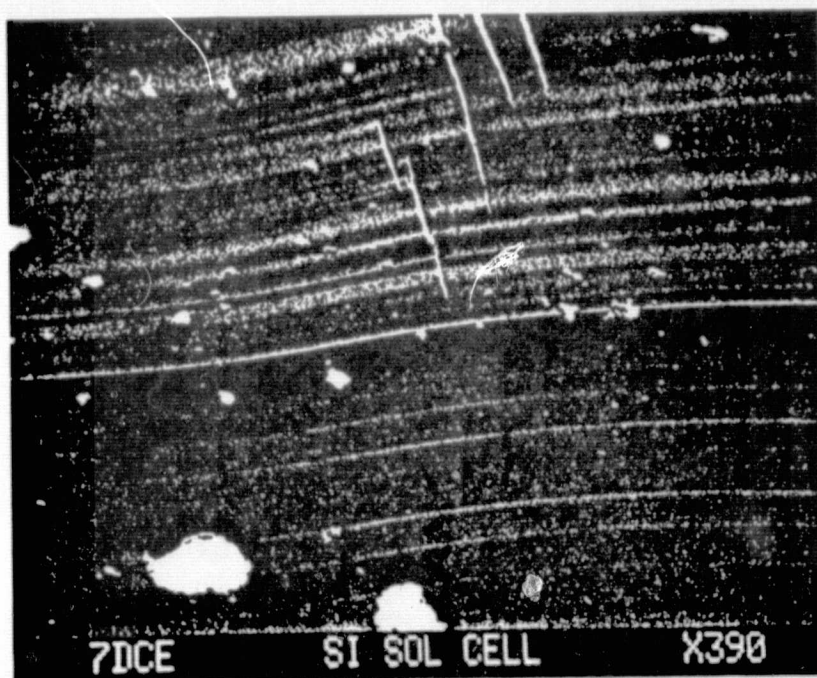


Fig. 3-12 Silicon Fracture Surface, 390 X, Away From Metal Trace

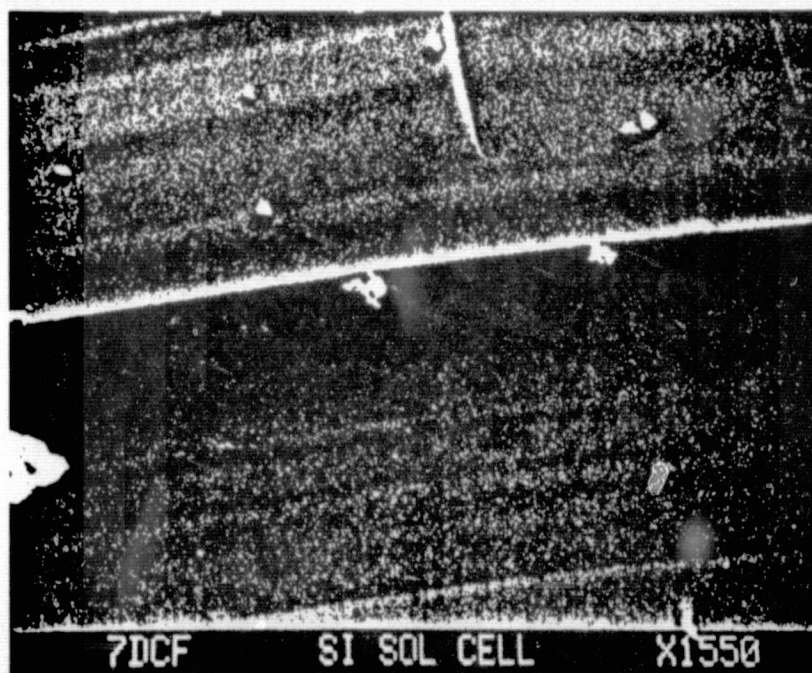


Fig. 3-13 Silicon Fracture Surface, 1000 X, Away From Metal Trace

from the trace line indicates that the step formation is probably closely related to a particular crystallographic plane in the silicon crystal. The pattern of fracture indicates a macrocrack which ran vertically upward during the spalling process. The separation distance of the lines running perpendicular to the crack front versus those in the finer trace cracks indicates a much faster propagation rate of the crack in the latter.

Figures 3-14 and 3-16 show a vapor-deposited metal trace cross section in an area which did not spall. Figure 3-15 shows a trace near a running spall. The inplane component of spall crack propagation is from left to right, while secondary cracks are found running perpendicularly toward the metal trace.

The following conclusions can be drawn:

- The cause of cell delamination is not associated with the metal traces.
- The existence of secondary cracks with closely spaced propagation lines below the traces and running toward the trace indicates that high local tensile stresses exist in the region below the trace which increase the propagation rate of the microcracks.
- It is likely that variation in temperature of the silicon during the vapor-deposition process introduces the local tensile stresses. These stresses are locked in because of the constraint of the cooling metal trace which is bonded to the silicon surface.

It is concluded that the "ghosts" are real but do not impact the thermal stability of solar cells.

### 3.4 REDIRECTION OF ENCAPSULANT MATERIAL EVALUATION PROGRAM

The program was redirected to an evaluation and assessment of candidate encapsulant materials which included G.E. RTV 655 silicone being developed and qualified by General Electric for JPL, glass resin systems being developed and qualified by Owens-Illinois, and other promising encapsulant materials including Spraylon.

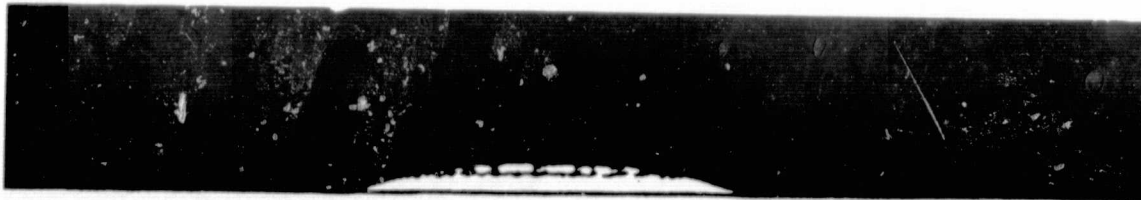


Fig. 3-14 Metal Trace of Current Collection Grid on Solar Cell, in Cross-Section,  
500 X (Non-Spalling Area)

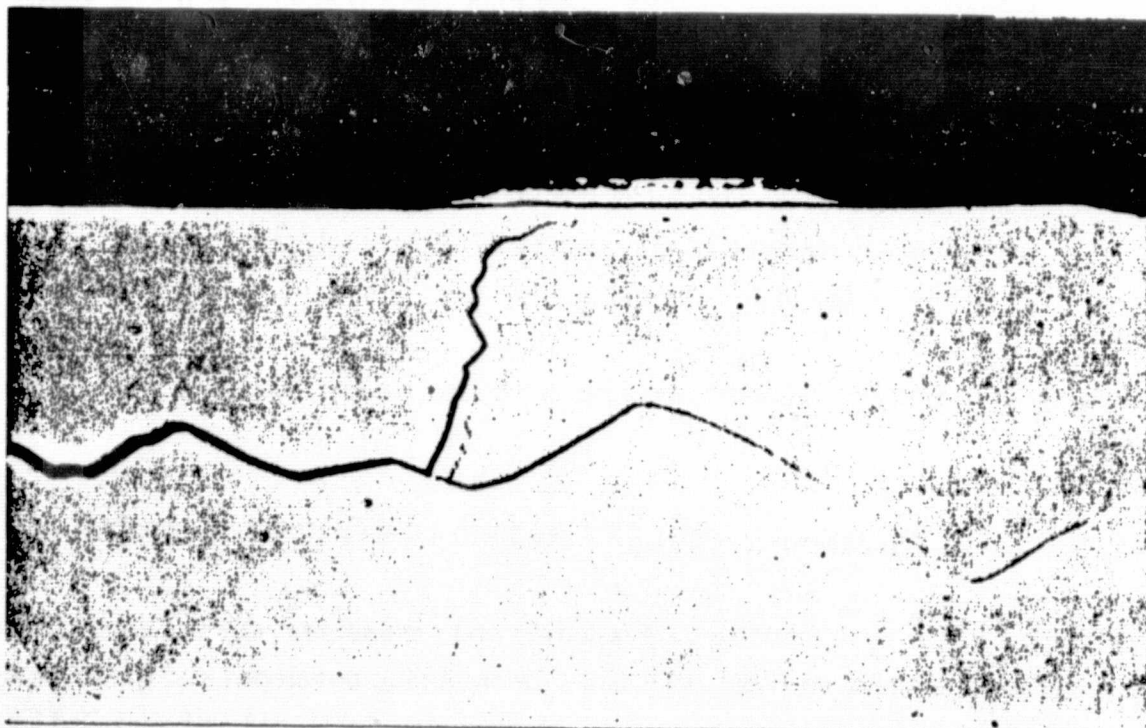


Fig. 3-15 Metal Trace of Current Collection Grid on Solar Cell, in Cross-Section,  
500 X (in Spalling Area)





Fig. 3-16 Metal Trace of Current Collection Grid on Solar Cell, in Cross-Section, 500 X (in Non-Spalling Area)

ORIGINAL PAGE IS  
OF POOR QUALITY

During the course of the extended program, many changes occurred in candidate materials considered, fabrication methods, and test requirements.

The assessment and evaluation program included the following:

- UV exposure at +120°C coordinated with ongoing tests at NASA-LeRC and at GE
- Thermal cycling tests at +120°C to -190°C (coordinated with ongoing tests at NASA-LeRC and GE)
- UV exposure combined with low-energy proton and electrons exposure. These tests were performed at the Boeing Company.
- Compatibility of the encapsulant with the module design using the computer-developed program

### 3.5 EVALUATION ASSESSMENT OF CANDIDATE ENCAPSULANTS

The proposed GE and NASA-LeRC and LPARL (Lockheed Palo Alto Research Laboratory) candidate materials to be used for solar cell covers and their laminar structures were:

- General Electric
  - 1-mil RTV 655 (cover)
  - 2-mil silicon cell
  - 6- $\mu$ m silver electrode
  - 1/2-mil RTV 655 adhesive
  - 1-mil Kapton (substrate)
- NASA-LeRC
  - 1-mil, glass resin (not specified)
  - 2-mil silicon cell
  - 1/2-mil GE RTV 655 adhesive
  - 1-mil Kapton (substrate)

- LPARL
  - 1-mil FEP-A Teflon (cover)
  - 2-mil silicon cell
  - 6- $\mu$ m silver electrode
  - 1/2-mil FEP-C Teflon substrate
  - 1-mil Kapton substrate

FEP Teflon was included as a candidate because it was one of the organic materials that could satisfy the requirements for a solar cell cover. It exhibited small changes in optical properties when subjected to high-intensity UV, short-term exposure to high-energy electrons, and low-energy protons at 120°C. Spectral reflectance and transmittance characteristics are shown in Appendix C. This material would probably satisfy all requirements except embrittlement from cross-linking due to high-energy electrons and/or UV (Refs. 3, 4, and 5). This effect is accelerated at higher temperatures.

This embrittlement is a serious problem. The approach taken is how to accommodate the solar cell cover to this difficulty. Observation of the TRW (Ref. 4) and NASA-LeRC (Ref. 5) test cells, which suffered large cracks and spallings of the FEP Teflon cell cover, showed a surprising similarity to the cracks and spallings of Spraylon after thermocycling when its thickness exceeded 3 mils on 8- or 12-mil silicon cells, when an inappropriate adhesion-promoter was used or an appropriate adhesion-promoter was not uniformly applied.

An approach to accommodate to the FEP Teflon embrittlement is to design the cell laminate structure in such a way as to lower the stress in the Teflon cover within the constraints of a functional design. The computer program for stress analysis of the individual laminum in the cell structure and, in particular, the interfacial silicon/FEP Teflon stress was used for the TRW design (Ref. 4) and for the LMSC proposed design. This analysis is shown in Section 3.8.

ORIGINAL PAGE IS  
OF POOR QUALITY

### 3.6 UV TEST RESULTS

To accumulate UV exposure data in a short time span, testing of materials was accelerated at 5 and 10 suns intensity. There was concern about the validity of accelerated testing in regard to degradation reciprocity of sun hours to intensity of exposure. Experience has shown, in general, that the order of 500 ESH at 10 suns intensity was adequate to show the relative degradation of most candidate materials. Exposures at 1 and 2 suns intensity were also included so as to determine reciprocity.

The following tests were performed in order to establish the qualification status and limitations of the candidate materials:

- Low-intensity UV, 1 and 2 suns
- High-intensity UV, 5 and 10 suns

#### 3.6.1 Low-Intensity UV Exposure Test Results of Candidate Encapsulants (1 and 2 Suns Intensity)

Tests were made on Spraylon-coated cells and G. E. RTV 655-coated cells at 120°C and at one and two suns intensity so as to verify degradation rate dependency as a function of UV intensity.

The test apparatus accommodates specimens placed in an arc on a temperature-controlled substrate holder. This fixed radius arc enables a 10 suns uniform exposure intensity of irradiance. To accommodate one- and two-sun exposure, a neutral density filter screen made by nickel-plating a fine-mesh stainless-steel screen was wrapped around the water-cooled fused silica UV lamp enclosure. This filter screen provided a one sun intensity to those specimens placed at the original fixed radial distance to the lamp. Copper block spacers were secured to the temperature-controlled substrate holder at a distance to provide a two sun intensity at the specimen position. Specimens were exposed for 808 hr (808 ESH at one sun intensity, and 1616 at two suns intensity).

The tests results are shown in Tables 3-3 and 3-4.

Table 3-3

**RESULTS OF LOW-INTENSITY UV IRRADIATION AT 120°C  
CANDIDATE SILICON SOLAR CELL COVERS**

Cell <sup>(a)</sup> No.	Cover Material Intensity (1 mil)	UV In- tensity	Current Short Circuit, $I_{sc}$ (mA)			Voltage, Open-Circuit, $V_{oc}$ (mV)			Current at $P_{max}$ , $I_{mp}$ <sup>(c)</sup> (mA)	Voltage at $P_{max}$ , $V_{mp}$ <sup>(c)</sup> (mV)	Power Maximum, $P_{max}$ (mW)		
			Pre-UV	Post-UV	Post- Thermal Cycles	Pre-UV	Post-UV	Post- Thermal Cycle	Pre-UV	Pre-UV	Pre-UV	Post-UV	Post- Thermal Cycle
X10	Spraylon <sup>(b)</sup>	1	152.0	140.3	139.9	586.6	580.0	578.7	139.8	473.0	66.13	60.0	60.5
X16	Spraylon	1	152.0	145.3	144.4	579.0	573.5	573.6	137.3	473.0	64.94	61.7	62.6
X20	Spraylon	1	152.7	137.0	138.0	591.6	583.5	583.9	140.4	490.0	68.80	59.7	59.5
X30	Spraylon	1	152.9	145.2	145.3	578.8	572.2	573.0	136.4	467.0	63.70	58.0	60.3
X40	Spraylon	1	151.7	137.5	138.1	587.2	578.7	578.9	140.8	480.0	67.58	60.0	61.0
X42	Spraylon	1	152.6	138.9	138.7	582.0	573.9	573.8	142.0	468.0	66.46	57.2	61.1
6-53-8	RTV 655 <sup>(b)</sup> Silicone	1	131.2	—	—	549.2	—	—	121.9	453.0	55.22	—	—
6-72-9	RTV 655 Silicone	1	133.8	94.2	95.8	543.7	534.0	531.9	120.2	441.0	53.00	36.1	36.2
X12	Spraylon	2	150.6	142.3	146.0	579.1	573.0	573.8	137.1	476.0	65.26	59.8	63.7
X17	Spraylon	2	150.8	142.0	141.0	591.4	582.6	581.9	137.0	479.0	65.62	62.0	62.8
X19	Spraylon	2	150.4	133.3	133.0	581.9	574.0	573.4	139.8	477.0	66.68	57.8	59.3
X21	Spraylon	2	151.9	142.1	143.0	581.7	573.0	573.0	138.2	469.0	64.82	53.7	61.8
X23	Spraylon	2	152.0	143.0	142.3	580.4	573.8	574.0	141.0	469.0	66.13	60.0	61.2
X44	Spraylon	2	152.0	139.9	144.2	585.7	577.5	578.2	140.0	470.0	65.80	60.9	62.9
6-61-8	RTV 655 Silicone	2	131.6	85.7	88.6	550.7	531.6	534.8	124.0	443.0	54.93	34.5	36.2
6-171-7	RTV 655	2	135.2	90.5	92.7	551.0	536.2	537.6	123.0	450.0	55.35	36.1	37.1

(a) Solar Cell: X10-X44 12-mil Spectrolab  
6-53-8 to 171-7 2-mil Solarex

(b) Spraylon coatings applied by LPARL  
G.E. RTV 655 coatings applied by  
General Electric

(c)  $I_{mp}$  at  $P_{max}$  and  $V_{mp}$  at  $P_{max}$ , Post UV  
and Post Thermal Cycle not available

Test Conditions: 808 hr UV exposure of 1 and 2 suns intensity  
(808 ESH and 1616 ESH)  
Cells at nominal 120°C

Cell Measurement  
Conditions: Irradiation Intensity - 140 mW/cm<sup>2</sup>  
Average Cell Temperature 28°C

Cell I/V Measurements made by NASA-JPL

Table 3-4

**SUMMARY OF RESULTS OF LOW-INTENSITY UV IRRADIATION  
CANDIDATE SILICON SOLAR CELL COVERS AT 120°C**

Cell No.	Cover Material (1 mil)	Source (a)	UV In-tensity	$\frac{P_{\max} \text{ (Post-UV)}}{P_{\max} \text{ (Pre-UV)}}$	$\frac{P_{\max} \text{ (Post-Thermal Cycle)}}{P_{\max} \text{ (Pre-UV)}}$	Average Maximum Power Lost (%)	Observations	
							Post UV	Post-Thermal Cycle
X10	Spraylon	LPARL	1	0.91	0.91	—	No visible change	No visible change
X16	Spraylon	LPARL	1	0.95	0.96	—	No visible change	No visible change
X20	Spraylon	LPARL	1	0.87	0.87	—	No visible change	No visible change
X30	Spraylon	LPARL	1	0.91	0.95	8	No visible change	No visible change
X40	Spraylon	SPARL	1	0.89	0.90	—	No visible change	No visible change
X42	Spraylon	SPARL	1	0.86	0.92	—	No visible change	No visible change
6-53-8	RTV 655	Gen. Elec.	1	—	—	—	Coating yellowed	No visible change
6-72-9	RTV 655	Gen. Elec.	1	0.68	0.68	32	Coating yellowed	No visible change
X12	Spraylon	LPARL	2	0.92	0.98	—	No visible change	No visible change
X17	Spraylon	LPARL	2	0.94	0.96	—	No visible change	No visible change
X18	Spraylon	LPARL	2	0.87	0.89	5	No visible change	No visible change
X21	Spraylon	LPARL	2	0.83	0.95	—	No visible change	No visible change
X23	Spraylon	LPARL	2	0.91	0.93	—	No visible change	No visible change
X44	Spraylon	LPARL	2	0.93	0.96	—	No visible change	No visible change
6-61-8	RTV 655	Gen. Elec.	2	0.63	0.66	33	Crazed coating — Yellowed	No visible change
6-171-7	RTV 655	Gen. Elec.	2	0.65	0.67	33	Crazed coating — Yellowed	No visible change

Test Conditions: UV 808-hr UV exposure of 1 and 2 suns intensity  
(808 ESH and 1616 ESH)  
Cells at 120°C

Thermal Cycle: 25 cycles from +100°C to -196°C  
(4 min from 100°C to liquid N<sub>2</sub> immersion)

(a) Lockheed Palo Alto Research Laboratory.

### 3.6.2 Accelerated UV Test Results of Candidate Encapsulants (5 and 10 Suns Intensity)

LPARL-prepared FEP Teflon-covered 2-mil silicon cells and G. E.-supplied silicone-covered 2-mil silicon cells were exposed to 285 hr of UV at 5 suns and 10 suns intensity (1425 ESH and 2850 ESH, respectively). The cells were removed for electrical measurements — current-voltage (I/V) characterization — and then replaced and exposed for an additional 165 hr. The total exposure was 5 suns for 2250 ESH and 10 suns for 4500 ESH. Glass resin-covered silicon cells prepared by NASA-LeRC were given the second exposure of 165 hr only because of late availability. The glass resin cell covers were of various formulations and thicknesses.

The LPARL and G. E. cell identification, processing, and primers used are shown in Table 3-5. The NASA-LeRC identification and test allocation are shown in Table 3-6.

Cell performances after 285 hr at 120°C for 5 and 10 suns intensity are shown in Table 3-7. It should be noted that the cell temperatures were monitored directly by means of thermocouples welded to measurement tabs 1/8 in. away from cells. Within the same laminate construction, the thermal resistance varied from cell to cell. The thermal resistance was higher for the G. E. cells which were adhesively bonded to the FEP/Kapton substrate and, in turn, adhesively bonded with double-backed adhesive Kapton tape to 0.040-in. Invar substrate. The LMSC cells were thermally bonded to FEP/Kapton substrates and then adhesively bonded to 0.040-in. Invar substrate using double-backed adhesive Kapton tape.

The cell temperature was very sensitive to power supply output variations, changes in UV lamps, and clamping pressure of Invar substrate to the constant temperature copper substrate holder. Typical variations in cell temperature during exposure are shown in Table 3-8 for which inconsistencies are attributed mainly to variations in clamping pressure.

The results of the second increment of UV exposure are shown in Table 3-9. The G. E. silicone-coated cells and the LPARL FEP-Teflon-coated cells approached degradation

**Table 3-5**  
**UV TEST CELLS IDENTIFICATION**

Cell No.	Process
V12	2-mil FEP/A Thermally Bonded to Cell at 290°C, 0.1% Z6020 Primer
V11	1-mil Spraylon Processed on Cell After Thermal Bonding Cell to Substrate
V13	1-mil FEP/A Thermally Bonded to Cell at 290°C, 5% A1100
V14	1-mil FEP/A Thermally Bonded to Cell at 290°C, 0.1% Z6020
V15	2-mil FEP/A Thermally Bonded to Cell at 290°C, 5% A1100
V18	2-mil FEP/A Thermally Bonded to Cell at 290°C, 0.1% Z6020
V20	1-mil Spraylon Processed on Cell After Thermal Bonding Cell to Substrate
V23	1-mil FEP/A Thermally Bonded to Cell at 290°C, 2-1/2% A1100
V27	2-mil FEP/A Thermally Bonded to Cell at 290°C, 2-1/2% A1100
V28	1-mil FEP/A Adhesive Bonded to Cell, 1/2-mil D.C. 93500, 0.1% A6020
V30	1-mil FEP/A Adhesive Bonded to Cell, 1/2-mil D.C. 93500, 0.1% Z6020
V31	1-mil FEP/A Thermally Bonded to Cell at 290°C, 0.1% Z6020
V52	1.4-mil D.C. 93500 Adhesive as Cell Cover, 0.1% Z6020
V53	1.5-mil D.C. 93500 Adhesive as Cell Cover, 0.1% Z6020
46	G.E.-Supplied Cell (6-46-8) RTV 655 Coating
161	G.E.-Supplied Cell (6-161-6) RTV 655 Coating
167	G.E.-Supplied Cell (6-167-6) RTV 655 Coating
170	G.E.-Supplied Cell (6-170-7) RTV 655 Coating

**Notes:**

1. Cell: 2-mil Silicon Cell, Solarex
2. Substrate: 1-mil Kapton/1/2-mil FEP/Type C Teflon
  - (a) V11 through V53 thermally bonded to substrate at 290°C for 5 min
  - (b) 46 through 170 adhesive bonded to substrate with RTV 655
3. Cells primed by dip, followed by vertical drain, followed by oven-dry at 365°F for 1 min. Cell then coated within 30 min.
4. Primers (or "adhesion promoter")
  - Z6020 - Dow Corning
  - A1100 - Union Carbide



Table 3-6  
NASA-LeRC GLASS RESIN CELLS  
TEST ALLOCATION

Cell No.	Composition No.	Cell Identification	Infrared Emittance at 300 K	Test <sup>(a)</sup>
20	G.R. 908M	Group 20, 3-1, 45 $\mu\text{m}$	0.883	Boeing - UV + p <sup>+</sup>
26	G.R. 100	Group 26, 6-2, 22 $\mu\text{m}$	0.865	Boeing - UV + p <sup>+</sup>
39A	G.R. 908	Group 39A, 15 $\mu\text{m}$	0.789	Boeing - UV + p <sup>+</sup>
17	G.R. 908M	Group 17, 1-5, 15 $\mu\text{m}$	0.800	Boeing - UV + p <sup>+</sup>
19	G.R. 908M	Group 19, 3-5, 35 $\mu\text{m}$	0.853	Boeing - UV + e <sup>-</sup>
22	G.R. 100	Group 22, 7-3, 28 $\mu\text{m}$	0.864	Boeing - UV + e <sup>-</sup>
39B	G.R. 908	Group 39B, 15 $\mu\text{m}$	0.763	Boeing - UV + e <sup>-</sup>
25	R.G. 908M	Group 25, 6-3, 18 $\mu\text{m}$	0.837	Boeing - UV + e <sup>-</sup>
24	G.R. 100	Group 24, 6-5	-	Lockheed - UV Test, 10 suns
38A	G.R. 908	Group 38A, 12 $\mu\text{m}$	-	Lockheed - UV Test, 10 suns
38B	G.R. 908	Group 38B	-	Lockheed - UV Test, 5 suns
27	G.R. 650M	Group 27, 85	-	Lockheed - UV Test, 5 suns

(a) Boeing Environmental Test:

- (1) UV + p<sup>+</sup> (ultraviolet plus 100-keV protons)  
intermittent proton irradiation with continuous UV at 5 suns intensity for 160 hr  
Total exposure -  $5 \times 10^{15}$  p/cm<sup>2</sup>  
Cell at 120°C
- (2) UV + e<sup>-</sup> (ultraviolet plus 1-meV electrons)  
intermittent electron irradiation with continuous UV at 5 suns intensity for 160 hr  
Total exposure -  $5 \times 10^{15}$  e/cm<sup>2</sup>  
Cell at 120°C

Table 3-7

**UV EXPOSURE TEST DATA - 1ST EXPOSURE INCREMENT (285 HR)  
SOLAR CELLS AT 120°C**

Cell No. (a)	UV Intensity	ESH	$I_{sc}$ (mA)	$V_{oc}$ (mV)	$I_{mp}$ (mA)	$V_{mp}$ (mV)	$P_{max}$ (mW)	$P_{max}$ (mW)	(Post-UV) (Pre-UV)	Infrared Emittance at 300K
									$\frac{P_{max}^{(Post)}}{P_{max}^{(Pre)}}$	
V11	10	2850	56.8	516.0	24.3	423.0	10.28	50.26	0.204	0.815
V12	5	1425	122.4	530.2	101.0	408.0	41.21	42.91	0.960	0.804
V13	5	1425	123.3	530.6	112.1	432.0	48.43	53.40	0.906	0.742
V14 <sup>(b)</sup>	10	2850	126.2	534.8	113.9	415.0	47.27	49.22	0.960	0.737
V15	5	1425	121.8	528.5	112.0	425.0	47.60	51.11	0.931	0.784
V18	10	2850	122.8	520.8	112.7	415.0	46.78	50.10	0.933	0.792
V20	5	1425	95.9	524.5	87.4	409.0	35.75	50.36	0.709	0.818
V23	10	2850	119.8	537.2	98.0	429.0	42.04	45.54	0.923	0.720
V27	10	2850	104.8	533.0	96.5	433.0	41.78	51.21	0.815	0.774
V28	5	1425	119.4	531.2	110.7	429.0	47.49	53.87	0.881	0.875
V30	10	2850	89.4	533.6	84.4	432.0	36.46	52.60	0.693	0.855
V31 <sup>(c)</sup>	5	1425	126.4	545.0	114.4	442.0	50.56	53.24	0.950	0.740
V52	10	2850	108.9	533.3	101.9	435.0	44.33	54.80	0.809	0.833
V53	5	1425	124.3	528.5	96.5	410.0	39.57	27.79	-	0.875
6-46-8 <sup>(b)</sup>	5	1425	112.7	546.4	107.0	451.0	48.26	33.59	0.853	0.893
6-161-6 <sup>(b)</sup>	10	2850	112.0	540.0	105.3	443.0	46.65	54.08	0.863	0.883
6-167-6	10	2850	109.0	541.9	102.0	450.0	45.90	54.66	0.840	0.885
6-170-7 <sup>(c)</sup>	5	1425	112.1	541.5	103.9	449.0	46.65	54.70	0.853	0.885

Notes:

1. Irradiation Intensity: 140 mW/cm<sup>2</sup>
2. Average Cell Temperature: 28°C
3. UV Test Time: 285 hr

(a) V cells are FEP Teflon covered; V11 and V20 are Spraylon covered; V52 and V53 are D. C. 93500 silicone covered; 6-46-8 to 6-170-7 are RTV 655 silicone covered.

(b) Cells V14, 46, and 161 were removed from this test series and subsequently used in UV/proton and UV/electron Boeing Test Series.

(c) Cell 170 was removed from this test series and sent to G. E. for evaluation.

Table 3-8

## CELL OPERATING TEMPERATURES FOR NOMINAL 120°C UV TEST

Cell Identification	Source	Exposure Intensity (suns)	Cell Temperature (°C)
G. R. 100, #24	NASA-LeRC	10	127
V15 (2-mil FEP)	Lockheed (LPARL)	5	101
G. R. 908, #38A	NASA-LeRC	10	121
G. R. 908, #38B	NASA-LeRC	5	96
G. R. 650M, #27	NASA-LeRC	5	96
161 (RTV 655)	G. E. 6-161-6	10	127
46 (RTV 655)	G. E. 6-46-8	5	108
V15 (2-mil FEP)	Lockheed (LPARL)	5	118
V14 (1-mil FEP)	Lockheed (LPARL)	10	108

Table 3-9

UV EXPOSURE TEST DATA (450 HR TOTAL)  
1ST EXPOSURE INCREMENT (285 HR); 2ND EXPOSURE INCREMENT (165 HR)  
SOLAR CELLS AT 120°C

Cell No.	UV Intensity	ESH	I <sub>sc</sub> (mA)	V <sub>oc</sub> (mV)	I <sub>mp</sub> (mV)	V <sub>mp</sub> (mV)	Post-UV (450ESH)	Pre-UV	$\frac{P_{max}(Post)}{P_{max}(Pre)}$ 285 hr	$\frac{P_{max}(Post)}{P_{max}(Pre)}$ 450 hr
							P <sub>max</sub> (mW)	P <sub>max</sub> (mW)		
V11	10	4500	52.0	513.0	44.1	418.0	18.44	50.26	0.204	0.366
V12	5	2250	120.3	529.2	100.0	399.0	39.9	42.91	0.960	0.930
V13	5	2250	120.3	529.5	110.0	422.0	46.4	53.40	0.906	0.869
V15	5	2250	118.3	527.4	107.0	418.0	44.7	51.11	0.931	0.875
V18	10	4500	120.7	521.8	110.0	411.0	45.2	50.10	0.933	0.902
V20	5	2250	87.3	522.1	79.0	408.0	32.2	50.36	0.709	0.639
V23	10	4500	118.0	534.4	96.2	420.0	40.4	45.54	0.923	0.887
V27	10	4500	101.3	531.9	94.4	430.0	40.6	51.21	0.815	0.793
V28	5	2250	114.0	528.0	106.0	430.0	45.6	53.87	0.881	0.846
V30	10	4500	89.5	531.5	83.0	435.0	36.1	52.60	0.693	0.686
V52	10	4500	109.7	532.6	101.9	437.0	44.5	54.80	0.809	0.812
V53	5	2250	110.0	510.0	78.2	386.0	30.2	27.79	—	—
6-167-6	10	4500	102.7	539.5	95.7	455.0	43.5	54.66	0.840	0.796
38A <sup>(a)</sup>	10	1650	112.0	534.0	98.0	347.0	33.33	54.60	0.610 <sup>(a)</sup>	—

**Notes:****Electrical Measurement**

1. Irradiation Intensity: 140 mW/cm<sup>2</sup>
2. Average Cell Temperature: 28°C
3. UV Test Time: 450 hr

(a) NASA-LeRC Cell #38A exposed to 165 hr (1650 ESH) only.

saturation as shown by comparing maximum power putput changes of cells exposed to 5 and 10 suns intensity for the same exposure time, and comparing this to the second exposure increment. Of the four NASA-LeRC cells, exposed only to the second increment of UV exposure, one cell, No. 38A (5 suns, 825 ESH), was measured. It showed yellowing and crazing and had a serious degradation of power output. Cell 38B (5 suns, 825 ESH) showed some yellowing and starting of crazing. Cell 27 (GR 650 M exposed to 5 suns, 825 ESH) yellowed badly. Cell 24 (GR 100 exposed to 10 suns, 1650 ESH) yellowed and crazed very badly.

### 3.7 COMBINED ENVIRONMENTAL EXPOSURES OF CANDIDATE MATERIALS

The candidate encapsulant materials were exposed as cell covers to UV plus electrons and UV plus protons environments at 120°C.

Candidate materials were provided for testing in addition to those specimens prepared by LPARL. The encapsulated cells and their configurations were:

- General Electric Space Division: 25- $\mu$ m G.E. RTV 655 Silicone Cover Coating on 2-mil Solarex Silicon Cell

Cell was adhesive-bonded to a 25- $\mu$ m Kapton film. In order to accommodate to a limited area space irradiation test plate and provide adequate heat transfer, the Kapton substrate was adhesively bonded to a 1-mm-thick Invar substrate. The invar substrate was used for easy removal from test plate for subsequent post-test electrical measurements. The use of the Invar substrate does not invalidate the later thermal cycling test results as the stress gradients are not significantly different (see Section 3.8.2).

- NASA-LeRC: Glass-Resin (GR) Cover Coating on a 2-mil Solarex Cell

The GR coated cells were applied in thickness of 15 to 35  $\mu$ m. Various formulations and modifications were supplied.

Because the cells were supplied unmounted, they were mounted to a 1-mm Invar plate using two thicknesses of adhesive Kapton tape so as to simulate the thermal impedance of the G.E. cells.

- LPARL: FEP (Type A) Teflon Thermal-Bonded onto a 2-mil Solarex Cell  
The cell was thermally bonded to a one-half-mil FEP Teflon -one-mil Kapton substrate. An Invar substrate was bonded to the Kapton.

One and 2-mil FEP Teflon covers were used with either A1100 or Z6020 primers.

Twelve various cells and one 4-cell coupon were mounted onto a 1/4-in. copper plate which was fabricated to fit the sample table of the Boeing Dynamitron.\* The Dynamitron was used for both electron and proton irradiations. Specimens were held at a nominal 120°C. The charged particle irradiations were done intermittently, while the UV irradiation was continuous at 5 suns intensity for 150 hr.

The electron beam profile map, electron fluence plot, proton beam profile map, and proton fluence plot were supplied by Boeing CRETC and are shown in Appendix B.

### 3.7.1 Combined Environmental Exposure Test Results

The results of high-energy electrons plus UV irradiation are shown in Tables 3-10 and 3-11. The results of low-energy protons plus UV irradiation are shown in Tables 3-12 and 3-13.

The I/V characteristics were measured after irradiation and again after thermal cycling. The power output degradation and short-circuit current changes as a result of these exposures are shown in the above tables as well as observations of mechanical changes.

### 3.8 PARAMETRIC STRESS ANALYSIS OF SOLAR ARRAY ELEMENTS

Limited computer analysis work done in Phase I confirmed the critical stresses in the Spraylon-silicon cell laminate during thermal cycling. It was shown that Spraylon thickness in excess of 3 mils on a conventional 8- or 12-mil cell resulted in unacceptable

---

\*The test irradiations were performed at the Boeing Combined Radiation Effects Test Laboratories (CRETL), Seattle, Washington.

Table 3-10

# RESULTS OF HIGH-ENERGY ELECTRONS PLUS UV IRRADIATION - CANDIDATE SILICON SOLAR CELL COVERS AT 120°C

Cell No.	Cell Cover	Identification	Emittance at 300 K UV Intensity	Current, Short-Circuit, $I_{sc}$ (mA)			Voltage, Open-Circuit, $V_{oc}$ (mV)			Current at $P_{max}$ , $I_{mp}$ (mA)	Voltage at $P_{max}$ , $V_{mp}$ (mV)	Power, Maximum ( $P_{max}$ ) (mW)		
				Pre-Irradiation	Post-Irradiation	Post-Thermal Cycle	Pre-Irradiation	Post-Irradiation	Post-Thermal Cycle	Pre-Irradiation	Pre-Irradiation	Pre-Irradiation	Post-Irradiation	Post-Thermal Cycle
V-51	Control		0.410	130.9	89.5	89.0	533.5	468.0	467.3	120.7	439.5	52.93	31.2	31.1
G-73-9	G.E. 25 $\mu$ m	RTV 655	0.870	134.0	71.9	71.9	553.9	473.0	470.9	124.0	460.0	57.04	15.3	25.9
G-161-6 (a)	G.E. 25 $\mu$ m	RTV 655	0.978	129.1	71.7	71.4	546.5	472.5	470.3	121.8	444.0	54.09	25.5	25.2
31	G.E. 4-Cell Coupon 25 $\mu$ m	RTV 655	-	261.9	146.7	148.7	1030.0	914.3	919.0	241.0	838.0	201.96	100.2	101.0
GR 19	NASA-LeRC 35 $\mu$ m	GR908M	0.853	129.9	-	-	550.2	-	-	121.1	459.0	55.59	-	-
GR 22	NASA-LeRC 25 $\mu$ m	GR100	0.864	132.5	-	-	549.6	-	-	123.3	454.0	55.99	-	-
GR 25	NASA-LeRC 18 $\mu$ m	GR903M	0.837	130.9	-	-	542.2	-	-	105.5	435.0	45.89	-	-
GR 39B	NASA-LeRC 15 $\mu$ m	GR909	0.763	131.2	-	-	549.4	-	-	121.0	457.0	55.30	-	-
V-7	LPARL 2-mil	FEP (A1160)	0.780	133.1	84.5	80.0	534.7	463.5	459.5	124.0	435.0	53.94	29.1	27.2
V-8	LPARL 1-mil	FEP (A1100)	0.724	134.0	86.2	70.0	537.0	463.0	456.0	123.8	438.0	54.22	29.5	20.0
V-9	LPARL 1-mil	FEP (Z6020)	0.803	119.6	76.0	85.3	526.9	460.6	461.5	107.0	420.0	44.94	24.8	29.1
V-11 (a)	LPARL 1-mil	FEP (Z6020)	0.734	132.1	80.9	76.1	536.3	459.4	456.1	119.6	415.0	49.22	25.7	22.9
V-24	LPARL 2-mil	FEP (Z6020)	0.794	123.9	89.0	82.5	528.9	471.1	468.6	111.8	426.5	47.65	30.0	25.6

(a) Previously exposed to 2850 ESH at 10 suns intensity.

Note: Specimen exposure map and relative fluence plot shown in Fig. B-4, Appendix B.

Test Conditions: UV 800 ESH at 5 suns intensity at 120°C plus  
 $5 \times 10^{15} \text{ e}^-/\text{cm}^2$  (1 MeV)

Thermal Cycle: 25 cycles, +100°C to -196°C  
 (4 min from +100 to liquid  $\text{N}_2$  immersion)

Cell I/V Measurements: Made by NASA-JPL  
 Average cell temperature 28°C

Irradiation Intensity 140 mW/cm<sup>2</sup>

Table 3-11

**SUMMARY OF RESULTS OF HIGH-ENERGY ELECTRONS PLUS UV IRRADIATION - CANDIDATE SILICON  
SOLAR CELL COVERS AT 120°C**

Cell No.	Cover Material	Source	$\frac{P_{max}}{P_{max}}$ (Post e <sup>-</sup> + UV)	$\frac{P_{max}}{P_{max}}$ (Post-Thermal Cycle)	Average Maximum Power Lost (%)	Observations	
			$\frac{P_{max}}{P_{max}}$ (Pre e <sup>-</sup> + UV)	$\frac{P_{max}}{P_{max}}$ (Pre e <sup>-</sup> + UV)		Post Irradiation - Pre-Thermal Cycling	Post Irradiation - Post-Thermal Cycling
V 51	Control		0.59	0.59	41		
6-73-9	RTV 655	G.E.	0.32	0.45		Crazed and yellowed	Some flaking - minor increase in crazing
161 <sup>(a)</sup>	RTV 655	G.E.	0.47	0.47	53	Yellowed	Minor flaking
31 (coupon)	RTV 655	G.E.	0.50	0.50		141-8 Badly crazed	Increased flaking in previously flaked areas
						143-8 Badly crazed	
						143-8 Badly crazed and flaking	Increased flaking in previously flaked areas
						140-8 Large area crazing	Increased flaking in previously flaked areas
						142-8 Large area crazing	Crazed areas - no significant changes
GR. 19	GR908M	NASA-LeRC	-	-	-	Visually OK	Some mottling
GR. 22	GR100	NASA-LeRC	-	-	-	Badly flaked - 10% left	No changes
GR. 25	GR908	NASA-LeRC	-	-	-	Visually OK - Small amount yellow	No change
GR. 39B	GR908	NASA-LeRC	-	-	-	Flaking surface	No change
V7 (2 mil)	FEP Teflon	LPARL <sup>(b)</sup>	0.54	0.50		Visually OK	Some flaking
V8 (1 mil)	FEP Teflon	LPARL	0.54	0.37	48	Visually OK	Minor flaking
V9 (1 mil)	FEP Teflon	LPARL	0.55	0.65		Flaking surface	Bad flaking
V14 <sup>(b)</sup> (1 mil)	FEP Teflon	LPARL	0.52	0.47		Visually OK	Minor flaking
V24 (2 mil)	FEP Teflon	LPARL	0.63	0.47		Visually OK	Flaking surface

Test Conditions:UV - 800 ESH at 5 suns intensity at 120°C plus  $5 \times 10^{10}$  e<sup>-</sup>/cm<sup>2</sup> (1 MeV)Thermal Cycle25 cycles from +100°C to -196°C (4 min from +100°C to liquid N<sub>2</sub> immersion)Cell I/V Measurements:(made by NASA/JPL) Average cell temperature: 28°C  
Irradiation intensity: 140 mW/cm<sup>2</sup>

(a) Previously exposed to 2850 ESH at 10 suns intensity.

(b) Lockheed Palo Alto Research Laboratory.



Table 3-12  
RESULTS OF LOW-ENERGY PROTONS PLUS UV IRRADIATION - CANDIDATE SILICON  
SOLAR CELL COVERS AT 120°C

Cell No.	Cell Cover	Ident.	Emittance at 300 K	Current, Short Circuit, $I_{sc}$ (mA)			Voltage, Open Circuit, $V_{oc}$ (mV)			Current at $P_{max}$ , $I_{mp}$ (mA)	Voltage at $P_{max}$ , $V_{mp}$ (mV)	Power, Max $P_{max}$ (mW)		
				Pre-irrad	Post-irrad	Post Thermal Cycle	Pre-irrad	Post-irrad	Post Thermal Cycle			Pre-irrad	Post-irrad	Post Thermal Cycle
V50	Control		0.448	109.0	—	—	104.4	—	—	65.0	42.0	2.73	—	—
6-46-9 <sup>(a)</sup>	G. E. 25 $\mu$ m	RTV655	0.890	131.4	96.8	98.3	553.4	542.9	541.5	123.3	459.0	56.59	40.9	41.5
6-66-9	G. E. 25 $\mu$ m	RTV655	0.868	131.9	108.9	110.3	549.8	542.3	542.6	123.0	451.0	55.47	45.4	46.0
28	G. E. 4 cell coupon 25 $\mu$ m	RTV655	—	261.8	229.3	226.0	1024.4	992.0	1022.0	242.0	823.0	199.17	153.9	161.3
GR 17	NASA-LeRC 15 $\mu$ m	GR908M	0.800	133.9	—	—	553.3	—	—	124.9	456.0	56.95	—	—
GR 20	NASA-LeRC 45 $\mu$ m	GR908M	0.883	130.4	—	—	551.1	—	—	122.0	457.0	55.75	—	—
GR 26	NASA-LeRC 22 $\mu$ m	GR100	0.865	130.8	—	—	533.2	—	—	121.0	439.0	53.12	—	—
GR 39A	NASA-LeRC 15 $\mu$ m	GR908	0.789	132.1	—	—	540.7	—	—	120.4	454.0	54.66	—	—
V1	LPARL 2 mil	FEP (A1100)	0.788	132.8	124.1	123.6	532.4	530.8	527.2	123.2	436.0	53.72	49.1	49.3
V2	LPARL 1 mil	FEP (Z6020)	0.706	134.5	128.0	126.8	536.6	533.2	533.7	123.0	427.5	52.59	49.1	49.2
V3	LPARL 2 mil	FEP (Z6020)	0.760	131.3	123.3	123.2	539.7	538.8	537.9	118.6	442.0	52.42	35.1	49.0
V6	LPARL 1 mil	FEP (A1100)	0.710	131.2	122.8	120.3	530.3	523.0	521.5	110.2	427.0	47.06	41.0	41.0
V31 <sup>(a)</sup>	LPARL 1 mil	FEP (Z6020)	0.727	133.2	123.9	123.1	544.4	539.3	538.1	118.7	448.5	53.24	47.0	46.5

(a) Previously exposed to 2850 ESH at 10 suns intensity

Test Conditions: UV 500 ESH at 5 Suns Intensity, 120°C Plus  $5 \times 10^{15}$  p<sup>+</sup>/cm<sup>2</sup> (100 KeV)

Thermal Cycle: 25 cycles + 100°C to -196°C (4 min + 100°C to LN<sub>2</sub> immersion)

Cell I/V Measurements (made by NASA-JPL). Average cell temperature: 28°C; irradiation intensity: 140 mW/cm<sup>2</sup>

Note: Specimen exposure map and relative fluence plot are shown in Fig. B-4, Appendix B.

Table 3-13

**SUMMARY OF RESULTS OF LOW-ENERGY PROTONS PLUS UV IRRADIATION - CANDIDATE SILICON  
SOLAR CELL COVERS AT 120°C**

Cell No.	Cover Material	Source	$\frac{P_{max}}{P_{max}} \text{ (Post } p^+ \text{ + UV)}$	$\frac{P_{max}}{P_{max}} \text{ (Post Thermal Cycle)}$	Average Maximum Power Lost (%)	Observations	
						Post Irradiation - Pre-Thermal Cycle	Post Irradiation - Post-Thermal Cycle
V50	Control		-	-	-	Visually OK	No change
6-46-8(a)	RTV 655	G. E.	0.72	0.74	-	General crazing - Yellowed	No significant change
6-66-9	RTV 655	G. E.	0.82	0.83	20	General crazing - Yellowed	No significant change
28 (coupon)	RTV 655	G. E.	0.77	0.83	-	General crazing - Yellowed	No significant change
GR. 17	GR908M	NASA-LeRC	-	-	-	Visually OK - Yellowed	Large major fracture
GR. 20	GR908M	NASA-LeRC	-	-	-	Visually OK - Yellowed	Large flakes - 50%
GR. 26	GR100	NASA-LeRC	-	-	-	Badly flaking - Yellowed	Large flakes - 50%
GR. 39A	GR908	NASA-LeRC	-	-	-	Crazing - Yellowed	Increased crazing
V1	FEP Teflon	LPARL <sup>(b)</sup>	0.91	0.91	-	Visually OK	No change
V2	FEP Teflon	LPARL	0.93	0.93	-	Visually OK - Some minor mottling	No change
V3	FEP Teflon	LPARL	0.87	0.93	7	Visually OK	No change
V6	FEP Teflon	LPARL	0.87	0.87	-	Visually OK	No change
V31(a)	FEP Teflon	LPARL	0.88	0.88	-	Visually OK	No change

Cell I/V Measurements: (made by NASA-JPL) Average cell temperature: 28°C  
Irradiation Intensity: 140 mW/cm<sup>2</sup>

Test Conditions: UV 800 ESH at 5 suns intensity, 120°C, plus  $5 \times 10^{15} p^+/\text{cm}$  (100 KeV)

Thermal Cycle: 25 cycles + 100°C to -196°C (4 min from +100°C to liquid N<sub>2</sub> immersion)

(a) Previously exposed to 2850 ESH at 10 suns intensity

(b) Lockheed Palo Alto Research Laboratory.

stress levels in the Spraylon and could cause major mechanical damage in the silicon as well as the cover. The Phase II program utilized thin (2-mil) solar cells which gave a cause for concern because of the potentially high induced stresses due to material incompatibility. In addition, the 2-mil silicon cell is very fragile. The major concerns were high stresses at the cell edges, as well as the cell interconnect stresses. The computer modeling, in Phase II, were more extensive because there were numerous laminate configurations of differing materials to consider along with variations in interconnect design.

Parametric stress studies were made to encompass the various configurations of the laminate cell structures of the systems submitted to LPARL for evaluation.

Two means of computing stress and strain levels in the solar cells due to thermal cycling were used. The parameter studies generated by a nonlinear composite laminate code developed by LMSC were effective in the study of stress distributions away from the edges or interconnect areas of the cells (Ref. 7). This code accommodates time- and temperature-dependent material properties. Although materials used in cell construction exhibit time-dependent behavior, the inclusion of such effects was beyond the scope of the present study. The basic assumption of laminate analysis is that there exists a linear strain distribution induced through the thickness of the cell and its various encapsulating layers. Such an assumption is invalid in the edge and interconnect regions; consequently, a second type of analysis is required, namely, a two-dimensional plane strain finite element model which was constructed to study this area separately.

### 3.8.1 Laminate Studies

Solar cell failure due to mechanical stress is primarily due to the large mismatch of the thermal expansion characteristics of the cell component materials; this causes curvature changes (bowing). Such bowing produces a self-equilibrating system of stresses in the cell which acts to produce failure should they exceed ultimate stress levels in some critically loaded layer. The effect of such stresses, however, is generally minimized by the bowing since an unrestrained curvature change has a

stress-relieving effect. When the cell is prevented from bowing, the stress levels are raised, for example, as when it is bonded to a stiffer substrate material. In general, the greater the tendency of a cell to bow, the greater the stress levels will be when it is mounted and attached to others in an array. Hence, curvature change serves as a convenient indicator to be used in the following studies to evaluate a number of geometric and material cell parameters.

Figure 3-17 shows a family of curves with Spraylon thickness as the variable parameter. The reciprocal of radius of curvature is plotted as a function of temperature for the sandwich of Spraylon/0.002-in. silicon cell/6- $\mu$ m silver back surface/0.0005-in. FEP Teflon and 0.001-in. Kapton substrate. The significant result shown here is that a Spraylon thickness of about 1 mil minimizes the induced curvature over the expected operating temperature range. This finding confirms the experimental data which indicate thermal cycling survivability for Spraylon thicknesses less than 2 mils for thin cells.

Figure 3-18 shows the effect of silicon thickness variation with a 1-mil Spraylon coating. To minimize the induced curvature, it is apparent that the cell thickness should not be less than 2 mils. Figures 3-19, 3-20, and 3-21 show the effect of variations in thickness of silver-back electrode, FEP Teflon thickness, and Kapton substrate thickness. The curves show that a range of manufacturing tolerances in these parameters is permissible without causing significant problems.

Figure 3-22 shows the effect of using different cover materials having different solidification temperatures which are indicated by the zero curvature condition. The induced curvature is minimized by the Spraylon cover material.

Four different cell configurations\* were examined in detail:

---

\*The NASA-LeRC configuration was not analyzed because glass-resin film for characterization was not provided.

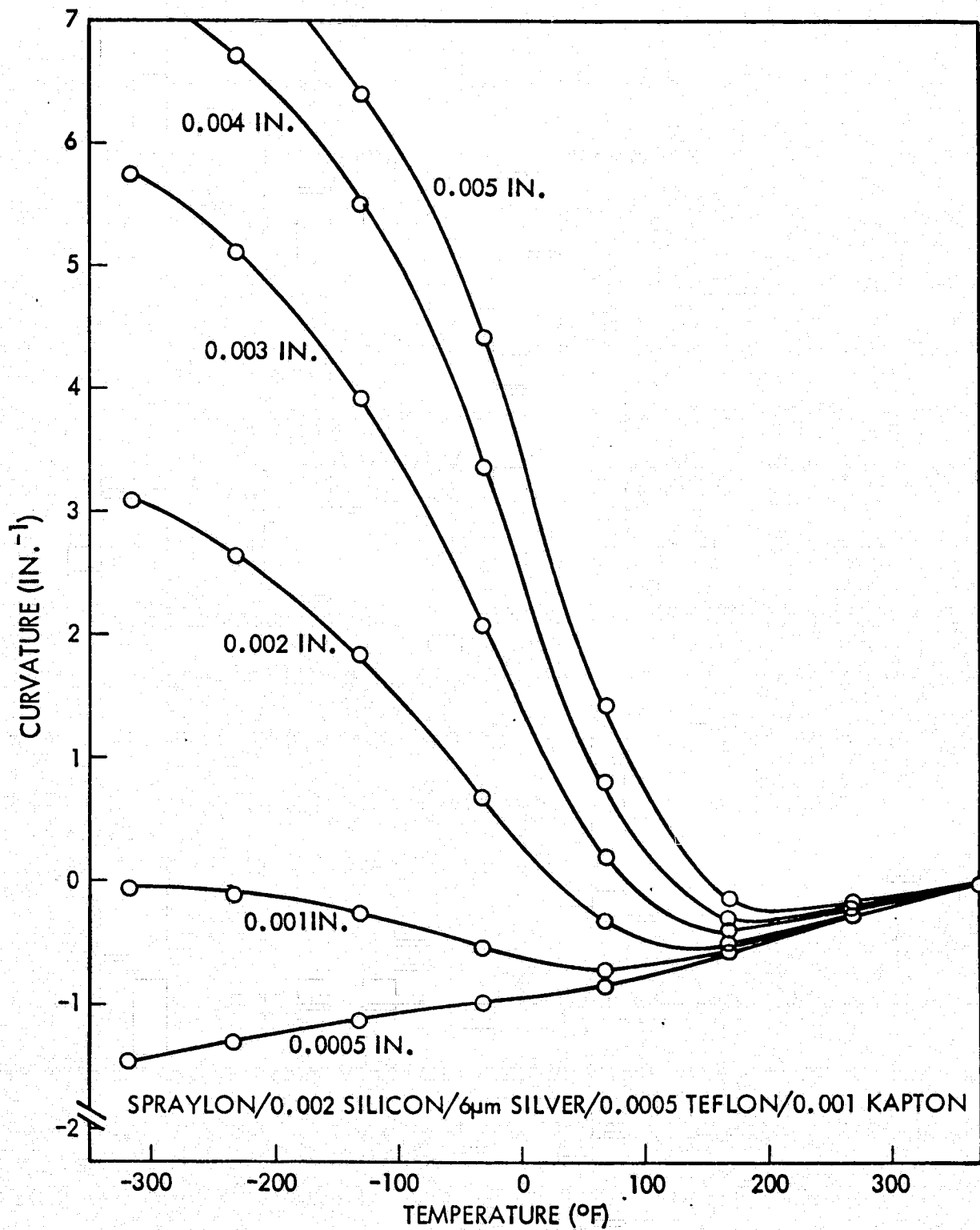


Fig. 3-17 Silicon Cell Curvature as a Function of Temperature - Spraylon Thickness  
Variable

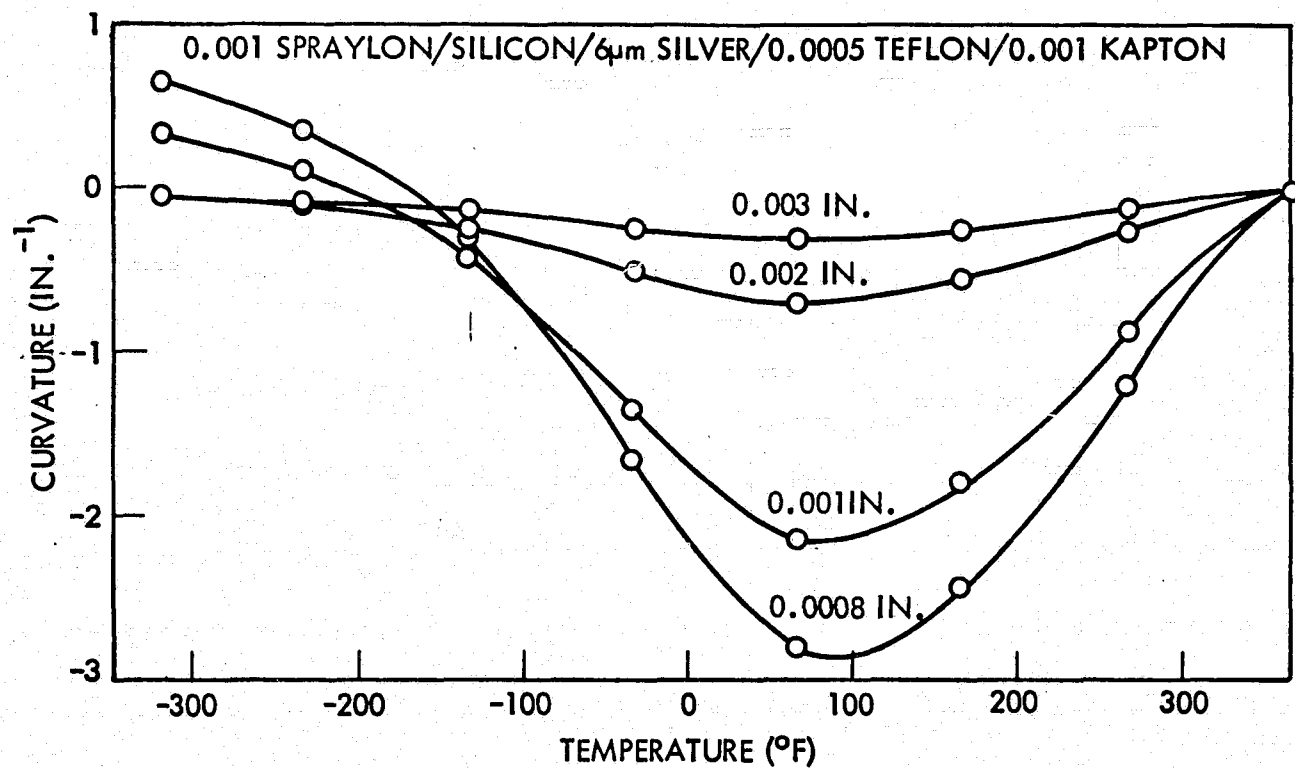


Fig. 3-18 Silicon Cell Curvature as a Function of Temperature - Silicon Thickness Variable

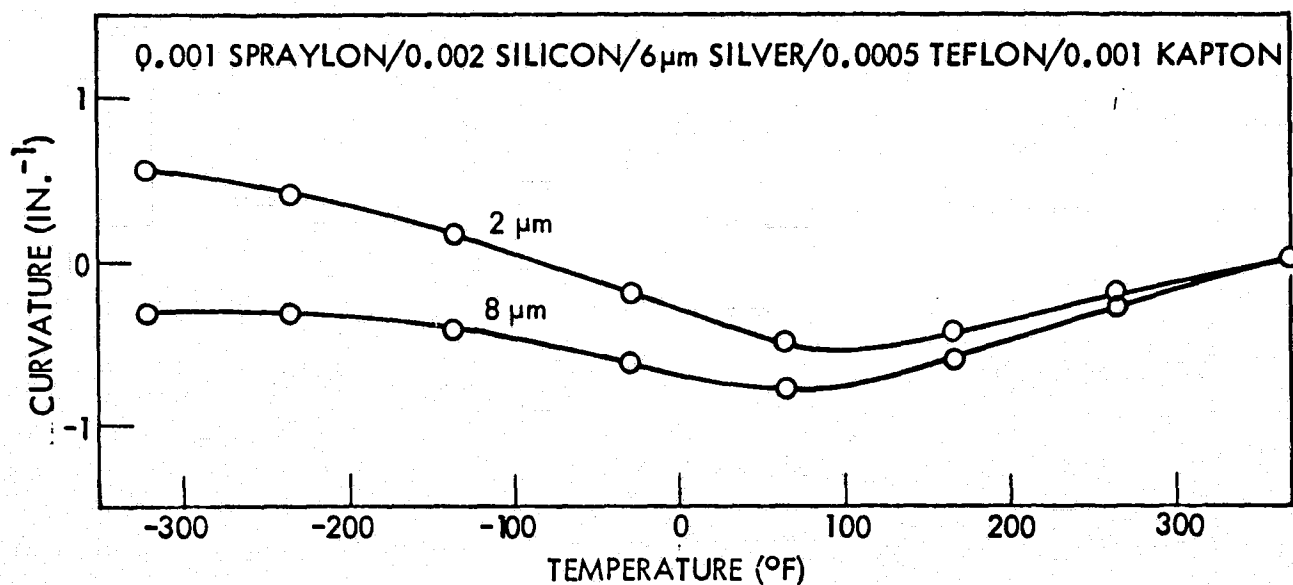


Fig. 3-19 Silicon Cell Curvature as a Function of Temperature -  
Silver Thickness Variable

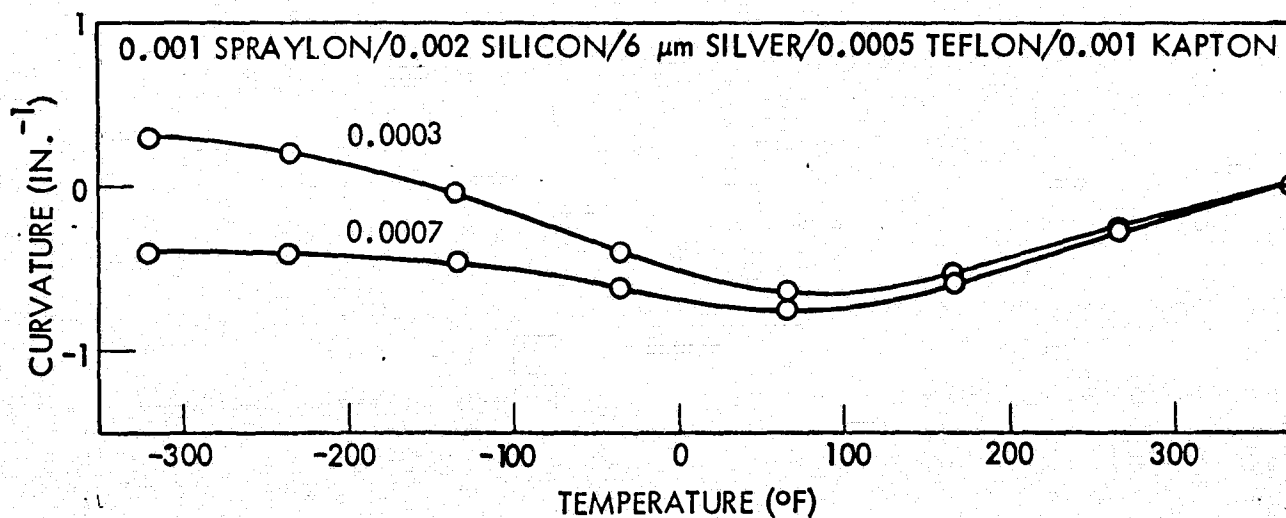


Fig. 3-20 Silicon Cell Curvature as a Function of Temperature -  
FEP Teflon Thickness Variable

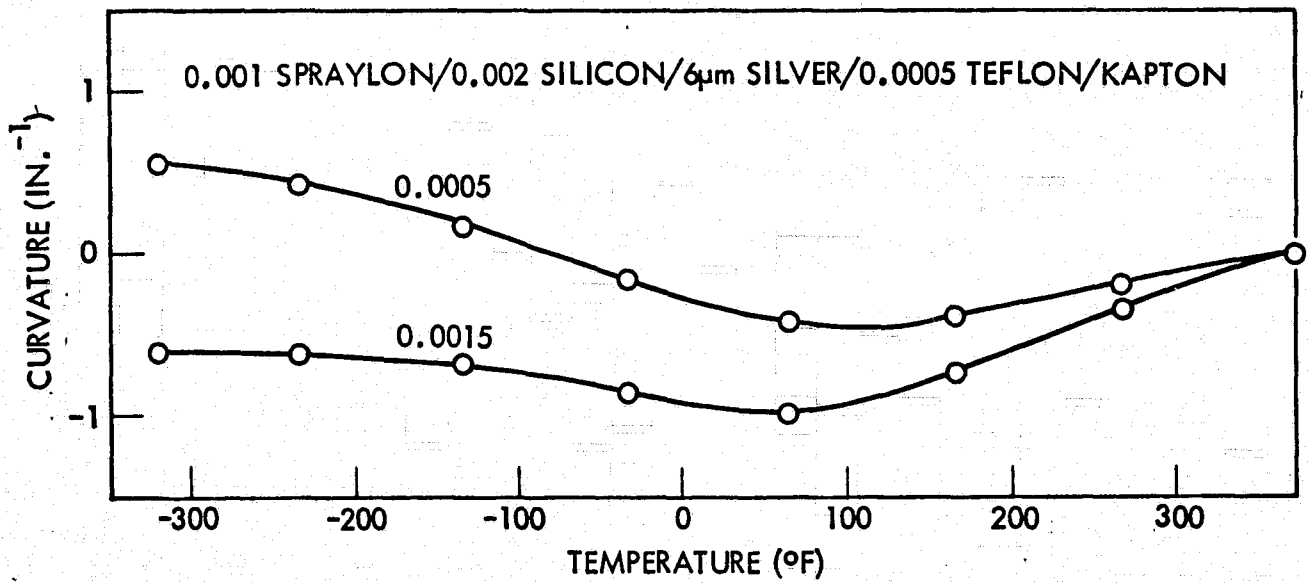


Fig. 3-21. Silicon Cell Curvature as a Function of Temperature -  
Kapton Thickness Variable



- 1 0.001 RTV 655/0.002 SILICON/6 $\mu$ m SILVER/0.0005 TEFLON/0.001 KAPTON
- 2 0.001 SPRAYLON/0.002 SILICON/6 $\mu$  SILVER/0.0005 TEFLON/0.001 KAPTON
- 3 0.001 TEFLON/0.002 SILICON/6 $\mu$ m SILVER/0.0005 TEFLON/0.001 KAPTON

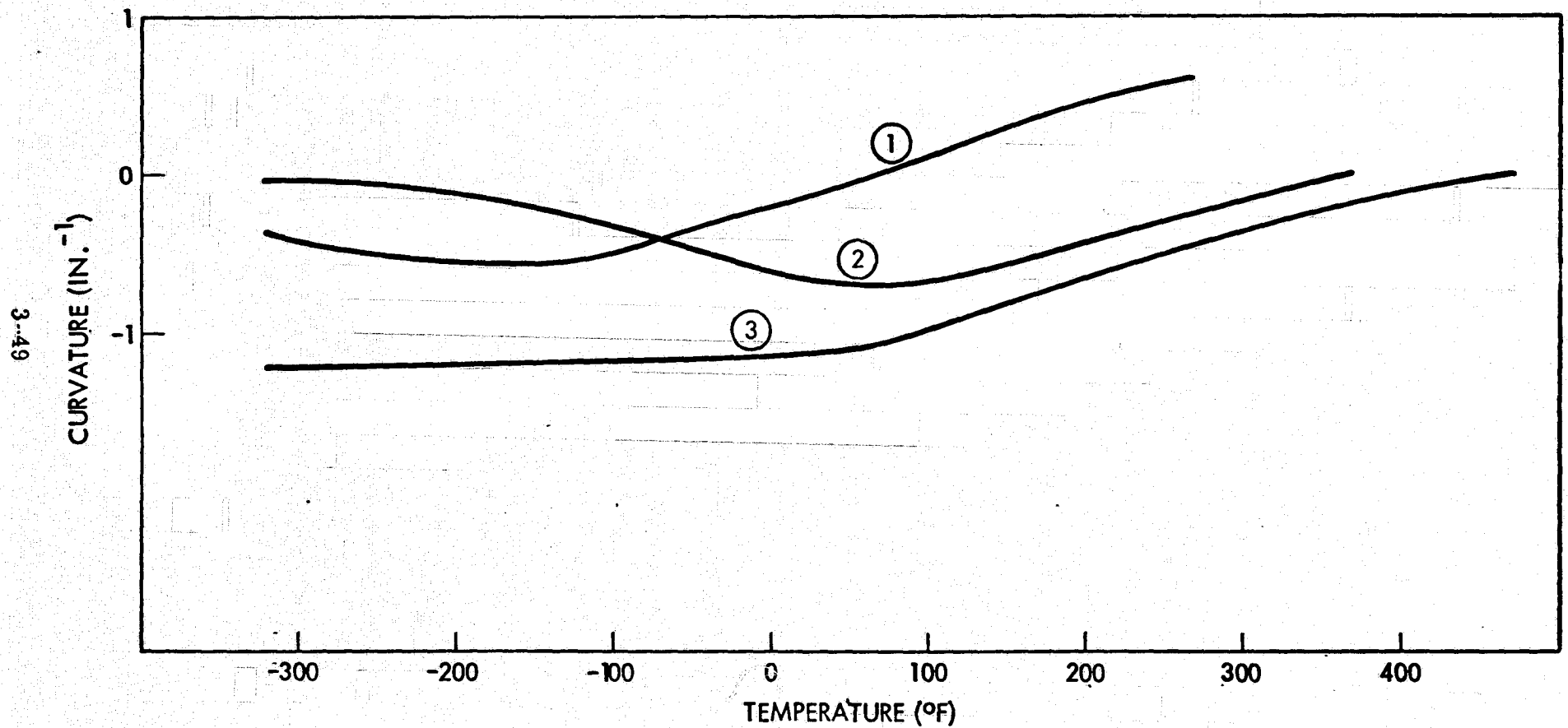


Fig. 3-22 Curvature of Silicon Cell as a Function of Temperature - Cover Material as a Variable

- **TRW Thermally Bonded Structure (Ref. 4)**

- 5-mil FEP-A Teflon cell cover

- 8-mil silicon cell

- 5- $\mu$ m silver back electrode

- 2-mil FEP-C Teflon

- 1-mil Kapton

- **LPARL Thermophysics Structure**

- 1-mil FEP-A Teflon cell cover

- 2-mil silicon cell

- 6- $\mu$ m silver electrode

- 1/2-mil FEP-C Teflon

- 1-mil Kapton

- **Spraylon Cover Structure**

- 1-mil Spraylon cell cover

- 2-mil silicon cell

- 6- $\mu$ m silver electrode

- 1/2-mil FEP Teflon

- 1-mil Kapton

- **G. E. Structure**

- 1-mil RTV 655 cell cover

- 2-mil silicon cell

- 6- $\mu$ m silver electrode

- 1/2-mil RTV 655 adhesive

- 1-mil Kapton

It should be noted that there has been some extrapolation of the physical properties of the materials for the temperature ranges considered since reliable thermophysical and mechanical properties data are not available for these extreme conditions.

Figure 3-23 shows those thermal expansion properties which were measured and used in the stress analysis.

ORIGINAL PAGE IS  
OF POOR QUALITY

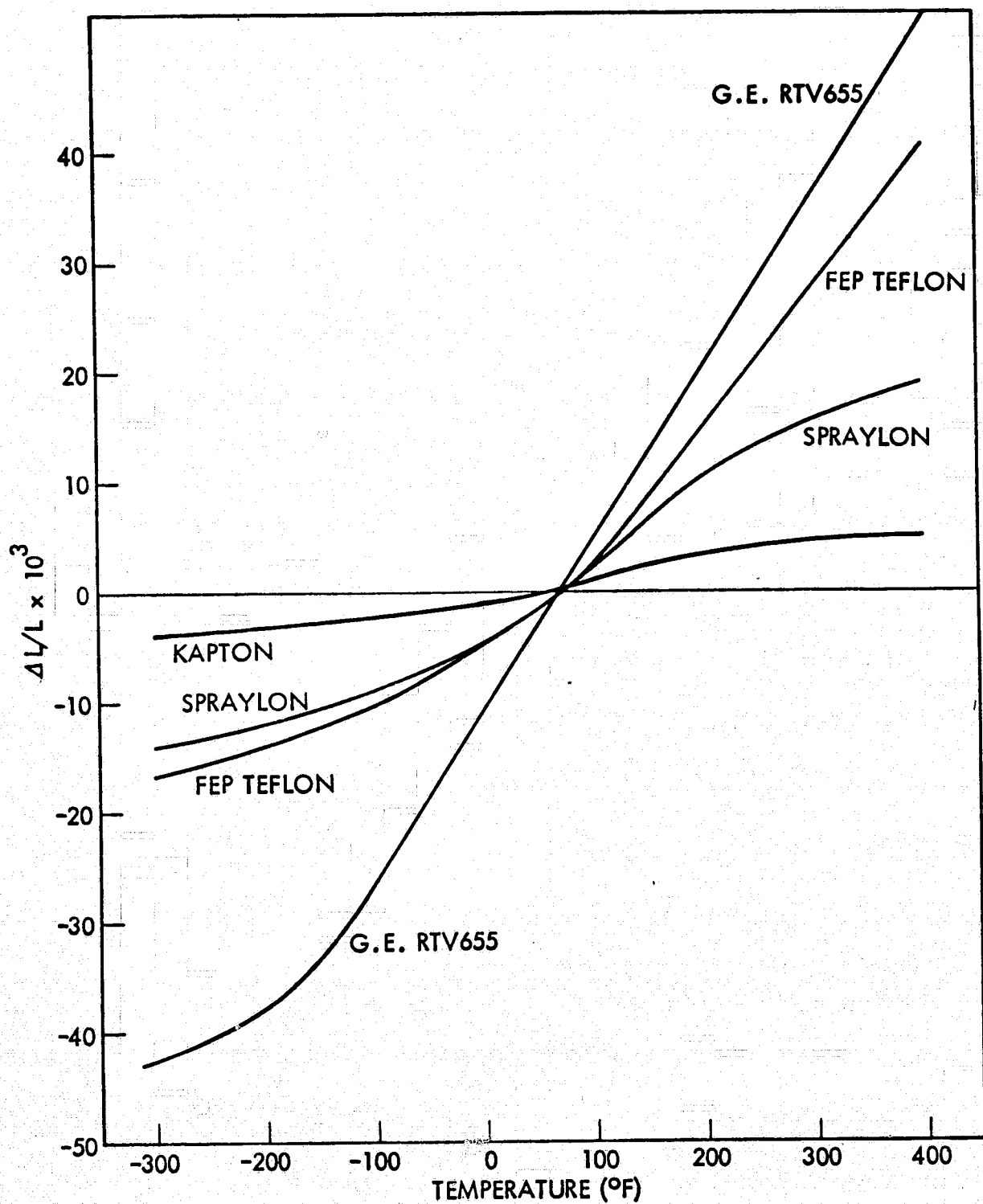


Fig. 3-23 Thermal Expansion Properties of Solar Cell Cover Materials

The stress profiles at each layer of the four-cell configurations are shown in Figs. 3-24 to 3-28 for which it can be seen that the stress levels are comparable in all cases except for the G.E. model. Since the zero stress state of the G.E. model is at room temperature, 65°F, its overall stress level is lower than the others. Figure 3-25 shows that the LPARL Teflon model has the smallest stress difference between the maximum and minimum stresses experienced during a thermal cycle so that the LPARL Teflon model is less likely to cause fatigue failure.

### 3.8.2 Thermal Cycling Analysis of Solar Cell Configurations

Thermal cycling (and irradiation exposures at 120°C) required a rigid substrate whose thermal conductance ensured uniform thermal conductance without damage to the test specimens. For test purposes, a 0.040-in. Invar substrate was used. To determine the stress contribution induced in the cover by the Invar substrate, the stresses, at different temperatures, were determined analytically for the following cell configurations:

- G.E. Configuration

- 1-mil RTV 655 cover
- 2-mil silicon cell
- 6- $\mu$ m silver electrode
- 1/2-mil RTV 655 adhesive
- 1-mil Kapton
- 2-mil RTV 655 adhesive
- 1-mil Kapton
- 2-mil RTV 655 adhesive
- 4-mil Invar

} Substrate

- LPARL Teflon Configuration

- 2-mil FEP-A Teflon cover
- 2-mil silicon cell
- 6- $\mu$ m silver electrode
- 1/2-mil FEP-C Teflon
- 1-mil Kapton
- 2-mil RTV 655 adhesive
- 1-mil Kapton
- 2-mil RTV 655 adhesive
- 40-mil Invar

} Substrate

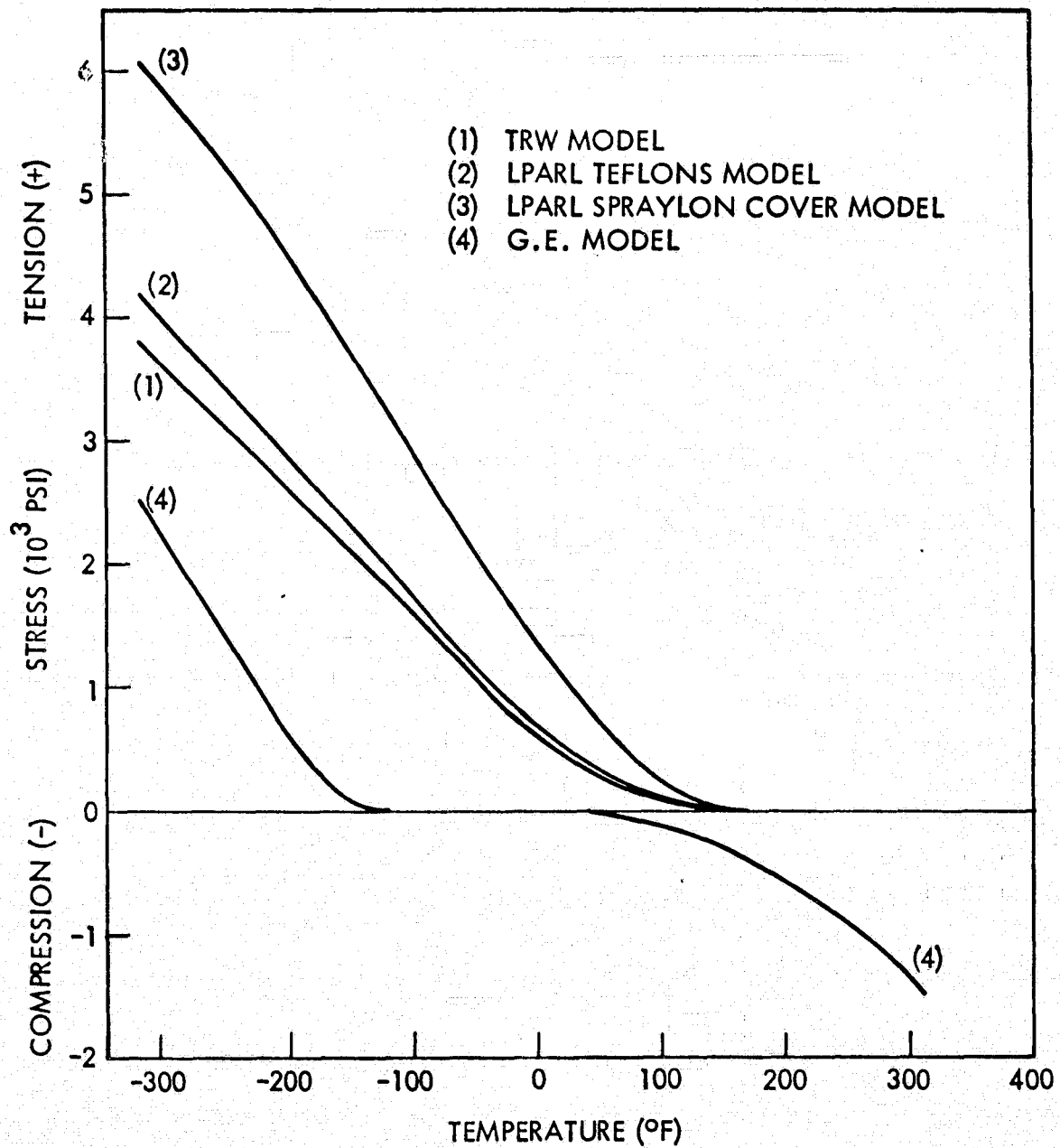


Fig. 3-24 Stress Profile in Cover Layer of Silicon Cell

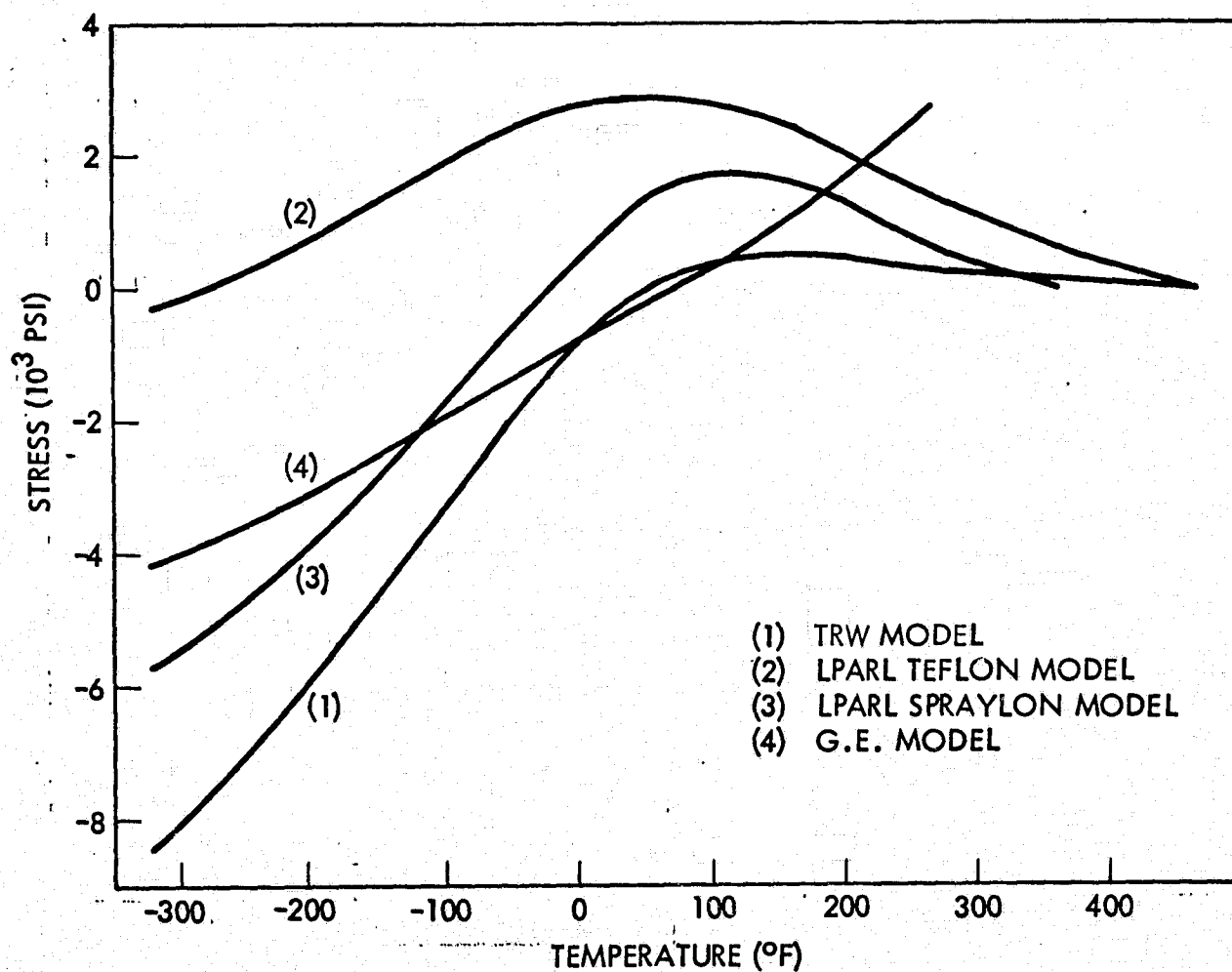


Fig. 3-25 Stress Profile in Silicon Cell Layer

ORIGINAL PAGE IS  
OF POOR QUALITY

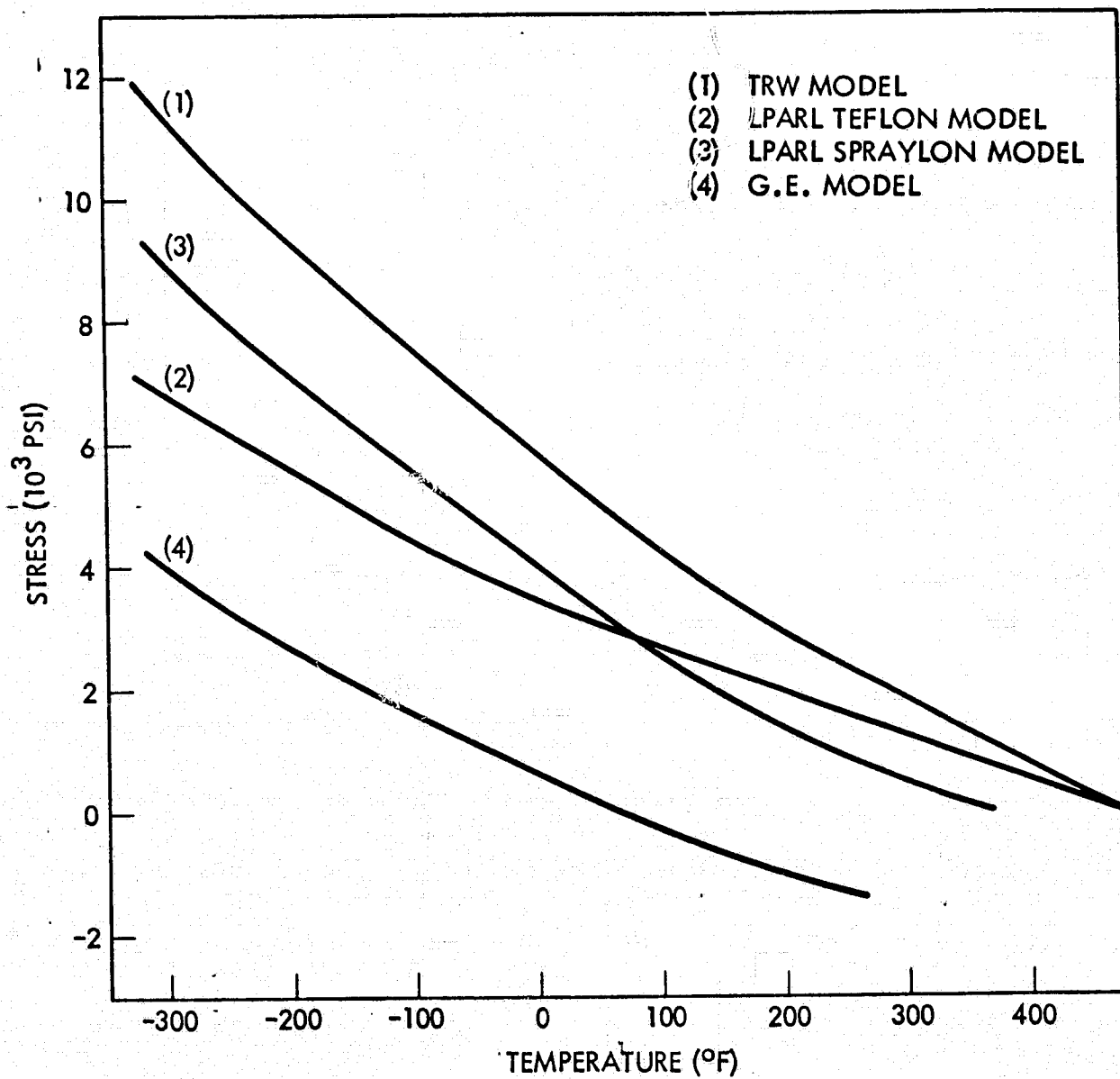


Fig. 3-26 Stress Profile in Silver Electrode Layer

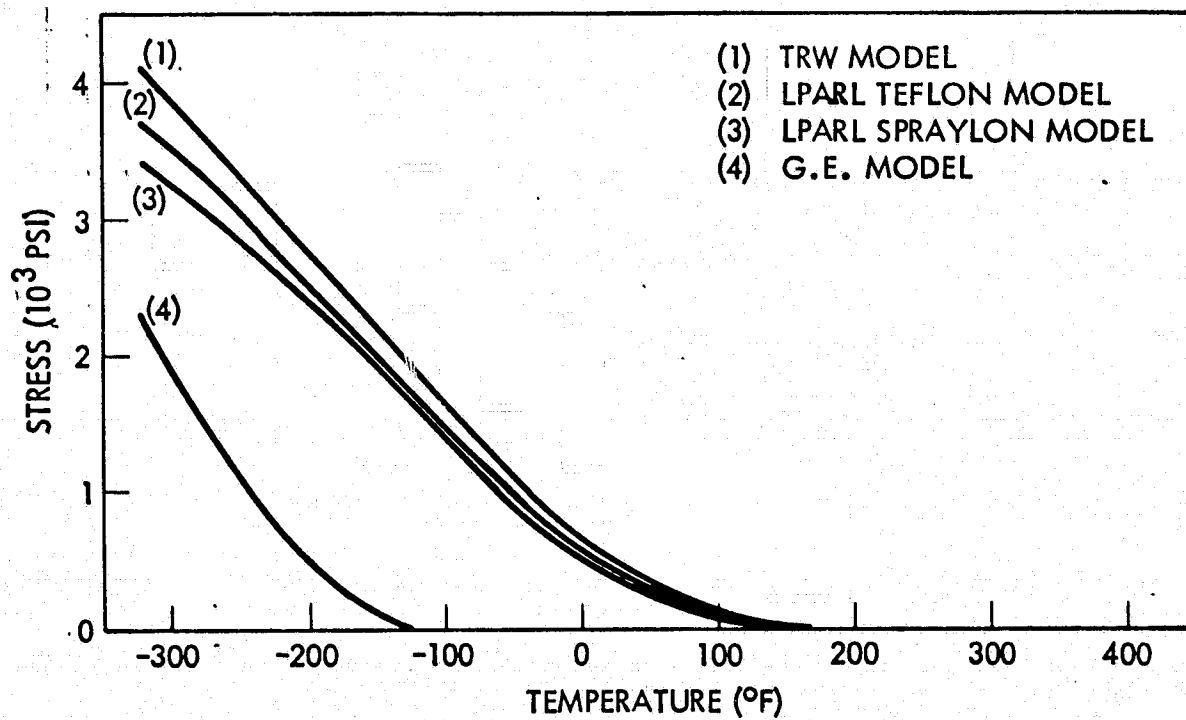


Fig. 3-27 Stress Profile in Adhesive Layer



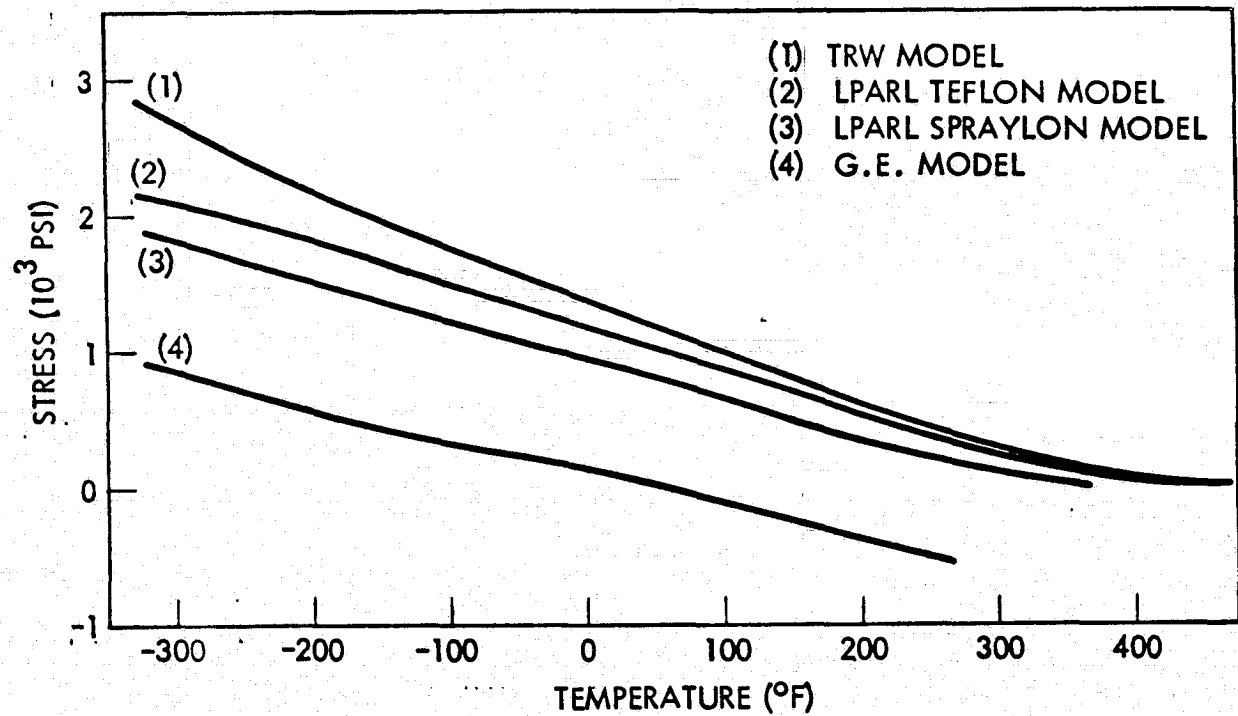


Fig. 3-28 Stress Profile in Kapton Layer

Table 3-14 shows the stresses in the cover layer with and without an Invar substrate. Although there is only a small change in cover stress with or without Invar substrate, there are, however, large changes in the silicon cell stresses.

### 3.8.3 Plane Strain Analysis

Plane strain finite element structural models were used to generate the stress analysis in the interconnect area using the SPAR code (Ref. 8). Two cross sections were studied, one in which there is no Invar interconnect (Fig. 3-29), and the other in which there is an Invar interconnect (Fig. 3-30). These two cross sections correspond to the areas (1) and (2) in Fig. 3-31, which shows an overall cross section of a cell structure at an interconnect area. As expected, the in-plane stresses approach the values obtained by the previously mentioned composite laminate code away from the edge. However, at the edge area, all three components of stresses are present. The primary concern is the shear stress and tensile stress in the thickness direction because these stresses may cause delamination of the composite. It was found that at the area of the silicon cell edge, a large shear stress exists for all cases. For example, at the element A in Fig. 3-29, shear stresses of the silicon cell at  $-320^{\circ}\text{F}$  are 11,600 psi for the Teflon-covered structure, 9,800 psi for the RTV 665 structure, and 23,400 psi for the Spraylon-covered structure. These shear stresses diminish very rapidly away from the edge. At element B (Fig. 3-29), which is only five elements from edge element A, the shear stresses reduce to less than 10% of those at element A. However, if the adhesion is not good, these localized shear stresses may cause delamination of the composite which then results in cracking of the cover.

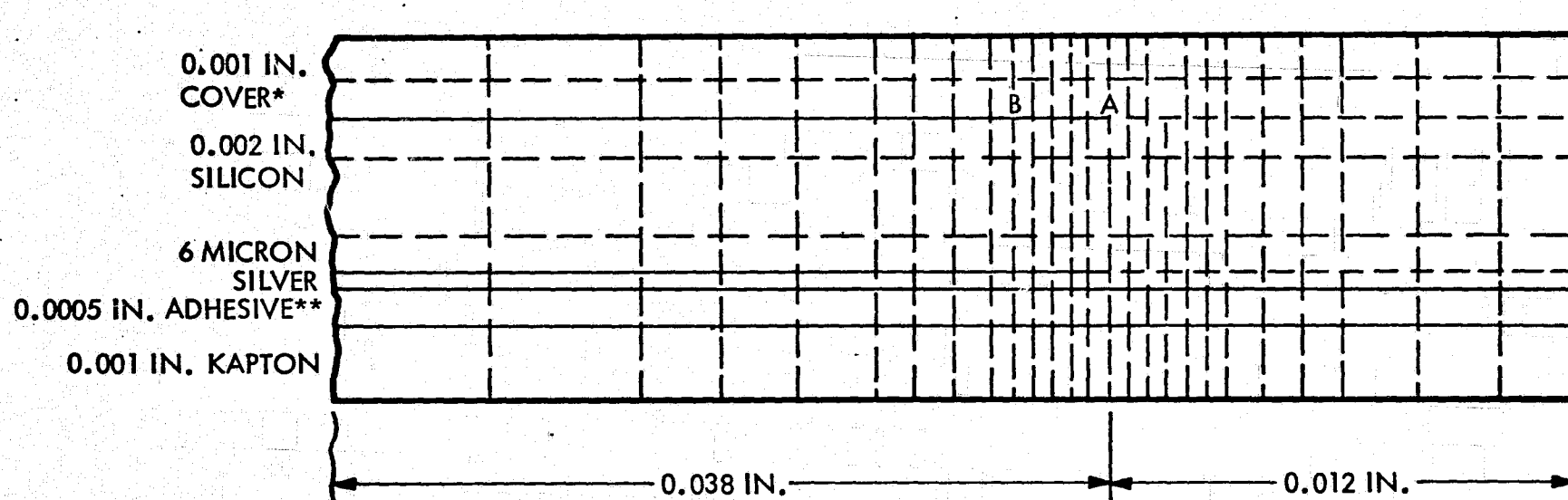
Figure 3-32 shows the shear stress variation of the silicon cell at  $-320^{\circ}\text{F}$  in the edge area. The stresses in the thickness direction are found to be relatively unimportant because they are mostly compressive. The maximum out-of-plane tensile stresses of the silicon cell at  $-320^{\circ}\text{F}$  in the edge area are 2,300 psi for the Teflon-covered structure, 50 psi for the G.E. RTV 655-covered structure, and essentially no tensile stress for the Spraylon-covered structure. The shear stresses between the Invar interconnect and the cover are fairly small; however, those between the Invar interconnect and the silicon cell at the edge area are very high. For example, at the

Table 3-14

## STRESSES IN THE CELL COVER WITH AND WITHOUT INVAR SUBSTRATE

Temperature (°F)	Stresses (psi)			
	FEP Teflon Cover With Invar Substrate	FEP Teflon Cover Without Substrate	RTV 655 Covers With Invar Substrate	RTV 655 Covers Without Substrate
365	0	0		
265	33	39	-10	-11
165	226	259	-3	-4
65	2,020	2,200	0	0
-35	8,250	8,330	2	34
-135	18,100	17,300	27	120
-235	27,900	26,300	10,740	11,300
-320	35,300	33,100	23,700	24,900

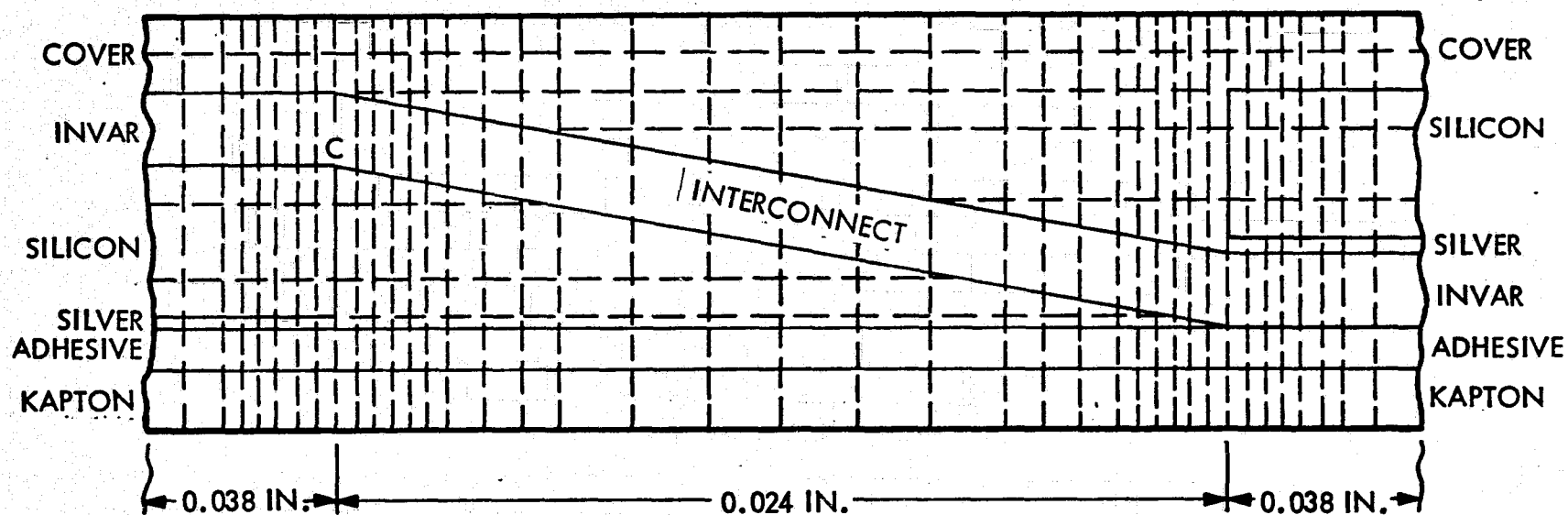
3-60



\*SPRAYLON, FEP-A TEFLON OR G.E. RTV 655  
\*\*FEP-C TEFLON OR G.E. RTV 655

Fig. 3-29 Finite Element Structural Model of an Interconnect Area

ORIGINAL PAGE IS  
OF POOR QUALITY



SPRAYLON, G.E. RTV655, OR FEP-A TEFLON COVER 0.001 IN.  
 INVAR 0.001 IN.  
 SILICON CELL 0.002 IN.  
 SILVER 6  $\mu$ m  
 FEP-C TEFLON OR G.E. RTV 655 ADHESIVE 0.0005 IN.  
 KAPTON 0.001 IN.

Fig. 3-30 Finite Element Structural Model of an Interconnect Area With Invar Connection

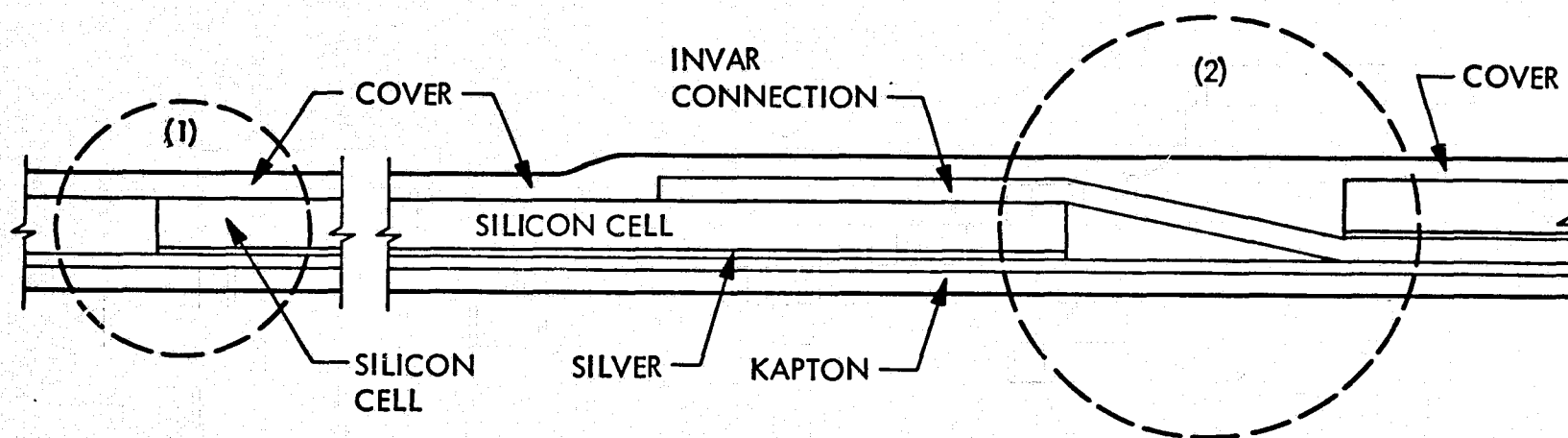


Fig. 3-31 Cross Section of a Cell Structure at Interconnected Area

ORIGINAL PAGE IS  
OF POOR QUALITY

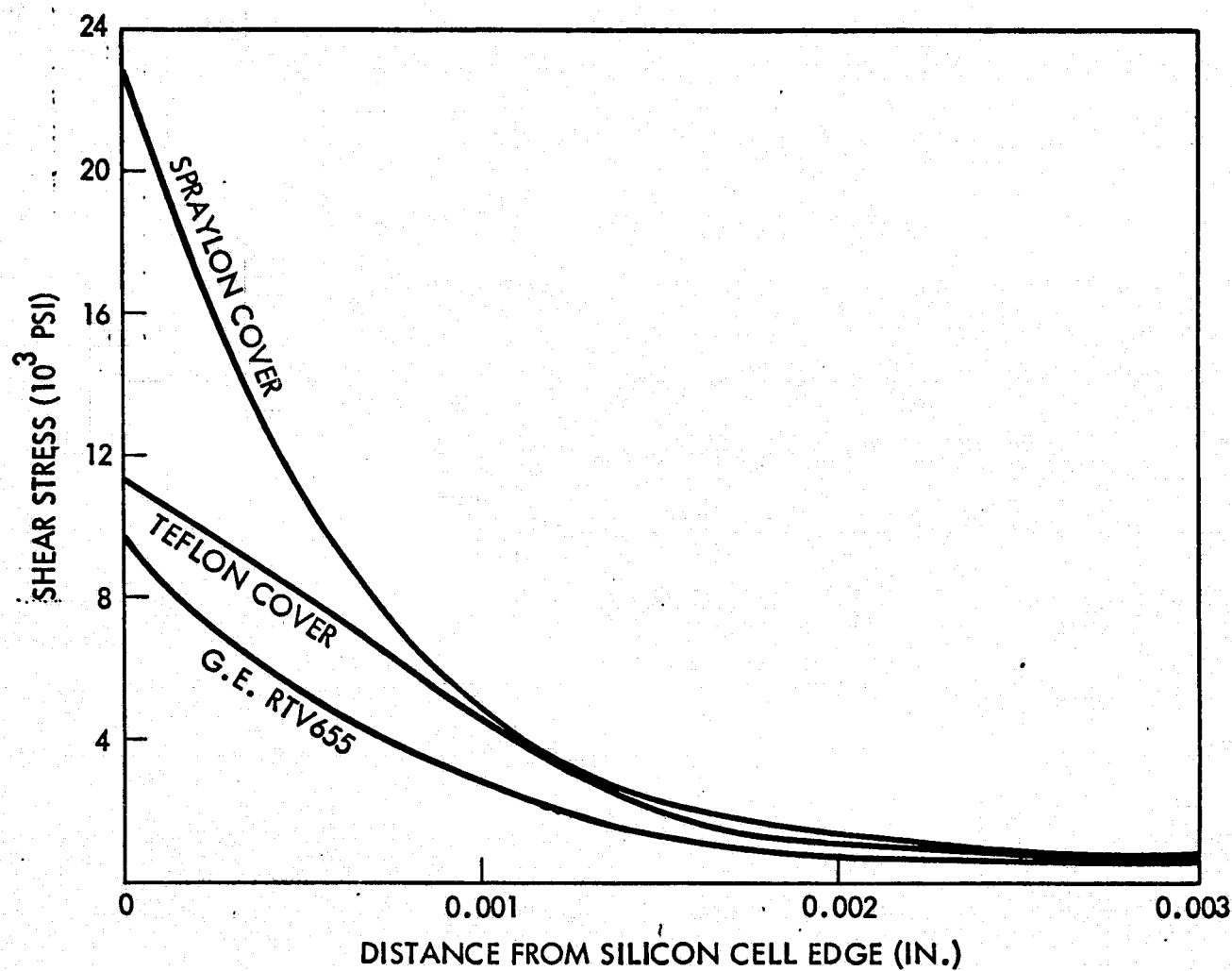


Fig. 3-32 Shear Stresses of the Silicon Cell in the Edge Area at 320°F for Different Cover Materials.

element C in Fig. 3-30, shear stresses at  $-320^{\circ}\text{F}$  are 53,000 psi for the RTV 655 cover; 60,000 psi, for the Teflon cover; and 80,000 psi, for the Spraylon cover. The results indicate that the bonding between the Invar interconnect and the silicon cell must be very strong to prevent separation. Figure 3-33 shows the shear stress variations between the Invar interconnect and the silicon cell at the interconnected area at  $-320^{\circ}\text{F}$ .

According to this finite element analysis of the edge area, it is found that the stress levels are comparable for all three cases. If one has to rank these from a stress point of view, a G.E. RTV 655 cover is the best, the FEP Teflon cover is second, while the Spraylon cover is least favorable.

It is important to recognize that the stress levels for these analyses are computed on the basis of a linear elastic response of the cover materials. In fact, stress relaxation and plastic deformation act to reduce the high localized stresses.



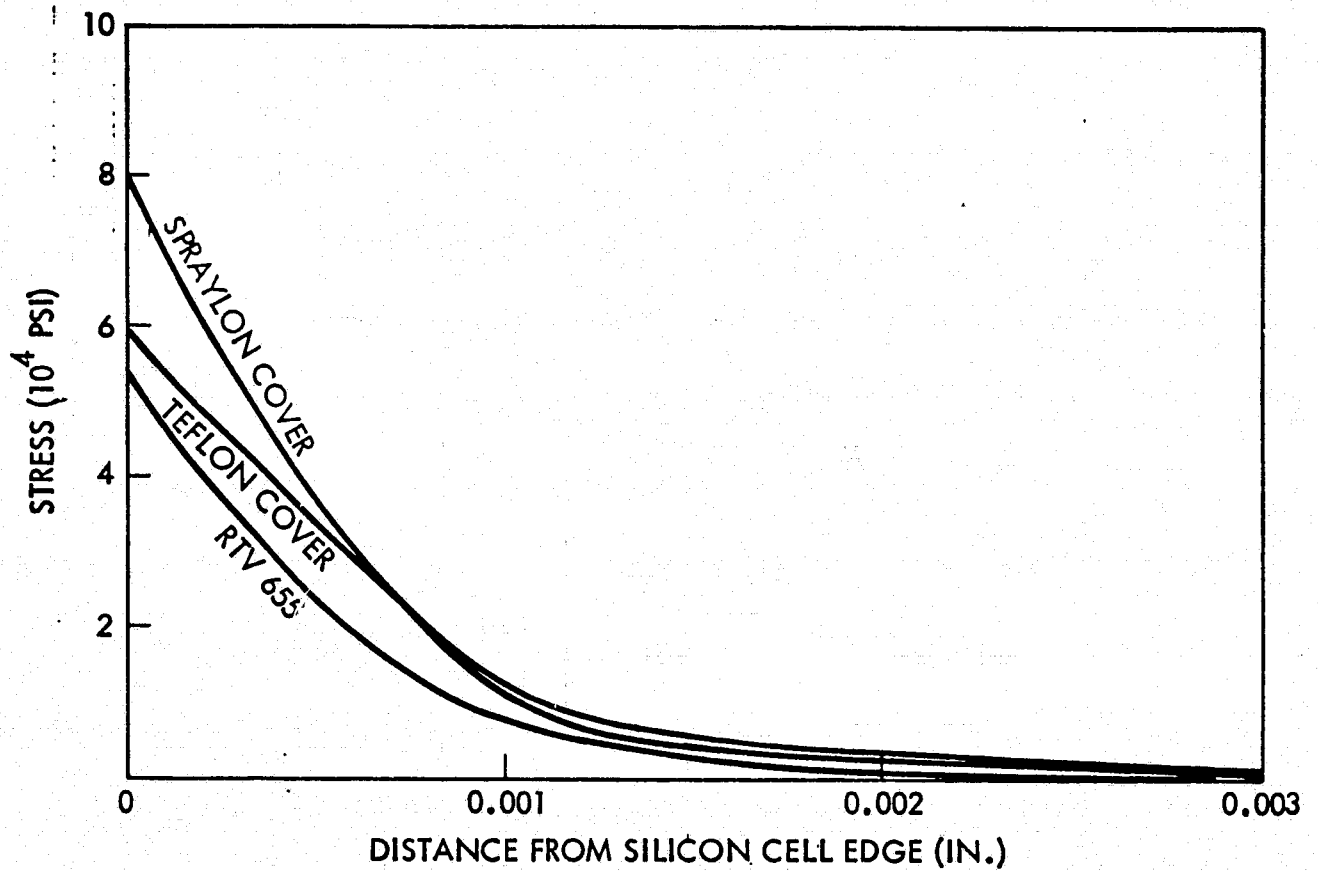


Fig. 3-33 Shear Stresses Between Invar and Silicon Cell at the Interconnected Area for Different Cover Materials at  $-320^{\circ}\text{F}$

## Section 4

### DISCUSSION OF TEST RESULTS AND OBSERVATIONS

#### 4.1 SELECTION OF MATERIALS

Consideration of a replacement for the costly fused silica-cover glass for silicon solar cells has led to a primary emphasis on stable organic materials of high transmittance in the spectral region of solar-cell response. The organic materials that can be considered are mostly silicones or fluorocarbons (or modifications thereof). These materials have shown excellent stabilities in most harsh environments. However, these materials have their limitations. In particular, the stabilities of these materials are strongly influenced not only by total incident energy (fluence) but also by rate (flux) of the electromagnetic and charged-particle radiations. In addition, reaction temperature during irradiation plays an important role in optical as well as mechanical properties degradation.

An analysis of the test data has been made to assess the attributes and the deficiencies of the candidate solar-cell cover materials tested for their application in various mission environments. The usefulness of these materials in specified environments will be dependent upon the expected life in the mission environment. Because most testing is accelerated, the validity of reciprocity between intensity and exposure time cannot be assumed. More real-time testing would have to be done to establish reasonable confidence levels. There will be obvious limitations in attempts at extrapolation because the test conditions are so varied. An additional caveat is that the results reported are also for those materials which were supplied for testing by others. No judgment is made as to whether those materials supplied are optimum.

## 4.2 SPRAYLON ENCAPSULANT TEST RESULTS

- Low-Intensity UV Exposure

1 sun at 120°C

808 ESH - 10% maximum power loss

2 suns at 120°C

1616 ESH - 10% maximum power loss

- High-Intensity UV Exposure

10 suns at 120°C

800 ESH - 10% maximum power lost

1870 ESH - 15% maximum power lost

3000 ESH - 26% maximum power lost

4280 ESH - 51% maximum power lost

Figure 4-1 shows the cell performance (maximum power output) degradation as a function of the equivalent sun hours of exposure for conditions of 1, 2, 5, and 10 suns intensity. It is evident that there is no reciprocity of suns intensity and equivalent sun hours for the range of intensities investigated. Replotting the data in the form of degradation as a function of hours of exposure (Fig. 4-2), the evidence is very strong that Spraylon stability is dependent on solar intensity.

## 4.3 SILICONE ENCAPSULANT TEST RESULTS

Silicones are not intensity-dependent. Their degradation is dependent upon net hours of exposure at elevated temperature.

### Test Results of G.E. RTV 655 and Dow Corning 93500 Silicones

- Low-Intensity UV Exposure (G.E. RTV 655)

808 ESH at 1 sun intensity and 120°C

32% maximum power lost

1616 ESH at 2 suns intensity and 120°C

33% maximum power lost

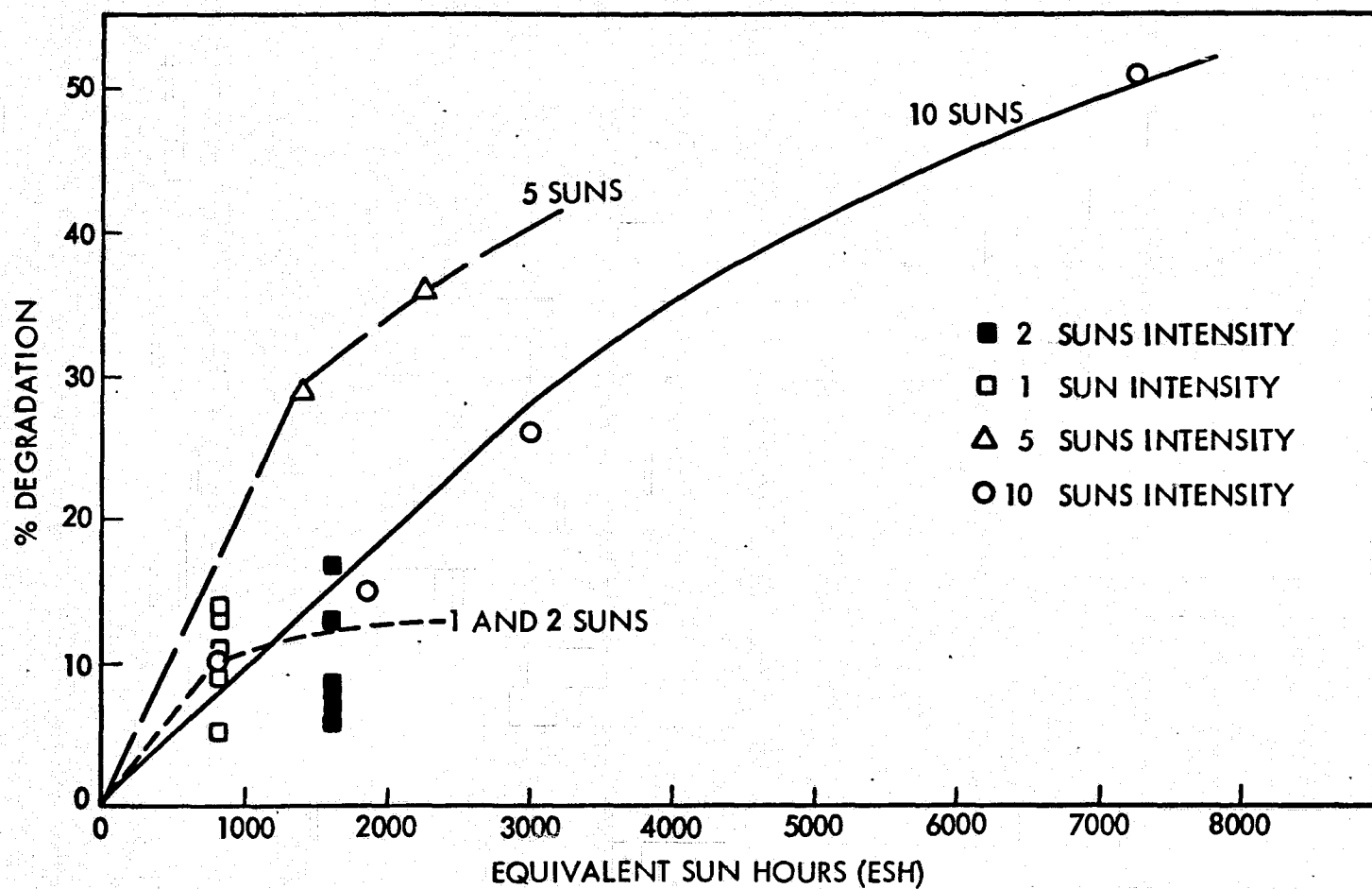


Fig. 4-1 UV Degradation of Silicon Cell Maximum Power as a Function of Equivalent Sun Hours (ESH) at 120° C for Spraylon Cover

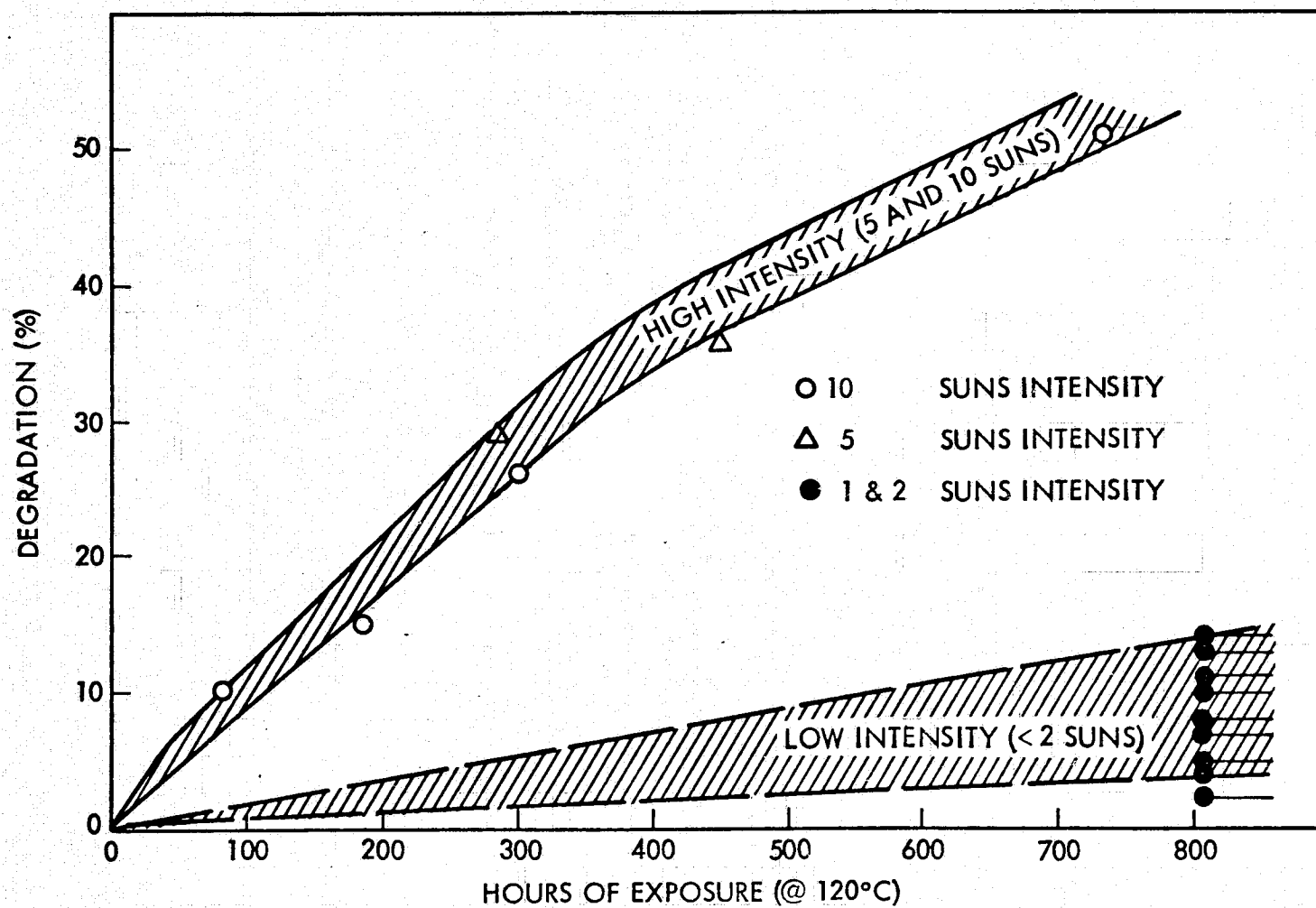


Fig. 4-2 UV Degradation of Silicon Cell Maximum Power as a Function of Hours of Exposure at 120° C for Spraylon Cover

- High-Intensity UV Exposure
  - a. G.E. RTV 655 Silicone  
7280 ESH at 10 suns intensity and 120°C  
24.2% maximum power lost
  - b. Dow Corning 93500 Silicone  
2850 ESH at 10 suns intensity and 120°C  
19% maximum power lost  
4500 ESH at 10 suns intensity and 120°C  
19% maximum power lost
- UV Plus High-Energy Electrons Environment  
G.E. RTV 655 Silicone  
1 MeV electrons -  $5 \times 10^{15} \text{ e}^-/\text{cm}^2$   
5 suns UV at 120°C, 800 ESH  
53% maximum power lost
- UV Plus Low-Energy Protons Environment  
G.E. RTV 655 Silicone  
100 keV -  $5 \times 10^{15} \text{ p}^+/\text{cm}^2$   
5 suns at 120°C, 800 ESH  
20% maximum power lost

Figure 4-3 shows the cell performance as a function of equivalent sun hours of exposure for 1, 2, 5, and 10 suns intensity. Figure 4-4 shows that there is approximate reciprocity between sun intensity and equivalent sun hours of exposure.

#### 4.4 FEP TEFLON ENCAPSULANT TEST RESULTS

- UV Environment at 120°C  
The results show no intensity dependence; degradation is a function of equivalent sun hours of exposure. The test results showed a maximum power loss of 12% for FEP Teflon at 120°C and 4500 ESH.

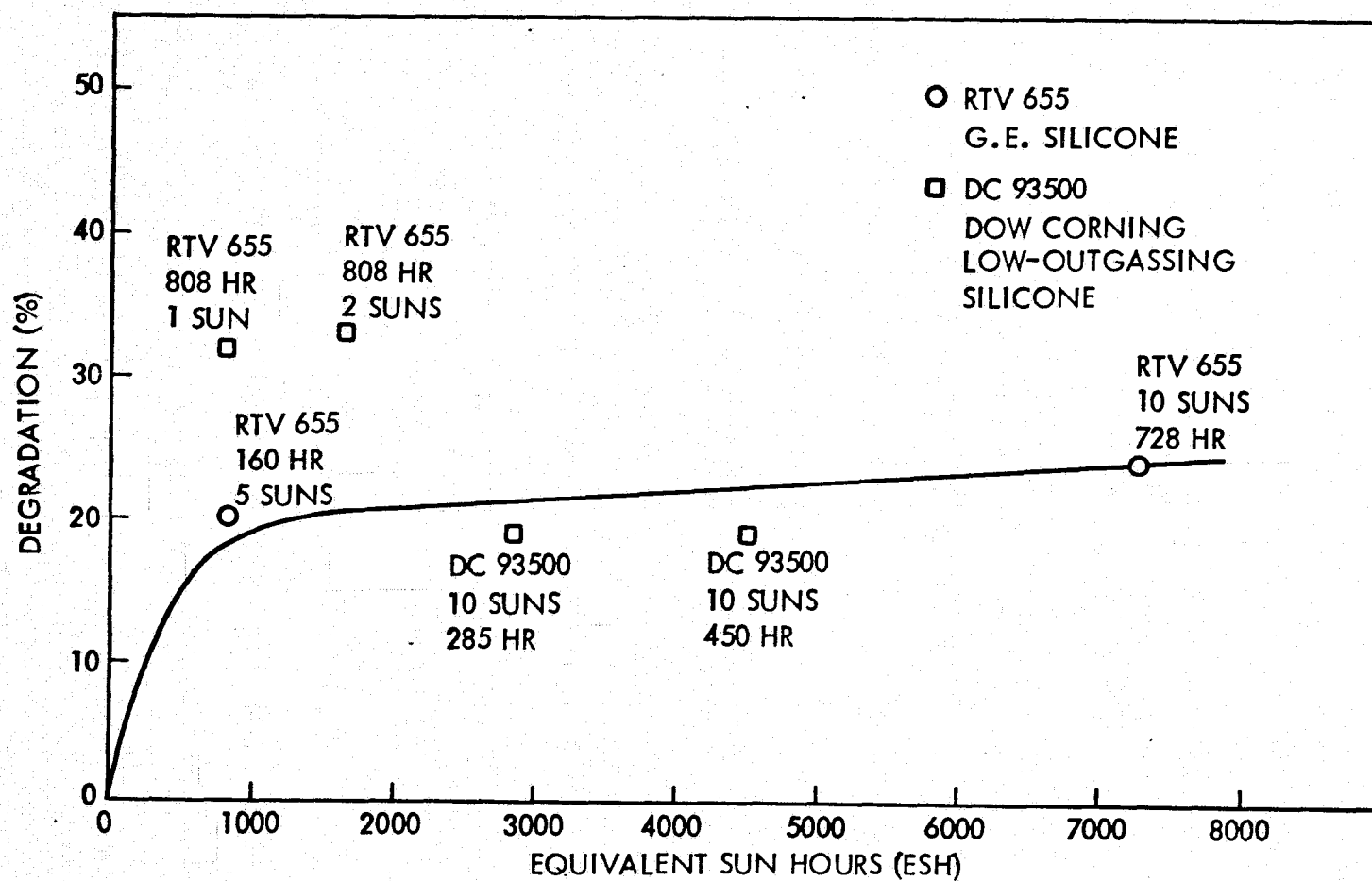


Fig. 4-3 UV Degradation of Silicon Cell Maximum Power as a Function of Equivalent Sun Hours (ESH) at 120°C for Silicone Cover

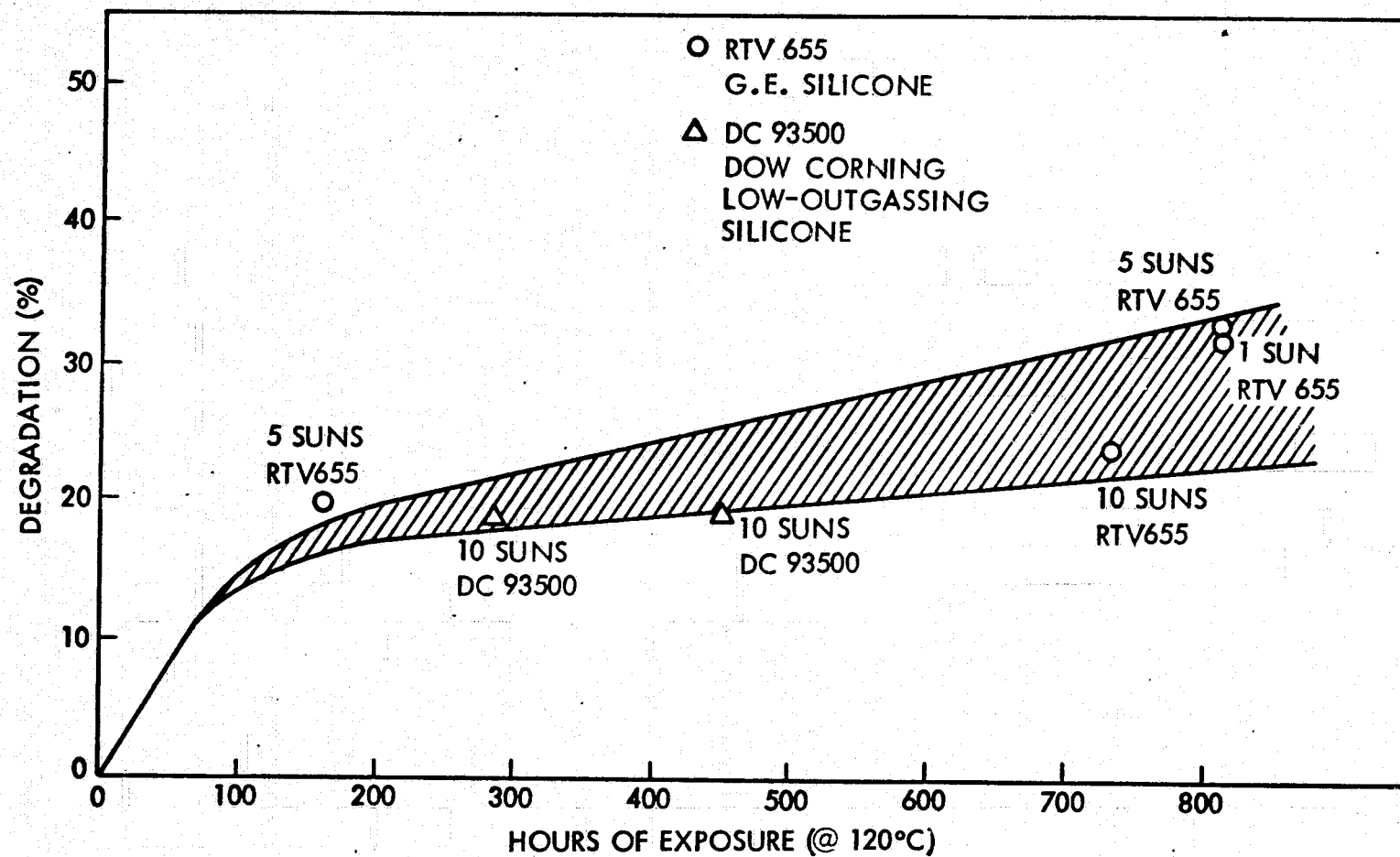


Fig. 4-4 UV Degradation of Silicon Cell Maximum Power as a Function of Hours of Exposure at 120° C for Silicone Cover 1 to 10 Suns Intensity



FEP Teflon is the most stable of the organic materials. The data from Table 4-1 show considerable scatter and inconsistencies, i.e., 1-mil FEP Teflon shows higher power loss than 2-mil FEP Teflon.

- UV + High-Energy Electrons (1 MeV)  $5 \times 10^{15} \text{ e}^-/\text{cm}^2$  at 120°C  
800 ESH at 5 suns

An average power loss of 48% was measured for this environment. This is consistent with results of other materials. In addition to silicone damage to electron penetration, the FEP Teflon suffers serious mechanical failure due to cracking and flaking.

- UV + Low-Energy Protons (100 KeV)  $5 \times 10^{15} \text{ p}^+/\text{cm}^2$  at 120°C  
800 ESH at 5 suns

Maximum power loss is less than 10% and represents mainly UV damage.

FEP Teflon is the most stable candidate for silicon solar cells in the environments considered. The exception to the acceptability of its use is in a high-energy electron radiation environment. This is true of all other candidate organic materials evaluated.

#### 4.5 GLASS RESIN ENCAPSULANT TEST RESULTS

It was anticipated that the optimum formulation would be provided for the testing that was to be done. A number of differing formulations of limited quantities were provided.

Referring to Tables 3-9, 3-11, and 3-12, the data show serious mechanical damage in addition to yellowing. The following summarizes the test data:

- High-Intensity UV Exposure  
10 suns, 1650 ESH, 120°C  
GR908 coating yellowed  
39% loss in maximum power output

Table 4-1

## SUMMARY OF RESULTS OF UV IRRADIATION - FEP TEFLON AT 120°C

Cell No.	Teflon Thickness (mils)	UV Intensity (suns)	ESH	Maximum Power Lost (%)
V12	2	5	2250	7
	2	5	1425	4
V15	2	5	2250	12
	2	5	1425	7
V18	2	10	4500	10
	2	10	2850	7
V13	1	5	2250	13
	1	5	1425	9
V23	1	10	4500	11
	1	10	2850	8

- UV Plus Low-Energy Proton Environment

(100 KeV)  $5 \times 10^{15} \text{ p}^+/\text{cm}^2$

800 ESH at 5 suns at 120°C

- a. GR908M glass resin yellowed after UV + protons; gross flaking and crazing after thermal cycling
- b. 

GR100 and GR908	}	glass resin	{	yellowing and flaking after UV + protons; gross flaking and increased crazing after thermal cycling
-----------------------	---	-------------	---	--

- UV Plus High-Energy Electrons Environment

(1 MeV)  $5 \times 10^{15} \text{ e}^-/\text{cm}^2$

800 ESH at 5 suns and 120°C

- a. GR908M — Small amount of yellowing
- b. GR100 — Badly flaked, 10% residual
- c. GR908 — Flaking surface

The glass-resin coatings showed poor stability in all test environments. In general, the modified glass-resin coatings were mechanically superior to the unmodified. The unmodified showed extensive crazing and flaking. Changes in power output of the glass resin-coated cells were not reported since post-test I/V characteristics were not measured.

#### 4.6 COMPARATIVE ENCAPSULANT EVALUATION

The performance characteristics of the candidate materials are compared in Table 4-2.

Extrapolation of the test data to long-term solar-array performance necessarily requires some major assumptions with respect to the damage mechanisms and kinetics of the candidate encapsulant materials. As a first approximation, it is generally necessary to establish whether reciprocity exists between incident ultraviolet intensity and exposure time in order to determine the validity of accelerated testing. In this study, the data obtained for Spraylon and silicone materials indicate that this simple

Table 4-2  
SUMMARY OF RADIATION EFFECTS ON CANDIDATE MATERIALS

Material	Environment (at 120° C)	Test Period (Equivalent Sun Hours ESH)	Maximum Power Lost (%)
Spraylon	Low-Intensity UV <sup>(b)</sup>	1600	10
	High-Intensity UV	7800	51
Silicone	Low-Intensity UV	1600	33
	High-Intensity UV	7800	24
	5 Sun Intensity UV + 1 MeV Electrons <sup>(b)</sup>	800	53
	5 Sun Intensity UV + 100 KeV Protons <sup>(c)</sup>	800	20
FEP Teflon	High-Intensity UV	4500	13
	5 Sun Intensity UV + 1 MeV Electrons	800	48
	5 Sun Intensity UV + 100 KeV Protons	800	7
Glass Resin	High-Intensity UV	1650	39

(a) Intensity: Low: 1 to 2 Suns  
High: 5 to 10 Suns

(b) Electron Fluence:  $5 \times 10^{15} \text{ e/cm}^2$

(c) Proton Fluence:  $5 \times 10^{15} \text{ p/cm}^2$

assumption of reciprocity is not valid, since presentation of the data (Figs. 4-1 and 4-3) shows that degradation does not correlate well with equivalent sun hours of exposure.

The demonstrated deviations from reciprocity indicate that the damage mechanisms for the candidate materials are complex and that first-order kinetic processes are not operative. Presentation of the degradation with respect to total hours of UV

exposure at 120° C (Figs. 4-2 and 4-4) provides some insight into the photolytic processes. For the silicone materials, despite some data scatter, there exists a direct correlation with exposure duration, independent of incident intensity. This type of behavior can be qualitatively explained in terms of a primary process that generates chromophoric groups followed by time and temperature-dependent non-photochemically activated processes (rearrangement, cross linking, etc.).

For Spraylon photodegradation, there is strong evidence for a free radical mechanism. The dissociation energies for the C-F and C-H bonds are 107 kcal/mole and 87 kcal/mole, respectively, which correspond to wavelengths of approximately 3300 Å and 2600 Å. Since there is significant output of the UV lamps in this spectral region and appreciable absorption by the Spraylon, it is reasonable to assume that both H· and F· radicals can be formed in the primary photochemical process. The reactive radicals can easily abstract additional H or F atoms forming hydrofluoric acid (HF). Irradiated Spraylon films stripped from aluminum substrates showed definite evidence of etching of the metal, substantiating the existence of a dehydrohalogenation process.

Figure 4-2 demonstrates that two distinct stages in degradation occur, in that degradation kinetics differ drastically for high (5 to 10 suns) and low (1 to 2 suns) intensities. By analogy to the photolysis of polyvinyl chloride films, it is postulated that the relatively fast initial stage depends upon intensity of irradiation and temperature, while the second slower stage is less dependent on both these parameters. This effect may be connected with the inhibition of polymer degradation by dissolved HF through readdition to the carbon-carbon double bonds.

The browning observed during high-temperature UV exposure of Spraylon is attributed to formation of conjugated double bonds (polymers), with increased extent of conjugation moving the absorption band further into the visible spectral region. The rate of discoloration formation may therefore be related to the diffusion characteristics of the generated HF. This would account for the apparently greater degradation rate at 5 suns compared to 10 suns (Fig. 4-1), since at the higher intensity, the probability of readdition of HF across the double bonds would be enhanced through increased HF concentration.

From a phenomenological viewpoint, the degradation mechanisms and kinetics of the Spraylon and silicone materials are sufficiently dissimilar so as to preclude direct intercomparison and extrapolation for all exposure parameters. Consequently, the extrapolations of long-term performance characteristics have been based more on direct data projections for specific exposures than for generalized properties.

#### 4.7 PARAMETRIC STRESS ANALYSIS

Part of the stress analysis investigation was the nature of cell fracturing in the area of the front-surface current collection grid. The conclusions were that the existence of microcracks did not affect the thermal-mechanical stability of the silicon cell. However, it is important to note that this observation applies only to the 12-mil Spectrolab cell and the particular metal grid vacuum deposition process used. In this cell, the macroscopic fracture plane extended to a depth of 4 mils. This may not be a problem for a 12-mil cell but could be a serious problem in the case of a 2-mil cell. Since the 2-mil, Solarex cell has a sintered metal coating, the observed fracturing may not be a problem. The grid-structure adhesion was not good for the cells tested. The grid could be lifted relatively easily - this implies, the adhesion being poor, that there was little induced stress that could cause fracturing. Process change resulting in good adhesion could cause fracture problems in the 2-mil cells.

The stresses in the solar cell laminate structure were investigated for the conditions of thermal cycling to  $-320^{\circ}\text{F}$ . The critical areas of concern were the cell cover and the silicon cell and, specifically, cell edges and interconnect areas. In addition, stress reversal during cycling could lead to problems of fatigue failure in the cover as well as the interconnect. By use of a developed LMSC composite laminate code, stress distributions in the cell composites of various designs were calculated. The results showed the range of cover, cell, and substrate thicknesses allowable to prevent excessively high stresses. The test results of free standing cells or small submodules in thermocycling tests may not be adequate to judge the validity of these tests in larger arrays where freedom to bow may be inhibited.

The plane-strain analysis for edge stresses points out the very large shear stress at the cell edge which rapidly falls off away from edge. This characteristic shows the importance of having good cover to cell bonding to prevent delamination. Similarly, it is desirable to weld interconnects as far away from edge as is practical. In the case of soldered interconnects, the solder bus is usually at the edge. From a stress point of view, it would be desirable also to locate the bus bar away from the edge. In almost all cases of cover failure in thermocycling, the failure was initiated at the solder bus bar.

## Section 5

### CONCLUSIONS AND RECOMMENDATIONS

#### 5.1 CONCLUSIONS

A number of candidate materials have been evaluated with respect to performance as solar cell covers operating at 120°C. The major conclusions of this program based on the limited test data are:

- Finite element analysis techniques permit definition of solar-array configurations consistent with thermal cycling constraints. The experimental results quantitatively confirm the analytical predictions of thermally-induced stress failure regimes for specific configurations.
- At high solar intensities (5 to 10 equivalent suns), Spraylon, RTV-655, and glass resin systems exhibited substantial degradation of optical properties, leading to reductions in solar cell power outputs exceeding 20% for a one-month exposure.
- At high solar intensity, FEP Teflon exhibited the best stability of all materials tested.
- Both Spraylon and RTV-655 showed complex time-intensity degradation kinetics, which precludes extrapolation of degradation by conventional reciprocity considerations using accelerated testing data.
- At low solar intensities (1 to 2 suns), Spraylon appears to be more stable than the silicone materials; however, the test data are insufficient to establish long-term performance characteristics.

#### 5.2 RECOMMENDATIONS

The requirements of advanced state-of-the-art low-cost, lightweight solar arrays are consistent with the use of polymeric solar cell cover systems. To demonstrate the



utility of this approach, the following recommendations for future work are proposed:

- Test and evaluate radiation stability of candidate cover materials for specific environmental requirements using real-time testing at temperature.
- Perform mechanical testing of single cell and multicell modules for cell restraint effects on cell stress.
- Evaluate test cell interconnect configurations for thermal cycling survivability.
- Investigate the feasibility of incorporating UV inhibitors in the polymer films to retard optical degradation.
- Investigate the use of electrical conductive additives to the polymer films to ameliorate electrical discharge damage related to surface charging from charged-particle irradiation.
- Explore alternative cover materials including inorganic films applied by chemical or physical vapor deposition processes including ion plating, sputtering, and thermal evaporation with prestressed silicon solar cells.

**Appendix A**  
**TABLE OF THERMAL-UV STABILITY**  
**OF SILANE PRIMER/SPRAYLON**

Table A-1

**THERMAL - UV STABILITY  
SILANE PRIMER/SPRAYLON  
ALCLAD 6061 SUBSTRATES**

**Parameters:** Silane Composition and Concentration, Spraylon Material/Processing, Time, Temperature, and UV Intensity During UV Exposure

**Primer:** D.C., Dow Corning - G.E., General Electric - U.C., Union Carbide (Primers Diluted in MeOH)

Primer	Concentration (%)	Spraylon Material and Treatment	Temperature (°C)	Time UV Exposure (ESH)	Solar Intensity (suns)	Spraylon Thickness (mils)	Comments
D.C. Z6020	0.1	Primer only (No Spraylon) ↓	120	120	10	0	No discoloration
D.C. Z6020	0.1		>180	240	20	0	Light straw color
D.C. Z6011	0.1		>200	480	40	0	No discoloration (primer volatilized off)
D.C. Z6011	1.0		120	120	10	0	No discoloration
D.C. Z6011	1.0		>180	240	20	0	Brown/blue discoloration
D.C. Z6011	1.0		>200	480	40	0	Light straw color
D.C. Z6011	2.0		120	120	10	0	Slight straw color
D.C. Z6011	2.0		>180	240	20	0	Gray-blue color
D.C. Z6011	2.0		>200	480	40	0	Light straw color
D.C. Z6011	2.0		120	900	20	0	Few straw color spots

A-2

ORIGINAL PAGE IS  
OF POOR QUALITY

Table A-1 (Cont.)

Primer	Concentration (%)	Spraylon Material and Treatment	Temperature (°C)	Time UV Exposure (ESH)	Solar Intensity (suns)	Spraylon Thickness (mils)	Comments
D.C. Z6082	2.0	Primer only (No Spraylon)	180	312	5	0	No discoloration
D.C. Z6082	2.0	↓	180	624	10	0	Minor spots, straw-colored
G.E. 4120	5.0	↓	18	323	5	0	No discoloration
G.E. 4120	10.0	↓	18	323	5	0	No discoloration
G.E. 4120	33.0	↓	18	323	5	0	Minor discoloration
D.C. Z6020	0.2	↓	18	323	5	0	No discoloration
D.C. Z6020	10.0	↓	18	323	5	0	No discoloration
U.C. A1100	5.0	Primer only (No Spraylon)	18	323	5	0	No discoloration
D.C. Z6082	2.0	1201 Spraylon	18	312	5	3	No discoloration
D.C. Z6082	2.0	↓	280	2496	40	3	Light brown
D.C. Z6020	0.1	↓	> 200	480	40	3	Dark brown color
D.C. Z6011	1.0	↓	> 200	480	40	3	Black
D.C. Z6011	2.0	1201 Spraylon	> 200	480	40	3	Black

Table A-1 (Cont.)

Primer	Concentration (%)	Spraylon Material and Treatment	Temperature (°C)	Time UV Exposure (ESH)	Solar Intensity (suns)	Spraylon Thickness (mils)	Comments
D.C. Z6020	0.1	1201 Spraylon	> 180	240	20	3	Black
No Primer	—		18	323	5	2	No discoloration
G.E. 4120	5.0		18	323	5	5	No discoloration
D.C. Z6020	0.1		18	323	5	3	No discoloration
U.C. A1100	5.0		18	323	5	3	No discoloration
D.C. Z6020	10.0		18	323	5	3	No discoloration
D.C. Z6020	0.2		18	323	5	3	No discoloration
D.C. Z6020	0.2		180	624	10	3	Straw color
D.C. Z6011	1.0		120	900	20	3	Straw color
D.C. Z6011	2.0		120	900	20	3	Light straw color
D.C. Z6011	1.0		120	450	10	3	Slight straw color
D.C. Z6011	2.0		120	450	10	3	Slight straw color
D.C. Z6020	0.1	1201 Spraylon	120	450	10	3	Slight straw color

A-4

ORIGINAL PAGE IS  
OF POOR QUALITY

Table A-1 (Cont.)

Primer	Concentration (%)	Spraylon Material and Treatment	Temperature (°C)	Time UV Exposure (ESH)	Solar Intensity (suns)	Spraylon Thickness (mils)	Comments
D.C. Z6020	0.1	1201 Spraylon	120	900	20	3	Light straw color
No Primer	—	1201 Spraylon	120	900	20	3	Light straw color; poor Spraylon adhesion
No Primer	—	1201 Spraylon	120	450	10	3	Light straw color; poor Spraylon adhesion
No Primer	—	Nov 1976 Batch 1201 Spraylon	155	310	5	3	Straw color (delamination)
No Primer	—	New batch 1201 Spraylon	155	310	5	3	Straw color (delamination)
No Primer	—	New batch 1201 Spraylon	155	620	10	3	Straw color (delamination)
No Primer	—	Nov 1976 batch 1201 Spraylon	155	620	10	3	Straw color (delamination)
D.C. Z6020	0.1	New batch 1201 Spraylon	155	310	5	3	Light straw color
D.C. Z6020	0.1	New batch 1201 Spraylon	155	620	10	3	Light straw color
D.C. Z6020	0.1	New batch 1201 Spraylon	135	190	10	3	Slight straw color
D.C. Z6020	0.1	Old batch + 1/4-gm glacial acetic acid	135	190	10	3	Slight straw color

Table A-1 (Cont.)

Primer	Concentration (%)	Spraylon Material and Treatment	Temperature (°C)	Time UV Exposure (ESH)	Solar Intensity (suns)	Spraylon Thickness (mils)	Comments
No Primer	—	New batch 1201 Spraylon	135	190	10	3	Slight straw color
D.C. Z6011	1.0	Old batch Spraylon	135	190	10	3	Straw color (delaminated)
D.C. Z6011	1.0	Old batch Spraylon	135	380	20	3	Straw color (delaminated)
D.C. Z6011	0.1	Old batch Spraylon + 1/4 acetic acid	135	380	20	3	Light straw
D.C. Z6020	0.1	Old batch	135	380	20	3	Light straw
No Primer	—	Old batch Spraylon	135	380	20	3	Light straw (delaminated)
No Primer	—	Old batch + 1/4 acetic acid	135	380	20	3	Light brown (delaminated)
D.C. Z6020	0.1	15% 1201 Spraylon	146	160	10	3	Very slight straw color
D.C. Z6020	0.1	15% 1201 Spraylon + acetic acid	146	160	10	3	Slight straw color
D.C. Z6020	0.1	15% 1201 Spraylon + 1/3 acetic acid	146	160	10	3	Very slight straw color

A-6

ORIGINAL PAGE IS  
OF POOR QUALITY

Table A-1 (Cont.)

Primer	Concentration (%)	Spraylon Material and Treatment	Temperature (°C)	Time UV Exposure (ESH)	Solar Intensity (suns)	Spraylon Thickness (mils)	Comments
D.C. Z6020	0.1	15% 1201 Spraylon	146	320	20	3	Very slight straw color
D.C. Z6020	0.1	15% 1201 Spraylon	146	320	20	3	Very slight straw color
D.C. Z6020	0.1	15% 1201 Spraylon	146	320	20	3	Light straw color
D.C. Z6020	0.1	15% 1201 Spraylon + 1/3 acetic acid	146	320	20	3	Slight straw
D.C. Z6011	1.0	15% 1201 Spraylon + acetic acid	146	320	20	3	Light straw
D.C. Z6011	1.0	15% 1201 Spraylon	146	160	10	3	Light straw color
D.C. Z6011	1.0	15% 1201 Spraylon + 1/3 acetic acid	146	160	10	3	Light straw color
D.C. Z6020	0.1	15% 1201 Spraylon	156	160	10	3	Light straw color
D.C. Z6020	0.1	15% 1201 Spraylon + 0.05% Tinuvin P	156	160	10	3	Light straw color



Table A-1 (Cont.)

Primer	Concentration (%)	Spraylon Material and Treatment	Temperature (°C)	Time UV Exposure (ESH)	Solar Intensity (suns)	Spraylon Thickness (mils)	Comments
D.C. Z6020	0.1	15% 1201 Spraylon + 0.1% Tinuvin P	156	160	10	3	Light straw color
D.C. Z6020	0.1	15% 1201 Spraylon + 1.0% Tinuvin P	156	160	10	3	Light straw color
D.C. Z6020	0.1	15% 1201 Spraylon + 1% Tinuvin P	156	320	20	3	Medium straw color
D.C. Z6020	0.1	15% 1201 Spraylon + 1% Tinuvin 328	156	320	20	3	Straw color
D.C. Z6020	0.1	15% 1201 Spraylon + 1% Tinuvin 328	156	160	10	3	Straw
D.C. Z6020	0.1	15% 1201 Spraylon + HCl	156	160	10	3	Light straw
D.C. Z6020	0.1	15% 1201 Spraylon + HCl	156	320	20	3	Straw

A-8 ORIGINAL PAGE IS OF POOR QUALITY

Table A-1 (Cont.)

Primer	Concentration (%)	Spraylon Material and Treatment	Temperature (°C)	Time UV Exposure (ESH)	Solar Intensity (suns)	Spraylon Thickness (mils)	Comments
D.C. Z6020	0.1	15% 1201 Spraylon + HCl	156	320	20	3	Straw
D.C. Z6020	0.1	15% 1201 Spraylon + Trace Hydroquinone	125	140	10	3	Dark straw color
D.C. Z6020	0.1	15% 1201 Spraylon + Trace Hydroquinone	125	280	20	3	Dark straw color
D.C. Z6020	0.1	15% 1201 Spraylon + Trace Hydroquinone	125	280	20	3	Dark straw color
D.C. Z6020	0.1	15% 1201 Spraylon + Trace HQ + Tinuvin P	125	140	10	3	Dark straw color
D.C. Z6020	0.1	15% 1201 Spraylon + Trace HQ + Tinuvin P	120	280	20	3	Dark straw color
D.C. Z6020	0.1	15% 1201 Spraylon +2X Trace HQ	125	140	10	3	Straw color

Table A 1 (Cont.)

Primer	Concentration (%)	Spraylon Material and Treatment	Temperature (°C)	Time UV Exposure (ESH)	Solar Intensity (suns)	Spraylon Thickness (mils)	Comments
No Primer	—	15% 1201 Spraylon Deionized Water Washed	111	150	10	3	Slight straw
No Primer	—	15% 1201 Spraylon Deionized Water Washed	121	300	20	3	Light straw
D.C. Z6020	0.1	15% 1201 Spraylon Deionized Water Washed	111	150	10	3	Light straw
D.C. Z6020	0.1	15% 1201 Spraylon Deionized Water Washed	121	300	20	3	Light straw
No Primer	—	15% 1201 Spraylon + 0.1% BaO	111	150	10	3	Slight straw
D.C. Z6020	0.1	15% 1201 Spraylon +0.1% BaO	111	150	10	3	Slight straw

A-10

ORIGINAL PAGE IS  
OF POOR QUALITY

Table A-1 (Cont.)

Primer	Concentration (%)	Spraylon Material and Treatment	Temperature (°C)	Time UV Exposure (ESH)	Solar Intensity (suns)	Spraylon Thickness (mils)	Comments
D.C. Z6020	0.1	15% 1201 Spraylon + 0.1% BaO	121	300	20	3	Slight straw
D.C. Z6020	0.1	15% 1201 Spraylon + 0.5% BaO	111	150	10	3	Light straw
Un-primed	—	15% 1201 Spraylon	108	170	10	3	Slight straw color
D.C. Z6020	0.1	15% 1201 Spraylon	108	170	10	3	Slight straw color
D.C. Z6020	0.1	15% 1201 Spraylon HCl Acid Washed	116	340	20	3	Slight straw color
D.C. Z6020	0.1	15% 1201 Standard Spraylon	108	600	10	3	Slight straw color
D.C. Z6020	0.1	15% 1201 Standard Spraylon	113	1200	20	3	Light straw color
D.C. Z6020	0.1	15% 1201 Spraylon HCl Washed	108	600	10	3	Slight straw

Table A-1 (Cont.)

Primer	Concentration (%)	Spraylon Material and Treatment	Temperature (°C)	Time UV Exposure (ESH)	Solar Intensity (suns)	Spraylon Thickness (mils)	Comments
D.C. Z6020	0.1	15% 1201 Spraylon HCl Washed	113	1200	20	3	Light straw
D.C. Z6020	0.1	15% 1201 Spraylon Acetic Acid Washed	108	600	10	3	Slight straw
D.C. Z6020	0.1	15% 1201 Spraylon Acetic Acid Washed	113	1200	20	3	Light straw
D.C. Z6020	0.1	15% 1881 Spraylon HCl Washed Powder	108	600	10	3	Medium straw color
D.C. Z6020	0.1	15% 1881 Spraylon HCl Washed Powder	113	1200	20	3	Straw color
D.C. Z6020	0.1	15% 1901 Spraylon HCl Washed	108	600	10	3	Light straw color
D.C. Z6020	0.1	15% 1901 Spraylon HCl Washed	113	1200	20	3	Light straw color

A-12

ORIGINAL PAGE IS  
OF POOR QUALITY

Table A-1 (Cont.)

Primer	Concentration (%)	Spraylon Material and Treatment	Temperature (°C)	Time UV Exposure (ESH)	Solar Intensity (suns)	Spraylon Thickness (mils)	Comments
D.C. Z6020	0.1	15% A Spraylon (11-3-76)	119	170	10	3	Slight straw color
D.C. Z6020	0.1	15% A Spraylon (11-3-76)	124	340	20	3	Light straw
D.C. Z6020	0.1	1201 Spraylon HCl Washed MeOH Washed Vac Oven Dry Sintered Glass Filter	119	170	10	3	Slight straw color
D.C. Z6020	0.1	1201 HCl Washed MeOH Washed Vac Oven Dry Sintered Glass Filter	124	340	20	3	Slight straw color
D.C. Z6020	0.1	1201 Spraylon + Oxalic Acid (1/2 gm)	119	170	10	3	Light straw color
D.C. Z6020	0.1	1201 Spraylon + Oxalic Acid (1/2 gm)	124	340	20	3	Light straw color
D.C. Z6020	0.1	1201 Spraylon + Oxalic Acid (1/4 gm)	119	170	10	3	Light straw color

Table A-1 (Cont.)

Primer	Concentration (%)	Spraylon Material and Treatment	Temperature (°C)	Time UV Exposure (ESH)	Solar Intensity (suns)	Spraylon Thickness (mils)	Comments
D.C. Z6020	0.1	1201 Spraylon + Oxalic Acid (1/4 gm)	124	340	20	3	Straw color
D.C. Z6020	0.1	1201 Spraylon + Acetic Acid	119	170	10	3	Slight straw color
D.C. Z6020	0.1	1201 Spraylon + Acetic Acid (1/4 gm)	124	340	20	3	Light straw color
D.C. Z6020	0.1	1201 Spraylon HCl Washed	118	170	10	3	Slight straw color
D.C. Z6020	0.1	1201 Spraylon HCl Washed	122	340	20	3	Slight straw color
D.C. Z6020	0.1	1201 Spraylon + Nickel Dibutyldithio Carbamate	118	170	10	3	Light straw color
D.C. Z6020	0.1	1201 Spraylon + Nickel Dibutyldithio Carbamate	122	340	20	3	Straw color
D.C. Z6020	0.1	1201 Spraylon + Nickel Dimethyl	118	170	10	3	Light straw color
D.C. Z6020	0.1	1201 Spraylon + Nickel Cyclopenta	118	170	10	3	Straw color

A-14

ORIGINAL PAGE IS  
OF POOR QUALITY

Table A-1 (Cont.)

Primer	Concentration (%)	Spraylon Material and Treatment	Temperature (°C)	Time UV Exposure (ESH)	Solar Intensity (suns)	Spraylon Thickness (mils)	Comments
D.C. Z6020	0.1	1201 Spraylon + di-t-Butyl Hydroperoxide	118	170	10	3	Slight straw
D.C. Z6020	0.1	1201 Spraylon + di-t-Butyl Hydroperoxide	122	340	20	3	Light straw color
D.C. Z6020	0.1	1201 Spraylon Powder Vac. Degassed 1 hr at 125°C	118	170	10	3	Slight straw color
D.C. Z6020	0.1	1201 Spraylon Powder Vac. Degassed 1 hr at 125°C	122	340	20	3	Light straw color
D.C. Z6020	0.1	1201 Spraylon Press Sintered Powder at 390°F	118	170	10	16	Straw color
D.C. Z6020	0.1	1201 Spraylon Press Sintered Powder at 390°F	122	340	20	16	Straw color

ORIGINAL PAGE IS  
OF POOR QUALITY

A-15



Table A-1 (Cont.)

Primer	Concentration (%)	Spraylon Material and Treatment	Temperature (°C)	Time UV Exposure (ESH)	Solar Intensity (suns)	Spraylon Thickness (mils)	Comments
D.C. Z6020	0.1	1201 Spraylon Cast from MeOH Powder Cured at 360°F	118	170	10	1.5	Slight straw color
D.C. Z6020	0.1	1201 Spraylon HCl Washed	117	130	10	5.5	Slight straw color
D.C. Z6020	0.1	1201 Spraylon Powder Vac. Dried at 125°C	117	130	10	4.5	Slight straw color
D.C. Z6020	0.1	1201 Spraylon Powder Vac. Dried at 125°C	119	260	20	5	Slight straw color
D.C. Z6020	0.1	1201 Spraylon Powder Washed in Freon Benzene HCl Deionized Water Vac. Dried at 125°C	117	130	10	3	Slight straw color
D.C. Z6020	0.1	1201 Spraylon Powder Washed in Freon Benzene HCl Deionized Water Vac. Dried at 125°C	119	260	20	3	Slight straw color

Table A-1 (Cont.)

Primer	Concentration (%)	Spraylon Material and Treatment	Temperature (°C)	Time Exposure (ESH)	Solar Intensity (suns)	Spraylon Thickness (mils)	Comments
SS4120 Followed With E910		1201 Spraylon	117	130	10	4	Light straw color
SS4120 Followed With E910		1201 Spraylon	119	260	20	5	Medium straw color
D. C. Z6020	0.1	1201 Spraylon Powder Vac. Dried Powder Dried 1 hr at 125°C	122	250	10	3	Slight straw color
D. C. Z6020	0.1	1201 Spraylon Powder Vac. Dried Powder Dried 1 hr at 125°C	127	500	20	2	Light straw color
D. C. Z6020	0.1	1201 Spraylon Powder Washed Freon Benzene Vac. Dried Filtered at 125°C	122	250	10	2	Slight straw color

A-17

Table A-1 (Cont.)

Primer	Concentration (%)	Spraylon Material and Treatment	Temperature (°C)	Time UV Exposure (ESH)	Solar Intensity (suns)	Spraylon Thickness (mils)	Comments
D.C. Z6020	0.1	1201 Spraylon Powder Washed Freon Benzene Vac. Dried Filtered at 125°C	127	500	20	2	Light straw color
D.C. Z6020	0.1	1201 Spraylon E-910 Adhesive	122	250	10	2	Light straw color
D.C. Z6020	0.1	1201 Spraylon 0.1% E-910 No. SS	122	250	10	2	Light straw color
D.C. Z6020	0.1	1301 Spraylon Powder Vac. Dried 3 hr at 125°C	122	250	10	1.5	Slight straw color
D.C. Z6020	0.1	1301 Spraylon Powder Vac. Dried 3 hr at 125°C	127	500	20	2	Light straw color

A-18

ORIGINAL PAGE IS  
OF POOR QUALITY

Appendix B  
TEST REPORT  
UV/CHARGED PARTICLE IRRADIATIONS\*

by  
D. A. Russell  
(Boeing Company)

The program consisted of two major parts, the first part being 1-MeV electron exposure to  $5 \times 10^{15}$  e/cm<sup>2</sup> and ultraviolet exposure with 800 ESH at 5 suns intensity, and the second part being 100-keV proton exposure to  $5 \times 10^{15}$  p/cm<sup>2</sup> and ultraviolet exposure with 800 ESH at 5 suns intensity. Each part had its own set of samples with each 8 cm × 8 cm set consisting of a group of 12.2 cm × 2 cm cells and one 4-cell module.

The supplied cells and sample plates were mounted to a rotatable copper heat sink in the vacuum test chamber for the irradiations. The main features of the vacuum test chamber are shown in Figs. B-1 and B-2. The figures show the placement of the foil holder, rotating Faraday cup, sample plane Faraday cup, current-collecting tabs, and test samples. The vacuum test chamber is a diffusion-pumped system with a liquid nitrogen cold trap. The temperature of the sample plate was monitored during the irradiations with copper-constantan thermocouples mounted on the sample substrates.

ELECTRONS AND ULTRAVIOLET IRRADIATIONS

The electron beam was scattered by an aluminum foil. The electron dosimetry was done with the samples rotated 180° from the direction of the beam. The required current from the accelerator was set using the reading in the sample plane Faraday cup (see Fig. B-1). The reading in the sample plane Faraday cup was calculated from a predetermined flux at the sample plane. The following is an example of this calculation for a sample flux of  $1 \times 10^{11}$  e/cm<sup>2</sup>-s.

---

\*Performed by the Boeing Company, Seattle, Washington, August 1977.

B-2

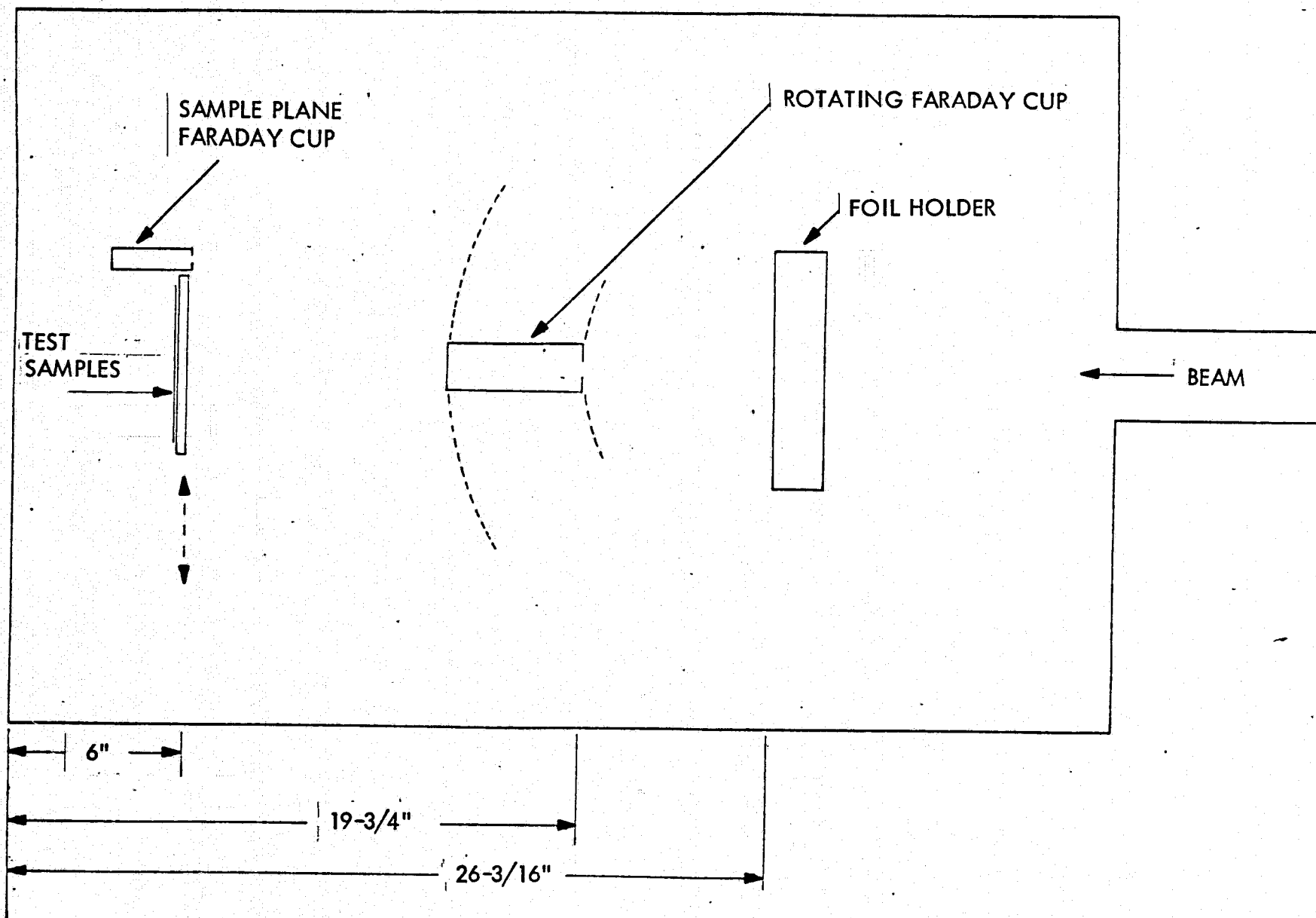


Fig. B-1 Top View of Vacuum Test Chamber

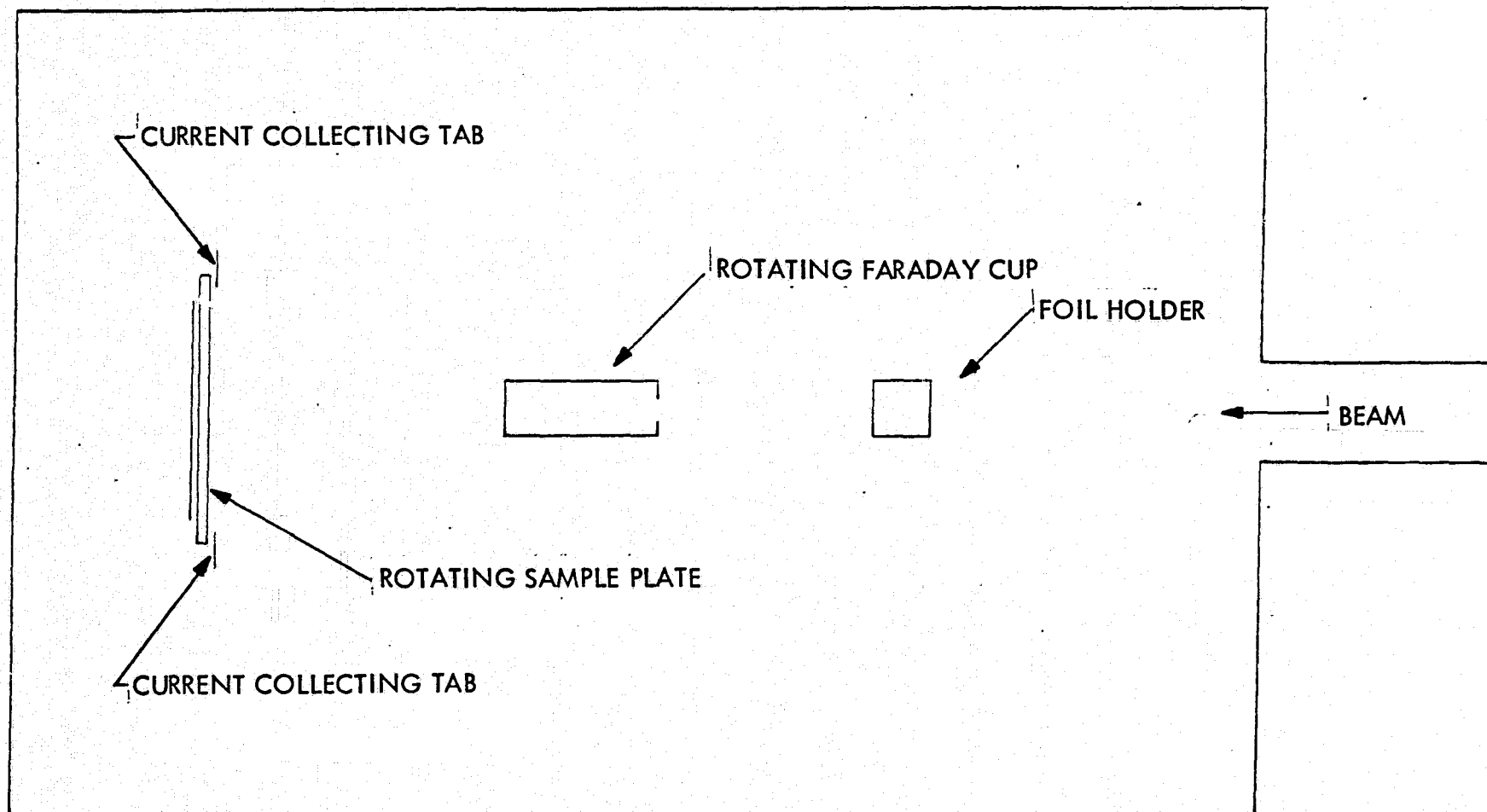


Fig. B-2 Side View of Vacuum Test Chamber

$$1 \times 10^{11} \text{ e/cm}^2\text{-sec} \times 1.6 \times 10^{-19} \text{ coule/e} \times 0.625 \text{ cm}^2 = 1 \times 10^{-8} \text{ amps}$$

$$1.6 \times 10^{-19} \text{ coule/e} = \text{the charge of an electron in coulombs}$$

$$0.625 \text{ cm}^2 = \text{the area of the sample plane Faraday cup.}$$

A beam profile map was made using the rotating Faraday cup for each run once an accelerator current was set. A profile point was taken every  $0.9^\circ$  so that a total of 21 points make up a plot of beam uniformity over the sample area. Figure B-3 is the plot of the beam profile. Although a mapping was made before each run only one is shown because they were all essentially the same. Figure B-4 is a plot of relative fluence across the sample as they were positioned in the chamber as determined by the beam profile map.

Having achieved a given flux at the sample plane, the required fluence was reached by integrating the current collected on the current collecting tabs. The number of integrator counts was calculated by the following equation:

$$\# \text{ counts} = \frac{\text{required fluence} \times 1.6 \times 10^{-19} \text{ coule/e}}{\# \text{ coul/count}} \times \frac{\text{reading on integrator}}{\text{flux at sample}}$$

# coul/count = the conversion from integrator counts to coulombs (1000 for the integrator used)

The tolerance of the Faraday cups is  $\pm 15\%$  and the tolerance of the Keithley 610 electrometer is  $\pm 3\%$ ; therefore, the probable error in the flux is  $\sqrt{(0.15)^2 + (0.03)^2}$ , or  $\pm 15.3\%$ . The tolerance of the current integrator is  $\pm 2\%$ . Therefore, the probable error in the fluence is  $\sqrt{(0.15)^2 + (0.03)^2 + (0.02)^2}$ , or  $\pm 15.4\%$ .

The source of the ultraviolet radiation was a X25L solar simulator set up and calibrated to give 5 equivalent ultraviolet suns at the sample plane. The temperature of the samples was monitored by a thermocouple mounted under cell position number

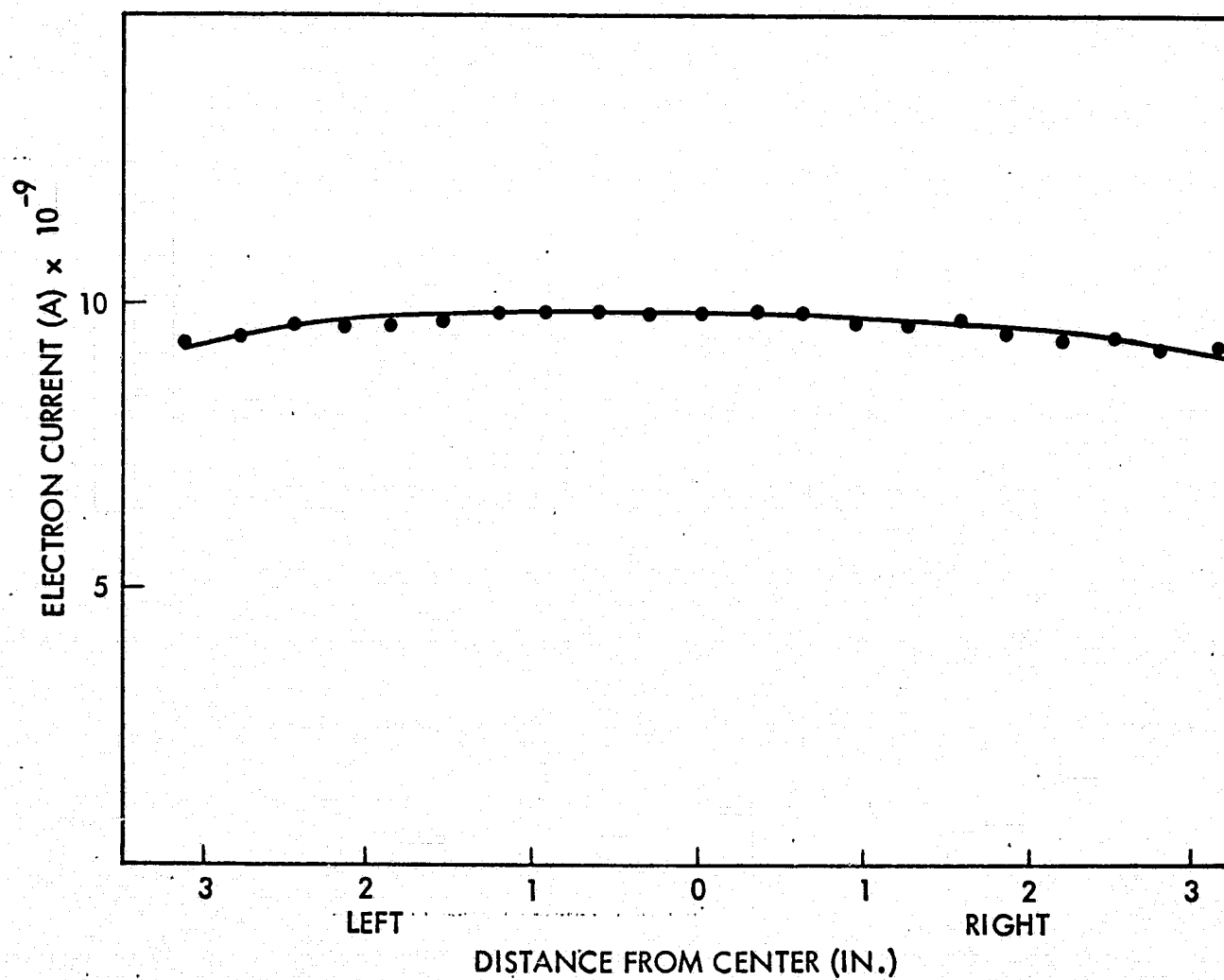


Fig. B-3 Electron Beam Profile Map



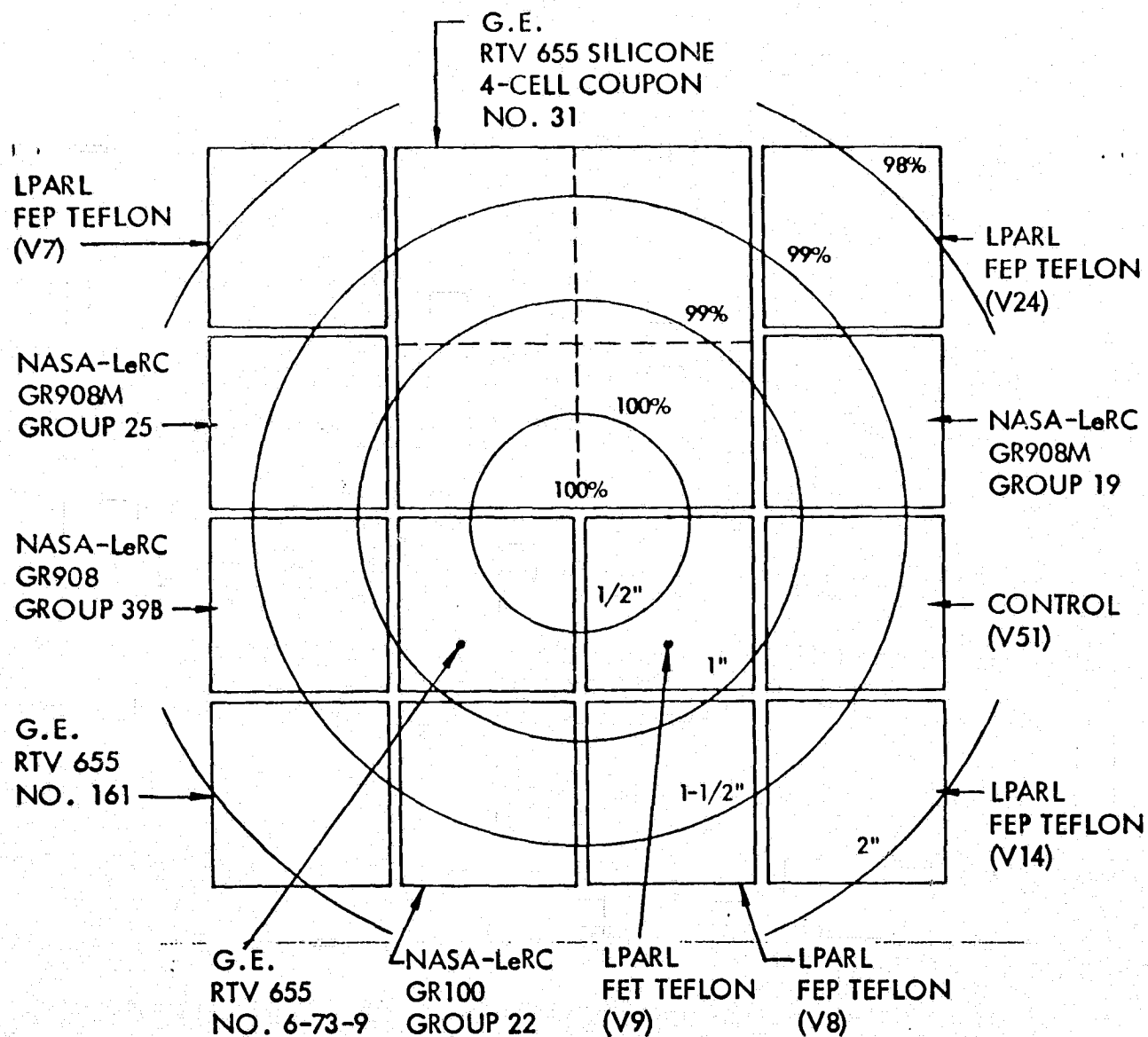


Fig. B-4 Relative Fluence Plot and Specimen Map for Electron Irradiation

four. The thermal mounting of the cells was such that the samples were cooled during UV exposure and heated during the electron exposure to maintain the 120° C temperature. Figure B-5 shows the time history of the sample. The electron irradiations were alternated with the UV exposure. The total UV hours at 5 equivalent UV suns was 161.86 hours, and the total electron fluence was  $5 \times 10^{15}$  e/cm<sup>2</sup>.

#### PROTONS AND ULTRAVIOLET IRRADIATIONS

The proton beam was scattered by an aluminum foil. The proton dosimetry was done with the samples rotated 180° from the direction of the beam. The required current from the accelerator was set using the reading in the sample plane Faraday cup (see Fig. B-1). The reading in the sample plane Faraday cup was calculated from a predetermined flux at the sample plane. The following is an example of this calculation for a sample flux of  $5 \times 10^{10}$  p/cm<sup>2</sup>-sec.

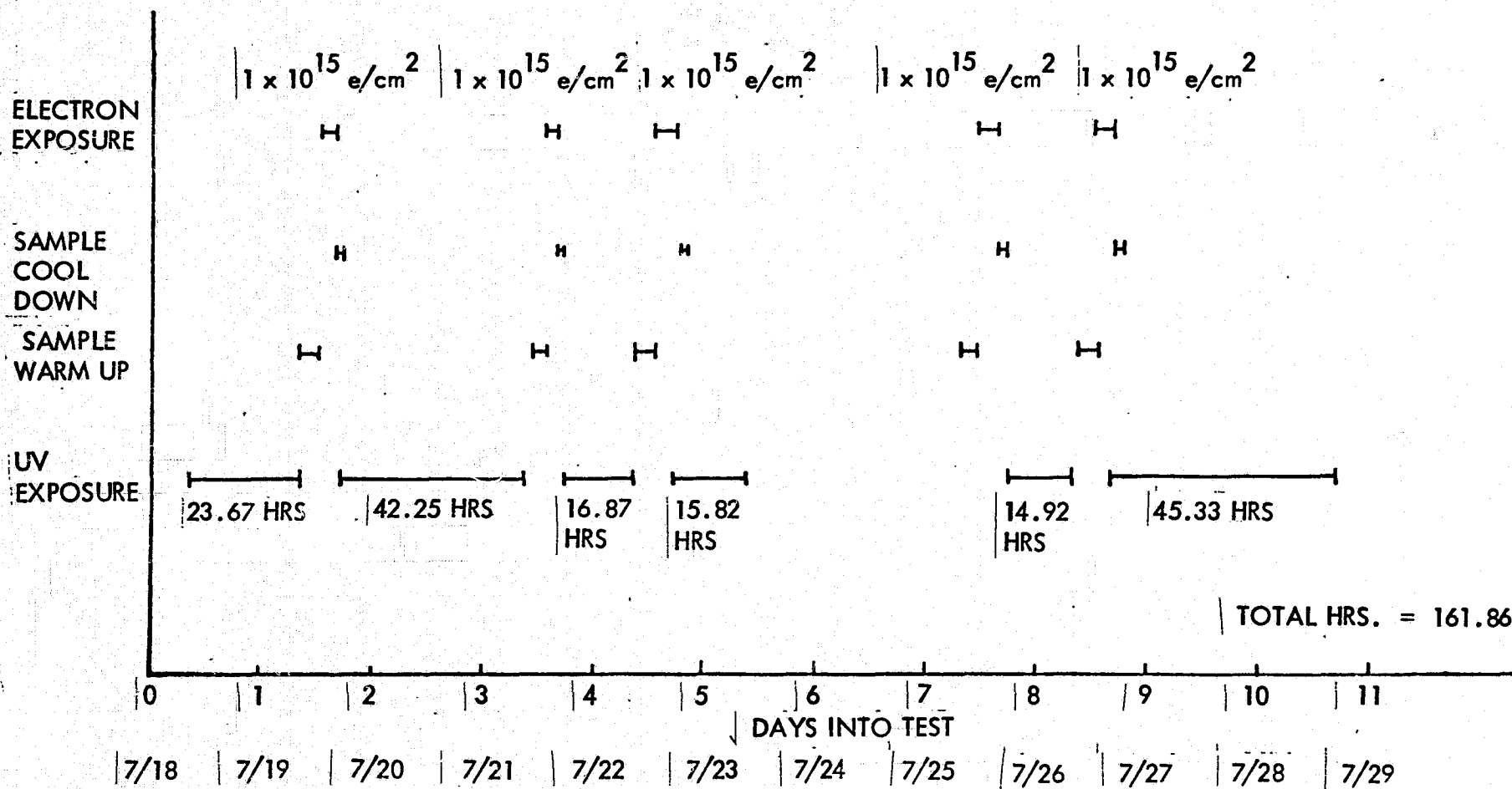
$$5 \times 10^{10} \text{ p/cm}^2\text{-sec} \times 1.6 \times 10^{-19} \text{ coul/p} \times 0.625 \text{ cm}^2 = 5 \times 10^{-9} \text{ amps}$$

$$1.6 \times 10^{-19} \text{ coul/p} = \text{the charge of a proton in coulombs}$$

$$0.625 \text{ cm}^2 = \text{the area of the sample plane Faraday cup}$$

A beam profile map was made using the rotating Faraday cup for each run once an accelerator current was set. A profile point was taken every 0.9° so that a total of 21 points make up a plot of beam uniformity over the sample area. Figure B-6 is the plot of the beam profile. Although a mapping was made before each run, only one is shown because they were all essentially the same. Figure B-7 is a plot of relative fluence across the sample as they were positioned in the chamber as determined by the beam profile map.

ORIGINAL PAGE IS  
OF POOR QUALITY



B-8

Fig. B-5 Sample History - Electron and UV Test

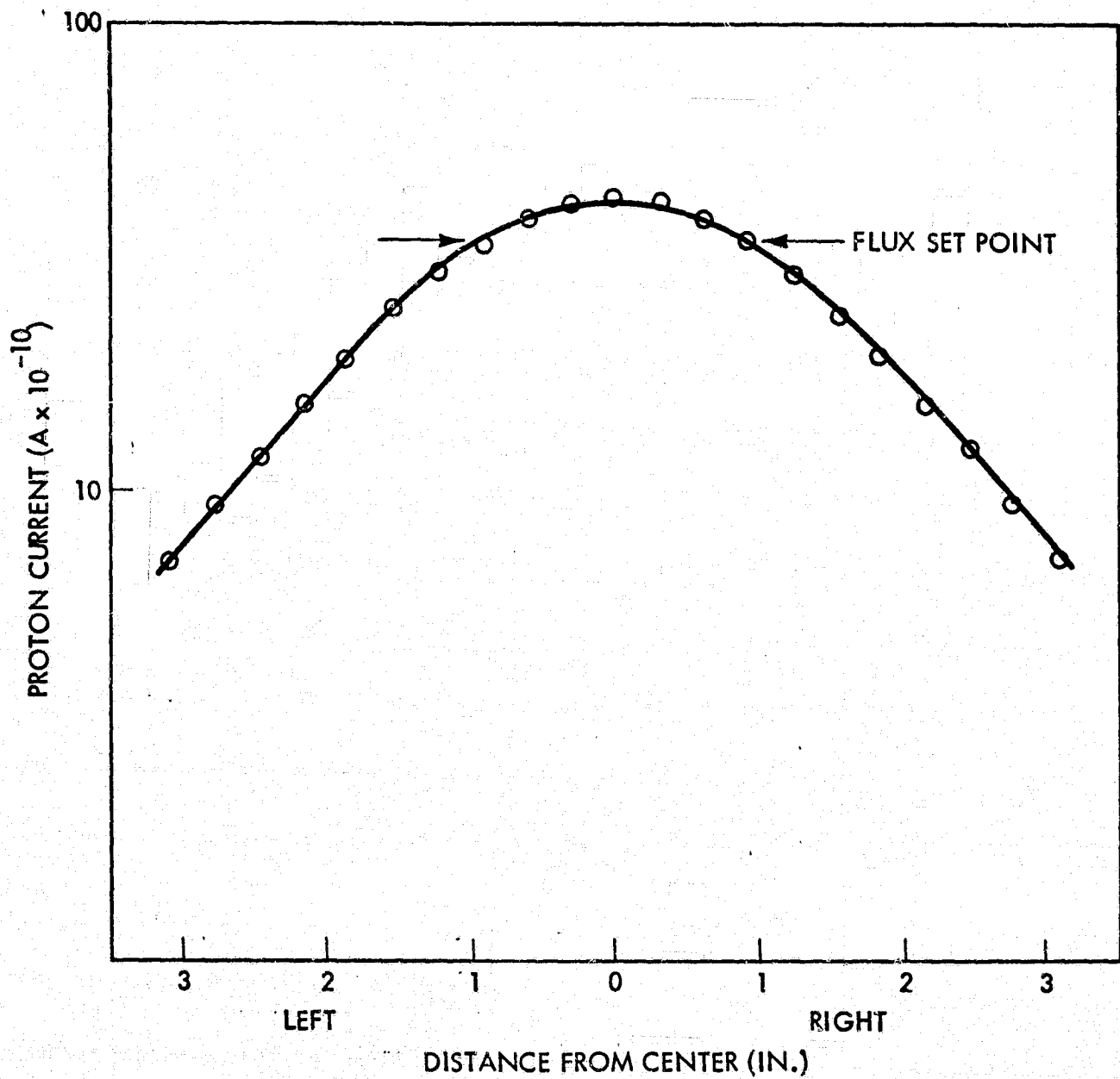


Fig. B-6 Proton Beam Profile Map

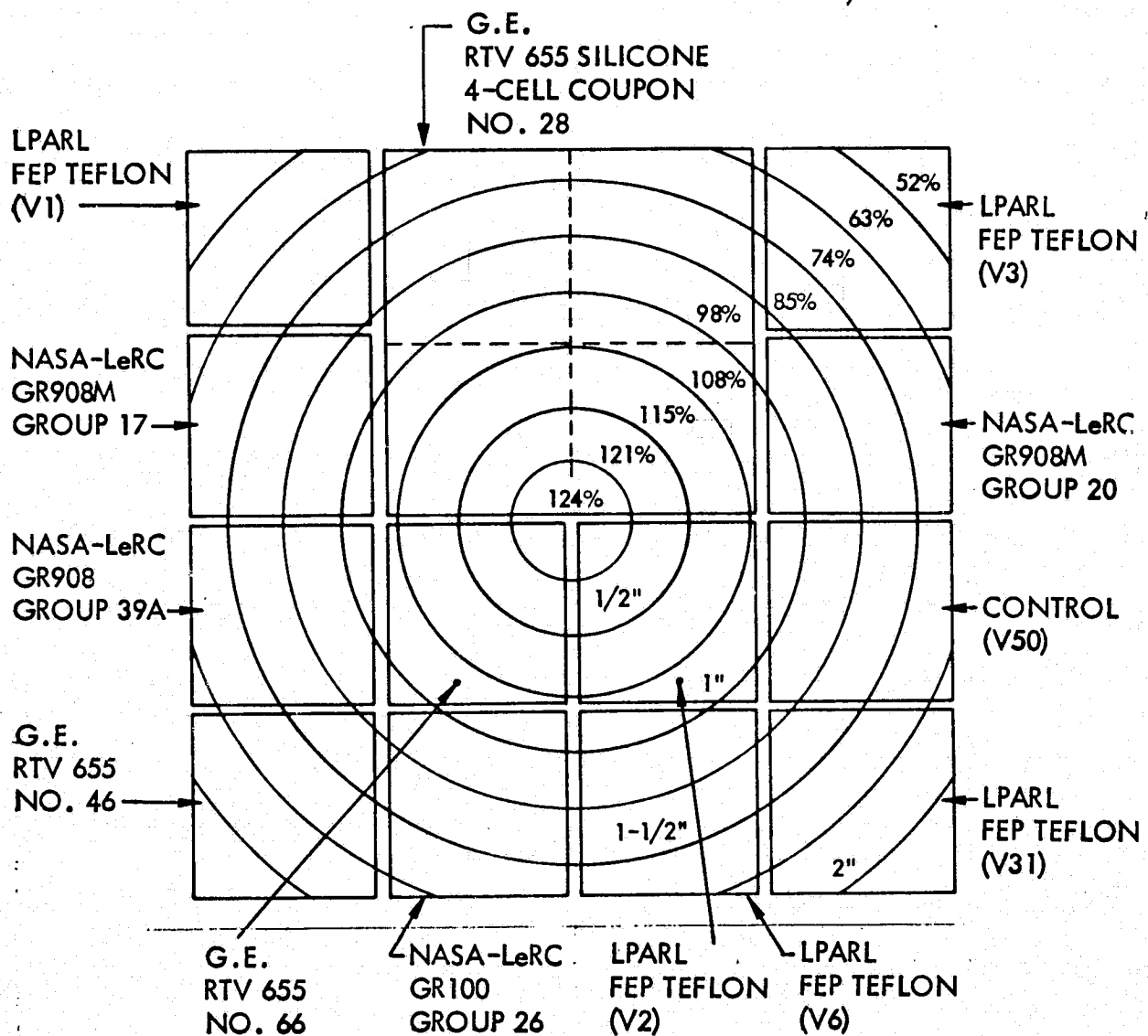


Fig. B-7 Relative Fluence Plot and Specimen Map for Proton Irradiations

C-6

Having achieved a given flux at the sample plane, the required fluence was reached by integrating the current collected on the current-collecting tabs. The number of integrator counts was calculated by the following equations:

$$\# \text{ counts} = \frac{\text{required fluence} \times 1.6 \times 10^{-19} \text{ coul/p}}{\# \text{ coul/count}} \times \frac{\text{reading on integrator}}{\text{flux at sample}}$$

# coul/count = the conversion from integrator counts to coulombs (1000 for the integrator used)

The tolerance of the Faraday cups is  $\pm 15\%$ , and the tolerance of the Keithley 610 electrometer is  $\pm 3\%$ ; therefore, the probable error in the flux is  $\sqrt{(0.15)^2 + (0.03)^2}$ , or  $\pm 15.3\%$ . The tolerance of the current integrator is  $\pm 2\%$ . Therefore, the probable error in the fluence is  $\sqrt{(0.15)^2 + (0.03)^2 + (0.02)^2}$ , or  $\pm 15.4\%$ .

The source of the ultraviolet radiation was a X25L solar simulator set up and calibrated to give 5 equivalent ultraviolet suns at the sample plane. The temperature of the samples was monitored by a thermocouple mounted under cell position number four. The thermal mounting of the cells was such that the samples were cooled during UV exposure and heated during the proton exposure to maintain the  $120^\circ\text{C}$  temperature. Figure B-8 shows the time history of the sample. The proton irradiations were alternated with the UV exposure. The total UV hours at 5 equivalent UV suns was 175.07 hours, and the total proton fluence was  $5 \times 10^{15} \text{ p/cm}^2$ .

21-8

PROTON  
EXPOSURE

SAMPLE  
COOL  
DOWN

SAMPLE  
WARM UP

UV  
EXPOSURE

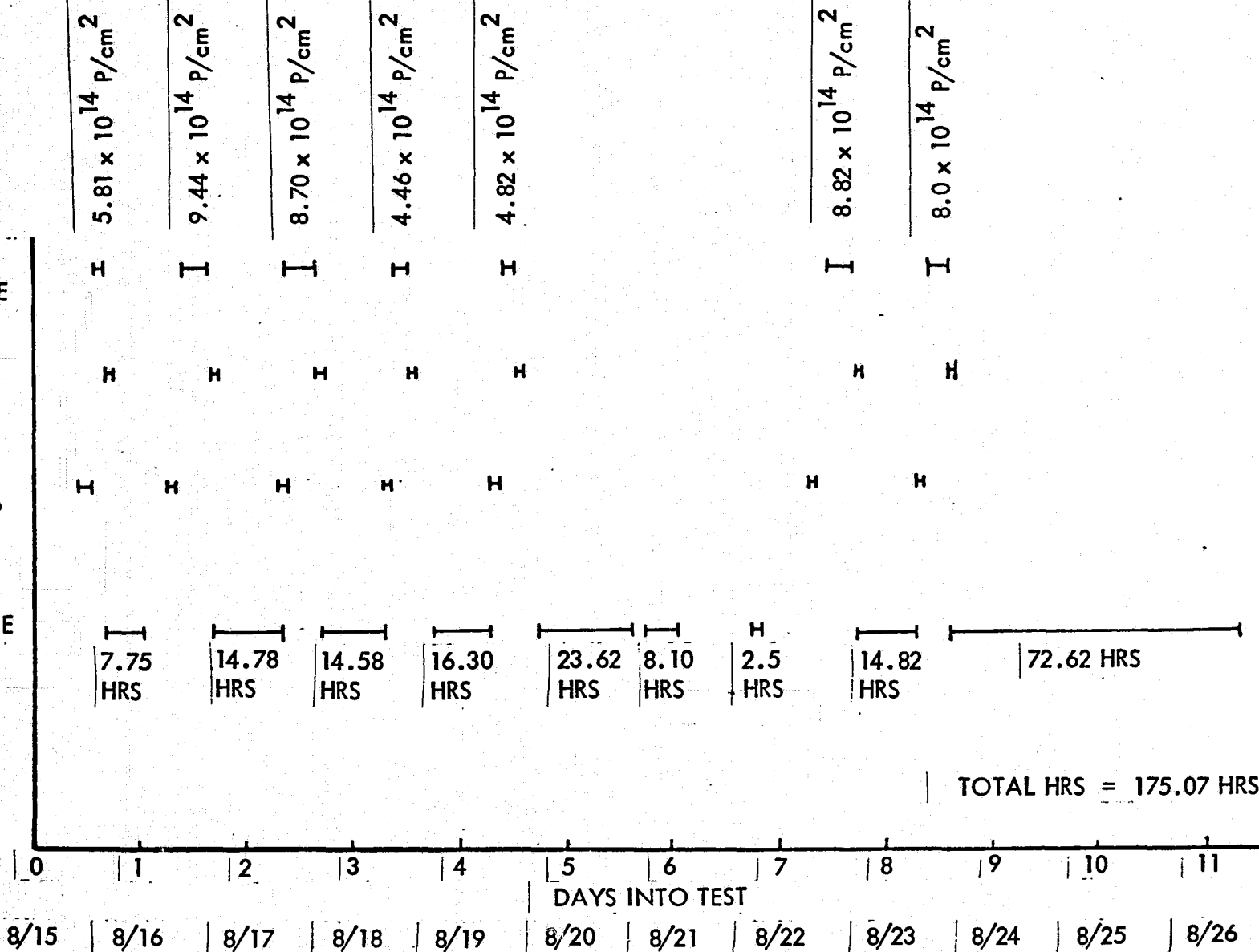


Fig. B-8 Sample History - Proton and UV Test

Appendix C  
OPTICAL DATA FOR FEP TEFLON

Spectral reflectance measurements of FEP Teflon films were made between  $0.35\ \mu\text{m}$  and  $2.4\ \mu\text{m}$  using a Gier-Dunkle Model SP-210 Integrating Sphere Reflectometer. Spectral transmittance measurements (normal and hemispherical) were made which showed the relative amount of scattered normal incident energy.

Spectral reflectance and transmission data for 1-, 5-, and 10-mil FEP Teflon films are shown in Figs. C-1 and C-2.

For the case of the FEP-covered solar cell, the combined emittance of the solar cell with 1-mil FEP is 0.72/0.74, while the emittance of a 2-mil FEP is 0.77/0.80. The bare solar cell has an emittance of 0.420. Measurements were made on a Gier-Dunkle DB-100.

ORIGINAL PAGE IS  
OF POOR QUALITY



C-2  
ORIGINAL PAGE IS  
OF POOR QUALITY

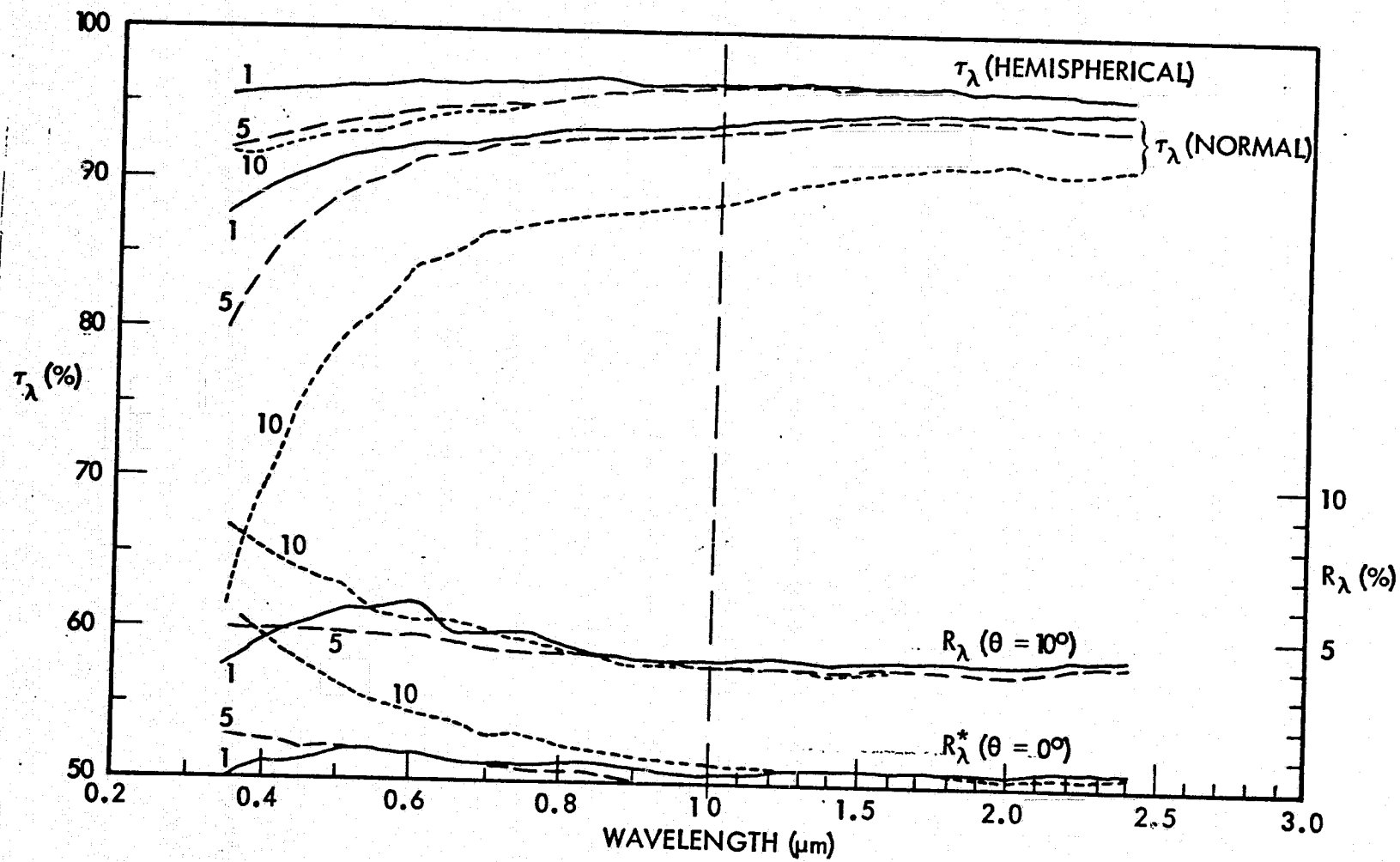


Fig. C-1 Spectral Reflectance and Transmittance Data for 1-, 5-, and 10-mil Thicknesses of Teflon Films in the Solar Region

C-3

ORIGINAL PAGE IS  
OF POOR QUALITY

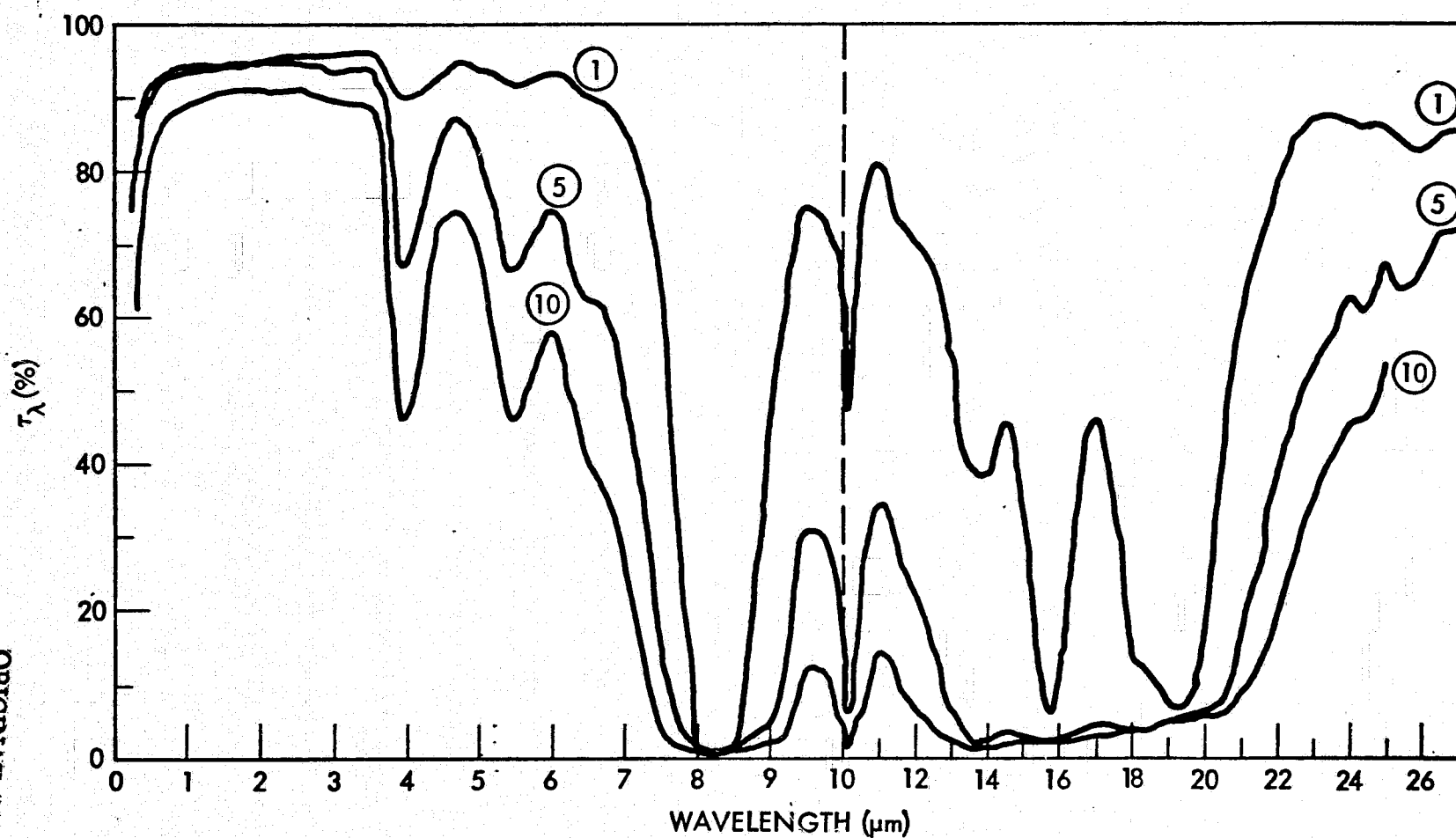


Fig. C-2 Spectral Normal Transmittance Data for 1-, 5-, and 10-mil-Thick Teflon Films

Appendix D  
REFERENCES

1. Lockheed Palo Alto Research Laboratories, Spraylon Fluorocarbon Encapsulation for Silicon Solar Cells Array, Phase I, LMSC-D55813, Palo Alto, Calif., Jun 1977
2. S. J. Marsik, C. K. Swartz, and C. R. Barona, Testing of Encapsulant Materials for Halley's Comet SEP Mission, NASA-LeRC Test Report, prepared for NASA-JPL, May 27, 1977
3. F. G. Cunningham, B. L. Bean, and S. G. Park, "Ultraviolet and Charged Particle Degradation of Aluminum and Silver Coated FEP Teflon Second Surface Mirrors," Fifth Space Simulation Conference, ASTM/IES/AIAA, Sep 1970, pp. 345 - 358
4. H. S. Rauschenbach and M. D. Cannady, Flexible FEP-Teflon Covered Solar Cell Module Development, TRW Report - NASA/Lewis, NAS 3-16742, Oct 1976
5. S. J. Marsik and J. D. Broder, "Effect of Electron Irradiation in Vacuum on FEP-A silicon Solar Cell Covers," Eleventh Photovoltaic Specialists Conference IEEE, Phoenix, Arizona, 6 - 8 May 1975 (NASA TMX-71713)
6. L. B. Fogdall and S. S. Cannaday, "Effects of Space Radiation on Thin Polymers and Nonmetallics," AIAA 12th Thermophysics Conference, Albuquerque, New Mexico, 27 - 29 Jun 1977
7. J. A. DeRuntz, Jr., Time, Temperature and Nonlinear Effects in Laminated Composites, LMSC-D464026, Lockheed Missiles & Space Company, Inc., Sunnyvale, California, 8 Dec 1975
8. W. D. Whetstone, SPAR Structural Analysis System Reference Manual, NASA CR 145098-1, Feb 1977

NASA - OAST  
TECHNOLOGY ASSESSMENT  
OF  
CONCENTRATOR SOLAR ARRAYS

3 June '77  
Meeting Report

## FOREWORD

This document records the proceedings of an early peer group assessment of concentrator solar array technology. This meeting was held in early June 1977 to provide additional insight into planning and conducting a technology development program through mission readiness for comet Halley and later missions. We intend to have a second meeting at which time the concerns of the peer group will be assessed.

ORIGINAL PAGE IS  
ON POOR QUALITY

Minutes of OAST Concentrator Solar Array  
Initial Assessment Meeting

June 3, 1977

The initial peer group assessment of concentrator solar array technology for the SEP Halley mission was held at the Marshall Space Flight Center on Friday, June 3, 1977. In attendance were representatives from the responsible NASA organizations and their contractors as well as specialists from COMSAT and the Air Force (see attached list). Due to a full agenda (attached), the meeting commenced at 0800 hours. Questions were entertained during each presentation resulting in healthy discussions. Although the meeting ran several minutes behind, the entire agenda was accomplished and all relevant views received full discussion.

The meeting began with Mr. Mullin (NASA - HQ) discussing the need for the meeting and the criticality of obtaining an early peer group assessment of the technology base for concentrator solar arrays for the Halley mission. Mr. Austin (MSFC) discussed briefly the mission analyses that led to the requirement for concentrator solar arrays and outlined in general terms what those performance requirements were. Dr. Brandhorst (LeRC) discussed silicon solar cell technology in general and made the recommendation that a 13% efficient 6 mil thick cells was a reasonable technology objective for this mission. Mr. Costoge (JPL) presented preliminary design and performance information on the "Winston" collector approach which offers an attractive low weight. Mr. Nixon (MSFC) discussed a planar reflector approach to concentrator solar arrays, and Mr. Elms (LMSC) gave details on the status of the extended performance SEP solar array contract study which includes the planar reflector concentrators. Mr. Hule (MSFC) discussed projected performances of solar arrays with concentration ratios as high as 4:1 and related these performance estimates to the respective component technology readiness. Mr. Moss (MSFC) discussed thermal test data and showed that within a reasonable tolerance, it compared favorably to predicted temperatures. However, he pointed out that this tolerance could be tightened with additional and higher fidelity thermal testing. Mr. Horton (MSFC) reported on the materials test activities supporting the general SEP solar array technology program and showed some preliminary results of reflectance change of reflector materials after exposure to energetic

ORIGINAL PAGE IS  
OF POOR QUALITY

particle radiation. He pointed out that reflectance observations were made after removal from the chamber to obtain preliminary information but that refined test data should be obtained in-situ. Mr. Young (MSFC) reported on concentration ratio tests conducted on single cell models and on maldistribution of light consequence tests conducted on surplus Skylab panel hardware. These tests indicate that the electrical consequence of maldistribution of illumination is minimal; however, they do not address the electrical power loss due to thermal gradients resulting from maldistributed light. Mr. Brantley (MSFC) discussed the totality of the testing to date and identified test objectives yet to be accomplished and Mr. Young (MSFC) concluded the formal presentations by presenting a technology plan accomplishing technology readiness by mid FY 79 with cost reduction activities extending into FY80. The total resource value of the plan is \$6.4M. Mr. Mullin (NASA HQ) concluded the meeting at 1645 hours by reviewing observation and criticisms in six areas as follows:

1. Fundamental Barriers
2. Testing and Interpretation of Data
3. Areas of Risk
4. Adequacy of Technology Program
5. Further Tests Required
6. Other Areas of Concern

These observations and critiques are summarized in the following section

SILICON SOLAR CELL  
CONCENTRATOR SOLAR ARRAY  
OAST TECHNOLOGY ASSESSMENT

JUNE 3, 1977  
ATTENDANCE LIST

Jim Miller	MSFC	453-2113
Jerry Mullin	OAST	755-3276
John Goldsmith	J.P.L.	213-354-3180
Denis Curtin	COMSAT	301-428-4564
Henry Oman	Boeing	206-773-9014
Lowell D. Massie	AFAPL/POE-2	513-255-6235
Larry Chidester	Lockheed	408-742-2270
Rick Elms	Lockheed	408-742-3268
Bill Szmyd	Lockheed	408-742-2474
Dale Lindberg	Lockheed	408-742-4931
Les Fero	NASA/OSF	202-755-3740
Ken Atkins	JPL	213-354-6293 FTS-792-6293
Chuck Terwilliger	Boeing	206-773-9509
Henry Brandhorst	NASA-Lewis	216-433-4000 x 309 FTS-294-6309
Bob Aden	MSFC-EC11	453-4950
Ken Ling	Optical Coating	213-968-6581
Whitt Brantley	MSFC PD14	205-453-3666



Gene Young	MSFC EC12	205-453-2110
Geo. E. Smith	MSFC EC12	205-453-4642
William L. Crabtree	MSFC EC12	205-453-2110
James L. Sanders	MSFC PD13	453-3229
Robert F. Nixon	MSFC PD21	453-4165
Walter Johanson	MSFC PD24	453-4260
R. Nixon	MSFC PD21	
O. D. Meredith	MSFC PD23	453-3569
Peter Fono	HAC	213-448-1471
George J. Rayl	GE Co. Space Div.	215-962-5585
Kevin Speight	GE Co. Space Div.	215-962-4158
Walter Hasbach	JPL	213-354-5300
Jim R. Stuart	JPL (233-307)	213-354-4191
Ron Boain	JPL (156-220)	213-354-2947
Joe O'Gallagher	U. of Chicago	312-753-8637
Roland Winston	U. Of Chicago	312-753-8654
E. N. Costogue	JPL (125-147)	213-354-4166
Richard J. Boehme	MSFC PD14	453-5726
Doug Moss	MSFC EP45	453-3627
T. M. White	MSFC EP45	453-3627
J. C. Horton	MSFC EH11	453-5090

ORIGINAL PAGE IS  
OF POOR QUALITY

SILICON SOLAR CELL  
CONCENTRATOR SOLAR ARRAY  
OAST TECHNOLOGY ASSESSMENT

JUNE 3, 1977  
MEETING AGENDA

8:00 - 8:05 a.m.	OPENING COMMENTS	MULLIN
8:05 - 8:10 a.m.	AGENDA & DETAILS	MILLER
8:10 - 8:25 a.m.	HALLEY MISSION REQUIREMENTS	AUSTIN
8:25 - 9:00 a.m.	CELL AVAILABILITY & PERFORMANCE	BRANDHORST
9:00 - 10:00 a.m.	CONCENTRATOR DESIGNS & TECHNOLOGY STATUS	COSTOGUE
10:00 - 10:30 a.m.	CONCENTRATOR S/A PROJ. PERF. & TECHNOLOGY REQ.	HUIE
10:30 - 10:50 a.m.	PRELIM. CONC. SYSTEM DESIGNS	NIXON
10:50 - 11:50 a.m.	EXTENDED PERF. SEP SOLAR ARRAY	ELMS
11:50 - 12:50 a.m.	TESTING	
	CONCENTRATION RATIO	YOUNG
	CONSEQUENCE OF ILLUMINATION MALDISTRIBUTION	YOUNG
	THERMAL TESTS	MOSS
	MATERIALS DEGRADATION	WHITAKER
12:50 - 1:30 p.m.	LUNCH	
1:30 - 2:00 p.m.	TEST RESULTS ASSESSMENT	BRANTLEY
2:00 - 2:30 p.m.	TECHNOLOGY PLAN	YOUNG
2:30 - 3:45 p.m.	DISCUSSIONS AND RECOMMENDATIONS	MULLIN
3:45 - 4:00 p.m.	CONCLUDING COMMENTS	MULLIN

ORIGINAL PAGE IS  
OF POOR QUALITY

## OBSERVATIONS AND CRITIQUE

### SUMMARY

ARE THERE ANY FUNDAMENTAL BARRIERS TO MEETING  
THE CONCENTRATOR ARRAY REQUIREMENTS AS  
DEFINED FOR THE HALLEY MISSION?

There are no known fundamental barriers. However, there are four areas of concern which could possibly become barriers depending upon what the actual concentrator array requirements are for the Halley mission. They are listed below in order of their potential for becoming a barrier:

1. Solar array weight
2. Degradation (primarily of the solar array blanket, but also reflector and other materials)
3. Limited time available to achieve technology readiness
4. Solar cell development

All of the above concerns are interrelated. The degradation concern refers primarily to the solar array blanket and reflectors, but appears to be largely based upon the assumption that a degradation of only 10 to 12% can be tolerated. If the degradation which can be tolerated is in the neighborhood of 20 to 25%, then this would no longer be of any significant concern.

A lesser concern was in meeting the schedule with the large volume of individual uncertainties such as thermal extremes, unknown degradations, material problems, and the present state of definition of the requirements.

Of least concern, but still a possible potential barrier is the availability of thin wraparound cells.

ARE THERE CONCERNS REGARDING ADEQUACY OF  
TESTING OR INTERPRETATION OF DATA

Almost every area of testing is of concern. For example, adequacy of solar simulation, similarity of cells tested to those proposed for concentrator array use, adequacy of test samples, scatter in test results, and adequacy of thermal modeling.

ORIGINAL PAGE IS  
OF POOR QUALITY

### WHAT ARE THE SPECIFIC AREAS OF GREATEST RISK?

The two major areas of greatest risk appear to be related to the solar cell and thermal effects. The greatest area of concern seems to center around the cell. Specific areas are achievement of required efficiency with cells of the required thinness, wraparound contacts, establishing production of the cells, achieving low cost, and handling feasibility.

In the thermal area, the concerns are thermal stability of concentrator materials, coverslides, cells and interconnectors since additional thermal distortions could dramatically alter the chances for success of the mission.

Whether failures will result from long term low temperature effects on the array and whether overall thermal expansion/contraction of the system will be within acceptable limits is of concern. Also, the thermal/optical effects of non-uniform illumination do not seem to be well characterized at this time for an entire array.

Questions regarding charging of the array from the ion engines and concern about deployment mechanisms reliability were two areas needing further definition. In the area of array charging from the ion engine, the concern is that large charge buildup on Kapton surfaces can be detrimental to the solar cell circuits when the Kapton discharges. Of particular concern in the deployment mechanisms area is the reliability of deployment and retraction of the array blanket and reflectors, the ability to achieve the required orientation, and the ability of the drive mechanisms to survive the full mission.

Other areas of concern are that the performance will be too optimistically predicted due to overall uncertainty in such things as reflectance, temperature distribution, power prediction, structural rigidity, and radiation resistance. Irradiation stability of concentrator materials, coverslides, cells, and inter connects need to be closely and accurately defined.

Concern is also expressed for choice of the coverglass since it needs to have very low degradation.

Structural weight requirements were felt to be "edge of the art" or beyond.

There was some concern regarding adequate ground test procedures including handling and a good collimated light source, and how on-orbit

performance is verified by ground tests. Also, reflector degradation from solar flare protons, non-uniformity of illumination of cells in series and its effect upon performance and solar pressure perturbations to trajectory were felt to be areas of some risk.

IS THE PLANNED TECHNOLOGY ADEQUATE TO  
REDUCE RISK TO AN ACCEPTABLE LEVEL?

The general attitude seems to be that the program is going in the right direction, but additional task definitions were needed. There was concern that the time allowances, and funding for various developments may not be adequate to meet the mission goals.

The following were suggested as additional tasks need to meet the mission goals:

Assessment of the probable fluence from solar flare protons during the mission

Develop cells that perform consistently and predictably at low intensities and temperatures

Testing BSF cells with radiation from the back

Testing of reflectors with non-uniform heating, for wrinkling

The opinion was expressed that considerable emphasis should be placed upon understanding thermal-structural interactions and electrical-thermal performance. This understanding should be gained by data from large scale tests and extensive material property data taken over the appropriate ranges.

WHAT FURTHER TESTS ARE REQUIRED, SHORT OF  
FULL SCALE IN SPACE DEMONSTRATION,  
TO ESTABLISH TECHNOLOGICAL FEASIBILITY?

The following types of tests were proposed:

1. Testing of typical type of panel for Halley mission with typical

concentrators in real thermal conditions

2. Large scale, collimated sunlight electrical, thermal tests of models in a thermal vacuum environment
3. Low temperature/low pressure testing
4. High temperature/low pressure testing
5. U.V. and particle irradiation testing
6. Roll-up tests with thin cells
7. Produce 20,000 cells for test and carefully evaluate yield and cost to evaluate production feasibility of thin cells as soon as possible
8. Fabricate several segments (2000 cells each) to evaluate handling and cell attrition for panel assembly of thin cells.
9. Extensive tests on degradation of cells and optical components in the expected environment, including combined effects as feasible
10. Motion testing to Shuttle/IUS environment
11. Space test of several thousand thin cells in concentrator configuration
12. OFT test should be carried out
13. Test to see plume effects from ion engines on array

ADDITIONAL COMMENTS THAT MAY CONTRIBUTE  
TO THE OVERALL ASSESSMENT

Most of the comments related to the cell. It was felt that production techniques for fabrication of the wraparound cells should be established. An understanding of the anomalous behavior of certain cells at low light intensities and temperatures is needed. Electrical performance of the solar cell after application of the plastic encapsulant was felt to be needed. Cell performance as a function of

ORIGINAL PAGE IS  
OF POOR QUALITY

temperature, light level and 1MeV fluence should be determined, and the cells should probably be low resistivity with more grids than the normal 1 sun cell, perhaps a deeper diffused junction with BSF.

Several suggestions and comments were made which varied in nature and in most cases were unrelated. They are as follows:

1. Maximum allowable power/weight needed for the array needs to be established.
2. Extensive test and analysis will be needed, and it may be necessary to work several design alternatives simultaneously in order to evaluate the margin and uncertainties in each design.
3. Power requirements as a function of Heliocentric Distance need definition.
4. Set cell performance/thickness etc. (and reflector material) and see if mission can be done (e.g., 13.5%, 6 mil w/a).
5. Care needs to be taken in dynamics and control calculations due to the widely ranging environment.
6. Thermal bending and effects on control system for orientation mechanism need to be considered.
7. Guidance and stability, e.g., cancellation of moments of inertia needs to be considered.
8. All alternative concepts for an array concentrator system should be eliminated systematically.



OBSERVATION AND CRITIQUE

COMMENTS

## CONCENTRATOR SOLAR ARRAY INITIAL ASSESSMENT

JUNE 3, 1977

Question 1 - IN YOUR OPINION ARE THERE ANY FUNDAMENTAL BARRIERS TO MEETING THE CONCENTRATOR ARRAY REQUIREMENTS AS DEFINED TODAY FOR THE HALLEY MISSION?

- 1-1    o    The relationship between array efficiency and mass may require solar cell performance beyond the capability of silicon solar cell technology.
- 1-2    o    Probably no show stoppers but solar array and reflector degradations in the environment are probably greater than assumed. This strongly impacts mission feasibility (conversely if we can only tolerate 10-12% losses then we've got a lot of technology development to do).
- 1-3    o    No fundamental barriers. However, it is not clear to me that cells having sufficient efficiency and thinness can be developed, consistent with the highest tolerable array weight for the mission.
- 1-4    o    Weight is a key problem - how heavy can the array be before it's no go?
- 1-5    o    At this time the feasibility of the mission depends on the achievement of weight and performance goals. I did not get a feeling of great confidence from the weight estimates that were presented.
- 1-6    o    Even with 3 to 1 concentration it will be extremely difficult to develop and fabricate an array that will do the mission in the time frame allotted. The combination of low solar input, large thermal extremes and their consequent mismatches, unknown degradation, material problems, etc. combined with what presently seem to be fuzzy requirements make success problematical.
- 1-7    o    The coverslide problem on the JPL/GE array could be a stopper because those materials will degrade. The 3 mil CMS material will be expensive and difficult to handle but should be usable.

- 1-8    o    A 4-6 mil cell at 14% will be difficult to achieve in a short time.
- 1-9    o    The ability to produce a 5-6 mil wraparound at 13-14% efficiency seems crucial and not yet shown to be feasible at high yield and low cost.

Question 2 -- PLEASE LIST SPECIFIC QUESTIONS YOU MIGHT HAVE ABOUT TEST RESULTS OR THEIR INTERPRETATION AS PRESENTED OR DISCUSSED AT THIS MEETING.

- 2-1 o The Marshall materials data that was presented is not at all useful. The testing has to be done in vacuum with in situ measurements under realistic irradiation rates.
- 2-2 o Test results very limited.
- 2-3 o Significant scatter in results: both intensity and temperature distribution.
- 2-4 o Concern about the use of simulation that may not provide good columnated light.
- 2-5 o Material, particularly reflecting surfaces, properties and associated structural support needs considerable, detailed evaluation.
- 2-6 o Will reflectors having the light weight used in performance estimates provide the optical quality assumed in the power output calculations?
- 2-7 o Need high quality tests of good test articles.
- 2-8 o The NASA Lewis data under 10 suns is questionable. People who do U.V. testing regularly say that 1 sun conditions should be used. Therefore, the status of the plastic and glass resin material is still unknown.
- 2-9 o Primary question is with regard to cell behavior at low light level and temperature.
- 2-10 o The cells tested were not optimized for concentration.
- 2-11 o The cells tested were not advanced thin cells of the type that would be required.
- 2-12 o Verification of thermal models has not been adequately done - do we have confidence as to their accuracy and with the idea that only 1° distortions can occur in these arrays?
- 2-13 o What is the advantage of CPC reflector over simple planar reflectors? -- It seems more complex.

- 2-14    o    What would the concentrator test results be like under real thermal conditions? There could be considerably more distortion, hot spots, etc.
- 2-15    o    Marshall Space Flight Center did a good job in honestly evaluating the data it had at hand.

Question 3 - IN YOUR OPINION WHAT ARE THE SPECIFIC AREAS OF GREATEST RISK?

- 3-1     o    The major concern is that performance will be too optimistically predicted. There may be significant cause for uncertainty in design -- reflectance, temperature distribution, power prediction, structural rigidity, radiation resistance, that reasonable margin must be provided for degradation and uncertainties.
- 3-2     o    The use of non-flight proven concentration techniques for a 3-4 year mission. There are many unknowns that make the problem difficult.
- 3-3     o    The thermal and irradiation stability of the concentrator materials, coverslides, cells, interconnectors need to be closely and accurately defined. One is left with the impression that everything is very tight. Consequently, any additional degradation in reflecting materials, cells, covers etc., like 5-10% or more or thermal distortions could dramatically alter the chances for success of the mission.
- 3-4     o    What happens to an array left at a very low temperature for a long time -- will there be failures?
- 3-5     o    Reliable mechanization of deployment of reflectors to required configuration and orientation.
- 3-6     o    Achievement of required efficiency with cells of required thinness.
- 3-7     o    Thin advanced cells: production feasibility; handling feasibility; roll-up feasibility
- 3-8     o    Obtaining 14-15%, 5 or 6 mil wraparound contact cells
- 3-9     o    Establishing production of solar cells having required performance and low cost.
- 3-10    o    Choice of cover glass -- (3 mil or 4 mil ceria micro sheet, etc.) having lowest possible degradation and/or polymers/rosins and their ability to be supplied.
- 3-11    o    Fabrication of the array and production of cells that meet the requirements of this mission.

- 3-12 o Leakage current through charge-exchange plasma.
- 3-13 o Charging of the solar array from the ion engines should be looked at. Large charge buildup on Kapton surfaces can be detrimental to the solar cell circuits when the Kapton discharges.
- 3-14 o Structure weight requirements may be "Edge-of-the-Art" or beyond.
- 3-15 o Reliability of drive mechanisms for full mission duration.
- 3-16 o Thermal expansion/contraction of system.
- 3-17 o Thermal distortion of structures, creating wrinkles in reflectors.
- 3-18 o Adequate ground test procedures including handling and good collimated light source. (How do we verify on-orbit performance based on ground tests).
- 3-19 o Thermal/optical effects of non-uniform illumination do not seem well characterized yet for entire array and cells.
- 3-20 o Reflector degradation from solar flare protons, particularly in the region of solar cell spectral response.
- 3-21 o Non-uniformly illuminated cells in series, some of which become reverse biased.
- 3-22 o Diode Isolation
- 3-23 o Long duration operation at high injection level (life test data needed).
- 3-24 o Solar pressure perturbations of trajectory.

Question 4 - IN YOUR ESTIMATION IS THE PLANNED TECHNOLOGY PROGRAM AS PRESENTED ADEQUATE TO REDUCE RISK TO ACCEPTABLE LEVELS?

- 4-1 o Right now the program is not really well thought out. Many of the present time allowances for various developments may not be adequate to meet the mission goals (e.g., can solar cell development work still be underway in late 1980?). On the other side though will they be ready to do a lot of full scale wing testing by March, 1978. The goals and actual requirements for the technology development need to be closely defined and then a program should be planned out. At a minimum though a program like this is needed but it must be tightly defined with a very specific goal.
- 4-2 o Yes, if the following items are added.
- o Assessment of the probable fluence from solar flare protons during the mission.
  - o Develop cells that perform consistently and predictably at low intensities and temperatures.
  - o Testing BSF cells with radiation from the back.
  - o Testing of reflectors with non-uniform heating, for wrinkling.
- The construction of test models may be very costly, and may consume most of the proposed budget.
- 4-3 o Difficult to determine with little exposure. The plan is in the right direction. Considerable emphasis should be placed in understanding thermal-structural interactions, uncertainties in actual electrical-thermal performance based upon empirically derived large scale tests and extensive material property ranges, e.g., optical-structural, etc., as function of exposure.
- 4-4 o Appears adequate technically but not adequate from the standpoint of development time and resources. FRUSA cost was \$4.4M and 4.5 years (1.5 kWe). HASPS cost was \$4.0M and 5 years (2.0 kWe).

ORIGINAL PAGE IS  
OF POOR QUALITY



4-5

- o The thermal testing of array segments and degradation of optics, etc., need additional study. Perhaps some additional \$ for array material component thermal efficiency matching. Otherwise program seems funded reasonably well but not clear what is the amount of money required to do the job.

Question 5 - WHAT FURTHER TESTS ARE REQUIRED, SHORT OF FULL SCALE IN SPACE DEMONSTRATION, TO ESTABLISH TECHNOLOGICAL FEASIBILITY?

- 5-1 o A test is needed on a typical type panel for this kind of mission with typical concentrators in real thermal conditions.
- 5-2 o The biggest problems will be in margin analysis, testing and packaging given the availability of the basic solar cell converter technology required. Large scale, collimated sunlight electrical, thermal tests of models in a thermal vacuum environment would help considerably. Also large scale thermal vacuum test to aid in the evaluation of thermal deflection at various temperature.
- 5-3 o Thermal vacuum tests of large systems.
- 5-4 o Low temperature/low pressure testing.
- 5-5 o High temperature/low pressure testing.
- 5-6 o U.V. and particle irradiation testing.
- 5-7 o Do roll-up tests with thin cells.
- 5-8 o Evaluate production feasibility of thin cells as soon as possible. Produce 20,000 cells for test and carefully evaluate yield and cost.
- 5-9 o Demonstrate panel assembly feasibility using thin cells. Fabricate several segments (2000 cells each) to evaluate handling and cell attrition.
- 5-10 o Extensive tests on degradation of cells and optical components in the expected environment, including combined effects as feasible.
- 5-11 o Tests of thin cells, with substrate, with expected proton fluences, irradiated from front and back.
- 5-12 o Realistic testing of the various parts of the system is crucial.
- 5-13 o Motion tests to the Shuttle/IUS environment.
- 5-14 o Space test of several thousand thin cells in concentrator configuration.

- 5-15    o    If possible the OFT test should be carried out. Even if this is a small array the data would be extremely useful.
- 5-16    o    Space flight test of reflector surfaces, particularly for degradation of reflectance at wavelengths where solar cells are most responsive.
- 5-17    o    Confirm that plume from ion engines does not impact arrays.
- 5-18    o    Will there be any charging of the arrays etc., from the thrusters? (aside from metal deposition?)

Question 6 - PLEASE ADD COMMENTS THAT YOU FEEL MAY CONTRIBUTE TO THIS ASSESSMENT.

- 6-1 o The problem of cells to operate efficiently at low temperature and low intensity is known and the solution is also unknown. However, these cells have not yet been built. Wraparound cells have been made periodically for the past 12-13 years. Production techniques for fabrication needs to be established.
- 6-2 o An understanding and solution of the anomalous behavior problem in certain types of cells at low light levels and temperatures.
- 6-3 o The electrical performance of solar cell after application of plastic encapsulant needs to be determined.
- 6-4 o Cell performance (including temporary coefficients) as a function of not only light level and temperature but also 1 mev electron fluence needs to be established.
- 6-5 o Where did the radiation fluence estimate come from? How was the proton fluence from solar flare proton predicted?
- 6-6 o Radiation environment needs to be defined closely: electrons, solar wind protons (and their effect on reflectors), and solar flare protons.
- 6-7 o A method to reduce  $\alpha$  needs investigation.
- 6-8 o Cells should probably be low resistivity with more grids than the normal 1 sun cell, perhaps a deeper diffused junction with BSF.
- 6-9 o There seems to be no focussing yet in the most promising array designs or on what the maximum allowable power/weight for the array must be to succeed.
- 6-10 o The problem for this mission probably will not be basic solar cell - structures technology but the understanding needed to evaluate the margin and uncertainties in the design. Extensive test and analysis will be necessary and it may be necessary to carry several design alternatives on simultaneously. Solar cell covers, their production and control needs to be firmed up early and a commitment to a design may really drive the entire power systems design.

- 6-11    o    Power requirements as a function of Heliocentric Distance need definition.
- 6-12    o    Set cell performance/thickness, CG, (and reflector material) and see if mission can be done (e.g., 13.5%, 6 mil w/a).
- 6-13    o    The dynamics and control of systems like this seems hard, especially in such a widely ranging environment, are the calculations being done sufficiently, realistically to ensure that nothing is being overlooked?
- 6-14    o    Thermal bending and effects on control system for orientation mechanism need to be considered.
- 6-15    o    Guidance and stability, e.g., cancellation of moments of inertia needs to be considered.
- 6-16    o    A better assessment of orientation requirements and constraint power regulation and control, thermal control and conditions, is needed.
- 6-17    o    Were all estimates of weights made on a consistent basis, with all elements carefully checked?
- 6-18    o    Need analysis of interconnection scheme.
- 6-19    o    Have all the alternative concepts been eliminated systemically For example, conflicting photovoltaic concepts operating at C.F.'s of 10, 15 or perhaps 25 to 1 with a distributed heat pipe radiator and selective optics. Selective concentration will improve the performance and provide minimum cost at 1 AU with a distributed heat pipe radiator to cell panel area ratio of 4 to 1  $AR = 4$ . Maximum CR is used consistent with HPR ability  $\overline{AF}$  to reject heat.